

LAR 9261-5

ATTACHMENT 3

to

Holtec Letter 5014666

LIST OF EFFECTIVE PAGES

and

PROPOSED SAR

REVISION 13, 13a, and 13b

LIST OF EFFECTIVE PAGES FOR PROPOSED REVISION 13b (RAI Response #2)

<u>Page(s)</u>	<u>Revision</u>
i through xxxiii	11

1.0-1 through 1.0-11	PR13b
1.1-1	PR13
Fig. 1.1.1	7
Fig. 1.1.2	10
Fig. 1.1.3	10
Fig. 1.1.4	10
Fig. 1.1.5	10
1.2-1 through 1.2-76	PR13b
Fig. 1.2.1	7
Fig. 1.2.2	7
Fig. 1.2.3	10
Fig. 1.2.4	10
Fig. 1.2.5	10
Fig. 1.2.6	7
Fig. 1.2.7	7
Fig. 1.2.8	10
Fig. 1.2.9	10
Fig. 1.2.10	PR13
Fig. 1.2.10A	10
Fig. 1.2.10B	10
Fig. 1.2.10C	10
Fig. 1.2.10D	10
Fig. 1.2.11	9
Fig. 1.2.11A	9
Fig. 1.2.12	Deleted
Fig. 1.2.13	4
Fig. 1.2.13A	10
Fig. 1.2.14	4
Fig. 1.2.15	10
Fig. 1.2.16	10
Fig. 1.2.17	10
1.3-1 through 1.3-20	PR13
1.4-1	PR13b
1.4-2	PR13b
Drawings	See Section 1.4
1.5-1	PR13
1.5-2	PR13
1.6-1	PR13a
1.6-2	PR13a
1.6-3	PR13a
1.1-1 through 1.1-10	PR13b
Fig. 1.1.1	PR13
1.A-1 through 1.A-7	10
Fig. 1.A.1 through Fig. 1.A.5	4
1.B-1 through 1.B-3	10
1.B-4 through 1.B-20	Deleted
1.C-1	10
1.C-2 through 1.C-8	7

LIST OF EFFECTIVE PAGES FOR PROPOSED REVISION 13b (RAI Response #2)

<u>Page(s)</u>	<u>Revision</u>
App. 1.D (Total of 9 Pages)	11
2.0-1 through 2.0-6	10
2.1-1 through 2.1-43	PR13
Fig. 2.1.1	7
Fig. 2.1.2	6
Fig. 2.1.3	10
Fig. 2.1.4	10
Fig. 2.1.5	4
Fig. 2.1.6	4
Fig. 2.1.7	4
Fig. 2.1.8	4
Fig. 2.1.9	4
Fig. 2.1.10	6
Fig. 2.1.11	4
Fig. 2.1.12	4
Fig. 2.1.13	4
Fig. 2.1.14	6
2.2-1 through 2.2-5	10
Fig. 2.2.1	4
2.3-1 through 2.3-11	PR13
Fig. 2.3.1	4
Fig. 2.3.2	7
2.4-1 through 2.4-7	PR13b
2.5-1 through 2.5-18	10
Fig. 2.5.1	10
Fig. 2.5.2	10
Fig. 2.5.3 through 2.5.11	Deleted
Fig. 2.5.12	10
Fig. 2.5.13	10
2.6-1 through 2.6-67	PR13
Fig. 2.6.1	4
Fig. 2.6.2	4
Fig. 2.6.3	10
Fig. 2.6.4	10
Fig. 2.6.5	6
Fig. 2.6.6	10
Fig. 2.6.7	10
Fig. 2.6.8	6
Fig. 2.6.9	10
Fig. 2.6.10	10
Fig. 2.6.11	6
Fig. 2.6.12	7
Fig. 2.6.13	7
Fig. 2.6.14	7
Fig. 2.6.15	4
Fig. 2.6.16	8
Fig. 2.6.17	8
Fig. 2.6.18	8
Fig. 2.6.19	8

LIST OF EFFECTIVE PAGES FOR PROPOSED REVISION 13b (RAI Response #2)

<u>Page(s)</u>	<u>Revision</u>
Fig. 2.6.19A	8
Fig. 2.6.19B	8
Fig. 2.6.19C	8
Fig. 2.6.20	10
Fig. 2.6.21	7
Fig. 2.6.22	6
Fig. 2.6.23	8
Fig. 2.6.24	10
Fig. 2.6.25	10
2.7-1 through 2.7-47	PR13a
Fig. 2.7.1	10
Fig. 2.7.2	10
Fig. 2.7.3	10
Fig. 2.7.4	10
Fig. 2.7.5	6
Fig. 2.7.6	6
Fig. 2.7.7	8
Fig. 2.7.8	8
Fig. 2.7.9	8
Fig. 2.7.10	8
Fig. 2.7.11	8
Fig. 2.7.12	8
Fig. 2.7.13	8
Fig. 2.7.14	8
Fig. 2.7.15	8
Fig. 2.7.16	8
Fig. 2.7.17	8
Fig. 2.7.18	8
Fig. 2.7.19 through -22	Deleted
2.8-1	7
2.9-1 through 2.9-19	10
Fig. 2.9.1 through Fig. 2.9.9	8
2.10-1	10
2.10-2	10
2.11-1	10
2.11-2	10
2.11-3	10
2.I-1 through 2.I-16	PR13b
2.A-1 through 2.A-28	PR13a
Fig. 2.A.1.1	10
Fig. 2.A.1.2	10
Fig. 2.A.1.3	10
Fig. 2.A.2.1	10
Fig. 2.A.3.1	10
Fig. 2.A.4.1	10
Fig. 2.A.4.2	10
Fig. 2.A.4.3	10
Fig. 2.A.4.4	10
Fig. 2.A.5.1	10
Fig. 2.A.5.2	10

LIST OF EFFECTIVE PAGES FOR PROPOSED REVISION 13b (RAI Response #2)

<u>Page(s)</u>	<u>Revision</u>
Fig. 2.A.5.3	10
Fig. 2.A.5.4	10
Fig. 2.A.5.5	10
Fig. 2.A.5.6	10
Fig. 2.A.5.7	10
Fig. 2.A.5.8	10
Fig. 2.A.5.9	10
Fig. 2.A.5.10	10
Fig. 2.A.5.11	10
Fig. 2.A.5.12	10
Fig. 2.A.5.13	10
Fig. 2.A.5.14	10
Fig. 2.A.5.15	10
Fig. 2.A.5.15A	10
Fig. 2.A.5.15B	10
Fig. 2.A.5.15C	10
Fig. 2.A.5.16	10
Fig. 2.A.5.17	10
Fig. 2.A.5.17A	10
Fig. 2.A.5.18	10
Fig. 2.A.5.19	10
Fig. 2.a.5.19A	10
Fig. 2.A.5.20	10
Fig. 2.A.5.21	10
Fig. 2.A.5.21A	10
Fig. 2.A.6.1	10
Fig. 2.A.6.2	10
Fig. 2.A.6.3	10
Fig. 2.A.6.4	10
Fig. 2.A.6.5	10
Fig. 2.A.6.6	10
Fig. 2.A.7.1	10
Fig. 2.A.7.2	10
Fig. 2.A.7.3	10
Fig. 2.A.10.1	10
Fig. 2.A.10.2	10
Fig. 2.A.10.3	10
2.B-1	10
2.B-2	10
2.B-3	10
Appendices 2.C through 2.AO	Deleted
3.0-1	11
3.0-2	11
3.1-1 through 3.1-3	PR13b
3.2-1 through 3.2-10	PR13b
3.3-1 through 3.3-4	PR13a
3.4-1 through 3.4-71	PR13b
Fig. 3.4.1	6
Fig. 3.4.2	7

LIST OF EFFECTIVE PAGES FOR PROPOSED REVISION 13b (RAI Response #2)

<u>Page(s)</u>	<u>Revision</u>
Fig. 3.4.3	7
Fig. 3.4.4	4
Fig. 3.4.5	7
Fig. 3.4.6	10
Fig. 3.4.7	6
Fig. 3.4.8	6
Fig. 3.4.9	Deleted
Fig. 3.4.10	10
Fig. 3.4.11	6
Fig. 3.4.12	7
Fig. 3.4.13	7
Fig. 3.4.14	6
Fig. 3.4.15	Deleted
Fig. 3.4.16	6
Fig. 3.4.17	6
Fig. 3.4.18	Deleted
Fig. 3.4.19	7
Fig. 3.4.20	7
Fig. 3.4.21	Deleted
Fig. 3.4.22	7
Fig. 3.4.23	7
Fig. 3.4.24	8
Fig. 3.4.25	8
Fig. 3.4.26	8
Fig. 3.4.27	8
Fig. 3.4.28	8
3.5-1 through 3.5-10	10
Fig. 3.5.1	7
Fig. 3.5.2	6
Fig. 3.5.3	6
Fig. 3.5.4	6
Fig. 3.5.5	6
Fig. 3.5.6	7
Fig. 3.5.7	7
Fig. 3.5.8	7
Fig. 3.5.9	7
3.6-1 through 3.6-4	PR13
3.7-1 through 3.7-4	PR13b
3.I-1 through 3.I-6	PR13b
3.A-1 through 3.A-6	10
3.B-1 through 3.B-4	10
Fig 3.B-1	10
<hr/>	
4.0-1	PR13
4.0-2	PR13
4.1-1 through 4.1-6	PR13
Fig. 4.1.1	8
Fig. 4.1.2	8
Fig. 4.1.3	8
Fig. 4.1.4	PR13-Deleted

LIST OF EFFECTIVE PAGES FOR PROPOSED REVISION 13b (RAI Response #2)

<u>Page(s)</u>	<u>Revision</u>
4.2-1 through 4.2-30	PR13b
4.3-1	PR13
4.3-2	PR13
4.4-1	PR13
4.I-1 through 4.I-16	PR13b
4.A-1 through 4.A-3	8
4.B-1 through 4.B-5	10

5.0-1	10
5.0-2	10
5.1-1 through 5.1-21	PR13
Fig. 5.1.1	10
Fig. 5.1.2	6
5.2-1 through 5.2-59	PR13
5.3-1 through 5.3-11	10
Fig. 5.3.1	10
Fig. 5.3.2	10
Fig. 5.3.3	4
Fig. 5.3.4	10
Fig. 5.3.5	10
Fig. 5.3.6	7
Fig. 5.3.7	6
Fig. 5.3.8	6
Fig. 5.3.9	10
Fig. 5.3.10	10
Fig. 5.3.11	8
Fig. 5.3.12	8
5.4-1 through 5.4-46	PR13a
Fig. 5.4.1	8
Fig. 5.4.2	10
5.5-1 through 5.5-4	PR13
5.6-1 through 5.6-3	10
5.I-1 through 5.I-5	PR13b
5.A-1	7
5.A-2	7
5.A-3	7
5.B-1 through 5.B-6	7
5.C-1 through 5.C-33	10

6.1-1 through 6.1-17	PR13b
6.2-1 through 6.2-58	PR13b
6.3-1 through 6.3-18	PR13b
Fig. 6.3.1	10
Fig. 6.3.1A	10
Fig. 6.3.2	10
Fig. 6.3.3	10
Fig. 6.3.4	10
Fig. 6.3.5	10
Fig. 6.3.6	4
Fig. 6.3.7	10

LIST OF EFFECTIVE PAGES FOR PROPOSED REVISION 13b (RAI Response #2)

<u>Page(s)</u>	<u>Revision</u>
6.4-1 through 6.4-38	PR13b
Fig. 6.4.1	9
Fig. 6.4.2	9
Fig. 6.4.3	9
Fig. 6.4.4	9
Fig. 6.4.5	9
Fig. 6.4.6	9
Fig. 6.4.7	9
Fig. 6.4.8	9
Fig. 6.4.9	10
Fig. 6.4.10	9
Fig. 6.4.11	10
Fig. 6.4.12	10
6.5-1	10
6.6-1	10
6.7-1	10
6.7-2	10
6.I-1 through 6.I-10	PR13b
Fig. 6.I.1 through Fig. 6.I.4	PR13b
6.A-1 through 6.A-22	10
Fig. 6.A.1	7
Fig. 6.A.2	7
Fig. 6.A.3	7
Fig. 6.A.4	7
Fig. 6.A.5	7
Fig. 6.A.6	7
Fig. 6.A.7	10
6.B-1	7
6.B-2	7
Appendix 6.C	Deleted
6.D-1 through 6.D-46	10
6.E-1	10

7.0-1 through 7.0-2	PR13a
7.1-1 through 7.1-8	PR13b
Fig. 7.1.1	PR13b
Fig. 7.1.2a	Deleted
Fig. 7.1.2b	Deleted
Fig. 7.1.2c	Deleted
Fig. 7.1.3	Deleted
Fig. 7.1.4	Deleted
Fig. 7.1.5	Deleted
Fig. 7.1.6	Deleted
Fig. 7.1.7	Deleted
Fig. 7.1.8	Deleted
Fig. 7.1.9	Deleted
Fig. 7.1.10	Deleted
Fig. 7.1.11	Deleted
Fig. 7.1.12	Deleted
Fig. 7.1.13	Deleted

LIST OF EFFECTIVE PAGES FOR PROPOSED REVISION 13b (RAI Response #2)

<u>Page(s)</u>	<u>Revision</u>
Fig. 7.1.14	Deleted
Fig. 7.1.15	Deleted
Fig. 7.1.16	Deleted
Fig. 7.1.17	Deleted
Fig. 7.1.18	Deleted
Fig. 7.1.19	Deleted
Fig. 7.1.20	Deleted
Fig. 7.1.21	Deleted
Fig. 7.1.22	Deleted
Fig. 7.1.23	Deleted
Fig. 7.1.24	Deleted
Fig. 7.1.25	Deleted
Fig. 7.1.26	Deleted
Fig. 7.1.27	Deleted
Fig. 7.1.28	Deleted
Fig. 7.1.29	Deleted
Fig. 7.1.30	Deleted
7.2-1 through 7.2-2	PR13b
Fig. 7.2.1	Deleted
Fig. 7.2.2a	Deleted
Fig. 7.2.2b	Deleted
Fig. 7.2.2c	Deleted
Fig. 7.2.3	Deleted
Fig. 7.2.4	Deleted
Fig. 7.2.5	Deleted
7.3-1 through 7.3-2	PR13a
7.4-1	PR13
7.5-1	PR13a
7.6-1	Deleted
7.I-1	PR13b
<hr/>	
8.1-1 through 8.1-8	PR13b
Fig. 8.1.1	Deleted
Fig. 8.1.2	Deleted
Fig. 8.1.3	Deleted
Fig. 8.1.4	Deleted
8.2-1 through 8.2-3	PR13b
Fig. 8.2.1	Deleted
8.3-1	PR13b
8.4-1	Deleted
8.I-1	PR13

CHAPTER 1: GENERAL INFORMATION

1.0 GENERAL INFORMATION

This Safety Analysis Report (SAR) for Holtec International's HI-STAR 100 packaging is a compilation of information and analyses to support a United States Nuclear Regulatory Commission (NRC) licensing review as a spent nuclear fuel transportation package (Docket No. 71-9261) under requirements specified in 10CFR71 [1.0.1] and 49CFR173 [1.0.2]. This SAR supports NRC approval and issuance of Certificate of Compliance No. 9261, issued under the provisions and definitions in 10CFR71, Subpart D, for the design Model: HI-STAR 100 as an acceptable Type B(U)F-8596 packaging for transport by exclusive use shipment (10CFR71.47).

The HI-STAR 100 packaging complies with the requirements of 10CFR71 for a Type B(U)F-8596 package. The HI-STAR 100 packaging does not have a maximum normal operating pressure (MNOP) greater than 700 kPa (100 lb/in²). The HI-STAR 100 internal design pressure is specified in Table 2.1.1 as 100 psig to calculate bounding stress values. Section 3.4 calculates the MNOP (reported in Table 3.4.15) and demonstrates that the value remains below the design value specified in Table 2.1.1. No pressure relief device is provided on the HI-STAR 100 containment boundary, as discussed in Subsection 1.2.1.8. Therefore, there is no pressure relief device that would allow the release of radioactive material under the tests specified in 10CFR71.73. Analyses that demonstrate that the HI-STAR 100 packaging complies with the requirements of Subparts E and F of 10CFR71 are provided in this SAR. Specific reference to each section of the SAR that is used to specifically address compliance to 10CFR71 is provided in Table 1.0.2. Therefore, the HI-STAR 100 packaging to transport spent nuclear fuel should be designated B(U)F-8596.

The HI-STAR 100 ~~transport index for nuclear criticality control~~ *Criticality Safety Index (CSI)* is zero, as an unlimited number of packages is subcritical under the procedures specified in 10CFR71.59(a). Section 6.1 provides the determination of the ~~transport index for nuclear criticality control~~ *CSI*. The Transport Index (*TI*) based on radiation is in excess of 10 for the HI-STAR 100 Packaging with design basis fuel contents. Therefore, the HI-STAR 100 Packaging must be transported by exclusive use shipment (10CFR71.47).

The HI-STAR 100 packaging design, fabrication, assembly, and testing shall be performed in accordance with Holtec International's quality assurance program. Holtec International's quality assurance program was originally developed to meet NRC requirements delineated in 10CFR50, Appendix B, and was expanded to include provisions of 10CFR71, Subpart H, and 10CFR72, Subpart G, for structures, systems, and components designated as important to safety. NRC approval of Holtec International's quality assurance program is documented by the Quality Assurance Program Approval for Radioactive material Packages (NRC Form 311), Approval Number 0784, Docket No. 71-0784.

This SAR has been prepared in the format and content suggested in NRC Regulatory Guide 7.9 [1.0.3]. The purpose of this chapter is to provide a general description of the design features and transport capabilities of the HI-STAR 100 packaging including its intended use. This chapter provides a summary description of the packaging, operational features, and contents, and provides

reasonable assurance that the package will meet the regulations and operating objectives. Table 1.0.1 contains a listing of the terminology and notation used in preparing this SAR.

This SAR was initially prepared prior to the issuance of the draft version of NUREG-1617 [1.0.5]. To aid NRC review, additional tables and references have been added to facilitate the location of information needed to demonstrate compliance with 10CFR71 as outlined by NUREG-1617. Table 1.0.2 provides a matrix of the 10CFR71 requirements as outlined in NUREG-1617, the format requirements of Regulatory Guide 7.9, and reference to the applicable SAR section(s) that address(es) each topic.

The HI-STAR 100 System is a dual purpose system, certified under 10 CFR 71 and 10 CFR 72. The HI-STAR 100 Final Safety Analysis Report (FSAR) [1.0.6] supports Certificate of Compliance No. 1008 for HI-STAR 100 to store spent nuclear fuel at an Independent Spent Fuel Storage Installation (ISFSI) facility under requirements of 10CFR72, Subpart L [1.0.4] (Docket Number 72-1008).

Within this report, all figures, tables and references cited are identified by the double decimal system m.n.i, where m is the chapter number, n is the section number, and i is the sequential number. Thus, for example, Figure 1.1.1 is the first figure in Section 1.1 of Chapter 1 (which is the next section in this chapter).

Revision of this document was made on a section level. Therefore, if any change occurs on a page, the entire section was updated to the current revision. The locations of specific text changes are indicated by revision bars in the margin of the page. Figures are controlled individually at the latest SAR revision level for that particular figure. Sections and figures unchanged in the latest SAR revision indicate the revision level corresponding to the last changes made in the section/figure. Drawings are also controlled individually within the Holtec International drawing control system. The revisions of drawings included in this revision of this SAR are the same as those incorporated by reference into CoC No. 9261, Amendment 3 46.

This revision of this SAR includes information pertaining to the MPC-32 basket. However, the MPC-32 is not certified for transportation at this time. MPC-32 is under review by the NRC and will be certified in a future CoC amendment.

The HI-STAR 100 Version HB (also called HI-STAR HB) is a shorter variation of the HI-STAR 100 specifically designed for Humboldt Bay fuel [1.0.8]. Information pertaining to the HI-STAR HB System is generally contained in supplements to each chapter identified by a Roman numeral "I" (i.e., Chapter 1 and Supplement 1.I). Certain sections of the main SAR are also affected and are appropriately modified for continuity with the "I" supplements. Unless superseded or specifically modified by information in the "I" supplements, the information in the main SAR chapters is applicable to the HI-STAR HB System.

Through revision 11 of this SAR, discussions were presented that described MPC designs called the MPC-24EF, and MPC-68F. These designs contain features required to classify them as secondary containments, which was necessary for transportation of fuel debris under an earlier version of 10 CFR 71, and were the only MPC designs allowed to be loaded with fuel debris. Recent changes to 10 CFR 71 have eliminated the need for secondary containment of fuel debris. The F-canister

designs have been retained in this SAR; however, any requirements regarding the secondary containment function of these canisters have been removed.

1.0.1 Engineering Change Orders

The changes authorized by the following Holtec Engineering Change Orders (ECOs) are reflected in this revision of this SAR:

MPC-68/68F: ~~ECO 1021-62, 63, 64, 78, None.~~

MPC-24: ~~ECO 1022-58, 59, 67, 68 None.~~

MPC-24E/24EF: ~~ECO 1022-67, 68 None.~~

MPC-32: ~~ECO 1023-31, 32, 33, 43, 45, 46 None.~~

HI-STAR overpack: ECO 1020-48, 50.

MPC Enclosure Vessel: ECO 1023-42, 1021-77, 83.

HI-STAR 100 Assembly for Transport: ECO 1020-51.

Ancillary Equipment: ECO 1027-64, 5014-146, 5014-160.

Table 1.0.1

TERMINOLOGY AND NOTATION

ALARA is an acronym for As Low As Reasonably Achievable.

AL-STAR™ is the trademark name of the HI-STAR 100 impact limiter.

Boral is a generic term to denote an aluminum-boron carbide cermet manufactured in accordance with U.S. Patent No. 4027377. The individual material supplier may use another trade name to refer to the same product.

Boral™ means Boral manufactured by AAR Advanced Structures.

BWR is an acronym for boiling water reactor.

C.G. is an acronym for center of gravity.

Commercial Spent Fuel or CSF refers to nuclear fuel used to produce energy in a commercial nuclear power plant.

Containment System Boundary means the enclosure formed by the overpack inner shell welded to a bottom plate and top flange plus the bolted closure plate with dual seals and the vent and drain port plugs with seals. ~~It is also called the primary containment boundary when used with the inner (secondary) containment boundary of the MPC 68F and MPC 24EF.~~

Containment System means the HI-STAR 100 overpack that forms the containment boundary of the packaging intended to contain the radioactive material during transport.

Cooling Time (or post-irradiation cooling time) for a spent fuel assembly is the time between reactor shutdown and the time the spent fuel assembly is loaded into the MPC.

***Critical Characteristic** means a feature of a component or assembly that is necessary for the proper safety function of the component or assembly. Critical characteristics of a material are those attributes that have been identified, in the associated material specification, as necessary to render the material's intended function.*

***Criticality Safety Index (CSI)** is the dimensionless number (rounded up to the next tenth) assigned to and placed on the label of a fissile material package, to designate the degree of control of accumulation of packages containing fissile material during transportation.*

Damaged Fuel Assembly is a fuel assembly with known or suspected cladding defects, as determined by a review of records, greater than pinhole leaks or hairline cracks, empty fuel rod locations that are not filled with dummy fuel rods, *missing structural components such as grid spacers, whose structural integrity has been impaired such that geometric rearrangement of fuel or*

gross failure of the cladding is expected based on engineering evaluations, or those that cannot be handled by normal means. Fuel assemblies which that cannot be handled by normal means due to fuel cladding damage are considered Fuel Debris FUEL DEBRIS.

Damaged Fuel Container (or Canister) means a specially designed enclosure for damaged fuel assemblies or fuel debris which permits gaseous and liquid media to escape while minimizing dispersal of gross solid particulates.

Enclosure Vessel (or MPC Enclosure Vessel) means the pressure vessel defined by the cylindrical shell, baseplate, port cover plates, lid, closure ring, and associated welds that provides confinement for the helium gas contained within the MPC. The Enclosure Vessel (EV) and the fuel basket together constitute the multi-purpose canister.

Exclusive use means the sole use by a single consignor of a conveyance for which all initial, intermediate, and final loading and unloading are carried out in accordance with the direction of the consignor or consignee. The consignor and the carrier must ensure that loading or unloading is performed by personnel having radiological training and resources appropriate for safe handling of the consignment. The consignor must issue specific instructions, in writing, for maintenance of exclusive use shipment controls, and include them with the shipping paper information provided to the carrier by the consignor.

FSAR is an acronym for Final Safety Analysis Report (10CFR72).

Fuel Basket means a honeycomb structural weldment with square openings which can accept a fuel assembly of the type for which it is designed.

Fuel Debris is ruptured fuel rods, severed fuel rods, loose fuel pellets, or fuel assemblies with known or suspected defects which cannot be handled by normal means due to fuel cladding damage, *including containers and structures supporting these parts*. Fuel debris also includes certain Trojan plant-specific fuel material contained in Trojan Failed Fuel Cans.

HI-STAR 100 overpack or overpack means the cask that receives and contains the sealed multi-purpose canisters containing spent nuclear fuel. It provides the containment boundary for radioactive materials, gamma and neutron shielding, and a set of lifting trunnions for handling. Certain overpack models also include optional pocket trunnions for upending and downending.

HI-STAR 100 System or HI-STAR 100 Packaging consists of the MPC sealed within the HI-STAR 100 overpack with impact limiters installed.

Holtite™ is the trade name for all present and future neutron shielding materials formulated under Holtec International's R&D program dedicated to developing shielding materials for application in dry storage and transport systems. The Holtite development program is an ongoing experimentation effort to identify neutron shielding materials with enhanced shielding and temperature tolerance characteristics. Holtite-A™ is the first and only shielding material qualified under the Holtite R&D program. As such, the terms Holtite and Holtite-A may be used interchangeably throughout this

SAR.

Holtite™-A is a trademarked Holtec International neutron shield material.

***Humboldt Bay Damaged Fuel Container (or Canister)** is a Holtec damaged fuel container custom-designed for Humboldt Bay plant damaged fuel and fuel debris.*

Impact Limiter means a set of fully-enclosed energy absorbers that are attached to the top and bottom of the overpack during transport. The impact limiters are used to absorb kinetic energy resulting from normal and hypothetical accident drop conditions. The HI-STAR impact limiters are called AL-STAR.

Important to Safety (ITS) means a function or condition required to transport spent nuclear fuel safely; to prevent damage to spent nuclear fuel, and to provide reasonable assurance that spent nuclear fuel can be received, handled, packaged, transported, and retrieved without undue risk to the health and safety of the public.

Intact Fuel Assembly is defined as a fuel assembly without known or suspected cladding defects greater than pinhole leaks and hairline cracks, and which can be handled by normal means. Fuel assemblies without fuel rods in fuel rod locations shall not be classified as Intact Fuel Assemblies unless dummy fuel rods are used to displace an amount of water greater than or equal to that displaced by the original fuel rod(s).

Load-and-Go is a term used in this SAR that means the practice of loading spent fuel into the HI-STAR 100 System packaging and placing the packaging into transportation service under 10 CFR 71, without first deploying the system at an Independent Spent Fuel Storage Installation (ISFSI) under 10 CFR 72.

Maximum Normal Operating Pressure (MNOP) means the maximum gauge pressure that would develop in the containment system in a period of 1 year under the heat condition specified in 10CFR71.71(c)(1), in the absence of venting, external cooling by an ancillary system, or operational controls during transport.

Maximum Reactivity means the highest possible k-effective including bias, uncertainties, and calculational statistics evaluated for the worst-case combination of fuel basket manufacturing tolerances.

MGDS is an acronym for Mined Geological Depository System.

MPC Fuel Basket means the honeycombed composite cell structure utilized to maintain subcriticality of the spent nuclear fuel. The number and size of the storage cells depends on the type of spent nuclear fuel to be transported. Each MPC fuel basket has sheathing welded to the storage cell walls for retaining the ~~Boral~~ neutron absorber. *The neutron absorber ~~Boral~~* is a commercially-available thermal neutron poison material composed of boron carbide and aluminum.

Multi-Purpose Canister (MPC) means the sealed canister consisting of a honeycombed fuel basket for spent nuclear fuel storage, contained in a cylindrical canister shell (the MPC Enclosure Vessel). There are different MPCs with different fuel basket geometries for storing PWR or BWR fuel. All MPCs except the Trojan and Humboldt Bay plant MPCs have identical exterior dimensions. The Trojan plant MPCs have the same outside diameter, but are approximately nine inches shorter than the generic MPC design. *The Humboldt Bay plant MPCs have the same outside diameter, but are approximately 6.3 feet shorter.* MPC is an acronym for multi-purpose canister. ~~The~~ Many of the MPCs used as part of the HI-STAR 100 Packaging are identical to the MPCs authorized for use in the HI-STAR 100 Storage (Docket No. 72-1008) and HI-STORM 100 Storage (72-1014) [1.0.7] CoCs to the extent that *many of* the particular MPC models are authorized for use under both CoCs.

Neutron Absorber Material is a generic term used in this SAR to indicate any neutron absorber material qualified for use in the HI-STAR 100 System MPCs.

Neutron Shielding means Holtite, a material used in the overpack to thermalize and capture neutrons emanating from the radioactive spent nuclear fuel.

Neutron Sources means specially designed inserts for fuel assemblies that produce neutrons for startup of the reactor. The specific types of neutron sources authorized for transportation in the HI-STAR 100 System are discussed in Section 1.2.3.

Non-fuel Hardware, or NFH, means Burnable Poison Rod Assemblies (BPRAs), Thimble Plug Devices (TPDs), Control Rod Assemblies (CRAs), Axial Power Shaping Rods (APSRs), Wet Annular Burnable Absorbers (WABAs), Rod Cluster Control Assemblies (RCCAs), Control Element Assemblies (CEAs), water displacement guide tube plugs, orifice rod assemblies, and vibration suppressor inserts. The specific types of NFH authorized for transportation in the HI-STAR 100 System are discussed in Section 1.2 of this SAR.

Packaging means the HI-STAR 100 System consisting of a single HI-STAR 100 overpack, a set of impact limiters, and a multi-purpose canister (MPC). It excludes all lifting devices, rigging, transporters, saddle blocks, welding machines, and auxiliary equipment (such as the drying and helium backfill system) used during fuel loading operations and preparation for off-site transportation.

Package means the HI-STAR 100 System plus the licensed radioactive contents loaded for transport.

Planar-Average Initial Enrichment is the average of the distributed fuel rod initial enrichments within a given axial plane of the assembly lattice.

PWR is an acronym for pressurized water reactor.

Reactivity is used synonymously with effective multiplication factor or k-effective.

SAR is an acronym for Safety Analysis Report (10CFR71).

~~**Secondary Containment Boundary** means the Enclosure Vessel of the "F" model MPC. The secondary containment boundary of the "F" model MPC provides the separate inner container for the transport of fuel debris. The "F" model MPC, in conjunction with the overpack containment system boundary, is designed to meet the double barrier requirement of 10CFR71.63(b) for plutonium shipments.~~

Single Failure Proof means that the handling system is designed so that a single failure will not result in the loss of the capability of the system to safely retain the load.

SNF is an acronym for spent nuclear fuel.

STP is Standard Temperature (298°K) and Pressure (1 atm) conditions.

Transport index (TI) means the dimensionless number (rounded up to the next tenth) placed on the label of a package, to designate the degree of control to be exercised by the carrier during transportation. The transport index is ~~determined for fissile material packages as the number determined by multiplying the maximum radiation level in millisievert per hour at one meter (3.3 ft) from the external surface of the package by 100 (equivalent to the maximum radiation level in millirem per hour at one meter (3.3 ft)); or, for criticality control purposes, the number obtained as described in 10CFR71.59, whichever is larger.~~

Trojan Damaged Fuel Container (or Canister) is a Holtec damaged fuel container custom-designed for Trojan plant damaged fuel and fuel debris. Trojan plant damaged fuel and fuel debris not loaded into a Trojan Failed Fuel Can must be loaded into a Trojan Damaged Fuel Container.

Trojan Failed Fuel Can (FFC) is a non-Holtec designed Trojan plant-specific damaged fuel container that may be loaded with Trojan plant damaged fuel assemblies, Trojan fuel assembly metal fragments (e.g., portions of fuel rods, grid assemblies, bottom nozzles, etc.), a Trojan fuel rod storage container, a Trojan Fuel Debris Process Can Capsule, or a Trojan Fuel Debris Process Can.

Trojan Failed Fuel Can Spacer is a square, structural steel tube with a baseplate designed to be placed inside one Trojan Failed Fuel Can to occupy any space between the top of the contents and the top of the FFC in order to minimize movement of the FFC contents during transportation.

Trojan Fuel Debris Process Can is a Trojan plant-specific canister containing fuel debris (metal fragments) and was used to process organic media removed from the Trojan plant spent fuel pool during cleanup operations in preparation for spent fuel pool decommissioning. Trojan Fuel Debris Process Cans are loaded into Trojan Fuel Debris Process Can Capsules or directly into Trojan Failed Fuel Cans.

Trojan Fuel Debris Process Can Capsule is a Trojan plant-specific canister that contains up to five Trojan Fuel Debris Process Cans and is vacuumed, purged, backfilled with helium, and then seal-welded closed.

Undamaged fuel assemblies are fuel assemblies where all the exterior rods in the assembly are visually inspected and shown to be intact. The interior rods of the assembly are in place; however the cladding of these rods is of unknown condition. This definition only applies to Humboldt Bay fuel assembly array/class 6x6D and 7x7C.

ZR means any zirconium-based fuel cladding material authorized for use in a commercial nuclear power plant reactor. Any reference to Zircaloy fuel cladding in this SAR applies to any zirconium-based fuel cladding material.

Table 1.0.2

HI-STAR 100 SAR CORRELATION WITH 10CFR71 AND REGULATORY GUIDE 7.9

RG 7.9 Section	10CFR Part 71 Section	HI-STAR SAR Section
1.1	71.31(a)(1), 71.31(a)(2), 71.31(a)(3), 71.31(c), 71.33(a)(1), 71.33(a)(3), 71.35(b), 71.37, 71.59	1.0, 1.1, 1.2, 1.5
1.2	71.31(a)(1), 71.33(a)(2), 71.33(a)(4), 71.33(a)(5), 71.33(a)(6), 71.33(b), 71.43(b)	1.2, 1.3, 1.4
None	71.31(a)(2), 71.35(a), 71.41(a)	1.5
1.3	None	Appendices 1.A, 1.B, and 1.C
2.1, 2.2	71.31(a)(1), 71.31(c), 71.33	2.1, 2.2
2.3, 2.4	71.43(d)	2.3, 2.4
2.5	71.45	2.5
2.6, 2.7	71.31(a)(2), 71.35(a), 71.41(a), 71.61, 71.71, 71.73	2.6, 2.7
2.6	71.35(a), 71.41(a), 71.43(f), 71.51(a)(1), 71.55(d)(4), 71.71	2.6
2.7	71.35(a), 71.41(a), 71.73	2.7
None	71.61	2.7
None	71.85(b)	8.1.2.2 8.1.3
2.10	None	2.10
3.1	71.31(a)(1), 71.31(c), 71.33(a)(5), 71.33(a)(6), 71.33(b)(1), 71.33(b)(3), 71.33(b)(5), 71.33(b)(7), 71.33(b)(8), 71.51(c)	Chapters 1 & 2, Sections 3.0, 3.1, 3.4, 3.6
3.2, 3.3	71.31(a)(1), 71.33(a)(5)	Chapters 1 & 2, Sections 3.0, 3.1, 3.4, 3.6
None	71.31(a)(2), 71.35(a), 71.41(a)	3.0, 3.1, 3.4, 3.5, 3.6
None	71.43(g)	3.0, 3.4, 3.6
3.4	71.43(f), 71.51(a)(1), 71.71	3.0, 3.4, 3.6
3.5	71.73	3.0, 3.5, 3.6
3.6	None	N/A
4.1	71.31(a)(1), 71.31(c), 71.33(a)(4), 71.33(a)(5), 71.33(b)(1), 71.33(b)(3), 71.33(b)(5), 71.33(b)(7), 71.43(c), 71.43(d), 71.43(e)	4.0, 4.1, 4.2, 4.3
4.2	71.31(a)(2), 71.35(a), 71.41(a), 71.43(f), 71.43(h), 71.51(a)(1), 71.51(c)	4.2, 4.3
4.3	71.31(a)(2), 71.35(a),	4.2, 4.3

Table 1.0.2 (continued)

HI-STAR 100 SAR CORRELATION WITH 10CFR71 AND REGULATORY GUIDE 7.9

RG 7.9 Section	10CFR Part 71 Section	HI-STAR SAR Section
	71.41(a), 71.51(a)(2), 71.51(c)	
4.4	71.63	4.2, 4.3
4.5	None	-
5.1	71.31(a)(1), 71.31(c), 71.33(a)(5)	5.1
5.2	71.31(a)(1), 71.33(b)(1), 71.33(b)(2), 71.33(b)(3)	5.2
5.3	71.31(a), 71.31(b)	5.3
5.4	71.31(a)(2), 71.35(a), 71.41(a), 71.43(f), 71.47(b), 71.51(a)(1), 71.51(a)(2)	5.1, 5.4, 5.5
5.5	None	Appendices 5.A, 5.B, 5.C
6.1	71.31(a)(1), 71.31(c), 71.33(a)(5), 71.35(b), 71.59(b)	6.1
6.2	71.31(a)(1), 71.33(b)(1), 71.33(b)(2), 71.33(b)(3), 71.83	6.2
6.3	71.31(a)(2), 71.35(a), 71.41(a)	6.3
6.4	71.35, 71.43(f), 71.51(a)(1), 71.55(b), 71.55(d), 71.55(e), 71.59	6.4
6.5	71.31(a)(2), 71.35	6.5, Appendix 6.A
6.6	None	6.2, 6.4, Appendices 6.B, 6.C, 6.D
7.1	71.31(c), 71.35(c), 71.43(g), 71.47(b), 71.47(c), 71.47(d), 71.87, 71.89	7.4, 7.1.3, 7.1.7 7.1
7.2	71.35(c)	7.1.7 7.2
7.3	71.87(i)	7.1.7 7.3
None	71.35(c)	7.1.7 7.0
7.4	None	-
8.1	71.31(c), 71.37(b), 71.85(a), 71.85(b), 71.85(c), 71.87(g), 71.93(b)	8.1
8.2	71.31(c), 71.37(b), 71.87(b), 71.87(g), 71.93(b)	8.2

Notes:

“-“ There is no HI-STAR SAR section that addresses this.

1.1 INTRODUCTION

HI-STAR 100 (acronym for Holtec International Storage, Transport and Repository) is a spent nuclear fuel (SNF) packaging designed to be in general compliance with the U.S. Department of Energy's (DOE) original design procurement specifications for multi-purpose canisters and large transportation casks [1.1.1], [1.1.2].

The HI-STAR 100 System consists of a sealed, metal multi-purpose canister, herein abbreviated as the "MPC", contained within an overpack with impact limiters. Figure 1.1.1 provides a pictorial view of the HI-STAR 100 System. The HI-STAR 100 System is designed to accommodate a wide variety of spent fuel assemblies in a single overpack design by utilizing different MPC basket designs. The exterior dimensions of all MPCs (except the custom-designed Trojan plant and Humboldt Bay MPCs) are identical to allow the use of a single overpack design. The Trojan plant MPCs are approximately nine inches shorter than the generic Holtec MPC design and have the same outer diameter. *The Humboldt Bay MPCs are approximately 6.3 feet shorter than the generic Holtec MPC design and have the same outer diameter.* Each of the MPCs has different design features (e.g., fuel baskets) to accommodate distinct fuel characteristics. Each MPC is identified by the maximum quantity of fuel assemblies it is capable of receiving. The MPC-24, -24E, and -24EF each can contain a maximum of 24 PWR assemblies; the MPC-32 can contain up to 32 PWR assemblies; and the MPC-68 and -68F each can contain a maximum of 68 BWR fuel assemblies; *and the MPC-HB for Humboldt Bay can contain up to 80 fuel assemblies.* Figure 1.1.2 depicts the HI-STAR 100 with two of its major constituents, the MPC and the overpack, in a cutaway view. This view does not include depiction of the spacer required for the Trojan version of the MPC-24E/EF design, which is shorter than the Holtec generic MPC-24E/EF design. The spacer is required for the shorter MPC to ensure the design characteristics of the HI-STAR 100 System (e.g., center-of-gravity, MPC lid-to-overpack closure plate gap, etc.) remain bounded by the supporting analyses. See Figure 1.1.5 for a depiction of the Trojan MPC spacer. A drawing of the Trojan MPC spacer is also included in Section 1.4. A summary of the qualification of the spacer for performing its design function is provided in Section 2.7.1.1.

Figure 1.1.2 also indicates that the overpack pocket trunnions are optional appurtenances. Overpack serial numbers 1020-001 through 1020-007 include the pocket trunnions, while later serial number overpacks do not. The impact of this design change on vehicle tie down methods and qualification analyses are discussed in Section 2.5 of this SAR. The pocket trunnions are not part of the qualified vehicle tie-down system for the package. Figure 1.1.3 provides an elevation cross sectional view of an MPC, and Figure 1.1.4 contains an elevation cross sectional view of the HI-STAR 100 overpack.

The HI-STAR 100 System is designed for both storage and transport. The HI-STAR 100 System's multi-purpose design reduces SNF handling operations and thereby enhances radiological protection. Once SNF is loaded and the MPC and overpack are sealed, the HI-STAR 100 System can be positioned on site for temporary or long-term storage or transported directly off-site. The HI-STAR 100 System's ability to both store and transport SNF eliminates repackaging.

1.2 PACKAGE DESCRIPTION

1.2.1 Packaging

The HI-STAR 100 System consists of an MPC designed for BWR or PWR spent nuclear fuel, an overpack that provides the containment boundary and a set of impact limiters that provide energy absorption capability for the normal and hypothetical accident conditions of transport. Each of these components is described below, including information with respect to component fabrication techniques and designed safety features. This discussion is supplemented by a set of drawings in Section 1.4. Section 1.3 provides the HI-STAR 100 design code applicability and details any alternatives to the ASME Code.

Before proceeding to present detailed physical data on HI-STAR 100, it is contextual to summarize the design attributes that set it apart from the prior generation of spent fuel transportation packages.

There are several features in the HI-STAR 100 System design that increase its effectiveness with respect to the safe transport of spent nuclear fuel (SNF). Some of the principal features of the HI-STAR 100 System that enhance its effectiveness are:

- the honeycomb design of the MPC fuel basket
- the effective distribution of neutron and gamma shielding materials within the system
- the high heat rejection capability
- the structural robustness of the multi-shell overpack construction

The honeycomb design of the MPC fuel baskets renders the basket into a multi-flanged plate weldment where all structural elements (box walls) are arrayed in two orthogonal sets of plates. Consequently, the walls of the cells are either completely coplanar (no offset) or orthogonal with each other. There is complete edge-to-edge continuity between contiguous cells.

Among the many benefits of the honeycomb construction is the uniform distribution of the metal mass over the body of the basket (in contrast to the "box and spacer disk" construction where the support plates are localized mass points). Physical reasoning suggests that a uniformly distributed mass provides a more effective shielding barrier than can be obtained from a non-uniform (box and spacer disk) basket. In other words, the honeycomb basket is a more effective radiation attenuation device.

The complete cell-to-cell connectivity inherent in the honeycomb basket structure provides an uninterrupted heat transmission path, making the HI-STAR 100 MPC an effective heat rejection device.

The multi-layer shell construction in the overpack provides a natural barrier against crack propagation in the radial direction across the overpack structure. If, during a hypothetical

accident (impact) event, a crack was initiated in one layer, the crack could not propagate to the adjacent layer. Additionally, it is highly unlikely that a crack would initiate as the thinner layers are more ductile than a thicker plate.

In this Safety Analysis Report the HI-STAR 100 System design is demonstrated to have predicted responses to accident conditions that are clearly acceptable with respect to certification requirements for post-accident containment system integrity, maintenance of subcriticality margin, dose rates, and adequate heat rejection capability. Table 1.2.18 presents a summary of the HI-STAR 100 System performance against these aspects of post-accident performance at two levels. At the first level, the integrity of the MPC boundary prevents release of radioactive material or helium from the MPC, and ingress of moderator. The integrity of the MPC is demonstrated by the analysis of the response of this high quality, ASME Code, Section III, Subsection NB-designed, pressure vessel to the accident loads while in the overpack. With this demonstration of MPC integrity, the excellent performance results listed in the second column of Table 1.2.18 constitute an acceptable basis for certification of the HI-STAR 100 System for the safe transport of spent nuclear fuel. However, no credit is taken for MPC integrity for certification of the HI-STAR 100 System for the transport of intact or damaged fuel assemblies. ~~Credit is only taken for the additional containment boundary of the MPC 68F and MPC 24EF for the transport of fuel classified as fuel debris in order to meet the requirements of 10 CFR 71.63(b).~~

The HI-STAR 100 System provides a large margin of safety. The third column in Table 1.2.18 summarizes the performance if the MPC is postulated to suffer gross failure in the post-accident analysis. Even with this postulated failure, the performance of the HI-STAR 100 System is acceptable for the transport of intact and damaged fuel assemblies, showing the defense-in-depth methodology incorporated into the HI-STAR 100 System.

The containment boundary of the HI-STAR 100 System is shown to satisfy the special requirements of 10CFR71.61 for irradiated nuclear fuel shipments.

~~To meet the requirements of 10CFR71.63(b) for plutonium shipments, which is considered applicable for the transport of fuel classified as fuel debris, double containment is provided by the containment boundary of the overpack and the secondary containment boundary of the MPC 68F and MPC 24EF, serving as a separate inner container.~~

1.2.1.1 Gross Weight

The gross weight of the HI-STAR 100 System depends on which of the MPCs is loaded into the HI-STAR 100 overpack for shipment. Table 2.2.1 summarizes the maximum calculated component weights for the HI-STAR 100 overpack, impact limiters, and each MPC loaded to maximum capacity with design basis SNF. The maximum gross transport weight of the HI-STAR 100 System is to be marked on the packaging nameplate.

1.2.1.2 Materials of Construction, Dimensions, and Fabrication

All materials used to construct the HI-STAR 100 System are ASME Code materials, except the neutron shield, neutron poison, optional aluminum heat conduction elements, thermal expansion foam, seals, pressure relief devices, aluminum honeycomb, pipe couplings, and other material classified as Not Important to Safety. The specified materials of construction along with outline dimensions for important-to-safety items are provided in the drawings in Section 1.4.

The materials of construction and method of fabrication are further detailed in the subsections that follow. Section 1.3 provides the codes applicable to the HI-STAR 100 packaging for materials, design, fabrication, and inspection, including NRC-approved alternatives to the ASME Code.

1.2.1.2.1 HI-STAR 100 Overpack

The HI-STAR 100 overpack is a heavy-walled steel cylindrical vessel. ~~A single overpack design is provided that is capable of transporting each type of MPC.~~ The inner diameter of the overpack is approximately 68-3/4 inches and the height of the internal cavity is ~~approximately usually~~ 191-1/8 inches, *however, shorter overpacks are available to meet site-specific requirements. Refer to Supplement 1.1 for details of the Humboldt Bay HI-STAR HB.* The overpack inner cavity is sized to accommodate the MPCs. The outer diameter of the overpack is approximately 96 inches and the height is approximately 203-1/4 inches, *however, shorter overpacks are available to meet site-specific requirements. Refer to Supplement 1.1 for details of the Humboldt Bay HI-STAR HB.*

Figure 1.2.1 provides a cross sectional elevation view of the overpack containment boundary. The overpack containment boundary is formed by a steel inner shell welded at the bottom to a bottom plate and, at the top, to a heavy top flange with a bolted closure plate. Two concentric grooves are machined into the closure plate for the seals. The closure plate is recessed into the top flange and the bolted joint is configured to protect the closure bolts and seals in the event of a drop accident. The closure plate has test and vent ports that are closed by a threaded port plug with a seal. The bottom plate has a drain port that is also closed by a threaded port plug with a seal. The containment boundary forms an internal cylindrical cavity for housing the MPC.

The outer surface of the overpack inner shell is buttressed with intermediate shells of gamma shielding that are installed in a manner to ensure a permanent state of contact between adjacent layers. Besides serving as an effective gamma shield, these layers provide additional strength to the overpack to resist puncture or penetration. *Except in the HI-STAR HB (refer to Supplement 1.1),* radial channels are vertically welded to the outside surface of the outermost intermediate shell at equal intervals around the circumference. These radial channels act as fins for improved heat conduction to the overpack outer enclosure shell surface and as cavities for retaining and protecting the neutron shielding. The enclosure shell is formed by welding enclosure shell panels between each of the channels to form additional cavities. Neutron shielding material is placed into each of the radial cavity segments formed by the radial channels, the outermost intermediate shell, and the enclosure shell panels. The exterior flats of the radial channels and enclosure shell panels form the overpack outer enclosure shell (Figure 1.2.2). Atop the outer enclosure shell, pressure relief devices (e.g., rupture disks) are positioned in a recessed area. The relief devices

relieve internal pressure that may develop as a result of the fire accident and subsequent off-gassing of the neutron shield material. Within each radial channel, a layer of silicone sponge is positioned to act as a thermal expansion foam to compress as the neutron shield expands in the axial direction. Appendix 1.C provides material information on the thermal expansion foam. Figure 1.2.2 provides a mid-plane cross section view of the overpack, depicting the inner shell, intermediate shells, radial channels, outer enclosure shell, and neutron shield. *Refer to drawings in Supplement 1.1 for HI-STAR HB.*

The exposed steel surfaces (except seal seating surfaces) of the overpack and the intermediate shell layers are coated to prevent corrosion. Coating materials are chosen based on the expected service conditions, considering the dual purpose certification status of the HI-STAR 100 System under 10 CFR 72 for spent fuel storage as well as transportation. The coatings applied to the overpack exposed exterior and interior surfaces are specified on the drawings in Section 1.4. The material data on the coatings is provided in Appendix 1.C. The inner cavity of the overpack is coated with a material appropriate to its high temperatures and the exterior of the overpack is coated with a material appropriate for fuel pool operations and environmental exposure. The coating applied to the intermediate shells acts as a surface preservative and is not exposed to the fuel pool or ambient environment.

Lifting trunnions are attached to the overpack top flange for lifting and rotating the cask body between vertical and horizontal positions. The lifting trunnions are located 180° apart in the sides of the top flange. On overpack serial numbers 1020-001 through 1020-007, pocket trunnions are welded to the lower side of the overpack 180° apart to provide a pivoting axis for rotation. The pocket trunnions are slightly off-center to ensure proper rotation direction of the overpack. As shown in Figure 1.1.4, the trunnions do not protrude beyond the cylindrical envelope of the overpack outer enclosure shell. This feature reduces the potential for direct impact on a trunnion in the event of an overpack side impact. After fabrication of HI-STAR overpack serial number 1020-007, the pocket trunnions were deleted from the overpack design.

1.2.1.2.2 Multi-Purpose Canisters

1.2.1.2.2.1 General Description

In this subsection, discussion of those attributes applicable to all of the MPC models is provided. Differences among the models are discussed in subsequent subsections. Specifications for the authorized contents of each MPC model, including non-fuel hardware and neutron sources are provided in Section 1.2.3.

The HI-STAR 100 MPCs are welded cylindrical structures with flat ends. Each MPC is an assembly consisting of a honeycombed fuel basket, a baseplate, a canister shell, a lid with vent and drain ports and cover plates, and a closure ring. The outer diameter of all MPCs and cylindrical height of each generic design MPC is fixed (see discussion in Subsection 1.2.1.2.2.3 regarding Trojan plant-specific MPCs and *Supplement 1.1 for Humboldt Bay plant-specific MPCs*). The number of spent nuclear fuel storage locations in each of the MPCs depends on the fuel assembly characteristics. As the generic MPCs are interchangeable, they correspondingly have identical exterior dimensions. The outer dimension of the MPC is nominally 68-3/8 inches

and the length is nominally 190-1/4 inches. Figures 1.2.3-1.2.5 depict the cross sectional views of the different MPCs. Drawings of the MPCs are provided in Section 1.4. Key system data for the HI-STAR 100 System are outlined in Tables 1.2.2 and 1.2.3.

The generic MPC-24/24E/24EF and Trojan plant MPC-24E/EF differ in construction from the MPC-32 and MPC-68/68F in one important aspect: the fuel cells are physically separated from one another by a flux trap between each cell for criticality control (Figures 1.2.3 and 1.2.4). All MPC baskets are formed from an array of plates welded to each other, such that a honeycomb structure is created that resembles a multi-flanged, closed-section beam in its structural characteristics.

The MPC fuel basket is positioned and supported within the MPC shell by a series of basket supports welded to the inside of the MPC shell. In the peripheral area created by the basket, the MPC shell, and the basket supports, optional aluminum heat conduction elements are installed in some early production MPC-68 and MPC-68F models (see Figure 1.2.3). These heat conduction elements are fabricated from thin aluminum alloy 1100 in shapes and a design that allows a snug fit in the confined spaces and ease of installation. The heat conduction elements are along the full length of the MPC basket, except at the drain pipe location, to create a nonstructural thermal connection that facilitates heat transfer from the basket to the shell. In their operating condition, the heat conduction elements conform to, and contact the MPC shell and basket walls. In SAR Revision 10, a refined thermal analysis, described in Chapter 3, has allowed the elimination of these heat conduction elements from the MPC design, thus giving this design feature "optional" status.

Lifting lugs attached to the inside surface of the MPC canister shell serve to permit placement of the empty MPC into the overpack, and are considered non-structural, non-pressure retaining attachments to the MPC pressure boundary. The lifting lugs also serve to axially locate the MPC lid prior to welding. These internal lifting lugs are not used to handle a loaded MPC, since the MPC lid blocks access to the lifting lugs.

The top of the HI-STAR 100 MPC incorporates a redundant closure system. Figure 1.2.6 provides a sketch of the MPC closure details. The MPC lid is a circular plate (fabricated from one piece, or two pieces - split top and bottom) that is edge-welded to the MPC shell. If the two-piece lid design is employed, only the top piece is analyzed as part of the enclosure vessel pressure boundary. The bottom piece acts primarily as a radiation shield and is attached to the top piece with a non-structural, non-pressure retaining weld, as depicted on the MPC enclosure vessel drawing in Section 1.4. The MPC lid is equipped with vent and drain ports that are used to remove moisture and gas from the MPC and backfill the MPC with a specified pressure of inert gas (helium). The vent and drain ports are sealed closed by cover plates welded to the MPC lid before the closure ring is installed. The closure ring is a circular ring edge-welded to the MPC shell and MPC lid. The MPC lid provides sufficient rigidity to allow the entire MPC loaded with SNF to be lifted by the threaded holes in the MPC lid during transfer from the storage-only HI-STORM 100 System to the HI-STAR 100 overpack for transportation. Threaded insert plugs are installed to provide shielding when the threaded holes are not in use.

All MPCs are designed to handle intact fuel assemblies, damaged fuel assemblies, and fuel classified as fuel debris. Damaged fuel and fuel debris must be transported in damaged fuel containers or other approved damaged/failed fuel canister. At this time, ~~only~~ BWR damaged fuel and fuel debris from ~~the Dresden Unit 1 and Humboldt Bay plants~~ is certified for transportation in the MPC-68 and the MPC-68F. *Humboldt Bay damaged fuel and fuel debris will be transported in the MPC-HB (refer to Supplement 1.1).* Similarly, only PWR damaged fuel and fuel debris from the Trojan plant is certified for transportation in the Trojan plant-specific MPC-24E and the MPC-24EF. The definitions, and applicable specifications for all authorized contents, including the requirements for canning certain fuel, are provided in Subsection 1.2.3.

Intact SNF can be placed directly into the MPC. Damaged SNF and fuel debris must be placed into a Holtec damaged fuel container or other authorized canister for transportation inside the MPC and the HI-STAR 100 overpack. Figures 1.2.10 through 1.2.11 provide sketches of the containers authorized for transportation of damaged fuel and fuel debris in the HI-STAR 100 System. One Dresden Unit 1 Thoria rod canister, shown in Figure 1.2.11A, is also authorized for transportation in HI-STAR 100.

~~In order to qualify the MPC-68F and MPC-24EF shells as a secondary containment boundary for the transportation of Dresden Unit 1/Humboldt Bay and Trojan plant fuel debris, respectively,~~ †The MPC-68 and MPC-24E enclosure vessels have been slightly modified to further strengthen the lid-to-shell joint area. These ~~fuel debris~~-MPCs are given the "F" suffix (hence, MPC-68F and MPC-24EF)†. The differences between the standard and "F-model" MPC lid-to-shell joints are shown on Figure 1.2.17, and include a thickened upper shell, a larger lid-to-shell weld size, and a correspondingly smaller lid diameter. The design of the rest of the enclosure vessel is identical between the standard MPC and the "F-model" MPC.

~~The MPC-68F and MPC-24EF provide the separate inner container per 10CFR71.63(b) for the HI-STAR 100 System transporting fuel classified as fuel debris to ensure double containment. The overpack containment boundary provides the primary containment boundary.~~

1.2.1.2.2.2 MPC-24/24E/24EF

The MPC-24 is designed to transport up to 24 PWR intact fuel assemblies meeting the limits specified in Subsection 1.2.3. The MPC 24E is designed to transport up to 24 PWR intact and up to four PWR damaged fuel assemblies in damaged fuel containers. The MPC-24EF is designed to transport up to 24 PWR intact fuel assemblies and up to four PWR damaged fuel assemblies or fuel assemblies classified as fuel debris. At this time, however, generic PWR damaged fuel and fuel debris are not authorized for transportation in the MPC-24E/EF.

All MPC-24-series fuel baskets employ the flux trap design for criticality control, as shown in the drawings in Section 1.4. The fuel basket design for the MPC-24E is an enhanced MPC-24 basket layout designed to improve the fuel storage geometry for criticality control. The fuel basket design of the MPC-24EF is identical to the MPC-24E. The MPC-24E/EF basket designs

† The drawing in Section 1.4 also denotes an MPC-68FF ~~fuel debris~~ canister design. However, the MPC-68FF is not authorized for use in transportation under the HI-STAR 100 10 CFR 71 CoC.

also employ a higher ¹⁰B loading than the MPC-24, as shown in Table 1.2.3. The differences between the MPC-24EF enclosure vessel design and the MPC-24/24E enclosure vessel are discussed in Subsection 1.2.1.2.2.1.

1.2.1.2.2.3 Trojan Plant MPC-24E/EF

The Trojan plant MPC-24E and -24EF models are designs that have been customized for that plant's fuel and the concrete storage cask being used at the Trojan plant Independent Spent Fuel Storage Installation (ISFSI) (Docket 72-0017). The design features that are unique to the Trojan plant MPCs are specifically noted on the MPC enclosure vessel and MPC-24E/EF fuel basket drawings in Section 1.4. These differences include:

- a shorter MPC fuel basket and cavity length to match the shorter Trojan fuel assembly length
- shorter corner fuel storage cell lengths to accommodate the Trojan Failed Fuel Cans
- a different fuel storage cell and flux trap dimension in the corner cells to accommodate the Trojan Failed Fuel Cans
- a different configuration of the flow holes at the bottom of the fuel basket (rectangular vs. semi-circular)

All other design features in the Trojan MPCs are identical to the generic MPC-24E/EF design. The HI-STAR 100 overpack design has not been modified for the Trojan MPC design.

The technical analyses described in this SAR were verified in most cases to bound the Trojan-specific design features. Where necessary, Trojan plant-specific evaluations were performed and are summarized in the appropriate SAR section. To accommodate the shorter Trojan plant MPC length in a standard-length HI-STAR 100 overpack, a spacer was designed for installation into the overpack above the Trojan MPC (see Figure 1.1.5 and the drawing in Section 1.4) for transportation in the standard-length HI-STAR 100 overpack. This spacer prevents the MPC from moving more than the MPC was analyzed to move in the axial direction and serves to transfer the axial loads from the MPC lid to the overpack top closure plate within the limits of the supporting analyses. See Section 2.7.1.1 for additional discussion of the spacer used with the Trojan MPC design. Hereafter in this SAR, the Trojan plant-specific MPC design is only distinguished from the generic MPC-24E/EF design when necessary to describe unique evaluations performed for those MPCs.

1.2.1.2.2.4 MPC-32

NOTE: The MPC-32 is not certified for transportation at this time.

The MPC-32 is designed to transport up to 32 PWR intact fuel assemblies meeting the specifications in Subsection 1.2.3. Damaged fuel and fuel debris are not permitted to be transported in the MPC-32. The MPC-32 enclosure vessel design is identical to the MPC-24/24E

enclosure vessel design as shown on the drawings in Section 1.4. The MPC-32 fuel basket does not employ flux traps for criticality control. Credit for burnup of the fuel is taken in the criticality analyses for accident conditions and to meet the requirements of 10 CFR 71.55(b). Because the MPC is designed to preclude the intrusion of moderator under all normal and credible accident conditions of transport, the moderator intrusion condition analyzed as required by 10 CFR 71.55(b) is a non-mechanistic event for the HI-STAR 100 System.

1.2.1.2.2.5 MPC-68/68F

The MPC-68 is designed to transport up to 68 BWR intact fuel assemblies and damaged fuel assemblies meeting the specifications in Subsection 1.2.3. Zircaloy channels are permitted. At this time, only damaged fuel from the Dresden Unit 1 and Humboldt Bay plants is authorized for transportation in the MPC-68. The MPC-68F is designed to transport only fuel and other authorized material from the Dresden Unit 1 and Humboldt Bay plants meeting the specifications in Subsection 1.2.3. The sole difference between the MPC-68 and MPC-68F fuel basket design is a reduction in the required ^{10}B areal density in the ~~Boral~~ *neutron absorber*. A reduction in the required ^{10}B areal density of the ~~Boral~~ *neutron absorber* is possible for the MPC-68F due to limited types of fuel and low enrichments permitted to be transported in this MPC model. The differences between the MPC-68F enclosure vessel design and the MPC-68 enclosure vessel are discussed in Subsection ~~1.2.1.2.2.1~~ 1.0.

1.2.1.2.2.6 Alloy X

The HI-STAR MPC is constructed entirely from stainless steel alloy materials (except for the neutron absorber and aluminum vent and drain cap seal washers in all MPCs, and the aluminum heat conduction elements in the first several production units of MPC-68 and MPC-68F). No carbon steel parts are used in the design of the HI-STAR 100 MPC. Concerns regarding interaction of coated carbon steel materials and various MPC operating environments [1.2.1] are not applicable to the HI-STAR MPCs. All structural components in a HI-STAR MPC will be fabricated of Alloy X, a designation that warrants further explanation.

Alloy X is a fictitious material that should be acceptable as a Mined Geological Depository System (MGDS) waste package and that meets the thermophysical properties set forth in this document.

At this time, there is considerable uncertainty with respect to the material of construction for an MPC that would be acceptable as a waste package for the MGDS. Candidate materials being considered for acceptability by the DOE include:

- Type 316
- Type 316LN
- Type 304
- Type 304LN

The DOE material selection process is primarily driven by corrosion resistance in the potential environment of the MGDS. As the decision regarding a suitable material to meet disposal

requirements is not imminent, this application requests approval for use of any one of the four Alloy X materials.

For the MPC design and analysis, Alloy X (as defined in this SAR) may be one of the following materials. Any steel part in an MPC may be fabricated from any of the acceptable Alloy X materials listed below, except that all steel pieces comprising the MPC shell (i.e., the 1/2" thick cylinder) must be fabricated from the same Alloy X stainless steel type:

- Type 316
- Type 316LN
- Type 304
- Type 304LN

The Alloy X approach is accomplished by qualifying the MPC for all mechanical, structural, neutronic, radiological, and thermal conditions using material thermophysical properties that are the least favorable for the entire group for the analysis in question. For example, when calculating the rate of heat rejection to the outside environment, the value of thermal conductivity used is the lowest for the candidate material group. Similarly, the stress analysis calculations use the lowest value of the ASME Code allowable stress intensity for the entire group. Stated differently, we have defined a material, which is referred to as Alloy X, whose thermophysical properties, from the MPC design perspective, are the least favorable of the candidate materials group. The evaluation of the Alloy X constituents to determine the least favorable properties is provided in Appendix I.A.

The Alloy X approach is conservative because no matter which material is ultimately utilized, the Alloy X approach guarantees that the performance of the MPC will exceed the analytical predictions contained in this document.

1.2.1.3 Impact Limiters

The HI-STAR 100 overpack is fitted with aluminum honeycomb impact limiters, termed AL-STAR™, one at each end, once the overpack is positioned and secured in the transport frame. The impact limiters ensure the inertia loadings during the normal and hypothetical accident conditions of transport are maintained below design levels. The impact limiter design is discussed further in Chapter 2 and drawings are provided in Section 1.4.

1.2.1.4 Shielding

The HI-STAR 100 System is provided with shielding to minimize personnel exposure. The HI-STAR 100 System will be transported by exclusive use shipment to ensure the external radiation requirements of 10CFR71.47 are met. During transport, a personnel barrier is installed to restrict access to the overpack to protect personnel from the HI-STAR 100 exterior surface temperature in accordance with 10CFR71.43(g). The personnel barrier provides a stand-off equal to the exterior radial dimension of the impact limiters. Figure 1.2.8 provides a sketch of the personnel barrier being installed.

The initial attenuation of gamma and neutron radiation emitted by the radioactive spent fuel is provided by the MPC fuel basket structure built from inter-welded plates and Boral neutron poison panels with sheathing attached to the fuel cell walls. The MPC canister shell, baseplate, and lid provide additional thicknesses of steel to further reduce gamma radiation and, to a smaller extent, neutron radiation at the outer MPC surfaces. No shielding credit is taken for the aluminum heat conduction elements installed in some of the early production MPC-68 and MPC-68F units.

The primary HI-STAR 100 shielding is located in the overpack and consists of neutron shielding and additional layers of steel for gamma shielding. Neutron shielding is provided around the outside circumferential surface of the overpack. Gamma shielding is provided by the overpack inner, intermediate and enclosure shells with additional axial shielding provided by the bottom plate and the top closure plate. During transport, the impact limiters will provide incremental gamma shielding and provide additional distance from the radiation source at the ends of the package. An additional circular segment of neutron shielding is contained within each impact limiter to provide neutron attenuation.

1.2.1.4.1 Neutron Absorber Materials

Both Boral and Metamic are neutron absorber materials made of B₄C and Aluminum. Boral is used in the MPC-24/24E/24EF, MPC-68/68F, and Trojan MPC-24E/24EF. Metamic is used in the MPC-HB.

1.2.1.4.1.1 Boral Neutron Absorber

Boral is a thermal neutron poison material composed of boron carbide and aluminum alloy 1100. Boron carbide is a compound having a high boron content in a physically stable and chemically inert form. The boron carbide contained in Boral is a fine granulated powder that conforms to ASTM C-750-80 nuclear grade Type III. The aluminum alloy 1100 is a lightweight metal with high tensile strength that is protected from corrosion by a highly resistant oxide film. The two materials, boron carbide and aluminum, are chemically compatible and ideally suited for long-term use in the radiation, thermal, and chemical environment of a nuclear reactor, spent fuel pool, or dry cask.

The documented historical applications of Boral, in environments comparable to those in spent fuel pools and fuel storage casks, dates to the early 1950s (the U.S. Atomic Energy Commission's AE-6 Water-Boiler Reactor [1.2.2]). Technical data on the material was first printed in 1949, when the report "Boral: A New Thermal Neutron Shield" was published [1.2.3]. In 1956, the first edition of the "Reactor Shielding Design Manual" [1.2.4], contains a section on Boral and its properties.

In the research and test reactors built during the 1950s and 1960s, Boral was frequently the material of choice for control blades, thermal-column shutters, and other items requiring very good thermal-neutron absorption properties. It is in these reactors that Boral has seen its longest service in environments comparable to today's applications.

Boral found other uses in the 1960s, one of which was a neutron poison material in baskets used in the shipment of irradiated, enriched fuel rods from Canada's Chalk River laboratories to Savannah River. Use of Boral in shipping containers continues, with Boral serving as the poison in many cask designs.

Boral has been licensed by the NRC for use in numerous BWR and PWR spent fuel storage racks and has been extensively used in international nuclear installations.

Boral has been exclusively used in fuel storage applications in recent years. Its use in spent fuel pools as the neutron absorbing material can be attributed to its proven performance and several unique characteristics, such as:

- The content and placement of boron carbide provides a very high removal cross section for thermal neutrons.
- Boron carbide, in the form of fine particles, is homogeneously dispersed throughout the central layer of the Boral panels.
- The boron carbide and aluminum materials in Boral do not degrade as a result of long-term exposure to radiation.
- The neutron absorbing central layer of Boral is clad with permanently bonded surfaces of aluminum.
- Boral is stable, strong, durable, and corrosion resistant.

Boral absorbs thermal neutrons without physical change or degradation of any sort from the anticipated exposure to gamma radiation and heat. The material does not suffer loss of neutron attenuation capability when exposed to high levels of radiation dose.

Holtec International's QA Program ensures that Boral is manufactured under the control and surveillance of a Quality Assurance/Quality Control Program that conforms to the requirements of 10CFR71, Subpart H and 10CFR72, Subpart G. Holtec International has procured over 200,000 panels of Boral from AAR Advanced Structures for over 20 projects. Boral has always been purchased with a minimum ^{10}B loading requirement. Coupons extracted from production runs were tested using the "wet chemistry" procedure. The actual ^{10}B loading, out of thousands of coupons tested, has never been found to fall below the design specification. The size of this coupon database is sufficient to provide confidence that all future procurements will continue to yield Boral with full compliance with the stipulated minimum loading. Furthermore, the surveillance, coupon testing, and material tracking processes that have so effectively controlled the quality of Boral are expected to continue to yield Boral of similar quality in the future. Nevertheless, to add another layer of insurance, only 75% ^{10}B credit of the fixed neutron absorber is assumed in the criticality analysis.

Operating experience in nuclear plants with fuel loading of Boral equipped MPCs as well as laboratory test data indicate that the aluminum used in the manufacture of the Boral may react

with water, resulting in the generation of hydrogen. The numerous variables (i.e., aluminum particle size, pool temperature, pool chemistry, etc.) that influence the extent of the hydrogen produced make it impossible to predict the amount of hydrogen that may be generated during MPC loading or unloading at a particular plant. Therefore, due to the variability in hydrogen generation from the Boral-water reaction, the operating procedures in Chapter 7 require monitoring for combustible gases and either exhausting or purging the space beneath the MPC lid during loading and unloading operations when an ignition event could occur (i.e., when the space beneath the MPC lid is open to the welding or cutting operation).

1.2.1.4.1.2 METAMIC[®]

METAMIC[®] is a neutron absorber material developed by the Reynolds Aluminum Company in the mid-1990s for spent fuel reactivity control in dry and wet storage applications. Metallurgically, METAMIC[®] is a metal matrix composite (MMC) consisting of a matrix of 6061 aluminum alloy reinforced with Type 1 ASTM C-750 boron carbide. METAMIC[®] is characterized by extremely fine aluminum (325 mesh or better) and boron carbide powder. Typically, the average B₄C particle size is between 10 and 15 microns. As described in the U.S. patents held by METAMIC, Inc.^{1,2}, the high performance and reliability of METAMIC[®] derives from the particle size distribution of its constituents, rendered into a metal matrix composite by the powder metallurgy process. This yields excellent and uniform homogeneity.

The powders are carefully blended without binders or other additives that could potentially adversely influence performance. The maximum percentage of B₄C that can be dispersed in the aluminum alloy 6061 matrix is approximately 40 wt.%, although extensive manufacturing and testing experience is limited to approximately 31 wt.%. The blend of powders is isostatically compacted into a green billet under high pressure and vacuum sintered to near theoretical density.

According to the manufacturer, billets of any size can be produced using this technology. The billet is subsequently extruded into one of a number of product forms, ranging from sheet and plate to angle, channel, round and square tube, and other profiles. For the METAMIC[®] sheets used in the MPCs, the extruded form is rolled down into the required thickness.

METAMIC[®] has been subjected to an extensive array of tests sponsored by the Electric Power Research Institute (EPRI) that evaluated the functional performance of the material at elevated temperatures (up to 900°F) and radiation levels (1E+11 rads gamma). The results of the tests documented in an EPRI report (Ref. [1.2.17]) indicate that METAMIC[®] maintains its physical and neutron absorption properties with little variation in its properties from the unirradiated state. The main conclusions provided in the above-referenced EPRI report are summarized below:

¹ U.S. Patent No. 5,965,829, "Radiation Absorbing Refractory Composition".

² U.S. Patent No. 6,042,779, "Extrusion Fabrication Process for Discontinuous Carbide Particulate Metal Matrix Composites and Super, Hypereutectic Al/Si."

- The metal matrix configuration produced by the powder metallurgy process with a complete absence of open porosity in METAMIC[®] ensures that its density is essentially equal to the theoretical density.
- The physical and neutronic properties of METAMIC[®] are essentially unaltered under exposure to elevated temperatures (750° F - 900° F).
- No detectable change in the neutron attenuation characteristics under accelerated corrosion test conditions has been observed.

In addition, independent measurements of boron carbide particle distribution show extremely small particle-to-particle distance[†] and near-perfect homogeneity.

An evaluation of the manufacturing technology underlying METAMIC[®] as disclosed in the above-referenced patents and of the extensive third-party tests carried out under the auspices of EPRI makes METAMIC[®] an acceptable neutron absorber material for use in the MPCs. Holtec's technical position on METAMIC[®] is also supported by the evaluation carried out by other organizations.

Consistent with its role in reactivity control, all METAMIC[®] material procured for use in the Holtec MPCs will be qualified as important-to-safety (ITS) Category A item. ITS category A manufactured items, as required by Holtec's NRC-approved Quality Assurance program, must be produced to essentially preclude the potential of an error in the procurement of constituent materials and the manufacturing processes. Accordingly, material and manufacturing control processes must be established to eliminate the incidence of errors, and inspection steps must be implemented to serve as an independent set of barriers to ensure that all critical characteristics defined for the material by the cask designer are met in the manufactured product.

All manufacturing and in-process steps in the production of METAMIC[®] shall be carried out using written procedures. As required by the company's quality program, the material manufacturer's QA program and its implementation shall be subject to review and ongoing assessment, including audits and surveillances as set forth in the applicable Holtec QA procedures to ensure that all METAMIC[®] panels procured meet with the requirements appropriate for the quality genre of the MPCs. Additional details pertaining to the qualification and production tests for METAMIC[®] are summarized in Subsection 9-1.5.38.1.5.5.2.

Because of the absence of interconnected porosities, the time required to dehydrate a METAMIC[®]-equipped MPC is expected to be less compared to an MPC containing Boral.

NUREG/CR-5661 (Ref. [1.2.20]) recommends limiting poison material credit to 75% of the minimum ¹⁰B loading because of concerns for potential "streaming" of neutrons, and allows for

[†] Medium measured neighbor-to-neighbor distance is 10.08 microns according to the article, "METAMIC Neutron Shielding", by K. Anderson, T. Haynes, and R. Kazmier, EPRI Boraflex Conference, November 19-20, 1998.

greater percentage credit in criticality analysis "if comprehensive acceptance tests, capable of verifying the presence and uniformity of the neutron absorber, are implemented". The value of 75% is characterized in NUREG/CR-5661 as a very conservative value, based on experiments with neutron poison containing relatively large B₄C particles, such as BORAL with an average particle size in excess of 100 microns. METAMIC[®], however, has a much smaller particle size of typically between 10 and 15 microns on average. Any streaming concerns would therefore be drastically reduced.

Analyses performed by Holtec International show that the streaming due to particle size is practically non-existent in METAMIC[®]. Further, EPRI's neutron attenuation measurements on 31 and 15 B₄C weight percent METAMIC[®] showed that METAMIC[®] exhibits very uniform ¹⁰B areal density. This makes it easy to reliably establish and verify the presence and microscopic and macroscopic uniformity of the ¹⁰B in the material. Therefore, 90% credit can be applied to the minimum ¹⁰B areal density in the criticality calculations, i.e. a 10% penalty can be applied. This 10% penalty is considered conservative since there are no significant remaining uncertainties in the ¹⁰B areal density. In Chapter 98 the qualification and on-production tests for METAMIC[®] to support 90% ¹⁰B credit are specified. With 90% credit, the target weight percent of boron carbide in METAMIC[®] is 31 for all MPCs, as summarized in Table 1.2.378, consistent with the test coupons used in the EPRI evaluations [1.2.17]. The maximum permitted value is 33.0 wt% to allow for necessary fabrication flexibility.

Because METAMIC[®] is a solid material, there is no capillary path through which spent fuel pool water can penetrate METAMIC[®] panels and chemically react with aluminum in the interior of the material to generate hydrogen. Any chemical reaction of the outer surfaces of the METAMIC[®] neutron absorber panels with water to produce hydrogen occurs rapidly and reduces to an insignificant amount in a short period of time. Nevertheless, combustible gas monitoring for METAMIC[®]-equipped MPCs and purging or exhausting the space under the MPC lid during welding and cutting operations, is required until sufficient field experience is gained that confirms that little or no hydrogen is released by METAMIC[®] during these operations.

Mechanical properties of 31 wt.% METAMIC[®], based on coupon tests of the material in the as-fabricated condition and after 48 hours of an elevated temperature state at 900°F, are summarized below from the EPRI report [1.2.17].

Mechanical Properties of 31wt.% B ₄ C METAMIC		
Property	As-Fabricated	After 48 hours of 900°F Temperature Soak
Yield Strength (psi)	32937 ± 3132	28744 ± 3246
Ultimate Strength (psi)	40141 ± 1860	34608 ± 1513
Elongation (%)	1.8 ± 0.8	5.7 ± 3.1

The required flexural strain of the neutron absorber to ensure that it will not fracture when the supporting basket wall flexes, due to the worst case lateral inertial loading is 0.2%, which is the

flexural strain of the Alloy X basket panel material. The 1% minimum elongation of 31wt.% B₄C METAMIC[®] indicated by the above table means that a large margin of safety against cracking exists, so there is no need to perform testing of the METAMIC[®] for mechanical properties.

EPRI's extensive characterization effort [1.2.17], which was focused on 15 and 31 wt.% B₄C METAMIC[®] served as the principal basis for a recent USNRC SER for 31wt.% B₄C METAMIC for used in wet storage [1.2.18]. Additional studies on METAMIC[®] [1.2.19], EPRI's and others work provide the confidence that 31wt.% B₄C METAMIC[®] will perform its intended function in the MPCs. Finally to further substantiate the performance of Metamic (with maximum B₄C of up to 33%), Holtec has performed robust independent qualification testing as documented in Holtec Proprietary Report [1.2.21].

1.2.1.4.2 Holtite-A[™] Neutron Shielding

The specification for the overpack and impact limiter neutron shield material is predicated on functional performance criteria. These criteria are:

- Attenuation of neutron radiation and associated neutron capture to appropriate levels;
- Durability of the shielding material under normal conditions, in terms of thermal, chemical, mechanical, and radiation environments;
- Stability of the homogeneous nature of the shielding material matrix;
- Stability of the shielding material in mechanical or thermal accident conditions to the desired performance levels; and
- Predictability of the manufacturing process under adequate procedural control to yield an in-place neutron shield of desired function and uniformity.

Other aspects of a shielding material, such as ease of handling and prior nuclear industry use, are also considered, within the limitations of the main criteria. Final specification of a shield material is a result of optimizing the material properties with respect to the main criteria, along with the design of the shield system, to achieve the desired shielding results.

Holtite-A is the only approved neutron shield material that fulfills the aforementioned criteria. Holtite-A is a poured-in-place solid borated synthetic neutron-absorbing polymer. Holtite-A is specified with a nominal B₄C loading of 1 weight percent for the HI-STAR 100 System. Appendix 1.B provides the Holtite-A material properties germane to its function as a neutron shield. Holtec has performed confirmatory qualification tests on Holtite-A under the company's QA program.

In the following, a brief summary of the performance characteristics and properties of Holtite-A is provided.

Density

The nominal specific gravity of Holtite-A is 1.68 g/cm^3 as specified in Appendix 1.B. To conservatively bound any potential weight loss at the design temperature and any inability to reach the theoretical density, the density is reduced by 4% to 1.61 g/cm^3 . The density used for the shielding analysis is assumed to be 1.61 g/cm^3 to underestimate the shielding capabilities of the neutron shield.

Hydrogen

The nominal weight concentration of hydrogen is 6.0%. However, all shielding analyses conservatively assume 5.9% hydrogen by weight in the calculations.

Boron Carbide

Boron carbide dispersed within Holtite-A in finely dispersed powder form is present in 1% (nominal) weight concentration. Holtite-A may be specified with a B_4C content of up to 6.5 weight percent. For the HI-STAR 100 System, Holtite-A is specified with a nominal B_4C weight percent of 1%.

Design Temperature

The design temperature of Holtite-A is set at 300°F . The maximum spatial temperature of Holtite-A under all normal operating conditions must be demonstrated to be below this design temperature.

Thermal Conductivity

It is evident from Figure 1.2.2 that Holtite-A is directly in the path of heat transmission from the inside of the overpack to its outside surface. For conservatism, however, the design basis thermal conductivity of Holtite-A under heat rejection conditions is set equal to zero, *except for HI-STAR HB*. The reverse condition occurs under a postulated fire event when the thermal conductivity of Holtite-A aids in the influx of heat to the stored fuel in the fuel basket. The thermal conductivity of Holtite-A is conservatively set at $1 \text{ Btu/hr-ft-}^\circ\text{F}$ for all fire accident analyses.

The Holtite-A neutron shielding material is stable at normal design temperatures over the long term and provides excellent shielding properties for neutrons.

1.2.1.4.3 Gamma Shielding Material

For gamma shielding, HI-STAR 100 utilizes carbon steel in plate stock form. Instead of utilizing a thick forging, the gamma shield design in the HI-STAR 100 overpack borrows from the concept of layered vessels from the field of ultra-high pressure vessel technology. The shielding is made from successive layers of plate stock. The fabrication of the shell begins by rolling the inner shell plate and making the longitudinal weld seam. Each layer of the intermediate shells is

constructed from two halves. The two halves of the shell are precision sheared, beveled, and rolled to the required radii. The two halves of the second layer are wrapped around the first shell. Each shell half is positioned in its location and while applying pressure using a specially engineered fixture, the halves are tack welded. The beveled edges to be joined are positioned to make contact or have a slight gap. The second layer is made by joining the two halves using two longitudinal welds. Successive layers are assembled in a like manner. Thus, the welding of every successive shell provides a certain inter-layer contact (Figure 1.2.7).

A thick structural component radiation barrier is thus constructed with four key features, namely:

- The number of layers can be increased as necessary to realize the required design objectives.
- The layered construction is ideal to stop propagation of flaws.
- The thinner plate stock is much more ductile than heavy forgings used in other designs.
- Post-weld heat treatment is not required by the ASME Code, simplifying fabrication.

1.2.1.5 Lifting and Tie-Down Devices

The HI-STAR 100 overpack is equipped with two lifting trunnions located in the top flange. The lifting trunnions are designed in accordance with 10CFR71.45, NUREG-0612 [1.2.11], and ANSI N14.6 [1.3.3], manufactured from a high strength alloy, and are installed in threaded openings. The lifting trunnions may be secured in position by optional locking pads, shaped to make conformal contact with the curved overpack. Once the locking pad is bolted in position, the inner diameter is sized to restrain the trunnion from backing out. The two off-center pockets located near the overpack bottom plate on overpack serial numbers 1020-001 through 1020-007 are pocket trunnions. The pocket trunnions were eliminated from the design after serial number 1020-007 was fabricated and are no longer considered qualified tie-down devices. However, the pocket trunnions on these overpacks may still be used for normal handling activities such as upending and downending.

The lifting, upending, and downending of the HI-STAR 100 System requires the use of external handling devices. A lifting yoke is utilized when the cask is to be lifted or set in a vertical orientation. For those overpacks that have been fabricated with the pocket trunnions, transport and rotation cradles may include rotation trunnions that interface with the pocket trunnions to provide a pivot axis. A lift yoke may be connected to the lifting trunnions and the crane hook used for upending or downending the HI-STAR 100 System by rotating on the pocket trunnions for these overpacks. For those overpacks fabricated without pocket trunnions, the overpack must be transferred into the transport saddle with appropriate lift rigging. If an overpack having pocket trunnions is secured to the transport vehicle without engaging the pocket trunnions, plugs are required to be installed in the pocket to provide radiation shielding (see the overpack drawing in Section 1.4).

For transportation, the HI-STAR 100 System is engineered to be mounted on a transport frame secured to the transporter bed. Figure 1.2.8 provides a sketch of the HI-STAR 100 System secured for transport and the drawing in Section 1.4 provides additional details. The transport frame has a lower saddle with attachment points for belly slings around the cask body designed to prevent excessive vertical or lateral movement of the cask during normal transportation. The impact limiters affixed to both ends of the cask are designed to transmit the design basis axial loads into the cradle structure. See Section 2.5 for discussion of the qualification of tie-down devices.

The top of the MPC lid is equipped with four threaded holes that allow lifting of the loaded MPC. These holes allow the loaded MPC to be raised and/or lowered from the HI-STAR overpack. For users of the HI-STORM 100 Dry Storage System, MPC handling operations are performed using a HI-TRAC transfer cask of the HI-STORM 100 System (Docket No. 72-1014). The HI-TRAC transfer cask allows the sealed MPC loaded with spent fuel to be transferred from the HI-STORM 100 overpack (storage-only) to the HI-STAR 100 overpack, or vice versa. The threaded holes in the MPC lid are designed in accordance with NUREG-0612 and ANSI N14.6 and are plugged during transportation to prevent radiation streaming.

1.2.1.6 Heat Dissipation

The HI-STAR 100 System can safely transport SNF by maintaining the fuel cladding temperature below the limits specified in Table 1.2.3 for normal and accident conditions. These limits have been established consistent with the guidance in NRC Interim Staff Guidance (ISG) document No. 11, Revision 2 (Ref. [1.2.14]). The temperature of the fuel cladding is dependent on the decay heat and the heat dissipation capabilities of the cask. The total heat load per BWR and PWR MPC is identified in Table 1.2.3. The SNF decay heat is passively dissipated without any mechanical or forced cooling.

The HI-STAR 100 System must meet the requirements of 10 CFR 71.43(g) for the accessible surface temperature limit. To meet this requirement the HI-STAR 100 System is shipped as an exclusive use shipment and includes an engineered personnel barrier during transport.

The primary heat transfer mechanisms in the HI-STAR 100 System are conduction and surface radiation.

The free volume of the MPC and the annulus between the external surface of the MPC and the inside surface of the overpack containment boundary are filled with 99.995% pure helium gas during fuel loading operations. Table 1.2.3 specifies the acceptance criteria for helium fill pressure in the MPC internal cavity. Besides providing an inert dry atmosphere for the fuel cladding, the helium also provides conductive heat transfer across any gaps between the metal surfaces inside the MPC and in the annulus between the MPC and overpack containment boundary. Metal conduction transfers the heat throughout the MPC fuel basket, through the MPC aluminum heat conduction elements (if installed) and shell, through the overpack inner shell, intermediate shells, steel radial connectors and finally, to the outer neutron shield enclosure shell. The most adverse temperature profiles and thermal gradients for the HI-STAR 100 System with each of the MPCs are discussed in detail in Chapter 3. The thermal analysis in Chapter 3 no

longer takes credit for the aluminum heat conduction elements and they have been designated as optional equipment.

1.2.1.7 Coolants

There are no coolants utilized in the HI-STAR 100 System. As discussed in Subsection 1.2.1.6 above, helium is sealed within the MPC internal cavity. The annulus between the MPC outer surface and overpack containment boundary is also purged and filled with helium gas.

1.2.1.8 Pressure Relief Systems

No pressure relief system is provided on the HI-STAR 100 packaging containment boundary.

The sole pressure relief devices are provided in the overpack outer enclosure (Figure 1.1.4). The overpack outer enclosure contains the neutron shield material. Normal loadings will not cause the rupture disks to open. The rupture disks are installed to relieve internal pressure in the neutron shield cavities caused by the fire accident. The overpack outer enclosure is not designed as a pressure vessel. Correspondingly, the rupture disks are designed to open at relatively low pressures as stated below.

Relief Device location	Set pressure, psig
Overpack outer enclosure	30, +/- 5

1.2.1.9 Security Seal

The HI-STAR 100 packaging provides a security seal that while intact, provides evidence that the package has not been opened by unauthorized persons. When installed, the impact limiters cover all penetrations into the HI-STAR 100 packaging containment boundary. Therefore, the security seal is placed to ensure that the impact limiters are not removed which thereby ensures that the package has not been opened. As shown on the HI-STAR transport assembly drawing in Section 1.4, security seals are provided on one impact limiter attachment bolt on the top impact limiter and through two adjacent bolts on the bottom impact limiter. A hole is provided in the head of the bolt and the impact limiter. Lock wire shall be threaded through the hole and joined with a security seal.

1.2.1.10 Design Life

The design life of the HI-STAR 100 System is 40 years. This is accomplished by using materials of construction with a long proven history in the nuclear industry and specifying materials known to withstand their operating environments with little to no degradation. A maintenance program, as specified in Chapter 8, is also implemented to ensure the HI-STAR 100 System will exceed its design life of 40 years. The design considerations that assure the HI-STAR 100 System performs as designed throughout the service life include the following:

HI-STAR Overpack

- Exposure to Environmental Effects
- Material Degradation
- Maintenance and Inspection Provisions

MPC

- Corrosion
- Structural Fatigue Effects
- Maintenance of Helium Atmosphere
- Allowable Fuel Cladding Temperatures
- Neutron Absorber Boron Depletion

1.2.2 Operational Features

Table 1.2.7 provides the sequence of basic operations necessary to load fuel and prepare the HI-STAR 100 System for transport. More detailed guidance for transportation-related loading, unloading, and handling operations is provided in Chapter 7 and is supported by the drawings in Section 1.4. A summary of the loading and unloading operations is provided below. Figures 1.2.9 and 1.2.16 provide a pictorial view of the loading and unloading operations, respectively.

1.2.2.1 Applicability of Operating Procedures for the Dual-Purpose HI-STAR 100 System

The HI-STAR 100 System is a dual-purpose system certified for use as a dry storage cask under 10 CFR 72 and a transportation package under 10 CFR 71. In addition, the MPC is certified for use under 10 CFR 72 in the storage-only HI-STORM 100 System (a ventilated concrete cask system). Therefore, it is possible that the HI-STAR 100 overpack and/or the MPC may be loaded, prepared, and sealed under the operating procedures for storage, delineated in the HI-STAR 100 storage FSAR (Docket 72-1008) or the HI-STORM 100 storage FSAR (Docket 72-1014) *or under a site specific storage license*. In those cases, the operating procedures governing MPC and overpack preparation for storage would apply. The MPC and HI-STAR 100 overpack, as applicable, must be confirmed to meet all requirements of the Part 71 Certificate of Compliance before being released for shipment.

For those instances where the MPC is being loaded and shipped off-site in a HI-STAR 100 overpack under 10 CFR 71 without first being deployed at an ISFSI (known as “load-and-go” operations), the operating procedures in Chapter 7 (and summarized below) apply for preparation of the MPC and HI-STAR overpack. For those cases where the MPC is transferred from storage in a HI-STORM overpack to a HI-STAR overpack for shipment, the operating procedures in Chapter 7 (and summarized below) govern the preparation activities for the HI-STAR overpack.

Loading Operations

At the start of loading operations, the overpack is configured with the closure plate removed. The lift yoke is used to position the overpack in the designated preparation area or setdown area for overpack inspection and MPC insertion. The annulus is filled with plant demineralized water and

an ~~inflatable~~ annulus seal is installed. The ~~inflatable~~ seal prevents contact between spent fuel pool water and the MPC shell reducing the possibility of contaminating the outer surfaces of the MPC. The MPC is then filled with spent fuel pool water or plant demineralized water (~~borated as required for MPC 32~~). The overpack and MPC are lowered into the spent fuel pool for fuel loading using the lift yoke. Pre-selected assemblies are loaded into the MPC and a visual verification of the assembly identification is performed.

While still underwater, a thick shielding lid (the MPC lid) is installed. The lift yoke is remotely engaged to the overpack lifting trunnions and is used to lift the overpack close to the spent fuel pool surface. The MPC lift bolts (securing the MPC lid to the lift yoke) are removed. As the overpack is removed from the spent fuel pool, the lift yoke and overpack are sprayed with demineralized water to help remove contamination.

The overpack is removed from the pool and placed in the designated preparation area. The top surfaces of the MPC lid and the top flange of the overpack are decontaminated. The ~~inflatable~~ annulus seal is removed, and an annulus shield is installed. The annulus shield provides additional personnel shielding at the top of the annulus and also prevents small items from being dropped into the annulus (foreign material exclusion). If used, the Automated Welding System (AWS) is installed. The MPC water level is lowered slightly and the space under the MPC lid is purged or exhausted and monitoring is performed. The MPC lid is seal-welded using the AWS. Liquid penetrant examinations are performed on the root and final passes and ultrasonic examination is also performed on the MPC lid-to-shell weld or, in place of the ultrasonic examination, the weld may be inspected by multiple-pass liquid penetrant examination at approximately every 3/8 inch of weld depth. ~~Then a small volume of the water is displaced with helium gas. The helium gas is used for leakage testing. A helium leakage rate test is performed on the MPC lid confinement weld (lid to shell) to verify weld integrity and to ensure that the leakage rates are within acceptance criteria. The MPC water is displaced from the MPC by blowing pressurized helium or nitrogen gas into the vent port of the MPC, thus displacing the water through the drain line.~~ At the appropriate time in the sequence of activities, based on the type of test performed (hydrostatic or pneumatic), a pressure test of the MPC enclosure vessel is performed.

The Forced Helium Dehydration (FHD) System is connected to the MPC and is used to remove residual water from the MPC and reduce the level of moisture in the MPC to acceptable levels. This is accomplished by recirculating dry, heated helium through the MPC cavity to absorb the moisture. When the helium exiting the MPC is determined to meet the required moisture limit, the MPC is considered sufficiently dried for transportation (see Section 3.4.1.1.16 for a description of the FHD System).

Following MPC drying operations, the MPC is backfilled with a predetermined amount of helium gas. The helium backfill ensures adequate heat transfer, *and* provides an inert atmosphere for fuel cladding integrity, ~~and provides the means of future leakage rate testing of the MPC enclosure vessel boundary welds. Cover plates are installed and seal-welded over the MPC vent and drain ports with liquid penetrant examinations performed on the root and/or final passes, depending on the number of weld passes required. That is, if only a single weld pass is required,~~

~~only a final liquid penetrant examination is performed. The cover plates are helium leakage tested to confirm that they meet the established leakage rate criteria.~~

The MPC closure ring is then placed on the MPC, aligned, tacked in place, and seal welded, providing redundant closure of the MPC enclosure vessel closure welds. Tack welds are visually examined, and the root and/or final welds (depending on the number of weld passes required) are inspected using the liquid penetrant examination technique to ensure weld integrity. The annulus shield is removed and the remaining water in the annulus is drained. The AWS is removed. The overpack closure plate is installed and the bolts are torqued. The overpack annulus is dried using the vacuum drying system (VDS).

~~If the MPC being transported is an "F model" canister, a helium leakage test on the canister must be performed to confirm the integrity of the secondary containment boundary prior to backfilling the overpack annulus.~~

The overpack annulus is backfilled with helium gas for heat transfer and seal testing. Concentric metallic seals in the overpack closure plate prevent the leakage of the helium gas from the annulus and provide the containment boundary to the release of radioactive materials. The seals on the overpack vent and drain port plugs are leak tested along with the overpack closure plate inner seal. Cover plates with metallic seals are installed over the overpack vent and drain ports to provide redundant closure of the overpack penetrations. A port plug with a metallic seal is installed in the overpack closure plate test port to provide fully redundant closure of all overpack penetrations.

The overpack is surveyed for removable contamination and secured on the transport vehicle with impact limiters installed, the security seals are attached, and the personnel barrier is installed. The HI-STAR 100 packaging is then ready for transport.

Unloading Operations

The HI-STAR 100 System unloading procedures describe the general actions necessary to prepare the MPC for unloading, cool the stored fuel assemblies in the MPC (if necessary), flood the MPC cavity, remove the lid welds, unload the spent fuel assemblies, and recover the overpack and empty MPC. Special precautions are outlined to ensure personnel safety during the unloading operations, and to prevent the risk of MPC overpressurization and thermal shock to the stored spent fuel assemblies.

After removing the impact limiters, the overpack and MPC are positioned in the designated preparation area. At the site's discretion, a gas sample is drawn from the overpack annulus and analyzed. The gas sample provides an indication of MPC enclosure vessel performance. The annulus is depressurized, the overpack closure plate is removed, and the annulus is filled with plant demineralized water. The annulus shield is installed to protect the annulus from debris produced from the lid removal process. Similarly, overpack top surfaces are covered with a protective fire-retarding blanket.

The Weld Removal System (WRS) is positioned on the MPC lid. The MPC closure ring is core drilled over the locations of the vent and drain port cover plates. The MPC closure ring and vent and drain port cover plates are core drilled to the extent necessary to allow access by the Remote Valve Operating Assemblies (RVOAs). Local ventilation is established around the vent and drain ports. The RVOAs are connected to allow access to the MPC cavity for re-flooding operations.

The MPC cavity gas is verified to be below an appropriate temperature (approximately 200°F) to allow water flooding. Depending on the time since initial fuel loading and the age and burnup of the contained fuel, mechanical cooling of the MPC cavity gas may or may not be required to ensure the cavity gas temperature meets the acceptance criterion. A thermal evaluation should be performed to determine the MPC bulk cavity gas temperature at the time of unloading. Based on that thermal evaluation, if the MPC cavity gas temperature does not already meet the acceptance limit, any appropriate means to cool the cavity gas may be employed to reduce the gas temperature to the acceptance criterion. Typically, this may involve intrusive means, such as recirculation cooling of the MPC cavity helium, or non-intrusive means, such as cooling of the exterior surface of the MPC enclosure vessel with water or air. The thermal evaluation should include an evaluation of the cooling process, if required, to determine the appropriate criteria for the cooling process, such as fluid flow rate(s), fluid temperature(s), and the cooling duration required to meet the acceptance criterion. Following fuel cool-down (if required), the MPC is flooded with water. The WRS is positioned for MPC lid-to-shell weld removal. The WRS is then removed with the MPC lid left in place.

The annulus shield is removed and the ~~inflatable~~ annulus seal is installed and pressurized. The MPC lid is rigged to the lift yoke and the lift yoke is engaged to overpack lifting trunnions. The overpack is placed in the spent fuel pool and the MPC lid is removed. All fuel assemblies are returned to the spent fuel storage racks. The overpack and MPC are returned to the designated preparation area. The annulus water is drained and the MPC and overpack are dispositioned for re-use or waste.

1.2.3 Contents of Package

The HI-STAR 100 packaging is classified as a Type B package under 10CFR71. As the HI-STAR 100 System is designed to transport spent nuclear fuel, the maximum activity of the contents requires that the HI-STAR 100 packaging be classified as Category I in accordance with Regulatory Guide 7.11 [1.2.10]. This section delineates the authorized contents permitted for shipment in the HI-STAR 100 System, including fuel assembly types; non-fuel hardware; neutron sources; physical parameter limits for fuel assemblies and sub-components; enrichment, burnup, cooling time, and decay heat limits; location requirements; and requirements for canning the material. *See Supplement I for the contents of the HI-STAR HB.*

1.2.3.1 Determination of Design Basis Fuel

The HI-STAR 100 package is designed to transport most types of fuel assemblies generated in the commercial U.S. nuclear industry. Boiling-water reactor (BWR) fuel assemblies have been supplied by General Electric (GE), Siemens (SPC), Exxon Nuclear, ANF, UNC, ABB

Combustion Engineering, Allis-Chalmers (AC) and Gulf Atomic. Pressurized-water reactor (PWR) fuel assemblies are generally supplied by Westinghouse, Babcock & Wilcox, ANF, and ABB Combustion Engineering. ANF, Exxon, and Siemens are historically the same manufacturing company under different ownership. Within this report, SPC is used to designate fuel manufactured by ANF, Exxon, or Siemens. Publications such as Refs. [1.2.6], [1.2.7], and [1.2.15] provide a comprehensive description of fuel discharged from U.S. reactors. A central object in the design of the HI-STAR 100 System is to ensure that a majority of SNF discharged from the U.S. reactors can be transported in one of the MPCs.

The cell openings in the fuel basket have been sized to accommodate all BWR and PWR assemblies listed in Refs. [1.2.6], [1.2.7], and [1.2.15], except as noted below. Similarly, the cavity length of the MPC has been set at a dimension that permits transportation of most types of PWR fuel assemblies and BWR fuel assemblies with or without fuel channels. The one exception is as follows:

- The South Texas Units 1 & 2 SNF, and CE 16x16 System 80TM SNF are too long to be accommodated in the available MPC cavity length.

In addition to satisfying the cross sectional and length compatibility, the active fuel region of the SNF must be enveloped in the axial direction by the neutron absorber located in the MPC fuel basket. Alignment of the neutron absorber with the active fuel region is ensured by the use of upper and lower fuel spacers suitably designed to support the bottom and restrain the top of the fuel assembly. The spacers axially position the SNF assembly such that its active fuel region is properly aligned with the neutron absorber in the fuel basket. Figure 1.2.15 provides a pictorial representation of the fuel spacers positioning the fuel assembly active fuel region. Both the upper and lower fuel spacers are designed to perform their function under normal and hypothetical accident conditions of transport. Due to the shorter, custom MPC design for Trojan plant fuel, only lower fuel spacers are needed for certain fuel assemblies that do not contain integral control rod assemblies. This creates the potential for a slight misalignment between the active fuel region of a fuel assembly and the neutron absorber panels affixed to the cell walls of the Trojan MPCs. This condition is addressed in the criticality evaluations described in Chapter 6.

In summary, the geometric compatibility of the SNF with the MPC designs does not require the definition of a design basis fuel assembly. This, however, is not the case for structural, containment, shielding, thermal-hydraulic, and criticality criteria. In fact, the same fuel type in a category (PWR or BWR) may not control the cask design in all of the above-mentioned criteria. To ensure that no SNF listed in Refs. [1.2.6], [1.2.7], and [1.2.15] that is geometrically admissible in the HI-STAR MPC is precluded from loading, it is necessary to determine the governing fuel specification for each analysis criteria. To make the necessary determinations, potential candidate fuel assemblies for each qualification criteria were considered. Table 1.2.8 lists the PWR fuel assemblies evaluated. These fuel assemblies were evaluated to define the governing design criteria for PWR fuel. The BWR fuel assembly designs evaluated are listed in Table 1.2.9. Tables 1.2.10 and 1.2.11 provide the fuel characteristics determined to be acceptable for transport in the HI-STAR 100 System. Each "array/class" listed in these tables represents a bounding set of parameters for one or more fuel assembly types. The array/classes are defined in SAR Section 6.2. Table 1.2.12 lists the BWR and PWR fuel assembly designs that are found to

govern for the qualification criteria, namely reactivity, shielding, and thermal. Thermal is broken down into three criteria, namely: 1) fuel assembly effective planar conductivity, 2) fuel basket effective axial conductivity, and 3) MPC density and heat capacity. Substantiating results of analyses for the governing assembly types are presented in the respective chapters dealing with the specific qualification topic. Tables 1.2.10, 1.2.11, and 1.2.21 through 1.2.36 provide the specific limits for all material authorized to be transported in the HI-STAR 100 System. Additional information on the design basis fuel definition is presented in the following subsections.

1.2.3.2 Design Payload for Intact Fuel

Intact fuel assemblies are defined as fuel assemblies without known or suspected cladding defects greater than pinhole leaks and hairline cracks, and which can be handled by normal means. The design payload for intact fuel to be transported in the HI-STAR 100 System is provided in Tables 1.2.10, 1.2.11, and 1.2.22 through 1.2.36. The placement of a single stainless steel clad fuel assembly in an MPC necessitates that all fuel assemblies (stainless steel clad or Zircaloy clad) stored in that MPC meet the maximum heat generation requirements for stainless steel clad fuel. Stainless steel clad fuel assemblies are not authorized for transportation in the MPC-68F or MPC-32.

Fuel assemblies without fuel rods in fuel rod locations cannot be classified as intact fuel unless dummy fuel rods, which occupy a volume equal to or greater than the original fuel rods, replace the missing rods prior to loading. Any intact fuel assembly that falls within the geometric, thermal, and nuclear limits established for the design basis intact fuel assembly can be safely transported in the HI-STAR 100 System.

Some Trojan fuel assemblies not loaded into DFCs or FFCs show conditions of minor impairments on some grid straps [1.2.16]. These conditions, as determined by visual inspection of the assemblies, consist of small portions of grid straps that are missing or bent. The worst condition is the exposure of a single fuel rod on the periphery of one grid strap. These conditions do not meet the definition of damaged fuel in the CoC, since the impairment is minor, no grid spacers are missing, and the overall structural integrity of the assembly is not affected. Such assemblies are therefore classified as intact assemblies.

The fuel characteristics specified in Tables 1.2.10, 1.2.11, and 1.2.21 have been evaluated in this SAR and are acceptable for transport in the HI-STAR 100 System.

1.2.3.3 Design Payload for Damaged Fuel and Fuel Debris

Damaged fuel and fuel debris are defined in Table 1.0.1. The only PWR damaged fuel and fuel debris authorized for transportation in the HI-STAR 100 System is that from the Trojan plant. The only BWR damaged fuel and fuel debris authorized for transportation in the HI-STAR 100 System is that from the Dresden Unit 1 and Humboldt Bay plants.

Damaged fuel may only be transported in the MPC-24E, MPC-24EF, MPC-68, or MPC-68F as shown in Tables 1.2.23 through 1.2.26. Fuel debris may only be transported in the MPC-24EF

and the MPC-68F as shown in Tables 1.2.24 and 1.2.26. Damaged fuel and fuel debris must be transported in stainless steel Holtec damaged fuel containers (DFCs) or other approved stainless steel damaged/failed fuel canister in the HI-STAR 100 System. The list of approved damaged/failed fuel canisters and associated SAR figures are provided below:

- Holtec-designed Dresden Unit 1 ~~and Humboldt Bay~~ Damaged Fuel Container (Figure 1.2.10)
- Sierra Nuclear-designed Trojan Failed Fuel Can (Figure 1.2.10A) containing Trojan damaged fuel, fuel debris, or Trojan Fuel debris process cans; or containing Trojan Fuel Debris Process Can Capsules (Figure 1.2.10C), which themselves contain Trojan Fuel Debris Process Cans (Figure 1.2.10B).
- Holtec-designed Damaged Fuel Container for Trojan plan fuel (Figure 1.2.10D)
- Dresden Unit 1's TN Damaged Fuel Container (Figure 1.2.11)
- Dresden Unit 1's Thoria Rod Canister (Figure 1.2.11A)
- *Holtec-designed Humboldt Bay Damaged Fuel Container (refer to Supplement 1.I)*

1.2.3.3.1 BWR Damaged Fuel and Fuel Debris

Dresden Unit 1 (UO₂ fuel rods and MOX fuel rods) ~~and Humboldt Bay~~ fuel arrays (Assembly Classes 6x6A, 6x6B, 6x6C, 7x7A, and 8x8A) are authorized for transportation as damaged fuel in the MPC-68 and damaged fuel or fuel debris in the MPC-68F. No other BWR damaged fuel or fuel debris is authorized for transportation.

The limits for transporting Dresden Unit 1 ~~and Humboldt Bay~~ damaged fuel and fuel debris are given in Table 1.2.23 and 1.2.24. The placement of a single damaged fuel assembly in an MPC-68 or MPC-68F, or a single fuel debris damaged fuel container in an MPC-68F necessitates that all fuel assemblies (intact, damaged, or debris) placed in that MPC meet the maximum heat generation requirements specified in Tables 1.2.23 and 1.2.24.

The fuel characteristics specified in Tables 1.2.11, 1.2.23 and 1.2.24 for Dresden Unit 1 ~~and Humboldt Bay~~ fuel arrays have been evaluated in this SAR and are acceptable for transport as damaged fuel or fuel debris in the HI-STAR 100 System. Because of the long cooling time, small size, and low weight of spent fuel assemblies qualified as damaged fuel or fuel debris, the DFC and its contents are bounded by the structural, thermal, and shielding analyses performed for the intact BWR design basis fuel. Separate criticality analysis of the bounding fuel assembly for the damaged fuel and fuel debris has been performed in Chapter 6.

~~As Dresden Unit 1 and Humboldt Bay fuel assemblies classified as fuel debris have significant cladding damage, no cladding integrity is assumed. To meet the double containment criteria of 10CFR71.63(b) for plutonium shipments, the MPC 68F provides the secondary containment~~

~~boundary (separate inner container), while the overpack provides the primary containment boundary.~~

The fuel characteristics specified in Table 1.2.11 for the Dresden Unit 1 ~~and Humboldt Bay~~ fuel arrays (Assembly Classes 6x6A, 6x6B, 6x6C, 7x7A, and 8x8A) have been evaluated in this SAR and are acceptable for transport as damaged fuel or fuel debris in the HI-STAR 100 System after being placed in a damaged fuel container.

Refer to Supplement 1.1 for information regarding Humboldt Bay damaged fuel and fuel debris.

1.2.3.3.2 PWR Damaged Fuel and Fuel Debris

The PWR damaged fuel and fuel debris authorized for transportation in the HI-STAR 100 System is limited to that from the Trojan plant. The limits for transporting Trojan plant damaged fuel and fuel debris in the Trojan MPC-24E/EF are given in Tables 1.2.10, 1.2.25 and 1.2.26. All Trojan plant damaged fuel, and fuel debris listed below is authorized for transportation in the HI-STAR 100 System [1.2.12]:

- Damaged fuel assemblies in Trojan failed fuel cans
- Damaged fuel assemblies in Holtec's Trojan plant PWR damaged fuel container
- Fuel assemblies classified as fuel debris in Trojan failed fuel cans
- Trojan fuel assemblies classified as fuel debris in Holtec's Trojan damaged fuel container
- Fuel debris consisting of loose fuel pellets, fuel pellet fragments, and fuel assembly metal fragments (portions of fuel rods, portions of grid assemblies, bottom nozzles, etc.) in Trojan failed fuel cans
- Trojan fuel debris process cans loaded into Trojan fuel debris process can capsules and then into Trojan failed fuel cans. The fuel debris process cans contain fuel debris (metal fragments) and were used to process organic media removed from the Trojan spent fuel pool during cleanup operations in preparation for decommissioning the pool. The fuel debris process cans have metallic filters in the can bottom and lid that allowed removal of water and organic media using high temperature steam, while retaining the solid residue from the processed media and fuel debris inside the process can[†]. Up to five process cans can be loaded into a process can capsule, which is vacuumed, purged, backfilled with helium, and seal-welded closed to provide a sealed containment for the fuel debris.

[†] The Trojan Fuel Debris Process Cans were used in the spent fuel pool cleanup effort conducted as part of plant decommissioning. This project is complete and not associated with certification of Trojan fuel debris for transportation in the HI-STAR 100 System under 10 CFR 71.

One Trojan Failed Fuel Can is not completely filled with fuel debris. Therefore, a stainless steel failed fuel can spacer is installed in this FFC to minimize movement of the fuel debris during normal transportation and hypothetical accident conditions. The spacer is a long, square tube with a baseplate that rests atop the fuel debris inside the Trojan FFC. A drawing of the Trojan failed fuel can spacer is provided in Section 1.4. A summary of the structural analysis of the FFC spacer is provided in Section 2.6.1.3.1.3.

1.2.3.4 Structural Payload Parameters

The main physical parameters of an SNF assembly applicable to the structural evaluation are the fuel assembly length, envelope (cross sectional dimensions), and weight. These parameters, which define the mechanical and structural design, are listed in Tables 1.2.22 through 1.2.27 for the various MPC models. The centers of gravity reported in Chapter 2 are based on the maximum fuel assembly weight. Upper and lower fuel spacers (as appropriate) maintain the axial position of the fuel assembly within the MPC basket and, therefore, the location of the center of gravity. The upper and lower spacers are designed to withstand normal and accident conditions of transport. An axial clearance of approximately 2 inches is provided to account for the irradiation and thermal growth of the fuel assemblies. The suggested upper and lower fuel spacer lengths are listed in Tables 1.2.16 and 1.2.17. Due to the custom design of the Trojan MPCs, only lower fuel spacers are required with Trojan plant fuel assemblies not containing non-fuel hardware or neutron sources. In order to qualify for transport in the HI-STAR 100 MPC, the SNF must satisfy the physical parameters listed in Tables 1.2.21 through 1.2.36, as applicable.

1.2.3.5 Thermal Payload Parameters

The principal thermal design parameter for the fuel is the peak fuel cladding temperature, which is a function of the maximum heat generation rate per assembly and the decay heat removal capabilities of the HI-STAR 100 System. The maximum heat generation rate per assembly for the design basis fuel assembly is based on the fuel assembly type with the lowest thermal performance characteristics. The parameters that define this decay heat design basis fuel are listed in Table 1.2.12. The governing thermal parameters to ensure that the range of SNF discussed previously are bounded by the thermal analysis discussed in detail and specified in Chapter 3. By utilizing these bounding thermal parameters, the calculated peak fuel rod cladding temperatures are conservative for the actual spent fuel assemblies, which are apt to have a higher thermal conductivity.

The peak fuel cladding temperature limit for normal conditions of transport is 400°C (752°F), which is consistent with the guidance in ISG-11, Revision 2 [1.2.14]. Tables 1.2.21 through 1.2.27 provide the maximum heat generation for all fuel assemblies authorized for transportation in the HI-STAR 100 System. The basis for these limits is discussed in Chapter 3.

Finally, the axial variation in the heat emission rate in the design basis fuel is defined based on the axial burnup distribution. For this purpose, the data provided in Refs. [1.2.8], [1.2.9], and [1.2.12] are utilized and summarized in Table 1.2.15 and Figures 1.2.13, 1.2.13A, and 1.2.14, for reference. These distributions are representative of fuel assemblies with the design burnup levels

considered. These distributions are used for analysis only, and do not provide a criteria for fuel assembly acceptability for transport in the HI-STAR 100 System.

1.2.3.6 Radiological Payload Parameters

The principal radiological design criteria are the 10CFR71.47 and 10CFR71.51 radiation dose rate and release requirements for the HI-STAR 100 System. The radiation dose rate is directly affected by the gamma and neutron source terms of the SNF assembly.

The gamma and neutron sources are separate and are affected differently by enrichment, burnup, and cool time. It is recognized that, at a given burnup, the radiological source terms increase monotonically as the initial enrichment is reduced. The shielding design basis fuel assembly is, therefore, evaluated for different combinations of maximum burnup, minimum cooling time, and minimum enrichment. The shielding design basis intact fuel assembly thus bounds all other intact fuel assemblies.

The design basis dose rates can be met by a variety of burnup levels, cooling times, and minimum enrichments. Tables 1.2.21 through 1.2.36 include the burnup and cooling time values that meet the radiological dose rate requirements for all authorized contents to be transported in each MPC model. The allowable maximum burnup, minimum cooling time, and minimum enrichment limits were chosen strictly based on the dose rate requirements. All allowable burnup, cooling time, and minimum enrichment combinations result in calculated dose rates less than the regulatory dose rate limits.

Table 1.2.15 and Figures 1.2.13, 1.2.13A, and 1.2.14 provide the axial distribution for the radiological source term for PWR and BWR fuel assemblies, and for Trojan plant-specific fuel, based on the actual burnup distribution. The axial burnup distributions are representative of fuel assemblies with the design basis burnup levels considered. These distributions are used for analysis only, and do not provide criteria for fuel assembly acceptability for transport in the HI-STAR 100 System.

Thoria rods placed in Dresden Unit 1 Thoria Rod Canisters meeting the requirements of Table 1.2.21 and Dresden Unit 1 fuel assemblies with one Antimony-Beryllium neutron source have been qualified for transport. Up to one Dresden Unit 1 Thoria Rod Canister plus any combination of damaged fuel assemblies in damaged fuel containers and intact fuel, up to a total of 68 may be transported.

1.2.3.7 Criticality Payload Parameters

As discussed earlier, the MPC-68/68F and MPC-32 feature a basket without flux traps. In these fuel baskets, there is one panel of neutron absorber between adjacent fuel assemblies. The MPC-24/24E/24EF employs a construction wherein two neighboring fuel assemblies are separated by two panels of neutron absorber with a water gap between them (flux trap construction). The MPC-24 flux trap basket can accept a much higher enrichment fuel than a non-flux trap basket without taking credit for fuel assembly burnup in the criticality analysis. The maximum initial ²³⁵U enrichment for PWR and BWR fuel authorized for transport is specified by fuel array/class

in Tables 1.2.10 and 1.2.11, respectively. Trojan plant fuel is limited to a lower maximum initial enrichment of 3.7 wt.% ^{235}U compared to other fuel in its array/class, based on the specific analysis performed for the custom-designed Trojan MPCs containing only Trojan plant fuel.

~~The MPC 24 Boral ^{10}B areal density is specified at a minimum loading of 0.0267 g/cm². The MPC 24E/EF, MPC 32, and MPC 68 Boral ^{10}B areal density is specified at a minimum loading of 0.0372 g/cm². The MPC 68F Boral ^{10}B areal density is specified at a minimum loading of 0.01 g/cm².~~

The minimum ^{10}B areal density in the neutron absorber panels for each MPC model is shown in Table 1.2.3. Values for MPC-HB are found in Supplement 1.1.

For all MPCs, the ^{10}B loading areal density used for analysis is conservatively established *below the minimum values shown in Table 1.2.3. For Boral, the value used in the analysis is at 75% of the minimum ^{10}B areal density, while for METAMIC, it is 90% of the minimum value can be used* to demonstrate that the reactivity under the most adverse accumulation of tolerances and biases is less than 0.95. The reduction in ^{10}B areal density credit meets NUREG-1617 [1.0.5], which requires *up to* a 25% reduction in ^{10}B areal density credit. A large body of sampling data accumulated by Holtec from thousands of manufactured Boral panels indicates the average ^{10}B areal densities to be approximately 15% greater than the specified minimum.

Credit for burnup of the fuel, in accordance with the intent of the guidance in Interim Staff Guidance Document 8 (ISG-8) [1.2.13], is taken in the criticality analysis to allow the transportation of certain PWR fuel assemblies in MPC-32. Burnup credit is a required input to qualify PWR fuel for transportation in the MPC-32, considering the inleakage of moderator (i.e., unborated water) under accident conditions. This hypothetical event is non-credible given the double barrier design engineered into the HI-STAR 100 System with the fully welded MPC enclosure vessel (designed for 60 g's) surrounded by the sealed overpack, which is designed for deep submersion under water (greater than 650 feet submersion) without breach. The details of the burnup credit analyses are provided in Chapter 6, including detailed discussion of how the recommendations of ISG-8 were implemented. Exceptions to some of the recommendations in ISG-8 were necessary (e.g., partial credit for fission products) in order to develop burnup versus enrichment curves that can be practically implemented at the plants. These exceptions are described in Chapter 6.

1.2.3.8 Non-Fuel Hardware and Neutron Sources

BWR fuel is permitted to be stored with or without Zircaloy channels. Control blades and stainless steel channels are not authorized for transportation in the HI-STAR 100 System. Dresden Unit 1 (D-1) neutron sources are authorized for transportation as shown in Tables 1.2.23 and 1.2.24. The D-1 neutron sources are single, long rods containing Sb-Be source material that fits into a water rod location in a D-1 fuel assembly.

Except for Trojan plant fuel, no PWR non-fuel hardware or neutron sources are authorized for transportation in the HI-STAR 100 System. For Trojan plant fuel only, the following non-fuel

hardware and neutron sources are permitted for transportation in specific quantities as shown in Tables 1.2.25 and 1.2.26:

- Rod Cluster Control Assemblies (RCCAs) with cladding made of Type 304 stainless steel and Ag-In-Cd neutron absorber material.
- Burnable Poison Rod Assemblies (BPRAs) with cladding made of Type 304 stainless steel and borosilicate glass tube neutron poison material.
- Thimble Plug Devices made of Type 304 stainless steel.
- Neutron source assemblies with cladding made of Type 304 stainless steel - two (2) californium primary source assemblies and four (4) antimony-beryllium secondary source assemblies.

These devices are designed with thin rods of varying length and materials as discussed above, that fit into the fuel assembly guide tubes within the fuel rod lattice. The upper fittings for each device can vary to accommodate the handling tool (grapple) design. During reactor operation, the positions of the RCCAs are controlled by the operator using the control rod drive system, while the BPRAs, TPDs, and neutron sources stay fully inserted.

A complete list of the authorized non-fuel hardware and neutron sources, including appropriate limits on the characteristics of this material, is provided in Tables 1.2.23 through 1.2.36, as applicable.

1.2.3.9 Summary of Authorized Contents

The criticality safety index for the HI-STAR 100 Package is zero. A fuel assembly is acceptable for transport in a HI-STAR 100 System if it fulfills the following criteria.

- a. It satisfies the physical parameter characteristics listed in Tables 1.2.10 or 1.2.11, as applicable.
- b. It satisfies the cooling time, decay heat, burnup, enrichment, and other limits specified in Tables 1.2.21 through 1.2.36, as applicable.
- c. Deleted.
- d. Deleted.

A damaged fuel assembly shall be transported in a damaged fuel container or other authorized damaged/failed fuel canister, and shall meet the characteristics specified in Tables 1.2.23 through 1.2.26 for transport in the MPC-68, MPC-68F, MPC-24E, or MPC-24EF. Fuel classified as fuel debris shall be placed in a damaged fuel container or other authorized damaged/failed fuel canister and shall meet the characteristics specified in Tables 1.2.24 or 1.2.26 for transport in the MPC-68F or MPC-24EF.

Stainless steel clad fuel assemblies shall meet the characteristics specified in Tables 1.2.22 through 1.2.33 for transport in the MPC-24, MPC-24E, MPC-24EF, or MPC-68.

MOX BWR fuel assemblies shall meet the requirements of Tables 1.2.23 or 1.2.24 for intact and damaged fuel/fuel debris.

Thoria rods placed in Dresden Unit 1 Thoria Rod Canisters meeting the requirements of Table 1.2.21 and Dresden Unit 1 fuel assemblies with one Antimony-Beryllium neutron source have been qualified for transport. Up to one Dresden Unit 1 Thoria Rod Canister plus any combination of damaged fuel assemblies in damaged fuel containers and intact fuel, up to a total of 68 may be transported.

Dresden Unit 1 fuel assemblies with one Antimony-Beryllium neutron source are authorized for loading in the MPC-68 or MPC-68F.

Table 1.2.2 summarizes the key system data for the HI-STAR 100 System. Table 1.2.3 summarizes the key parameters and limits for the HI-STAR 100 MPCs. Tables 1.2.10, 1.2.11, and 1.2.21 through 1.2.367 and other tables referenced from these tables provide the limiting conditions for all material to be transported in the HI-STAR 100 System. *Refer to Supplement 1.1 for HI-STAR HB.*

Table 1.2.1

TABLE INTENTIONALLY DELETED

Table 1.2.2

SUMMARY OF KEY SYSTEM DATA FOR HI-STAR 100

PARAMETER	VALUE (Nominal)	
Types of MPCs in this SAR	6†	4 for PWR 2 for BWR
MPC capacity	MPC-24	Up to 24 intact ZR or stainless steel clad PWR fuel assemblies
	MPC-24E	Up to 24 intact ZR or stainless steel clad PWR fuel assemblies. Up to four (4) Trojan plant fuel assemblies classified as damaged fuel, each in a Trojan Failed Fuel Can or a Holtec damaged fuel container, and the complement intact fuel assemblies.
	MPC-24EF	Up to 24 intact ZR or stainless steel clad PWR fuel assemblies. Up to four (4) Trojan plant fuel assemblies classified as damaged fuel or fuel debris, each in a Trojan Failed Fuel Can or a Holtec damaged fuel container; or other Trojan fuel debris stored in Trojan Process Cans either placed directly into a Trojan Failed Fuel Can or placed inside Trojan Process Can Capsules and then in Trojan Failed Fuel Cans; and the complement intact fuel assemblies.
	MPC-32	Up to 32 intact ZR clad PWR fuel assemblies.
	MPC-68	Up to 68 intact ZR or stainless steel clad BWR fuel assemblies or damaged ZR clad fuel assemblies* in damaged fuel containers within an MPC-68
	MPC-68F	Up to 4 damaged fuel containers with ZR clad BWR fuel debris* and the complement intact or damaged* ZR clad BWR fuel assemblies within an MPC-68F. *Only damaged fuel and fuel debris from Dresden Unit 1 or Humboldt Bay is authorized for transportation in the MPC-68 and MPC-68F.

† - excluding MPC-HB. See Supplement I.

Table 1.2.3
KEY PARAMETERS FOR HI-STAR 100 MULTI-PURPOSE CANISTERS

PARAMETER	PWR	BWR
Unloaded MPC weight (lb)	See Table 2.2.1	See Table 2.2.1
Minimum <i>Boral</i> neutron absorber ¹⁰ B loading (g/cm ²)	0.0267 (MPC-24) 0.0372 (MPC-24E/EF) 0.0372 (MPC-32)	0.0372 (MPC-68) 0.01 (MPC-68F)
Minimum <i>Metamic</i> neutron absorber ¹⁰ B loading (g/cm ²)	N/A	N/A
Pre-disposal service life (years)	40	40
Design temperature, max./min. (°F)	725 [†] /-40 ^{††}	725 [†] /-40 ^{††}
Design Internal pressure (psig)		
Normal Conditions	100	100
Off-normal Conditions	100	100
Accident Conditions	200	200
Total heat load, max. (kW)	20.0	18.5
Maximum permissible peak fuel cladding temperature (°F)	752° (normal conditions) 1058° (accident conditions)	752° (normal conditions) 1058° (accident conditions)
MPC internal environment Helium filled (psig)	≥ 0 and ≤ 44.8 psig ^{†††} at a reference temperature of 70°F	≥ 0 and ≤ 44.8 psig ^{†††} at a reference temperature of 70°F
MPC external environment/overpack internal environment Helium filled initial pressure (psig, at STP)	≥ 10 and ≤ 14	≥ 10 and ≤ 14
Maximum permissible reactivity including all uncertainty and biases	<0.95	<0.95
End closure(s)	Welded	Welded
Fuel handling	Opening compatible with standard grapples	Opening compatible with standard grapples
Heat dissipation	Passive	Passive

† Maximum normal condition design temperature for the MPC fuel basket. A complete listing of design temperatures for all components is provided in Table 2.1.2

†† Temperature based on minimum ambient temperature (10CFR71.71(c)(2)) and no fuel decay heat load.

††† This value represents the nominal backfill value used in the thermal analysis, plus 2 psig operating tolerance. Based on the MPC pressure results in Table 3.4.15 and the pressure limits specified in Table 2.1.1, there is sufficient analysis margin to accommodate this operating tolerance.

Tables 1.2.4 through 1.2.6

INTENTIONALLY DELETED

Table 1.2.7

HI-STAR 100 LOADING OPERATIONS DESCRIPTION

Site-specific handling and operating procedures will be prepared, reviewed, and approved by each owner/user.	
1	Overpack and MPC lowered into the fuel pool without closure plate and MPC lid
2	Fuel assemblies transferred to the MPC fuel basket
3	MPC lid lowered onto the MPC
4	Overpack/MPC assembly moved to the decon pit and MPC lid welded in place, examined, <i>and</i> pressure tested, and leak tested
5	MPC dewatered, dried, backfilled with helium, and the vent/drain port cover plates and closure ring welded
6	Overpack drained and external surfaces decontaminated
7	Overpack seals and closure plate installed and bolts pre-tensioned
8	Overpack cavity dried, backfilled with helium, and helium leak tested
9	HI-STAR 100 System transferred to transport bay
10	HI-STAR 100 placed onto transport saddles, tied down, impact limiters and personnel barrier installed, and package surveyed for release for transport.

Table 1.2.8

PWR FUEL ASSEMBLIES EVALUATED TO DETERMINE DESIGN BASIS SNF

Assembly Class	Array Type
B&W 15x15	All
B&W 17x17	All
CE 14x14	All
CE 16x16	All except System 80™
WE 14x14	All
WE 15x15	All
WE 17x17	All
St. Lucie	All
Ft. Calhoun	All
Haddam Neck (Stainless Steel Clad)	All
San Onofre 1 (Stainless Steel Clad, except MOX)	All
Indian Point 1	All

Table 1.2.9

BWR FUEL ASSEMBLIES EVALUATED TO DETERMINE DESIGN BASIS SNF

Assembly Class	Array Type			
GE BWR/2-3	All 7x7	All 8x8	All 9x9	All 10x10
GE BWR/4-6	All 7x7	All 8x8	All 9x9	All 10x10
Humboldt Bay	All 6x6	All 7x7 (Zircaloy Clad)		
Dresden-1	All 6x6	All 8x8		
LaCrosse (Stainless Steel Clad)	All			

Table 1.2.10
PWR FUEL ASSEMBLY CHARACTERISTICS (Note 1)

Fuel Assembly Array/Class	14x14A	14x14B	14x14C	14x14D	14x14E
Clad Material (Note 2)	ZR	ZR	ZR	SS	SSZR
Design Initial U (kg/assy.) (Note 3)	≤ 407	≤ 407	≤ 425	≤ 400	≤ 206
Initial Enrichment (MPC-24, 24E, and 24EF) (wt % ²³⁵ U)	≤ 4.6 (24) ≤ 5.0 (24E/24EF)	≤ 4.6 (24) ≤ 5.0 (24E/24EF)	≤ 4.6 (24) ≤ 5.0 (24E/24EF)	≤ 4.0 (24) ≤ 5.0 (24E/24EF)	≤ 5.0
Initial Enrichment (MPC-32) (wt % ²³⁵ U) (Note 5)	N/A	N/A	N/A	N/A	N/A
No. of Fuel Rod Locations	179	179	176	180	173
Fuel Clad O.D. (in.)	≥ 0.400	≥ 0.417	≥ 0.440	≥ 0.422	≥ 0.3415
Fuel Clad I.D. (in.)	≤ 0.3514	≤ 0.3734	≤ 0.3880	≤ 0.3890	≤ 0.3175
Fuel Pellet Dia. (in.)	≤ 0.3444	≤ 0.3659	≤ 0.3805	≤ 0.3835	≤ 0.3130
Fuel Rod Pitch (in.)	≤ 0.556	≤ 0.556	≤ 0.580	≤ 0.556	Note 6
Active Fuel Length (in.)	≤ 150	≤ 150	≤ 150	≤ 144	≤ 102
No. of Guide and/or Instrument Tubes	17	17	5 (Note 4)	16	0
Guide/Instrument Tube Thickness (in.)	≥ 0.017	≥ 0.017	≥ 0.038	≥ 0.0145	N/A

Table 1.2.10 (continued)
PWR FUEL ASSEMBLY CHARACTERISTICS (Note 1)

Fuel Assembly Array/Class	15x15A	15x15B	15x15C	15x15D	15x15E	15x15F
Clad Material (Note 2)	ZR	ZR	ZR	ZR	ZR	ZR
Design Initial U (kg/assy.) (Note 3)	≤ 464	≤ 464	≤ 464	≤ 475	≤ 475	≤ 475
Initial Enrichment (MPC-24, 24E, and 24EF (wt % ²³⁵ U))	≤ 4.1 (24) ≤ 4.5 (24E/24EF)					
Initial Enrichment (MPC-32) (wt % ²³⁵ U) (Note 5)	N/A	N/A	N/A	≤ 5.0	≤ 5.0	≤ 5.0
No. of Fuel Rod Locations	204	204	204	208	208	208
Fuel Clad O.D. (in.)	≥ 0.418	≥ 0.420	≥ 0.417	≥ 0.430	≥ 0.428	≥ 0.428
Fuel Clad I.D. (in.)	≤ 0.3660	≤ 0.3736	≤ 0.3640	≤ 0.3800	≤ 0.3790	≤ 0.3820
Fuel Pellet Dia. (in.)	≤ 0.3580	≤ 0.3671	≤ 0.3570	≤ 0.3735	≤ 0.3707	≤ 0.3742
Fuel Rod Pitch (in.)	≤ 0.550	≤ 0.563	≤ 0.563	≤ 0.568	≤ 0.568	≤ 0.568
Active Fuel Length (in.)	≤ 150	≤ 150	≤ 150	≤ 150	≤ 150	≤ 150
No. of Guide and/or Instrument Tubes	21	21	21	17	17	17
Guide/Instrument Tube Thickness (in.)	≥ 0.0165	≥ 0.015	≥ 0.0165	≥ 0.0150	≥ 0.0140	≥ 0.0140

Table 1.2.10 (continued)
PWR FUEL ASSEMBLY CHARACTERISTICS (Note 1)

Fuel Assembly Array/Class	15x15G	15x15H	16x16A	17x17A	17x17B	17x17C
Clad Material (Note 2)	SS	ZR	ZR	ZR	ZR	ZR
Design Initial U (kg/assy.) (Note 3)	≤ 420	≤ 475	≤ 443	≤ 467	≤ 467	≤ 474
Initial Enrichment (MPC-24, 24E, and 24EF) (wt % ²³⁵ U)	≤ 4.0 (24) ≤ 4.5 (24E/24EF)	≤ 3.8 (24) ≤ 4.2 (24E/24EF)	≤ 4.6 (24) ≤ 5.0 (24E/24EF)	≤ 4.0 (24) ≤ 4.4 (24E/24EF)	≤ 4.0 (24) ≤ 4.4 (24E/24EF) (Note 7)	≤ 4.0 (24) ≤ 4.4 (24E/24EF)
Initial Enrichment (MPC-32) (wt % ²³⁵ U) (Note 5)	N/A	≤ 5.0	N/A	≤ 5.0	≤ 5.0	≤ 5.0
No. of Fuel Rod Locations	204	208	236	264	264	264
Fuel Clad O.D. (in.)	≥ 0.422	≥ 0.414	≥ 0.382	≥ 0.360	≥ 0.372	≥ 0.377
Fuel Clad I.D. (in.)	≤ 0.3890	≤ 0.3700	≤ 0.3320	≤ 0.3150	≤ 0.3310	≤ 0.3330
Fuel Pellet Dia. (in.)	≤ 0.3825	≤ 0.3622	≤ 0.3255	≤ 0.3088	≤ 0.3232	≤ 0.3252
Fuel Rod Pitch (in.)	≥ 0.563	≥ 0.568	≥ 0.506	≥ 0.496	≥ 0.496	≥ 0.502
Active Fuel Length (in.)	≤ 144	≤ 150	≤ 150	≤ 150	≤ 150	≤ 150
No. of Guide and/or Instrument Tubes	21	17	5 (Note 4)	25	25	25
Guide/Instrument Tube Thickness (in.)	≥ 0.0145	≥ 0.0140	≥ 0.0400	≥ 0.016	≥ 0.014	≥ 0.020

Table 1.2.10 (continued)
PWR FUEL ASSEMBLY CHARACTERISTICS

Notes:

1. All dimensions are design nominal values. Maximum and minimum dimensions are specified to bound variations in design nominal values among fuel assemblies within a given array/class.
2. ZR designates any zirconium-based fuel cladding material authorized for use in a commercial power reactor.
3. Design initial uranium weight is the nominal uranium weight specified for each assembly by the fuel manufacturer or reactor user. For each PWR fuel assembly, the total uranium weight limit specified in this table may be increased up to 2.0 percent for comparison with users' fuel records to account for manufacturer's tolerances.
4. Each guide tube replaces four fuel rods.
5. Minimum assembly average burnup is required per Table 1.2.34.
6. This fuel assembly array/class includes only the Indian Point Unit 1 fuel assembly. This fuel assembly has two pitches in different sectors of the assembly. These pitches are 0.441 inches and 0.453 inches.
7. Trojan plant-specific fuel is governed by the limits specified for array/class 17x17B and will be transported in the custom-designed Trojan MPC-24E/EF canisters. The Trojan MPC-24E/EF design is authorized to transport only Trojan plant fuel with a maximum initial enrichment of 3.7 wt.% ²³⁵U.

Table 1.2.11
BWR FUEL ASSEMBLY CHARACTERISTICS (Note 1)

Fuel Assembly Array/Class	6x6A	6x6B	6x6C	7x7A	7x7B	8x8A
Clad Material (Note 2)	ZR	ZR	ZR	ZR	ZR	ZR
Design Initial U (kg/assy.) (Note 3)	≤ 110	≤ 110	≤ 110	≤ 100	≤ 195	≤ 120
Maximum Planar-Average Initial Enrichment (wt % ²³⁵ U)	≤ 2.7	≤ 2.7 for the UO ₂ rods. See Note 4 for MOX rods.	≤ 2.7	≤ 2.7	≤ 4.2	≤ 2.7
Initial Maximum Rod Enrichment (wt % ²³⁵ U)	≤ 4.0	≤ 4.0	≤ 4.0	≤ 5.5	≤ 5.0	≤ 4.0
No. of Fuel Rod Locations	35 or 36	35 or 36 (up to 9 MOX rods)	36	49	49	63 or 64
Fuel Clad O.D. (in.)	≥ 0.5550	≥ 0.5625	≥ 0.5630	≥ 0.4860	≥ 0.5630	≥ 0.4120
Fuel Clad I.D. (in.)	≤ 0.5105	≤ 0.4945	≤ 0.4990	≤ 0.4204	≤ 0.4990	≤ 0.3620
Fuel Pellet Dia. (in.)	≤ 0.4980	≤ 0.4820	≤ 0.4880	≤ 0.4110	≤ 0.4910	≤ 0.3580
Fuel Rod Pitch (in.)	≤ 0.710	≤ 0.710	≤ 0.740	≤ 0.631	≤ 0.738	≤ 0.523
Active Fuel Length (in.)	≤ 120	≤ 120	≤ 77.5	≤ 80	≤ 150	≤ 120
No. of Water Rods (Note 11)	1 or 0	1 or 0	0	0	0	1 or 0
Water Rod Thickness (in.)	> 0	> 0	N/A	N/A	N/A	≥ 0
Channel Thickness (in.)	≤ 0.060	≤ 0.060	≤ 0.060	≤ 0.060	≤ 0.120	≤ 0.100

Table 1.2.11 (continued)
BWR FUEL ASSEMBLY CHARACTERISTICS (Note 1)

Fuel Assembly Array/Class	8x8B	8x8C	8x8D	8x8E	8x8F	9x9A
Clad Material (Note 2)	ZR	ZR	ZR	ZR	ZR	ZR
Design Initial U (kg/assy) (Note 3)	≤ 185	≤ 185	≤ 185	≤ 185	≤ 185	≤ 177
Maximum Planar-Average Initial Enrichment (wt % ²³⁵ U)	≤ 4.2	≤ 4.2	≤ 4.2	≤ 4.2	≤ 4.0	≤ 4.2
Initial Maximum Rod Enrichment (wt % ²³⁵ U)	≤ 5.0	≤ 5.0	≤ 5.0	≤ 5.0	≤ 5.0	≤ 5.0
No. of Fuel Rod Locations	63 or 64	62	60 or 61	59	64	74/66 (Note 5)
Fuel Clad O.D. (in.)	≥ 0.4840	≥ 0.4830	≥ 0.4830	≥ 0.4930	≥ 0.4576	≥ 0.4400
Fuel Clad I.D. (in.)	≤ 0.4295	≤ 0.4250	≤ 0.4230	≤ 0.4250	≤ 0.3996	≤ 0.3840
Fuel Pellet Dia. (in.)	≤ 0.4195	≤ 0.4160	≤ 0.4140	≤ 0.4160	≤ 0.3913	≤ 0.3760
Fuel Rod Pitch (in.)	≤ 0.642	≤ 0.641	≤ 0.640	≤ 0.640	≤ 0.609	≤ 0.566
Design Active Fuel Length (in.)	≤ 150	≤ 150	≤ 150	≤ 150	≤ 150	≤ 150
No. of Water Rods (Note 11)	1 or 0	2	1 - 4 (Note 7)	5	N/A (Note 12)	2
Water Rod Thickness (in.)	≥ 0.034	> 0.00	> 0.00	≥ 0.034	≥ 0.0315	> 0.00
Channel Thickness (in.)	≤ 0.120	≤ 0.120	≤ 0.120	≤ 0.100	≤ 0.055	≤ 0.120

Table 1.2.11 (continued)
BWR FUEL ASSEMBLY CHARACTERISTICS (Note 1)

Fuel Assembly Array/Class	9x9 B	9x9 C	9x9 D	9x9 E (Note 13)	9x9 F (Note 13)	9x9 G
Clad Material (Note 2)	ZR	ZR	ZR	ZR	ZR	ZR
Design Initial U (kg/assy.) (Note 3)	≤ 177	≤ 177	≤ 177	≤ 177	≤ 177	≤ 177
Maximum Planar-Average Initial Enrichment (wt % ²³⁵ U)	≤ 4.2	≤ 4.2	≤ 4.2	≤ 4.0	≤ 4.0	≤ 4.2
Initial Maximum Rod Enrichment (wt % ²³⁵ U)	≤ 5.0	≤ 5.0	≤ 5.0	≤ 5.0	≤ 5.0	≤ 5.0
No. of Fuel Rod Locations	72	80	79	76	76	72
Fuel Clad O.D. (in.)	≥ 0.4330	≥ 0.4230	≥ 0.4240	≥ 0.4170	≥ 0.4430	≥ 0.4240
Fuel Clad I.D. (in.)	≤ 0.3810	≤ 0.3640	≤ 0.3640	≤ 0.3640	≤ 0.3860	≤ 0.3640
Fuel Pellet Dia. (in.)	≤ 0.3740	≤ 0.3565	≤ 0.3565	≤ 0.3530	≤ 0.3745	≤ 0.3565
Fuel Rod Pitch (in.)	≤ 0.572	≤ 0.572	≤ 0.572	≤ 0.572	≤ 0.572	≤ 0.572
Design Active Fuel Length (in.)	≤ 150	≤ 150	≤ 150	≤ 150	≤ 150	≤ 150
No. of Water Rods (Note 11)	1 (Note 6)	1	2	5	5	1 (Note 6)
Water Rod Thickness (in.)	> 0.00	≥ 0.020	≥ 0.0300	≥ 0.0120	≥ 0.0120	≥ 0.0320
Channel Thickness (in.)	≤ 0.120	≤ 0.100	≤ 0.100	≤ 0.120	≤ 0.120	≤ 0.120

Table 1.2.11 (continued)
BWR FUEL ASSEMBLY CHARACTERISTICS (Note 1)

Fuel Assembly Array/Class	10x10 A	10x10 B	10x10 C	10x10 D	10x10 E
Clad Material (Note 2)	ZR	ZR	ZR	SS	SS
Design Initial U (kg/assy.) (Note 3)	≤ 186	≤ 186	≤ 186	≤ 125	≤ 125
Maximum Planar-Average Initial Enrichment (wt % ²³⁵ U)	≤ 4.2	≤ 4.2	≤ 4.2	≤ 4.0	≤ 4.0
Initial Maximum Rod Enrichment (wt % ²³⁵ U)	≤ 5.0	≤ 5.0	≤ 5.0	≤ 5.0	≤ 5.0
No. of Fuel Rod Locations	92/78 (Note 8)	91/83 (Note 9)	96	100	96
Fuel Clad O.D. (in.)	≥ 0.4040	≥ 0.3957	≥ 0.3780	≥ 0.3960	≥ 0.3940
Fuel Clad I.D. (in.)	≤ 0.3520	≤ 0.3480	≤ 0.3294	≤ 0.3560	≤ 0.3500
Fuel Pellet Dia. (in.)	≤ 0.3455	≤ 0.3420	≤ 0.3224	≤ 0.3500	≤ 0.3430
Fuel Rod Pitch (in.)	≤ 0.510	≤ 0.510	≤ 0.488	≤ 0.565	≤ 0.557
Design Active Fuel Length (in.)	≤ 150	≤ 150	≤ 150	≤ 83	≤ 83
No. of Water Rods (Note 11)	2	1 (Note 6)	5 (Note 10)	0	4
Water Rod Thickness (in.)	≥ 0.030	> 0.00	≥ 0.031	N/A	≥ 0.022
Channel Thickness (in.)	≤ 0.120	≤ 0.120	≤ 0.055	≤ 0.080	≤ 0.080

Table 1.2.11 (continued)
BWR FUEL ASSEMBLY CHARACTERISTICS

NOTES:

1. All dimensions are design nominal values. Maximum and minimum dimensions are specified to bound variations in design nominal values among fuel assemblies within a given array/class.
2. ZR designates any zirconium-based fuel cladding material authorized for use in a commercial power reactor.
3. Design initial uranium weight is the nominal uranium weight specified for each assembly by the fuel manufacturer or reactor user. For each BWR fuel assembly, the total uranium weight limit specified in this table may be increased up to 1.5 percent for comparison with users' fuel records to account for manufacturer tolerances.
4. ≤ 0.635 wt. % ^{235}U and ≤ 1.578 wt. % total fissile plutonium (^{239}Pu and ^{241}Pu), (wt. % of total fuel weight, i.e., UO_2 plus PuO_2).
5. This assembly class contains 74 total rods; 66 full length rods and 8 partial length rods.
6. Square, replacing nine fuel rods.
7. Variable.
8. This assembly contains 92 total fuel rods; 78 full length rods and 14 partial length rods.
9. This assembly class contains 91 total fuel rods; 83 full length rods and 8 partial length rods.
10. One diamond-shaped water rod replacing the four center fuel rods and four rectangular water rods dividing the assembly into four quadrants.
11. These rods may also be sealed at both ends and contain ZR material in lieu of water.
12. This assembly is known as "QUAD+." It has four rectangular water cross segments dividing the assembly into four quadrants.
13. For the SPC 9x9-5 fuel assembly, each fuel rod must meet either the 9x9E or the 9x9F set of limits or clad O.D., clad I.D., and pellet diameter.

Table 1.2.12

DESIGN BASIS FUEL ASSEMBLY FOR EACH DESIGN CRITERION

Criterion	MPC-68/68F	MPC-24/24E/24EF/32
Reactivity	SPC 9x9-5 (Array/Class 9x9E/F)	B&W 15x15 (Array/Class 15x15F)
Shielding (Source Term)	GE 7x7	B&W 15x15
Fuel Assembly Effective Planar Thermal Conductivity	GE 11 9x9	<u>W</u> 17x17 OFA
Fuel Basket Effective Axial Thermal Conductivity	GE 7x7	<u>W</u> 14x14 OFA
MPC Density and heat Capacity	Dresden 6x6	<u>W</u> 14x14 OFA

Tables 1.2.13 and 1.2.14

INTENTIONALLY DELETED

Table 1.2.15

NORMALIZED DISTRIBUTION BASED ON BURNUP PROFILE

GENERIC FUEL DISTRIBUTION[†]			
Interval	Axial Distance From Bottom of Active Fuel (% of Active Fuel Length)	PWR Fuel Normalized Distribution	BWR Fuel Normalized Distribution
1	0% to 4-1/6%	0.5485	0.2200
2	4-1/6% to 8-1/3%	0.8477	0.7600
3	8-1/3% to 16-2/3%	1.0770	1.0350
4	16-2/3% to 33-1/3%	1.1050	1.1675
5	33-1/3% to 50%	1.0980	1.1950
6	50% to 66-2/3%	1.0790	1.1625
7	66-2/3% to 83-1/3%	1.0501	1.0725
8	83-1/3% to 91-2/3%	0.9604	0.8650
9	91-2/3% to 95-5/6%	0.7338	0.6200
10	95-5/6% to 100%	0.4670	0.2200
TROJAN PLANT FUEL DISTRIBUTION^{††}			
Interval	Axial Distance From Bottom of Active Fuel (% of Active Fuel Length)	Normalized Distribution	
1	0% to 5%	0.59	
2	5% to 10%	0.89	
3	10% to 15%	1.03	
4	15% to 20%	1.07	
5	20% to 25%	1.09	
6	25% to 45%	1.10	
7	45% to 70%	1.09	
8	70% to 75%	1.07	
9	75% to 80%	1.05	
10	80% to 85%	1.02	
11	85% to 90%	0.96	
12	90% to 95 %	0.82	
13	95% to 100%	0.56	

[†] References [1.2.8] and [1.2.9]

^{††} Reference [1.2.12]

Table 1.2.16

SUGGESTED PWR UPPER AND LOWER FUEL SPACER LENGTHS (Note 1)

Fuel Assembly Type	Assembly Length w/o NFH [†] (in.)	Location of Active Fuel from Bottom (in.)	Max. Active Fuel Length (in.)	Upper Fuel Spacer Length (in.)	Lower Fuel Spacer Length (in.)
CE 14x14	157	4.1	137	9.5	10
CE 16x16	176.8	4.7	150	0	0
BW 15x15	165.7	8.4	141.8	6.7	4.1
W 17x17 OFA	159.8	3.7	144	8.2	8.5
W 17x17S	159.8	3.7	144	8.2	8.5
W 17x17V5H	160.1	3.7	144	7.9	8.5
W 15x15	159.8	3.7	144	8.2	8.5
W 14x14S	159.8	3.7	145.2	9.2	7.5
W 14x14 OFA	159.8	3.7	144	8.2	8.5
Ft. Calhoun	146	6.6	128	10.25	20.25
St. Lucie 2	158.2	5.2	136.7	10.25	8.05
B&W 15x15 SS	137.1	3.873	120.5	19.25	19.25
W 15x15 SS	137.1	3.7	122	19.25	19.25
W 14x14 SS	137.1	3.7	120	19.25	19.25
Indian Point 1	137.2	17.705	101.5	18.75	20.0

Notes: 1. These fuel spacer lengths are not applicable to Trojan plant fuel. Trojan plant fuel spacer lengths are determined uniquely for the custom-designed Trojan MPC-24E/EF, as necessary, based on the presence of non-fuel hardware. They are sized to maintain the active fuel within the envelope of the neutron absorber affixed to the cell walls and allow for an approximate 2-inch gap between the fuel and the MPC lid. See Chapter 6 for discussion of potential misalignments between the active fuel and the neutron absorber.

[†] NFH is an abbreviation for non-fuel hardware, including control components. Fuel assemblies with control components may require shorter fuel spacers.

Table 1.2.17

SUGGESTED BWR UPPER AND LOWER FUEL SPACER LENGTHS (Note 1)

Fuel Assembly Type	Assembly Length (in.)	Location of Active Fuel from Bottom (in.)	Max. Active Fuel Length (in.)	Upper Fuel Spacer Length (in.)	Lower Fuel Spacer Length (in.)
GE/2-3	171.2	7.3	150	4.8	0
GE/4-6	176.2	7.3	150	0	0
Dresden 1	134.4	11.2	110	18	28.0
Humboldt Bay	95	8	79	40.5	40.5
Dresden 1 Damaged Fuel or Fuel Debris	142.1 [†]	11.2	110	17	16.9
Humboldt Bay Damaged Fuel or Fuel Debris	105.5 [†]	8	79	35.25	35.25
LaCrosse	102.5	10.5	83	37	37.5

Notes: 1. Each user shall specify the fuel spacer lengths based on their fuel length and allowing an approximate 2-inch gap between the fuel and the MPC lid. See Chapter 6 for discussion of potential misalignments between the active fuel and the neutron absorber.

[†] Fuel length includes the damaged fuel container.

Table 1.2.18

SUMMARY OF HI-STAR 100 SYSTEM POST-ACCIDENT PERFORMANCE

Aspect of Post-Accident Performance	Results with Demonstrated Integrity of MPC Enclosure Vessel	Results with Postulated Gross Failure of MPC Enclosure Vessel
Containment Boundary Integrity	The MPC enclosure vessel is leak tested to 5.0×10^{-6} atm cm^3/s (helium). The overpack containment boundary is standard air leak tested to 4.3×10^{-6} atm cm^3/s (helium). Both boundaries are shown to withstand all hypothetical accident conditions. Therefore, there will be no detectable release of radioactive materials.	The overpack containment boundary is leak tested to 4.3×10^{-6} atm cm^3/s (helium). The overpack containment boundary is shown to withstand all hypothetical accident conditions. Therefore, the overpack containment boundary meets the accident condition leakage rates.
Maintenance of Subcritical Margins (Maximum k_{eff})	The MPC enclosure vessel is seal welded and there is no breach of the MPC. The bolted closure overpack containment boundary has been shown to prevent water immersion. Therefore, the maximum reactivity of the fuel in a dry MPC is less than 0.5.	The bolted closure overpack containment boundary has been shown to prevent water immersion. Therefore, the maximum reactivity of the fuel in a dry MPC is less than 0.5. Assuming the MPC is fully flooded with water, the reactivity is shown to be below the regulatory requirement of 0.95 including uncertainties and bias.
Adequate Shielding	The MPC enclosure vessel boundary has no effect on the dose rates of the HI-STAR 100 System.	Failure of the MPC enclosure vessel to maintain a release boundary has no effect on the dose rates of the HI-STAR 100 System.
Adequate Heat Rejection (Peak Fuel Cladding Temperature)	The MPC enclosure vessel maintains the helium and the peak fuel cladding temperature is demonstrated to remain below 800°F in the post-fire hypothetical accident condition.	Assuming the MPC internal helium fill pressure is released into the overpack containment, the pressure within the small annulus would rise to equalize with the MPC internal pressure. There would be a corresponding slight pressure decrease in the MPC enclosure vessel. The comparatively small volume of the annulus and pressure differential results in the slight pressure change. This will have a negligibly small effect on the peak fuel cladding temperature. The overpack containment boundary is demonstrated to withstand all hypothetical accident conditions. Therefore, there is no credible mechanism for the release of the helium.

Tables 1.2.19 and 1.2.20

INTENTIONALLY DELETED

Table 1.2.21

DESIGN CHARACTERISTICS FOR THORIA RODS IN D-1 THORIA ROD CANISTERS

PARAMETER	MPC-68 or MPC-68F
Cladding Type	ZR
Composition	98.2 wt.% ThO ₂ , 1.8 wt.% UO ₂ with an enrichment of 93.5 wt. % ²³⁵ U
Number of Rods Per Thoria Canister	≤ 18
Decay Heat Per Thoria Canister	≤ 115 watts
Post-Irradiation Fuel Cooling Time and Average Burnup Per Thoria Canister	Cooling time ≥ 18 years and average burnup ≤ 16,000 MWD/MTIHM
Initial Heavy Metal Weight	≤ 27 kg/canister
Fuel Cladding O.D.	≥ 0.412 inches
Fuel Cladding I.D.	≤ 0.362 inches
Fuel Pellet O.D.	≤ 0.358 inches
Active Fuel Length	≤ 111 inches
Canister Weight	≤ 550 lbs., including Thoria Rods
Canister Material	Type 304 SS

Table 1.2.22

LIMITS FOR MATERIAL TO BE TRANSPORTED IN MPC-24

PARAMETER	VALUE
Fuel Type	Uranium oxide, PWR intact fuel assemblies meeting the limits in Table 1.2.10 for the applicable array/class
Cladding Type	ZR or Stainless Steel (SS) as specified in Table 1.2.10 for the applicable array/class
Maximum Initial Enrichment	As specified in Table 1.2.10 for the applicable array/class
Post-irradiation Cooling Time, Average Burnup, and Minimum Initial Enrichment per Assembly	ZR clad: As specified in Table 1.2.28 or Table 1.2.29, as applicable SS clad: As specified in Table 1.2.30
Decay Heat Per Assembly	ZR clad: ≤ 833 Watts SS clad: ≤ 488 Watts
Fuel Assembly Length	≤ 176.8 in. (nominal design)
Fuel Assembly Width	≤ 8.54 in. (nominal design)
Fuel Assembly Weight	$\leq 1,680$ lbs
Other Limitations	<ul style="list-style-type: none"> ▪ Quantity is limited to up to 24 PWR intact fuel assemblies. ▪ Non-fuel hardware and neutron sources not permitted. ▪ Damaged fuel assemblies and fuel debris not permitted. ▪ Trojan plant fuel not permitted.

Table 1.2.23

LIMITS FOR MATERIAL TO BE TRANSPORTED IN MPC-68

PARAMETER	VALUE (Note 1)			
Fuel Type(s)	Uranium oxide, BWR intact fuel assemblies meeting the limits in Table 1.2.11 for the applicable array/class, with or without Zircaloy channels	Uranium oxide, BWR damaged fuel assemblies meeting the limits in Table 1.2.11 for array/class 6x6A, 6x6C, 7x7A, or 8x8A, with or without Zircaloy channels, placed in Damaged Fuel Containers(DFCs)	Mixed Oxide (MOX) BWR intact fuel assemblies meeting the limits in Table 1.2.11 for array/class 6x6B, with or without Zircaloy channels	Mixed Oxide (MOX) BWR damaged fuel assemblies meeting the limits in Table 1.2.11 for array/class 6x6B, with or without Zircaloy channels, placed in Damaged Fuel Containers (DFCs)
Cladding Type	ZR or Stainless Steel (SS) as specified in Table 1.2.11 for the applicable array/class	ZR	ZR	ZR
Maximum Initial Planar-Average and Rod Enrichment	As specified in Table 1.2.11 for the applicable array/class	As specified in Table 1.2.11 for the applicable array/class	As specified in Table 1.2.11 for array/class 6x6B	As specified in Table 1.2.11 for array/class 6x6B
Post-irradiation Cooling Time, Average Burnup, and Minimum Initial Enrichment per Assembly	ZR clad: As specified in Table 1.2.31 except as provided in Notes 2 and 3 SS clad: Note 4	Cooling time ≥ 18 years, average burnup $\leq 30,000$ MWD/MTU, and minimum initial enrichment ≥ 1.458 wt. % ^{235}U .	Cooling time ≥ 18 years, average burnup $\leq 30,000$ MWD/MTIHM, and minimum initial enrichment ≥ 1.8 wt. % ^{235}U .	Cooling time ≥ 18 years, average burnup $\leq 30,000$ MWD/MTIHM, and minimum initial enrichment ≥ 1.8 wt. % ^{235}U .
Decay Heat Per Assembly	ZR clad: ≤ 272 Watts (Note 5) SS clad: ≤ 83 Watts	≤ 115 Watts	≤ 115 Watts	≤ 115 Watts

Table 1.2.23 (cont'd)

LIMITS FOR MATERIAL TO BE TRANSPORTED IN MPC-68

PARAMETER	VALUE (Note 1)			
Fuel Assembly Length	≤ 176.2 in. (nominal design)	≤ 135.0 in. (nominal design)	≤ 135.0 in. (nominal design)	≤ 135.0 in. (nominal design)
Fuel Assembly Width	≤ 5.85 in. (nominal design)	≤ 4.70 in. (nominal design)	≤ 4.70 in. (nominal design)	≤ 4.70 in. (nominal design)
Fuel Assembly Weight	≤ 700 lbs (including channels)	≤ 550 lbs, (including channels and DFC)	≤ 400 lbs, (including channels)	≤ 550 lbs, (including channels and DFC)
Quantity per MPC	Up to 68 BWR intact fuel assemblies	Up to 68 BWR damaged and/or intact fuel assemblies	Up to 68 BWR intact fuel assemblies	Up to 68 BWR damaged and/or intact fuel assemblies
Other Limitations	<ul style="list-style-type: none"> ▪ Quantity is limited to up to one (1) Dresden Unit 1 thoria rod canister meeting the specifications listed in Table 1.2.21 plus any combination of Dresden Unit 1 or Humboldt Bay damaged fuel assemblies in DFCs and intact fuel assemblies up to a total of 68. ▪ Stainless steel channels are not permitted. ▪ Fuel debris is not permitted. ▪ Dresden Unit 1 fuel assemblies with one antimony-beryllium neutron source are permitted. The antimony-beryllium neutron source material shall be in a water rod location. 			

Notes:

1. A fuel assembly must meet the requirements of any one column and the other limitations to be authorized for transportation.
2. Array/class 6x6A, 6x6C, 7x7A, and 8x8A fuel assemblies shall have a cooling time ≥ 18 years, an average burnup ≤ 30,000 MWD/MTU, and a minimum initial enrichment ≥ 1.458 wt. % ²³⁵U.
3. Array/class 8x8F fuel assemblies shall have a cooling time ≥ 10 years, an average burnup ≤ 27,500 MWD/MTU, and a minimum initial enrichment ≥ 2.4 wt. % ²³⁵U.
4. SS-clad fuel assemblies shall have a cooling time ≥ 16 years, an average burnup ≤ 22,500 MWD/MTU, and a minimum initial enrichment ≥ 3.5 wt. % ²³⁵U.
5. Array/class 8x8F fuel assemblies shall have a decay heat ≤ 183.5 Watts.

Table 1.2.24

LIMITS FOR MATERIAL TO BE TRANSPORTED IN MPC-68F

PARAMETER	VALUE (Notes 1 and 2)			
Fuel Type(s)	Uranium oxide, BWR intact fuel assemblies meeting the limits in Table 1.2.11 for array/class 6x6A, 6x6C, 7x7A, or 8x8A, with or without Zircaloy channels	Uranium oxide, BWR damaged fuel assemblies or fuel debris meeting the limits in Table 1.2.11 for array/class 6x6A, 6x6C, 7x7A, or 8x8A, with or without Zircaloy channels, placed in Damaged Fuel Containers(DFCs)	Mixed Oxide (MOX) BWR intact fuel assemblies meeting the limits in Table 1.2.11 for array/class 6x6B, with or without Zircaloy channels	Mixed Oxide (MOX) BWR damaged fuel assemblies or fuel debris meeting the limits in Table 1.2.11 for array/class 6x6B, with or without Zircaloy channels, placed in Damaged Fuel Containers (DFCs))
Cladding Type	ZR	ZR	ZR	ZR
Maximum Initial Planar-Average and Rod Enrichment	As specified in Table 1.2.11 for the applicable array/class	As specified in Table 1.2.11 for the applicable array/class	As specified in Table 1.2.11 for array/class 6x6B	As specified in Table 1.2.11 for array/class 6x6B
Post-irradiation Cooling Time, Average Burnup, and Minimum Initial Enrichment per Assembly	Cooling time ≥ 18 years, average burnup $\leq 30,000$ MWD/MTU, and minimum initial enrichment ≥ 1.458 wt. % ^{235}U .	Cooling time ≥ 18 years, average burnup $\leq 30,000$ MWD/MTU, and minimum initial enrichment ≥ 1.458 wt. % ^{235}U .	Cooling time ≥ 18 years, average burnup $\leq 30,000$ MWD/MTIH M, and minimum initial enrichment ≥ 1.8 wt. % ^{235}U .	Cooling time ≥ 18 years, average burnup $\leq 30,000$ MWD/MTIHM, and minimum initial enrichment ≥ 1.8 wt. % ^{235}U .
Decay Heat Per Assembly	≤ 115 Watts	≤ 115 Watts	≤ 115 Watts	≤ 115 Watts

Table 1.2.24 (cont'd)

LIMITS FOR MATERIAL TO BE TRANSPORTED IN MPC-68F

PARAMETER	VALUE (Note 1)			
Fuel Assembly Length	≤ 135.0 in. (nominal design)	≤ 135.0 in. (nominal design)	≤ 135.0 in. (nominal design)	≤ 135.0 in. (nominal design)
Fuel Assembly Width	≤ 4.70 in. (nominal design)	≤ 4.70 in. (nominal design)	≤ 4.70 in. (nominal design)	≤ 4.70 in. (nominal design)
Fuel Assembly Weight	≤ 400 lbs (including channels)	≤ 550 lbs (including channels and DFC)	≤ 400 lbs (including channels)	≤ 550 lbs (including channels and DFC)
Other Limitations	<ul style="list-style-type: none"> ▪ Quantity is limited to up to four (4) DFCs containing Dresden Unit 1 or Humboldt Bay uranium oxide or MOX fuel debris. The remaining fuel storage locations may be filled with array/class 6x6A, 6x6B, 6x6C, 7x7A, and 8x8A fuel assemblies of the following type, as applicable: <ul style="list-style-type: none"> - uranium oxide BWR intact fuel assemblies - MOX BWR intact fuel assemblies - uranium oxide BWR damaged fuel assemblies in DFCs - MOX BWR damaged fuel assemblies in DFCs - up to one (1) Dresden Unit 1 thoria rod canister meeting the specifications listed in Table 1.2.21 ▪ Stainless steel channels are not permitted. ▪ Dresden Unit 1 fuel assemblies with one antimony-beryllium neutron source are permitted. The antimony-beryllium neutron source material shall be in a water rod location. 			

Notes:

1. A fuel assembly must meet the requirements of any one column and the other limitations to be authorized for transportation.
2. Only fuel from Dresden Unit 1 and Humboldt Bay plant are is permitted for transportation in the MPC-68F.

Table 1.2.25

LIMITS FOR MATERIAL TO BE TRANSPORTED IN MPC-24E

PARAMETER	VALUE (Note 1)	
Fuel Type	Uranium oxide PWR intact fuel assemblies meeting the limits in Table 1.2.10 for the applicable array/class	Trojan plant damaged fuel meeting the limits in Table 1.2.10 for array/class 17x17B, placed in a Holtec Damaged Fuel Container (DFC) designed for Trojan plant fuel or a Trojan Failed Fuel Can (FFC)
Cladding Type	ZR or Stainless Steel (SS) assemblies as specified in Table 1.2.10 for the applicable array/class	ZR
Maximum Initial Enrichment	As specified in Table 1.2.10 for the applicable array/class	3.7 wt. % ²³⁵ U
Post-irradiation Cooling Time, Average Burnup, and Minimum Initial Enrichment per Assembly (except Trojan plant fuel and non-fuel hardware)	ZR clad: As specified in Table 1.2.28 or 1.2.29, as applicable SS clad: As specified in Table 1.2.30	Not applicable
Post-irradiation Cooling Time, Average Burnup, and Minimum Initial Enrichment per Assembly for Trojan plant fuel	As specified in Table 1.2.35	As specified in Table 1.2.35
Post-irradiation Cooling Time and Burnup for Trojan plant Non-fuel Hardware and Neutron Sources	As specified in Table 1.2.36	Not applicable
Decay Heat Per Assembly (except for Trojan plant fuel)	ZR clad: ≤ 833 Watts SS clad: ≤ 488 Watts	Not applicable
Decay heat per Assembly for Trojan plant fuel	≤ 725 Watts	≤ 725 Watts

Table 1.2.25 (cont'd)

LIMITS FOR MATERIAL TO BE TRANSPORTED IN MPC-24E

PARAMETER	VALUE (Note 1)	
Fuel Assembly Length	≤ 176.8 in. (nominal design)	≤ 169.3 in. (nominal design)
Fuel Assembly Width	≤ 8.54 in. (nominal design)	≤ 8.43 in. (nominal design)
Fuel Assembly Weight	≤ 1680 lbs (including non-fuel hardware)	≤ 1680 lbs (including DFC or Failed Fuel Can)
Other Limitations	<ul style="list-style-type: none"> ▪ Quantity per MPC: up to 24 PWR intact fuel assemblies. For Trojan plant fuel only, up to four (4) damaged fuel assemblies may be stored in fuel storage locations 3, 6, 19, and/or 22. The remaining fuel storage locations may be filled with Trojan plant intact fuel assemblies. ▪ Trojan plant fuel must be transported in the custom-designed Trojan MPCs with the MPC spacer installed (see Figure 1.1.5). Fuel from other plants is not permitted to be transported in the Trojan MPCs. ▪ Except for Trojan plant fuel, the fuel assemblies shall not contain non-fuel hardware. Trojan intact fuel assemblies containing non-fuel hardware may be transported in any fuel storage location. ▪ Trojan plant damaged fuel assemblies must be transported in a Holtec DFC for Trojan plant fuel or a Trojan plant FFC. ▪ One (1) Trojan plant Sb-Be and/or two (2) Cf neutron sources, each in a Trojan plant intact fuel assembly may be transported in any one MPC. Each neutron source may be transported in any fuel storage location. ▪ Fuel debris is not authorized for transportation in the MPC-24E. ▪ Trojan plant non-fuel hardware and neutron sources may not be transported in the same fuel storage location with damaged fuel assemblies. 	

Notes:

1. A fuel assembly must meet the requirements of any one column and the other limitations to be authorized for transportation.

Table 1.2.26

LIMITS FOR MATERIAL TO BE TRANSPORTED IN MPC-24EF

PARAMETER	VALUE (Note 1)		
Fuel Type	Uranium oxide PWR intact fuel assemblies meeting the limits in Table 1.2.10 for the applicable array/class	Trojan plant damaged fuel meeting the limits in Table 1.2.10 for array/class 17x17B, placed in a Holtec Damaged Fuel Container (DFC) designed for Trojan plant fuel or a Trojan Failed Fuel Can (FFC)	Trojan plant Fuel Debris Process Can Capsules and/or Trojan plant fuel assemblies classified as fuel debris, for which the original fuel assemblies meet the applicable criteria in Table 1.2.10 for array/class 17x17B, placed in a Holtec Damaged Fuel Container (DFC) designed for Trojan plant fuel or a Trojan Failed Fuel Can (FFC)
Cladding Type	ZR or Stainless Steel (SS) assemblies as specified in Table 1.2.10 for the applicable array/class	ZR	ZR
Maximum Initial Enrichment	As specified in Table 1.2.10 for the applicable array/class	≤ 3.7 wt. % ^{235}U	≤ 3.7 wt. % ^{235}U
Post-irradiation Cooling Time, Average Burnup, and Minimum Initial Enrichment per Assembly (except Trojan plant fuel and non-fuel hardware)	ZR clad: As specified in Table 1.2.28 or 1.2.29, as applicable SS clad: As specified in Table 1.2.30	Not applicable	Not applicable
Post-irradiation Cooling Time, Average Burnup, and Minimum Initial Enrichment per Assembly for Trojan plant fuel	As specified in Table 1.2.35	As specified in Table 1.2.35	As specified in Table 1.2.35

Table 1.2.26 (cont'd)

LIMITS FOR MATERIAL TO BE TRANSPORTED IN MPC-24EF

PARAMETER	VALUE (Note 1)		
Post-irradiation Cooling Time and Burnup for Trojan plant Non-fuel Hardware and Neutron Sources	As specified in Table 1.2.36	As specified in Table 1.2.36	As specified in Table 1.2.36
Decay Heat Per Assembly (except for Trojan plant fuel)	ZR clad: ≤ 833 Watts SS clad: ≤ 488 Watts	Not applicable	Not applicable
Decay heat per Assembly for Trojan plant fuel	≤ 725 Watts	≤ 725 Watts	≤ 725 Watts
Fuel Assembly Length	≤ 176.8 in. (nominal design)	≤ 169.3 in. (nominal design)	≤ 169.3 in. (nominal design)
Fuel Assembly Width	≤ 8.54 in. (nominal design)	≤ 8.43 in. (nominal design)	≤ 8.43 in. (nominal design)
Fuel Assembly Weight	≤ 1680 lbs (including non-fuel hardware)	≤ 1680 lbs (including DFC or Failed Fuel Can)	≤ 1680 lbs (including DFC or Failed Fuel Can)

Table 1.2.26 (cont'd)

LIMITS FOR MATERIAL TO BE TRANSPORTED IN MPC-24EF

<p>Other Limitations</p>	<ul style="list-style-type: none"> ▪ Quantity per MPC: Up to 24 PWR intact fuel assemblies. For Trojan plant fuel only, up to four (4) damaged fuel assemblies, fuel assemblies classified as fuel debris, and/or Trojan Fuel Debris Process Can Capsules may be stored in fuel storage locations 3, 6, 19, and/or 22. The remaining fuel storage locations may be filled with Trojan plant intact fuel assemblies. ▪ Trojan plant fuel must be transported in the custom-designed Trojan MPCs with the MPC spacer installed (see Figure 1.1.5). Fuel from other plants is not permitted to be transported in the Trojan MPCs. ▪ Except for Trojan plant fuel, the fuel assemblies shall not contain non-fuel hardware or neutron sources. Trojan intact fuel assemblies containing non-fuel hardware may be transported in any fuel storage location. ▪ Trojan plant damaged fuel assemblies, fuel assemblies classified as fuel debris, and Fuel Debris Process Can Capsules must be transported in a Trojan Failed Fuel Can or a Holtec DFC for Trojan plant fuel. ▪ One (1) Trojan plant Sb-Be and/or two (2) Cf neutron sources, each in a Trojan plant intact fuel assembly may be transported in any one MPC. Each neutron source may be transported in any fuel storage location.
--------------------------	--

Notes:

1. A fuel assembly must meet the requirements of any one column and the other limitations to be authorized for transportation.

Table 1.2.27

LIMITS FOR MATERIAL TO BE TRANSPORTED IN MPC-32 (Note 1)

PARAMETER	VALUE
Fuel Type	Uranium oxide, PWR intact fuel assemblies meeting the limits in Table 1.2.10 for array/classes 15x15D, E, F, and H and 17x17A, B, and C
Cladding Type	ZR
Maximum Initial Enrichment	As specified in Table 1.2.10
Post-irradiation Cooling Time, Average Burnup, and Minimum Initial Enrichment per Assembly	As specified in Table 1.2.32 or Table 1.2.33, as applicable
Decay Heat Per Assembly	≤ 625 Watts
Minimum Burnup per Assembly	As specified in Table 1.2.34 for the applicable array/class
Fuel Assembly Length	≤ 176.8 in. (nominal design)
Fuel Assembly Width	≤ 8.54 in. (nominal design)
Fuel Assembly Weight	≤ 1,680 lbs
Other Limitations	<ul style="list-style-type: none"> ▪ Quantity is limited to up to 32 PWR intact fuel assemblies in the above-specified array/classes only. ▪ Non-fuel hardware and neutron sources not permitted. ▪ Damaged fuel assemblies and fuel debris not permitted. ▪ Trojan plant fuel not permitted.

NOTES:

1. The MPC-32 is not authorized for transportation in the HI-STAR 100 System at this time.

Table 1.2.28

FUEL ASSEMBLY COOLING, AVERAGE BURNUP, AND MINIMUM ENRICHMENT
LIMITS FOR TRANSPORTATION IN MPC-24/24E/24EF; PWR FUEL WITH ZR
CLADDING AND WITH NON-ZIRCALOY IN-CORE GRID SPACERS

ASSEMBLY POST-IRRADIATION COOLING TIME (years)	ASSEMBLY BURNUP (MWD/MTU)	ASSEMBLY ENRICHMENT (wt. % ²³⁵ U)
≥ 9	≤ 24,500	≥ 2.3
≥ 11	≤ 29,500	≥ 2.6
≥ 13	≤ 34,500	≥ 2.9
≥ 15	≤ 39,500	≥ 3.2
≥ 18	≤ 44,500	≥ 3.4

Table 1.2.29

FUEL ASSEMBLY COOLING, AVERAGE BURNUP, AND MINIMUM ENRICHMENT
LIMITS FOR TRANSPORTATION IN MPC-24/24E/24EF;PWR FUEL WITH ZR
CLADDING AND WITH ZIRCALOY IN-CORE GRID SPACERS

ASSEMBLY POST-IRRADIATION COOLING TIME (years)	ASSEMBLY BURNUP (MWD/MTU)	ASSEMBLY ENRICHMENT (wt. % ²³⁵ U)
≥ 6	≤ 24,500	≥ 2.3
≥ 7	≤ 29,500	≥ 2.6
≥ 9	≤ 34,500	≥ 2.9
≥ 11	≤ 39,500	≥ 3.2
≥ 14	≤ 44,500	≥ 3.4

Table 1.2.30

FUEL ASSEMBLY COOLING, AVERAGE BURNUP, AND MINIMUM ENRICHMENT
LIMITS FOR TRANSPORTATION IN MPC-24/24E/24EF; PWR FUEL WITH
STAINLESS STEEL CLADDING

ASSEMBLY POST-IRRADIATION COOLING TIME (years)	ASSEMBLY BURNUP (MWD/MTU)	ASSEMBLY ENRICHMENT (wt. % ²³⁵ U)
≥ 19	≤ 30,000	≥ 3.1
≥ 24	≤ 40,000	≥ 3.1

Table 1.2.31

FUEL ASSEMBLY COOLING, AVERAGE BURNUP, AND MINIMUM ENRICHMENT
LIMITS FOR TRANSPORTATION IN MPC-68

ASSEMBLY POST-IRRADIATION COOLING TIME (years)	ASSEMBLY BURNUP (MWD/MTU)	ASSEMBLY ENRICHMENT (wt. % ²³⁵ U)
≥ 5	≤ 10,000	≥ 0.7
≥ 7	≤ 20,000	≥ 1.35
≥ 8	≤ 24,500	≥ 2.1
≥ 9	≤ 29,500	≥ 2.4
≥ 11	≤ 34,500	≥ 2.6
≥ 14	≤ 39,500	≥ 2.9
≥ 19	≤ 44,500	≥ 3.0

Table 1.2.32

FUEL ASSEMBLY COOLING, AVERAGE BURNUP, AND MINIMUM ENRICHMENT LIMITS FOR TRANSPORTATION IN MPC-32; PWR FUEL WITH ZR CLADDING AND WITH NON-ZIRCALOY IN-CORE GRID SPACERS (Note 1)

ASSEMBLY POST-IRRADIATION COOLING TIME (years)	ASSEMBLY BURNUP (MWD/MTU)	ASSEMBLY ENRICHMENT (wt. % ²³⁵ U)
≥ 12	≤ 24,500	≥ 2.3
≥ 14	≤ 29,500	≥ 2.6
≥ 16	≤ 34,500	≥ 2.9
≥ 19	≤ 39,500	≥ 3.2
≥ 20	≤ 42,500	≥ 3.4

NOTES:

1. MPC-32 is not authorized for transportation at this time.

Table 1.2.33

FUEL ASSEMBLY COOLING, AVERAGE BURNUP, AND MINIMUM ENRICHMENT
LIMITS FOR TRANSPORTATION IN MPC-32; PWR FUEL WITH ZR CLADDING
AND WITH ZIRCALOY IN-CORE GRID SPACERS (Note 1)

ASSEMBLY POST-IRRADIATION COOLING TIME (years)	ASSEMBLY BURNUP (MWD/MTU)	ASSEMBLY ENRICHMENT (wt. % ²³⁵ U)
≥ 8	≤ 24,500	≥ 2.3
≥ 9	≤ 29,500	≥ 2.6
≥ 12	≤ 34,500	≥ 2.9
≥ 14	≤ 39,500	≥ 3.2
≥ 19	≤ 44,500	≥ 3.4

NOTES:

1. MPC-32 is not authorized for transportation at this time.

Table 1.2.34

FUEL ASSEMBLY MINIMUM BURNUP REQUIREMENTS FOR TRANSPORTATION IN MPC-32 (Note 1)

FUEL ASSEMBLY ARRAY/CLASS	MINIMUM BURNUP (B) AS A FUNCTION OF INITIAL ENRICHMENT (E) (Note 2) (GWD/MTU)
15x15D, E, F, and H	Later
17x15A, B, and C	Later

Notes:

1. MPC-32 is not authorized for transportation at this time.
2. E = Initial enrichment from the fuel vendor's data sheet, i.e., for 4.05wt. %, E = 4.05.

Table 1.2.35

TROJAN PLANT FUEL ASSEMBLY COOLING, AVERAGE BURNUP, AND MINIMUM ENRICHMENT LIMITS (Note 1)

Post-irradiation Cooling Time (years)	Assembly Burnup (MWD/MTU)	Assembly Minimum Enrichment (wt. % ²³⁵ U)
≥ 16	≤ 42,000	≥ 3.09
≥ 16	≤ 37,500	≥ 2.6
≥ 16	≤ 30,000	≥ 2.1

Notes:

1. Each fuel assembly must only meet one set of limits (i.e., one row).

Table 1.2.36

TROJAN PLANT NON-FUEL HARDWARE AND NEUTRON SOURCE COOLING AND
BURNUP LIMITS

Type Of Hardware or Neutron Source	Burnup (MWD/MTU)	Post-irradiation Cooling Time (years)
BPRAs	≤ 15,998	≥ 24
TPDs	≤ 118,674	≥ 11
RCCAs	≤ 125,515	≥ 9
Cf neutron source	≤ 15,998	≥ 24
Sb-Be neutron source with 4 source rods, 16 burnable poison rods, and 4 thimble plug rods	≤ 45,361	≥ 19
Sb-Be neutron source with 4 source rods and 20 thimble plug rods	≤ 88,547	≥ 9

Table 1.2.37

METAMIC[®] DATA FOR HOLTEC MPCs

MPC Type	Min. B-10 areal density required by criticality analysis (g/cm ²)	Nominal Weight Percent of B ₄ C and Reference <i>METAMIC</i> [®] Panel Thickness			
		100% Credit	90% Credit	75% Credit	Ref. Thickness (inch) (see note)
MPC 24	0.020	27.6	31	37.2	0.075
MPC 68, 32, 24E, and 24EF	0.0279	27.8	31	37.4	0.104

Note: The drawings in Section 1.4 show slightly larger thickness to ensure that the minimum B-10 areal density is conservative under all conditions.

Figure Withheld Under 10 CFR 2.390

FIGURE 1.2.10; HOLTEC DAMAGED FUEL CONTAINER FOR
DRESDEN UNIT-1 SNF

1.3 DESIGN CODE APPLICABILITY

The ASME Boiler and Pressure Vessel Code (ASME Code), 1995 Edition with Addenda through 1997 [1.3.1], is the governing code for the construction of the HI-STAR 100 System, as clarified in Table 1.3.2. The ASME Code is applied to each component consistent with the function of the component. Table 1.3.3 lists each structure, system and component (SSC) of the HI-STAR 100 System that are labeled Important to Safety (ITS), along with its function and governing Code. Some components perform multiple functions and in those cases, the most restrictive Code is applied. In accordance with NUREG/CR-6407, "Classification of Transportation Packaging and Dry Spent Fuel Storage System Components" [1.3.2] and according to importance to safety, components of the HI-STAR 100 System are classified as A, B, C, or NITS (not important to safety) in Table 1.3.3. Table 1.3.3 may not include all NITS items associated with the HI-STAR 100 Package.

Table 1.3.1 lists the applicable ASME Code section and paragraph for material procurement, design, fabrication and inspection of the components of the HI-STAR 100 System that are governed by the ASME Code. The ASME Code section listed in the design column is the section used to define allowable stresses for structural analyses.

Table 1.3.2 lists the alternatives to the ASME Code for the HI-STAR 100 System and the justification for those alternatives.

The MPC is classified as important to safety. The MPC structural components include the internal fuel basket and the enclosure vessel. The fuel basket is designed and fabricated as a core support structure, in accordance with the applicable requirements of Section III, Subsection NG of the ASME Code, with certain NRC-approved alternatives, as discussed in Table 1.3.2. The enclosure vessel is designed and fabricated as a Class 1 component pressure vessel in accordance with Section III, Subsection NB of the ASME Code, with certain NRC-approved alternatives, as discussed in Table 1.3.2. The principal exceptions are the MPC lid, vent and drain cover plates, and closure ring welds to the MPC lid and shell, as discussed in Table 1.3.2. In addition, the threaded holes in the MPC lid are designed in accordance with the requirements of ANSI N14.6 [1.3.3] for critical lifts to facilitate vertical MPC transfer.

The MPC closure welds are partial penetration welds that are structurally qualified by analysis, as presented in Chapter 2. The MPC closure ring welds are inspected by performing a liquid penetrant examination of the root pass (if more than one weld pass is required) and final weld surface, in accordance with the requirements contained in Section 8.1. The MPC lid weld may be examined by either volumetric or multi-layer liquid penetrant examination. If volumetric examination is used, it shall be the ultrasonic method and shall include a liquid penetrant examination of the root and final weld layers. If multi-layer liquid penetrant examination is used alone, at a minimum, it must include the root and final weld layers and each approximately 3/8 inch of weld to detect critical weld flaws. The integrity of the MPC lid weld is further verified by performing a pressure test (hydrostatic or pneumatic) ~~and a helium leak test~~ in accordance with the requirements contained in Section 8.1.

The structural analysis of the MPC, in conjunction with the redundant closures and nondestructive examination, *and* pressure testing, ~~and helium leak testing~~ performed during MPC fabrication and MPC closure, provides assurance of canister closure integrity in lieu of the specific weld joint requirements of the ASME Code, Section III, Subsection NB.

The HI-STAR overpack is classified as important to safety. The HI-STAR overpack top flange, closure plate, inner shell, and bottom plate are designed and fabricated in accordance with the requirements of ASME Code, Section III, Subsection NB, to the maximum extent practical (see Table 1.3.2). The remainder of the HI-STAR overpack steel structure is designed and fabricated in accordance with the requirements of ASME Code, Section III, Subsection NF, to the maximum extent practical (see Table 1.3.2).

Table 1.3.1

HI-STAR 100 ASME BOILER AND PRESSURE VESSEL CODE APPLICABILITY

HI-STAR 100 Component	Material Procurement	Design	Fabrication	Inspection
Overpack containment boundary	Section II; and Section III, Subsection NB, NB-2000	Section III, Subsection NB, NB-3200	Section III, Subsection NB, NB-4000	Section III, Subsection NB, NB-5000 and Section V
Overpack intermediate shells, radial channels, outer enclosure	Section II; and Section III, Subsection NF	Section III, Subsection NF, NF-3300	Section III, Subsection NF, NF-4000	Section III, Subsection NF, NF-5360 and Section V
MPC helium retention boundary	Section II; and Section III, Subsection NB, NB-2000	Section III, Subsection NB, NB-3200	Section III, Subsection NB, NB-4000	Section III, Subsection NB, NB-5000 and Section V
MPC fuel basket	Section II; and Section III, Subsection NG, NG-2000 for core support structures (NG-1121)	Section III, Subsection NG, NG-3300 and NG-3200 for core support structures (NG-1121)	Section III, Subsection NG, NG-4000 for core support structures (NG-1121)	Section III, Subsection NG, NG-5000 and Section V for core support structures (NG-1121)
Lifting Trunnions	Section II; and Section III, Subsection NF, NF-2000	ANSI N14.6	Section III, Subsection NF, NF-4000	ANSI 14.6 See Chapter 8
MPC Basket Supports (Angled Plates)	Section II, and Section III, Subsection NG, NG-2000 for internal structures (NG-1122)	Section III, Subsection NG, NG-3300 and NG-3200 for internal structures (NG-1122)	Section III, Subsection NG, NG-4000 for internal structures (NG-1122)	Section III, Subsection NG, NG-5000 and Section V for internal structures (NG-1122)
Damaged Fuel Container	Section II, and Section III, Subsection NG, NG-2000	Section III, Subsection NG, NG-3300 and NG-3200	Section III, Subsection NG, NG-4000	Section III, Subsection NG, NG-5000 and Section V

Table 1.3.2

LIST OF ASME CODE ALTERNATIVES FOR HI-STAR 100 SYSTEM

Component	Reference ASME Code Section/Article	Code Requirement	Alternative, Justification & Compensatory Measures
MPC, MPC basket assembly, and HI-STAR overpack steel structure.	Subsection NCA	General Requirements. Requires preparation of a Design Specification, Design Report, Overpressure Protection Report, Certification of Construction Report, Data Report, and other administrative controls for an ASME Code stamped vessel.	<p>Because the MPC and overpack are not ASME Code stamped vessels, none of the specifications, reports, certificates, or other general requirements specified by NCA are required. In lieu of a Design Specification and Design Report, the HI-STAR SAR includes the design criteria, service conditions, and load combinations for the design and operation of the HI-STAR 100 System as well as the results of the stress analyses to demonstrate that applicable Code stress limits are met. Additionally, the fabricator is not required to have an ASME-certified QA program. All important-to-safety activities are governed by the NRC-approved Holtec QA program.</p> <p>Because the cask components are not certified to the Code, the terms "Certificate Holder" and "Inspector" are not germane to the manufacturing of NRC-certified cask components. To eliminate ambiguity, the responsibilities assigned to the Certificate Holder in the various articles of Subsections NB, NG, and NF of the Code, as applicable, shall be interpreted to apply to the NRC Certificate of Compliance (CoC) holder (and by extension, to the component fabricator) if the requirement must be fulfilled. The Code term "Inspector" means the QA/QC personnel of the CoC holder and its vendors assigned to oversee and inspect the manufacturing process.</p>
MPC	NB-1100	Statement of requirements for Code stamping of components.	MPC vessel is designed and will be fabricated in accordance with ASME Code, Section III, Subsection NB to the maximum practical extent, but Code stamping is not required.
MPC	NB-2000	Requires materials to be supplied by ASME-approved material supplier.	Materials will be supplied by Holtec approved suppliers with Certified Material Test Reports (CMTRs) in accordance with NB-2000 requirements.

Table 1.3.2 (continued)

LIST OF ASME CODE ALTERNATIVES FOR HI-STAR 100 SYSTEM

Component	Reference ASME Code Section/Article	Code Requirement	Alternative, Justification & Compensatory Measures
MPC basket supports and lift lugs	NB-1130	<p>NB-1132.2(d) requires that the first connecting weld of a nonpressure-retaining structural attachment to a component shall be considered part of the component unless the weld is more than $2t$ from the pressure-retaining portion of the component, where t is the nominal thickness of the pressure-retaining material.</p> <p>NB-1132.2(e) requires that the first connecting weld of a welded nonstructural attachment to a component shall conform to NB-4430 if the connecting weld is within $2t$ from the pressure-retaining portion of the component.</p>	<p>The MPC basket supports (nonpressure-retaining structural attachments) and lift lugs (nonstructural attachments used exclusively for lifting an empty MPC) are welded to the inside of the pressure-retaining MPC shell, but are not designed in accordance with Subsection NB. The basket supports and associated attachment welds are designed to satisfy the stress limits of Subsection NG and the lift lugs and associated attachment welds are designed to satisfy the stress limits of Subsection NF, as a minimum. These attachments and their welds are shown by analysis to meet the respective stress limits for their service conditions. Likewise, non-structural items, such as shield plugs, spacers, etc. if used, can be attached to pressure-retaining parts in the same manner.</p>
MPC, MPC basket assembly, and HI-STAR overpack steel structure.	NB-3100 NG-3100 NF-3100	Provides requirements for determining design loading conditions, such as pressure, temperature, and mechanical loads.	These requirements are not applicable. The HI-STAR SAR, serving as the Design Specification, establishes the service conditions and load combinations for the storage system.

Table 1.3.2 (continued)

LIST OF ASME CODE ALTERNATIVES FOR HI-STAR 100 SYSTEM

Component	Reference ASME Code Section/Article	Code Requirement	Alternative, Justification & Compensatory Measures
MPC	NB-3350	NB-3352.3 requires, for Category C joints, that the minimum dimensions of the welds and throat thickness shall be as shown in Figure NB-4243-1.	<p>The MPC shell-to-baseplate weld joint design (designated Category C) may not include a reinforcing fillet weld or a bevel in the MPC baseplate, which makes it different than any of the representative configurations depicted in Figure NB-4243-1. The transverse thickness of this weld is equal to the thickness of the adjoining shell (1/2 inch). The weld is designed as a full penetration weld that receives VT and RT or UT, as well as final surface PT examinations. Because the MPC shell design thickness is considerably larger than the minimum thickness required by the Code, a reinforcing fillet weld that would intrude into the MPC cavity space is not included. Not including this fillet weld provides for a higher quality radiographic examination of the full penetration weld.</p> <p>From the standpoint of stress analysis, the fillet weld serves to reduce the local bending stress (secondary stress) produced by the gross structural discontinuity defined by the flat plate/shell junction. In the MPC design, the shell and baseplate thicknesses are well beyond that required to meet their respective membrane stress intensity limits.</p>
MPC, MPC basket assembly, and HI-STAR overpack steel structure	NB-4120 NG-4120 NF-4120	NB-4121.2, NG-4121.2, and NF-4121.2 provide requirements for repetition of tensile or impact tests for material subjected to heat treatment during fabrication or installation.	<p>In-shop operations of short duration that apply heat to a component, such as plasma cutting of plate stock, welding, machining, coating, and pouring of Holtite are not, unless explicitly stated by the Code, defined as heat treatment operations.</p> <p>For the steel parts in the HI-STAR 100 System components, the duration for which a part exceeds the off-normal temperature limit shall be limited to 24 hours in a particular manufacturing process (such as the Holtite pouring process).</p>

Table 1.3.2 (continued)

LIST OF ASME CODE ALTERNATIVES FOR HI-STAR 100 SYSTEM

Component	Reference ASME Code Section/Article	Code Requirement	Alternative, Justification & Compensatory Measures
MPC and HI-STAR overpack steel structure	NB-4220 NF-4220	Requires certain forming tolerances to be met for cylindrical, conical, or spherical shells of a vessel.	The cylindricity measurements on the rolled shells are not specifically recorded in the shop travelers, as would be the case for a Code-stamped pressure vessel. Rather, the requirements on inter-component clearances (such as the MPC-to-overpack) are guaranteed through fixture-controlled manufacturing. The fabrication specification and shop procedures ensure that all dimensional design objectives, including inter-component annular clearances are satisfied. The dimensions required to be met in fabrication are chosen to meet the functional requirements of the dry storage components. Thus, although the post-forming Code cylindricity requirements are not evaluated for compliance directly, they are indirectly satisfied (actually exceeded) in the final manufactured components.
MPC Lid and Closure Ring Welds	NB-4243	Full penetration welds required for Category C Joints (flat head to main shell per NB-3352.3)	MPC lid and closure ring are not full penetration welds. They are welded independently to provide a redundant seal. Additionally, a weld efficiency factor of 0.45 has been applied to the analyses of these welds.
MPC Lid-to-Shell Weld	NB-5230	Radiographic (RT) or ultrasonic (UT) examination required.	Only UT or multi-layer liquid penetrant (PT) examination is permitted. If PT alone is used, at a minimum, it will include the root and final weld layers and each approximately 3/8 inch of weld depth.
MPC Closure Ring, Vent and Drain Cover Plate Welds	NB-5230	Radiographic (RT) or ultrasonic (UT) examination required.	Root (if more than one weld pass is required) and final liquid penetrant examination to be performed in accordance with NB-5245. The MPC vent and drain cover plate welds are leak tested. The closure ring provides independent redundant closure for vent and drain cover plates.

Table 1.3.2 (continued)

LIST OF ASME CODE ALTERNATIVES FOR HI-STAR 100 SYSTEM

Component	Reference ASME Code Section/Article	Code Requirement	Alternative, Justification & Compensatory Measures
MPC Enclosure Vessel and Lid	NB-6111	All completed pressure retaining systems shall be pressure tested.	The MPC vessel is seal welded in the field following fuel assembly loading. The MPC vessel shall then be pressure tested as defined in Chapter 8. Accessibility for leakage inspections precludes a Code compliant pressure test. All MPC vessel welds (except closure ring and vent/drain cover plate) are inspected by volumetric examination, except that the MPC lid-to-shell weld shall be verified by volumetric or multi-layer PT examination. If PT alone is used, at a minimum, it must include the root and final layers and each approximately 3/8 inch of weld depth. For either UT or PT, the maximum undetectable flaw size must be demonstrated to be less than the critical flaw size. The critical flaw size must be determined in accordance with ASME Section XI methods. The critical flaw size shall not cause the primary stress limits of NB-3000 to be exceeded. The inspection results, including relevant findings (indications) shall be made a permanent part of the user's records by video, photographic, or other means which provide an equivalent retrievable record of weld integrity. The video or photographic records should be taken during the final interpretation period described in ASME Section V, Article 6, T-676. The vent/drain cover plate welds are confirmed by helium leakage testing and liquid penetrant examination and the closure ring weld is confirmed by liquid penetrant examination. The inspection of the weld must be performed by qualified personnel and shall meet the acceptance requirements of ASME Code Section III, NB-5350 for PT or NB-5332 for UT.
MPC Enclosure Vessel	NB-7000	Vessels are required to have overpressure protection.	No overpressure protection is provided. The function of MPC vessel is as a helium retention boundary. MPC vessel is designed to withstand maximum internal pressure considering 100% fuel rod failure and maximum accident temperatures.

Table 1.3.2 (continued)

LIST OF ASME CODE ALTERNATIVES FOR HI-STAR 100 SYSTEM

Component	Reference ASME Code Section/Article	Code Requirement	Alternative, Justification & Compensatory Measures
MPC Enclosure Vessel	NB-8000	States requirements for nameplates, stamping and reports per NCA-8000.	HI-STAR 100 System to be marked and identified in accordance with 10CFR71 and 10CFR72 requirements. Code stamping is not required. QA data package to be in accordance with Holtec approved QA program.
Overpack Containment Boundary	NB-1100	Statement of requirements for Code stamping of components.	Overpack containment boundary is designed, and will be fabricated in accordance with ASME Code, Section III, Subsection NB to the maximum practical extent, but Code stamping is not required.
Overpack Containment Boundary	NB-2000	Requires materials to be supplied by ASME-approved material supplier.	Materials will be supplied by Holtec approved suppliers with CMTRs per NB-2000.
Overpack Containment Boundary	NB-7000	Vessels are required to have overpressure protection.	No overpressure protection is provided. Function of overpack vessel is as a radionuclide containment boundary under normal and hypothetical accident conditions. Overpack vessel is designed to withstand maximum internal pressure and maximum accident temperatures.
Overpack Containment Boundary	NB-8000	States requirements for nameplates, stamping and reports per NCA-8000.	HI-STAR 100 System to be marked and identified in accordance with 10CFR71 and 10CFR72 requirements. Code stamping is not required. QA data package to be in accordance with Holtec's approved QA program.
MPC Basket Assembly	NG-2000	Requires materials to be supplied by ASME-approved material supplier.	Materials will be supplied by Holtec approved supplier with CMTRs in accordance with NG-2000 requirements.

Table 1.3.2 (continued)

LIST OF ASME CODE ALTERNATIVES FOR HI-STAR 100 SYSTEM

Component	Reference ASME Code Section/Article	Code Requirement	Alternative, Justification & Compensatory Measures
MPC Basket Assembly	NG-4420	NG-4427(a) allows a fillet weld in any single continuous weld to be less than the specified fillet weld dimension by not more than 1/16 inch, provided that the total undersize portion of the weld does not exceed 10 percent of the length of the weld. Individual undersize weld portions shall not exceed 2 inches in length.	<p>Modify the Code requirement (intended for core support structures) with the following text prepared to accord with the geometry and stress analysis imperatives for the fuel basket: For the longitudinal MPC basket fillet welds, the following criteria apply: 1) The specified fillet weld throat dimension must be maintained over at least 92 percent of the total weld length. All regions of undersized weld must be less than 3 inches long and separated from each other by at least 9 inches. 2) Areas of undercuts and porosity beyond that allowed by the applicable ASME Code shall not exceed 1/2 inch in weld length. The total length of undercut and porosity over any 1-foot length shall not exceed 2 inches. 3) The total weld length in which items (1) and (2) apply shall not exceed a total of 10 percent of the overall weld length. The limited access of the MPC basket panel longitudinal fillet welds makes it difficult to perform effective repairs of these welds and creates the potential for causing additional damage to the basket assembly (e.g., to the neutron absorber and its sheathing) if repairs are attempted. The acceptance criteria provided in the foregoing have been established to comport with the objectives of the basket design and preserve the margins demonstrated in the supporting stress analysis.</p> <p>From the structural standpoint, the weld acceptance criteria are established to ensure that any departure from the ideal, continuous fillet weld seam would not alter the primary bending stresses on which the design of the fuel baskets is predicated. Stated differently, the permitted weld discontinuities are limited in size to ensure that they remain classifiable as local stress elevators ("peak stress", F, in the ASME Code for which specific stress intensity limits do not apply).</p>
MPC Basket Assembly	NG-8000	States requirements for nameplates, stamping and reports per NCA-8000.	The HI-STAR 100 System will be marked and identified in accordance with 10CFR71 and 10CFR72 requirements. No Code stamping is required. The MPC basket data package will be in conformance with Holtec's QA program.
Overpack Intermediate Shells	NF-2000	Requires materials to be supplied by ASME-approved material supplier.	Materials will be supplied by Holtec approved supplier with CMTRs in accordance with NF-2000 requirements.

Table 1.3.2 (continued)

LIST OF ASME CODE ALTERNATIVES FOR HI-STAR 100 SYSTEM

Component	Reference ASME Code Section/Article	Code Requirement	Alternative, Justification & Compensatory Measures
Overpack Containment Boundary	NB-2330	Defines the methods for determining the T_{NDT} for impact testing of materials.	T_{NDT} shall be defined in accordance with Regulatory Guides 7.11 and 7.12 for the containment boundary components.
Overpack Containment Boundary	NF-3320 NF-4720	NF-3324.6 and NF-4720 provide requirements for bolting.	<p>These Code requirements are applicable to linear structures wherein bolted joints carry axial, shear, as well as rotational (torsional) loads. The overpack bolted connections in the structural load path are qualified by design based on the design loadings defined in the SAR. Bolted joints in these components see no shear or torsional loads under normal storage conditions. Larger clearances between bolts and holes may be necessary to ensure shear interfaces located elsewhere in the structure engage prior to the bolts experiencing shear loadings (which occur only during side impact scenarios).</p> <p>Bolted joints that are subject to shear loads in accident conditions are qualified by appropriate stress analysis. Larger bolt-to-hole clearances help ensure more efficient operations in making these bolted connections, thereby minimizing time spent by operations personnel in a radiation area. Additionally, larger bolt-to-hole clearances allow interchangeability of the lids from one particular fabricated cask to another.</p>

Table 1.3.2 (continued)

LIST OF ASME CODE ALTERNATIVES FOR HI-STAR 100 SYSTEM

Component	Reference ASME Code Section/Article	Code Requirement	Alternative, Justification & Compensatory Measures
MPC-68 Serial #1021-023, 036, 037 Closure Rings	NB-2531	Requires UT inspection of plate.	The sole deviation of the 3/8" thick austenitic stainless steel material used for the MPC closure ring is the omission of a straight beam UT inspection as required by NB-2531. The ASME Code required straight beam inspection for vessels because the predominant indication in plates is laminations. Straight beam inspection cannot detect indications perpendicular to the surface of the plate. With respect to maintaining confinement, an indication perpendicular to the surface of the plate is the most critical. Laminations in the plate parallel to the surface of the plate cannot cause leakage through the plate. Therefore, the straight beam UT inspection does not add any value for detecting a defect in the thin closure ring with respect to its confinement function.

Table 1.3.3

MATERIALS AND COMPONENTS OF THE HI-STAR 100 SYSTEM

OVERPACK ^(1,2)

Primary Function	Component ⁽³⁾	Safety Class ⁽⁴⁾	Codes/Standards (as applicable to component)	Material	Strength (ksi)	Special Surface Finish/Coating	Contact Matl. (if dissimilar)
Containment	Inner Shell	A	ASME Section III; Subsection NB	SA203-E or SA350-LF3	Table 2.3.4	Paint inside surface with Thermaline 450 (Note 5). External surface to be coated with a surface preservative.	NA
Containment	Bottom Plate	A	ASME Section III; Subsection NB	SA350-LF3	Table 2.3.4	Paint inside surface with Thermaline 450 (Note 5).	NA
Containment	Top Flange	A	ASME Section III; Subsection NB	SA350-LF3	Table 2.3.4	Paint inside surface with Thermaline 450. Paint outside surface with Carboline 890 (Note 5).	NA
Containment	Closure Plate	A	ASME Section III; Subsection NB	SA350-LF3	Table 2.3.4	Paint inside surface with Thermaline 450. Paint outside surface with Carboline 890 (Note 5).	NA
Containment	Closure Plate Bolts	A	ASME Section III; Subsection NB	SB637-N07718	Table 2.3.5	NA	NA
Containment	Port Plug	A	Non-code	SA193-B8	Not required	NA	NA
Containment	Port Plug Seal	A	Non-code	Alloy X750	Not required	NA	NA
Containment	Closure Plate Seal	A	Non-code	Alloy X750	Not required	NA	NA
Containment	Port Cover Seal	B	Non-code	Alloy X750	Not required	NA	NA

- Notes: 1) There are no known residuals on finished component surfaces.
- 2) All welding processes used in welding the components shall be qualified in accordance with the requirements of ASME Section IX. All welds shall be made using welders qualified in accordance with ASME Section IX. Weld material shall meet the requirements of ASME Section II and the applicable Subsection of ASME Section III. For parts beyond the purview of ASME Section III, compliance with Section IX and Section II of the Code shall be observed to the extent practicable.
- 3) Component nomenclature taken from drawings in Chapter I.
- 4) A,B and C denote important to safety classifications as described in NUREG/CR-6407. NITS stands for Not Important To Safety.
- 5) Thermaline 450 and Carboline 890 were the product names at the time of initial licensing. Chemically identical products with different names are permitted. For example, Carboline 890 was re-named Carboguard 890 in 2000, with no change to the coating material and is, therefore, acceptable for use where Carboline 890 is specified.

TABLE 1.3.3 (continued)

MATERIALS AND COMPONENTS OF THE HI-STAR 100 SYSTEM

OVERPACK ^(1,2)

Primary Function	Component ⁽³⁾	Safety Class ⁽⁴⁾	Codes/Standards (as applicable to component)	Material	Strength (ksi)	Special Surface Finish/Coating	Contact Matl. (if dissimilar)
Shielding	Intermediate Shells	B	ASME Section III; Subsection NF	SA516-70	Table 2.3.2	Internal surfaces to be coated with a silicone encapsulant (Dow-Corning SYLGARD 567 or equivalent) for surface preservation, <i>except for HI-STAR HB</i> . Exposed areas of fifth intermediate shell to be painted with Carboline 890 (Note 5).	NA
Shielding	Neutron Shield	B	Non-code	Holtite-A	Not required	NA	Holtite/CS
Shielding	Plugs for Drilled Holes	NITS	Non-code	SA193-B7	Not required	NA	NA
Shielding	Removable Shear Ring	B	ASME Section III; Subsection NF	SA203-E <i>Carbon Steel</i>	Table 2.3.4 <i>Not required</i>	Paint external surface with Carboline 890 (Note 5).	NA
Shielding	Pocket Trunnion Plug Plate	C	Non-code	SA240-304	Not required	NA	NA
Heat Transfer	Radial Channels (<i>not used on the HI-STAR HB</i>)	B	ASME Section III; Subsection NF	SA515-70	Table 2.3.3	Paint outside surface with Carboline 890 (Note 5).	NA

- Notes:
- 1) There are no known residuals on finished component surfaces.
 - 2) All welding processes used in welding the components shall be qualified in accordance with the requirements of ASME Section IX. All welds shall be made using welders qualified in accordance with ASME Section IX. Weld material shall meet the requirements of ASME Section II and the applicable Subsection of ASME Section III. For parts beyond the purview of ASME Section III, compliance with Section IX and Section II of the Code shall be observed to the extent practicable.
 - 3) Component nomenclature taken from drawings in Chapter 1.
 - 4) A,B and C denote important to safety classifications as described in NUREG/CR-6407. NITS stands for Not Important To Safety.
 - 5) Thermaline 450 and Carboline 890 were the product names at the time of initial licensing. Chemically identical products with different names are permitted. For example, Carboline 890 was re-named Carboguard 890 in 2000, with no change to the coating material and is, therefore, acceptable for use where Carboline 890 is specified.

TABLE 1.3.3 (continued)

MATERIALS AND COMPONENTS OF THE HI-STAR 100 SYSTEM

OVERPACK ^(1,2)

Primary Function	Component ⁽³⁾	Safety Class ⁽⁴⁾	Codes/Standards (as applicable to component)	Material	Strength (ksi)	Special Surface Finish/Coating	Contact Matl. (if dissimilar)
Rotation Pivot and Shielding	Pocket Trunnion	B	Non-Code	SA705-630 17-4 PH or SA564-630 17-4 PH	Table 2.3.5	NA	NA
Structural Integrity	Lifting Trunnion	A	ANSI N14.6	SB637- N07718	Table 2.3.5	NA	NA
Structural Integrity	Relief Device	C	Non-code	Commercial	Not required	NA	Brass-C/S
Structural Integrity	Relief Device Plate	C	Non-code	SA 516 Grade 70 or A569	Not required	NA	NA
Structural Integrity	Removable Shear Ring Bolt	C	Non-code	SA193-B7	Not required	NA	NA
Structural Integrity	Thermal Expansion Foam	NITS	Non-code	Silicone Foam	Not required	NA	Silicone with CS, brass, and Holtite
Structural Integrity	Closure Bolt Washer	NITS	Non-code	ASTM A564, 17-7 PH	Not required	NA	NA
Structural Integrity	Enclosure Shell Panels	B	ASME Section III; Subsection NF	SA515-70	Table 2.3.3	Paint outside surface with Carboline 890 (Note 5).	NA

- Notes: 1) There are no known residuals on finished component surfaces.
- 2) All welding processes used in welding the components shall be qualified in accordance with the requirements of ASME Section IX. All welds shall be made using welders qualified in accordance with ASME Section IX. Weld material shall meet the requirements of ASME Section II and the applicable Subsection of ASME Section III. For parts beyond the purview of ASME Section III, compliance with Section IX and Section II of the Code shall be observed to the extent practicable.
- 3) Component nomenclature taken from drawings in Chapter 1.
- 4) A,B and C denote important to safety classifications as described in NUREG/CR-6407. NITS stands for Not Important To Safety.
- 5) Thermaline 450 and Carboline 890 were the product names at the time of initial licensing. Chemically identical products with different names are permitted. For example, Carboline 890 was re-named Carboguard 890 in 2000, with no change to the coating material and is, therefore, acceptable for use where Carboline 890 is specified.

TABLE 1.3.3 (continued)

MATERIALS AND COMPONENTS OF THE HI-STAR 100 SYSTEM

OVERPACK ^(1,2)

Primary Function	Component ⁽³⁾	Safety Class ⁽⁴⁾	Codes/Standards (as applicable to component)	Material	Strength (ksi)	Special Surface Finish/Coating	Contact Matl. (if dissimilar)
Structural Integrity	Enclosure Shell Return	B	ASME Section III; Subsection NF	SA515-70	Table 2.3.3	Paint outside surface with Carboline 890 (Note 5).	NA
Structural Integrity	Port Cover	B	ASME Section III; Subsection NF	SA203E or SA350-LF3	Table 2.3.4	Paint outside surface with Carboline 890 (Note 5).	NA
Structural Integrity	Port Cover Bolt	C	Non-code	SA193-B7	Not required	NA	NA
Operations	Trunnion Locking Pad and End Cap Bolt	C	Non-code	SA193-B7	Not required	NA	NA
Operations	Lifting Trunnion End Cap	C	Non-code	SA516-70 or SA515 Gr. 70	Table 2.3.2	Paint exposed surfaces with Carboline 890 (Note 5).	NA
Operations	Lifting Trunnion Locking Pad	C	Non-code	SA516-70	Table 2.3.2	Paint exposed surfaces with Carboline 890 (Note 5).	NA
Operations	Nameplate	NITS	Non-code	S/S	Not required	NA	NA

- Notes:
- 1) There are no known residuals on finished component surfaces.
 - 2) All welding processes used in welding the components shall be qualified in accordance with the requirements of ASME Section IX. All welds shall be made using welders qualified in accordance with ASME Section IX. Weld material shall meet the requirements of ASME Section II and the applicable Subsection of ASME Section III. For parts beyond the purview of ASME Section III, compliance with Section IX and Section II of the Code shall be observed to the extent practicable.
 - 3) Component nomenclature taken from drawings in Chapter 1.
 - 4) A,B and C denote important to safety classifications as described in NUREG/CR-6407. NITS stands for Not Important To Safety.
 - 5) Thermaline 450 and Carboline 890 were the product names at the time of initial licensing. Chemically identical products with different names are permitted. For example, Carboline 890 was re-named Carboguard 890 in 2000, with no change to the coating material and is, therefore, acceptable for use where Carboline 890 is specified.

Table 1.3.3 (cont'd)

MATERIALS AND COMPONENTS OF THE HI-STAR 100 SYSTEM

MPC ^(1,2)

Primary Function	Component ⁽³⁾	Safety Class ⁽⁴⁾	Codes/Standards (as applicable to component)	Material	Strength (ksi)	Special Surface Finish/Coating	Contact Matl. (if dissimilar)
Helium Retention (Secondary Containment)	Shell	A	ASME Section III; Subsection NB	Alloy X ⁽⁵⁾	See Appendix 1.A	NA	NA
Helium Retention (Secondary Containment)	Baseplate	A	ASME Section III; Subsection NB	Alloy X	See Appendix 1.A	NA	NA
Helium Retention (Secondary Containment)	Lid (One-piece design and top portion of optional two-piece design)	A	ASME Section III; Subsection NB	Alloy X	See Appendix 1.A	NA	NA
Helium Retention (Secondary Containment)	Closure Ring	A	ASME Section III; Subsection NB	Alloy X	See Appendix 1.A	NA	NA
Helium Retention (Secondary Containment)	Port Cover Plates	A	ASME Section III; Subsection NB	Alloy X	See Appendix 1.A	NA	NA
Criticality Control	Basket Cell Plates	A	ASME Section III; Subsection NG; core support structures (NG-1121)	Alloy X	See Appendix 1.A	NA	NA
Criticality Control	Boral	A	Non-code	NA	NA	NA	Aluminum/SS
Shielding	Drain and Vent Shield Block	C	Non-code	Alloy X	See Appendix 1.A	NA	NA
Shielding	Plugs for Drilled Holes	NITS	Non-code	Alloy X	See Appendix 1.A	NA	NA

Notes: 1) There are no known residuals on finished component surfaces.

2) All welding processes used in welding the components shall be qualified in accordance with the requirements of ASME Section IX. All welds shall be made using welders qualified in accordance with ASME Section IX. Weld material shall meet the requirements of ASME Section II and the applicable Subsection of ASME Section III. For parts beyond the purview of ASME Section III, compliance with Section IX and Section II of the Code shall be observed to the extent practicable.

3) Component nomenclature taken from Bill of Materials in Chapter 1.

4) A, B and C denote important to safety classifications as described in NUREG/CR-6407. NITS stands for Not Important To Safety.

5) For details on Alloy X material, see Appendix 1.A.

TABLE 1.3.3 (continued)

MATERIALS AND COMPONENTS OF THE HI-STAR 100 SYSTEM

MPC^(1,2)

Primary Function	Component ⁽³⁾	Safety Class ⁽⁴⁾	Codes/Standards (as applicable to component)	Material	Strength (ksi)	Special Surface Finish/Coating	Contact Matl. (if dissimilar)
Shielding	Bottom portion of optional two-piece MPC lid design	B	Non-code	Alloy X	See Appendix 1.A	NA	NA
Heat Transfer	Optional Heat Conduction Elements	B	Non-code	Aluminum; Alloy 1100	NA	Sandblast Specified Surfaces	Aluminum/SS
Structural Integrity	Upper Fuel Spacer Column	B	ASME Section III; Subsection NG (only for stress analysis)	Alloy X	See Appendix 1.A	NA	NA
Structural Integrity	Sheathing	A	Non-code	Alloy X	See Appendix 1.A	Aluminum/SS	NA
Structural Integrity	Shims	NITS	Non-code	Alloy X	See Appendix 1.A	NA	NA
Structural Integrity	Basket Supports (Angled Plates)	A	ASME Section III; Subsection NG; internal structures (NG-1122)	Alloy X	See Appendix 1.A	NA	NA
Structural Form	Basket Supports (Flat Plates)	NITS	Non-code	Alloy X	See Appendix 1.A	NA	NA
Structural Integrity	Upper Fuel Spacer Bolt	NITS	Non-code	A193-B8	Per ASME Section II	NA	NA
Structural Integrity	Upper Fuel Spacer End Plate	B	Non-code	Alloy X	See Appendix 1.A	NA	NA

Notes: 1) There are no known residuals on finished component surfaces.

2) All welding processes used in welding the components shall be qualified in accordance with the requirements of ASME Section IX. All welds shall be made using welders qualified in accordance with ASME Section IX. Weld material shall meet the requirements of ASME Section II and the applicable Subsection of ASME Section III. For parts beyond the purview of ASME Section III, compliance with Section IX and Section II of the Code shall be observed to the extent practicable.

3) Component nomenclature taken from Bill of Materials in Chapter 1.

4) A, B and C denote important to safety classifications as described in NUREG/CR-6407. NITS stands for Not Important To Safety.

5) For details on Alloy X material, see Appendix 1.A.

TABLE 1.3.3 (continued)

MATERIALS AND COMPONENTS OF THE HI-STAR 100 SYSTEM

MPC^(1,2)

Primary Function	Component ⁽³⁾	Safety Class ⁽⁴⁾	Codes/Standards (as applicable to component)	Material	Strength (ksi)	Special Surface Finish/Coating	Contact Matl. (if dissimilar)
Structural Integrity	Lower Fuel Spacer Column	B	ASME Section III; Subsection NG (only for stress analysis)	S/S	See Appendix 1.A	NA	NA
Structural Integrity	Lower Fuel Spacer End Plate	B	Non-code	Alloy X	See Appendix 1.A	NA	NA
Structural Integrity	Vent Shield Block Spacer	C	Non-code	Alloy X	See Appendix 1.A	NA	NA
Structural Integrity	Trojan MPC Spacer	B	Non-code	304 S/S	Per ASME Section II	NA	NA
Structural Integrity	Trojan Failed Fuel Can Spacer	B	ASME Section III, Subsection NF	304 or 304LN S/S	Per ASME Section II	NA	NA
Operations	Vent and Drain Tube	C	Non-code	S/S	Per ASME Section II	Thread area surface hardened	NA
Operations	Vent & Drain Cap	C	Non-code	S/S	Per ASME Section II	NA	NA
Operations	Vent & Drain Cap Seal Washer	NITS	Non-code	Aluminum	NA	NA	Aluminum/SS
Operations	Vent & Drain Cap Seal Washer Bolt	NITS	Non-code	Aluminum	NA	NA	NA
Operations	Reducer	NITS	Non-code	Alloy X	See Appendix 1.A	NA	NA
Operations	Drain Line	NITS	Non-code	Alloy X	See Appendix 1.A	NA	NA

Notes: 1) There are no known residuals on finished component surfaces.

2) All welding processes used in welding the components shall be qualified in accordance with the requirements of ASME Section IX. All welds shall be made using welders qualified in accordance with ASME Section IX. Weld material shall meet the requirements of ASME Section II and the applicable Subsection of ASME Section III. For parts beyond the purview of ASME Section III, compliance with Section IX and Section II of the Code shall be observed to the extent practicable.

3) Component nomenclature taken from Bill of Materials in Chapter 1.

4) A, B and C denote important to safety classifications as described in NUREG/CR-6407. NITS stands for Not Important To Safety.

5) For details on Alloy X material, see Appendix 1.A.

TABLE 1.3.3 (continued)

MATERIALS AND COMPONENTS OF THE HI-STAR 100 SYSTEM

MPC^(1,2)

Primary Function	Component ⁽³⁾	Safety Class ⁽⁴⁾	Codes/Standards (as applicable to component)	Material	Strength (ksi)	Special Surface Finish/Coating	Contact Matl. (if dissimilar)
Operations	Damaged Fuel Container	C	ASME Section III; Subsection NG	Primarily 304 S/S	See Appendix 1.A	NA	NA
Operations	Trojan Failed Fuel Can	C	ASME Section III; Subsection NG	304 S/S	Per ASME Section II	NA	NA
Operations	Drain Line Guide Tube	NITS	Non-code	S/S	NA	NA	NA

- Notes:
- 1) There are no known residuals on finished component surfaces.
 - 2) All welding processes used in welding the components shall be qualified in accordance with the requirements of ASME Section IX. All welds shall be made using welders qualified in accordance with ASME Section IX. Weld material shall meet the requirements of ASME Section II and the applicable Subsection of ASME Section III. For parts beyond the purview of ASME Section III, compliance with Section IX and Section II of the Code shall be observed to the extent practicable.
 - 3) Component nomenclature taken from Bill of Materials in Chapter 1.
 - 4) A,B and C denote important to safety classifications as described in NUREG/CR-6407. NITS stands for Not Important To Safety.
 - 5) For details on Alloy X material, see Appendix 1.A.

1.4 DRAWINGS

The following drawings provide sufficient detail to describe the HI-STAR 100 packaging. *Refer to Supplement 1.1 for drawings related to the HI-STAR HB.*

The classification of all components important to safety in accordance with Regulatory Guide 7.10 and NUREG/CR-6407 is provided in Table 1.3.3. Operational information, such as bolt torque and pressure-relief specifications are provided in Chapters 7 and 8. The maximum weight of the package and the maximum weight of the contents is provided in Table 2.2.1.

The following HI-STAR 100 System design drawings are provided in this section.

Drawing Number/Sheet	Description	Rev.
3913	Licensing Drawing for HI-STAR 100 Overpack Assembly	79
3923	Licensing Drawing for MPC Enclosure Vessel	1416
3925	Licensing Drawing for MPC-24E/EF Fuel Basket Assembly	5
3926	Licensing Drawing for MPC-24 Fuel Basket Assembly	5
3927	Licensing Drawing for MPC-32 Fuel Basket Assembly	6
3928	Licensing Drawing for MPC-68/68F/68FF Fuel Basket Assembly	5
5014-C1765 Sht 1/7 [†]	HI-STAR 100 Impact Limiter	24
5014-C1765 Sht 2/7 [†]	HI-STAR 100 Bottom Impact Limiter	23
5014-C1765 Sht 3/7 [†]	HI-STAR 100 Top Impact Limiter	14
5014-C1765 Sht 4/7 [†]	HI-STAR 100 Top Impact Limiter	24
5014-C1765 Sht 5/7 [†]	HI-STAR 100 Top Impact Limiter Detail of Item #6	12
5014-C1765 Sht 6/7 [†]	HI-STAR 100 Impact Limiter Honeycomb Details	13
5014-C1765 Sht 7/7 [†]	HI-STAR 100 Bottom Impact Limiter	01
3930	HI-STAR 100 Assembly For Transport	12
4111	Licensing Drawing for Trojan MPC Spacer Ring	0
4119	Licensing Drawing for Holtec Damaged Fuel Container for Trojan Plant Fuel	1

[†] These drawing titles include the term "CoC No. 9261, Appendix B." Rather than appending the drawings directly to the CoC, they are incorporated into the CoC by reference. The "Appendix B" will be removed from each drawing as part of its next normal revision.

Drawing Number/Sheet	Description	Rev.
4122	Licensing Drawing for Trojan FFC Spacer	0
PFFC-001	Failed Fuel Can Assembly	8
PFFC-002	Failed Fuel Can Shell and Lid Assembly	7

Figure Withheld Under 10 CFR 2.390

 HOLTEC INTERNATIONAL HOLTEC CENTER 535 LINCOLN DRIVE WEST MARLTON, NJ 08053	CLIENT	GENERAL					
	DESCRIPTION	HI-STAR 100 OVERPACK					
PROJECT NO.	1020	DRAWING NO.	3913	SHEET	1	TOTAL SHEETS	9
P.O. NO.	N/A	FILE PATH	E:\ADMINISTR\HQP\3913.D				

Figure Withheld Under 10 CFR 2.390

 HOLTEC INTERNATIONAL HOLTEC CENTER 555 LINCOLN DRIVE WEST MARLTON, NJ 08053	CLIENT	GENERAL		
	DESCRIPTION	HI-STAR 100 OVERPACK ELEVATION VIEW		
CONTRACT NUMBER	REV	ORDER NO.	SHEET	NO.
	D	3913	2	9
	SCALE	NTS	FILE PATH	6:\V\200801\108P\2013

Figure Withheld Under 10 CFR 2.390

 HOLTEC INTERNATIONAL HOLTEC CENTER 555 LINCOLN DRIVE WEST MARTLTON, NJ 08053	CLIENT GENERAL			
	DESCRIPTION HI-STAR 100 OVERPACK DETAIL OF TOP FLANGE AT 0° & 180°			
COMPANY STANDARD	SIZE D	DESIGN NO. 3913	SHEET NO. 3	TOTAL SHEETS 9
SCALE NTS		FILE PATH G:\VIBRATION\1182\LIB\13		

Figure Withheld Under 10 CFR 2.390

 HOLTEC INTERNATIONAL HOLTEC CENTER 333 LINCOLN DRIVE WEST MARLTON, NJ 08053	CLIENT			
	GENERAL			
ACCOUNT NO.		HI-STAR 100 OVERPACK MID-PLANE SECTION "E" - "E"		
SECTION NUMBER	SIZE	ORDER NO.	SHEET	NO.
	D	3913	6	9
SCALE		NTS	FILE PATH: @\\J0000001\1007\3113	

Figure Withheld Under 10 CFR 2.390

 HOLTEC INTERNATIONAL HOLTEC CENTER 555 LINCOLN DRIVE WEST MARLTON, NJ 08053	CLIENT GENERAL			
	DESCRIPTION HI-STAR 100 OVERPACK TEST, VENT AND DRAIN PORT DETAILS			
CONTRACT NUMBER	REV D	DESIGN NO. 3913	SHEET NO. 7	TOTAL SHEETS 9
SCALE NTS		FILE PATH <small>\\VOLUME001\1029\3913</small>		

Figure Withheld Under 10 CFR 2.390

 HOLTEC INTERNATIONAL HOLTEC CENTER 555 LINCOLN DRIVE WEST MARLTON, NJ 08053	CLIENT	GENERAL		
	DESCRIPTION	HI-STAR 100 OVERPACK DETAIL "H"		
COMPANY NUMBER	SIZE D	PACKAGE NO. 3913	SHEET 8	REV 9
SCALE	NTS	FILE PATH	G:\UNSWER\1103P_2013	

Figure Withheld Under 10 CFR 2.390

		TITLE	
HOLTEC INTERNATIONAL		GENERAL	
HOLTEC CENTER 835 LINCOLN DRIVE WEST MARLTON, NJ 08053		DESCRIPTION	
COMPANY DRAWING		POCKET TRUNNION DETAIL	
SIZE	DRAWING NO.	SHEET	OF
D	3913	9	9
SCALE	NTS	FILE PATH	BY/ISSUED/1807/3913

Figure Withheld Under 10 CFR 2.390

 HOLTEC INTERNATIONAL HOLTEC CENTER 550 LINCOLN DRIVE WEST MARTIN, NJ 08053	CLASSIFICATION	GENERAL					
	DESCRIPTION	MPC ENCLOSURE VESSEL					
PROJECT NO.	5014	CONTAINER NO.	3923	SHEET	1	TOTAL SHEETS	7
DATE	N/A	REVISED		© ORNL 2014			

Figure Withheld Under 10 CFR 2.390

 HOLTEC INTERNATIONAL <small>HOLTEC CENTER 8501 ROCKAWAY DRIVE WEST MABLETON, NJ 08050</small>	CLASSIFICATION		
	GENERAL		
<small>CONTAINER IDENTIFICATION NO.</small> 3925, 3926, 3927, 3928	DESCRIPTION		
	MPC ENCLOSURE VESSEL GENERAL ARRANGEMENT		
	SCALE	FIGURE NO.	SHEET NO.
	D	3923	2
	SCALE	FILE NO.	FIGURE NO.
	NONE		16

© 2014 Holtec International

Figure Withheld Under 10 CFR 2.390

 HOLTEC INTERNATIONAL HOLTEC CENTER 555 LINDSEY DRIVE WEST MADISON NJ 07052	GENERAL			
	DESCRIPTION MPC ENCLOSURE ENCLOSURE VESSEL ELEVATION DETAILS			
COMMISSION/OPERATION 3925, 3926, 3927, 3928	SCALE NONE	DRWG NO. 3923	REV 3	PAGE 16
		FILE NO.		© 1994 HPI/014-0222

Figure Withheld Under 10 CFR 2.390

 HOLTEC INTERNATIONAL HOLTEC CENTER 555 LINCOLN DRIVE WEST MANLTON, NJ 08053	GENERAL			
	FUEL SPACER DETAILS			
3925, 3926, 3927, 3928	D	3923	5	16
SCALE	NONE	DATE PLOTTED	C:\WORK\950518\223823	

Figure Withheld Under 10 CFR 2.390

 HOLTEC INTERNATIONAL HOLTEC CENTER 550 PINECORN DRIVE WEST MARCLOFTON, NJ 08053	GENERAL			
	MPC SERIAL #1021-040 ENCLOSURE VESSEL LID DETAILS			
COMPONENT NUMBER 3925, 3926, 3927, 3928	SIZE D	DRAWING NO. 3923	SHEET 6	TOTAL 16
SCALE	ALONE	REF PCH	C:\DRAWING\3923\3923.DWG	

Figure Withheld Under 10 CFR 2.390

 HOLTEC INTERNATIONAL HOLTEC CENTER 555 LINCOLN DRIVE WEST MORRISTOWN, NJ 07960	CLASS	GENERAL		
	DESCRIPTION	MPC ENCLOSURE VESSEL LID DETAILS (SMDR 1269 / 1364)		
COMPANY PARTS 3925, 3926, 3927, 3928	SIZE	CLASSIFICATION	REV	REV
	D	3923	16	16
	SCALE	NONE	REF ID: A	© 2014 WILCOX DESIGN LLC

Figure Withheld Under 10 CFR 2.390

THIS DRAWING IS AN INTELLECTUAL PROPERTY OF HOLTEC INTERNATIONAL. IT IS PROVIDED TO THE RECIPIENT UNDER THE EXPLICIT CONDITION THAT IT WILL NOT BE DUPLICATED IN WHOLE OR IN PART OR GIVEN TO OTHERS WITHOUT WRITTEN CONSENT OF HOLTEC INTERNATIONAL.	
	EQUIPMENT DESIGN ANALYSIS CONSULTING
DESCRIPTION HI-STAR 100 IMPACT LIMITER 	
CLIENT VARIOUS	
COMPANION DRAWINGS NONE	REV. 4
PROJECT No. 5014	DRAWING No.
P.D. No. VARIOUS	C1765 (E.I.D. 4420) SH. 1 OF 7

Figure Withheld Under 10 CFR 2.390

THIS DRAWING IS AN INTELLECTUAL PROPERTY OF HOLTEC INTERNATIONAL. IT IS PROVIDED TO THE RECIPIENT UNDER THE EXPLICIT CONDITION THAT IT WILL NOT BE DUPLICATED IN WHOLE OR IN PART, OR GIVEN TO OTHERS WITHOUT WRITTEN CONSENT OF HOLTEC INTERNATIONAL.	
	EQUIPMENT DESIGN ANALYSIS CONSULTING
DESCRIPTION HI-STAR 100 BOTTOM IMPACT LIMITER 	
CLIENT VARIOUS	
COMPANION DRAWINGS NONE	REV. 3
PROJECT No. 5014 P.O. No. VARIOUS	DRAWING No. C1765 (E.I.D. 4421) SHI. 2 OF 7

Figure Withheld Under 10 CFR 2.390

THIS DRAWING IS AN INTELLECTUAL PROPERTY OF HOLTEC INTERNATIONAL. IT IS PROVIDED TO THE RECIPIENT UNDER THE EXPLICIT CONDITION THAT IT WILL NOT BE DUPLICATED IN WHOLE OR IN PART, OR GIVEN TO OTHERS WITHOUT WRITTEN CONSENT OF HOLTEC INTERNATIONAL.	
	EQUIPMENT DESIGN ANALYSIS CONSULTING
DESCRIPTION HI-STAR 100 TOP IMPACT LIMITER 	
CLIENT VARIOUS	
COMPANION DRAWINGS NONE	REV. 4
PROJECT No. 5014 P.O. No. VARIOUS	DRAWING No. C1765 (E.I.D. 4798) SHT. 3 OF 7

Figure Withheld Under 10 CFR 2.390

THIS DRAWING IS AN INTELLECTUAL PROPERTY OF HOLTEC INTERNATIONAL. IT IS PROVIDED TO THE RECIPIENT UNDER THE EXPLICIT CONDITION THAT IT WILL NOT BE DUPLICATED IN WHOLE OR IN PART, OR GIVEN TO OTHERS WITHOUT WRITTEN CONSENT OF HOLTEC INTERNATIONAL.		
		EQUIPMENT DESIGN ANALYSIS CONSULTING
DESCRIPTION HI-STAR 100 TOP IMPACT LIMITER 		
CLIENT VARIOUS		
COMPANION DRAWINGS NONE		REV. 4
PROJECT No. 5014	DRAWING No. C1765	
P.O. No. VARIOUS	(E.I.D. 4422) SH. 4 OF 7	

Figure Withheld Under 10 CFR 2.390

THIS DRAWING IS AN INTELLECTUAL PROPERTY OF HOLTEC INTERNATIONAL. IT IS PROVIDED TO THE RECIPIENT UNDER THE EXPLICIT CONDITION THAT IT WILL NOT BE DUPLICATED, IN WHOLE OR IN PART, OR GIVEN TO OTHERS WITHOUT WRITTEN CONSENT OF HOLTEC INTERNATIONAL.	
	EQUIPMENT DESIGN ANALYSIS CONSULTING
DESCRIPTION HI-STAR 100 TOP IMPACT LIMITER DETAIL OF ITEM #6 	
CLIENT VARIOUS	
COMPANION DRAWINGS NONE	REV. 2
PROJECT No. 5014 P.D. No. VARIOUS	DRAWING No. C1765 (E.I.D. 6116) SHT. 5 OF 7

Figure Withheld Under 10 CFR 2.390

THIS DRAWING IS AN INTELLECTUAL PROPERTY OF HOLTEC INTERNATIONAL. IT IS PROVIDED TO THE RECIPIENT UNDER THE EXPLICIT CONDITION THAT IT WILL NOT BE DUPLICATED IN WHOLE OR IN PART, OR GIVEN TO OTHERS WITHOUT WRITTEN CONSENT OF HOLTEC INTERNATIONAL.	
	EQUIPMENT DESIGN ANALYSIS CONSULTING
DESCRIPTION HI-STAR 100 IMPACT LIMITER HONEYCOMB DETAILS 	
CLIENT VARIOUS	
COMPANION DRAWINGS NONE	REV. 3
PROJECT No. 5014	DRAWING No. (E.I.D. 5372)
P.D. No. VARIOUS	C1765 SHIT. 6 OF 7

Figure Withheld Under 10 CFR 2.390

THIS DRAWING IS AN INTELLECTUAL PROPERTY OF HOLTEC INTERNATIONAL. IT IS PROVIDED TO THE RECIPIENT UNDER THE EXPLICIT CONDITION THAT IT WILL NOT BE DUPLICATED IN WHOLE OR IN PART, OR GIVEN TO OTHERS WITHOUT WRITTEN CONSENT OF HOLTEC INTERNATIONAL.	
	EQUIPMENT DESIGN ANALYSIS CONSULTING
DESCRIPTION HI-STAR 100 BOTTOM IMPACT LIMITER 	
CLIENT VARIOUS	
COMPANION DRAWINGS NONE	REV. 1
PROJECT No. 5014 P.D. No. VARIOUS	DRAWING No. (E.D. 6117) C1765 SH. 7 OF 7

Figure Withheld Under 10 CFR 2.390

		CLIENT		GENERAL	
HOLTEC INTERNATIONAL		DESCRIPTION			
HOLTEC CENTER 353 LINCOLN DRIVE WEST MARLTON, NJ 08053		HI-STAR 100 ASSEMBLY FOR TRANSPORT			
PROJECT NO.	1020	ISSUE NO.	3930	SHEET	1
P/A NO.	N/A			TOTAL SHEETS	3
		FILE PATH		G:\VENDOR\100P\1020	

Figure Withheld Under 10 CFR 2.390

 HOLTEC INTERNATIONAL HOLTEC CENTER 505 LINCOLN DRIVE WEST MARLTON, NJ 08053	CLASS: GENERAL			
	DESCRIPTION: HI-STAR 100 ASSEMBLY FOR TRANSPORT			
CONTRACT NUMBER:	REV: D	DESIGN NO: 3930	SHEET: 2	TOT: 2
SCALE: NTS		FILE PATH: 01/000001/0001/0001		

Figure Withheld Under 10 CFR 2.390

		CLASS		GENERAL	
HOLTEC INTERNATIONAL HOLTEC CENTER 333 LINCOLN DRIVE WEST MARTON, NJ 08053		DESCRIPTION			
CONFIDENTIAL OR RESTRICTED		HI-STAR 100 TRANSPORT CONFIGURATION			
REV	ISSUED BY	ISSUE NO.	REV.	DATE	BY
D		3930	3		2
SCALE	NTS	FILE NO.	6-12-1984-1487-3100		

1.5 Compliance with 10CFR71

The HI-STAR 100 packaging complies with the requirements of 10CFR71 for a Type B(U)F-8596 package. Analyses which demonstrate that the HI-STAR 100 packaging complies with the requirements of Subparts E and F of 10CFR71 are provided in this SAR. Specific reference to each section of the SAR that is used to specifically address compliance is provided in Table 1.0.2. The HI-STAR 100 packaging complies with the general standards for all packages, 10CFR71.43, as demonstrated in Section 2.4. Under the tests specified in 10CFR71.71 (normal conditions of transport) the HI-STAR 100 packaging is demonstrated to sustain no degradation in its safety function allowing the HI-STAR 100 packaging to meet the requirements of 10CFR71, Paragraphs 71.45, 71.51, and 71.55. Under the tests specified in 10CFR71.73 (hypothetical accident conditions) and 10CFR71.61 (special requirement for irradiated nuclear fuel shipments), the degradation sustained by the HI-STAR 100 packaging is shown not to cause the HI-STAR 100 packaging to exceed the requirements of 10CFR71, Paragraphs 71.51, 71.55, and 71.63(b).

The HI-STAR 100 packaging meets the structural, thermal, containment, shielding and criticality requirements of 10CFR71, as described in Chapters 2 through 6. The operational procedures and acceptance tests and maintenance program provided in Chapters 7 and 8 ensure compliance with the requirements of 10CFR71.

The following is a summary of the information provided in Chapter 1 that is directly applicable to verifying compliance with 10CFR71:

- The HI-STAR 100 packaging has been described in sufficient detail to provide an adequate basis for its evaluation.
- Drawings provided in Section 1.4 contain information that provides an adequate basis for evaluation of the HI-STAR 100 packaging against the 10CFR71 requirements. Each drawing is identified, consistent with the text of the SAR, and contains keys or annotation to explain and clarify information on the drawing.
- Section 1.0 includes a reference to the NRC-approved Holtec International quality assurance program for the HI-STAR 100 packaging.
- Section 1.3 identifies the applicable codes and standards for the HI-STAR 100 packaging design, fabrication, assembly, and testing.
- The HI-STAR 100 packaging meets the general requirements of 10CFR71.43(a) and 10CFR71.43(b), as demonstrated by the drawings provided in Section 1.4 and the discussion provided in Subsection 1.2.1.9, respectively.
- The drawings provided in Section 1.4 provide a detailed packaging description that can be evaluated for compliance with 10CFR71 for each technical discipline.

- Any restrictions on the use of the HI-STAR 100 packaging are specified in Subsection 1.2.3 and Chapter 7.

1.6 REFERENCES

- [1.0.1] 10CFR Part 71, "Packaging and Transportation of Radioactive Materials", Title 10 of the Code of Federal Regulations, Office of the Federal Register, Washington, D.C.
- [1.0.2] 49CFR173, "Shippers - General Requirements For Shipments and Packagings", Title 49 of the Code of Federal Regulations, Office of the Federal Register, Washington, D.C.
- [1.0.3] Regulatory Guide 7.9, "Standard Format and Content of Part 71 Applications for Approval of Packaging for Radioactive Material", Proposed Revision 2, USNRC, May 1986.
- [1.0.4] 10CFR Part 72, "Licensing Requirements for the Storage of Spent Fuel in an Independent Spent Fuel Storage Installation", Title 10 of the Code of Federal Regulations, Office of the Federal Register, Washington, D.C.
- [1.0.5] NUREG-1617, "Standard Review Plan for Transportation Packages for Spent Nuclear Fuel", , U.S. Nuclear Regulatory Commission, March 2000.
- [1.0.6] HI-STAR 100 Final Safety Analysis Report, Holtec Report No. HI-2012610, Revision 1, Docket No. 72-1008.
- [1.0.7] HI-STORM 100 Final Safety Analysis Report, Holtec Report No. HI-2002444, Revision 1, Docket No. 72-1014.
- [1.0.8] *Pacific Gas & Electric Company HIL-06-001, "Humboldt Bay ISFSI Final Safety Analysis Report", Revision 0, January 2006, USNRC Docket 72-27.*
- [1.1.1] U.S. Department of Energy, "Multi-Purpose Canister (MPC) Subsystem Design Procurement Specification", Document No. DBG000000-01717-6300-00001, Rev. 5, January 11, 1996.
- [1.1.2] U.S. Department of Energy, "MPC Transportation Cask Subsystem Design Procurement Specification", Document No. DBF 000000-01717-6300-00001, Rev. 5, January 11, 1996.
- [1.2.1] U.S. NRC Information Notice 96-34, "Hydrogen Gas Ignition During Closure Welding of a VSC-24 Multi-Assembly Scale Basket".
- [1.2.2] Directory of Nuclear Reactors, Vol. II, Research, Test & Experimental Reactors, International Atomic Energy Agency, Vienna, 1959.
- [1.2.3] V.L. McKinney and T. Rockwell III, Boral: A New Thermal-Neutron Shield,

USAEC Report AECD-3625, August 29, 1949.

- [1.2.4] Reactor Shielding Design Manual, USAEC Report TID-7004, March 1956.
- [1.2.5] Deleted.
- [1.2.6] ORNL/TM-10902, "Physical Characteristics of GE BWR Fuel Assemblies", by R.S. Moore and K.J. Notz, Martin Marietta (1989).
- [1.2.7] U.S. DOE SRC/CNEAF/95-01, Spent Nuclear Fuel Discharges from U.S. Reactors 1993, Feb. 1995.
- [1.2.8] S.E. Turner, "Uncertainty Analysis - Axial Burnup Distribution Effects," presented in "Proceedings of a Workshop on the Use of Burnup Credit in Spent Fuel Transport Casks", SAND-89-0018, Sandia National Laboratory, Oct., 1989.
- [1.2.9] Commonwealth Edison Company, Report No. NFS-BND-95-083, Chicago, Illinois.
- [1.2.10] Regulatory Guide 7.11, "Fracture Toughness Criteria of Base Material for Ferritic Steel Shipping Cask Containment Vessels with a Maximum Wall Thickness of 4 Inches (0.1m)", U.S. Nuclear Regulatory Commission, Washington, D.C., June 1991.
- [1.2.11] NUREG-0612, "Control of Heavy Loads at Nuclear Power Plants", U.S. Nuclear Regulatory Commission, Washington, D.C., July 1980.
- [1.2.12] Trojan ISFSI Safety Analysis Report, Revision 3, USNRC Docket 72-0017.
- [1.2.13] NRC Interim Staff Guidance Document No. 8, "Burnup Credit in the Criticality Safety Analyses of PWR Spent Fuel in Transportation and Storage Casks", Revision 2.
- [1.2.14] NRC Interim Staff Guidance Document No. 11, "Cladding Considerations for the Transportation and Storage of Spent Fuel", Revision 2.
- [1.2.15] DOE/RW-0184, Volume 3, "Characteristics of Spent Fuel, High Level Waste, and Other Radioactive Wastes Which May Require Long-Term Isolation," Appendix 2.A, "Physical Descriptions of LWR Fuel Assemblies," U.S. Department of Energy, Office of Civilian Radioactive Waste Management, December 1987.
- [1.2.16] PGE Letter ISFSI-004-04L, dated June 17, 2004, "Change to the Definition of Damaged Fuel – Detailed Trojan Fuel Assembly Damage", from S. B.

Nichols (PGE) to Eric G. Lewis (Holtec)

- [1.2.17] *"Qualification of METAMIC[®] for Spent Fuel Storage Application," EPRI, 1003137, Final Report, October 2001.*
- [1.2.18] *"Safety Evaluation by the Office of Nuclear Reactor Regulation Related to Holtec International Report HI-2022871 Regarding Use of Metamic in Fuel Pool Applications," Facility Operating License Nos. DPR-51 and NPF-6, Entergy Operations, Inc., Docket No. 50-313 and 50-368, USNRC, June 2003.*
- [1.2.19] *"Metamic 6061+40% Boron Carbide Metal Matrix Composite Test", California Consolidated Tech. Inc. Report dated August 21, 2001 to NAC International.*
- [1.2.20] *"Recommendations for Preparing the Criticality Safety Evaluation for Transportation Packages", NUREG/CR-5661, USNRC, Dyer and Parks, ORNL.*
- [1.2.21] *Holtec Proprietary Report HI-2043215, "Sourcebook for Metamic Performance Assessment", Revision 2.*
- [1.3.1] American Society of Mechanical Engineers, "Boiler and Pressure Vessel Code", 1995 with Addenda through 1997.
- [1.3.2] NUREG/CR-6407, "Classification of Transportation Packaging and Dry Spent Fuel Storage System Components According to Importance to Safety", U.S. Nuclear Regulatory Commission, Washington D.C., February 1996.
- [1.3.3] ANSI N14.6-1993, "Special Lifting Devices for Shipping Containers Weighing 10,000 Pounds (4500 Kg) or More", June 1993.

SUPPLEMENT 1.1

GENERAL DESCRIPTION OF THE HI-STAR 100 SYSTEM FOR HUMBOLDT BAY

1.1.0 GENERAL INFORMATION

The HI-STAR 100 System has been expanded to include options specific for use at PG&E's Humboldt Bay (HB) plant for dry storage and future transportation of spent nuclear fuel (SNF)[1.0.8]. HB fuel assemblies are considerably shorter in length than the typical BWR fuel assemblies. As a result, the HI-STAR 100 system now includes an overpack assembly and MPC for use at HB; the HI-STAR 100 Version HB (also called HI-STAR HB) and the MPC-HB. Note that the HB fuel has a cooling time of more than 25 years and relatively low burnup. The heat load and nuclear source terms of this fuel are therefore substantially lower than the design basis fuel described in the main part of this chapter. Consequently, peak cladding temperatures and dose rates are below the regulatory limits with a substantial margin. Nevertheless, all major dimensions and features, such as diameter, wall thickness, flange design, top and bottom thicknesses, are maintained identical to the standard design. Therefore, from a structural perspective, the HI-STAR HB will be even more robust than the standard overpack, due to its shorter length. Information pertaining to the HI-STAR HB System is generally contained in the "I" supplements to each chapter of this SAR. Certain sections of the main SAR are also affected and are appropriately modified for continuity with the "I" supplements. Unless superseded or specifically modified by information in the "I" supplements, the information in the main SAR is applicable to the HI-STAR System for use at HB.

1.1.1 INTRODUCTION

The HI-STAR 100 System as deployed at Humboldt Bay will consist of a HI-STAR HB overpack, an MPC-HB that includes a fuel basket assembly and enclosure vessel specific to HB, and impact limiters. The HB specific components are described below and key parameters for HI-STAR HB are presented in Table 1.1.1. Section 1.1.3 provides the HI-STAR HB design code applicability and details any alternatives to the ASME Code if different than HI-STAR 100. All discussion is supplemented by a set of drawings in Section 1.1.4.

1.1.2 PACKAGE DESCRIPTION

1.1.2.1 Packaging

1.1.2.1.1 Gross Weight

Table 2.1.2.1 summarizes the maximum calculated weights for the HI-STAR HB overpack, impact limiters, and each MPC loaded to maximum capacity with design basis SNF. Table 2.1.2.1 also provides the location of the center of gravity of the fully loaded package.

1.1.2.1.2 Materials of Construction, Dimensions, and Fabrication

Humboldt Bay specific materials of construction along with outline dimensions for important-to-safety items are provided in the drawings in Section 1.1.4.

1.1.2.1.2.1 HI-STAR HB Overpack

The HI-STAR HB overpack is a heavy-walled, steel cylindrical vessel identical to the standard HI-STAR, except that the outer and inner heights are approximately 128 and 115 inches, respectively. Unlike the HI-STAR 100, the HI-STAR HB overpack does not contain radial channels vertically welded to the outside surface of the outermost intermediate shell.

1.1.2.1.2.2 MPC-HB

MPC-HB is similar to the MPC-68F except it is approximately 114 inches high. Key parameters of the MPC-HB are given in Table 1.1.2. The MPC-HB is designed to transport up to 80 Humboldt Bay BWR spent nuclear fuel assemblies meeting the specifications in Table 1.1.4. Damaged SNF and fuel debris must be placed into a Holtec damaged fuel container or other authorized canister for transportation inside the MPC-HB and the HI-STAR HB overpack. Figure 1.1.1 provides a sketch of the container authorized for transportation of damaged fuel and fuel debris in the HI-STAR HB System.

1.1.2.2 Operational Features

The sequence of basic operations necessary to load fuel and prepare the HI-STAR HB system for transport is identical to that of HI-STAR 100. The supporting drawings for HB can be found in Section 1.1.4.

1.1.2.3 Contents of Package

This section delineates the authorized contents permitted for shipment in the HI-STAR HB System, including fuel assembly types; non-fuel hardware; neutron sources; physical parameter limits for fuel assemblies and sub-components; enrichment, burnup, cooling time, and decay heat limits; location requirements; and requirements for canning the material, as applicable.

1.1.2.3.1 Determination of Design Basis Fuel

The HI-STAR HB package is designed to transport Humboldt Bay fuel assemblies. The HB fuel assembly designs evaluated are listed in Table 1.1.3. Table 1.1.4 provides the fuel characteristics determined to be acceptable for transport in the HI-STAR HB System. Each "array/class" listed in this table represents a bounding set of parameters for one or more fuel assembly types. The array/classes are defined for HB in Section 6.1.2. Table 1.1.5 lists the fuel assembly designs that are found to govern for the qualification criteria. Tables 1.1.4 and 1.1.7 provide the specific limits for all material authorized to be transported in the HI-STAR HB System.

1.I.2.3.2 Design Payload for Intact and/or Undamaged Fuel

The fuel characteristics specified in Table 1.I.4 have been evaluated in this SAR and are acceptable for transport in the HI-STAR HB System. Holtec considers that almost all of the Humboldt Bay fuel assemblies not classified as damaged are intact, however the inspection records of the Humboldt Bay fuel assemblies precludes classifying the assemblies as intact fuel since the interior rods of the assembly are in an unknown condition. This fuel is therefore classified as undamaged and can still perform all fuel specific and system related functions, even with possible breaches or defects. Except where specifically noted, throughout this document references to Humboldt Bay fuel as intact or undamaged are equivalent.

1.I.2.3.3 Design Payload for Damaged Fuel and Fuel Debris

Limits for transporting HB damaged fuel and fuel debris are given in Table 1.I.7. Damaged HB fuel and fuel debris must be transported in the Holtec designed Humboldt Bay Damaged Fuel Container (DFC) as shown in Figure 1.I.1.

1.I.2.3.4 Structural Payload Parameters

The main physical parameters of an SNF assembly applicable to the structural evaluation are the fuel assembly length, envelope (cross sectional dimensions), and weight. In order to qualify for transport in the HI-STAR HB MPC, the SNF must satisfy the physical parameters listed in Table 1.I.7. The center of gravity for HB, reported in Chapter 2.I, is based on the maximum fuel assembly weight. Upper fuel spacers (as appropriate) in the form of welded I-beams, approximately 4 inches high, maintain the axial position of the fuel assembly within the MPC basket and, therefore, the location of the center of gravity. The upper spacers are designed to withstand normal and accident conditions of transport. An axial clearance of approximately 2 inches is provided to account for the irradiation and thermal growth of the fuel assemblies.

1.I.2.3.5 Thermal Payload Parameters

Table 1.I.7 provides the maximum heat generation for all fuel assemblies authorized for transportation in the HI-STAR HB System.

1.I.2.3.6 Radiological Payload Parameters

The design basis dose rates are met by the burnup level, cooling time, and minimum enrichment presented in Table 1.I.6 for HI-STAR HB.

1.I.2.3.7 Criticality Payload Parameters

The neutron absorber's minimum ^{10}B areal density loading for MPC-HB is specified in Table 1.I.2.

1.1.2.3.8 Non-Fuel Hardware and Neutron Sources

None.

1.1.2.3.9 Summary of Authorized Contents

Table 1.1.1 summarizes the key system data for the HI-STAR HB. Table 1.1.2 summarizes the key parameters and limits for the MPC-HB. Tables 1.1.4 and 1.1.7 and other tables referenced from these tables provide the limiting conditions for all material to be transported in the HI-STAR HB.

1.1.3 DESIGN CODE APPLICABILITY

Design code applicability for the HI-STAR HB is identical to HI-STAR 100 as presented in Section 1.3, except that the internal surfaces of the intermediate shells will not be coated with a silicone encapsulant due to its lower heat loads.

1.1.4 DRAWINGS

Drawing Number/Sheet	Description	Rev.
4082	Licensing Drawing for HI-STAR HB Overpack Assembly	3
4102	Licensing Drawing for MPC HB Enclosure Vessel	1
4103	Licensing Drawing for MPC HB Fuel Basket Assembly	5
4113	Licensing Drawing for Damaged Fuel Container	1

1.1.5 COMPLIANCE WITH 10CFR71

Same as in Section 1.5.

1.1.6 REFERENCES

Same as in Section 1.6.

Table 1.1.1

SUMMARY OF KEY SYSTEM DATA FOR HI-STAR HB

PARAMETER	VALUE (Nominal)	
<i>Types of MPCs in this Supplement</i>	1	MPC HB
<i>MPC capacity</i>	MPC HB	<ul style="list-style-type: none"> - Up to 80 intact and/or undamaged ZR Humboldt Bay fuel assemblies. - Up to 28 Damaged Fuel Assemblies/Fuel Debris in DFCs located in the peripheral basket cells, remaining cells loaded with intact and/or undamaged ZR Humboldt Bay fuel assemblies; or, - Up to 40 Damaged Fuel Assemblies/Fuel Debris in DFCs arranged in a checkerboard pattern with 40 intact and/or undamaged ZR Humboldt Bay fuel assemblies

Table 1.1.2
KEY PARAMETERS FOR MPC-HB

PARAMETER	VALUE (Nominal)
Unloaded MPC weight (lb)	See Table 2.1.2.1
Fixed neutron absorber (Metamic) ¹⁰ B loading density (g/cm ²)	0.01
Pre-disposal service life (years)	40
Design temperature, max. /min. (°F)	725°/-40°
Design Internal pressure (psig)	
Normal Conditions	100
Off-normal Conditions	100
Accident Conditions	200
Total heat load, max. (kW)	2
Maximum permissible peak fuel cladding temperature (°F)	752 (Normal conditions) 1058 (Accident conditions).
MPC internal environment Helium filled (psig)	≥ 0 and ≤ 48.8 psig at a reference temperature of 70°F
MPC external environment/overpack internal environment Helium filled initial pressure (psig, at STP)	≥ 10 and ≤ 14
Maximum permissible reactivity including all uncertainty and biases	<0.95
End closure(s)	Welded
Fuel handling	Opening compatible with standard grapples
Heat dissipation	Passive

Table 1.1.3

HUMBOLDT BAY FUEL ASSEMBLIES EVALUATED TO DETERMINE DESIGN BASIS SNF

<i>Assembly Class</i>	<i>Array Type</i>	
<i>Humboldt Bay</i>	<i>All 6x6</i>	<i>All 7x7</i>

Table 1.1.4

HUMBOLDT BAY FUEL ASSEMBLY CHARACTERISTICS

<i>Fuel Assembly Array/Class</i>	<i>6x6D</i>	<i>7x7C</i>
<i>Clad Material</i>	<i>ZR</i>	<i>ZR</i>
<i>Design Initial U (kg/assy.)</i>	≤ 78	≤ 78
<i>Initial Maximum Rod Enrichment (wt.% ²³⁵U)</i>	≤ 4.0 <i>(see Note 1)</i>	≤ 4.055
<i>Maximum planar-average initial enrichment (wt.% ²³⁵U)</i>	≤ 2.6	≤ 2.6
<i>No. of Fuel Rod Locations</i>	<i>36</i>	<i>49</i>
<i>Fuel Clad O.D. (in.)</i>	≥ 0.5585	≥ 0.4860
<i>Fuel Clad I.D. (in.)</i>	≤ 0.5050	≤ 0.426
<i>Fuel Pellet Dia. (in.)</i>	≤ 0.4880	≤ 0.4110
<i>Fuel Rod Pitch (in.)</i>	≤ 0.740	≤ 0.631
<i>Active Fuel Length (in.)</i>	≤ 80	≤ 80
<i>No. of Water Rods</i>	<i>0</i>	<i>0</i>
<i>Channel Thickness (in.)</i>	≤ 0.060	≤ 0.060

Note 1: Two 6x6D assemblies contain one high power test rod with an initial enrichment of 5.5%.

Table 1.1.5

DESIGN BASIS FUEL ASSEMBLY FOR EACH DESIGN CRITERION

<i>Criterion</i>	<i>MPC-HB</i>
<i>Reactivity</i>	<i>6x6D and 7x7C</i>
<i>Shielding (Source Term)</i>	<i>6x6D</i>
<i>Fuel Assembly Effective Planar Thermal Conductivity</i>	<i>7x7C</i>
<i>Fuel Basket Effective Axial Thermal Conductivity</i>	<i>6x6D</i>

Table 1.1.6

HUMBOLDT BAY FUEL ASSEMBLY COOLING, AVERAGE BURNUP, AND MINIMUM ENRICHMENT LIMITS

<i>Post-irradiation Cooling Time (years)</i>	<i>Assembly Burnup (MWD/MTU)</i>	<i>Assembly Minimum Enrichment (wt. % ²³⁵U)</i>
<i>≥ 29</i>	<i>≤ 23,000</i>	<i>≥ 2.09</i>

Table 1.1.7
LIMITS FOR MATERIAL TO BE TRANSPORTED IN MPC-HB

PARAMETER	VALUE (Note 1)	
<i>Fuel Type (Note 2)</i>	<i>Uranium oxide, HB BWR intact and/or undamaged fuel assemblies meeting the limits in Table 1.1.4 for the applicable array/class, with or without Zircaloy channels</i>	<i>Uranium oxide, HB BWR damaged fuel assemblies or fuel debris meeting the limits in Table 1.1.4 for array/class 6x6D or 7x7C with or without Zircaloy channels, placed in HB Damaged Fuel Containers (DFCs)</i>
<i>Cladding Type</i>	ZR	ZR
<i>Maximum Initial Enrichment</i>	<i>As specified in Table 1.1.4 for the applicable array/class</i>	<i>As specified in Table 1.1.4 for the applicable array/class</i>
<i>Post-irradiation Cooling Time, Average Burnup, and Minimum Initial Enrichment per Assembly</i>	<i>As specified in Table 1.1.6.</i>	<i>As specified in Table 1.1.6.</i>
<i>Decay Heat Per Assembly</i>	≤ 50 Watts	<i>Fuel debris up to a maximum of one equivalent fuel assembly is allowed (Note 4)</i>
<i>Fuel Assembly Length</i>	≤ 96.91 in. (nominal design)	≤ 96.91 in. (nominal design)
<i>Fuel Assembly Width</i>	≤ 4.70 in. (nominal design)	≤ 4.70 in. (nominal design)
<i>Fuel Assembly Weight</i>	≤ 400 lbs (including channels)	≤ 400 lbs, (including channels and DFC)(Note 3)
<i>Quantity per MPC</i>	<i>Up to 80 HB BWR intact and/or undamaged fuel assemblies</i>	<i>Up to 28 DFCs loaded in the peripheral cells of the basket with 52 intact and/or undamaged assemblies in the remainder (figure 6.1.3) <u>or</u> Up to 40 DFCs with 40 intact and/or undamaged assemblies loaded in a checkerboard pattern (figure 6.1.4)</i>
<i>Other Limitations</i>	<i>Stainless steel channels are not permitted.</i>	

Table 1.1.7 (cont.)
LIMITS FOR MATERIAL TO BE TRANSPORTED IN MPC-HB

Notes:

1. *A fuel assembly must meet the requirements of any one column and the other limitations to be authorized for transportation.*
2. *Fuel assemblies with channels may be stored in any fuel cell location.*
3. *The total quantity of damaged fuel permitted in a single DAMAGED FUEL CONTAINER is limited to the equivalent weight and special nuclear material quantity of one intact or undamaged assembly.*
4. *Fuel debris in the form of loose debris consisting of zirconium clad pellets, stainless steel clad pellets, unclad pellets or rod segments up to a maximum of one equivalent fuel assembly is allowed. A maximum of 1.5 kg of stainless steel clad is allowed per cask.*

Figure Withheld Under 10 CFR 2.390

FIGURE 1.I.1; HOLTEC DAMAGED FUEL CONTAINER
FOR HUMBOLDT BAY SNF IN MPC-HB

Figure Withheld Under 10 CFR 2.390

 HOLTEC INTERNATIONAL HOLTEC CENTER 355 LINCOLN DRIVE WEST MARLTON, NJ 08053		CLIENT PG&E	
		DESCRIPTION HI-STAR HB OVERPACK	
PROJECT NO. 1125	ISSUE NO. 4082	SHEET 1	TOTAL SHEETS 7
P.O. NO. 3500120394		FILE PATH H:\2008\1125\4082	

Figure Withheld Under 10 CFR 2.390

 HOLTEC INTERNATIONAL HOLTEC CENTER 353 LINCOLN DRIVE WEST MARLTON, NJ 08053	CLIENT PG&E			
	PROJECT HI-STAR HB OVERPACK ELEVATION VIEW			
COMPANY NUMBER	SCALE D	DESIGN NO. 4082	SHEET 2	TOTAL 3
DATE NTS		FILE PATH <small>414000001110P.000</small>		

Figure Withheld Under 10 CFR 2.390

 HOLTEC INTERNATIONAL HOLTEC CENTER 555 LINCOLN DRIVE WEST MARLTON, NJ 08053	CLIENT	PG&E		
	DESCRIPTION	HI-STAR HB OVERPACK DETAIL OF TOP FLANGE AT 0' & 180'		
COMPANY NUMBER	SIZE	DRAWING NO.	DWGT.	REV.
	D	4082	3	3
	SCALE	NTS	FILE NO.	H:\00000011\01_002

Figure Withheld Under 10 CFR 2.390

 HOLTEC INTERNATIONAL <small>HOLTEC CENTER 555 LINCOLN DRIVE WEST WARLTON, NJ 08087</small>	CLIENT PG&E			
	DESCRIPTION HI-STAR HB OVERPACK TOP PLAN VIEW "D" - "D"			
COMPANY NUMBER	SIZE D	PROJECT NO. 4082	SHEET 5	REV 3
SCALE NTS		FILE NO. HJ0000011107_002		

Figure Withheld Under 10 CFR 2.390

		Client	
HOLTEC INTERNATIONAL		PG&E	
HOLTEC CENTER 555 LINCOLN DRIVE WEST MARLTON, NJ 08053		DESCRIPTION HI-STAR HB OVERPACK TEST, VENT AND DRAIN PORT DETAILS	
COMPANY DRAWING	SIZE D	DRAWING NO. 4082	SHEET 7
	SCALE NTS	FILE NO.	REV 3

Figure Withheld Under 10 CFR 2.390

		PG&E					
HOLTEC INTERNATIONAL		MPC-HB ENCLOSURE VESSEL					
HOLTEC CENTER 5501 PISCATAWAY DRIVE WEST MARLTON, NJ 08053							
PROJECT NO.	1125	DESCRIPTION	4102	WEEK	1	SHEET	4
P.O. NO.	3500120394	REVISED		© 2004 BY PG&E HOLDINGS, INC.			

Figure Withheld Under 10 CFR 2.390

 HOLTEC INTERNATIONAL HOLTEC CENTER 555 LINDEN DRIVE WEST MARLTON, NJ 08053	CLASS			PG&E	
	DESCRIPTION			MPC-HB ENCLOSURE VESSEL	
CONTRACT NUMBER	SIZE	DESCRIPTION	QTY	UNIT	PCY
	D	4102	2	1	
	NONE		© 2000 AMERICAN ELECTRIC		

Figure Withheld Under 10 CFR 2.390

 HOLTEC INTERNATIONAL HOLTEC CENTER 501 BRUCE A DRIVE WEST MARLTON, NJ 08053	CLIENT	PG&E					
	DESCRIPTION	MPC-HB ENCLOSURE VESSEL ELEVATION DETAILS					
ISSUE	D	DRAWING NO.	4102	SHEET	3	REV.	1
SCALE	NONE		REF ID:	G:\DRAWINGS\11-25-102			

Figure Withheld Under 10 CFR 2.390

 HOLTEC INTERNATIONAL <small>HOLTEC CENTER 855 LINCOLN DRIVE WEST MARTIN, UT 84053</small>	CLASSIFICATION: PG&E			
	DESCRIPTION: MPC-HB ENCLOSURE VESSEL LID DETAILS			
COMPILED BY: DVA/HGA	SCALE: D	DRAWING NO.: 4102	SHEET: 4	OF: 1
	REVISION: NONE	DATE: 6/10/2010	DRAWING: 81125-4102	

Figure Withheld Under 10 CFR 2.390

 HOLTEC INTERNATIONAL HOLTEC CENTER 550 LINCOLN DRIVE WEST MARLTON, NJ 08053		PG&E	
		DESCRIPTION MPC-HB FUEL BASKET	
PROJECT NO. 1125	DRAWING NO. 4103	SHEET 1	TOTAL SHEETS 3
PG. NO. 3500120394		FILE NO. G:\ORIG\PG&E\11254\10	

Figure Withheld Under 10 CFR 2.390

 HOLTEC INTERNATIONAL HOLTEC CENTER 350 LINCOLN DRIVE WEST MARLTON, NJ 08053	CLASSIFICATION		PG&E	
	DESCRIPTION		MPC-HB FUEL BASKET	
COMPONENT NUMBER	UNIT	GROUP NO.	GROUP	REV.
	D	4103	2	5
	SCALE	TICK MARKS		© 10/04/99 PG&E 112041102
	NONE			

Figure Withheld Under 10 CFR 2.390

 HOLTEC INTERNATIONAL HOLTEC CENTER 550 LITTLETON DRIVE WEST MARTIN, NJ 08058	FILE# PG&E			
	DESCRIPTION MPC-HB FUEL BASKET LAYOUT AND WELD DETAILS			
CLASSIFICATION	REV D	DRAWING NO. 4103	SHEET 3	TOTAL SHEETS 5
SCALE NONE	TOLERANCE		G. DRAWINGS 1125-8151	

Figure Withheld Under 10 CFR 2.390

 HOLTEC INTERNATIONAL HOLTEC CENTER 555 LINGEN DRIVE WEST MARTON, NJ 08053		PLANT PG & E HUMBOLDT BAY					
		DESCRIPTION DAMAGED FUEL CONTAINER					
PROJECT NO.	1125	DAMAGE NO.	4113	WEEK	1	SHEET	2
P.O. NO.	3500120394	DATE		© 2004 HANBROS 1125-0113			

Figure Withheld Under 10 CFR 2.390

 HOLTEC INTERNATIONAL <small>HOLTEC CENTER 555 LINCOLN DRIVE WEST MARTINEZ, NJ 08953</small>	TITLE PG & E HUMBOLDT BAY			
	DESCRIPTION DAMAGED FUEL CONTAINER			
DATE -	REV D	REV NO. 4113	REV 2	REV 1
SCALE 1:2		DRAWING NO. 0000000000 11204113		

2.1 STRUCTURAL DESIGN

2.1.1 Discussion

The HI-STAR 100 System (also designated as the HI-STAR 100 Package) consists of three principal components: the multi-purpose canister (MPC), the overpack assembly, and a set of impact limiters. The overpack confines the MPC and provides the containment boundary for transport conditions. The MPC is a hermetically sealed, welded structure of cylindrical profile with flat ends and an internal honeycomb fuel basket for SNF. A complete description of the HI-STAR MPC is provided in Section 1.2.1.2.2 wherein its design and fabrication details are presented with the aid of figures. A discussion of the HI-STAR 100 overpack is presented in Subsection 1.2.1.2.1. Drawings for the HI-STAR 100 System are provided in Section 1.4. In this section, the discussion is directed to characterizing and establishing the structural features of the MPC and the transport overpack.

The design of the HI-STAR 100 MPC seeks to attain three objectives that are central to its functional adequacy, namely;

- **Ability to Dissipate Heat:** The thermal energy produced by the spent fuel must be transported to the outside surface of the MPC such that the prescribed temperature limits for the fuel cladding and the fuel basket metal walls are not exceeded.
- **Ability to Withstand Large Impact Loads:** The MPC with its payload of nuclear fuel must be sufficiently robust to withstand large impact loads associated with the hypothetical accident conditions during transportation of the system. Furthermore, the strength of the MPC must be sufficiently isotropic to assure structural qualification under a wide variety of drop orientations.
- **Restraint of Free End Expansion:** The membrane and bending stresses produced by restraint of free end expansion of the fuel basket are conservatively categorized as primary stresses. In view of the concentration of heat generation in the fuel basket, it is necessary to ensure that structural constraints to its external expansion do not exist.

Where the first two criteria call for extensive inter-cell connections, the last criterion requires the opposite. The design of the HI-STAR 100 MPC seeks to realize all of the above three criteria in an optimal manner.

As the description presented in Chapter 1 indicates, the MPC enclosure vessel is a spent nuclear fuel (SNF) pressure vessel designed to meet ASME Code, Section III, Subsection NB stress limits. The enveloping canister shell, the MPC baseplate, and the closure lid system form a complete closed pressure vessel referred to as the "enclosure vessel". This enclosure vessel serves as the helium retention boundary when the HI-STAR 100 is within the purview of 10CFR71. Within this cylindrical vessel is an integrally welded assemblage of cells of square cross sectional openings, referred to herein as the "fuel basket". The fuel basket is analyzed under the provisions of Subsection NG of Section III of the ASME Code. There are different multi-purpose canisters that are exactly alike in their external dimensions. The essential difference between the MPCs lies in the fuel baskets. Each fuel storage MPC is designed to house fuel assemblies with different characteristics.

Although all HI-STAR 100 MPC fuel baskets are configured to maximize structural ruggedness through extensive inter-cell connectivity, they are sufficiently dissimilar in structural details to warrant separate evaluations. Therefore, analyses for the different MPC types are presented, as appropriate, throughout this chapter.

The HI-STAR 100 overpack provides the containment function for the stored SNF. There is an undivided reliance on the structural integrity of this containment vessel to maintain complete isolation of its contained radioactive contents from the environment under all postulated accident scenarios, even though the MPC is a completely autonomous, ASME Section III Class 1 pressure vessel which provides an unbreachable enclosure for the fuel. The containment boundary is made up of the inner shell, the bottom plate, the top flange, and the closure plate.

Components of the HI-STAR 100 System that are important to safety and their applicable design codes are defined in Chapter 1.

The structural function of the MPC in the transport mode is:

1. To maintain position of the fuel in a sub-critical configuration.
2. To maintain a helium confinement boundary.

The structural function of the overpack in the transport mode is:

1. To serve as a penetration and puncture barrier for the MPC.
2. To provide a containment boundary.
3. To provide a structurally robust support for the radiation shielding.

The structural function of the impact limiters in the transport mode is:

1. To cushion the HI-STAR 100 overpack and the contained MPC with fuel during normal transport handling and in the event of a hypothetical drop accident during transport.

Some structural features of the MPCs that allow the system to perform their structural functions are summarized below:

- There are no external or gasketed ports or openings in the MPC. The MPC does not rely on any sealing arrangement except welding. The absence of any gasketed or flanged joints precludes joint leaks. The MPC enclosure vessel contains no valves or other pressure relief devices.

- The closure system for the MPCs consists of two components, namely, the MPC lid and the closure ring. The MPC lid is a thick circular plate continuously welded to the MPC shell along its circumference. The MPC closure system is shown in the drawings in Section 1.4. The MPC lid-to-MPC shell weld is a J-groove weld that is subject to root and final pass liquid penetrant examinations and finally, a volumetric examination to ensure the absence of unacceptable flaws and indications. The MPC lid is equipped with vent and drain ports which are utilized for evacuating moisture and air from the MPC following fuel loading and subsequent backfilling with an inert gas (helium) in a specified quantity. The vent and drain ports are covered by a cover plate and welded before the closure ring is installed. The closure ring is a thin circular annular plate edge-welded to the MPC shell and to the MPC lid. Lift points for the MPC are provided in the MPC lid.
- The MPC fuel basket consists of an array of interconnecting plates. The number of storage cells formed by this interconnection process varies depending on the type of fuel being transported. Basket designs for different PWR and BWR cell configurations have been designed and are explained in detail in Subsection 1.2. All baskets are designed to fit into the same MPC shell. Welding the plates along their edges essentially renders the fuel basket into a multi-flange beam. For example, Figure 2.1.1 provides an isometric illustration of a fuel basket for the MPC-68 design.
- The MPC basket is separated from the longitudinal supports installed in the enclosure vessel by a small gap. The gap size decreases as a result of thermal expansion (depending on the magnitude of internal heat generation from the stored spent fuel). The provision of a small gap between the basket and the basket support structure is consistent with the natural thermal characteristics of the MPC. The planar temperature distribution across the basket, as shown in Chapter 3, approximates a shallow parabolic profile. This profile will create high thermal stresses unless structural constraints at the interface between the basket and the basket support structure are removed.

The MPCs will be loaded with fuel assemblies with widely varying heat generation rates. The basket/basket support structure gap tends to be reduced for higher heat generation rates due to increased thermal expansion rates. The basket/basket support structure gap tends to be reduced due to thermal expansion from decay heat generation. Gaps between the fuel basket and the basket support structure are specified to be sufficiently large such that a gap exists around the periphery under all normal or accident conditions of transport.

A small number of optional flexible thermal conduction elements (thin aluminum tubes) may be interposed between the basket and the MPC shell. The elements are designed to be resilient. They do not provide structural support for the basket, and thus their resistance to thermal growth is negligible.

Structural features of the overpack that allow the HI-STAR 100 package to perform its safety function are summarized below:

- The overpack features a thick inner shell welded to a bottom plate which forms a load bearing surface for the HI-STAR 100 System. A solid metal top flange welded at the top of the inner shell provides the attachment location for the lifting trunnions. The top flange is designed to provide a recessed ledge for the closure plate to protect the bolts from direct shear loading resulting from an impulsive load at the top edge of the overpack (Figure 2.1.2). In the transport mode the overpack inner shell, bottom plate, top flange, and closure plate with metallic seals constitute the containment boundary for the HI-STAR 100 System. The HI-STAR 100 overpack is subject to the stress limits of the ASME Code, Section III, Subsection NB [2.1.5].
- The inner shell (containment boundary) is reinforced by multi-layered intermediate shells. The multi-layer approach eliminates the potential for a crack in any one layer, developed by any postulated mechanical loading or material flaw, to travel uninterrupted through the vessel wall. The intermediate shells also buttress the overpack inner shell against buckling. The intermediate shells of the HI-STAR 100 overpack are subject to the stress limits of the ASME Code, Section III, Subsection NF, Class 3 [2.1.7].
- To facilitate handling of the loaded package, the HI-STAR 100 overpack is equipped with two lifting trunnions at the top of the overpack. The initial seven HI-STAR 100 overpacks are also equipped with pocket trunnions, embedded in the overpack intermediate shells, just above the bottom plate. HI-STAR 100 overpacks fabricated after the initial seven do not have pocket trunnions (see Subsection 2.5 for further discussion). Lifting trunnions are conservatively designed to meet the design safety factor requirements of NUREG-0612 [2.1.9] and ANSI N14.6-1993 [2.1.10] for single failure proof lifting equipment.
- A circular recess is incorporated on the inner surface of the overpack closure plate. The purpose of this recess is to reduce the moment applied to the flanged joint from MPC impact during a hypothetical top end drop accident. During a hypothetical drop accident where the top end of the overpack impacts first, the MPC contacts the inner surface of the overpack closure plate. Because of the recess, the MPC will only contact an annular region of the inner surface of the overpack closure plate. Thus, the load on the overpack closure plate from the MPC is located closer to the bolt circle, and the moment on the flanged joint is reduced.
- A small circular gap between the MPC external surface and the inside surface of the overpack is provided to allow insertion and removal of the MPC. This gap diminishes monotonically with the increase in the heat generation rate in the MPC, but is sized to avoid metal-to-metal contact between the MPC and the overpack cylindrical surface as a result of thermal expansion under the most adverse thermal conditions.
- There are no valves in the HI-STAR 100 overpack containment boundary. The vent and drain ports used during HI-STAR 100 overpack loading and unloading operations are closed with port plugs and metallic seals. The port plugs are recessed and are suitably protected with a cover plate with seal. These small penetrations equipped with dual seals are not deemed to be particularly vulnerable locations in the HI-STAR 100 System.

The HI-STAR 100 System is equipped with a set of impact limiters (AL-STAR) attached to the top and bottom ends of the overpack. The structural function of the impact limiters is to cushion the HI-STAR 100 overpack and the contained MPC with fuel in the event of a hypothetical drop accident during transport, and to provide the necessary resistance to the longitudinal decelerations experienced during normal rail transport. The design of the impact limiter is independent of the design of the MPC and overpack. This is achieved by establishing design basis deceleration limits for normal transport and for the hypothetical 30-foot drop accident and demonstrating that impact limiter performance limits the deceleration levels imposed on the cask.

Table 1.3.3 provides a listing of the applicable design codes for all structures, systems, and components that are designated as Important to Safety (ITS).

2.1.2 Design Criteria

Regulatory Guide 7.6 provides design criteria for the structural analysis of shipping casks [2.1.4]. Loading conditions and load combinations that must be considered for transport are defined in 10CFR71 [2.1.1] and in USNRC Regulatory Guide 7.8 [2.1.2]. Consistent with the provisions of these documents, the central objective of the structural analysis presented in this chapter is to ensure that the HI-STAR 100 System possesses sufficient structural capability to meet the demands of normal conditions and hypothetical accident conditions of transport.

The following table provides a synoptic matrix to demonstrate our explicit compliance with the seven regulatory positions stated in Regulatory Guide 7.6.

REGULATORY GUIDE 7.6 COMPLIANCE	
Regulatory Position	Compliance in HI-STAR 100 SAR
1. Material properties, design stress intensities, and fatigue curves are obtained from the ASME Code	Tables 2.1.12-2.1.20 for allowable stresses/stress intensities and Tables 2.3.1-2.3.5 for material properties are obtained from the ASME Code (the 1995 Code tables are used). Section 2.6.1.3.3 uses the appropriate fatigue data from the Code.
2. Under normal conditions of transport, the limits on stress intensity are those limits defined by the ASME Code for primary membrane and for primary membrane plus bending for Level A conditions.	Tables 2.1.3-2.1.5 define the correct stress intensity limits for normal conditions of transport as stated in the ASME Code for Level A conditions.
3. Perform fatigue analysis for normal conditions of transport using ASME Code Section III methodology (NB) and appropriate fatigue curves.	Section 2.6.1.3.3 considers the potential for fatigue using accepted ASME Code methodology and fatigue data from the ASME Code.
4. The stress intensity S_n associated with the range of primary plus secondary stresses under normal conditions should be less than $3S_m$ where S_m is the primary membrane stress intensity from the Code.	Section 2.6.1.3.3 considers the fatigue potential of the HI-STAR 100 Package based on the $3S_m$ limit.
5. Buckling of the containment vessel should not occur under normal or accident conditions.	The methodology used is Code Case N-284; this has been accepted by the NRC as an appropriate vehicle to evaluate buckling of the containment.

REGULATORY GUIDE 7.6 COMPLIANCE	
Regulatory Position	Compliance in HI-STAR 100 SAR
6. Under accident conditions, the values of primary membrane stress intensity should not exceed the lesser of $2.4S_m$ and $0.7S_u$ (ultimate strength), and primary membrane plus bending stress intensity should not exceed the lesser of $3.6S_m$ and S_u .	Tables 2.1.3-2.1.5 of the SAR state these requirements.
7. The extreme total stress intensity range should be less than S_a at 10 cycles as given by the appropriate fatigue curves.	Subsection 2.6.1.3.3 demonstrates compliance by conservatively bounding the total stress intensity range and demonstrating that the bounding value is less than S_a at 10 cycles as given by the appropriate fatigue curves.

Note that Regulatory Guide 7.6 references ASME Code Sections in the 1977 code year. This SAR has been prepared using the identical information on allowable stress intensities and fatigue data as listed in the 1995 ASME Code.

Table 1.3.1, in Chapter 1, summarizes the ASME pressure vessel code applicability to HI-STAR 100 components. Table 1.3.2 in Chapter 1 provides a statement of exceptions taken to the ASME Code requirements.

Stresses arise in the components of the HI-STAR 100 System due to various loads that originate under normal and hypothetical accident conditions of transport. These individual loads are combined to form load combinations. Stresses and stress intensities resulting from the load combinations are compared to allowable stresses and stress intensities. The following subsections present loads, load combinations, and allowable strengths for use in the structural analyses of the MPC and the HI-STAR 100 overpack.

2.1.2.1 Loading and Load Combinations

10CFR71 and Regulatory Guide 7.6 define two conditions that must be considered for qualification of a transport package. These are defined as "Normal Conditions of Transport" and "Hypothetical Accident Conditions", which are related herein to the ASME Code Service Levels for the purposes of quantifying allowable stress limits. In terms of the ASME terminology, the following parallels are applicable.

Normal Conditions of Transport = ASME Design Condition and ASME Level A or B Service Condition

Hypothetical Accident Condition = ASME Level D Service Condition

To establish the appropriate loadings and load combinations that require evaluation, the pressure and temperatures used for the design analyses must be defined. Table 2.1.1 establishes the design pressures for the two transport conditions that must be evaluated. Table 2.1.2 establishes reference hot temperature limits for the two conditions of transport. The ASME Code does not prescribe a metal temperature limit for Level D (also called "faulted") conditions. Under the provisions of the ASME Code, large strains (such as deformations resulting from a thermal shock) are acceptable if

the post-event structural configuration of the component is within the limits prescribed for it subsequent to the faulted event (ASME Code Section III, Subsection NCA-2142.4). In the case of the cask, it is required that the containment boundary continues to perform its function and that the outer skin continues to provide an enclosure for the radiation shielding. For conservatism, the peak metal bulk temperature during and after the fire transient in the overpack containment structure is required to be limited to the maximum temperature limit prescribed in the ASME Section II Part D allowable stress /stress intensity tables. That is, the maximum bulk metal temperature is equal to the maximum temperature for which the allowable stress intensity, S_m , is listed in the Code for the applicable Code Class. For the external skin of the overpack that is directly exposed to the fire no specific temperature limits are enforced by the governing documents. The performance expectation of the HI-STAR 100 package, however, is that the skin does not melt, slump, or sever from the overpack structure. This performance objective is considered to be fulfilled with adequate margin if the metal temperature of the enclosure shell at any section does not exceed 50% of the melting point of the shell material. Tables 2.1.3 and 2.1.4 set forth the allowable strength bases for the two conditions of transport based on their designation as Level A, B, or D.

For its qualification as an acceptable packaging component, the following types of loads are defined for the HI-STAR 100 MPC.

- Dead load (lb.), D ;
- Internal design pressure (psi), P_i ;
- External design pressure (psi), P_o ;
- Accident internal pressure (psi), P_i^* ;
- Accident external pressure (psi), P_o^* ;
- Thermal load due to design basis heat generation in the MPC, T , and under most adverse external environmental conditions, T' ;
- Side drop at 0° basket circumferential orientation under normal conditions of transport, H ;
- Side drop at 45° basket circumferential orientation under normal conditions of transport, H ;
- Drop at 0° fuel basket circumferential orientation under design basis deceleration for hypothetical accident conditions, H' (angle of inclination that the package longitudinal axis makes with the horizontal plane varies);
- Drop at 45° fuel basket circumferential orientation under design basis deceleration for hypothetical accidental conditions, H' (angle of inclination that the package longitudinal axis makes with the horizontal plane varies);
- Vertical drop under design basis deceleration for hypothetical accident conditions, H' .

Insofar as the fuel basket is not radially symmetric, the orientation of the basket cross section with respect to the direction of side drop will affect the state of stress induced by the deceleration produced by the impact. Heretofore, two horizontal drop circumferential orientations are considered which are referred to as the 0 degree drop and 45 degree drop, respectively. Figures 2.1.3 and 2.1.4, showing an MPC-68 fuel basket, illustrate the two orientations. In the 0-degree drop, the basket drops with its two sets of panels, respectively; parallel and normal to the vertical (Figure 2.1.3). The 45-degree drop implies that the basket's honeycomb section is rotated meridionally by 45 degrees (Figure 2.1.4).

For the above loads, a series of load combinations for the fuel baskets and the enclosure vessel are compiled in Tables 2.1.6 and 2.1.7, respectively. These load combinations represent both normal conditions of transport and the hypothetical accident conditions.

The loadings and load combinations applicable to the overpack are more numerous, because all external loads directly bear on it and several potentially limiting oblique drop orientations exist. In the following, each individual overpack loading which enters in subsequent load combinations is explained.

- **Internal Design Pressure, P_i :** An internal design pressure is defined for the containment cavity of the overpack pressure vessel (Figure 2.1.5). The coincident external pressure is assumed to be atmospheric (0 psig) (Table 2.1.1). For conservatism, the design value is set equal to the MPC internal pressure under normal conditions of transport.
- **External Design Pressure, P_o :** An external design pressure with the cavity depressurized (0 psig) is defined for the overpack pressure vessel as the second design condition loading (Figure 2.1.6), (Table 2.1.1).
- **Accident External Pressure, P_o^* :** An external accident design pressure with cavity depressurized (Figure 2.1.6) (Table 2.1.1). This loading in conjunction with the buckling analysis of the overpack inner shell, is intended to demonstrate that the containment boundary is in compliance with the requirements of 10CFR71.61. This loading condition bounds the external pressure specified by 10CFR71.73(c) (5) and (6).
- **Accident Internal Pressure, P_i^* :** An internal accident design pressure is defined for the containment cavity of the overpack pressure vessel (Figure 2.1.5). The coincident external pressure is assumed to be atmospheric (0 psig) (Table 2.1.1). The design value is based on conservatively assuming that the MPC enclosure vessel is breached.
- **Thermal Conditions:** Thermal conditions pertain to the stresses that develop due to thermal gradient in the overpack. The temperature field in the overpack under the maximum heat generation scenario is developed in Chapter 3. The effect of this temperature field, T_h , is included in all load cases, as appropriate.

The condition where the overpack is subject to a -40°F ambient environment and maximum decay heat is labeled as T_s . Likewise, the condition when the overpack is subject to a -20°F ambient environment is denoted by T_c . Finally, the thermal load during and after 30 minutes of exposure to a 1475°F enveloping fire is referred to as T_f .

- **Overpack Joint Sealing Load, W_s :** The pre-load applied to the overpack closure plate bolts seat the metallic seals and create a contact pressure on the inside land which serves to protect the joint from leakage under postulated impact loading events. The bolt pre-load, however, produces a state of stress in the overpack top closure plate, the overpack top flange, and the overpack inner and intermediate shell region adjacent to the flange. The pre-load, W_s , is, therefore, treated as a distinct loading type.
- **Fabrication Loads, F :** The internal loads induced due to the method of fabrication employed in building the overpack are included in the load combinations.
- **Bottom End Drop, D_{ba} :** This is the first of six drop accident scenarios, wherein the packaging is assumed to drop vertically with its overpack bottom plate sustaining the impulsive load transmitted through the bottom impact limiter. The weight of the package is included in all drop load cases. A schematic of the external forces working on the overpack under this drop scenario is illustrated in Figure 2.1.7. The deceleration load under the 30 ft drop event (accident event) is labeled D_{ba} . (The design basis deceleration is given in Table 2.1.10).
- **Top End Drop, D_{ta} :** This drop condition is the opposite of the preceding case. The top closure plate withstands the impact load transmitted through the impact limiter. This loading is illustrated in Figure 2.1.8. The design basis deceleration is given in Table 2.1.10.
- **Side Drop, D_{sn} and D_{sa} :** The overpack along with its contents drops with its longitudinal axis horizontal. The loaded MPC bears down on the overpack as it decelerates under the resistance offered by the two impact limiters pressing against an essentially unyielding surface (Figure 2.1.9). The subscripts "n" and "a" denote normal transport and hypothetical accident conditions, respectively. The design basis deceleration is given in Table 2.1.10.
- **Bottom C.G.-Over-the-Corner Drop, D_{ca} :** In this drop scenario, the HI-STAR 100 System is assumed to impact an essentially unyielding surface with its center-of-gravity directly above its bottom corner (Figure 2.1.10) under the hypothetical drop accident condition. The design basis deceleration is given in Table 2.1.10.
- **Top Center-of-Gravity Over-the-Corner Drop, D_{ca} :** This loading case is identical to the preceding case, except that the package is assumed to be dropping with its top end down and its center-of-gravity is aligned with the corner of the top closure plate (Figure 2.1.11). The design basis deceleration is given in Table 2.1.10.

- **Side Puncture Force Event, P_s :** This event consists of a free drop of the packaging for 1 meter (40 in.) on to a stationary and vertical mild steel bar of 6 in. diameter with its leading edge (top edge) rounded to 1/4 in. radius. The bar is assumed to be of such a length as to cause maximum damage to the overpack. The package is assumed to be dropping horizontally with the penetrant force being applied at the mid-length of the cask (Figure 2.1.12).
- **Top End Puncture Force, P_t :** This event is similar to the preceding case except the penetrant force is assumed to act at the center of the top closure plate (Figure 2.1.13).
- **Bottom End Puncture Force, P_b :** This is the third of the bar puncture events configured to create a condition of maximum damage to the package. The loading event is identical to the preceding two cases, except that the puncture load acts on the center of the bottom plate of the overpack (Figure 2.1.14).
- **Vibration and Shock, V :** Vibration and shock loads arise during transport of the packaging. The vibratory loads transmitted to the HI-STAR 100 System will produce negligibly small stresses in comparison with stresses that will be produced by the loadings described previously. Therefore, this loading is neglected in the analyses performed herein.

The foregoing loadings are combined in the manner of Table 1 of Regulatory Guide 7.8 to form four (4) distinct load combinations for the normal condition of transport and nineteen (19) load combinations for the hypothetical accident conditions. These load combinations are summarized in Tables 2.1.8 and 2.1.9.

Two concluding observations are relevant with respect to a Flange Seating Condition and to the External Pressure Condition:

- **Flange Seating Condition:** The stress field in the overpack under the bolt pre-stress load condition is evaluated with the elastic constants of the finite element gridwork in the overpack set at its coincident hot environment condition (100°F ambient). The bolt pre-load and material elastic constants under the cold environment condition (-20°F) will be different, resulting in a slightly different stress field. However, the consequence of this refinement is considered to be a second order effect and is, therefore, neglected.
- **External Pressure Condition:** The condition of 20 psia external pressure in Table 1 of Regulatory Guide 7.8 is conservatively bounded by the deep submergence pressure under 200 meters of water. Likewise, the internal design pressure of 100 psig with outside at ambient is assumed to conservatively bound the minimum external pressure (3.5 psia) service condition.

In the load cases considered (Tables 2.1.6-2.1.9), material behavior is always considered to be linearly elastic. To facilitate review, the following matrix is provided to relate the load combinations specifically addressed in Table 1 of Regulatory Guide 7.8 to the load combinations defined in this SAR by Tables 2.1.6-2.1.9. Also included in the matrix are locations in the SAR where particular results are presented that are germane to demonstrating compliance with the intent of Regulatory Guide 7.8.

Compliance of HI-STAR 100 SAR With Regulatory Guide 7.8 Load Combinations		
Reg. Guide Load Combination	HI-STAR 100 Explicit Load Combination (Tables 2.1.6-2.1.9)	Location in SAR for Results
NORMAL CONDITIONS		
Hot Environment	Table 2.1.7(Case E1.c) Table 2.1.8(Case 1)	2.6.1.3.1.2; Tables 2.6.6,2.6.7 Table 2.6.5; Table 2.6.9
Cold Environment	Table 2.1.8(Case 2)	Table 2.6.12
Increased External Pressure	Table 2.1.9 (Case 18 bounds)	2.6.4
Minimum External Pressure	---	2.6.3
Vibration and Shock	---	2.6.5
One-Foot Free Drop	Table 2.1.6(Case F2) Table 2.1.7(Case E2) Table 2.1.8(Cases 3,4)	Tables 2.6.2,2.6.8 Table 2.6.3 Tables 2.6.9,2.6.12
ACCIDENT CONDITIONS		
Thirty-Foot Free Drop	Table 2.1.6(Case F3) Table 2.1.7(Case E3) Table 2.1.9(Cases 1-5;9-13)	Tables 2.7.1,2.7.4,2.7.7 Tables 2.7.2,2.7.4,2.7.7 Tables 2.7.3,2.7.5,2.7.6-2.7.8
Puncture by Bar	Table 2.1.9(Cases 6-8;14-16)	Tables 2.7.3,2.7.5,2.7.6-2.7.8
Fire Accident	Table 2.1.9(Cases 17,19)	Tables 2.7.3,2.7.8

2.1.2.2 Allowables

Components of the HI-STAR 100 System Important to Safety (ITS) are listed in Table 1.3.3. Allowable stresses are tabulated for these components for all applicable service levels. The applicable service level from the ASME Code for determination of allowables is listed in Subsection 2.1.2.1.

Allowable stress limits for the overpack containment structure and for the MPC enclosure vessel are obtained from the ASME Code, Section III, Division 1, Subsection NB [2.1.5]. The MPC fuel basket is subject to the stress limits of ASME Section III, Division 1, Subsection NG [2.1.6].

All non-containment parts of the overpack (e.g., intermediate shells, outer enclosure shells, radial channels), are subject to the stress limits of ASME Section III, Subsection NF [2.1.7] for mechanical loadings. The overpack containment boundary and the MPC enclosure vessel are also evaluated for stability in accordance with ASME Code Case N-284 [2.1.8]. Overpack closure bolts are subject to the stress limits of ASME Section III, Subsection NB. Finally, lifting trunnions and other lifting components are subject to the stress limits of NUREG-0612 [2.1.9], which references ANSI N14.6 [2.1.10].

Allowable stresses and stress intensities are calculated using the data provided in the ASME Code, Section II, Part D [2.1.11] and Tables 2.1.3 through 2.1.5. Tables 2.1.11 through 2.1.20 contain numerical values of the allowable stresses/stress intensities for all MPC and overpack load-bearing materials as a function of temperature.

In all tables, the terms S_m , S_y , and S_u , respectively, denote the design stress intensity, minimum yield strength, and the ultimate strength. Property values at intermediate temperatures that are not reported in the ASME Code are obtained by linear interpolation as allowed by paragraph NB-3229. Property values are not extrapolated beyond the limits of the Code in any structural analysis.

Additional terms relevant to the analyses are extracted from the ASME Code (Figure NB-3222-1) as follows.

<u>Symbol</u>	<u>Description</u>	<u>Notes</u>
P_m	Average primary stress across a solid section.	Excludes effects of discontinuities and concentrations. Produced by pressure and mechanical loads.
P_L	Average stress across any solid section.	Considers effects of discontinuities but not concentrations. Produced by pressure and mechanical loads, including inertia earthquake effects.
P_b	Primary bending stress.	Component of primary stress proportional to the distance from the centroid of a solid section. Excludes the effects of discontinuities and concentrations. Produced by pressure and mechanical loads, including inertia earthquake effects.
P_e	Secondary expansion stress.	Stresses which result from the constraint of free-end displacement. Considers effects of discontinuities but not local stress concentration. (Not applicable to vessels.)
Q	Secondary membrane plus bending stress.	Self-equilibrating stress necessary to satisfy continuity of structure. Occurs at structural discontinuities. Can be caused by pressure, mechanical loads, or differential thermal expansion.
F	Peak stress.	Increment added to primary or secondary stress by a concentration (notch), or, certain thermal stresses that may cause fatigue but not distortion. This value is not used in the tables.

It is shown in this report that there is no interference between component parts due to free thermal expansion. Therefore, P_e does not develop within any HI-STAR 100 component. A summary of the allowable limits for normal conditions of transport and for the hypothetical accident conditions as they apply to various components of the package is presented in Table 2.1.3 for the overpack and MPC enclosure vessel (shell, lid, and baseplate), in Table 2.1.4 for the MPC fuel basket, and in Table 2.1.5 for the non-containment parts of the overpack.

It is recognized that the planar temperature distribution in the fuel basket and the overpack under the maximum heat load condition is the highest at the cask center and drops monotonically, reaching its lowest value at the outside surface. Strictly speaking, the allowable stresses/stress intensities at any location in the basket, the enclosure vessel, or the overpack should be based on the coincident metal temperature under the specific operating condition. However, in the interest of conservatism, reference temperatures may be established for each component that are upper bounds on the metal temperature for each situational condition. Table 2.1.21 provides the reference temperatures for the MPC and the overpack and, utilizing Tables 2.1.11 through 2.1.20, provides conservative numerical limits for the stresses and stress intensities for all loading cases.

Summarizing the previous discussions, in accordance with the Regulatory Guide 7.6 and with ASME Code Section III, Subsection NB, the allowable stress limits for the overpack containment boundary are based on design stress intensities (S_m), yield strengths (S_y) and ultimate strengths (S_u). These limits govern the design of the overpack (including the inner shell, the top flange, the bottom plate, and the closure plate), and also govern the design of the MPC enclosure vessel. The stress limits for the MPC fuel basket are based on stress intensities as set forth in ASME, Section III, Subsection NG. For applicable accident conditions, Appendix F of the ASME Code applies [2.1.12]. Stress limits for closure bolts conform to those given in Table 2.1.24.

The lifting devices in the HI-STAR 100 overpack and the multi-purpose canisters, collectively referred to as "trunnions", are subject to specific limits set forth by NUREG-0612: the primary stresses in a trunnion must be less than the smaller of 1/10 of the material ultimate strength and 1/6 of the material yield strength while loaded by the lifted load that includes an appropriate dynamic load amplifier.

The region around the trunnion is part of the NF structure in HI-STAR 100 and an NB pressure boundary in the MPC, and as such, must satisfy the applicable stress (or stress intensity) limits for the load combination. In addition to meeting the applicable Code limits, it is further required that the local primary stresses at the trunnion/mother structure interface must not exceed the material yield stress at three times the handling condition load. This criterion eliminates the potential of local yielding at the trunnion/structure interface.

Impact limiters are not designed to any stress or deformation criteria. Rather, their function is solely to absorb the impact energy by plastic deformation. The impact limiter must perform its energy absorption function over the range of environmental temperatures.

Allowable stresses derived from other authoritative sources are summarized in Table 2.1.24.

2.1.2.3 Brittle Fracture Failure

The MPC canister and basket are constructed from a series of stainless steels termed Alloy X. These stainless steel materials do not undergo a ductile-to-brittle transition in the minimum temperature range of the HI-STAR 100 System. Therefore, brittle fracture is not a concern for the MPC components. However, the HI-STAR 100 overpack is composed of ferritic steel materials, which will be subject to impact loading in a cold environment and, therefore, must be evaluated and/or subjected to impact testing in accordance with the ASME Code to ensure protection against brittle fracture.

Tables 2.1.22 and 2.1.23 provide the fracture toughness test criteria for the HI-STAR 100 overpack components in accordance with the applicable ASME Codes and Regulatory Guide requirements for prevention of brittle fracture. Regulatory Guides 7.11 [2.1.13] and 7.12 [2.1.14] are used to determine drop test requirements for the containment boundary components, as discussed below.

All containment boundary materials subject to impact loading in a cold environment must be evaluated and/or tested for their propensity for brittle fracture. The overpack baseplate, top flange, and closure plate have thicknesses greater than four inches. Table 1 of Regulatory Guide 7.12 requires that the Nil Ductility Transition temperature, T_{NDT} (for the lowest service temperature of -20°F), be -129°F for 6-inch thick material, and linear interpolation of the table shows that for 7-inch thick material, the T_{NDT} is -132°F . SA350-LF3 has been selected as the material for these overpack components based on the material's capability to perform at low temperatures with excellent ductility properties.

The overpack inner shell has a thickness of 2.5 inches. SA203-E has been selected as the material for this item due to its capability to perform at low temperatures (Table A1.15 of ASME Section IIA). Regulatory Guide 7.11 requires that the T_{NDT} for this material be less than -70°F (at the lowest service temperature of -20°F).

The overpack closure plate bolts are fabricated from SB-637 Grade N07718, a high strength nickel alloy material. Section 5 of NUREG/CR-1815 [2.1.15] indicates that bolts are generally not considered a fracture critical component. Nevertheless, this material has a high resistance to fracture at low temperatures, as can be shown by calculating the transition temperature of the material and assessing its performance as indicated in NUREG/CR-1815.

The Aerospace Structural Metals Handbook [2.1.16] shows that minimum impact absorption energy for SB-637 Grade N07718 at -320°F is 18.5 ft-lb. This may be transferred into a fracture toughness value by using the relationship (presented in Section 4.2 of NUREG/CR-1815) between Charpy impact measurement, C_v (ft-lb), and dynamic fracture toughness, K_{ID} (psi $\sqrt{\text{in.}}$)

$$K_{ID} = (5 E C_v)^{1/2}$$

where $E = 31 \times 10^6$ psi at -320°F and C_v (minimum) = 18.5 ft-lb.

Therefore,

$$K_{ID} = 53.5 \text{ ksi}\sqrt{\text{in.}}$$

Using Figure 2 of NUREG/CR-1815 yields

$$(T - T_{NDT}) = 32 \text{ degrees F}$$

Since the data used is for $T = -320^{\circ}\text{F}$, then $T_{NDT} = -320^{\circ}\text{F} - 32^{\circ}\text{F} = -352^{\circ}\text{F}$

Using Figure 3 of NUREG/CR-1815 where thickness is defined as the bolt diameter (1.5 inch), and $\sigma/\sigma_{yd} = 1$ per Regulatory Guide 7.11, A (degrees F) is found to be 60 degrees F. Therefore, the required maximum nil ductility transition temperature per NUREG/CR-1815 for the closure bolts is:

$$\begin{aligned} T_{NDT} &= T_{LT} - A \\ &= -40^{\circ} - 60^{\circ} = -100^{\circ}\text{F} \end{aligned}$$

where T_{LT} = lowest temperature of -40°F (conservatively below the lowest service temperature).

The large margin between the calculated T_{NDT} and the required maximum Nil Ductility Transition temperature leads to the conclusion that SB-637 Grade N07718 possesses appropriate fracture toughness for use as closure lid bolting.

ASME Code Section III, Subsection NF requires Charpy V-notch tests for materials of certain noncontainment components of the overpack. The intermediate shells used for gamma shielding are fabricated from normalized SA516-70. Table A1.15 of ASME Section IIA shows that normalized SA516-70 should have minimum energy absorption of 12 ft-lb at -40°F for a Charpy V-notch test. The lowest anticipated temperature the overpack is to experience is conservatively set at -40°F . Therefore, these tests on the normalized SA516-70 materials of the intermediate shells will confirm the minimum energy absorption of 12 ft-lb at -40°F and the ability of the intermediate shells to perform their intended function at the lowest service temperature.

The pocket trunnions in the initial seven HI-STAR 100 overpacks are fabricated from 17-4PH (or equivalent) material that is precipitation hardened to condition H1150. ARMCO Product Data Bulletin S-22 [2.1.17] shows that Charpy V-notch testing of 17-4PH H1150 material at -110°F gives energy absorption values of approximately 48 ft-lbs. Using the same methodology as used for the closure bolts,

$$K_{ID} = 83 \text{ ksi}\sqrt{\text{in.}}$$

where $E = 28.7 \times 10^6$ psi and $C_v = 48$ ft-lbs.

Using Figure 2 of NUREG/CR-1815 yields

$$T - T_{NDT} = 65^{\circ}\text{F}$$

and therefore

$$T_{\text{NDT}} = -110^{\circ}\text{F} - 65^{\circ}\text{F} = -175^{\circ}\text{F}$$

While the optional pocket trunnions are not part of the containment for the overpack, Regulatory Guide 7.12 is used to define the required T_{NDT} for the trunnion pocket thickness ($T_{\text{NDT}} = -140^{\circ}\text{F}$). The 35°F margin between the calculated T_{NDT} and the T_{NDT} defined in Regulatory Guide 7.12 provides assurance that brittle fracture failure of the 17-4 material will not occur at the lowest service temperature.

2.1.2.4 Impact Limiter

The impact limiters are designed as energy absorbers to ensure that the maximum impact deceleration applied to the package is limited to values less than the design basis deceleration, as applicable.

2.1.2.5 Buckling

Certain load combinations subject structural sections with relatively large slenderness ratios (such as the MPC enclosure vessel shell) to compressive stresses that may actuate buckling instability before the allowable stress is reached. Tables 2.1.7 and 2.1.9 list load combinations for the MPC enclosure vessel and the HI-STAR 100 overpack structure; the cases that warrant stability (buckling) check are listed therein.

Table 2.1.1

DESIGN PRESSURES

Pressure Location	Condition	Pressure (psig)
MPC Internal Pressure	Normal Condition of Transport	100
	Hypothetical Accident	200 [†]
MPC External Pressure	Normal Condition of Transport	40
	Hypothetical Accident	60 ^{††}
Overpack External Pressure	Normal Condition of Transport	(0) Ambient
	Hypothetical Accident	300
Overpack Internal Pressure	Normal Condition of Transport	-Same as MPC Internal Pressure
	Hypothetical Accident	Same as MPC Internal Pressure
Overpack Enclosure Shell Internal Pressure	Normal Condition of Transport	30
	Hypothetical Accident	30

[†] This pressure is only associated with the hypothetical accident where 100% rod rupture is assumed to occur. For all other accident events, such as a 30-ft drop, the applicable MPC internal pressure is the design pressure under normal conditions of transport.

^{††} For transport, this represents the differential pressure limit for elastic/plastic stability calculations.

Table 2.1.2

NORMAL REFERENCE TEMPERATURES AND ACCIDENT BULK METAL
TEMPERATURE LIMITS

HI-STAR 100 Component	Normal Operating Condition Reference Temp. Limits [†] (Deg.F)	Hypothetical Accident Condition Metal Bulk Temp. Limits ^{††} (Deg.F)
MPC shell	450	550
MPC basket	725	950
MPC lid	550	775
MPC closure ring	400	775
MPC baseplate	400	775
MPC Boron neutron absorber	800	950
MPC heat conduction elements	725	950
Overpack inner shell	400	500
Overpack bottom plate	350	700
Overpack closure plate	400	700
Overpack top flange	400	700
Overpack closure plate seals	400	1200
Overpack closure plate bolts	350	600
Port plug seals (vent and drain)	400	1600
Port cover seals (vent and drain)	400	932
Neutron shielding	300	†††
Overpack Intermediate Shells	350	700
Overpack Outer Enclosure Shell	350	1350
Optional Pocket Trunnion	200	700
Impact Limiter	150	1105

[†] These temperatures are maximum possible temperatures for the normal operating condition. They bound the actual calculated temperatures.

^{††} These temperatures are maximum possible temperatures for the postulated fire accident. They must bound the actual calculated temperatures.

^{†††} For shielding analysis, the neutron shield is conservatively assumed to be lost during the fire accident.

Table 2.1.3

OVERPACK CONTAINMENT STRUCTURE AND MPC ENCLOSURE VESSEL STRESS INTENSITY LIMITS
FOR DIFFERENT LOADING CONDITIONS (ELASTIC ANALYSIS PER NB-3220)[†]

STRESS CATEGORY	NORMAL CONDITIONS OF TRANSPORT	HYPOTHETICAL ACCIDENT ^{††}
Primary Membrane, P_m	S_m	AMIN ($2.4S_m, .7S_u$)
Local Membrane, P_L	$1.5S_m$	150% of P_m Limit
Membrane plus Primary Bending	$1.5S_m$	150% of P_m Limit
Primary Membrane plus Primary Bending	$1.5S_m$	150% of P_m Limit
Membrane plus Primary Bending plus Secondary	$3S_m$	N/A
Average ^{†††} Primary Shear (Section in Pure Shear)	$0.6S_m$	$0.42S_u$

[†] Stress combinations including F (peak stress) apply to fatigue evaluations only.

^{††} Governed by Appendix F, Paragraph F-1331 of the ASME Code, Section III. Stress limited to S_u .

^{†††} Governed by NB-3227.2 or F-1331.1(d) of the ASME Code, Section III (NB or Appendix F)

Table 2.1.4

MPC BASKET STRESS INTENSITY LIMITS
FOR DIFFERENT LOADING CONDITIONS (ELASTIC ANALYSIS PER NG-3220)

STRESS CATEGORY	NORMAL CONDITIONS OF TRANSPORT	HYPOTHETICAL ACCIDENT [†]
Primary Membrane, P_m	S_m	AMIN ($2.4S_m, .7S_u$) ^{††}
Primary Membrane plus Primary Bending	$1.5S_m$	150% of P_m Limit (Limited to S_u)
Primary Membrane plus Primary Bending plus Secondary	$3S_m$	N/A

[†] Governed by Appendix F, Paragraph F-1331 of the ASME Code, Section III.

^{††} Average primary shear stress across a section loaded in pure shear shall not exceed $0.42S_u$.

Table 2.1.5

STRESS INTENSITY LIMITS FOR DIFFERENT
LOADING CONDITIONS FOR THE EXTERNAL STRUCTURALS IN THE HI-STAR OVERPACK
(ELASTIC ANALYSIS PER NF-3260 - CLASS 3)
(ELASTIC ANALYSIS PER NF-3220 - CLASS 1)

STRESS CATEGORY	NORMAL CONDITION OF TRANSPORT [†]	HYPOTHETICAL ACCIDENT ^{††}
Primary Membrane, P_m	S (Class 3) S_m (Class 1)	AMAX ($1.2S_y, 1.5S_m$) but $< .7S_u$
Primary Membrane, P_m , plus Primary Bending, P_b	1.5S (Class 3) 1.5 S_m (Class 1)	150% of P_m (Limited to S_u)
Shear Stress	N/A (Class 3) .6 S_m (Class 1)	$< 0.42S_u$

Definitions:

- S = Allowable Stress Value for Table 1A, ASME Section II, Part D
- S_m = Allowable Stress Intensity Value from Table 2A, ASME Section II, Part D
- S_u = Ultimate Strength

[†] Limits for Normal Condition of Transport are on stress for Class 3 and on stress intensity for Class 1, upper value in column is for Class 3; lower value in column is for Class 1.

^{††} Governed by Appendix F, Paragraph F-1332 of the ASME Code, Section III. Class 1 and Class 3 use same stress intensity limits.

Table 2.1.6

LOADING CASES FOR THE MPC FUEL BASKET

Case Number	Load Combination [†]	Notes
F1	T or T'	Demonstrate that the most adverse of the temperature distributions in the basket will not cause fuel basket to expand and contact the enclosure vessel wall. Compute the stress intensity and show that it is less than allowable.
F2		
F2.a	D+H	1 ft. side drop, 0 degrees circumferential orientation (Figure 2.1.3)
F2.b	D+H	1 ft. side drop, 45 degrees circumferential orientation (Figure 2.1.4)
F3		
F3.a	D + H'	30 ft. vertical axis drop
F3.b	D + H'	30 ft. side Drop, 0 degrees circumferential orientation (Figure 2.1.3)
F3.c	D + H'	30 ft. side Drop, 45 degrees circumferential orientation (Figure 2.1.4)

[†] The symbols used for loads are defined in Subsection 2.1.2.1.

Table 2.1.7

LOADING CASES FOR THE MPC ENCLOSURE VESSEL

Case Number	Load Combination [†]	Notes
E1		
E1.a	Design internal pressure, P_i	Primary Stress intensity
E1.b	Design external pressure, P_o	Primary stress intensity limits, buckling stability
E1.c	Design internal pressure plus Temperature, $P_i + T$	Primary plus secondary stress intensity under Level A condition
E2		
E2.a	$(P_i, P_o) + D + H$	1 ft. side drop, 0° circumferential orientation (Figure 2.1.3)
E2.b	$(P_i, P_o) + D + H$	1 ft. side drop, 45° circumferential orientation (Figure 2.1.4)

[†] The symbols used for loads are defined in Subsection 2.1.2.1. Note that in the analyses, the bounding pressure (P_i, P_o) is applied, e.g., in stability calculations P_o is bounding, whereas in stress calculations both P_o and P_i are appropriate.

Table 2.1.7 (continued)

Case Number	Load Combination [†]	Notes
E3		
E3.a	$D + H' + P_o$ (Stability of the shell considers internal pressure plus drop deceleration)	30 ft. vertical axis drop
E3.b	$D + H' + P_i$	30 ft. side drop, 0° circumferential orientation (Figure 2.1.3)
E3.c	$D + H' + P_i$	30 ft. side drop, 45° circumferential orientation (Figure 2.1.4)
E4	T or T'	Demonstrate that interference with the overpack will not develop for T
E5	$(P_i^*, P_o^*) + D + T'$	Demonstrate compliance with level D stress limits - buckling stability

[†] The symbols used for loads are defined in Subsection 2.1.2.1. Note that in the analyses, the bounding pressure (P_i , P_o) is applied, e.g., in stability calculations P_o is bounding, whereas in stress calculations both P_o and P_i are appropriate.

Table 2.1.8

OVERPACK LOAD CASES FOR NORMAL CONDITION OF TRANSPORT

Case Number	Load Combination [†]	Notes
1	$T_h + P_i + F + W_s$	Hot Environment
2	$T_s + P_o + F + W_s$	Super-Cold Environment
3	$T_h + D_{sn} + P_i + F + W_s$	Free One Foot Side Drop - Hot Environment
4	$T_c + D_{sn} + P_o + F + W_s$	Free One Foot Side Drop - Cold Environment
5	T_c and $T_h + P_i + V$	Rapid Ambient Temperature Change

Note that load case 5 is outside of the load combinations of Reg. Guide 7.8

[†] The symbols used here are defined in Subsection 2.1.2.1.

Table 2.1.9

OVERPACK LOAD CASES FOR HYPOTHETICAL ACCIDENT CONDITIONS OF TRANSPORT

Case Number	Load Combination [†]	Notes
1	$T_h + D_{ba} + P_i + F + W_s$	Bottom End 30 ft. Drop - Hot
2	$T_h + D_{ta} + P_i + F + W_s$	Top End 30 ft Drop - Hot
3	$T_h + D_{sa} + P_i + F + W_s$	Side 30 ft Drop - Hot
4	$T_h + D_{ea} + P_i + F + W_s$	30 ft C.G. Over-the-Bottom-Corner Drop - Hot
5	$T_h + D_{ga} + P_i + F + W_s$	30 ft C.G. Over-the-Top-Corner Drop Hot
6	$T_h + P_s + P_i + F + W_s$	Side Puncture - Hot
7	$T_h + P_t + P_i + F + W_s$	Top End Puncture - Hot
8	$T_h + P_b + P_i + F + W_s$	Bottom End Puncture - Hot
9	$T_c + D_{ba} + P_o + F + W_s$	Case 1 - Cold
10	$T_c + D_{ta} + P_o + F + W_s$	Case 2 - Cold
11	$T_c + D_{sa} + P_o + F + W_s$	Case 3 - Cold
12	$T_c + D_{ea} + P_o + F + W_s$	Case 4 - Cold
13	$T_c + D_{ga} + P_o + F + W_s$	Case 5 - Cold
14	$T_c + P_s + P_o + F + W_s$	Case 6 - Cold
15	$T_c + P_t + P_o + F + W_s$	Case 7 - Cold
16	$T_c + P_b + P_o + F + W_s$	Case 8 - Cold
17	$T_f + P_i + F + W_s$	Fire Event (Bolt unloading)
18	P_o^*	Containment Stability - Hot Deep Submergence
19	$P_i^* + T_f + F + W_s$	Fire Accident Internal Pressure - Hot
20	$T_h + D_{ga} + P_i + F + W_s$	30 ft C.G. Oblique Drop (30 Degree) on Top Forging - Hot
21	$T_c + D_{ga} + P_i + F + W_s$	30 ft C.G. Oblique Drop (30 Degree) on Top Forging - Cold
22	$T_c + D_{ga} + P_i + F + W_s$	30 ft Drop -Slapdown Secondary Impact Limiter at Top Forging - Hot

[†] The symbols used here are defined in Subsection 2.1.2.1.

Table 2.1.10
BOUNDING DECELERATIONS FOR DROP EVENTS

Event	Deceleration Value (in multiples of acceleration due to gravity)
Normal conditions of transport, drop from 1 ft. height (any circumferential orientations)	17
Transport hypothetical accident conditions; drop from 30 ft. height (any axial and circumferential orientations)	60

Table 2.1.11

DESIGN, LEVELS A AND B: STRESS INTENSITY

Code: ASME NB
 Material: SA203-E
 Service Conditions: Normal Conditions of Transport
 Item: Stress Intensity

Temp. (degree F)	Classification and Value (ksi)					
	S_m	P_m^\dagger	P_L^\dagger	$P_L + P_b^\dagger$	$P_L + P_b + Q$	$P_e^{\dagger\dagger}$
-20 to 100	23.3	23.3	35.0	35.0	69.9	69.9
200	23.3	23.3	35.0	35.0	69.9	69.9
300	23.3	23.3	35.0	35.0	69.9	69.9
400	22.9	22.9	34.4	34.4	68.7	68.7
500	21.6	21.6	32.4	32.4	64.8	64.8

Definitions:

- S_m = Stress intensity values per ASME Code
- P_m = Primary membrane stress intensity
- P_L = Local membrane stress intensity
- P_b = Primary bending stress intensity
- P_e = Expansion stress
- Q = Secondary stress
- $P_L + P_b$ = Either primary or local membrane plus primary bending

Definitions for Table 2.1.11 apply to all following tables unless modified.

† Evaluation required for Design condition only.

†† P_e not applicable to vessels.

Table 2.1.12

LEVEL D: STRESS INTENSITY

Code: ASME NB
 Material: SA203-E
 Service Condition: Hypothetical Accident
 Item: Stress Intensity

Temp. (degree F)	Classification and Value (ksi)		
	P_m	P_L	$P_L + P_b$
-20 to 100	49.0	70.0	70.0
200	49.0	70.0	70.0
300	49.0	70.0	70.0
400	48.2	68.8	68.8
500	45.4	64.9	64.9

Notes:

1. Level D allowables per NB-3225 and Appendix F, Paragraph F-1331.
2. Average primary shear stress across a section loaded in pure shear may not exceed $0.42 S_u$.
3. Limits on values are presented in Table 2.1.3.

Table 2.1.13

DESIGN, LEVELS A AND B: STRESS INTENSITY

Code: ASME NB
 Material: SA350-LF3
 Service Conditions: Normal Conditions of Transport
 Item: Stress Intensity

Temp. (degree F)	Classification and Value (ksi)					
	S_m	P_m^\dagger	P_L^\dagger	$P_L + P_b^\dagger$	$P_L + P_b + Q$	P_e^{**}
-20 to 100	23.3	23.3	35.0	35.0	69.9	69.9
200	22.8	22.8	34.2	34.2	68.4	68.4
300	22.2	22.2	33.3	33.3	66.6	66.6
400	21.5	21.5	32.3	32.3	64.5	64.5
500	20.2	20.2	30.3	30.3	60.6	60.6
600	18.5	18.5	27.75	27.75	55.5	55.5
700	16.8	16.8	25.2	25.2	50.4	50.4

Notes:

1. Source for S_m is ASME Code.
2. Limits on values are presented in Table 2.1.3.

[†] Evaluation required for Design condition only.

^{**} P_e not applicable to vessels.

Table 2.1.14

LEVEL D, STRESS INTENSITY

Code: ASME NB
 Material: SA350-LF3
 Service Conditions: Hypothetical Accident
 Item: Stress Intensity

Temp. (degree F)	Classification and Value (ksi)		
	P_m	P_L	$P_L + P_b$
-20 to 100	49.0	70.0	70.0
200	48.0	68.5	68.5
300	46.7	66.7	66.7
400	45.2	64.6	64.6
500	42.5	60.7	60.7
600	38.9	58.4	58.4
700	35.3	53.1	53.1

Notes:

1. Level D allowables per NB-3225 and Appendix F, Paragraph F-1331.
2. Average primary shear stress across a section loaded in pure shear may not exceed $0.42 S_u$.
3. Limits on values are presented in Table 2.1.3.

Table 2.1.15

DESIGN AND LEVEL A: STRESS AND STRESS INTENSITY

Code:	ASME NF (Class 3)	ASME NF (Class 1)
Material:	SA515, Grade 70	SA515, Grade 70
	SA516, Grade 70	SA516, Grade 70
Service Conditions:	Normal Conditions of Transport	Normal Conditions of Transport
Item:	Stress	Stress Intensity

Temp. (degree F)	Classification and Value (ksi)					
	S (Class 3)	S _m (Class 1)	Membrane Stress (Class 3)	P _m (Class 1)	Membrane plus Bending Stress (Class 3)	P _m +P _b (Class 1)
-20 to 100	17.5	23.3	17.5	23.3	26.3	34.95
200	17.5	23.1	17.5	23.1	26.3	34.65
300	17.5	22.5	17.5	22.5	26.3	33.75
400	17.5	21.7	17.5	21.7	26.3	32.55
500	17.5	20.5	17.5	20.5	26.3	30.75
600	17.5	18.7	17.5	18.7	26.3	28.05
650	17.5	18.4	17.5	18.4	26.3	27.6
700	16.6	18.3	16.6	18.3	24.9	27.45

Notes:

1. S = Maximum allowable stress values from Table 1A of ASME Code, Section II, Part D.
2. Stress classification per Paragraph NF-3260.
3. Limits on values are presented in Table 2.1.5.
4. Level A allowable stress intensities per NF.3221.1.
5. S_m = Stress intensity values per Table 2A of ASME, Section II, Part D.

Table 2.1.16

LEVEL D: STRESS INTENSITY

Code: ASME NF
 Material: SA515, Grade 70
 SA516, Grade 70
 Service Conditions: Hypothetical Accident
 Item: Stress Intensity

Temp. (degree F)	Classification and Value (ksi)		
	S_m	P_m	$P_m + P_b$
-20 to 100	23.3	45.6	68.4
200	23.1	41.5	62.3
300	22.5	40.4	60.6
400	21.7	39.1	58.7
500	20.5	36.8	55.3
600	18.7	33.7	50.6
650	18.4	33.1	49.7
700	18.3	32.9	49.3

Notes:

1. Level D allowable stress intensities per Appendix F, Paragraph F-1332.
2. S_m = Stress intensity values per Table 2A of ASME, Section II, Part D.
3. Limits on values are presented in Table 2.1.5.

Table 2.1.17

DESIGN, LEVELS A AND B: STRESS INTENSITY

Code: ASME NB
 Material: Alloy X
 Service Conditions: Normal Conditions of Transport
 Item: Stress Intensity

Temp. (degree F)	Classification and Numerical Value					
	S_m	P_m^\dagger	P_L^\dagger	$P_L + P_b^\dagger$	$P_L + P_b + Q$	$P_e^{\dagger\dagger}$
-20 to 100	20.0	20.0	30.0	30.0	60.0	60.0
200	20.0	20.0	30.0	30.0	60.0	60.0
300	20.0	20.0	30.0	30.0	60.0	60.0
400	18.7	18.7	28.1	28.1	56.1	56.1
500	17.5	17.5	26.3	26.3	52.5	52.5
600	16.4	16.4	24.6	24.6	49.2	49.2
650	16.0	16.0	24.0	24.0	48.0	48.0
700	15.6	15.6	23.4	23.4	46.8	46.8
750	15.2	15.2	22.8	22.8	45.6	45.6
800	14.9	14.9	22.4	22.4	44.7	44.7

Notes:

1. S_m = Stress intensity values per Table 2A of ASME II, Part D.
2. Alloy X S_m values are the lowest values for each of the candidate materials at temperature.
3. Stress classification per NB-3220.
4. Limits on values are presented in Table 2.1.3.

† Evaluation required for Design condition only.

†† P_e not applicable to vessels.

Table 2.1.18

LEVEL D: STRESS INTENSITY

Code: ASME NB
 Material: Alloy X
 Service Conditions: Hypothetical Accident
 Item: Stress Intensity

Temp. (degree F)	Classification and Value (ksi) [†]		
	P _m	P _L	P _L + P _b
-20 to 100	48.0 (48.0)	72.0 (72.0)	72.0 (72.0)
200	48.0 (46.3)	72.0 (69.5)	72.0 (69.5)
300	46.2 (43.1)	69.3 (64.7)	69.3 (64.7)
400	44.9 (42.0)	67.4 (63.0)	67.4 (63.0)
500	42.0 (41.5)	63.0 (62.3)	63.0 (62.3)
600	39.4 (39.4)	59.1 (59.1)	59.1 (59.1)
650	38.4 (38.4)	57.6 (57.6)	57.6 (57.6)
700	37.4 (37.4)	56.1 (56.1)	56.1 (56.1)
750	36.5 (36.5)	54.8 (54.8)	54.8 (54.8)
800	35.8 (35.8)	53.7 (53.7)	53.7 (53.7)

Notes:

1. Level D stress intensities per ASME NB-3225 and Appendix F, Paragraph F-1331.
2. The average primary shear strength across a section loaded in pure shear may not exceed 0.42 S_u.
3. Limits on values are presented in Table 2.1.3.

[†] Values in parentheses apply strictly to the one-piece construction MPC lids, which are made from SA-336 forging material rather than SA-240 plate material.

Table 2.1.19

DESIGN, LEVELS A AND B: STRESS INTENSITY

Code: ASME NG
 Material: Alloy X
 Service Conditions: Normal Conditions of Transport
 Item: Stress Intensity

Temp. (degree F)	Classification and Value (ksi)				
	S_m	P_m	P_m+P_B	P_m+P_b+Q	P_e
-20 to 100	20.0	20.0	30.0	60.0	60.0
200	20.0	20.0	30.0	60.0	60.0
300	20.0	20.0	30.0	60.0	60.0
400	18.7	18.7	28.1	56.1	56.1
500	17.5	17.5	26.3	52.5	52.5
600	16.4	16.4	24.6	49.2	49.2
650	16.0	16.0	24.0	48.0	48.0
700	15.6	15.6	23.4	46.8	46.8
750	15.2	15.2	22.8	45.6	45.6
800	14.9	14.9	22.4	44.7	44.7

Notes:

1. S_m = Stress intensity values per Table 2A of ASME, Section II, Part D.
2. Alloy X S_m values are the lowest values for each of the candidate materials at temperature.
3. Classifications per NG-3220.
4. Limits on values are presented in Table 2.1.4.

Table 2.1.20

LEVEL D: STRESS INTENSITY

Code: ASME NG
 Material: Alloy X
 Service Conditions: Hypothetical Accident
 Item: Stress Intensity

Temp. (degrees F)	Classification and Value (ksi)		
	P_m	P_L	$P_L + P_b$
-20 to 100	48.0	72.0	72.0
200	48.0	72.0	72.0
300	46.2	69.3	69.3
400	44.9	67.4	67.4
500	42.0	63.0	63.0
600	39.4	59.1	59.1
650	38.4	57.6	57.6
700	37.4	56.1	56.1
750	36.5	54.8	54.8
800	35.8	53.7	53.7

Notes:

1. Level D stress intensities per ASME NG-3225 and Appendix F, Paragraph F-1331.
2. The average primary shear strength across a section loaded in pure shear may not exceed $0.42 S_u$.
3. Limits on values are presented in Table 2.1.4.

Table 2.1.21

REFERENCE TEMPERATURES AND STRESS LIMITS
FOR THE VARIOUS LOAD CASES

Load Case Number	Material	Reference Temperature [†] , (°F)	Stress Intensity Allowables, ksi		
			P _m	P _L + P _b	P _L + P _b + Q
F1	Alloy X	725	15.4	23.1	46.2
F2	Alloy X	725	15.4	23.1	46.2
F3	Alloy X	725	36.9	55.4	NL ^{††}
E1	Alloy X	450 ^{†††}	18.1	27.2	NL
E2	Alloy X	450 ^{†††}	18.1	27.2	54.3
E3	Alloy X	450 ^{†††}	43.4	65.2	NL
E4	Alloy X	450 ^{†††}	18.1	27.2	54.3
E5	Alloy X	775 ^{†††}	36.15	54.25	NL

[†] Values for reference temperatures are taken as the design temperatures (Table 2.1.2).

^{††} NL: No specific limit in the Code.

^{†††} Levels used for enclosure vessel top closure and baseplate only.

Table 2.1.21 (continued)

REFERENCE TEMPERATURES AND STRESS LIMITS
FOR THE VARIOUS LOAD CASES

Condition	Material	Reference Temperature, (°F)	Stress Intensity Allowables, ksi		
			P _m	P _L + P _b	P _L + P _b + Q
Normal	SA203-E	400 [†]	22.9	34.4	68.7
	SA350-LF3	400 [†]	21.5	32.3	64.5
	SA516 Gr. 70 SA515 Gr. 70	400 [†]	17.5	26.3	52.5
	SA203-E	-20	23.3	35.0	69.9
	SA350-LF3	-20	23.3	35.0	69.9
	SA516 Gr. 70 SA515 Gr. 70	-20	17.5	26.3	52.5
Hypothetical Accident - Mechanical Loads	SA203-E	400 [†]	48.2	68.8	NL ^{††}
	SA350-LF3	400 [†]	45.2	64.6	NL
	SA516 Gr. 70 SA515 Gr. 70	400 [†]	39.1	58.7	NL
	SA203-E	-20	49.0	70.0	NL
	SA350-LF3	-20	49.0	70.0	NL
	SA516 Gr. 70 SA515 Gr. 70	-20	45.6	68.4	NL
Fire	SA203-E	500	45.4	64.9	NL
	SA350-LF3	700	35.3	53.1	NL
	SA516 Gr. 70	700	32.9	49.3	NL

[†] Values for reference temperatures are taken as the design temperatures (Table 2.1.2).

^{††} NL: No limit specified in the Code.

Table 2.1.22

FRACTURE TOUGHNESS TEST CRITERIA: CONTAINMENT BOUNDARY

Item	Material	Thickness (in.)	Charpy V-Notch Temperature [†]	Drop Test Temperature ^{††}
Weld Metal for NB Welds	As required	NA	As required per ASME Section III, Subsection NB, Article NB-2430 and Article NB-2330 Min. test temperature = -40°F	As required per ASME Section III, Subsection NB, Articles NB-2430 and Article NB-2330
Shell	SA203E or SA350-LF2 or SA350-LF3 or SA350-LF3	2-1/2	$T_{NDT} \leq -70^{\circ}\text{F}$ with testing and acceptance criteria per ASME Section III, Subsection NB, Article NB-2330	$T_{NDT} \leq -70^{\circ}\text{F}$ per Reg. Guide 7.11
Top Flange	SA350-LF3	8-3/4	$T_{NDT} \leq -136^{\circ}\text{F}$ with testing and acceptance criteria per ASME Section III, Subsection NB, Article NB-2330	$T_{NDT} \leq -136^{\circ}\text{F}$ per Reg. Guide 7.12

[†] Temperature is T_{NDT} unless noted.

^{††} Materials to be tested in accordance with ASTM E208-87a.

Table 2.1.22 (Continued)

FRACTURE TOUGHNESS TEST CRITERIA: CONTAINMENT BOUNDARY

Item	Material	Thickness (in.)	Charpy V-Notch Temperature [†]	Drop Test Temperature ^{††}
Bottom Plate	SA350-LF3	6	T _{NDT} ≤ -129 °F with testing and acceptance criteria per ASME Section III, Subsection NB, Article NB-2330	T _{NDT} ≤ -129 °F per Reg. Guide 7.12
Closure Plate	SA350-LF3	6	T _{NDT} ≤ -129 °F with testing and acceptance criteria per ASME Section III, Subsection NB, Article NB-2330	T _{NDT} ≤ -129 °F per Reg. Guide 7.12

[†] Temperature is T_{NDT} unless noted.

^{††} Materials to be tested in accordance with ASTM E208-87a.

Table 2.1.23

FRACTURE TOUGHNESS TEST CRITERIA: MISCELLANEOUS ITEMS

Item	Material	Thickness (in.)	Charpy V-Notch Temperature [†]	Drop Test Temperature
Intermediate Shells	SA516 Grade 70	1-1/4 and 1	Test temperature = -40 Deg. F with acceptance criteria per ASME Section III, Subsection NF, Table NF-2331(a)-3 and Figure NF-2331(a)-2, except BOM items 15 & 16 shall meet Table NF-2331(a)-1 and NF-2331 (a)-4	Not Required
Port Cover Plates	SA203-E or SA350-LF3 or SA350-LF2 or SA350-LF3	1-1/2	Test temperature = -40 Deg. F with acceptance criteria per ASME Section III, Subsection NF, Table NF-2331(a)-3 and Figure NF-2331(a)-2	Not Required
Weld Metal for NF Welds	As required	NA	As required per ASME Section III, Subsection NF, Article NF-2430 and Article NF-2330 Test temperature = -40 Deg. F	Not Required

[†] Temperature is T_{NDT} unless noted.

Table 2.1.24

ALLOWABLE STRESS CRITERIA FROM OTHER SOURCES

OVERPACK CLOSURE BOLTS[†]:

STRESS CATEGORY	NORMAL CONDITIONS OF TRANSPORT	HYPOTHETICAL ACCIDENT
Average Tensile Stress	$2/3 S_y$	$\text{AMIN}(S_y, 0.7 S_u)$
Average Shear Stress	$0.6 (2/3 S_y)$	$\text{AMIN}(0.6 S_y, 0.42 S_u)$
Combined Tensile and Shear Stress ^{††}	$R_t^2 + R_s^2 < 1.0$	$R_t^2 + R_s^2 < 1.0$

IMPACT LIMITER ATTACHMENT BOLTS:

STRESS CATEGORY	NORMAL CONDITIONS OF TRANSPORT	HYPOTHETICAL ACCIDENT
Average Tensile Stress	$2/3 S_y$	S_u
Average Shear Stress	$0.6 (2/3 S_y)$	S_u
Combined Tensile and Shear Stress	$R_t^2 + R_s^2 < 1.0$	$R_t^2 + R_s^2 < 1.0$

LIFTING TRUNNIONS AND LIFTING BOLTS:

The lifting trunnions and the lifting bolts, for the overpack closure plate and for the MPC lid, are designed in accordance with NUREG-0612 and ANSI N14.6. Specifically, the design must meet factors of safety of six based on the material yield stress and ten based on the material ultimate stress for non-redundant lifting devices.

[†] The overpack closure bolts are designed in accordance with NUREG/CR-6007, "Stress Analysis of Closure Bolts for Shipping Casks".

^{††} R_t and R_s are the ratios of actual stress to shear stress, respectively.

2.3 MECHANICAL PROPERTIES OF MATERIALS

This section provides the mechanical properties used in the structural evaluation. The properties include yield stress, ultimate stress, modulus of elasticity, Poisson's ratio, weight density, and coefficient of thermal expansion. The property values are presented for a range of temperatures for which structural calculations are performed.

The materials selected for use in the HI-STAR 100 MPC and overpack are presented in the Bills-of-Materials in Chapter 1, Section 1.4. In this chapter, the materials are divided into two categories, structural and nonstructural. Structural materials are those that serve a load bearing function. Materials that do not support mechanical loads are considered nonstructural. For example, the overpack inner shell is a structural material, while Holtite-A (neutron shield) is a nonstructural material.

2.3.1 Structural Materials

2.3.1.1 Alloy X

A hypothetical material termed Alloy X is defined for all MPC structural components. The material properties of Alloy X are the least favorable values from the set of candidate stainless alloys. The purpose of a "least favorable" material definition is to ensure that all structural analyses are conservative, regardless of the actual MPC material. For example, when evaluating the stresses in the MPC, it is conservative to work with the minimum values for yield strength and ultimate strength. This guarantees that the material used for fabrication of the MPC is of equal or greater strength than the hypothetical material used in the analysis. In the structural evaluation, the only property for which it is not always conservative to use the minimum values is the coefficient of thermal expansion. Two sets of values for the coefficient of thermal expansion are specified, a minimum set and a maximum set. For each analysis, the set of coefficients, minimum or maximum that causes the more severe load on the cask system is used. Table 2.3.1 lists the numerical values for the material properties of Alloy X versus temperature. These values, taken from the ASME Code, Section II, Part D [2.1.11], are used to complete all structural analyses. The maximum temperatures in MPC components may exceed the allowable limits of temperature during short time duration events. However, under no scenario does the maximum temperature of Alloy X material used in the helium confinement boundary exceed 1000°F. As shown in ASME Code Case N-47-33 (Class 1 Components in Elevated Temperature Service, 1995 Code Cases, Nuclear Components), the strength properties of austenitic stainless steels do not change due to exposure to 1000°F temperature for up to 10,000 hours. Therefore, there is no significant effect on mechanical properties of the helium confinement boundary or fuel basket material during the short time duration loading. Further description of Alloy X, including the materials from which it is derived, is provided in Appendix 1.A.

Two properties of Alloy X which are not included in Table 2.3.1 are weight density and Poisson's ratio. These properties are assumed constant for all structural analyses, regardless of the temperature. The values used are shown in the table below.

PROPERTY	VALUE
Weight Density (lb./in ³)	0.290
Poisson's Ratio	0.30

2.3.1.2 Carbon Steel, Low-Alloy, and Nickel Alloy Steel

The carbon steels used in the HI-STAR 100 System are SA516 Grade 70, SA515 Grade 70. These steels are not constituents of Alloy X. The material properties of SA516 Grade 70 and SA515 Grade 70 are shown in Tables 2.3.2 and 2.3.3, respectively. The nickel alloy and low-alloy steels are SA203-E and SA350-LF3, respectively. The material properties of SA203-E and SA350-LF3 are given in Table 2.3.4.

Two properties of these steels which are not included in Tables 2.3.2 through 2.3.4 are weight density and Poisson's ratio. These properties are assumed constant for all structural analyses. The values used are shown in the table below.

PROPERTY	VALUE
Weight Density (lb./in ³)	0.283
Poisson's Ratio	0.30

2.3.1.3 Bolting Materials

Material properties of the bolting materials used in the HI-STAR System are given in Table 2.3.5.

2.3.1.4 Weld Material

All weld filler materials utilized in the welding of the Code components will comply with the provisions of the appropriate ASME subsection (e.g., Subsection NB for the overpack and enclosure vessel) and Section IX. All non-Code welds shall also be made using weld procedures that meet Section IX of the ASME Code. All non-code welds shall also be made using weld procedures that meet Section IX of the ASME Code. The minimum tensile strength of the weld wire and filler material (where applicable) will be equal to or greater than the tensile strength of the base metal listed in the ASME Code.

2.3.1.5 Impact Limiter

The Impact Limiter for the HI-STAR 100 System has been named AL-STAR™. AL-STAR is composed of cross core and uni-directional aluminum honeycomb made by layering corrugated sheets of aluminum (Alloy 5052). For the cross core material, alternate layers of corrugated aluminum sheets are laid in orthogonal direction to each other (Figure 2.3.1). The layers are bonded together by a high-temperature epoxy. The Holtec drawing in Section 1.4 illustrates the

arrangement of the cross core and uni-directional honeycomb sectors in AL-STAR to realize adequate crush moduli in all potential impact modes. The external surface of AL-STAR consists of a stainless steel skin to provide long-term protection against weather and environmental conditions.

Rail transport considerations limit the maximum diameter of the impact limiter to 128 inches. The axial dimension of AL-STAR is limited by the considerations of maximum permissible packaging weight for rail transport. Within the limitations of space and weight, AL-STAR must possess sufficient energy absorption capacity so as to meet the design basis rigid body deceleration limits (Table 2.1.10) under all postulated drop orientations. The sizing of the AL-STAR internal structure is principally guided by the above considerations. For example, in order to ensure that a sufficient portion of the honeycomb structure participates in lateral impacts, a thick carbon steel shell buttressed with gussets provides a hard backing surface for the aluminum honeycomb to crush against.

Two properties of the cross core honeycomb germane to its function are the crush strength and the nominal density. The crush strength of AL-STAR is the more important of the two properties; the density is significant in establishing the total weight of the package. The crush strength increases monotonically with density. For example, the cross core honeycomb of 2500 psi crush strength has a nominal density of 27 lb. per cubic foot. At 2,000 psi crush strength, the change in aluminum honeycomb parameters lowers the density to approximately 22 lb. per cubic foot. The crush strength of the honeycomb can be varied within a rather wide range by adjusting the aluminum foil thickness and corrugation size. Drawings in Section 1.4 show the required crush strengths of the honeycomb sectors in the various regions of AL-STAR.

Like all manufactured materials, the crush strength and density of the honeycomb material are subject to slight variation within a manufactured lot. The crush strength will be held to a tolerance of approximately 15% (a nominal crush strength \pm 7.5%).

Hexcel Corporation's publication TSB 120, "Mechanical Properties of Hexcel Honeycomb Materials", [2.3.1] provides detailed information on the mechanical characteristics of aluminum honeycomb materials. Hexcel's experimental data shows that the load-deflection curve of aluminum honeycomb simulates the shape of elastic-perfectly plastic materials. The honeycomb crushes at a nearly uniform load (slowly applied) until solidity in the range of 30 to 40% is reached. It is the crushing at constant load characteristic of aluminum honeycomb along with its excellent crush strength-to-weight ratio that makes it an ideal energy absorption material. The cross layered honeycomb (cross-core) has an identical crush strength in two orthogonal directions. In other words, from a load-deflection standpoint, the cross-layered honeycomb is a transversely isotropic material.

A typical honeycomb pressure-strain curve is illustrated in Figure 2.A.2.1 in Appendix 2.A wherein additional discussion on the crush properties of the honeycomb material is provided.

However, three key properties of the honeycomb material which are central to its function as a near-ideal impact limiter crush material are summarized below.

- i. The honeycomb material can be used in the "un-crushed" or "pre-crushed" condition. The difference is in the initial "bump" in the pressure-strain curve shown in Figure 2.A.2.1. By pre-crushing the honeycomb, its pressure-strain relationship simulates that of an ideal elastic-perfectly-plastic material, which is most desirable in limiting abrupt peaks in the deceleration of the package under drop events.
- ii. Irrespective of the crush strength, under quasi-static loading, all honeycomb materials begin to strain harden at about 60% strain and lock up at about 70%. Thus, a 10-inch thick honeycomb column will crush down to a thickness of 4 inches at near constant force; crushing further will require progressively greater compression force. The six inches of available crush distance is referred to as the available "stroke" in the lexicon of impact limiter design technology.
- iii. Because the crush material is made entirely out of one of the most cryogenically competent industrial metals available, aluminum, the pressure-crush behavior of the ALSTAR honeycomb material is insensitive to the environmental temperature range germane to Part 71 transport (-20 degrees F to 100 degrees F). Table Y-1 of the ASME Code [2.1.11] lists the yield strength of the material (Alloy 5052) to be constant in the range -20 degrees F to 350 degrees F.

Independent confirmation of the invariance of the ALSTAR's crush properties with temperature in the range of temperatures applicable to the HI-STAR 100 packaging was provided by experiments conducted by Holtec International in June 1998 [2.3.2] using sample material obtained from Hexcell. The test objective was to evaluate the temperature sensitivity, if any, of the static compression strength of the honeycomb material. To that end, test specimens were cut from the sample material and were subject to static compression testing using a Q.A. validated procedure.

A series of specimens of two different strengths were tested at three different temperatures. The specimens were tested at -29 degrees C, 23 degrees C and 80 degrees C which represent "Cold", "Ambient", and "Heat" environmental conditions. Ten specimens were prepared for each crush strength, to allow for multiple data points at each test temperature. The specimens were not pre-crushed so the static compression-crush curves exhibited an initial peak. After discounting the initial peaks in the static force-crush curve, the constant force range for each specimen could be identified from the test data and a crush pressure for the specimen defined by dividing this constant force by the measured specimen loaded area.

The computed crush pressures showed no significant trending that could be ascribed to environmental effects. Figure 2.3.2 is a plot of the test results and plots the average of the calculated test crush pressures from the series of specimens at each of the three temperatures. The results for individual test samples at any given temperature were within manufacturing tolerance. It is clear from the plotted results that the effect of temperature is well within the data scatter due to manufacturing tolerance. Therefore, within the temperature range germane to the ALSTAR impact limiter, the force-crush characteristic is expected to be essentially unaffected by the coincident honeycomb metal temperature. This leads to the conclusion that environmental temperature effects will not influence impact limiter performance predictions.

Appendix 2.A contains further information on the AL-STAR honeycomb and its performance characteristics. The sensitivity of the package performance to variations in compression strength of the aluminum honeycomb is evaluated in Appendix 2.A.

In summary, the AL-STAR impact limiter is composed of a carbon steel inner shell structure, an assemblage of cross core and uni-directional aluminum honeycombs and a stainless steel external sheathing.

None of the structural materials has a low melting point or is flammable. A Holtite-A layer is situated deep in the honeycomb in such a manner that it does not participate in the crushing process, but provides neutron shielding in the axial direction.

2.3.2 Nonstructural Materials

2.3.2.1 Neutron Shield

The neutron shield in the overpack is not considered as a structural member of the HI-STAR 100 System. Its load carrying capacity is neglected in all structural analyses except where such omission would be nonconservative. The only material property of the neutron shield which is important to the structural evaluation is weight density (1.63 g/cm^2).

2.3.2.2 BoralTM-Solid Neutron Absorber

The fuel basket solid neutron absorber Boral is not a structural member of the HI-STAR 100 System. Its load carrying capacity is neglected in all structural analyses. The only material property of Boral-solid neutron absorber which is important to the structural evaluation is weight density. As the MPC fuel baskets can be constructed with Boral-neutron absorber panels of variable areal density, the weight that produces the most severe cask load is assumed in each analysis. (Density 2.644 g/cm^3).

2.3.2.3 Aluminum Heat Conduction Elements

The aluminum heat conduction elements are located between the fuel basket and MPC vessel in several of the early vintage MPC-68s and MPC-68Fs. They have since been removed from the MPC design and none were installed in the PWR MPCs. They are thin, flexible elements whose sole function is to transmit heat from the basket. They are not credited with any structural load capacity and are shaped to provide negligible resistance to basket thermal expansion. The total weight of the aluminum heat conduction elements is less than 1,000 lb. per MPC.

Table 2.3.1

ALLOY X MATERIAL PROPERTIES

Temp. (°F)	Alloy X				
	S_y	S_u^\dagger	α_{\min}	α_{\max}	E
-40	30.0	75.0 (70.0)	8.54	8.55	28.82
100	30.0	75.0 (70.0)	8.54	8.55	28.14
150	27.5	73.0 (68.1)	8.64	8.67	27.87
200	25.0	71.0 (66.2)	8.76	8.79	27.6
250	23.75	68.5 (63.85)	8.88	8.9	27.3
300	22.5	66.0 (61.5)	8.97	9.0	27.0
350	21.6	65.2 (60.75)	9.10	9.11	26.75
400	20.7	64.4 (60.0)	9.19	9.21	26.5
450	20.05	64.0 (59.65)	9.28	9.32	26.15
500	19.4	63.5 (59.3)	9.37	9.42	25.8
550	18.8	63.3 (59.1)	9.45	9.50	25.55
600	18.2	63.1 (58.9)	9.53	9.6	25.3
650	17.8	62.8 (58.6)	9.61	9.69	25.05
700	17.3	62.5 (58.4)	9.69	9.76	24.8
750	16.9	62.2 (58.1)	9.76	9.81	24.45
800	16.6	61.7 (57.6)	9.82	9.90	24.1

Definitions:

S_y = Yield Stress (ksi)

α = Mean Coefficient of thermal expansion (in./in. per degree F x 10^{-6})

S_u = Ultimate Stress (ksi)

E = Young's Modulus (psi x 10^6)

Notes:

1. Source for S_y values is Table Y-1 of [2.1.11].
2. Source for S_u values is Table U of [2.1.11].
3. Source for α_{\min} and α_{\max} values is Table TE-1 of [2.1.11].
4. Source for E values is material group G in Table TM-1 of [2.1.11].

[†] The ultimate stress of Alloy X is dependent on the product form of the material (i.e., forgings vs. plate). Values in parentheses are based on SA-336 forging materials (Type F304, F304LN, F316, and F316LN), which are used solely for the one-piece construction MPC lids. All other values correspond to SA-240 plate material.

Table 2.3.2

SA516, GRADE 70 MATERIAL PROPERTIES

Temp. (°F)	SA516, Grade 70			
	S _y	S _u	α	E
-40	38.0	70.0	5.53	29.34
100	38.0	70.0	5.53	29.34
150	36.3	70.0	5.71	29.1
200	34.6	70.0	5.89	28.8
250	34.15	70.0	6.09	28.6
300	33.7	70.0	6.26	28.3
350	33.15	70.0	6.43	28.0
400	32.6	70.0	6.61	27.7
450	31.65	70.0	6.77	27.5
500	30.7	70.0	6.91	27.3
550	29.4	70.0	7.06	27.0
600	28.1	70.0	7.17	26.7
650	27.6	70.0	7.30	26.1
700	27.4	70.0	7.41	25.5
750	26.5	69.3	7.50	24.85

Definitions:

S_y = Yield Stress (ksi)

α = Mean Coefficient of thermal expansion (in./in. per degree F x 10⁻⁶)

S_u = Ultimate Stress (ksi)

E = Young's Modulus (psi x 10⁶)

Notes:

1. Source for S_y values is Table Y-1 of [2.1.11].
2. Source for S_u values is Table U of [2.1.11].
3. Source for α values is material group C in Table TE-1 of [2.1.11].
4. Source for E values is "Carbon steels with C ≤ 0.30%" in Table TM-1 of [2.1.11].

Table 2.3.3

SA515, GRADE 70 MATERIAL PROPERTIES

Temp. (°F)	SA515, Grade 70			
	S _y	S _u	α	E
-40	38.0	70.0	5.53	29.34
100	38.0	70.0	5.53	29.34
150	36.3	70.0	5.71	29.1
200	34.6	70.0	5.89	28.8
250	34.15	70.0	6.09	28.6
300	33.7	70.0	6.26	28.3
350	33.15	70.0	6.43	28.0
400	32.6	70.0	6.61	27.7
450	31.65	70.0	6.77	27.5
500	30.7	70.0	6.91	27.3
550	29.4	70.0	7.06	27.0
600	28.1	70.0	7.17	26.7
650	27.6	70.0	7.30	26.1
700	27.4	70.0	7.41	25.5
750	26.5	69.3	7.50	24.85

Definitions:

S_y = Yield Stress (ksi)α = Mean Coefficient of thermal expansion (in./in. per degree F x 10⁻⁶)S_u = Ultimate Stress (ksi)E = Young's Modulus (psi x 10⁶)

Notes:

1. Source for S_y values is Table Y-1 of [2.1.11].
2. Source for S_u values is Table U of [2.1.11].
3. Source for α values is material group C in Table TE-1 of [2.1.11].
4. Source for E values is "Carbon steels with C ≤ 0.30%" in Table TM-1 of [2.1.11].

Table 2.3.4

SA350-LF3 AND SA203-E MATERIAL PROPERTIES

Temp. (°F)	SA350-LF3			SA350-LF3/SA203-E		SA203-E		
	S _m	S _y	S _u	E	α	S _m	S _y	S _u
-100	23.3	37.5	70.0	28.5	6.20	23.3	40.0	70.0
100	23.3	37.5	70.0	27.6	6.27	23.3	40.0	70.0
200	22.8	34.2	68.5	27.1	6.54	23.3	36.5	70.0
300	22.2	33.2	66.7	26.7	6.78	23.3	35.4	70.0
400	21.5	32.2	64.6	26.1	6.98	22.9	34.3	68.8
500	20.2	30.3	60.7	25.7	7.16	21.6	32.4	64.9
600	18.5	-	-	-	-	-	-	-
700	16.8	-	-	-	-	-	-	-

Definitions:

- S_m = Design Stress Intensity (ksi)
 S_y = Yield Stress (ksi)
 S_u = Ultimate Stress (ksi)
 α = Coefficient of Thermal Expansion (in./in. per degree F x 10⁻⁶)
 E = Young's Modulus (psi x 10⁶)

Notes:

1. Source for S_m values is Table 2A of [2.1.11].
2. Source for S_y values is Table Y-1 of [2.1.11].
3. Source for S_u values is ratioing S_m values.
4. Source for α values is material group E in Table TE-1 of [2.1.11].
5. Source for E values is material group B in Table TM-1 of [2.1.11].

Table 2.3.5

SB637-N07718, SA564-630, AND SA705-630 MATERIAL PROPERTIES

Temp. (°F)	SB637-N07718				
	S_y	S_u	E	α	S_m
-100	150.0	185.0	29.9	---	50.0
-20	150.0	185.0	---	---	50.0
70	150.0	185.0	29.0	7.05	50.0
100	150.0	185.0	---	7.08	50.0
200	144.0	177.6	28.3	7.22	48.0
300	140.7	173.5	27.8	7.33	46.9
400	138.3	170.6	27.6	7.45	46.1
500	136.8	168.7	27.1	7.57	45.6
600	135.3	166.9	26.8	7.67	45.1
SA705-630/SA564-630 (Age Hardened at 1075°F)					
Temp. (°F)	S_y	S_u	E	α	-
200	115.6	145.0	28.5	5.9	-
300	110.7	145.0	27.9	5.9	-
400	106.7	141	-	-	-
500	103.5	140	-	-	-
SA705-630/SA564-630 (Age Hardened at 1150°F)					
200	97.1	135.0	28.5	5.9	-
300	93.0	135.0	27.9	5.9	-
400	89.8	131.4	-	-	-
500	87	128.5	-	-	-

Definitions:

 S_m = Design Stress Intensity (ksi) S_y = Yield Stress (ksi) α = Mean Coefficient of thermal expansion (in./in. per degree F x 10^{-6}) S_u = Ultimate Stress (ksi)E = Young's Modulus (psi x 10^6)

Notes:

1. Source for S_m values is Table 4 of [2.1.11].
2. Source for S_y , S_u values is ratioing design stress intensity values.
3. Source for α values is Tables TE-1 and TE-4 of [2.1.11], as applicable.
4. Source for E values is Table TM-1 of [2.1.11].

Table 2.3.6

YIELD STRENGTH OF SA-193-B8S IMPACT LIMITER ATTACHMENT BOLTS

Yield Stress for Attachment Bolt Calculations [†]	
Item	Yield Stress (psi)
Yield Stress	50,000

[†] Source for stress is Table 3 of [2.1.11].

2.4 GENERAL STANDARDS FOR ALL PACKAGES

The compliance of the HI-STAR 100 System to the general standards for all packaging, specified in 10CFR71.43, is demonstrated in the following paragraphs.

2.4.1 Minimum Package Size

The HI-STAR 100 package meets the requirements of 10CFR71.43(a); the outer diameter of the overpack is approximately 96" and its length is approximately 203".

2.4.2 Tamperproof Feature

During transport operations, a wire tamper seal with a stamped identifier will be attached between the lower base of the upper impact limiter shell and the head of one of the impact limiter attachment bolts for the purpose of indicating possible tampering. In order to access the radioactive contents of the overpack, the upper impact limiter is required to be removed to access the closure plate bolting. This tamper seal satisfies the requirements of 10CFR71.43(b). A second wire tamper seal will be attached between the lower impact limiter and an attachment bolt head to indicate tampering. This seal will prevent access to the drain port. The assembly drawing in Section 1.4 depicts the security seals.

2.4.3 Positive Closure

There are no quick-connect/disconnect valves in the containment boundary of the HI-STAR 100 packaging. The only access to the overpack internals is through the closure plate on the overpack, which weighs over 7000 pounds, and the overpack vent and drain ports which are sealed and protected by bolted cover plates. This closure plate is fastened to the overpack flange with heavy bolts, which are torqued to closure values in Table 7.1.12. Opening of the overpack vent and drain port would require removal of the bolted cover plate and unthreading of the port plug. Inadvertent opening of the overpack is not feasible; opening an overpack requires mobilization of special tools and a source of power. The overpack containment boundary is analyzed for normal and accident condition internal pressure and demonstrates integrity under both conditions.

2.4.4 Chemical and Galvanic Reactions

There is no credible mechanism for significant chemical or galvanic reactions in the HI-STAR 100 System during loading operations.

The MPC, which is filled with helium, provides a nonaqueous and inert environment. Insofar as corrosion is a long-term time-dependent phenomenon, the inert gas environment in the MPC precludes the incidence of corrosion during transport. Furthermore, the only dissimilar material groups in the MPC are: (1) ~~Boral~~TM-the neutron absorber material and stainless steel and (2) aluminum and stainless steel. ~~Boral~~-Neutron absorber materials and stainless steel have been

used in close proximity in wet storage for over 30 years. Many spent fuel pools at nuclear plants contain fuel racks, which are fabricated from ~~Boral~~ *neutron absorber materials* and stainless steel materials, with geometries similar to the HI-STAR 100 MPC. Not one case of chemical or galvanic degradation has been found in fuel racks built by Holtec. This experience provides a sound basis to conclude that corrosion will not occur in these materials. Additionally, the aluminum heat conduction elements and stainless steel basket are very close on the galvanic series chart. Aluminum, like other metals of its genre (e.g., titanium and magnesium) rapidly passivates in an aqueous environment, leading to a thin ceramic (Al_2O_3) barrier, which renders the material essentially inert and corrosion-free over long periods of application. The physical properties of the material, e.g., thermal expansion coefficient, diffusivity, and thermal conductivity, are essentially unaltered by the exposure of the aluminum metal stock to an aqueous environment.

The aluminum in the optional heat conduction elements will quickly passivate in air and in water to form a protective oxide layer that prevents any significant hydrogen production during MPC cask loading and unloading operations. The aluminum in ~~the Boral neutron absorber material~~ ; ~~particularly in the core area,~~ *will* also react with water to generate hydrogen gas. The exact rate of generation and total amount of hydrogen generated is a function of a number of variables (see Section 1.2.1.4.1) and cannot be predicted with any certainty. Therefore, to preclude the potential for hydrogen ignition during lid welding or cutting, the operating procedures in Chapter 7 require monitoring for combustible gas and either exhausting or purging the space beneath the MPC lid with an inert gas during these activities. Once the MPC cavity is drained, dried, and backfilled with helium, the source of hydrogen gas (the aluminum-water reaction) is eliminated.

The HI-STAR 100 overpack combines low-alloy and nickel alloy steels, carbon steels, neutron and gamma shielding, thermal expansion foam, and bolting materials. All of these materials have a long history of nongalvanic behavior within close proximity of each other. The internal and external carbon steel surfaces of the overpack and closure plates are sandblasted and coated to preclude surface oxidation. The coating does not chemically react with borated water. Therefore, chemical or galvanic reactions involving the overpack materials are highly unlikely and are not expected.

The interfacing seating surfaces of the closure plate metallic seals are clad with stainless steel to assure long-term sealing performance and to eliminate the potential for localized corrosion of the seal seating surfaces.

In accordance with NRC Bulletin 96-04, a review of the potential for chemical, galvanic, or other reactions among the materials of the HI-STAR 100 System, its contents and the operating environment, which may produce adverse reactions, has been performed. Table 2.4.1 provides a listing of the materials of fabrication for the HI-STAR 100 System and evaluates the performance of the material in the expected operating environments during short-term loading/unloading operations and transport operations. As a result of this review, no operations were identified which could produce adverse reactions beyond those conditions already analyzed in this SAR.

The HI-STAR 100 System is composed of materials with a long proven history of use in the nuclear industry. The materials are not affected by the radiation levels caused by the spent nuclear fuel. Gamma radiation damage to metals (e.g., aluminum, stainless steel, and carbon steel) does not occur until the dose reaches 10^{18} rads or more. The gamma dose from the spent nuclear fuel transported in the HI-STAR 100 System is on the order of 10^{10} rads. Moreover, significant radiation damage due to neutron exposure does not occur for neutron fluences below approximately 10^{19} n/cm² [2.4.1, 2.4.2], which is far greater than the neutron fluence for which components of the HI-STAR 100 System will be exposed.

Table 2.4.1

HI-STAR 100 SYSTEM MATERIAL COMPATIBILITY
WITH OPERATING ENVIRONMENTS

Material/Component	Fuel Pool (Borated and Unborated Water) ¹	Transport (Open to Environment)
Alloy X: -MPC Fuel Basket -MPC Baseplate -MPC Shell -MPC Lid -MPC Fuel Spacers	Stainless steels have been extensively used in spent fuel storage pools with both borated and unborated water with no adverse reactions or interactions with spent fuel.	The MPC internal and external environment will be inert (helium) atmosphere. No adverse interactions identified.
Aluminum -Conduction Inserts	Aluminum and stainless steels form a galvanic couple. However, they are very close on the galvanic series chart and aluminum rapidly passivates in an aqueous environment forming a thin ceramic (Al ₂ O ₃) barrier. The aluminum will be installed in a passivated condition. Therefore, during the short time they are exposed to fuel pool water, corrosion is not expected.	In a non-aqueous atmosphere galvanic corrosion is not expected.
Boral Neutron Absorber Material: -Neutron Absorber	Extensive in-pool experience on spent fuel racks with no adverse reactions. See Chapter 7 for additional requirements for combustible gas monitoring and required actions for control of combustible gas accumulation under the MPC lid.	The Boral will be in a helium environment. No adverse reactions identified.

¹ HI-STAR 100 System short-term operating environment during loading and unloading.

Table 2.4.1 (continued)

HI-STAR 100 SYSTEM MATERIAL COMPATIBILITY
WITH OPERATING ENVIRONMENTS

Material/Component	Fuel Pool (Borated and Unborated Water) ²	Transport (Open to Environment)
<p>Steels:</p> <ul style="list-style-type: none"> -SA350-LF3 -SA203-E -SA515 Grade 70 -SA516 Grade 70 -SA750 630 17-4 PH -SA564 630 17-4 PH -SA106 -SA193-B7 <p>Overpack Body</p>	<p>All exposed steel surfaces (except seal areas, pocket trunnions, and bolt locations) will be coated with paint specifically selected for performance in the operating environments. Even without coating, no adverse reactions (other than nominal corrosion) have been identified.</p>	<p>Internal surfaces of the overpack will be painted and maintained in an inert atmosphere. Exposed external surfaces (except those listed in fuel pool column) will be painted and will be maintained with a fully painted surface. No adverse reactions identified.</p>
<p>Stainless Steels:</p> <ul style="list-style-type: none"> -SA240 304 -SA193 Grade B8 -18-8 S/S <p>Miscellaneous Components</p>	<p>Stainless steels have been extensively used in spent fuel storage pools with both borated and unborated water with no adverse reactions.</p>	<p>Stainless steel has a long proven history of corrosion resistance when exposed to the atmosphere. These materials are used for bolts and threaded inserts. No adverse reactions with steel have been identified. No impact on performance.</p>

² HI-STAR 100 System short-term operating environment during loading and unloading.

Table 2.4.1 (continued)

HI-STAR 100 SYSTEM MATERIAL COMPATIBILITY
WITH OPERATING ENVIRONMENTS

Material/Component	Fuel Pool (Borated and Unborated Water) ³	Transport (Open to Environment)
Nickel Alloy: -SB637-NO7718 Bolting	Bolts are not used in pool.	Exposed to weathering effects. No adverse reactions with overpack closure plate. No impact on performance.
Brass: -Rupture Disk	Small surface of rupture disk will be exposed. No significant adverse impact identified.	Exposed to external weathering. No loss of function expected. Disks inspected prior to transport.
Holtite-A: -Neutron Shield	The neutron shield is fully enclosed by the outer enclosure. No adverse reaction identified. No adverse reactions with thermal expansion foam or steel.	The neutron shield is fully enclosed in the outer enclosure. No adverse reaction identified. No adverse reactions with thermal expansion foam or steel.
Silicone Foam: -Thermal Expansion Foam	Fully enclosed in the outer enclosure. No adverse reaction identified. No adverse reactions with neutron shield or steel.	Foam is fully enclosed in outer enclosure. No adverse reaction identified. No adverse reactions with neutron shield or steel.

³ HI-STAR 100 System short-term operating environment during loading and unloading.

Table 2.4.1 (continued)

HI-STAR 100 SYSTEM MATERIAL COMPATIBILITY
WITH OPERATING ENVIRONMENTS

Material/Component	Fuel Pool (Borated and Unborated Water) ⁴	Transport (Open to Environment)
<p><u>Paint:</u></p> <ul style="list-style-type: none"> - Carboline 890 - Thermaline 450 	<p>Carboline 890 used for exterior surfaces. Acceptable performance for short-term exposure in mild borated pool water.</p> <p>Thermaline 450 selected for excellent high temperature resistance properties. Will only be exposed to demineralized water during in-pool operations as annulus is filled prior to placement in the spent fuel pool and the inflatable seal prevents fuel pool water in-leakage. No adverse interaction identified which could affect MPC/fuel assembly performance.</p>	<p>Good performance on exterior surfaces. Discoloration is not a concern.</p> <p>During transport, internal overpack surfaces will operate in an inert (helium) atmosphere. No adverse reaction identified.</p>
<p><u>Metallic Seals:</u></p> <ul style="list-style-type: none"> - Alloy X750 - 304 S/S 	<p>Not installed or exposed during in-pool handling.</p>	<p>Seals enclosed by closure plate or port cover plates.</p> <p>Closure plate seals seat against stainless steel overlay surfaces. No degradation of seal integrity due to corrosion is expected.</p>

⁴ HI-STAR 100 System short-term operating environment during loading and unloading.

2.6 NORMAL CONDITIONS OF TRANSPORT

The HI-STAR 100 package, when subjected to the normal conditions of transport specified in 10CFR71.71, meets the design criteria in Subsection 2.1.2 (derived from the stipulations in 10CFR71.43 and 10CFR71.51) as demonstrated in the following section.

2.6.1 Heat

Subsection 2.6.1, labeled “Heat” in Regulatory Guide 7.9, is required to contain information on all structural (including thermoelastic) analyses performed on the cask to demonstrate positive safety margins, except for lifting operations that are covered in the preceding Section 2.5. Accordingly, this subsection contains all necessary information on the applied loadings, differential thermal expansion considerations, stress analysis models, and results for all normal conditions of transport. Assessment of potential malfunction under “Cold” conditions is required to be presented in Subsection 2.6.2.

Consistent with Regulatory Guide 7.9, the thermal evaluation of the HI-STAR 100 Package is reported in Chapter 3. The thermal evaluation also establishes the material temperatures, which are used in the structural evaluations discussed in this section and in Section 2.7.

2.6.1.1 Summary of Pressures and Temperatures

Design pressures and design temperatures for all conditions of transport are listed in Tables 2.1.1 and 2.1.2, respectively.

Load cases F1 (Table 2.1.6) and E4 (Table 2.1.7) are defined to study the effect of differential thermal expansion among the constituent components in the HI-STAR 100 Package. Figures 2.6.1 and 2.6.2 provide the defining bounding temperature distributions used for the MPC and overpack finite element thermal stress calculations to maximize stresses that develop due to temperature gradients. The distribution T is applied conservatively to analyze its effect on the fuel basket, the enclosure vessel (helium retention boundary), and the overpack.

2.6.1.2 Differential Thermal Expansion

In addition to the finite element solutions for free expansion stress (due to temperature gradients), simplified closed form calculations are independently performed to demonstrate that a physical interference will not develop between the overpack and the MPC canister, and between the MPC canister and the fuel basket due to unconstrained thermal expansion of each component during normal conditions of transport. To assess this in the most conservative manner, the thermal solutions computed in Chapter 3 are surveyed for the following information.

- The radial temperature distribution in each of the fuel baskets at the location of peak center metal temperature.
- The highest and lowest mean temperatures of the canister shell for the hot environment condition.

- The inner and outer surface temperature of the overpack shell (inner shell, intermediate shells, neutron shield, and outer closure) at the location of highest and lowest surface temperature (which will produce the lowest mean temperature).

The thermal evaluation is performed in Chapter 3. Tables 3.4.17 and 3.4.18 present the resulting temperatures used in the deflection evaluation.

Using the temperature information in the above-mentioned tables, simplified thermoelastic solutions of equivalent axisymmetric problems are used to obtain conservative estimates of gap closures. The following procedure, which conservatively neglects axial variations in temperature distribution, is utilized.

1. Use the surface temperature information for the fuel basket to define a parabolic distribution in the fuel basket that bounds (from above) the actual temperature distribution. Using this result, generate a conservatively high estimate of the radial and axial growth of the different fuel baskets using classical closed form solutions for thermoelastic deformation in cylindrical bodies.
2. Use the temperatures obtained for the canister to predict an estimate of the radial and axial growth of the canister to check the canister-to-basket gaps.
3. Use the temperatures obtained for the canister to predict an estimate of the radial and axial growth of the canister to check the canister-to-overpack gaps.
4. Use the overpack surface temperatures to construct a logarithmic temperature distribution (characteristic of a thick walled cylinder) at the location used for canister thermal growth calculations; and use this distribution to predict an estimate of overpack radial and axial growth.
5. For given initial clearances, compute the operating clearances.

The results are summarized in the tables given below for normal conditions of transport.

THERMOELASTIC DISPLACEMENTS IN THE MPC AND OVERPACK UNDER HOT TEMPERATURE ENVIRONMENT CONDITION				
CANISTER - FUEL BASKET				
	Radial Direction (in.)		Axial Direction (in.)	
Unit	Initial Clearance	Final Gap	Initial Clearance	Final Gap
All PWR MPCs	0.1875	0.101	2.0	1.57
MPC-68	0.1875	0.104	2.0 (min)	1.586 (min)
CANISTER - OVERPACK				
	Radial Direction (in.)		Axial Direction (in.)	
Unit	Initial Clearance	Final Gap	Initial Clearance	Final Gap
All PWR MPCs	0.09375	0.058	0.625	0.422
MPC-68	0.09375	0.059	0.625	0.429

It can be verified by referring to the Design Drawings provided in Section 1.4 of this report, and the foregoing table, that the clearances between the MPC basket and canister structure, as well as those between the MPC shell and overpack inside surface, are sufficient to preclude a temperature induced interference from the thermal expansions listed above.

It is concluded that the HI-STAR 100 package meets the requirement that there be no restraint of free thermal expansion in any of the constituent components (i.e, the fuel basket, the enclosure vessel, and the overpack structure).

2.6.1.3 Stress Calculations

In this subsection, the normal conditions of transport associated with the thermal environment designated as "Heat" are considered. The stresses due to the combined effect of pressure, mechanical loads, and thermal gradient are evaluated. Within this subsection, the effects of fatigue and structure elastic/plastic stability under compression and lateral loading are also considered. Included in the subsection is a complete description of the finite element models developed to assess package performance under various loads. A two-dimensional finite element model of the fuel basket and the MPC enclosure shell is developed to evaluate the effect of pressure, radial temperature gradients and lateral deceleration induced inertia loads. A three-dimensional model of the overpack is also developed in this section to assess performance of the overpack under all load cases. Since both of

these finite element models are used again in Section 2.7, where hypothetical accident conditions of transport are examined, the explanation of the features of the model is presented herein in a general manner. Included in this description of the features of the model is a discussion of the loads applied, how they are chosen, and the methodology used to insure satisfaction of equilibrium. Where the loads, assumptions, geometry, etc. are common to both normal conditions of transport analyses and to hypothetical accident conditions of transport, the detailed description is presented in this section. Where the descriptions and discussions are relevant only for the hypothetical accident condition of transport, the detailed descriptions required for full understanding of the analysis are presented in Section 2.7.

This subsection presents the methodology for calculation of the stresses in the different components of the HI-STAR 100 Package from the load cases assembled in Section 2.1. Where the results are finite element based the methodology and the model is described in detail in this section. Results of finite element stress analyses are used for the comparison with allowable stresses performed in Subsection 2.6.1.4. Loading cases for the MPC fuel basket, the MPC enclosure vessel, and the HI-STAR 100 storage overpack are listed in Tables 2.1.6 through 2.1.8, respectively, for normal conditions of transport. An abbreviated description of each of the analyses is presented in the body of the chapter.

In general, as required by Regulatory Guide 7.9, the comparison of the calculated stresses with their corresponding allowables is presented in Subsection 2.6.1.4. However, for clarity in the narrative in this subsection (2.6.1.3), unnumbered summary tables are presented within the text. The key stress comparisons are subsequently reproduced in numbered tables in Subsection 2.6.1.4 to provide strict compliance with Regulatory Guide 7.9.

For all stress evaluations, the allowable stresses and stress intensities for the various HI-STAR 100 System components are based on bounding high metal temperatures to provide additional conservatism (Table 2.1.21 for the MPC basket and shell, for example). Elastic behavior is assumed for all stress analyses. Elastic analysis is based on the assumption of a linear relationship between stress and strain.

In Section 2.7, the same analytical models described here for normal conditions of transport are used to assess package performance under the hypothetical accident conditions. Therefore, the description of the models provided below is also applicable to the analysis performed in Section 2.7 except as previously noted.

In addition to the loading cases germane to stress evaluations mentioned above, cases pertaining to the elastic stability of the overpack are also considered.

The specific finite element models and component calculations described and reported in this subsection are:

1. MPC stress and stability calculations
2. HI-STAR 100 overpack stress and stability calculations

MPC stress and elastic stability analyses are considered in Subsection 2.6.1.3.1 wherein load cases from Tables 2.1.6 and 2.1.7 appropriate to normal conditions of transport are considered. The following analyses for the MPC are performed:

- a. Finite element analysis of the MPC fuel basket and MPC helium retention shell under lateral loads from handling loads during normal transport.
- b. Finite element and analytical analysis of the helium retention vessel (enclosure vessel) as an ASME Code pressure vessel.
- c. Analysis of the fuel support spacers under longitudinal inertia compression load appropriate to normal conditions of transport.
- d. Elastic stability and yielding of the MPC enclosure shell under axial and lateral loads arising from normal handling and external pressure.

Overpack stress and elastic stability analyses are considered in Subsection 2.6.1.3.2. Load cases from Table 2.1.8 are considered. The following analyses are performed to establish the structural adequacy of the overpack:

- a. Three-dimensional finite element analysis of the overpack subjected to load cases listed in Table 2.1.8 for normal conditions of transport.
- b. Consideration of fabrication stresses.
- c. Structural analysis of the closure bolting for normal condition of transport.
- d. Stress Analysis of overpack enclosure shell and return.

2.6.1.3.1 MPC Stress Calculations

The structural function of the MPC in the transport mode is stated in Section 2.1. The calculations presented here demonstrate the ability of the MPC to perform its structural function. Analyses are performed for each of the MPC designs. The following subsections describe the model, individual loads, load combinations, and analysis procedures applicable to the MPC.

2.6.1.3.1.1 Analysis of Load Cases F2 (Table 2.1.6) and E2, and E4 (Table 2.1.7)

The load cases considered herein pertain to lateral loading on the MPC components, namely the fuel basket and the enclosure vessel. For this purpose, a finite element model of the MPC is necessary. During normal conditions of transport, a bounding handling load is simulated by applying a deceleration induced inertia load from a 1' drop with impact limiters installed. During hypothetical accident conditions (see Section 2.7), the MPC is subject to the design basis decelerations from a 30' drop. The finite element model used to simulate both load cases is described here and is used for analyses for normal conditions of transport and later in Section 2.7 is used for the hypothetical accident analyses.

- Description of Finite Element Models of the MPCs under Lateral Loading

A finite element model of each MPC is used to assess the effects of normal and accident conditions of transport. The models are constructed using ANSYS [2.6.4], and they are identical to the models used in HI-STAR's 10CFR72 submittal under Docket Number 72-1008. The following model description is common to all MPCs.

The MPC structural model is two-dimensional. It represents a one-inch long cross section of the fuel basket and the MPC canister.

The MPC model includes the fuel basket, the basket support structures, and the MPC shell. A basket support is defined as any structural member that is welded to the inside surface of the MPC shell. A portion of the overpack inner surface is modeled to provide the correct boundary conditions for the MPC. Figures 2.6.3 through 2.6.11 show the MPC models.

The fuel basket support structure shown in the figures here, and in the design drawings in Section 1.4, is a multi-plate structure consisting of solid shims or support members having two separate compressive load supporting members. For conservatism in the finite element model some dual path compression members (i.e., "V" angles) are simulated as single columns. Therefore, the calculated stress intensities in the fuel basket supports from the finite element solution are conservatively overestimated in some locations.

The ANSYS model is not intended to resolve the detailed stress distributions in weld areas. Individual welds are not included in the finite element model.

No credit is taken for any load support offered by the ~~Boral~~ *neutron absorber* panels, sheathing, and the optional aluminum heat conduction elements. Therefore, these so-called non-structural members are not represented in the model. The bounding MPC weight used, however, does include the mass contributions of these non-structural components.

The model is built using five ANSYS element types: BEAM3, PLANE82, CONTAC12, CONTAC26, and COMBIN14. The fuel basket and MPC shell are modeled entirely with two-dimensional beam elements (BEAM3). Plate-type basket supports are also modeled with BEAM3 elements. Eight-noded plane elements (PLANE82) are used for the solid-type basket supports. The gaps between the fuel basket and the basket supports are represented by two-dimensional point-to-point contact elements (CONTAC12). Contact between the MPC shell and the overpack is modeled using two-dimensional point-to-ground contact elements (CONTAC26) with an appropriate clearance gap.

For each MPC type, three variations of the finite element model were prepared. The basic model includes only the fuel basket and the enclosure shell (Figures 2.6.3 through 2.6.5 show representative configurations) and is used only to study the free thermal expansion due to the temperature field developed in the system. The other two models include a representation of the overpack and are used for the two drop cases considered. Two orientations of the deceleration vector are considered. The 0-degree drop model includes the overpack-MPC interface in the basket

orientation illustrated in Figures 2.6.6 through 2.6.8. The 45-degree drop model represents the overpack interface with the basket oriented in the manner shown in Figures 2.6.9 through 2.6.11. Table 2.6.1 lists the element types and number of elements for all three models for all fuel storage MPC types.

A contact surface is provided in the models used for drop analyses to represent the overpack inner shell. As the MPC makes contact with the overpack, the MPC shell deforms to mate with the inside surface of the inner shell. The nodes that define the elements representing the fuel basket and the MPC shell are located along the centerline of the plate material. As a result, the line of nodes that forms the perimeter of the MPC shell is inset from the real boundary by a distance that is equal to half of the shell thickness. In order to maintain the specified MPC shell/overpack gap dimension, the radius of the overpack inner shell is decreased by an equal amount in the model.

Contact is simulated using two-dimensional point-to-ground elements (CONTAC26). The surface is tangent to the MPC shell at the initial point of impact and extends approximately 135 degrees on both sides. This is sufficient to capture the full extent of contact between the MPC and the overpack.

The three discrete components of the HI-STAR System, namely the fuel basket, the MPC shell, and the overpack, are engineered with small diametral clearances that are large enough to permit unconstrained thermal expansion of the three components under the rated (maximum) heat duty condition. A small diametral gap under ambient conditions is also necessary to assemble the system without physical interference between the contiguous surfaces of the three components. The required gap to ensure unrestricted thermal expansion between the basket and the MPC shell is less than 0.1 inch. This gap, too, will decrease under maximum heat load conditions, but will introduce a physical nonlinearity in the structural events involving lateral loadings (such as side drop of the system) under ambient conditions. It is evident from the system design drawings that the fuel basket, which is non-radially symmetric, is in proximate contact with the MPC shell at a discrete number of locations along the circumferences. At these locations, the MPC shell, backed by the massive overpack weldment, provides a virtually rigid support line to the fuel basket during lateral drop events. Because the fuel basket, the MPC shell, and the overpack are all three-dimensional structural weldments, their inter-body clearances may be somewhat uneven at different azimuthal locations. As the lateral loading is increased, clearances close at the support locations, resulting in the activation of the support from the overpack.

The bending stresses in the basket and the MPC shell at low lateral loading levels, which are too small to close the support location clearances, are secondary stresses since further increase in the loading will activate the overpack's support action, mitigating further increase in the stress. Therefore, to compute primary stresses in the basket and the MPC shell under lateral drop events, the gaps should be assumed to be closed. However, for conservatism, it is assumed that an initial gap of 0.1875" exists, in the direction of the applied deceleration, at all support locations between the basket and the shell, and the diametral gap between the shell and the overpack at the support locations is 3/32". All stresses produced by the applied loading on this configuration are compared with primary stress levels even though the self-limiting stresses should be considered secondary in the strict definition of the ASME Code. Therefore, many of the reported safety factors for conditions of normal transport are conservative in that secondary stress allowables are ignored in the

computation of safety factors. Similarly, in Section 2.7, the safety factors reported for the hypothetical accident conditions will also be conservative since the secondary stress is contained in the result.

- Description of Individual Loads and Boundary Conditions Applied to the MPCs

The method of applying each individual load to the MPC model is described in this subsection. The individual loads and the load combinations are shown in Tables 2.1.6 and 2.1.7. As an example, a free-body diagram of the MPC-68 corresponding to each individual load is given in Figures 2.6.12 through 2.6.14. In the following discussion, reference to vertical and horizontal orientations is made. Vertical refers to the direction along the cask axis, and horizontal refers to a radial direction.

Quasi-static structural analysis methods are used. The effect of any dynamic load factors (DLFs) is included in the final evaluation of safety factors. All analyses are carried out using the design basis decelerations in Table 2.1.10.

The MPC models used for side drop evaluations are shown in Figures 2.6.6 through 2.6.11. In each model, the fuel basket and the enclosure vessel are constrained to move only in the direction that is parallel to the acceleration vector. The overpack inner shell, which is defined by three nodes needed to represent the contact surface, is fixed in all degrees of freedom. The fuel basket, enclosure vessel, and overpack inner shell are all connected at one location by linear springs (see Figure 2.6.6, for example).

(a) Accelerations (Load Case F2 (Table 2.1.6) and E2 (Table 2.1.7))

During a side impact event, the stored fuel is directly supported by the cell walls in the fuel basket. Depending on the orientation of the drop, 0 or 45 degrees (see Figures 2.1.3 and 2.1.4), either one or two walls support the fuel. The effect of deceleration on the fuel basket and canister metal structure is accounted for by amplifying the gravity field in the appropriate direction. In the finite element model this load is introduced by applying a uniformly distributed pressure over the full span of the supporting walls. Figure 2.6.15 shows the pressure load on a typical cell for both the 0 degree and the 45 degree drop cases. The magnitude of the pressure is determined by the weight of the fuel assembly (Table 1.2.13), the axial length of the fuel basket support structure, the width of the cell wall, and the impact acceleration. It is assumed that the load is evenly distributed along an axial length of basket equal to the fuel basket support structure. For example, the pressure applied to an impacted cell wall during a 0-degree side drop event is calculated as follows:

$$p = \frac{a_v W}{L \ell}$$

where:

p = pressure

a_v = ratio of the impact acceleration to the gravitational acceleration

- W = weight of a stored fuel assembly
- L = axial length of the fuel basket support structure
- t = width of a cell wall

For the case of a 45-degree side drop the pressure on any cell wall equals p (defined above) divided by the square root of two. Figures 2.6.13, 2.6.14, and 2.6.15 show the details of the fuel assembly pressure load on the fuel basket.

(b) Internal/External Pressure (Load Case E1 (Table 2.1.7))

Design internal pressure in the MPC model is applied by specifying pressure on the inside surface of the enclosure vessel. The magnitude of the internal pressure applied to the model is taken from Table 2.1.1.

For this load condition, the center of the fuel basket is fixed in all degrees of freedom.

(c) Temperature (Load Cases F1 (Table 2.1.6) and E4 (Table 2.1.7))

Temperature distributions are developed in Chapter 3 and applied as nodal temperatures to the finite element model of the MPC enclosure vessel (confinement boundary). Maximum design heat load has been used to develop the temperature distribution used to demonstrate compliance with ASME Code stress intensity levels. A plot of the applied temperature distribution as a function of radius is shown in Figure 2.6.1. Figure 2.6.12 shows the MPC-68 with the typical boundary conditions for all thermal and pressure load cases.

- Analysis Procedure

The analysis procedure for this set of load cases is as follows:

1. The stress intensity and deformation field due to the combined loads is determined by the finite element solution. Results are then subject to post-processing.
2. The results for each load combination are compared to allowables. The comparison with allowable values is made in Subsection 2.6.1.4.

2.6.1.3.1.2 Analysis of Load Cases E1.a and E1.c (Table 2.1.7)

Load Cases E1.a and E1.c pertain to the performance of the helium retention boundary structure (enclosure vessel) considered as an ASME Section III, Subsection NB pressure vessel.

Since the MPC shell is a pressure vessel, the classical Lamé's calculations should be performed to demonstrate the shell's performance as a pressure vessel. Note that dead load has an insignificant effect on this stress state. Calculations for the shell under internal pressure are performed initially. Subsequently, a finite element analysis on the entire helium retention boundary as a pressure vessel

subject to both internal pressure and temperature gradients is performed. Finally, confirmatory hand calculations are performed to gain confidence in the finite element predictions,

- **Lame's Solution for the MPC Shell**

The stress from internal pressure is found using classical formulas:

Define the following quantities:

P = pressure, r = MPC radius, and t = shell thickness.

Using classical thin shell theory, the circumferential stress, $\sigma_1 = Pr/t$, the axial stress $\sigma_2 = Pr/2t$, and the radial stress $\sigma_3 = -P$ are computed for both normal and accident internal pressures. The results are given in the following table:

Classical Shell Theory Results for Normal and Accident Internal Pressures				
Item	σ_1 (psi)	σ_2 (psi)	σ_3 (psi)	$\sigma_1 - \sigma_3$ (psi)
P= 100 psi	6,838	3,419	-100	6,938
P= 200 psi	13,677	6,838	-200	13,877

Table 2.1.21 provides the allowable membrane stress for Load Case E1 for Alloy X under normal conditions of transport. It is seen that a safety factor greater than 1.0 exists

$$FS = \frac{18.1 \text{ ksi}}{6.938 \text{ ksi}} = 2.6$$

Subsection 2.7.3.3.1 develops the corresponding safety factor for the case of accident pressure.

- **Finite Element Analysis (Load Case E1.a and E1.c of Table 2.1.7)**

Having performed the classical "thin shell under pressure" evaluation, a finite element analysis is performed where the interaction between the end closures and the MPC shell is rigorously modeled.

The MPC shell, the top lid, and the baseplate together form the helium retention boundary (enclosure vessel) for storage of spent nuclear fuel. In this section, the operating condition consisting of dead weight, internal pressure, and thermal effects for the normal heat condition of transport is evaluated. The top and bottom plates of the MPC enclosure vessel (EV) are modeled using plane axisymmetric elements, while the shell is modeled using the axisymmetric thin shell element. The thickness of the top lid varies in the MPC types and can be either a single thick lid, or two lids, welded around their common periphery; the minimum thickness top lid is modeled in the finite element analysis. As applicable, the results for the MPC top lid are modified to account for the fact that in the dual lid configuration, the two lids act independently under mechanical loading. The temperature distributions for all MPC constructions are nearly identical in magnitude and gradient. Temperature

differences across the thickness of both the baseplate and the top lid exist during HI-STAR 100's operations. There is also a thermal gradient from the center of the top lid and baseplate out to the shell wall. The metal temperature profile is essentially parabolic from the centerline of the MPC out to the MPC shell. There is also a parabolic temperature profile along the length of the MPC canister. Figure 2.6.20 shows a sketch of the confinement boundary structure with identifiers A-I (also called locating points) where temperature input data is used to represent a continuous temperature distribution for analysis purposes. The overall dimensions of the confinement boundary are also shown in the figure.

Section 3.4 provides the desired temperatures for thermal stress analysis of the helium retention boundary. From the tables (3.4.22 and 3.4.23), it is seen that the distribution from PWRs provides the largest temperature gradients in the baseplate (from centerline to outer edge) and in the shell (from the joint at the baseplate to the half-height of the cask). It will be shown later that stress intensities are greatest in these components of the vessel. Because of the intimate contact between the two lid plates when the MPC lid is a two-piece unit, there is no significant thermal discontinuity through the thickness; thermal stresses arising in the MPC top lid will be bounding when there is only a single lid. Therefore, for thermal stresses, results from the analysis

that considers the lid as a one-piece unit are used and are amplified to reflect the increase in stress in the dual lid configuration

Figure 2.6.21 shows details of the finite element model of the top lid (considered as a single piece), canister shell, and baseplate. The top lid is modeled with 40 axisymmetric quadrilateral elements; the weld connecting the lid to the shell is modeled by a single element solely to capture the effect of the top lid attachment to the canister offset from the middle surface of the top lid. The MPC canister is modeled by 50 axisymmetric shell elements, with 20 elements concentrated in a short length of shell appropriate to capture the so-called "bending boundary layer" at both the top and bottom ends of the canister. The remaining 10 shell elements model the MPC canister structure away from the shell ends in the region where stress gradients are lower (from the physics of the problem). The baseplate is modeled by 20 axisymmetric quadrilateral elements. Deformation compatibility at the connections is enforced at the top by the single weld element, and deformation and rotation compatibility at the bottom by additional shell elements between nodes 106-107 and 107-108.

The geometry of the model is listed below (terms are defined in Figure 2.6.21):

$H_t =$	9.5" (the minimum total thickness lid is assumed)
$R_L =$	0.5 x 67.25" (Nominal dimension used for calculation)
$L_{MPC} =$	190.5" (Nominal dimension used for calculation)
$t_s =$	0.5" (MPC drawing in Section 1.4)
$R_S =$	0.5 x 68.375" (Nominal radius)
$t_{BP} =$	2.5" (MPC drawing in Section 1.4)

$$\beta L = 2\sqrt{R_s t_s} \approx 12" \text{ (The bending boundary layer)}$$

Stress analyses are carried out for two cases as follows:

- a. internal pressure = 100 psi
- b. internal pressure = 100 psi, plus applied temperature field

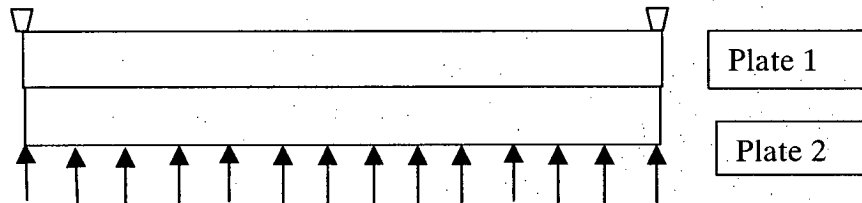
The dead weight of the top lid reduces the stresses due to pressure. For example, the equivalent pressure simulating the effect of the weight of the top lid is an external pressure of 3 psi, which reduces the pressure difference across the top lid to 97 psi. Thus, for conservatism, dead weight of the top lid is neglected to provide additional conservatism in the results. The dead weight of the baseplate, however, adds approximately 0.73 psi to the effective internal pressure acting on the base. The effect of dead weight is still insignificant compared to the 100 psi design pressure, and is therefore neglected. The thermal loading in the confinement vessel is obtained by developing a parabolic temperature profile to the entire length of the MPC canister and to the top lid and baseplate. The temperature data provided at locations A-I in Figures 2.6.20 and 2.6.21 are sufficient to establish the profiles. Through-thickness temperatures are assumed linearly interpolated between top and bottom surfaces of the top lid and baseplate. All material properties and expansion coefficients are considered to be temperature-dependent in the model.

Results for stress intensity are reported for the case of internal pressure alone and for the combined loading of pressure plus temperature (Load Case E1.c in Table 2.1.7). Tables 2.6.6 and 2.6.7 report results at the inside and outside surfaces of the top lid and baseplate at the centerline and at the extreme radius. Canister results are reported in the "bending boundary layer" and at a location near mid-length of the MPC canister. In the tables, the calculated value is the value from the finite element analysis, the categories are P_m = primary membrane; $P_L + P_b$ = local membrane plus primary bending; and $P_L + P_b + Q$ = primary plus secondary stress intensity. The allowable stress intensity value is obtained from the appropriate table in Section 2.1 for Level A conditions, and the safety factor SF is defined as the allowable strength divided by the calculated value. Allowable stresses for Alloy X are taken at 300° F, which bounds the normal heat condition of transport temperatures everywhere except at the mid-length position of the MPC shell (Location I in Figure 2.6.20) during the normal operation. At Location I, the allowable strength is taken at 400°F. The results given in Tables 2.6.6 and 2.6.7 demonstrate the ruggedness of the MPC as a confinement boundary. Since mechanically induced stresses in the top lid are increased when a dual lid configuration is considered, the stress results obtained from an analysis of a single top lid must be corrected to reflect the maximum stress state when a dual lid configuration is considered. The modifications required are based on the following logic:

Consider the case of a simply supported circular plate of thickness h under uniform lateral pressure "q". Classical strength of materials provides the solution for the maximum stress, which occurs at the center of the plate, in the form:

$$\sigma_s = 1.225q(a/h)^2 \quad \text{where } a \text{ is the radius of the plate and } h \text{ is the plate thickness.}$$

Now consider the MPC simply supported top lid as fabricated from two plates “1” and “2”, of thickness h_1 and h_2 , respectively, where the lower surface of plate 2 is subjected to the internal pressure “ q ”, the upper surface of plate 1 is the outer surface of the helium retention boundary, and the lower surface of plate 1 and the upper surface of plate 2 are in contact. The following sketch shows the dual lid configuration for the purposes of this discussion:



From classical plate theory, if it is assumed that the interface pressure between the two plates is uniform and that both plates deform to the same central deflection, then if

$$h_1 + h_2 = h, \text{ and if } h_2/h_1 = r$$

the following relations exist between the maximum stress in the two individual plates, σ_1 , σ_2 and the maximum stress σ_s in the single plate of thickness “ h ”:

$$\frac{\sigma_1}{\sigma_s} = \frac{(1+r)^2}{(1+r^3)} \qquad \frac{\sigma_2}{\sigma_s} = \frac{(1+r)^2}{(1+r^3)} r$$

Since the two lid thicknesses are the same in the dual lid configuration, $r = 1.0$ so that the stresses in plates 1 and 2 are both two times larger than the maximum stress computed for the single plate lid having the same total thickness. In Tables 2.6.6 and 2.6.7, bounding results for the dual lid configuration are reported by using these ratios at all locations in the top lid.

- Confirmatory Closed Form Solution

The results in Table 2.6.6 and 2.6.7 also show that the baseplate and the shell connection to the baseplate are the most highly stressed regions under the action of internal pressure. To confirm the finite element results, an alternate closed form solution is performed using classical plate and shell theory equations that are listed in or developed from the reference Timoshenko and Woinowsky-Krieger, Theory of Plate and Shells, McGraw Hill, Third Edition.

Assuming that the thick baseplate receives little support against rotation from the thin shell, the bending stress at the centerline is evaluated by considering a simply supported plate of radius a , and thickness h , subjected to lateral pressure p . The maximum bending stress is given by

$$\sigma = \frac{3(3+\nu)}{8} p \left(\frac{a}{h}\right)^2$$

where:

$$a = .5 \times 68.375''$$

$$h = 2.5''$$

$$\nu = 0.3 \text{ (Poisson's Ratio)}$$

$$p = 100 \text{ psi}$$

Calculating the stress in the plate gives $\sigma = 23,142$ psi.

Now consider the thin MPC shell ($t = 0.5''$) and first assume that the baseplate provides a clamped support to the shell. Under this condition, the bending stress in the thin shell at the connection to the plate is given as:

$$\sigma_{Bp} = 3p \frac{a}{t} \frac{(1-\nu/2)}{\sqrt{3}(1-\nu^2)^{1/2}} = 10,553 \text{ psi}$$

In addition to this stress, there is a component of stress in the shell due to the baseplate rotation that causes the shell to rotate. The joint rotation is essentially driven by the behavior of the baseplate as a simply supported plate; the shell offers little resistance because of the disparity in thickness and will essentially follow the rotation of the thick plate.

Using formulas from thin shell theory, the additional axial bending stress in the shell due to this rotation θ can be written in the form

$$\sigma_{B\theta} = 12 \beta D_s \frac{\theta}{t^2}$$

where

$$\theta = pa^3/8D(1+\nu) * \left(\frac{1}{1+\alpha}\right)$$

and

$$D = \frac{E h^3}{12(1-\nu^2)} \quad E = \text{plate Young's Modulus}$$

and

$$\alpha = \frac{2\beta at^3}{h^3(1+\nu)}$$

$$\beta^2 = \sqrt{3(1-\nu^2)}/at$$

$$D_s = \frac{Et^3}{12(1-\nu^2)}$$

Substituting the numerical values gives

$$\sigma_{B_} = 40,563 \text{ psi}$$

Note that the approximate solution is independent of the value chosen for Young's Modulus as long as the material properties for the plate and shell are the same.

Combining the two contributions to the shell bending stress gives the total extreme fiber stress in the longitudinal direction as 51,116 psi. Note that the same confirmatory solution can be obtained from Roark's Formulas for Stress and Strain, McGraw-Hill, 4th Edition, Table XIII. Case 30 in that text contains the solution for the bending moment at the intersection of a long cylinder and a flat plate due to internal pressures. Using the handbook formula, 53,090 psi is obtained.

The baseplate stress value, 23,142 psi, compares well with the finite element result 20,528 psi (Table 2.6.6). The shell joint stress, 51,116 psi, is greater than the finite element result (43,986 psi in Table 2.6.6). This is due to the local effects of the shell-to-baseplate connection offset. That is, the connection between shell and baseplate in the finite element model is at the surface of the baseplate, not at the middle surface of the baseplate. This offset will cause an additional bending moment that will reduce the rotation of the plate and hence, reduce the stress in the shell due to the rotation of the baseplate.

In summary, the approximate closed form solution confirms the accuracy of the finite element analysis in the MPC baseplate region.

2.6.1.3.1.3 Supplementary MPC Calculations

The MPC has been subject to extensive analysis in the companion HI-STAR 100 FSAR (storage) submittal (Docket Number 72-1008). For completeness, certain information from the FSAR has been repeated here and in Section 2.7 where the results are germane to normal conditions of transport and to hypothetical accident conditions of transport, respectively. Because of the different requirements for storage and transport submittals, some of the results presented here may not be directly

associated with a load case defined in Tables 2.1.6 and 2.1.7. Nevertheless, their inclusion here is warranted for completeness. In this subsection, results are summarized from these analyses that pertain to normal conditions of transport. In Section 2.7, additional results pertaining to the hypothetical accident conditions of transport are reported.

- Structural Analysis of the Fuel Support Spacers (Load Case F2)

Upper and lower fuel support spacers are utilized to position the active fuel region of the spent nuclear fuel within the poisoned region of the fuel basket. It is necessary to ensure that the spacers will continue to maintain their structural integrity during normal conditions of transport. Ensuring structural integrity implies that the spacer will not buckle under the maximum compressive load, and that the maximum compressive stress will not exceed the compressive strength of the spacer material (Alloy X). Detailed calculations demonstrate that large structural margins in the fuel spacers are available for the entire range of spacer lengths that may be used in HI-STAR 100 applications (for the various acceptable fuel types). The fuel spacers are shown to meet ASME Code Subsection NG stress limits (the spacers are not, however, required to be designed to any ASME Code, however). Standard Code design formulas are used to evaluate elastic stability limits. For normal conditions of transport (Level A Service Condition), a 10g deceleration load is applied and stress and stability issues are considered. The result is summarized below:

Fuel Spacers - Minimum Safety Factors (Load Cases F2)			
Item	Load (lb.)	Capacity (lb.)	Safety Factor
Axial Load - Level A	16,800	46,446	2.76

The safety factor is greater than 1.0, which demonstrates that the fuel spacers meet the requirements of Level A Service Conditions for the normal condition of transport.

The above result also represents a conservative minimum safety factor for the Trojan failed fuel can (FFC) spacer under normal conditions of transport. The reasons are (i) the FFC spacer has the same cross sectional area as the PWR lower fuel spacer and (ii) the FFC spacer supports less weight than the PWR lower fuel spacer. Whereas the PWR lower fuel spacer is designed and licensed to support the design fuel assembly weight of 1680 lb, the maximum weight that the FFC spacer supports is somewhat less than 1680 lb since the total weight of the Trojan FFC plus its contents, which includes the FFC spacer, is restricted to 1680 lb.

- MPC Shell Stability

The MPC shell is examined for elastic/plastic instability due to external pressure or compressive loads introduced as part of the load cases (design external pressure, normal transport). Each load component is examined separately. Design external pressure is applied to the outer surface of the enclosure vessel shell in the MPC model. The magnitude of the external pressure applied to the model is taken from Table 2.1.1. Analysis of the MPC under external pressure is performed using the methodology of ASME Code Case N-284 [2.1.8]. The following stability evaluations are performed for the MPC shell for normal transport conditions:

- a. Normal Transport Deceleration Load from 10CFR71.45(b).
- b. Design external pressure plus a 1g compressive dead load.

The following table summarizes the limiting result from the calculations:

MPC Shell - Elastic/Plastic Stability (ASME Code Case N-284) - Minimum Safety Factors			
Item	Value	Allowable	Safety Factor
Load Case 10CFR71.45(b) (Yield)	0.193	2.0	10.36
Load Case E1.b - Table 2.1.7 (Stability Interaction Curve)	0.832	1.0	1.20

Note that for the load case associated with the 10CFR71.45(b) requirement, the yield strength criteria in the Code Case N-284 method governs the “allowable” value. In this event, the safety factor 2.0, built into the Code Case, is included in the tabular result in order to obtain the actual safety factor with respect to the yield strength of the material.

The results demonstrate that the MPC shell meets the requirements of Code Case N-284. Note that the stability results presented above are very conservative. The stability analyses carried out for the MPC shell assumed no axial stiffening from the fuel basket supports that run the full length of the shell. An analysis that included the effect of the stiffening (and therefore, recognized the fact that instability will most likely occur between stiffeners) will give increased safety factors for Load Case E1.b.

2.6.1.3.2 Overpack Stress Calculations

The structural functions of the overpack are stated in Section 2.1. The analyses documented here demonstrate the ability of components of the HI-STAR 100 overpack to perform their structural functions under normal conditions of transport. Load cases applicable to the structural evaluation of the HI-STAR 100 overpack under these conditions are compiled in Table 2.1.8.

In this subsection, stresses and stress intensities in the HI-STAR 100 overpack due to the combined effects of thermal gradients, pressure, and mechanical loads are presented. The results are obtained from a series of finite element analyses on the complete overpack and separate analyses on overpack components.

2.6.1.3.2.1 Finite Element Analysis - Load Cases 1 to 4 in Table 2.1.8

Load Case 1 pertains to a demonstration of the containment boundary as an ASME “NB component under Design Pressure and Level A Service Condition thermal loading. Other cases pertain to handling inertia loads imposed during normal conditions of transport and an extreme environmental condition. To analyze these load cases, a suitable finite element model of the complete overpack is required. As noted earlier, since the identical finite element model is used in Section 2.7 to analyze

the hypothetical accident conditions of transport, the following discussion refers to both sets of analyses to avoid textual repetition.

- Description of Finite Element Model (Normal Conditions and Hypothetical Accident)

The purpose of the HI-STAR 100 overpack model is to calculate stresses and stress intensities resulting from the loadings defined in Subsection 2.1 and compiled into load cases in Table 2.1.8.

A three-dimensional finite element model of the HI-STAR 100 overpack is used to assess the effects of loads associated with normal conditions of transport. The same finite element model is used in Section 2.7 to evaluate the effects of loading due to hypothetical accident scenarios. The overpack is a large structure subject to a variety of complex loads and boundary conditions. The finite element model developed for this analysis allows efficient determination of the stresses in this complex structure.

The finite element model of the overpack is constructed using ANSYS [2.6.4]. This model is duplicated in the HI-STAR 100 FSAR (10CFR72) submittal for storage.

For structural analysis purposes, the overpack is assumed to be symmetric about a diametral mid-plane. This assumption is reasonable because the purpose of the model is to investigate global stresses in the model. The model is not intended to resolve effects due to small penetrations that produce peak stresses (which are significant only in cyclic fatigue conditions).

Element plots of the model are shown in a series of figures (Figures 2.6.16 through 2.6.19C). Figure 2.6.16 shows an overall view of half of the overpack subject to detailed finite element analysis. The view is directed toward the internal cavity and shows the surface of symmetry. To enforce symmetry, displacements normal to the plane of symmetry at all nodes on the plane of symmetry are not permitted. Out-of-plane rotations at the nodes on the plane of symmetry are also set to zero. The basic building blocks of the finite element model are 20-node brick (SOLID95), 8-node brick (SOLID45), and 6-node tetrahedron elements (SOLID45). These are 3-D solid elements with 3 degrees of freedom at each node (three linear displacement degrees of freedom). Element densities are increased towards the top and bottom of the model in order to provide increased resolution of the stress fields in those regions.

The top flange/closure plate interface is modeled using linear spring elements (COMBIN14). The concentric seals are not modeled explicitly. The model is not intended to resolve the stress field around the grooves for the seals. The status of joint seal is ascertained by “compression springs” that simulate the O-ring gaskets. Contact between the overpack top flange and closure plate is verified by checking the status of these spring elements. If contact between the closure plate and top flange is maintained under an applied loading (indicated by a compressive load in the “compression springs”), then the integrity of the seal is determined to have been maintained under that load.

The overpack closure bolts are modeled with beam elements (BEAM4). The top of the beam elements represent the bolt head and are connected to the overpack closure plate. The bottom of the elements represents the threaded region of the bolt and is connected to nodes of elements representing the top flange. Torsional displacements of the bolts are suppressed to conform to the

degrees of freedom permitted at the nodes of the connecting solid elements.

The inner shell of the overpack is modeled with two solid element layers through the thickness of the shell.

Each of the lifting trunnions is modeled as three rigid beam elements (BEAM4) connected to the top forging. The beams extend from the forging and meet at a single node location. Trunnion stress analysis is documented in Subsection 2.5; the inclusion of the trunnion herein is solely to provide the appropriate offset for handling loads. The beam elements representing the trunnions are not shown on any of the figures describing the finite element model.

The neutron shield material is not a load bearing or supporting component in the finite element model. However, the weight of the neutron shield material must be included in the model in order to obtain the proper inertia loads. The neutron shield material is modeled with SOLID45 elements having a weight density that is specified in Subsection 2.3.2.1. In the model herein, the neutron shield material is included as an element set to ensure that proper accounting of total weight (and accompanying deceleration loads) occurs. Therefore, the neutron shield material must be assigned a Young's Modulus in the model. A value approximately equal to 1% of the Modulus of the steel load carrying components is assigned to the neutron shield material to insure that the neutron shield material serves as a load rather than a structural member in the model.

Figure 2.6.17 shows the finite element grid used for the bottom plate.

Figure 2.6.18 provides the details of the solid element grid for the top forging. Also shown in the figure are the line elements that represent the lid bolts. Since the lid is not shown in this figure, the upper part of the line elements is not attached to any node point.

Figure 2.6.19 shows a view from above of the overpack lid and details the element grid around the 180-degree periphery modeled.

Figure 2.6.19A shows the finite element grid for the inner shell and the five intermediate shells. The inner shell is modeled with two layers of solid elements; each of the five intermediate shells is modeled by a single layer of solid elements to capture a linear stress distribution through the thickness.

Figure 2.6.19B presents the solid element distribution modeling the Holtite-A material. As noted previously, the structural effect of this material is neglected; the elements are included in the model to insure a proper mass distribution for the different analyses.

Finally, Figure 2.6.19C shows the shell element grid used to model the enclosure shell. Thin shell elements are used to simulate all components of the enclosure shell.

It is recognized that the layered shells of the overpack (shown in Figures 2.6.16 and 2.6.19A) are connected to each other and to the inner shell only at their top and bottom extremities. The finite element model must allow for separation between the intermediate shells in the non-connected regions under certain loading. Likewise, the intermediate shells cannot interpenetrate each other or

the inner shell structure. To simulate these competing effects without making the model non-linear because of the introduction of contact elements, radial coupling of adjacent intermediate shell nodes is used in appropriate locations of the model. It is necessary to utilize physical reasoning to establish the regions where a nodal coupling is warranted because the shells cannot separate from each other. For example, radial coupling over two 60-degree spans serves to prevent interpenetration where it may occur during an impact simulation. Similarly, where physical reasoning indicates that a separation between the shell layers may occur, the nodes are left uncoupled. For example, when ovalization of the shells may occur under a specified loading, no coupling between shells is assumed. Figure 2.6.22 illustrates the nodal coupling pattern. The intermediate shell nodes that lie in the 60-degree sector between the top and bottom portions of the model remain uncoupled. The intermediate shells, in the uncoupled region, are free to separate from one another as the overpack cross section ovalizes during side impact. This modeling approach ensures that load transfer in a drop with significant lateral deceleration loads is modeled correctly. With respect to the overpack model, "bottom portion" refers to the 60-degree segment of the model closest to the point of impact. Conversely, "top portion" refers to the 60-degree sector farthest from the point of impact. This nodal coupling arrangement conservatively represents the structural behavior of the intermediate shells. In addition, no axial or circumferential nodal coupling has been used between adjacent intermediate shells. Thus, axial bending stiffness of the composite shell structure is conservatively underestimated. This underestimation of stiffness provides additional conservatism to the predicted values for safety factors.

The rotation trunnions present in the first seven HI-STAR 100 units (see Subsection 2.5) are conservatively neglected in the finite element models. Separate calculations, where applicable, are summarized later.

Elements at locations of welds in the modeled components are assumed to have complete connectivity in all directions. Material in the model located at positions where welds exist is assumed to have material properties identical to the base material.

To summarize, the total number of nodes and elements in the overpack model are 11265 and 8642, respectively. The elements used are SOLID45, SOLID95, BEAM4, SHELL63, and COMBIN14.

For all structural analyses, material properties are obtained from the appropriate tables in Section 2.3. Property data for temperatures that are not listed in the material property tables are obtained by linear interpolation. Property values are not extrapolated beyond the limits of the code for any structural analysis.

- Description of Individual Loads and Boundary Conditions

The method of applying each individual load to the overpack model is described in this subsection. The individual loads are defined in Subsection 2.1.2.1 and are listed in Table 2.1.8 for normal conditions of transport. A free-body diagram of the overpack corresponding to each individual load is given in Figures 2.1.5 through 2.1.14. The figures presented in Section 2.1 present a general description of the loading but are lacking in specific details concerning the extent of the area exposed to the load. Therefore, in this subsection, each of the applied loadings for the various cases considered is further discussed and additional details on the specific application of the loads are

provided. In the following discussion, reference to vertical and horizontal orientations is made. Vertical refers to the longitudinal direction along the cask axis, and horizontal refers to a lateral direction.

Quasi-static methods of structural analysis are used. The effects of any dynamic load factors (DLF) are discussed in the final evaluation of safety factors. The load combinations are formed from the solution of individual load cases

(a) Accelerations (Used to Form Load Cases 3 and 4 in Table 2.1.8)

Table 2.1.10 provides the bounding values of the accelerations used for design basis structural evaluation. The loading is imposed by amplifying the gravity vector by the design basis deceleration. The proper distribution of the body forces induced by the accelerations is internally consistent based on the mass distribution associated with the different components of the finite element model. How these acceleration induced loadings are put in equilibrium with reaction loads from the impact limiters is discussed in detail in a later section.

In the following, appropriate boundary conditions for analyses for load cases associated with normal conditions of transport (Table 2.1.8) are discussed. However, since the same finite element model is used to evaluate hypothetical accident conditions of transport (Table 2.1.9) in Section 2.7, boundary conditions for Section 2.7 analyses are discussed here, as well, in the ongoing interest of conciseness of the presentation.

Boundary conditions for the model are as follows:

- i. End drop - In an end drop, displacement fixities are applied to the model on a cross-section through the top flange that is normal to the drop direction. Figures 2.1.7 and 2.1.8 show the free-body diagram for these load events. No reactions or internal body forces are shown. Further discussion is provided in Section 2.7.
- ii. Side drop - In a side drop, the inertia loads are reacted by the impact limiters. The overpack is in equilibrium with essentially end pinned supports. Figure 2.1.9 shows the configuration for this case. Further elaboration is provided in Section 2.7.

(b) Loads on the Overpack from the MPC

Pressures are applied on the inner surfaces of the overpack model to represent loads from the MPC for the drop loads.

- i. End drop - For a bottom end drop (Load Case1, Hypothetical Accident, Table 2.1.9), the pressure load on the inside surface of the overpack bottom plate is assumed to be uniform and represents the load from the heaviest MPC (Figure 2.1.7). Note that this analysis conservatively assumes that the drop angle is not exactly 90° from the horizontal; attention is focussed on the overpack baseplate subject to the deceleration load from the heaviest MPC (applied as a uniform pressure) without the ameliorating effect of opposing distributed reaction from the

impacted surface.

The magnitude of the pressure is the weight of the heaviest fully loaded MPC divided by the area of the faces of the elements over which the pressure is applied. The weight of the heaviest fully loaded MPC is taken from the tables in Section 2.2, and is amplified by the design basis deceleration. Amplified loads from the MPC (weight times 60g acceleration) are applied as a pressure load to the entire inner surface of the bottom plate or the lid depending on the drop orientation. Note that for a top end drop, the MPC inertia loads act only on an outer annulus of the lid due to the raised surface deliberately introduced to act as a "landing" area for the MPC and reduce lid stress and deformation. By neglecting this raised annular area on the lid and applying the MPC load as a uniform pressure, stresses in the lid and the bolts are maximized. Further discussion is provided in Section 2.7.

- ii. Side drop - The shape and extent of the pressure distribution is determined from the results of the structural analysis of the MPC under similar orientations. In the MPC structural analysis, the extent of the support conditions of the MPC shell is determined with contact elements. In the analysis of the MPC under amplified inertia loads, the overpack is represented as a rigid circular surface. Based on results from the MPC evaluations, the loaded region is taken as 72 degrees (measured from the vertical). The MPC load on the overpack model is applied uniformly along the axial length of the inner surface of the model. Further discussion is provided in Section 2.7.
- iii. Oblique drop - Figures 2.1.10 and 2.1.11 show the balance loading applied for the oblique drop. A fixed node is defined away from the assumed impact point to insure that the package is in equilibrium under the applied loads. This drop orientation is only considered for the hypothetical accident evaluation. Therefore, a detailed discussion as to the methodology used to apply the loads and insure overall equilibrium is provided in Section 2.7 (specifically 2.7.1.3 and 2.7.1.4).

(c) Temperature (Used to Form Load Case 05 in Table 3.1.5)

Based on the results of the thermal evaluation for the normal hot environment presented in Chapter 3, a temperature distribution with a bounding gradient is applied to the overpack model. The purpose is to determine the stress intensities that develop in the overpack under the applied thermal load. A plot of the applied temperature distribution as a function of radius is shown in Figure 2.6.2.

The temperature distribution is applied to the ANSYS finite element model at discrete nodes using a parabolic curve fit of the computed distribution.

(d) Internal Pressure (Used to Form Load Cases 1 in Table 2.1.8)

Design internal pressure is applied to the overpack model. All interior overpack surfaces, including the inner shell, the bottom of the closure plate, and the top of the bottom plate are loaded with pressure. The magnitude of the internal pressure applied to the model is taken from Table 2.1.1.

Figure 2.1.5 shows the displacement constraints for this load case. Figure 2.6.23 is a finite element grid plot showing the surfaces where internal pressure is applied.

(e) External Pressure (Used to Form Load Case 2 in Table 2.1.8)

Design external pressure is applied to the overpack model. External pressure is applied to the model as a uniform pressure on the outer surface of the model. The magnitude of the external pressure applied to the model is taken from Table 2.1.1. Figure 2.1.6 shows the displacement constraints for this load case. External pressures are imposed in the same manner as shown in Figure 2.6.23 except that the surfaces and magnitude are different.

(f) Bolt Pre-load (Used in all load cases in Tables 2.1.8 and 2.1.9)

The overpack closure bolts are torqued to values predicted to preclude separation. This torque generates a pre-load in the bolts and stresses in the closure plate and top flange in the region adjacent to the bolts. The finite element representation of the bolt elements is shown in Figure 2.6.18. The initial preload of the bolts is applied to the overpack model by applying an initial strain to the beam elements representing the bolts. This induces a tensile stress in each of the bolts and a corresponding compression in the seals (represented by spring elements). This load case is present in every load combination.

(g) Fabrication stresses

Fabrication stresses are conservatively computed for the inner shell and all of the intermediate shells. Fabrication effects are not easily introduced into the finite element model unless compression-only contact elements are used. Since the fabrication stresses are circumferential secondary stresses in the shells, the incorporation of this load case is best accomplished outside of the finite element analysis. Therefore, there is no fabrication load case associated with the finite element analyses.

- Finite Element Analysis Solution Procedure

The analysis procedure is as follows:

1. The stress and deformation field due to each individual load is determined.
2. The results from each individual load case are combined in a postprocessor to create each load case. The load cases analyzed are listed in Table 2.1.8 for normal conditions of transport and in Table 2.1.9 for hypothetical accident conditions of transport.
3. The results for each load case are compared to allowables. The calculated values are compared with allowable values in Subsection 2.6.1.4 for normal conditions of transport and in an appropriate subsection of Section 2.7 for hypothetical accident conditions.

2.6.1.3.2.2 Fabrication Stress

The fabrication stresses originate from welding operations to affix the intermediate shells in position. As the molten weld metal solidifies, it shrinks pulling the two parts of the shells together. Adjacent points at the weld location will close together after welding by an amount " δ " which is a complex function of the root opening, shape of the bevel, type of weld process, etc. The residual stresses generated by the welding process are largely confined to the weld metal and the "heat affected zone". The ASME Code recognizes the presence of residual stresses in the welds, but does not require their calculation. The Code also seeks to minimize fabrication stresses in the welds through controlled weld procedures. Nevertheless, fabrication stresses cannot be eliminated completely.

The computation of fabrication stresses is carried out to comply with the provisions of Regulatory Guide 7.8, Article C-1.5. The Regulatory Guide requires that "Fabrication and installation stresses in evaluating transportation loadings should be consistent with the joining, forming, fitting, and aligning processes employed during the construction of casks...the phrase fabrication stresses includes the stresses caused by interference fits and the shrinkage of bonded lead shielding during solidification but does not include the residual stresses due to plate formation, welding, etc."

A literal interpretation of the above-cited Regulatory Guide text exempts the HI-STAR 100 designer from computing the stresses in the containment and intermediate shells due to welding. However, in the interest of conservatism, an upper bound, on the stresses induced in the containment shell and in the intermediate shells, is computed for the fabrication process.

To calculate the so-called fabrication stresses, it is recalled that in affixing the intermediate shells to the cask body, the design objective does not call for a definite radial surface pressure between the layers. Rather, the objective is to ensure that the shells are not loosely installed. Fortunately, extensive experience in fabricating multi-layer shells has been acquired by the industry over the past half-century. The technology that was developed and has matured for fabrication in older industries (such as oil and chemical) is used in HI-STAR 100 fabrication of the multi-layered shells. Mock-up tests on carbon steel coupons indicate that the total shrinkage after welding can range from 0.010" to 0.0625" for the bevel and fit-up geometry in the HI-STAR 100 design drawings. Therefore, the evaluations are carried out using the upper bound gap of 0.0625". To bound the computed stresses even further, the inter-layer friction coefficient is set equal to zero. It is intuitively apparent that increasing the friction increases the localized stresses near the "point of pull" (i.e., the weld) while mitigating the stresses elsewhere. Since the object is to maximize the distributed (membrane) stress, the friction coefficient is set equal to zero in the analysis.

A two-dimensional finite element analysis of the inner confinement shell and the five intermediate shells is performed to establish the level of fabrication circumferential stress developing during the assembly process. A 180-degree section through the overpack, consisting of six layers of metal, is modeled. The ANSYS finite element code is used to model the fabrication process; each layer is modeled using PLANE42 four node quadrilateral elements. Contact (or lack of contact) is modeled by CONTAC48 point-to-surface elements. Symmetry boundary conditions apply at 90 degrees, and radial movement of the inner node point of the confinement layer is restrained. At -90 degrees, the inner confinement layer is restrained while the remaining layers are subject to a prescribed circumferential displacement d to stretch the layer and to simulate the shrinkage caused by the weld

process. Although the actual fabrication process locates the longitudinal weld in each layer at different circumferential orientation, in the analytical simulations all layer welds are located together. This is acceptable for analysis since the stress of interest is the primary membrane component. Figure 2.6.24 shows a partial free body of a small section of one of the layers. Normal pressures p develop between each layer due to the welding process; shear stresses due to friction between the layers also develop since there is relative circumferential movement between the layers. Figure 2.6.25 shows a free body of the forces that develop on each layer.

The fabrication stress distribution is a function of the coefficient-of-friction between the layers. For a large enough coefficient-of-friction the effects of the assembly process are localized near the weld. Localized stresses are not considered as primary stresses. For a coefficient-of-friction = 0.0, the membrane hoop stress in the component shells is non-local in nature. Therefore, the fabrication stress computation conservatively considers only the case coefficient of friction (COF) = 0.0 since this will develop the largest in-plane primary membrane stress in each layer. The simulation is nonlinear in that each of the contact elements is checked for closure during increments of applied loading (the weld displacement).

The results from the analyses are summarized in the table below:

Fabrication Stresses in Overpack Shells - Minimum Safety Factors (Level A Service Condition at Assembly Temperature)			
Item	Value (ksi)	Allowable (ksi) (Note3)	Safety Factor
First Intermediate Shell (Note 1)	11.22	52.5	4.68
Fourth Intermediate Shell (Note 1)	7.79	52.5	6.74
Inner Shell Mid Plane (Note 2)	10.6	69.9	6.59
Inner Shell Outer Surface (Note 2)	16.27	69.9	4.30

Notes:

1. The fabrication stress is a tensile circumferential stress.
2. The fabrication stress is a compressive circumferential stress
3. Fabrication stresses are self-limiting and are therefore classified as "secondary" and are compared to 3 times the allowable membrane stress or stress intensity.

The above table leads to the conclusion that the maximum possible values for stresses resulting from HI-STAR 100 fabrication process are only a fraction of the relevant ASME Code limit.

2.6.1.3.2.3 Structural Analysis of Overpack Closure Bolting (Load Case 1 - Table 2.1.8)

Stresses are developed in the closure bolts due to pre-load, pressure loads, temperature loads, and accident loads. Closure bolts are explored in detail in Reference [2.6.3] prepared for analysis of shipping casks. The analysis herein of the overpack closure bolts under normal conditions of transport and for the hypothetical accident conditions uses the methodology and the procedures defined and explained in Reference [2.6.3]; the sole exception is that some of the formulas in the reference are modified to account for the annulus on the inner surface of the overpack closure lid; this annulus exists for the sole purpose of ensuring that the interface area between the MPC lid and the overpack top closure is a peripheral ring area rather than the entire surface area of the MPC lid. This feature ensures a reduction in the computed bolt stress.

The following combined load case is analyzed for normal conditions of transport:

Normal: Pressure, temperature, and pre-load loads are included (Load Case 1 in Table 2.1.8).

Reference [2.6.3] reports safety factors defined as the calculated stress combination divided by the allowable stress for the load combination. This definition of safety factor is the inverse of the definition consistently used in this SAR. In summarizing the closure bolt analyses performed, results are reported using the safety factor definition of allowable stress divided by calculated stress. The following result for closure lid bolting for normal conditions of transport are obtained:

Overpack Closure Bolt - Safety Factor (Load Case 1 in Table 2.1.8)	
Combined Load Case	Safety Factor on Bolt Tension
Average Tensile Stress	1.44
Combined Tension, Shear, Bending, and Torsion	1.57

It is seen from the above table that the safety factor is greater than 1.0 as required. Note that the magnitude of the safety factors reflect the large preload required for successful performance of the bolts under a hypothetical accident drop event where the demand is more severe.

2.6.1.3.2.4 Stress Analysis of Overpack Enclosure Shell

The overpack enclosure shell and the overpack enclosure return are examined for structural integrity under a bounding internal pressure. Flat beam strips of unit width are employed to simulate the performance of the flat panels and the flat plate return section (see drawings in Subsection 1.4). It is shown that large safety factors exist against overstress due to an internal pressure developing from off-gassing of the neutron absorber material. The minimum safety factors are summarized below:

Location	Calculated Stress (ksi)	Allowable Stress (ksi)	Safety Factor
Enclosure Shell Return (bottom)	2.56	26.3	10.2
Enclosure Shell Return (top)	3.42	26.3	7.68
Enclosure Shell Flat Panels	5.58	26.3	4.71
Weld Shear	0.63	10.52	16.7

2.6.1.3.3 Fatigue Considerations

Regulatory Guide 2.9 requires consideration of fatigue due to cyclic loading during normal conditions of transport. Considerations of fatigue associated with long-term exposure to vibratory motions associated with normal conditions of transport are considered below where individual components of the package are assessed for the potential for fatigue.

- Overpack and MPC Fatigue Considerations

The temperature and pressure cycles within the MPC and the inner shell of the overpack are entirely governed by the mechanical and thermal-hydraulic conditions presented by the fuel. The external surfaces of the overpack, however, are in direct contact with the ambient environment. The considerations of cyclic fatigue due to temperature and pressure cycling of the HI-STAR 100 System, therefore, must focus on different locations depending on the source of the cyclic stress.

As shown in the following, the overpack and the MPCs in the HI-STAR 100 System do not require a detailed fatigue analysis because all applicable loadings are well within the range that permits exemption from fatigue analysis per the provisions of Section III of the ASME Code. Paragraph NB-3222.4 (d) of Section III of the ASME Code provides five criteria that are strictly material and design condition dependent to determine whether a component can be exempted from a detailed fatigue analysis. The sixth criterion is applicable only when dissimilar materials are involved, which is not the case in the HI-STAR 100 System.

The Design Fatigue curves for the overpack and MPC materials are given in Appendix I of Section III of the ASME Code. Each of the five criteria is considered in the following:

- Atmospheric to Service Pressure Cycle

The number of permissible cycles, n , is bounded by $f(3S_m)$, where $f(x)$ means the number of cycles from the appropriate fatigue curve at stress amplitude of x psi. In other words

$$n < f(3S_m)$$

From Tables 2.1.11 through 2.1.20 for normal conditions, and the fatigue curves, the number of permissible cycles is

n (overpack) ≤ 1600 ($3S_m = 68,700$ psi) (Figure I.9-1 of ASME Appendix I)
 n (MPC) $\leq 40,000$ ($3S_m = 46,200$ psi) (Figure I.9-2 of ASME Appendix I)

The MPC, which is an all-welded component, is unlikely to undergo more than one cycle, indicating that a huge margin of safety with respect to this criterion exists. The overpack, however, is potentially subject to multiple uses. However, 1000 pressurizations in the 40-year life of the overpack is an upper bound estimate. In conclusion, the projected pressurizations of the HI-STAR components do not warrant a usage factor evaluation.

ii. Normal Service Pressure Fluctuation

Fluctuations in the service pressure during normal operation of a component are considered if the total pressure excursion δ_p exceeds Δ_p .

where

$$\Delta_p = \text{Design pressure} * S / (3S_m)$$

$$S = \text{Value of } S_a \text{ for one million cycles}$$

Using the above mentioned tables and appropriate fatigue curves,

$$(\Delta p)_{\text{overpack}} = \frac{(100)(13000)}{(3)(22,900)} = 18.9 \text{ psi}$$

$$(\Delta p)_{\text{MPC}} = \frac{(100)(26000)}{(3)(16000)} = 54.2 \text{ psi}$$

During normal operation the pressure fields in the MPC and the overpack are steady state. Therefore, normal pressure fluctuations are negligibly small. Normal service pressure oscillations do not warrant a fatigue usage factor evaluation.

iii. Temperature Difference - Startup and Shutdown

Fatigue analysis is not required if the temperature difference ΔT between any two adjacent points on the component during normal service does not exceed $S_a / 2E\alpha$, where S_a is the cyclic stress amplitude for the specified number of startup and shutdown cycles. E and α are the Young's Modulus and instantaneous coefficients of thermal expansion (at the service temperature). Assuming 1000 startup and shutdown cycles, Tables 2.3.1 and 2.3.4 and the appropriate ASME fatigue curves in Appendix I or Section III of the ASME Code give:

$$(\Delta T)_{\text{overpack}} = \frac{90,000}{(2)(26.1)(6.98)} = 247^{\circ} \text{F}$$

$$(\Delta T)_{\text{MPC}} = \frac{130,000}{(2)(25)(9.69)} = 268^{\circ} \text{F}$$

There are no locations on either the overpack or MPC where ΔT between any two adjacent points approach these calculated temperatures. As reported in Tables 3.4.16-18, the maximum ΔT that occurs between two components, the MPC shell and the basket periphery, is only 115 degrees F. Therefore, it is evident this temperature criterion is satisfied for 1,000 startup and shutdown cycles.

iv. Temperature Difference - Normal Service

Significant temperature fluctuations that require consideration in this criterion are those in which the range of temperature difference between any two adjacent points under normal service conditions is less than $S/2E\alpha$ where S corresponds to 10^6 cycles. Substituting, gives

$$(\Delta T)_{\text{MPC}} = \frac{26,000}{(2)(25)(9.69)} = 53.7^{\circ} \text{F}$$

$$(\Delta T)_{\text{overpack}} = \frac{13,000}{(2)(26.1)(6.98)} = 35.7^{\circ} \text{F}$$

During normal operation, the temperature fields in the MPC and the overpack are steady state. Therefore, normal temperature fluctuations are negligibly small. Normal temperature fluctuations do not warrant a fatigue usage factor evaluation.

v. Mechanical Loads

Mechanical loadings of appreciable cycling occur in the HI-STAR 100 System only during transportation. The stress cycling under transportation conditions is considered significant if the stress amplitude is greater than S_a corresponding to 10^6 cycles. It, therefore, follows that the stress limits that exempt the overpack and MPC are 13,000 psi and 26,000 psi, respectively.

From Subsection 2.5.2.1, g-loads typically associated with rail transport will produce stress levels in the MPC and overpack which are a small fraction of the above limits. Therefore, no potential for fatigue expenditure in the MPC and overpack materials is found to exist under transportation conditions.

In conclusion, the overpack and the MPC do not require fatigue evaluation under the exemption criteria of the ASME Code.

- Fatigue Analysis of Closure Bolts:

The maximum tensile stress developed in the overpack closure bolts during normal operating conditions is shown by analyses not to exceed 93.0 ksi. The alternating stress in the bolt is equal to 1/2 of the maximum stress due to normal conditions, or 46.5 ksi. The design service temperature for the bolts per Table 2.1.2 is 350 degrees F. Per Table 2.3.5, the Young's Modulus at 350 degrees F is 27,000 ksi. Therefore, the effective stress intensity amplitude for calculating usage factor using

$$S_a = \frac{(46.5)(4)(30e+06)}{27.7e+06} \\ = 201.4 \text{ ksi}$$

Figure I-9.4 (ASME Code, Appendices) is (ratioing the modulus used in the figure to the modulus used here):

Using Figure I-9.4 (NB, loc. cit), the permissible number of cycles is 200.

This result indicates the main closure bolts should *not be torqued and untorqued more than 200 times. After 200 loading cycles, they must be replaced.*

The total shear area of the overpack closure bolt threads is $A_v = 9.528 \text{ in}^2$. Therefore, the shear stress in the top closure bolt threads is, (use the limiting bolt load for normal operation and the tensile stress area of a bolt = 1.680 in^2).

$$\sigma_v = \frac{93.0 \text{ ksi} \times 1.68 \text{ in}^2}{9.528 \text{ in}^2} = 16.4 \text{ ksi}$$

The shear stress developed in the threads of the overpack closure bolts is significantly less than the stress developed in the bolt. Therefore, fatigue of the overpack closure bolts is not controlled by shear stress in the bolt threads.

- Fatigue Considerations for Top Flange Closure Bolt Threads:

The shear area of the main flange closure bolt threads is 12.371 in^2 . Therefore, the shear stress in the flange threads under the limit load on the bolt is:

$$\sigma_v = \frac{93.0 \text{ ksi} \times 1.68 \text{ in}^2}{12.928 \text{ in}^2} = 12.6 \text{ ksi}$$

The primary membrane stress in the main flange threads is equal to twice the maximum shear stress, or 21.1 ksi. The alternating stress in the threads, S_a , is equal to 1/2 of the total stress range, or 10.56 ksi. At 400 degrees F design temperature (per Table 2.1.2) the Young's Modulus (Table 2.3.4) is 26.1×10^6 psi.

The effective stress amplitude accounting for the fatigue strength reduction and Young's Modulus effects is given by

$$S_a = \frac{(12.6)(4)(30)}{26.1} = 57.9 \text{ ksi}$$

Using Figure I-9.4 (of NB, loc. cit), the allowable number of cycles is equal to 1,800.

Therefore, the *maximum service life of the main flange threads is 1,800 cycles* of torquing and untorquing of the overpack closure system.

- MPC Fatigue Analysis

The maximum primary and secondary alternating stress range for normal transport conditions is conservatively assumed to be equal to the allowable alternating stress range of $0.5 \times 40,000$ psi. Conservatively using a Young's Modulus of 25×10^6 psi for the fatigue evaluation, yields

$$S = 20,000 \text{ psi} \times \frac{28.3 \times 10^6 \text{ psi}}{25 \times 10^6 \text{ psi}} = 22,640 \text{ psi}$$

Cyclic life is in excess of 1×10^6 cycles per Figure I-9.2.1 of Appendix I of the ASME Code.

- Satisfaction of Regulatory Guide 7.6 Commitment

The minimum alternating stress range, S_a , at 10 cycles from all appropriate fatigue curves is 600 ksi. All primary stresses under any of the analyses performed in this SAR under the required load combinations are shown to lead to stress intensities that are less than the ultimate strength of the containment vessel material (70 ksi). Fabrication stresses are conservatively evaluated and are summarized in Subsection 2.6.1.3.2.2. Maximum fabrication stress intensities are less than 17 ksi. Conservatively assuming a stress concentration of 4 regardless of specific location produces a stress intensity range below $4 \times (70 + 17) = 348$ ksi (< 600 ksi). Therefore, satisfaction of the Regulatory Guide 7.6 commitment is assured.

2.6.1.4 Comparison with Allowable Stresses

Consistent with the formatting guidelines of Regulatory Guide 7.9, calculated stresses and stress intensities from the finite element analyses are compared with the allowable stresses and stress intensities defined in Subsection 2.1 (Tables 2.1.11 through 2.1.21) as applicable for conditions of normal transport. The results of these comparisons are presented in the form of factors of safety (SF) defined as:

$$SF = \frac{\text{Allowable Stress}}{\text{Calculated Stress}}$$

Safety factors associated components identified as lifting and tie-down devices have been presented in Section 2.5 as required by Regulatory Guide 7.9.

Major conservatisms are inherent in the finite element models for both the MPC fuel basket and the enclosure vessel, and for the HI-STAR 100 overpack. These conservatisms are elucidated here with additional discussion as needed later in the text associated with each particular issue.

Conservative Assumptions in Finite Element Analyses and Evaluation of Safety Factors

1. Comparison with allowable stresses or stress intensities is made using the design temperature of the component rather than the actual operating temperature existing in the metal at that location. As an example, all comparisons with allowables for the Alloy X fuel basket material uses the allowable strength at 725 degrees F (Table 2.1.21). Under the normal heat conditions of transport, temperatures near the periphery of the fuel basket are below 450 degrees F. High stresses in the fuel basket generally occur at the basket periphery. From Table 2.1.19, the allowable stresses for primary membrane plus bending at the two temperatures are compared to evolve the additional margin in the computed safety factor as $27.2/23.1 = 1.18$. Therefore, the reported safety factors from the analysis have at least an additional 18% hidden component from this effect. Similar hidden margins from this kind of simplification arise in the various components of the overpack. Depending on the material, these hidden margins, which increase the reported safety factor, may be large or small. From Figures 3.4.17 and 3.4.18 in Chapter 3, it is concluded that the normal heat condition of transport maximum inner shell temperature is less than 300 degrees F. The allowable stresses are uniformly assumed at 400 degrees F per Table 2.1.21. From Table 2.1.11, the additional hidden safety factor multiplier is computed as $35/34.4 = 1.02$. In the inner shell of the overpack, the increase in the reported safety factor from this effect is only 2% for normal conditions of transport.
2. Comparisons with primary stress allowables are made with secondary stresses included. This has an adverse effect on the reported safety factor, especially in areas near discontinuities.
3. In the modeling of the HI-STAR 100 overpack, the full structural connectivity of the intermediate shells and the inner containment shell is not included in the finite element model in order to maintain the linear elastic analysis methodology. The neglect of such interaction means that the overall bending stiffness of the overpack is underestimated; this leads to over-prediction of stresses and consequent adverse effects on reported safety factors.
4. In the modeling of the MPC fuel basket, the local reinforcement of the fuel basket panel from the fillet welds is neglected. The increase in the section modulus at the weld location is ignored leading to a decrease in stiffness of the basket panel. Consequently, under mechanical loading, the stress state is overestimated at the basket panel connection.

2.6.1.4.1 MPC Fuel Basket and Enclosure Vessel

It is recalled that the stress analyses have been performed for the load cases applicable to normal conditions of transport as assembled in Tables 2.1.6 and 2.1.7 for the fuel basket and the enclosure vessel, respectively. Detailed analyses, including finite element model details and the necessary explanations to collate and interpret the voluminous numerical results have been archived. A compendium of finite element results for the fuel basket and enclosure vessel for each load case associated with normal conditions of transport has been developed. Tables 2.6.6 and 2.6.7 summarize results obtained from the analyses (for all baskets) of Load Cases E1.a and E1.c defined in Table 2.1.7. Table 2.6.8 contains a synopsis of all safety factors obtained from the results. To further facilitate perusal of results, another level of summarization is performed in Tables 2.6.2 and 2.6.3 where the global minima of safety factor for each load case are presented. Finally, miscellaneous safety factors associated with the fuel basket and the MPC enclosure vessel are reported in Table 2.6.10.

The following element of information is relevant in ascertaining the safety factors under the various load cases presented in the tables.

- In the interest of simplification of presentation and conservatism, the total stress intensities under mechanical loading are considered to be of the primary genre' even though, strictly speaking, a portion can be categorized as secondary (that have much higher stress limits).

A perusal of the results for Tables 2.6.2 and 2.6.3 under different load combinations for the fuel basket and the enclosure vessel reveals that all factors of safety are above 1.0. The relatively modest factor of safety for the fuel basket under side drop events (Load Case F2.a and F2.b) in Table 2.6.2 warrants further explanation.

The wall thickness of the storage cells, which is by far the most significant variable in the fuel basket's structural strength, is significantly greater in the HI-STAR 100 MPCs than in comparable fuel baskets licensed in the past. For example, the cell wall thickness in the TN-32 basket (Docket No. 72-1021; M-56), is 0.1 inch and that in the NAC-STC basket (Docket No. 71-7235) is 0.048 inch. In contrast, the cell wall thickness in the MPC-68 is 0.25 inch. In spite of their relatively high flexural rigidities, computed margins in the HI-STAR 100 fuel baskets are rather modest. This is because of some conservative assumptions in the analysis that lead to an overstatement of the state of stress in the fuel basket. For example:

- i. The section properties of longitudinal fillet welds that attach contiguous cell walls to each other are completely neglected in the finite element model (Figure 2.6.15). The fillet welds strengthen the cell wall section modulus at the very locations where maximum stresses develop.

- ii. The radial gaps at the fuel basket-MPC shell and at the MPC shell-overpack interface are explicitly modeled. As the applied loading is incrementally increased, the MPC shell and fuel basket deform until a "rigid" backing surface of the overpack is contacted, making further unlimited deformation under lateral loading impossible. Therefore, some portion of the fuel basket and enclosure vessel (EV) stress has the characteristics of secondary stresses (which by definition, are self-limited by deformation in the structure to achieve compatibility). For conservativeness in the incremental analysis, no distinction between deformation controlled (secondary) stress and load controlled (primary) stress in the stress categorization is made. All stresses, regardless of their origin, are considered as primary stresses. Such a conservative interpretation of the Code has a direct (adverse) effect on the computed safety factors.

The above remarks can be illustrated simply by a simple closed-form bounding calculation. If all deformation necessary to close the gaps is eliminated from consideration, then the capacity of the fuel basket cell wall under loads which induce primary bending stress can be ascertained by considering a clamped beam (cell wall) subject to a lateral pressure representing the amplified weight of fuel assembly plus self-weight of the cell wall (e.g., see Figure 2.6.15).

Using the cell wall thickness and an appropriate unsupported length for the MPC-68, for example, the fixed edge bending stress is computed as 238.22 psi (using the actual fuel weights, cell wall weights, cell wall thickness and unsupported length). This implies a safety factor of 5.704 for a Level A event (for a 17g deceleration, $SF = 23,100 / (238.22 \times 17) = 5.704$) where the allowable bending stress intensity for Alloy X at 725 degrees F (Table 2.1.21) has been used. The above simple calculation demonstrates that the inherent safety margin under accident loading is considerably greater than is implied by the result in Table 2.6.8 ($SF=2.42$) for the MPC-68 and 0-degree drop orientation. Similar conclusions can be reached for other MPCs by performing scoping calculations in a similar manner.

- iii. The SNF inertia loading on the cell panels is simulated by a uniform pressure, which is a most conservative approach for incorporating the SNF/cell wall structure interaction.

The above assumptions all act to depress the computed values of factors of safety in the fuel basket finite element analysis and render conservative results.

The reported values do not include the effect of dynamic load amplification. Calculations show that, for the duration of impact and the predominant natural frequency of the basket panels under lateral hypothetical accident conditions, the dynamic load factors (DLF) are bounded by 1.05. It is expected that for the normal condition of transport 1' drop, the amplification would be reduced further.

Table 2.6.8 does not report the safety factors associated with Load Case F1 in Table 2.1.6 where it is shown that secondary stresses due to the thermal gradients are below the allowable secondary stress intensity limits. A representative stress intensity level arising from fuel basket thermal gradients is

15.07 ksi. Using the allowable stress intensity limit for primary plus secondary components per Table 2.1.21, the following representative fuel basket safety factor appropriate to Load Case F1 is obtained as "SF", where:

$$SF = 46.2 \text{ ksi}/15.07 \text{ ksi} = 3.06 \quad (\text{Load Case F1 from Table 2.1.6})$$

It is concluded that since all reported factors of safety for the fuel basket panels (based on stress analysis) are greater than the DLF, the MPC fuel basket is structurally adequate for its intended functions during and after a postulated lateral drop event associated with the normal conditions of transport.

Tables 2.6.6 and 2.6.7 report stress intensities and safety factors for the helium retention boundary (enclosure vessel) subject to internal pressure alone and to internal pressure plus the normal operating condition temperature with the most severe thermal gradient (Load Cases E1.a and E1.c in Table 2.1.7). Table 2.6.8 reports safety factors from the finite element analyses of the 1' free drop simulating a normal handling condition of transport. The final values for safety factors in the various locations of the helium retention boundary provide assurance that the MPC enclosure vessel is a robust pressure vessel.

2.6.1.4.2 Overpack

2.6.1.4.2.1 Discussion

The overpack is subject to the load cases listed in Table 2.1.8 for normal conditions of transport. Results from the series of finite element analyses are tabulated for normal heat and cold conditions of transport. The tabular results include contributions from mechanical and thermal loading and are needed to insure satisfaction of primary plus secondary stress limits for normal conditions of transport. Results are also tabulated from analyses that neglect thermal stresses. These tables are used to check primary stress limits.

The following text is a brief description of how the results are presented for evaluation and how the evaluation is organized in final form:

- The stress intensity results are sorted by safety factor in ascending order for each component making up the overpack. In particular, results are sorted separately for locations in the lid, the inner shell, and the bottom plate that together make up the containment boundary.
- The extensive body of results is initially summarized in Table 2.6.9 wherein the minimum safety factor for different components of the overpack for each of the load cases is presented. This table lists minimum safety factors for the load cases associated with the normal heat conditions of transport. All safety factors are conservatively computed using allowable stresses based on the maximum normal operating temperatures (see Tables 2.1.2 and 2.1.21 for temperatures and for allowable stresses).
- The finite element analyses include the stress state induced by bolt preload but do not include the effect of secondary fabrication stresses. Table 2.6.5 presents results of re-calculation of the safety factors for the inner containment shell and for the intermediate

shells to include the "fabrication stresses" reported in Subsection 2.6.1.3.2.2. Table 2.6.5 summarizes these recomputed safety factors, based on limits for primary plus secondary stresses, and reports the limiting safety factors for the overpack shells for events subject to normal conditions of transport (Level A Service Conditions). The incorporation of the fabrication stress and the computation of revised safety factors begins with the individual principal stress components for the shells, conservatively adds the circumferential fabrication stress in the inner and intermediate shells to the principal stress having the same sign as the fabrication stress, and then re-computes the stress intensity and the safety factor. For the inner shell, the safety factors including fabrication stress are computed from principal stress data including mechanical and thermal loading. For the intermediate shell, however, the recomputed safety factors are based on principal stresses that only include mechanical loading (no thermal stresses need be evaluated for a component designed in accordance with ASME Code Section III, Subsection NF regardless of Class 1 or Class 3 designation (see paragraph NF-3121.11)).

- Finally, Table 2.6.4 summarizes the minimum values of safety factors (global minima) for the overpack components for the normal conditions of transport.

The modifications summarized in Table 2.6.5 are briefly discussed below for the normal heat conditions of transport. The same series of modifications are also performed for the normal cold conditions of transport.

Case 1 (Pressure) - Safety factors are summarized in Table 2.6.9 prior to inclusion of fabrication stress. Table 2.6.5 shows the modified safety factor resulting from "adding" the fabrication stress for the inner containment shell to the appropriate principal stress that includes the combination of mechanical plus thermal loads. The same conservative methodology is applied to modify the safety factor for the intermediate shell to include fabrication stress. However, since the intermediate shells are designed to ASME Code Section III, Subsection NF, no thermal stresses need be included in the strength evaluation.

Case 3 (1 foot drop): Results are tabulated including both thermal and mechanical loading. Safety factors for the inner containment shell are summarized in Table 2.6.9 prior to inclusion of fabrication stress. Table 2.6.5 shows modified safety factors that are computed in the same manner as reported for Case 1. For the intermediate shell, principal stress results that do not include thermal stress effects are conservatively modified to include fabrication effects.

2.6.1.4.3 Result Summary for the Normal Heat Condition of Transport

- Stress Results from Overall Finite Element Models of the MPC and Overpack

Tables 2.6.6 through 2.6.9 summarize minimum safety factors from load cases analyzed using the finite element models of the MPC fuel basket plus canister and the overpack described in Subsections 2.6.1.3.1 and 2.6.1.3.2. All safety factors are greater than 1.0 and are greater than any credible dynamic amplifier for the location. Table 2.6.5 provides a summary table that includes the effect of fabrication stress on safety factors for the intermediate and inner shells of the overpack. Table 2.6.5 reports safety factors based on primary plus secondary allowable strengths.

- Status of Lid Bolts and Seals on the Overpack

The finite element analysis for the overpack provides results at the lid-to-top flange interface. In particular, tabulated results for seals and lid bolts are examined. The output results for each load combination indicate that all seal springs remain closed (i.e. the loading in the elements representing the seal remains compressive) indicating that the sealworthiness of the bolted joint will not be breached during normal heat conditions of transport.

Each load combination results in a report of the total compressive force on the closure plate-overpack interface as well as the total tangential force ("friction force"). If the ratio "total friction force/total compressive force" is formed for each set of results, the maximum value of the ratio is 0.219. There will be no slip of the closure plate relative to the overpack if the interface coefficient of friction is greater than the value given above. Mark's Handbook for Mechanical Engineers [3.4.9] in Table 3.2.1 shows $\mu = 0.74-0.79$ for clean and dry steel on steel surfaces. Therefore, it is concluded that there is no propensity for relative movement.

Based on the results of the finite element analysis for normal heat conditions of transport, the following conclusions are reached.

No bolt overstress is indicated under any loading event associated with normal conditions of transport. This confirms the results of alternate closure bolt analyses, performed in accordance with NUREG/CR-6007 UCRL-ID-110637, "Stress Analysis of Closure Bolts for Shipping Casks", by Mok, Fischer, and Hsu, LLL, 1993.

The closure plate seals do not unload under any load combination; therefore, the seals continue to perform their function.

- Stress and Stability Results from Miscellaneous Component Analyses in Subsection 2.6.1.3

Tables 2.6.10 and 2.6.11 repeat summary results from additional analyses described and reported on in Subsection 2.6.1.3 for components of the MPC and the overpack. The safety factors are summarized in this subsection in accordance with the requirements of Regulatory Guide 7.9. The tables report comparisons of calculated values with allowable values for both stress and stability and represent a compilation of miscellaneous analyses.

- Overpack Internal Pressure Test

The overpack is considered as an ASME pressure vessel. A hydrostatic test of the overpack under 1.5 times internal pressure must result in no stresses in excess of the material yield strength at room temperature to meet the requirement of 10CFR71.85(b). In the following, the necessary results to support the conclusion that the HI-STAR 100 transport containment boundary meets the requirement are presented. Table 2.3.4 gives the material yield strengths of SA350 LF3 and SA 203-E as 37.5 ksi and 40.0 ksi, respectively, at 100 degrees F. A survey of the safety factors for the containment boundary reported in Table 2.6.9 gives the following minimum safety factors:

CONTAINMENT BOUNDARY SAFETY FACTORS - Internal Pressure	
Item	Safety Factor
Lid	2.87
Inner Shell	12.1
Baseplate	11.2

These safety factors are determined using allowable stress intensities at the reference temperatures listed in Table 2.1.21 that are less than the yield stress for the corresponding material at room temperature. From the large safety factors in the above table, it is concluded, without further analysis, that an increase in the internal pressure by 50% will not cause stresses in the containment boundary to exceed the material yield stress.

- Summary of Minimum Safety Factors for Normal Heat Conditions of Transport

Tables 2.6.2 through 2.6.4 present a concise summary of safety factors for the fuel basket, the enclosure vessel, and the overpack, respectively. Locations within this SAR from which the summary results are culled are also indicated in the above tables.

Based on the results of all analyses, with results presented or summarized in the text and in tables, it is concluded that:

- All safety factors reported in the text and in the summary tables are greater than 1.0.
- There is no restraint of free thermal expansion between component parts of the HI-STAR 100 System.

Therefore, the HI-STAR 100 System, under the normal heat conditions of transport, has adequate structural integrity to satisfy the subcriticality, containment, shielding, and temperature requirements of 10CFR71.

2.6.2 Cold

The Normal Cold Condition of Transport assumes an ambient environmental temperature of -20 degrees Fahrenheit and maximum decay heat. A special condition of extreme cold is also defined where the system and environmental temperature is at -40 degrees F and the system is exposed to increased external pressure with minimum internal pressure. A discussion of the resistance to failure due to brittle fracture is provided in Subsection 2.1.2.3.

The value of the ambient temperature has two principal effects on the HI-STAR 100 storage system, namely:

- i. The steady-state temperature of all material points in the cask system will go up or down by the amount of change in the ambient temperature.
- ii. As the ambient temperature drops, the absolute temperature of the contained helium will drop accordingly, producing a proportional reduction in the internal pressure in accordance with the Ideal Gas Law.

In other words, the temperature gradients in the cask system under steady-state conditions, will remain the same regardless of the value of the ambient temperature. The internal pressure, on the other hand, will decline with the lowering of the ambient temperature. Since the stresses under normal transport condition arise principally from pressure and thermal gradients, it follows that the stress field in the MPC under a bounding "cold" ambient would be smaller than the "heat" condition of normal transport, treated in the preceding subsection. Therefore, the stress margins computed in Section 2.6.1 can be conservatively assumed to apply to the "cold" condition as well. Calculations using the methodology outlined in NUREG/CR-6007 UCRL-ID-110637, "Stress Analysis of Closure Bolts for Shipping Casks", by Mok, Fischer, and Hsu, LLL, 1993 demonstrate that the overpack closure bolts will retain the helium seal under the cold ambient conditions.

In addition, allowable stresses generally increase with decreasing temperatures. Safety factors, therefore, will be greater for an analysis at cold temperatures than at hot temperatures. Therefore, the safety factors reported for the hot conditions in Subsection 2.6.1 provide the limiting margins. The overpack, however, is analyzed under cold conditions to ensure that the integrity of the seals is maintained.

As no liquids are included in the HI-STAR 100 System design, loads due to expansion of freezing liquids are not considered.

2.6.2.1 Differential Thermal Expansion

The methodology for determination of the effects of differential thermal expansion in the normal heat condition of transport has been presented in Subsection 2.6.1.2. The same methodology is applied to evaluate the normal cold condition of transport.

The results are summarized in the tables given below for normal cold condition of transport.

THERMOELASTIC DISPLACEMENTS IN THE MPC AND OVERPACK UNDER COLD TEMPERATURE ENVIRONMENT CONDITION				
CANISTER - FUEL BASKET				
	Radial Direction (in.)		Axial Direction (in.)	
Unit	Initial Clearance	Final Gap	Initial Clearance	Final Gap
All PWRs	0.1875	0.095	2.0	1.524
BWR	0.1875	0.101	2.0(min)	1.554 (min)
CANISTER - OVERPACK				
	Radial Direction (in.)		Axial Direction (in.)	
Unit	Initial Clearance	Final Gap	Initial Clearance	Final Gap
All PWRs	0.09375	0.069	0.625	0.487
BWR	0.09375	0.071	0.625	0.497

It can be verified by referring to the Design Drawings, and the foregoing table, that the clearances between the MPC basket and canister structure, as well as those between the MPC shell and overpack inside surface, are sufficient to preclude a temperature induced interference from the thermal expansions listed above.

It is concluded that the HI-STAR 100 package meets the requirement that there be no restraint of free thermal expansion that would lead to development of primary stresses under normal cold conditions of transport.

2.6.2.2 MPC Stress Analysis

The only significant load on the MPCs under cold conditions arises from the postulated 1-foot side drop. Since the allowable stress intensities are higher under the extreme cold condition, results for the MPCs are bounded by the analysis for heat; no additional solutions need to be considered. Since the MPCs are constructed of austenitic stainless steel, there is no possibility of a brittle fracture occurring in any of the MPCs

2.6.2.3 Overpack Stress Analysis

Table 1 of NRC Regulatory Guide 7.8 [2.1.2] mandates load cases at the extreme cold temperature. The overpack may not be bounded by the results of the heat condition load cases for these following conditions:

- increased external pressure with minimum internal pressure, and extreme cold at - 40 degrees F.
- minimal internal pressure plus 1 foot drop with extreme cold condition at - 20 degrees F.
- rapid ambient temperature change during normal condition of transport (note that this case is not explicitly listed as a load case in Regulatory Guide 7.8).

The first two bulleted items are presented in Table 2.1.8; the results of those analyses are presented here. Structural evaluation for the last bulleted item is performed in this subsection. The structural evaluation uses inputs from thermal transient analyses performed and reported in Chapter 3 subsection 3.4.3.1.

Results of finite element analyses for increased external pressure with minimum internal pressure, and for minimum internal pressure plus 1 foot drop (Load Cases 2 and 4 in Table 2.1.8)

Safety factors for Load Cases 2 and 4 in Table 2.1.8 are computed from the results tabulated from the archived finite element analyses Table 2.6.12 summarizes the safety factors obtained. The finite element analysis does not clearly elucidate the effect of temperature on bolt preload. Separate calculations, using the methodology outlined in NUREG/CR-6007 UCRL-ID-110637, "Stress Analysis of Closure Bolts for Shipping Casks", by Mok, Fischer, and Hsu, LLL, 1993 analyze the closure bolts under extreme cold ambient condition plus pressure and provides the appropriate change in bolt preload expected from operation at the extreme low temperature. A small decrease from the initial preload stress in the bolt results from this operating condition.

The computed change in stress due to the assumption of a severe local low temperature condition is insignificant compared to the initial bolt stress and to the change in the allowable bolt stress because of the lowered temperature. It is concluded that the small change in bolt preload stress has no effect on structural calculations and safety factors.

The overpack load cases for normal conditions of transport described for the hot condition are re-analyzed for the cold condition in accordance with the requirements of Regulatory Guide 7.9. Since higher allowable stresses apply to the overpack components, it is not expected that the re-analyses will result in lower safety factors than have been already reported for the heat condition. The purpose of the analyses is to demonstrate that the overpack seals remain intact under the cold condition. The results of the analyses for normal cold conditions of transport are summarized in Tables 2.6.12 and 2.6.13.

Stress Analysis for Rapid Lowering of Ambient Temperature from 100 degrees F to -40 degrees F (Load Case 5 in Table 2.1.8)

During transportation, the HI-STAR 100 packaging may experience changes in the ambient temperature. Since the HI-STAR 100 packaging is a passive heat rejection device, a change in the ambient temperature has a direct influence on the temperature of its metal parts. In the preceding sub-sections, all structural integrity evaluations have focused on the steady state thermal conditions

using 100°F and -40°F as the limiting upper and lower ambient steady state values. In this sub-section, the structural consequences of a rapid change from the hot (100°F) to cold (-40°F) ambient condition is considered. This scenario is labelled as ASME Code Service Condition A, which requires that the range of primary plus secondary stress intensity must be less than $3 S_m$ (S_m = allowable stress intensity at the mean metal temperature). The loadings assumed to exist coincidentally with the thermal stresses from the transient event are: (i) overpack internal design pressure, P_i and (ii) the inertial deceleration load during transport (10g's). The primary plus secondary stress intensity range from the simultaneous action of internal pressure, axial g-load (10 g's), and thermal transient must be shown to be less than $3 S_m$.

It should be noted that the reverse transient (i.e. rapid change from cold to hot will produce a less severe thermal stress gradient. Therefore, the magnitudes of the results of a "rapid cooldown" event bound the corresponding results for the "rapid heat up" event.

To perform a bounding evaluation, it is necessary to identify the material locations on the overpack where the thermal stresses are apt to be most adverse. The thick top forging, which is directly exposed to the ambient air during transport is clearly a candidate location. The other location is the planar cross section of the overpack at approximately mid-height where the heat emission rate from the SNF is at its maximum. These locations are identified in Figure 3.4.24 and further explained in sub-section 3.4.3.

To evolve thermal gradient results for the postulated rapid ambient temperature change, a transient temperature problem is formulated and solved in Chapter 3. The thermal problem and finite element model are fully articulated in Chapter 3 (Subsection 3.4.3.1) where a three-dimensional thermal transient analysis of the HI-STAR 100 Package is performed under a postulated rapid drop in ambient temperature (100 degree F to -40 degree F in one hour). The design basis decay heat load is imposed throughout the time span of the transient solution. The temperature profiles through the wall of the overpack and the top forging are determined as functions of time and the change in thermal gradient through the wall of the sections are documented in Chapter 3, Figures 3.4.25-3.4.27. These locations are limiting since there is direct exposure to the ambient temperature on the outer surface of these components. It is shown in the figures that the top forging experiences a change in through-wall thermal gradient of less than 2.5 degrees K (4.5 degrees F) and that other sections of the overpack experience an even weaker change in thermal gradient. The finite element analyses for normal conditions of transport report results and safety factors for all locations for the normal heat and cold conditions of storage (under assumed steady state thermal conditions). The following additional calculation provides the stress state due to the maximum through-wall thermal gradient in the top forging. This stress state is then combined with the stresses from other load cases and stress intensities formed.

Based on the results from the thermal solutions, the material properties for this calculation are obtained for a metal temperature of 150 degrees F. For the top forging material, the Young's Modulus, E , and the coefficient of linear thermal expansion, α , are (at 150 degrees F):

$$E = 27,400,000 \text{ psi}$$

$$\alpha = 6.405 \times 10^{-6} \text{ inch/inch-degree F}$$

As reported in sub-section 3.4.3.1, the maximum change in temperature difference in the top forging material is bounded by 4.5°F. The ASME Code, (paragraph NB-3222.4(a)(4)) defines a significant temperature change ΔT_s as

$$\Delta T_s = S/2E\alpha$$

Where S is the value of S_a from the applicable design fatigue curve for 1 million cycles. For the forging material, $S = 18,900$ psi, which yields

$$\Delta T_s = 18,900/(2 \times 27,400,000 \times 0.00000641) = 53.9 \text{ } ^\circ\text{F}$$

It therefore follows that the metal temperature gradient change produced by the rapid cooldown (or heat up event) does not lead to a significant stress adder. Nevertheless, the factor of safety under this loading condition is quantified.

The linear temperature profile gives a linear stress distribution through the wall thickness with compressive stresses at the inside surface of the top forging. The magnitude of the stress due to the maximum thermal gradient is:

$$\Delta\sigma = E\alpha(\Delta T)/(2(1-\nu))$$

For $\Delta T = (4.5 \text{ degrees F (change)} + 1.5 \text{ degrees F (initial)})$ and $\nu = 0.3$, the stress intensity is computed as:

$$\Delta\sigma = 752 \text{ psi}$$

This stress is now combined with transport longitudinal stress from a 10g deceleration plus longitudinal stress from the normal condition internal pressure. These stresses are computed below:

Pressure stress:

$$\begin{aligned} p &= 100 \text{ psi (internal pressure per Table 2.1.1)} \\ \text{inside radius of top forging} &= a = 34.375'' \\ \text{outside radius of top forging} &= b = 41.625'' \end{aligned}$$

The magnitude of the longitudinal and circumferential stresses at the inside surface is

$$\sigma_x = (a^2/(b^2-a^2))p = 2.14 \times p = 214 \text{ psi}$$

$$\sigma_h = ((a^2 + b^2)/(b^2-a^2))p = 5.289 \times p = 529 \text{ psi}$$

Axial stress from deceleration:

The package weight = 282,000 lb. (Table 2.2.4)

The direct stress due to the axial deceleration is

$$\sigma_d = 10g \times 282,000 \text{ lb/Area} \quad \text{where the cross-section area is Area} = 1731 \text{ sq. inch}$$

Therefore,

$$\sigma_d = 1,629 \text{ psi}$$

Adding the absolute values of the stresses (for conservatism), the maximum surface stress intensity is

$$SI = (\sigma_d + \sigma_x + \Delta\sigma) + p = 2,695 \text{ psi}$$

This value is compared against 3 x the allowable stress intensity since it involves a secondary thermal stress. From Table 2.1.13, the allowable primary plus secondary stress intensity is

$$SI(\text{allowable}) \quad 3 \times \text{allowable membrane stress intensity} = 69,100 \text{ psi}$$

$$\text{The safety factor is } 69,100/2,695 = 25.64$$

Therefore, the HI-STAR 100 overpack is shown to meet the Level A stress intensity limits under the rapid ambient temperature change event with a large margin of safety.

Conclusions

Based on the results of the finite element analysis and the calculations carried out within this subsection, the following conclusions are reached for normal cold conditions of transport:

- No bolt yielding is indicated under any loading event.
- The closure plate seal springs do not unload under any load combination; therefore, the seals continue to perform their function.
- The postulated rapid drop in the ambient temperature from hot (100 degrees F) to cold (-40 degrees F) conditions of transport has no appreciable effect on the stress intensities in the transport overpack. The top forging will experience a small increase in through-wall thermal gradient. Calculations show that the change in thermal stress induced by this through-wall thermal gradient is small; large safety factors are calculated when the secondary thermal stress is combined with the pressure stress and the longitudinal transport stress.

Relative movement between the top flange and the top closure lid has been examined for the normal cold condition of transport. Each load combination reported provides the total compressive force on the lands as well as the total tangential force on the lands ("friction force"). If the ratio "total friction force/total compressive force" is formed for each set of results appropriate to the cold condition of normal transport, the maximum value of the ratio is 0.138. There will be no slip of the closure plate

relative to the overpack if the coefficient of friction is greater than the value given above. Mark's Handbook for Mechanical Engineers [2.6.2] shows $\mu = 0.74-0.79$ for clean and dry steel on steel surfaces. Therefore, it is concluded that there is no propensity for relative movement.

Since the results show that all safety factors are greater than 1.0, it is concluded that the HI-STAR 100 System under the normal cold conditions of transport has adequate structural integrity to satisfy the subcriticality, containment, shielding, and temperature requirements of 10CFR71.

2.6.3 Reduced External Pressure

The effects of a reduced external pressure equal to 3.5 psia, which is required by USNRC Regulatory Guide 7.8 [2.1.2], are bounded by the effects of the accident internal pressure for the overpack (Table 2.1.1). This is considered in Subsection 2.7 for the overpack inner shell. This case does not provide any bounding loads for other components of the overpack containment boundary. Therefore, the only additional analysis performed here to demonstrate package performance for this condition is an analysis of the outer enclosure shell panels.

Under this load condition, the outer enclosure shell panels (see Section 1.4, Drawing) deform as long plates under the 3.5 psi pressure that tends to deform the panels away from the neutron absorber material. The stress developed in this situation can be determined by considering the panel as a clamped beam subject to lateral pressure. The appropriate dimensions are:

$L = \text{unsupported width of panel} = 7.875''$

$t = \text{panel thickness} = 0.5''$

$p = \text{differential pressure} = 3.5 \text{ psi}$

The stress is computed from classical strength of materials beam theory as:

$$\sigma = 0.5p\left(\frac{L}{t}\right)^2$$

Substituting the numerical values gives the stress as 434 psi. From Table 2.1.15, the allowable stress is 26.3 ksi for this condition. Therefore, the safety factor is

$$SF = 60.6$$

Clearly, this event is not a safety concern for package performance.

2.6.4 Increased External Pressure

The effects of an external pressure equal to 20 psia on the package, which is required by USNRC Regulatory Guide 7.8 [2.1.2], are bounded by the effects of the large value for the design external pressure specified for the hypothetical accident (Table 2.1.1). Instability of the overpack shells is examined in Section 2.7. Therefore, no additional analyses need be performed here to demonstrate package performance.

2.6.5 Vibration

During transport, vibratory motions occur which could cause low-level stress cycles in the system due to beam-like deformations. If any of the package components have natural frequencies in the flexible range (i.e., below 33 Hz), or near the flexible range, then resonance may amplify the low level input into a significant stress response.

As discussed in Section 2.1, there are no "flexible" beam-like members in the HI-STAR 100 MPC. The MPC is a fully welded, braced construction over its entire length and it is fully supported by the overpack during transport. Since the MPC is supported by the overpack, and is itself a rigid structure, any vibration problems would manifest themselves in the fuel basket walls.

It is shown below that the lowest frequency of the fuel basket walls and the overpack, acting as a beam, are well above 33 Hz. Therefore, additional stresses from vibration are not expected.

The lowest frequency of vibration during normal transport conditions will occur due to vibrations of a fuel basket cell wall. It is demonstrated that the lowest frequency of the component, computed based on the assumption that there is support sufficient to limit vibration to that representative of a clamped beam, is 658 Hz for a PWR basket and 1,200 Hz for a BWR basket.

These frequencies are significantly higher than the 33 Hz transition frequency for rigidity.

When in a horizontal position, the overpack is supported over a considerable length of the enclosure shell. Conservatively considering the HI-STAR as a supported beam at only the two ends of the enclosure shell, and assuming the total mass of the MPC moves with the overpack, an estimate of the lowest material frequency of the structure during transport is in excess of 469 Hz

Based on these frequency calculations, it is concluded that vibration effects are minimal and no new calculations are required.

2.6.6 Water Spray

The condition is not applicable to the HI-STAR 100 System per Reg. Guide 7.8 [2.1.2].

2.6.7 Free Drop

The structural analysis of a 1-foot side drop under heat and cold conditions has been performed in Subsections 2.6.1 and 2.6.2 for heat and cold conditions of normal transport. As demonstrated in Subsections 2.6.1 and 2.6.2, safety factors are well over 1.0.

2.6.8 Corner Drop

This condition is not applicable to the HI-STAR 100 System per [2.1.2].

2.6.9 Compression

The condition is not applicable to the HI-STAR 100 System per [2.1.2].

2.6.10 Penetration

The condition is not applicable to the HI-STAR 100 System per [2.1.2].

Table 2.6.1

FINITE ELEMENTS IN THE MPC STRUCTURAL MODELS

MPC Type Element Type	Model Type		
	Basic	0 Degree Drop	45 Degree Drop
MPC-24	1068	1179	1178
BEAM3	1028	1028	1028
CONTAC12	40	38	38
CONTAC26	0	110	110
COMBIN14	0	3	2
MPC-32	766	873	872
BEAM3	738	738	738
CONTAC12	28	27	24
CONTAC26	0	106	105
COMBIN14	0	2	5
MPC-68	1234	1347	1344
BEAM3	1174	1174	1174
PLANE82	16	16	16
CONTAC12	44	43	40
CONTAC26	0	112	111
COMBIN14	0	2	3

Table 2.6.1 Continued

FINITE ELEMENTS IN THE MPC STRUCTURAL MODELS

MPC Type Element Type	Model Type		
	Basic	0 Degree Drop	45 Degree Drop
MPC-24E/24EF	1070	1183	1182
BEAM3	1030	1030	1030
CONTAC12	40	38	38
CONTAC26	0	112	112
COMBIN14	0	3	2

Table 2.6.2

MINIMUM SAFETY FACTORS FOR THE MPC FUEL BASKET - NORMAL CONDITIONS OF TRANSPORT

Case Number	Load ¹ Combination	Safety Factor	Location in SAR where Details are Provided
F1	T or T'	3.06	2.6.1.4.1
F2			
F2.a	D+H, 1 ft side drop 0°	1.57	Table 2.6.8
F2.b	D+H, 1 ft side drop 45°	1.29	Table 2.6.8

¹ The symbols used for loads are defined in Subsection 2.1.2.1.

Table 2.6.3

MINIMUM SAFETY FACTORS FOR THE MPC ENCLOSURE VESSEL - NORMAL CONDITIONS OF TRANSPORT

Case Number	Load Combination ¹	Safety Factor	Location in SAR where Details are Provided or Safety Factors Extracted	
E1	E1.a	Design internal pressure, P_i	5.06 1.5 1.36	Lid Table 2.6.6 Baseplate Table 2.6.6 Shell Table 2.6.6
	E1.b	Design external pressure, P_o	NA NA 1.2	Lid P_i bounds Baseplate P_i bounds Shell Table 2.6.10
	E1.c	Design internal pressure plus temperature	8.50 2.67 1.5	Lid Table 2.6.7 Base Table 2.6.7 Shell Table 2.6.7
E2	E2.a	$(P_i, P_o) + D + H$, 1 ft side drop, 0 deg.	1.41	Table 2.6.8
	E2.b	$(P_i, P_o) + D + H$, 1 ft. side drop, 45 deg.	1.63	Table 2.6.8
E4	T or T'	Sections show expansion does not result in restraint of free thermal expansion	2.6.1.2	

¹ The symbols used for loads are defined in Subsection 2.1.2.1.

Table 2.6.4

MINIMUM SAFETY FACTORS FOR OVERPACK FOR NORMAL CONDITION OF TRANSPORT

Case Number	Load Combination ¹	Safety Factor	Location in SAR where Details are Provided
1	$T_h + P_i + F + W_s$	1.65	Table 2.6.5
2	$T_s + P_o + F + W_s$	3.38	Table 2.6.13
3	$T_h + D_{sn} + P_i + F + W_s$	1.68	Table 2.6.9
4	$T_c + D_{sn} + P_o + F + W_s$	2.41	Table 2.6.13

¹ The symbols used here are defined in Subsection 2.1.2.1.

Table 2.6.5

MINIMUM SAFETY FACTORS INCLUDING FABRICATION STRESSES –
PRIMARY PLUS SECONDARY STRESS INTENSITY, NORMAL HEAT CONDITIONS OF TRANSPORT

Case	Inner Shell Exterior Surface	Intermediate Shell
1 - Internal pressure	1.65*	4.12
3 - 1 ft. Side Drop	1.70*	2.42

* *Applicable to inner shell fabricated from SA203-E material. Safety factor must be multiplied by 0.93 if inner shell is fabricated from optional SA350-LF3 material.*

Note: Thermal stresses are included for inner containment shell per ASME Section III, Subsection NB, but excluded in intermediate shell per ASME Code, Section III, Subsection NF.

Table 2.6.6

STRESS INTENSITY RESULTS FOR CONFINEMENT BOUNDARY -
INTERNAL PRESSURE ONLY (Load Case E1.a in Table 2.1.7)

Component Locations (Per Fig. 2.6.20)	Calculated Value of Stress Intensity (psi)	Category	Table 2.1.19 Allowable Value (psi) [†]	Safety Factor (Allowable/Calculated)
<u>Top Lid^{††}</u>				
A	3,282	$P_L + P_b$	30,000	9.14
Neutral Axis	40.4	P_m	20,000	495
B	3,210	$P_L + P_b$	30,000	9.34
C	1,374	$P_L + P_b$	30,000	21.8
Neutral Axis	1,462	P_m	20,000	13.6
D	5,920	$P_L + P_b$	30,000	5.06
<u>Baseplate</u>				
E	19,683	$P_L + P_b$	30,000	1.5
Neutral Axis	412	P_m	20,000	48.5
F	20,528	$P_L + P_b$	30,000	1.5
G	9,695	$P_L + P_b$	30,000	3.1
Neutral Axis	2,278	P_m	20,000	8.8
H	8,340	$P_L + P_b$	30,000	3.5

[†] Stress intensity taken at 300 degrees F in this comparison.

^{††} The stresses in the top lid are reported for the dual lid configuration. The stresses for the single lid configuration are 50% less (see Subsection 2.6.1.3.1.2 for further details).

Table 2.6.6 Continued

STRESS INTENSITY RESULTS FOR CONFINEMENT BOUNDARY -
INTERNAL PRESSURE ONLY (Load Case E1.a in Table 2.1.7)

Component Locations (Per Fig.2.6.20)	Calculated Value of Stress Intensity (psi)	Category	Table 2.1.19 Allowable Value (psi) [†]	Safety Factor (Allowable/Calculated)
<u>Canister</u>				
I	6,860	P_m	18,700	2.72
Upper Bending Boundary Layer Region	7,189	$P_L + P_b + Q$	30,000	4.2
	7,044	$P_L + P_b$	20,000	2.8
Lower Bending Boundary Layer Region	43,986	$P_L + P_b + Q$	60,000	1.36
	10,621	$P_L + P_b$	30,000	2.82

[†] Allowable stress intensity based at 300 degrees F except for Location I where allowable stress intensity values are based on 400 degree F.

Table 2.6.7

PRIMARY AND SECONDARY STRESS INTENSITY RESULTS FOR
HELIUM RETENTION BOUNDARY - PRESSURE PLUS THERMAL LOADING (Load Case E1.c in Table 2.1.7)

Component Locations (Per Fig. 2.6.20)	Calculated Value of Stress Intensity (psi)	Category	Table 2.1.19 Allowable Value (psi) [†]	Safety Factor (Allowable/Calculated)
<u>Top Lid^{††}</u>				
A	4,634	$P_L + P_b + Q$	60,000	12.9
Neutral Axis	1,464	P_L	30,000	20.4
B	2,140	$P_L + P_b + Q$	60,000	28.0
C	1,942	$P_L + P_b + Q$	60,000	30.8
Neutral Axis	3,528	P_L	30,000	8.50
D	7,048	$P_L + P_b + Q$	60,000	8.51
<u>Baseplate</u>				
E	22,434	$P_L + P_b + Q$	60,000	2.67
Neutral Axis	1,743	P_L	30,000	17.2
F	18,988	$P_L + P_b + Q$	60,000	3.16
G	5,621	$P_m + P_L$	60,000	10.7
Neutral Axis	5,410	P_L	30,000	5.55
H	12,128	$P_L + P_b + Q$	60,000	4.95

[†] Allowable stresses based on temperature of 300 degrees F.

^{††} The stresses in the top lid are reported for the dual lid configuration. The stresses for the single lid configuration are 50% less (see Subsection 2.6.1.3.1.2 for further details).

Table 2.6.7 Continued

PRIMARY AND SECONDARY STRESS INTENSITY RESULTS FOR
 HELIUM RETENTION BOUNDARY - PRESSURE PLUS THERMAL LOADING (Load Case E1.c in Table 2.1.7)

Component Locations (Per Fig.2.6.20)	Calculated Value of Stress Intensity (psi)	Category	Table 2.1.19 Allowable Value (psi) ¹	Safety Factor (Allowable/Calculated)
<u>Canister</u>				
I	6,897	P _L	28,100	4.07
Upper Bending Boundary Layer Region	6,525	P _L + P _b + Q	60,000	9.2
	3,351	P _L	30,000	8.95
Lower Bending Boundary Layer Region	40,070	P _L + P _b + Q	60,000	1.5
	6,665	P _L	30,000	4.5

¹ Allowable stresses based on temperature of 300 degree F except at Location I where the temperatures are based on 400 degrees F.

Table 2.6.8 - FINITE ELEMENT ANALYSIS RESULTS
 MINIMUM SAFETY FACTORS FOR MPC COMPONENTS UNDER NORMAL CONDITIONS

Component - Stress Result	MPC-24		MPC-68	
	1 Ft. Side Drop, 0 deg Orientation	1 Ft. Side Drop, 45 deg Orientation	1 Ft. Side Drop, 0 deg Orientation	1 Ft. Side Drop, 45 deg Orientation
	Load Case F2.a or E2.a	Load Case F2.b or E2.b	Load Case F2.a or E2.a	Load Case F2.b or E2.b
Fuel Basket - Primary Membrane (P_m)	4.12	5.64	4.42	6.16
Fuel Basket - Local Membrane Plus Primary Bending ($P_L + P_b$)	1.73	1.87	2.42	1.50
Enclosure Vessel - Primary Membrane (P_m)	2.71	2.71	2.67	2.72
Enclosure Vessel - Local Membrane Plus Primary Bending ($P_L + P_b$)	3.30	3.29	2.17	1.80
Basket Supports - Primary Membrane (P_m)	N/A	N/A	5.33	5.34
Basket Supports - Local Membrane Plus Primary Bending ($P_L + P_b$)	N/A	N/A	1.67	2.16

Table 2.6.8 (Continued) - FINITE ELEMENT ANALYSIS RESULTS
 MINIMUM SAFETY FACTORS FOR MPC COMPONENTS UNDER NORMAL CONDITIONS

Component - Stress Result	MPC-32		MPC-24E/EF	
	1 Ft. Side Drop, 0 deg Orientation	1 Ft. Side Drop, 45 deg Orientation	1 Ft. Side Drop, 0 deg Orientation	1 Ft. Side Drop, 45 deg Orientation
	Load Case F2.a or E2.a	Load Case F2.b or E2.b	Load Case F2.a or E2.a	Load Case F2.b or E2.b
Fuel Basket - Primary Membrane (P_m)	4.05	5.65	4.05	5.56
Fuel Basket - Local Membrane Plus Primary Bending ($P_L + P_b$)	1.57	1.29	1.69	1.83
Enclosure Vessel - Primary Membrane (P_m)	2.55	2.69	2.71	2.71
Enclosure Vessel - Local Membrane Plus Primary Bending ($P_L + P_b$)	1.41	1.63	3.05	3.14
Basket Supports - Primary Membrane (P_m)	3.96	5.33	N/A	N/A
Basket Supports - Local Membrane Plus Primary Bending ($P_L + P_b$)	3.49	3.12	N/A	N/A

Table 2.6.9 - FINITE ELEMENT ANALYSIS RESULTS
 MINIMUM SAFETY FACTORS FOR OVERPACK COMPONENTS UNDER NORMAL CONDITIONS (Hot Environment)

Component – Stress Result	Hot Environment	1 Ft. Side Drop
	Load Case 1	Load Case 3
Lid - Local Membrane Plus Primary Bending ($P_L + P_b$)	2.87	2.14
Inner Shell - Local Membrane Plus Primary Bending ($P_L + P_b$)	12.1*	3.24*
Inner Shell - Primary Membrane (P_m)	13.7*	3.53*
Intermediate Shells - Local Membrane Plus Primary Bending ($P_L + P_b$)	17.3	2.51
Baseplate - Local Membrane Plus Primary Bending ($P_L + P_b$)	11.2	6.28
Enclosure Shell - Primary Membrane (P_m)	35.2	3.24

* *Applicable to inner shell fabricated from SA203-E material. Safety factor must be multiplied by 0.93 if inner shell is fabricated from optional SA350-LF3 material.*

Table 2.6.9 (Continued) - FINITE ELEMENT ANALYSIS RESULTS

MINIMUM SAFETY FACTORS FOR OVERPACK COMPONENTS UNDER NORMAL CONDITIONS (Hot Environment)

Component - Stress Result	Hot Environment	1 Ft. Side Drop
	Load Case 1	Load Case 3
Lid - Local Membrane Plus Primary Bending Plus Secondary ($P_L + P_b + Q$)	2.14	1.90
Inner Shell - Local Membrane Plus Primary Bending Plus Secondary ($P_L + P_b + Q$)	2.69*	2.84*
Intermediate Shells - Local Membrane Plus Primary Bending Plus Secondary ($P_L + P_b + Q$ excluding thermal stress)	34.5	5.01
Baseplate - Local Membrane Plus Primary Bending Plus Secondary ($P_L + P_b + Q$)	1.81	1.68
Enclosure Shell - Local Membrane Plus Primary Bending Plus Secondary ($P_L + P_b + Q$)	1.97	1.88

* *Applicable to inner shell fabricated from SA203-E material. Safety factor must be multiplied by 0.93 if inner shell is fabricated from optional SA350-LF3 material.*

Table 2.6.10

SAFETY FACTORS FROM MISCELLANEOUS MPC CALCULATIONS -
NORMAL CONDITIONS OF TRANSPORT - HOT ENVIRONMENT

Item	Loading	Safety Factor	Location in SAR Where Details are Provided
Fuel Support Spacers	1' Drop (Load Case F2 in Table 2.1.6)	2.76	Subsection 2.6.1.3.1.3
MPC Stability	Code Case N-284 (Load Case E1.b in Table 2.1.7)	1.2	Subsection 2.6.1.3.1.3

Table 2.6.11

MINIMUM SAFETY FACTORS FROM MISCELLANEOUS OVERPACK CALCULATIONS
 NORMAL HOT CONDITIONS OF TRANSPORT

Item	Loading	Safety Factor	Location in SAR Where Details are Provided
Fabrication Stress in Inner Shell	Fabrication	4.3	Subsection 2.6.1.3.2.2
Closure Bolt	Average Tensile Stress Including Pre-Load	1.44	Subsection 2.6.1.3.2.3

Table 2.6.12 - FINITE ELEMENT ANALYSIS RESULTS
 MINIMUM SAFETY FACTORS FOR OVERPACK COMPONENTS UNDER NORMAL CONDITIONS (Cold Environment)

Component - Stress Result	Super-Cold Environment Load Case 2	1 Ft. Side Drop Load Case 4
Lid - Local Membrane Plus Primary Bending ($P_L + P_b$)	4.55	2.97
Inner Shell - Local Membrane Plus Primary Bending ($P_L + P_b$)	14.4	3.37
Inner Shell - Primary Membrane (P_m)	16.5	3.53
Intermediate Shells - Local Membrane Plus Primary Bending ($P_L + P_b$)	21.7	2.48
Baseplate - Local Membrane Plus Primary Bending ($P_L + P_b$)	722.8	7.84
Enclosure Shell - Primary Membrane (P_m)	50.2	3.21

Table 2.6.12 (Continued)

FINITE ELEMENT ANALYSIS RESULTS
 MINIMUM SAFETY FACTORS FOR OVERPACK COMPONENTS UNDER NORMAL CONDITIONS (Cold Environment)

Component - Stress Result	Super-Cold Environment Load Case 2	1 Ft. Side Drop Load Case 4
Lid - Local Membrane Plus Primary Bending Plus Secondary ($P_L + P_b + Q$)	8.79	5.79
Inner Shell - Local Membrane Plus Primary Bending Plus Secondary ($P_L + P_b + Q$)	15.5	6.36
Intermediate Shells - Local Membrane Plus Primary Bending Plus Secondary ($P_L + P_b + Q$ excluding thermal stress)	43.24	4.95
Baseplate - Local Membrane Plus Primary Bending Plus Secondary ($P_L + P_b + Q$)	83.8	15.1
Enclosure Shell - Local Membrane Plus Primary Bending Plus Secondary ($P_L + P_b + Q$)	21.4	7.67

Table 2.6.13

MINIMUM SAFETY FACTORS INCLUDING FABRICATION STRESS - PRIMARY PLUS SECONDARY
STRESS INTENSITY, NORMAL COLD CONDITIONS OF TRANSPORT

Case	Inner Shell Exterior Surface	Intermediate Shell
2 Pressure (Secondary Stress)	3.38	4.22
4 1 ft. Side Drop (Secondary Stress)	2.58	2.41

Note: Thermal stresses are included for inner containment shell per ASME Section III, Subsection NB, but excluded in intermediate shell per ASME Code, Section III, Subsection NF.

Table 2.6.14

MISCELLANEOUS SAFETY FACTOR FOR OVERPACK			
Item	Loading	Safety Factor	Location in SAR Where Details are Provided
Outer Enclosure Panels	Reduced External Pressure	60.6	Subsection 2.6.3

It was shown in the preceding section that the load combinations for normal conditions of transport do not induce stresses or stress intensities in excess of allowables. Therefore, it is concluded that the effectiveness of the HI-STAR 100 System is not reduced under normal conditions of transport.

The hypothetical accident conditions, as defined in 10CFR71.73 and Regulatory Guide 7.9, are applied to the HI-STAR 100 System in the required sequence. The system is first subjected to a 9 meter (30 foot) drop in the most damaging orientation, then subject to a 1 meter (40 inch) drop onto a 6 inch diameter mild steel pin (of length sufficient to cause damage to the steel structure), followed by a 1475^oF temperature fire environment for 30 minutes, and finally to a water immersion test.

The overpack containment boundary is also subjected to deep immersion in accordance with 10CFR71.61.

It is shown in the following subsections that the HI-STAR 100 System meets the standards set forth in 10CFR71, when it is subjected to the hypothetical accident conditions specified in 10CFR71.73. In particular, sufficient analytical and experimental evidence is presented herein to support the conclusion that HI-STAR 100 packaging, when subjected to hypothetical accident conditions, has adequate structural integrity to satisfy the subcriticality, containment, shielding, and temperature requirements of 10CFR71.

2.7.1 Free Drop

In this section the performance and structural integrity of the HI-STAR 100 System is evaluated for the most severe drop events. The drop events that are potentially most damaging are the end drops (top or bottom), the side drop, the orientation for which the center of gravity is directly over the point of impact, an oblique drop where the angle of impact is somewhere between center of gravity over corner and a near side drop, and an orientation where package rotation after an impact at one end induces a larger impact deceleration when the other end impacts the target (e.g., slapdown).

The structural assessment of the package is performed in two parts. In the first part, a numerical model to simulate the drop events is prepared and benchmarked against 1/8 scale static tests of the HI-STAR 100 impact limiters, and 1/4-scale dynamic drop tests of the HI-STAR 100 Package. This numerical/experimental effort is carried out to confirm that the maximum rigid body decelerations experienced by the package are less than the design basis values set forth in Table 2.1.10. In the second part, the structural integrity of components under the inertia loads due to design basis deceleration levels is evaluated. The deceleration sustained by the internals, such as the fuel basket, are further amplified in recognition of the elasticity of the internal structures. The dynamic amplifier is considered as an added multiplier on the rigid body deceleration in the structural assessments. Dynamic amplifiers applicable to components of the package have been developed from evaluating the behavior of simplified models.

Part One: Maximum Rigid Body Deceleration Under 10CFR71.73 Free Drop Event

The determination of the AL-STAR impact limiter performance under postulated 10CFR71.73 free drop events was carried out in six phases as summarized below and further elaborated in Appendix 2.A.

- i. Characterize honeycomb material crush behavior: Coupons of both unidirectional and cross-core honeycomb materials at different nominal crush strength values were prepared and tested. A typical pressure vs. deflection curve is shown in Figure 2.A.2.1 in Appendix 2.A. The pressure in the flat portion of the curve denotes the crush pressure.

Mathematical correlation of the data from the population of coupons tested showed that the pressure/crush curve for a honeycomb stock can be represented by one equation wherein the crush pressure, p_c , is the sole variable. This commonality in the deformation characteristic of the AL-STAR honeycomb materials of different crush strength is extremely helpful in simplifying the dynamic model for the impact limiter.

- ii. AL-STAR Force-Crush Relationship: The AL-STAR impact limiter is a radially symmetric structure whose external and internal diameters are fixed: the I.D. is set by the overpack diameter at its extremities and the O.D. is limited by rail transport considerations to 128". Within this annular space, the arrangement of the aluminum honeycomb material is specified so that the impact limiter can absorb the kinetic energy from a 30' drop event in *any* orientation. The axial dimension of the impact limiter is also limited by considerations of the overall weight of the packaging. To design the impact limiter within the above-mentioned constraints called for a method to predict the force required to crush the impact limiter by a given amount in any given orientation. The mathematical model to define the force-crush (F-d) curve is described in Appendix 2.A. The F-d model was used to establish the nominal crush strengths of the honeycomb sectors used in the various locations of the AL-STAR honeycomb volume to obtain the desired energy absorption characteristics in the equipment.

- iii. Static Scale Model Tests: The static 1/8 scale model tests consisted of preparing 1/8 scale models of the AL-STAR impact limiter and subjecting them to static crush tests in various orientations under normal and abnormal temperature conditions. One object of these tests was to confirm the validity of the theoretical F-d model. Confirming the structural adequacy of the AL-STAR backing structure (which is a thick carbon steel weldment) and the external skin were also objectives of the scale model test. The 1/8 scale static tests, as described in Appendix 2.A, met all project goals: a weakness in the AL-STAR backing structure was identified and corrected in a redesign of the backing structure. The test data also showed that Holtec's F-d model provided a reasonably accurate analytical tool to predict the static crushing behavior of AL-STAR in the various potential crushing orientations. The adequacy of the F-d model to predict static crush behavior was an essential prerequisite for the dynamic test correlation effort that followed.

iv. Dynamic Scale Model Tests: A 1/4 scale model of the HI-STAR 100 Package, including AL-STAR impact limiters, was used for drop testing. The drawings for the 1/4 scale impact limiters are ~~provided in Section 1.4 [2.1.7.4].~~ Appendix 2.A herein provides a complete synopsis of the AL-STAR impact limiter design development program, including the 1/4 scale model drop tests which demonstrated the performance of the package. The objectives of the drop tests may be stated as follows:

- i. Select a sufficient number of drop orientations to ensure that under the worst-case orientations, the structural adequacy of the package is demonstrated by testing.
- ii. Prove that the peak rigid body decelerations experienced by the package in any of the tests is below the Table 2.1.10 design basis value.
- iii. Demonstrate that the impact limiters prevent the cask from direct contact with the unyielding surface and remain attached through the end of the drop event.

Four drop configurations, namely, vertical (top end), horizontal (side), center-of-gravity-over-corner (CGOC), and slap-down (fully described in Appendix 2.A) were identified as a complete set capable of realizing the aforementioned objectives. The tests were performed in two distinct series as described below.

The first test series, conducted in August 1997, indicated the need to modify the honeycomb material crush strength utilized. The first dynamic test series also helped quantify the dynamic multiplier applicable to the statically determined honeycomb crush strength under impact conditions.

The second test series showed that the peak deceleration in all four drop orientations tested met the Table 2.1.10 limits. Despite meeting deceleration limits, the attachment bolts between the bottom impact limiter and the overpack failed in the side drop test. This required an additional design improvement to the bottom impact limiter-to-overpack attachment design, and re-performance of the side drop test. For the final four tests used for evaluation in Appendix 2.A, no attachment bolts sustained a failure.

v. AL-STAR Dynamic Response Model: The 1/4 scale tests provided valuable information on the package response which was used to confirm the veracity of Holtec's dynamic simulation model developed for predicting the package response under the other drop conditions. Like all orthotropic materials, the crushing of the honeycomb requires greater force under an impact load than the load necessary to achieve the same extent of crush under static conditions. The conversion of the static "force (F) - crush (d)" model to dynamic conditions simply means applying a dynamic factor to the formula. In other words, under dynamic conditions, the relation between crush force "F" and crush "d" is given as:

$$F = Z f(d)$$

where $f(d)$ is the crush force corresponding to the compression "d" under static conditions and Z is the dynamic multiplier function. The value of Z was quantified by the first series of 1/4 scale dynamic scale model test, such that a dynamic response simulation model could be developed that satisfied all equilibrium expectations.

In addition to comparing the predicted peak decelerations with the measured value, the duration of crushing and crush depth predicted by the dynamic model were also compared with the measured test data. The comparisons, presented in Appendix 2.A, confirm the ability of the dynamic model to simulate the behavior of the package under a drop event.

- vi. Sensitivity Studies: A significant result from the 1/4 scale model dynamic tests was a complete validation of the dynamic model. For every test performed, the AL-STAR dynamic model was able to simulate the peak accelerations, total crush, and crush duration with reasonable agreement. The experimentally benchmarked mathematical model could now be used to simulate drop events for a variety of HI-STAR 100 package weights and honeycomb crush strengths. Results of the simulations to determine the effects of variations in aluminum honeycomb crush strengths and package weights are presented in Appendix 2.A.

The results summarized in Table 2.A.5 of Appendix 2.A demonstrates that the maximum rigid body deceleration experienced by the HI-STAR 100 package equipped with the AL-STAR impact limiter (see the applicable drawing in ~~Section 1.4 herein~~ [2.1.7.4]) will be less than 60g's regardless of the orientation of impact. Therefore, in the balance of analyses performed to evaluate the consequences of "free drop" under the provisions of 10CFR71.73, the package will be assumed to be subject to a rigid body deceleration equal to 60 g's. It is clear from inspection of the geometry of the package that the most vulnerable direction of inertia loading for the HI-STAR fuel basket is the transverse direction wherein the flat panels of the basket are subjected to lateral inertia loading from the contained SNF. As mentioned earlier, the flexibility of basket panel acts to further amplify the package deceleration, which must be considered in the evaluation of results from the stress analysis model. In summary, the net result of the work effort described in the foregoing and further elaborated in Appendix 2.A was to confirm the validity of 60g as the *design basis* rigid body deceleration for the 10CFR71.73 drop event.

In Appendix 2.A, additional supporting technical information requested in Paragraph 2.7 of Reg. Guide 7.9 is provided. Information provided includes free-body diagrams, sketches, governing equations, test method for model testing, scaling factors, discussion of the law of similitude, measurements of crush, impact duration, deceleration histograms, effect of tolerances on package response, and demonstration that the model test will give conservative results for peak g-force and maximum deformation.

Additionally, Reg. Guide 7.9 calls for evaluation of the response of the package in terms of stress and strain to components and structural members, including investigation of structural stability as well as the consequences of the combined effects of temperature gradients, pressure, and other loads. Part Two of the work effort, described in the following, fulfills the above Reg. Guide 7.9 stipulations.

Part Two: Stress Analysis

The second part of the analysis is performed using the ANSYS finite element software [2.6.4]. The MPC and overpack models used here are identical to those presented in Section 2.6. The loads are applied to the models in accordance with the load combinations defined in Table 2.1.6 (Load Cases F3), Table 2.1.7 (Load Cases E3), and Table 2.1.9 (Load Cases 1-16) for hypothetical accident conditions of transport. The detailed application of each load case is described in the subsections that follow. The presentation and content follows the formatting requirements of Regulatory Guide 7.9. The results from conditions of "Heat" and "Cold" are considered together in the following presentation.

The analysis of the different hypothetical accident conditions of transport are carried out using general finite element models of the MPC and the overpack as well as calculations based on simplified models amenable to strength of materials solutions. The analyses using strength of materials solutions focus on specific loading conditions applied to component parts of the MPC and/or the overpack. The finite element analysis of the overpack involves a complex 3-D model of the overpack to which a series of loads are applied. The results from the solutions are then combined in a post-processing phase to make up the different accident load combination. Given the complexity of the overpack finite element analysis model, some discussion of the stress report is presented to facilitate an understanding of the conclusions. For each of the load combinations, the following components are identified for reporting purposes:

1. Seal
2. Bolts
3. Lid
4. Inner Shell (including the top flange)
5. Intermediate Shells
6. Baseplate
7. Enclosure

The postprocessor collects the nodal stresses from the finite element solution, for each of the components in turn, and reports the principal stresses and the stress intensity at selected locations where physical reasoning suggests that high stresses may occur under the different postulated load combinations. In order to identify the minimum safety factor for each of the above components after the load cases are combined, the collection of nodes is sorted by stress intensity magnitude in descending order. Therefore, since the hypothetical accident condition load combinations involve a comparison of primary stress intensities, a minimum safety factor for each of the defined components in the model may be identified as occurring at the node point with the largest calculated stress intensity. Safety factors are computed using the allowable stress intensities for the material at the reference temperature identified for the component and reported under one of the seven groups identified above. The post-processor collects, sorts, and reports the necessary information to enable documentation of the satisfaction of the applicable requirements. The following items are collected and evaluated for each load combination:

Seals: The normal force in each of the springs representing the seal is reported and shown to remain in compression under the load. Maintaining a compressive load in the seal springs assures that there is no separation at the component interfaces.

Bolts: The bolts are initially preloaded by applying an initial strain sufficient to result in the desired pre-stress. Subsequent to the application of the different loads to form a specified load combination, the bolts are shown not to unload.

Lid: For each load combination, the lid primary membrane plus primary bending stress intensities are compared to the allowable values at the designated reference temperature.

Inner Shell: Primary membrane and primary membrane plus bending stress intensity distributions are examined and compared to allowable stress intensity values.

Intermediate Shells: The five intermediate shells are examined at stress location points and compared to allowable stress intensities at the appropriate reference temperature. Since accident conditions of transport represent a Level D condition (where the comparison of calculated value vs. allowable value is always based on stress intensity), there is no differentiation between intermediate shells considered as Class 1 or Class 3 components.

Baseplate: Primary membrane plus bending stress intensities are compared to allowable values at the component reference temperature.

Enclosure: The plate and shell elements making up the enclosure for the Holtite-A material are compared to primary membrane stress intensity allowable values.

In the finite element analysis of all load combinations associated with hypothetical accident events, the initial preload case of the bolts and the internal pressure case are included in the final combination. Since no secondary stresses need be evaluated per the ASME Code requirements for an accident level event, the thermal stress load case for the "Heat" condition is not included as a specific load case. However, the allowable stress intensities used for the safety factor evaluation are obtained at the appropriate "Heat" condition reference temperature. In the reporting of safety factors, the variation in allowable stress intensity with temperature is ignored; this introduces an additional measure of conservatism in the reported safety factors since the reference temperatures (Table 2.1.21) are higher than the actual calculated temperatures. For the "Cold" condition, there are no temperature gradients developed. The interaction stresses developed to maintain compatibility under the uniform ambient temperature change are included in the analysis and are treated as primary stresses in the evaluation of the safety factor.

2.7.1.1 End Drop

- Overpack Stress (Load Cases 1,2,9, and 10 in Table 2.1.9)

The overpack is evaluated under both a top end drop and a bottom end drop. In both cases, the impact limiter reaction is assumed to act over the entire area that is backed by structural metal. Given that the total dropped weight is W and that the maximum acceleration is A, the impact

$$|R| = \frac{WA}{g}$$

limiter total reaction load follows from force equilibrium.

This reaction load R is imposed on the appropriate region of the overpack (either lid outer surface or bottom plate outer surface as a uniform pressure load to maximize the bending of the lid or bottom plate.

Since the same finite element model described and used in Section 2.6 for evaluation of loading associated with normal conditions of transport is used here with different applied loads, no further discussion of the model or the analysis methodology is required. Figures 2.1.7 and 2.1.8 show the loading on the overpack in the bottom down and the top down configurations, respectively. The results of the analyses for the top end and bottom end drops are collected and safety factors from the limiting locations in the model are reported in Tables 2.7.5 and 2.7.6 for both heat and cold environments. Table 2.7.5 presents the minimum safety factors for each of the components identified above for the "Heat" condition and Table 2.7.6 presents the safety factors for the "Cold" condition. Within each table, the component is identified, and the minimum safety factor reported.

- Overpack Stability

Structural stability of the overpack containment inner shell under the end drop is assessed. The case of the accident end drop is evaluated for elastic and plastic stability in accordance with the methodology of ASME Code Case N-284 [2.1.8]. All required interaction equation requirements set by [2.1.8] are met. For this event, yield strength limits rather than instability limits govern the minimum safety factor. The minimum safety factor for this case is summarized below:

Code Case N-284 Minimum Safety Factors - (Load Case 1 and 2 in Table 2.1.9)			
Item	Calculated Interaction Value	Allowable Interaction Value [†]	Safety Factor against Yield [†]
Load Case 1 and 2 in Table 2.1.9	0.62*	1.34	2.16*

* *Applicable to inner shell fabricated from SA203-E material. Safety factor must be multiplied by 0.93 if inner shell is fabricated from optional SA350-LF3 material.*

† Note that in computing the safety factor against yield for this table, the safety factor implicit in the Code Case N-284 allowable interaction equation is included. Note also that the safety factors given above from the Code Case analysis are all safety factors against the circumferential or longitudinal

stresses reaching the material yield stress. The actual safety factors against instability are larger than the factors reported in the table. In other words, yield strength rather than stability is the limiting condition. Finally, note that fabrication stresses have been included in the stability calculations even though these stresses are self-limiting. Therefore, all results corresponding to the calculated stability interaction equations are very conservative.

The result for the heat environment bound the similar result for the cold environment since yield strengths and elastic modulus are higher. Therefore, no analysis is performed for stability under cold conditions.

- Closure Bolt Analysis

Stresses are developed in the closure bolts due to pre-load, pressure loads, temperature loads, and accident loads. Closure bolts are explored in detail in Reference [2.6.3], which deals with the analysis of shipping casks. The analysis of the overpack closure bolts under normal conditions of transport has been reported in Section 2.6. This subsection presents the results for the analysis for the hypothetical accident end drop. The analysis follows the procedures defined in Reference [2.6.3]. The allowable stresses used for the closure bolts follows that reference. Note that the analyses provide alternative confirmation of the results from the finite element analysis; namely, under any of the identified load combinations, the bolts do not unload.

The following combined load case is for the hypothetical top end drop accident condition of transport. This drop conservatively assumes a nearly vertical orientation with the impact limiter reaction load applied at the outermost location of the lid. This results in the closure bolts resisting the inertial load from the MPC plus contents in addition to the inertia load from the closure lid itself. In reality, the load from the MPC would not load the bolts.

Top End Drop: Pressure, temperature, and pre-load loads are included.

Reference [2.6.3] reports safety factors defined as the calculated stress divided by the allowable stress for the load combination. This definition of safety factor is the inverse of the definition consistently used in this SAR. In summarizing the closure bolt analyses, results are reported using the safety factor definition of allowable stress divided by calculated stress. The following result for closure lid bolting for the top end drop hypothetical accident condition of transport is obtained.

Overpack Closure Bolt - Safety Factor (Load Case 2 in Table 2.1.9)	
Combined Load Case	Safety Factor on Bolt Tension
Average Tensile Stress	1.30

It is seen from the above table that the safety factor is greater than 1.0 as required. Note that the average tensile stress reflects the preload stress required for successful performance of the bolts as well as the applied load from the hypothetical accident drop event.

- MPC Fuel Basket Stability and Stress (Load Case F3.a in Table 2.1.6)

Under top or bottom end drop in a hypothetical accident condition of transport, the MPC is subject to its own amplified self-weight, causing compressive longitudinal stress in the fuel basket cell walls. The following analysis demonstrates that stability or yield is not a credible safety concern in the fuel basket walls under a hypothetical end drop accident condition of transport.

- MPC Fuel Basket Stability

Stability of the basket panels, under longitudinal deceleration loading (Load Cases F3.a in Table 2.1.6), is demonstrated in the following manner. Table 2.2.1 provides the weight of each fuel basket (including sheathing and ~~Boral~~ neutron absorber panels). The corresponding metal areas of the basket bearing on the MPC baseplate or top lid can be computed for each MPC basket by direct calculation from the appropriate drawings. Dividing weight by bearing area and multiplying by the design basis deceleration for the hypothetical accident from Table 2.1.10 gives the axial stress in the load bearing walls. The results for each basket are compared and the bounding result (maximum weight/area) reported below:

Fuel Basket Compressive Stress For End Drop (Load Case F3.a)			
Item	Weight (lb.)	Bearing Area (sq. inch)	Stress (psi)
Bounding Basket (at 60g's deceleration)	23,535	346.61	4,074

To demonstrate that elastic instability in the basket panels is not credible, the flat panel buckling stress, σ_{cr} , (critical stress level at which elastic buckling may occur) is computed using the formula in reference [2.6.1].

For conservatism, the MPC fuel basket is modeled as a rectangular plate simply supported along two sides and uniformly compressed in the parallel direction. The width of the plate is equal to the maximum unsupported width of a panel from all fuel basket types. Reference [2.6.1] provides the critical stress formula for these conditions as

$$\sigma_{cr} = \frac{2.3 \pi^2 E}{12 (1 - \nu^2)} \left(\frac{T}{W} \right)^2$$

where T is the panel thickness and W is the width of the panel, E is the Young's Modulus at the metal temperature and ν is the metal Poisson's Ratio. The following table summarizes the calculation for the critical buckling stress using the formula given above:

Elastic Stability Result for a Flat Panel	
Reference Temperature	725 degrees F
T (bounding thickness)	9/32 inch
W (bounding width)	11.0 inch
E	24,600,000 psi
Critical Axial Stress	33,430 psi

It is noted that the critical axial stress is an order of magnitude greater than the computed basket axial stress reported in the foregoing. Therefore, it is demonstrated that elastic stability under hypothetical accident condition of transport longitudinal deceleration inertia load is not a concern.

- MPC Fuel Basket Stress

The safety factor against yielding of the basket under longitudinal compressive stress from a design basis inertial loading is given by

$$SF = 17,100/4,074 = 4.198$$

where the yield stress of Alloy X has been taken from Table 2.3.1 at 725 degrees F.

Therefore, plastic deformation of the fuel basket under design basis deceleration is not credible.

Analyses of the Damaged Fuel canisters to be transported in the HI-STAR 100 Package are performed to demonstrate structural integrity under an end drop condition. A summary of the methodology and the results for all canisters is provided in Appendix 2.B.

- MPC Enclosure Shell Stability

Structural stability of the MPC enclosure shell under the end drop is evaluated for elastic and plastic/stability in accordance with the ASME Code Case N-284 [2.1.8]. All required interaction equation requirements set by [2.1.8] are met. It is shown that yield strength limits rather than instability limits govern the minimum safety factor. The minimum safety factor for this case is summarized below:

MPC Shell Elastic/Plastic Stability (Load Case E3.a Table 2.1.7)			
Item	Value	Allowable*	Safety Factor
Yield	0.698	1.34	1.92

* For Load Case E3.a, the yield strength criteria in the Code Case N-284 method govern. In this event, the safety factor 1.34, built into the Code Case, is included in the tabular result in order to obtain the actual safety factor with respect to the yield strength of the material.

- MPC Closure Lid Stress (Load Case E3.a)

The closure lid, the closure lid peripheral weld, and the closure ring are examined for maximum stresses developed during the hypothetical end drop accident event.

The closure lid is modeled as a single simply supported plate and is subject to deceleration from an end drop plus appropriate design pressures. Results are presented for both the single and dual lid configurations (in parentheses) for top end and bottom end drops. For the dual lid configuration, the two plates each support their own amplified weight as simply supported plates under a bottom end drop. The inner lid transfers the total load to the outer plate through the peripheral weld between the two lids. Under a top end drop scenario, the inner lid is partially supported by the outer lid and the amplified load is transmitted by a combination of peripheral support and interface contact pressure. The results for minimum safety factor are reported in the table below:

MPC Top Closure Lid - Minimum Safety Factors - Load Case E3.a in Table 2.1.7			
Item	Stress(ksi) or Load(lb.)	Allowable Stress (ksi) or Load Capacity (lb.)	Safety Factor
Lid Bending Stress - Load Case E3.a (bottom end drop)	3.35/(7.94)	60.7	18.1/(7.65)
Lid Bending Stress* - Load Case E3.a (top end drop)	21.9/(43.8)	60.7	2.77/(1.39)
Lid-to-Shell Peripheral Weld Load - Load Case E3.a	624,000	1,477,000**	2.37
Lid-to-Lid Peripheral Weld Load - Load Case E3.a (bottom end drop)	312,000	443,200***	1.42

* Stress computation is conservatively based on peripheral support at the outer diameter of the MPC lid. For a top end drop, the actual support diameter is .77 of the outer diameter. Therefore, an analysis based on an overhung plate would provide stresses reduced by a multiplier of 0.59. Consequently, the safety factors would be amplified by the factor 1.69.

** Based on a 0.625" single groove weld and conservatively includes a quality factor of 0.45.

*** This is a non-Code weld; limit is based on a 0.1875 groove weld and includes a quality factor of 0.45 for additional conservatism

Safety factors are greater than 1.0 as required. The limiting condition for the lid bending evaluation is a top end hypothetical accident end drop because the lid supports the amplified fuel weight as well as the lid amplified self-weight.

- MPC Baseplate and Canister Stress (Load Case E3.a)

Load Case E3.a provides the limiting accident loading on the baseplate wherein the combined effect of a 60g deceleration plus external pressure is considered. The top end hypothetical accident condition is limiting in transport, and here it is conservatively assumed that accident external pressure acts simultaneously, which exceeds the requirements of Table 2.1.7. The results are summarized below:

MPC Baseplate Minimum Safety Factors – Load Cases E3, Table 2.1.7			
Item	Value (ksi)	Allowable (ksi)	Safety Factor
Center of Baseplate - Primary Bending (Load Case E3)	22.12	67.32	3.04
Shell Bending Stress at Connection to Baseplate	31.47	67.32	2.14

Note that all safety factors are greater than 1.0. Also, note that the calculated stress conservatively includes both primary and secondary self-limiting stress components. For the hypothetical transport drop accident, the safety factor computed for the shell bending stress intensity need only consider the effect of primary membrane plus bending stresses that are to be compared against the ultimate stress at temperature for this ASME Code Service Level D event. Since secondary stresses have been included in the evaluation, the reported result for safety factor is conservatively low.

- Trojan MPC Spacer

The Trojan MPC-24E/EF enclosure vessel is 9 inches shorter in length than the generic MPC-24E/EF enclosure vessel. Thus, when the Trojan MPC-24E/EF is transported inside the HI-STAR 100, the axial clearance between the MPC lid and the HI-STAR 100 closure plate is greater than 10 inches. In order to prevent the Trojan MPC from thrusting forward and impacting the closure plate during a top-end drop or a tip-over event (i.e., slapdown), a spacer device is positioned on top of the MPC lid. The Trojan MPC spacer, depicted in Figure 1.1.5, is fabricated from SA240-304 stainless steel in the shape of a circular I-beam. The web of the spacer measures 1-inch thick and has a mean diameter of 60 inches. The total height of the MPC spacer is 9 inches.

During a top end drop, the MPC spacer must support the amplified weight of a fully loaded Trojan MPC-24E/EF. Based on a bounding MPC weight of 90,000 lb (Table 2.2.4) and a bounding deceleration of 60g (Table 2.1.10), the maximum compressive stress in the web is computed as follows.

$$\text{Cross-sectional area of web (A)} = \pi \times D \times t = \pi (60) (1) = 188.5 \text{ in}^2$$

$$\text{Amplified weight of MPC (P)} = G \times W = (60) (90,000) = 5.4 \times 10^6 \text{ lb}$$

$$\text{Compressive stress in web} = P/A = (5.4 \times 10^6) / 188.5 = 28,647 \text{ psi}$$

From Table 2.1.18, the primary membrane stress intensity limit for Alloy X (of which SA240-304 is a member) under Level D conditions is 44.9 ksi at 400°F. Therefore, the safety factor against compressive failure of the Trojan MPC spacer, per ASME Code Subsection NB stress limits, is

$$SF = 44,900 / 28,647 = 1.56$$

2.7.1.2 Side Drop (Load Cases F3 in Table 2.1.6, E3 in Table 2.1.7, and 3 and 11 in Table 2.1.9)

- MPC Fuel Basket and Canister Finite Element Analysis (Load Cases E3.b, E3.c in Table 2.1.7 and Load Cases F3.b, F3.c in Table 2.1.6)

The MPC configurations are assessed for a hypothetical accident condition of transport side drop. All fuel cells are loaded with design basis spent nuclear fuel (SNF). Evaluations are performed for the 0 degree and the 45 degree circumferential orientations of the fuel basket as defined in Figures 2.1.3 and 2.1.4 and are obtained using the finite element model described in Section 2.6.

The results for each MPC configuration for the two different drop orientations are evaluated for each appropriate load case listed in Tables 2.1.6 and 2.1.7. Analyses are performed only for the hot ambient temperature condition since this is the bounding case for the MPC; as noted in Section 2.6, allowable stresses are lower for the “heat” environmental condition.

- Elastic/Plastic Stability of the MPC Fuel Basket

Following the provisions of Appendix F of the ASME Code [2.1.12] for stability analysis of Subsection NG structures, (F1331.5(a)(1)), a comprehensive buckling analysis is performed using ANSYS. For this analysis, ANSYS's large deformation capabilities are used. This feature allows ANSYS to account for large nodal rotations in the fuel basket, which are characteristic of column buckling. The large deflection option is “turned on” so that equilibrium equations for each load increment are computed based on the current deformed shape. The interaction between compressive and lateral loading, caused by the deformation, is included in a rigorous manner. Subsequent to the large deformation analysis, the basket panel that is most susceptible to buckling failure is identified by a review of the results. The lateral displacement of a node located at the mid-span of the panel is measured for the range of impact decelerations. The buckling or collapse load is defined as the impact deceleration for which a slight increase in its magnitude results in a disproportionate increase in the lateral displacement.

The stability requirement for the MPC fuel basket under lateral loading is satisfied if two-thirds of the collapse deceleration load is greater than the design basis horizontal acceleration (Table 2.1.10). Figures 2.7.1, through 2.7.6 are plots of lateral displacement versus impact deceleration for representative fuel baskets. It should be noted that the displacements in Figures 2.7.1, 2.7.2, 2.7.3, 2.7.4, and 2.7.5 are expressed in 1×10^{-1} inch and Figure 2.7.6 is expressed in 1×10^{-2} inch. The plots clearly show that the large deflection collapse load of the MPC fuel basket is greater than 1.5 times the inertia load corresponding to the design basis deceleration for all baskets in all orientations. Thus, the requirements of Appendix F are met for lateral deceleration loading under Subsection NG stress limits for faulted conditions. Therefore, it is concluded that stability of the spent fuel basket cell walls is assured under the hypothetical accident side drop (from 30') condition of transport.

An alternative solution for the stability of the fuel basket panel is obtained using the methodology espoused in NUREG/CR-6322 [2.7.3]. In particular, the fuel basket panels are considered as wide plates in accordance with Section 5 of NUREG/CR-6322. Eq.(19) in that section is utilized with the “K” factor set to the value appropriate to a clamped panel. Material properties are selected corresponding to a metal temperature of 500 degrees F which bounds computed metal temperatures at the periphery of the basket. The critical buckling stress is:

$$\sigma_{cr} = \left(\frac{\pi}{K}\right)^2 \frac{E}{12(1-\nu^2)} \left(\frac{h}{a}\right)^2$$

where h is the panel thickness, a is the unsupported panel length, E is the Young’s Modulus of Alloy X at 500 degrees F (Table 2.3.1), ν is Poisson’s Ratio, and K=0.65 (per Figure 6 of NUREG/CR-6322).

Parameters appropriate to a MPC-24E basket are used; the following table shows the results from the finite element stress analysis and from the stability calculation.

Panel Buckling Results From NUREG/CR-6322			
Item	Finite Element Stress (ksi)	Critical Buckling Stress (ksi)	Factor of Safety
Stress	13.339	49.826	3.74

For a stainless steel member under an accident condition load, the recommended safety factor is 2.12. It is seen that the calculated safety factor exceeds this value; therefore, an independent confirmation of the stability predictions of the large deflection analysis is obtained based on classical plate stability analysis.

- Overpack Stress Analysis (Load Cases 3 and 11 in Table 2.1.9)

The overpack is assumed to be subject to a 60g side drop in the manner of the load combinations of Table 2.1.9 for both heat and cold environmental conditions as prescribed by Regulatory Guide 7.9. Reaction loads provided by the impact limiters are imposed as vertical pressures at each end of the overpack on areas of the structure that serve as backing. The applied mechanical loading is internal pressure, inertia load from the MPC and inertia load from the overpack self-weight. Figure 2.1.9 shows the assumed loading for this simulation. Figures 2.7.7, and Figures 2.7.11-2.7.13 are useful to aid in understanding the methodology used to apply the MPC loads and the balancing impact limiter reactions. Figure 2.7.7 shows a view of the overpack looking along the longitudinal axis for the general case of an oblique drop. While the intent of the figure is to describe the reaction loads from the impact limiter under a general oblique drop orientation, only the features necessary to elaborate on the side drop reaction load are discussed here. A region defined by the angle θ supports the applied loading in a side drop.

This angle is 18 degrees for the side drop and is chosen based on two considerations. First, the predictions from the theoretical model at the time of maximum “g” loading are examined and a projected loaded area on the top forging and bottom plate estimated. Second, the post-drop evaluation of the tested impact limiters from the one-eighth scale static test and the one-quarter scale dynamic test were visually examined and provided insight into the extent of the loaded region of the overpack at the impact limiter-hard surface interface. From these two evaluations, a conservatively low angle estimate is made for the finite element analysis. Figure 2.7.12 shows the extent around the periphery of the loading imposed by the MPC. From Section 2.6, the angle over which the MPC load is applied to the inner shell of the overpack is 72 degrees from the vertical on each half of the overpack. This angle is determined from the detailed analysis of the MPC enclosure shell and the fuel basket under 60g loading. The inertia load from overpack self-weight is applied by imposing an amplified value for the gravitational constant. Details of the finite element model have been discussed in Section 2.6. The results of the finite element analyses for load cases 3 and 11 in Table 2.1.9, for the overpack, are post-processed as previously discussed; Tables 2.7.5 and 2.7.6 summarize the results for each overpack component and identify the minimum safety factors.

2.7.1.3 Corner Drop

Figures 2.1.10 and 2.1.11 show the assumed loading for the bottom center of gravity over corner (CGOC) drop and the top CGOC drop, respectively. The impact limiter reaction load is applied as a pressure loading acting on two surfaces. From the geometry of the cask, with impact limiters in place, the angle of impact is 67.5 degrees from the horizontal plane. Although the theoretical and tested deceleration levels are below 60g’s, the design basis 60g-deceleration load is used as the input loading and applied vertically. Therefore, a 55g load is applied along the longitudinal axis of the cask, and a 23g load is applied perpendicular to the cask longitudinal axis.

The lateral inertia load from the MPC, amplified by the appropriate multiplier corresponding to 23g’s, is applied in the manner shown in Figures 2.7.11 and 2.7.12. The longitudinal component of the load from the MPC, amplified by 55g, is applied as a pressure over the inside surface of the lid as shown in Figure 2.7.8. In reality, the load would be applied over a narrow annulus near the outside radius of the lid because of the raised “landing region”. To maximize lid and bolt stress, however, the load is applied as a uniform pressure in the finite element model. The corresponding lateral and longitudinal loads from the overpack self-weight are applied by imposing amplified gravitational accelerations in the appropriate directions.

The loading from the impact limiter at the other end of the overpack, not involved in the impact, is applied as a uniform pressure over the surface of the backed area at the other impact limiter. Figure 2.7.10 shows the loading on the outside surface of the bottom plate that arises from the bottom end impact limiter during simulation of a top end drop. The total bottom impact limiter weight is amplified by 55g’s and applied as a pressure load. At the top end, where the impact limiter provides the distributed crush force to balance the inertia forces, the balancing reaction loads from the impact limiter are applied as a distributed side pressure loading and a distributed end surface pressure. The extent of the loaded region for this drop orientation is defined by the angle θ in Figure 2.7.7. For this case, the angle is approximately 68 degrees since a large “backed” area of the impact limiter is involved in resisting the crush. The angle is consistent with the predictions from the intersection geometry analysis used to develop the force-deformation data used in Appendix 2.A. That force-

crush model has been successfully used to predict maximum decelerations and extent of crush. Static finite element models require setting a fixed origin to insure satisfaction of all equilibrium equations. The center of gravity-over-corner orientation, in theory, provides automatic satisfaction of moment equilibrium so that all forces and moments at such a fixed origin location should be zero.

In this analysis and in the general oblique drop analysis, the fixed point is assumed at a location at the end of the overpack not impacted. The results from the finite element simulation confirm that the computed reactions are negligibly small compared to the applied loads. The loads from internal pressure are self-balancing and do not alter the calculation of equilibrium reactions. Tables 2.7.5 and 2.7.6 summarize the results from these analyses.

Results for the MPC and its internals have been discussed in Subsections 2.7.1.1 and 2.7.1.2 for the end and side drops, respectively, under the action of 60g deceleration and appropriate pressure loading. Under an oblique drop at an angle θ with respect to the target plane ($\theta = 0$ degrees equals the side drop), the MPC and its internals experience deceleration loads parallel and perpendicular to the MPC longitudinal axis. Each of these deceleration components, however, is less than the 60g design basis deceleration used in the end and side drop analyses. For the pure end drop, all stresses in the fuel basket and in the MPC canister (enclosure vessel) are axial. For the pure side drop, the conservative analysis of a 2-D section of the fuel basket and enclosure vessel gives rise to stresses in a plane perpendicular to the longitudinal axis of the MPC/fuel basket.

The results for any oblique drop can be obtained by a linear combination of the results for pure end drop and pure side drop. That is, the combined stress intensity is formed from the results of the two individual cases, after adjustment for the actual lateral and longitudinal "g" levels experienced by the components.

The MPC lid and baseplate are thick plate components; as such, the stress intensities experienced in the end drop orientation (which loads the lid and/or the baseplate in flexure) bound all other cases. Therefore, in what follows; only the enclosure vessel and the fuel basket need be considered. For each of these structures, the result " R_θ ", at a general oblique drop angle θ , is expressed in terms of the result for an end drop " R_{90} " and the result obtained for a pure side drop " R_0 " as:

$$R_\theta = R_{90} \left(\frac{g_E}{60} \right) + R_0 \left(\frac{g_S}{60} \right)$$

where g_E and g_S are the axial and lateral decelerations imposed on the MPC canister and fuel basket during the oblique drop at angle θ .

Since $g_E = 60 \sin \theta$, and $g_S = 60 \cos \theta$,

for a design basis oblique drop where the vertical deceleration is 60 g's, the result for the oblique drop is always expressed in the form,

$$R_\theta = R_{90} \sin \theta + R_0 \cos \theta$$

The following results are obtained for the end drop and side drop analyses:

End Drop:

Fuel Basket – maximum longitudinal membrane stress = 4,074 psi

Enclosure Vessel – maximum longitudinal compressive stress = 11,260 psi

The enclosure vessel result is obtained from the Code Case N-284 evaluation for a bottom end drop and conservatively bounds the result for a top end drop. The longitudinal compressive stress in the enclosure vessel includes the effect of external pressure.

Side Drop:

Stress intensity results for the fuel basket and enclosure vessel are summarized in Table 2.7.4. From Table 2.7.4, for the pure side drop, the minimum safety factor for the fuel basket is 1.17 (primary membrane plus primary bending). The corresponding minimum safety factor for the enclosure vessel is 2.64 (again, for primary membrane plus primary bending). The preceding results are obtained by surveying the summary of minimum safety factors in Table 2.7.4 for all MPC's and both fuel basket orientations within the MPC.

For the pure side drop orientation, the stress intensities (SI) associated with the minimum safety factors are:

Fuel Basket SI = 47,060 psi

Enclosure Vessel SI = 24,650 psi

The stress intensities at the most limiting location for the general oblique drop orientation are then computed as:

Fuel Basket SI = $4,074 \sin \theta + 47,060 \cos \theta$

Enclosure Vessel SI = $11,260 \sin \theta + 24,650 \cos \theta$

For the corner drop, $\theta = 67.5^\circ$ leading to the following final results:

C.G. OVER CORNER DROP MPC SAFETY FACTORS			
Item	Calculated S.I.	Allowable S.I.	Safety Factor
Fuel Basket	21,773 psi	55,450 psi [†]	2.55
Enclosure Vessel	19,836 psi	65,200 psi ^{††}	3.29

[†] at 725°F

^{††} at 450°F

As expected, the safety factors obtained for the corner drop are larger than the corresponding values obtained for the side drop.

Results for general oblique drop angles are now considered for the overpack. In particular, a 30-degree oblique drop is deemed to be most representative of a scenario where only a primary impact is involved. The general formula utilized in the preceding for the specific case of center-of-gravity-over-corner can also be used for a 30-degree drop angle. The following results are reported for the fuel basket and enclosure vessel.

30 DEGREE OBLIQUE DROP MPC SAFETY FACTORS			
Item	Calculated S.I. (psi)	Allowable S.I. (psi)	Safety Factor
Fuel Basket	42,792	55,450 [†]	1.30
Enclosure Vessel	26,978	65,200 ^{††}	2.42

[†] at 725°F

^{††} at 450°F

2.7.1.3.1 MPC "F Class" Enclosure Vessel Lid-to-Shell Weld

The Holtec MPCs labeled with the suffix "F" (designated as "F Class" in this subsection) are intended to store non-intact fuel (defined as damaged fuel in the latest revision of ISG-1 and "failed fuel and fuel debris" in this SAR).

To be certified to store loose fuel debris, the MPC must fulfill the function of the "secondary containment" required by 10CFR71.63(b). To qualify as a "secondary containment", the MPC Enclosure Vessel must be able to withstand the accident condition loading without releasing its contents. The accident condition mechanical loading for the secondary containment is identical to those for the primary containment, namely the inertia forces produced by a 60g deceleration. From Table 2.1.7, the pressure loads applicable to the MPC Enclosure Vessel during a hypothetical vertical end drop (Load Case E3.a) are the normal condition pressures. Therefore, per Table 2.1.1, the maximum pressure differential that exists across the MPC shell when a drop occurs is 60 psig. For conservatism, however, the accident condition internal pressure of 200 psig is used to qualify the MPC Enclosure Vessel as a secondary containment. All candidate vulnerable locations in the MPC Enclosure Vessel must be analyzed to ensure that a thru-wall breach in the pressure-retaining boundary does not occur under the loading combination defined above. In the case of the primary containment (the HI-STAR 100 overpack), the location of containment vulnerability is the cask lid-to-body forging bolted joint; the evaluation of the lid-to-body closure bolt has been analyzed to demonstrate containment integrity and the results of the evaluation summarized in Subsection 2.7.1.1 of the SAR. For the MPC "F Class", considered as secondary containment, the corresponding locations of vulnerability are the two extremities of the Enclosure Vessel where the vessel shell is joined to flat (plate-like) members.

The top lid-to-shell joint, a J-groove (partial penetration) joint made at the plant after fuel loading, is one candidate location, as this weld cannot be volumetrically examined even though the top lid is relatively thick. The MPC baseplate to the shell weld, on the other hand, is a shop-fabricated and volumetrically examined junction. However, because the baseplate is thinner than

the top lid, it may experience greater flexural action under the accident condition mechanical loading, resulting in somewhat greater junction region stresses. Therefore, the weld joints at both extremities of the MPC Enclosure Vessel are denoted as candidate locations whose structural integrity under the load combination appropriate to the MPC's secondary containment function must be demonstrated.

a. Top lid-to-shell joint

For MPCs with the "F" designation, this joint has been buttressed with a thick tapered shell and deeper J-groove weld than that utilized in the standard MPC Enclosure Vessel. A Holtec proprietary position paper, DS-213, "Acceptable Flaw Size in MPC Lid-to-Shell Welds", submitted to the NRC in support of the original certification of HI-STAR 100 in 1999 demonstrates that the largest postulated flaw in the most adverse orientation in the lid-to-shell joint in the "F" canister will not propagate under the impulsive inertia loading arising from a 60g axial deceleration of the MPC's contents.

An elastic stress analysis in the spirit of the ASME Code documented below likewise shows a large margin of safety against joint failure. For conservatism, the following assumptions are made.

- i. The closure ring (the structural member present to provide a second welded barrier against leakage of the contents) is assumed to be absent.
- ii. Even though a thru-wall failure of the joint is the appropriate failure criterion for the joint, non-exceedance of the ASME Code Section III Subsection NB stress intensity limits appropriate to Level D limits, which will occur at a much lower loading level, is set down as the acceptance limit. However, no weld efficiency factor is applied to the lid-to-shell weld since it is not required by Subsection NB.
- iii. The MPC model with the heaviest contents (MPC-32) is used in the analysis to bound the results for all "Type F" MPC models.

The MPC top lid may be fabricated as a single thick circular plate, or may be fabricated as a dual lid with the outer lid attached to the shell with the "J" groove weld, and the inner lid attached to the outer lid around the common periphery. The dual lid configuration has been analyzed for both Normal Conditions of Transport and Hypothetical Accident Conditions of Transport for MPC's carrying intact fuel; the results are documented in Subsection 2.6.1.3.1.2, and 2.7.1.1, respectively. The evaluation for the "F Class" MPC to provide secondary containment capability utilizes the same analytical model but introduces additional assumptions into the analysis to direct load to the lid-to-shell weld. In particular, a top end drop is postulated with the dual lids subjected to a 60g deceleration loading from the fuel, fuel basket, and lid weight, together with the accident internal pressure of the MPC. During a top end drop, the MPC cannot rotate relative to the HI-STAR overpack because of close clearances between the vessel shell and the inner surface of the overpack cavity. Therefore, regardless of the angle of impact, the reaction load from the HI-STAR to equilibrate the applied loads on the lid is uniformly distributed around the circumference. A bounding condition for this analysis for secondary containment is presumed to

be a top end drop where the Enclosure Vessel shell is assumed to contact the support (the HI-STAR lid) before the Enclosure Vessel lid; with this conservative assumption, the peripheral weld is subject to the entire applied load. The key results from the analyses (the case of dual lids bounds the analysis assuming a single thick lid) to support qualification of the MPC "F Class" as secondary containment are summarized in the table below:

KEY RESULTS FOR SECONDARY CONTAINMENT QUALIFICATION OF F CLASS MPC's – Load Case E3.a in Table 2.1.7 (Top End Drop)			
Item	Stress Intensity (ksi) or Load (lb)	Allowable Stress Intensity @ 550 Degrees F (ksi) or Load Capacity (lb)	Safety Factor
Structural Lid Bending Stress Intensity	46.05	60.7	1.32
Shield Plug Bending Stress Intensity	46.65	60.7	1.30
Lid-to-Shell Weld Load	5,268,000	6,627,000	1.26
Primary Local Axial Membrane Stress Intensity at Shell Contact Interface	24.53	40.45	1.65

b. Baseplate-to-Shell Joint

Because the baseplate-to-shell connection is a volumetrically examined, full penetration joint, flaw propagation under the accident condition inertia loads is not a concern for this location. As in the case of the top lid-to-shell junction, the baseplate-to-shell joint is established to be sufficiently robust if the stress intensity limits under the above load combination (appropriate for §71.63(b)) are below their corresponding limits for level D condition for Section III Class 1 (NB) components. Since the baseplate-to-shell joint in the MPC "F Class" units is identical to the joint in the MPC's used for intact fuel, no new analyses are required. The results of evaluation of this joint are reported in Subsection 2.7.1.1 and demonstrate substantial safety factors.

The above analyses demonstrate that the Enclosure Vessel for "Type F" MPCs is capable of serving as a "secondary containment" as required by §71.63(b).

2.7.1.4 Oblique Drops

Appendix 2.A contains results of analytical simulations for various orientations of the cask at impact. In Appendix 2.A, it is shown that lateral decelerations are large for the near side drop (slapdown) and decrease as the angle of orientation, with respect to the horizontal plane, increases. Therefore, it is likely that results presented in Subsections 2.7.1.1 through 2.7.1.3 are bounding for all orientations other than the near side drop (slapdown) in that at any other angle, the resulting g-loads in each direction (longitudinal and lateral) are smaller than the bounding deceleration loads applied in the end, side, and corner drops. Nevertheless, based on the results obtained in Appendix 2.A, the case of an oblique drop with primary impact at 30 degrees from the horizontal is analyzed in detail. This case covers all orientations where the maximum deceleration load occurs and is reacted by the primary impact limiter. For this case, moment equilibrium includes inertia loads from overpack rotation as well as linear deceleration. For the 30-degree drop orientation at the primary impact location, the design basis deceleration load is applied with 52g lateral component and 30g longitudinal component. The loads are applied in the same manner as discussed in Subsection 2.7.1.3 with one additional complication. In contrast to the center of gravity over corner orientation where moment equilibrium is automatically satisfied when the loads are correctly applied, the applied loads and the reaction loads from the impact limiter are not initially in moment equilibrium. No inertial loading due to overpack rotational motion at the instant being considered is included. Without an additional inertial moment loading component, a large reaction force would develop at the far-removed arbitrary fixed reference point because the impact limiter reaction loads are offset from the overpack and MPC inertia loads from the linear decelerations. Figure 2.7.14 shows the overpack in a general oblique orientation. Appropriate arrows show the impact limiter reaction forces and the components of the applied linear decelerations. The loads from the MPC are not shown on the figure but they are applied as previously described for the corner drop. It is clear that moment equilibrium is not satisfied unless reaction loads develop at the arbitrarily chosen fixed support location far removed from the impact point. In the real drop scenario, since there is only a primary impact reaction, the cask must have angular accelerations imposed to insure moment equilibrium since the fixed point is an artifact to meet the requirements of the finite element analysis. To zero this reaction load at the point far-removed from the impact location, an additional load case with a unit angular velocity imposed at the mass center of the system and no other loads is developed. An angular acceleration is internally generated by ANSYS for this load case. The solution to this load case provides a reaction at the hypothetical fixed point assumed at the end of the overpack far removed from the impact location to balance the imposed inertial moment. The addition of this load case, with proper magnitude and sign ascribed to the input angular velocity, serves to eliminate all reactions at the far-removed fixed point. By adding this inertia moment load case, both force and moment equilibrium equations are satisfied for the oblique drop case where there is only a single impact limiter providing external forces to react the cask motion. With reference to Figure 2.7.7, the extent of the impact limiter loaded region on the overpack for this case is $\theta = 63$ degrees. This angle is estimated from the projected geometry from the theoretical analysis in Appendix 2.A. Figure 2.7.9 shows a side view of the top forging with the end loading from the impact limiter applied as a pressure over the loaded region.

The finite element solution provides stress intensity results for the hot and cold conditions. The safety factors are summarized in Tables 2.7.5 and 2.7.6 (identified as Load Cases 20 and 21 corresponding to the "heat" and "cold" environmental conditions).

The near side drop with impact at the secondary impact limiter (slapdown) is a special case that also merits detailed analysis. For this case, the angle of the cask with the target is near zero degrees, similar to that used for the side drop analysis. The nature of the equilibrium equations is quite different, however. For the side drop, Figure 2.7.17 shows that equilibrium is satisfied by impact limiter reaction pressures at both impact locations. The reaction lateral pressure distribution at each impact limiter is distributed in the manner described by Figure 2.7.7. For the side drop evaluation, no introduction of a rotational component to the overpack is required to insure moment equilibrium. For the analysis of the near side drop secondary impact case, all of the reaction force required to insure that force equilibrium is maintained under the inertia induced loads, is imposed at the location of the secondary impact limiter. Figure 2.7.18 shows a side view of the overpack with the reaction load applied over a specified arc in the same manner as described by Figure 2.7.7. At the time of peak secondary impact deceleration, the theoretical analysis predicted minimal axial deceleration. Therefore, to perform the stress analysis using the finite element model, no axial deceleration is imposed. Referring to Figure 2.7.7, the angle θ for this evaluation is chosen on the basis of observed experimental results and theoretical prediction. The angle is related to the angle associated with the observed crush depth of the impact limiter itself. For a near side drop, the outer diameter of the impact limiter is known, and if the crush depth is observed, calculated, or measured, the angular extent of impact limiter crushed material is easily determined. The outer radius, "Ri" of the impact limiter, and the observed and calculated crush depth (see results in Appendix 2.A for a full scale impact limiter), "d", are:

$$R_i = 64"; \quad d = 15"$$

Therefore, the angle " ϕ " (on either side of a vertical diameter through the impact limiter) that is associated with the extent of loaded crushed surface of the impact limiter is obtained from simple geometry as:

$$\text{Cos}(\phi) = 1 - d/R_i$$

The angle over which the load is applied at the crushed surface of the impact limiter is calculated to be:

$$\phi = 40 \text{ degrees (measured from the vertical, on both sides of the vertical centerline).}$$

The angle of significant reaction loads on the interface surface of the top forging, is greater than this angle. However, it is conservative to perform the finite element analysis of the "slapdown" secondary impact event, using the load angle

$$\theta = \phi = 40 \text{ degrees.}$$

Note that this angle used for the "slapdown" evaluation is larger than the conservative value used to evaluate the side drop. This reflects the increased crush imparted to the impact limiter since the entire amplified load is reacted at the top end. The load from the MPC is imposed on the appropriate inside surface of the inner shell as a uniform load in the same manner as for the side drop analysis. Moment equilibrium is provided by imposing the additional pure rotation on the overpack sufficient to generate opposite reaction forces that zero out the combined reactions at the "balance point" from

the applied inertia decelerations plus the pure rotation case. Because the MPC is constrained within the overpack, no departure from a uniform load transfer to the overpack is anticipated. Therefore, the enforcement of moment equilibrium for this condition is ensured solely by the determination of a proper balancing moment by determining an appropriate angular acceleration for the overpack. This assumption has little effect on the computation of the primary stress intensity distribution that results from the impact.

The results of the analysis are tabulated and combined with other load conditions, and the combined load case is designated as "Load Case 22". Bolt preload, internal pressure, and the inertia loads are combined to form this "slapdown" simulation. The top-end secondary impact analysis reported herein bounds a similar analysis of the bottom end secondary impact case. Summary results for minimum safety factors are reported in Table 2.7.5 only for the "Heat" environmental condition as previous results have demonstrated that this case produces the minimum safety factors. Only primary stress intensities are surveyed and reported in accordance with ASME requirements. Also evaluated is the bolt stress, the net friction force, and the state of the seals and lands. From the post-processed results, it is concluded that no bolts are overstressed, no portion of the seals suffer unloading, and that there is sufficient frictional force to insure that the lid is maintained in position.

The preceding discussion focussed on the transport overpack analyses. The minimum safety factors for the MPC fuel basket and enclosure vessel, for arbitrary drop orientation, are obtained from the general formulation in the preceding subsection 2.7.1.3. The angle that provides the maximum combined stress intensity (S.I.) can be determined by classical means, and the minimum safety factor established. The results are summarized in the table below:

GENERAL OBLIQUE DROP ORIENTATION MPC – SAFETY FACTORS				
Item	Drop Orientation Angle (Degrees)	Calculated S.I. (psi)	Allowable S.I. (psi)	Safety Factor
Fuel Basket	4.54	47,208	55,450	1.17
Enclosure Vessel	24.55	27,100	65,200	2.41

2.7.1.5 Comparison with Allowable Stresses

Tables 2.7.4 through 2.7.8 summarize the limiting safety factor obtained for each hypothetical free drop accident condition of transport defined by the requirements of Regulatory Guide 7.9. In particular, Table 2.7.4 is a summary of safety factors from the analyses of the MPC fuel basket and enclosure vessel, and Tables 2.7.5 and 2.7.6 report safety factors from the overpack analyses. Finally, Tables 2.7.7 and 2.7.8 contain safety factor summary results from miscellaneous evaluations reported within the text. From these results, tables are constructed that summarize limiting safety factors for all of the hypothetical accident conditions of transport that are associated with drop events. Tables 2.7.1 through Tables 2.7.3 present the overall summary of the most limiting safety factor for each of the components of interest for all hypothetical accident conditions of transport. It is concluded from these tables that large factors of safety exist in the fuel basket, in the MPC shell, and in the various components of the overpack under all hypothetical accident conditions of

transport associated with free drop events.

It is noted that the overpack finite element results are developed using a 3-D model of the overpack. Even though symmetry conditions reduce the size of the model, there are over 8000 elements and 11000 nodes.

The postulated accident conditions all tend to load localized regions of the overpack. As an illustration, consider Load Case 20, the 30-degree oblique top-end impact with the target. The limiting results for safety factors are reported in Table 2.7.5. Figures 2.7.15 and 2.7.16 show stress intensity distributions for the inner shell and for the assemblage of intermediate shells, respectively. As expected, the regions of highest stress intensity are naturally concentrated near the impacted region.

2.7.2 Puncture

- Overpack Structural Components

10CFR71 mandates that a puncture event be considered as a hypothetical accident condition. For this event, it is postulated that the package falls freely through a distance of 1 meter and impacts a 6 inch diameter mild steel bar. The effects of the puncture drop are most severe when the steel bar is perpendicular to the impact surface. Therefore, all puncture analyses assume that the bar is perpendicular to the impact surface. It is assumed that the steel bar has a flow stress equal to 48,000 psi, which is representative of mild steel. The maximum resisting force can then be calculated as

$$F_R = \frac{\pi D^2}{4} \times 48,000 \text{ psi} = 1.357 \times 10^6 \text{ lb}$$

where D equals the diameter of the steel bar.

$$|A_p| = \frac{F_R g}{W}$$

Since the maximum force applied to the cask is limited to the above value, the average deceleration of the cask can be computed assuming it to be rigid. The average deceleration of the cask (plus contents) (weight = W) is determined as:

For a bounding (low) weight of 230,000 lb. (Table 2.2.1), for example, the rigid body average deceleration over the time duration of impact, is 5.9g.

Candidate locations for impact that have the potential to cause the most severe damage are near the center of the closure plate (top-end puncture), the center of the bottom plate (bottom puncture), and the center height of the overpack shells (side puncture). In accordance with Regulatory Guide 7.9, local damage near the point of impact and the overall effect on the package must be assessed.

An estimate of local puncture resistance is obtained by using Nelms' equation [2.7.1] that is

generally applicable only for lead backed shells. Nevertheless, it is useful to obtain an indication as to whether a potential problem exists in the HI-STAR 100 System. The equation is applied using an ultimate strength of 70,000 psi that is appropriate for the selected impact regions. Nelms' equation predicts a minimum thickness of material necessary to preclude significant puncture damage. For the HI-STAR 100 System,

$$t_m = \left(\frac{W}{S_u} \right)^{0.71} = 2.65 \text{ inch}$$

Inasmuch as the HI-STAR 100 overpack has substantially more material thickness in the baseplate, the closure plate, the top flange and the inner plus the initial intermediate shell, the overpack meets local puncture requirements as required by Nelms' equation.

The global effects of puncture are calculated using the overpack model described in Section 2.6, which is the same model that is used for the drop assessments. Figures 2.1.12 through 2.1.14 show free body diagrams of the overpack for the side, top, and bottom puncture events, respectively. In each case, the nodes on the surface of the overpack that directly impact the steel bar are fixed in all degrees of freedom. By then applying acceleration, A_p , a reaction force develops at those nodes equal in magnitude with F_R . Tables 2.7.5 and 2.7.6 summarize the safety factors for the overpack components obtained for the puncture acceleration computed above for both heat and cold environmental conditions. Note that for the stress intensities in the lid and baseplate, the highest stresses are exactly under the impact point. The results include the effect of the interface contact stress between the puncture pin and the plate surface. This local effect is not required to be included in the stress intensity comparison with allowable values for the hypothetical accident. Therefore, in the reporting of safety factors, the effect of local surface pressure is not included; rather, the radial and tangential stresses at the load point are used to form the stress intensity and set the lateral surface stress to zero. Tables 2.7.5 and 2.7.6 specifically identify this item by a note. Figure 2.7.17 shows the stress intensity distribution in the lid resulting from a top-end puncture analysis. The localized nature of the stress intensity distribution is clearly evident. The reported safety factors in the summary tables are adjusted to eliminate the effect of non-primary stress components.

- Closure Bolts

The methodology to analyze closure bolts is provided in reference [2.6.3] prepared for analysis of shipping casks. The analysis of the overpack closure bolts under normal conditions of transport, in accordance with the provisions of [2.6.3], has been reported in Section 2.6. In this subsection, the similar analysis for the hypothetical puncture accident is summarized. The analysis follows the procedures defined in Reference [2.6.3] and uses the allowable stresses for the closure bolts in that reference.

The following combined load case is analyzed for the hypothetical pin puncture accident condition of transport.

Puncture: Pressure, temperature, and pre-load loads are included.

Reference [2.6.3] reports safety factors defined as the calculated stress combination divided by the allowable stress for the load combination. This definition of safety factor is the inverse of the definition consistently used in this SAR. In summarizing the closure bolt analysis, results are reported using the SAR safety factor definition of allowable stress divided by calculated stress. The following result for closure lid bolting for the top end drop hypothetical accident condition of transport is obtained.

Overpack Closure Bolt - Safety Factor (Load Case 7 in Table 2.1.9)	
Item	Safety Factor on Bolt Tension
Average Tensile Stress in Bolt	1.86

2.7.3 Thermal

In this subsection, the structural consequences of the thirty-minute fire event are evaluated using the metal temperature data from Section 3.5 where a detailed analysis of the fire and post-fire condition is presented. Specifically, it desired to establish that:

1. The metal temperature, averaged across any section of the containment boundary, remains below the maximum permissible temperature for the Level A condition in the ASME Code for NB components. Strictly speaking, the fire event is a Level D condition for which Subsection NB of the ASME Code, Section III does not prescribe a specific metal temperature limit. The Level A limit is imposed herein for convenience because it obviates the need for creep considerations to ascertain post-fire containment integrity.
2. The external skin of the overpack, directly exposed to the fire will not slump (i.e., suffer rapid primary creep). This condition is readily ruled out for steel components if the metal temperature remains below 50% of the metal melting point.
3. Internal interferences among the constituents of the HI-STAR 100 System do not develop due to their differential thermal expansion during and after the fire transient.
4. Overpack closure bolts will not unload during a transport fire.
5. The helium retention boundary and the containment boundary both continue to perform their function as ASME "NB" pressure vessels.

2.7.3.1 Summary of Pressures and Temperatures

The following peak temperatures (per Tables 3.5.4 and 3.4.11) and pressures are used in Subsections 2.7.3.2, 2.7.3.3, and 2.7.3.4.

Overpack closure plate/bolts	514 degrees F (post-fire)
Overpack bottom plate	662 degrees F (post-fire)

Overpack outer closure	226 degrees F (initial pre-fire cold temperature); 1348 degrees F (maximum)
Overpack containment shell	395 degrees F (MPC –Shell post-fire temp. - increment of 24 degrees F (from data in Table 3.4.11))
MPC-Shell	419 degrees F (post-fire)
Basket (center)	751 degrees F (post-fire)
Basket (periphery)	478 degrees F (MPC-Shell post fire + 59 degrees F - (from data in Table 3.4.11))

It should be noted that the overpack containment shell, closure plate, and bottom plate temperatures are not specifically reported in Table 3.5.4. The temperatures listed above are based on the closest temperature report location. The overpack containment shell temperature is the lowest temperature that occurs prior to the fire accident and is used for the differential thermal expansion analysis. The overpack containment shell temperature falls (post-fire) below the outside basket temperature and subsequently lags the basket temperature by 24 degrees F. The 24 degree F lag is the same lag that occurs in the normal heat condition listed in Table 3.4.11 (i.e., 306 degrees F for the MPC outer shell surface - 282 degrees F for the overpack inner surface). This will maximize the potential for interference between the overpack and the MPC. Similarly, the temperature difference between the MPC shell and the fuel basket periphery will be essentially the same exists in the normal heat conditions of transport. Therefore, from Table 3.4.11, the basket peripheral temperature for the fire event analyses is set as the MPC shell temperature plus the maximum difference (365-306) degrees F from the table.

Subsection 3.5.3 contains a discussion of the peak bulk temperatures occurring during and after the fire transient. It is concluded in that section that:

1. The containment boundary protected by the intermediate shells remains below 500 degrees F (SA-203-E material).
2. The containment boundary that is within the confines of the impact limiters remains below 700 degrees F (SA-350 LF3 material).
3. The portion of the containment boundary directly exposed to the fire may have local outer surface temperatures in excess of 700 degrees F, but the bulk metal temperature of the material volume remains under 700 degrees F (SA-350 LF3 material).

The conclusions in Subsection 3.5.3 enable the statement that the containment boundary metal bulk temperatures remain at or below the upper limits permitted by the ASME Code. Therefore, stress evaluations that make comparisons to allowable stresses to demonstrate that the containment boundary continues to perform as a viable pressure vessel use allowable stresses that are given in the ASME Code (i.e., there is no extrapolation of allowable stresses beyond the recognized code limits). For the helium retention boundary stress calculations, however, allowable stresses for a conservatively high temperature (see Table 2.1.2 and 2.1.21) are used when pressure vessel code compliance is demonstrated.

From Table 3.5.4 in Subsection 3.5.4 of Chapter 3, it is concluded that:

The maximum temperature of the ferritic steel material in the body of the HI-STAR 100 overpack (the outer enclosure and the intermediate shells outside of the containment boundary is well below 50% of the material melting point. (The melting point of carbon and low alloy steels is approximately 2750 degrees F, per Mark's Standard Handbook, Ninth Edition, pp 6-11.)

The shielding experiences temperatures above its stated limit for effectiveness. This means that a limited loss of shielding effectiveness may occur. The shielding analysis in Chapter 5 (Subsection 5.1.2) recognizes this and conservatively assumes that all shielding is lost in post-fire shielding analyses.

Pressures during the fire transient are bounded by the internal and the external design pressures for accident conditions for the MPC shell as stated in Section 2.1. For internal pressure, Table 3.5.3 supports this conclusion. The following calculation is presented to support the conclusion for MPC external pressure.

The overpack annulus initial fill pressure is 14 psig (max.) per the specification in Chapter 7. The overpack annulus lower bound fill temperature is 70 degrees F. The fire condition MPC shell peak temperature is 419 degrees F per Table 3.5.4 and the use of this as the average gas temperature in the annulus is conservative.

Using the above data, the fire condition peak pressure in the annulus between the overpack and the MPC shell is calculated by using the ideal gas law with constant volume assumed in the gap as:

$$p_{\text{fire}} = (14 + 14.7) \times (419 + 460) / (70 + 460) = 47.6 \text{ psia} = 32.9 \text{ psig.}$$

2.7.3.2 Differential Thermal Expansion

The methodology for establishing that there will be no restraint of free thermal expansion has been presented in Subsection 2.6.1.2 for normal conditions of transport. The same methodology is applied in this subsection to evaluate the potential for component interference during and after the postulated hypothetical fire. For conservatism, use the temperatures in the overpack and the MPC temperatures that will maximize the potential for interference between the overpack and the MPC regardless of at what point in time the temperatures occurred. It is shown that there is no structural restraint of free-end expansion in the axial or radial directions under the most limiting temperature difference between the hot basket and the colder overpack/enclosure vessel. Thus, the ability to remove fuel by normal means is not inhibited by structural constraint of free-end expansion. The table below summarizes the results obtained for the limiting MPC temperature distributions assumed.

THERMOELASTIC DISPLACEMENTS IN THE MPC AND OVERPACK UNDER FIRE CONDITION				
CANISTER - FUEL BASKET				
	Radial Direction(in.)		Axial Direction (in.)	
Worst Case Unit	Initial Clearance	Final Gap	Initial Clearance	Final Gap
Bounding MPC	0.1875	0.117	2.0	1.672

CANISTER – OVERPACK				
	Radial Direction (in.)		Axial Direction (in.)	
Worst Case Unit	Initial Clearance	Final Gap	Initial Clearance	Final Gap
Bounding MPC	0.09375	0.004	0.625	0.291

Using the most conservative assumptions (i.e., do not consider a real “snapshot” in time during and after the fire, but rather assume the most detrimental temperature distribution occurs at the same instant in time) that maximize the potential for interference, it is demonstrated that no restraint of free thermal expansion in either the radial or axial directions occurs.

2.7.3.3 Stress Calculations

Under the fire accident, pressures in the MPC and overpack increase simultaneously, while the allowable strengths of the material may decrease from their values under normal conditions of transport. The MPC and overpack stresses are shown below (allowables are taken from Tables 2.1.21). It is required that both the helium retention boundary and the containment boundary meet Level D Service Limits of the ASME Code and continue to function as pressure vessels.

2.7.3.3.1 MPC

- Top Closure

The MPC Top Closure analysis for the fire condition is Load Case E5 in Table 2.1.7. The top closure is conservatively modeled as a simply supported plate considered to be loaded by the accident internal pressure plus self-weight acting in the same direction. For determination of the safety factor, the value of allowable stress from Table 2.1.20 appropriate to the fire temperature is used. The table below summarizes the result (where a multiplier of 2.0 has been incorporated to reflect the bounding dual lid design):

MPC Top Closure Safety Factor for Load Case E5 in Table 2.1.7			
Item	Value (ksi)	Allowable (ksi)	Safety Factor
Bending Stress	3.158 x 2	54.23	8.59

• Baseplate

Under the fire accident condition, the baseplate is subject to accident internal pressure (200 psi). If the HI-STAR 100 is assumed to be in the vertical position, then the baseplate also may support the weight of the fuel basket and the fuel loading. If the HI-STAR 100 is assumed to be oriented in the horizontal position, then the baseplate supports only internal pressure. For a conservative analysis, it is assumed that the internal pressure stress and the stress from basket weight and from fuel weight add. This Load Case E5 is summarized below. The second row is the result that is obtained if the basket and fuel weight is neglected.

MPC Baseplate Safety Factor under Hypothetical Fire Accident			
Item	Value (ksi)	Allowable (ksi)	Safety Factor
Baseplate Bending Stress (Including Basket and Fuel Weight)	46.32	54.23	1.17
Baseplate Bending Stress (Neglecting Basket, Fuel, and Self Weight)	42.28	54.23	1.28

• Shell

The MPC shell is examined for elastic/plastic stability under the fire accident external pressure using the ASME Code Case N-284 analysis method. The result from the stability analysis for Load Case E5 in Table 2.1.7 is summarized below:

MPC Canister Safety Factor - Stability under External Accident Pressure			
Item	Calculated Interaction Factor	Allowable Interaction Factor	Safety Factor
Elastic Stability	0.845	1.00	1.18

The shell is also analyzed for stress under the accident internal pressure by using the Lamé' solution previously used in Section 2.6. The stress due to the internal accident pressure of 200 psi is (P = pressure, r = MPC radius, t = shell thickness):

$$\sigma_1 = \frac{Pr}{t} = \frac{(200 \text{ psi})(68.375 \text{ in}/2)}{0.5 \text{ in}} = 13,675 \text{ psi}$$

$$\sigma_2 = \frac{Pr}{2t} = 6,838 \text{ psi}$$

$$\sigma_3 = -P = -200 \text{ psi}$$

The maximum stress intensity is $\sigma_1 - \sigma_3 = 13,875 \text{ psi}$

The safety factor is,

$$SF = \frac{36.15 \text{ ksi}}{13.875 \text{ ksi}} = 2.61$$

2.7.3.3.2 Overpack

The overpack stresses for normal heat conditions of transport are reported in Section 2.6. Since these stress solutions are based on linear elasticity, the stresses reported can be scaled up to account for the accident internal pressure and the safety factor computed based on the allowable stress for the fire temperature.

Generally, in the fire accident case, only primary stresses are of interest to demonstrate continued containment. Secondary stresses may be included in the evaluation, but they merely demonstrate additional levels of conservatism. Table 2.6.4 gives the minimum safety factor for the primary stress case of $T_h + P_i + F + W_s$.

The highest stress occurs in the inner shell, and has the value 2,832 psi.

The ratio of the accident pressure to normal pressure is (see Table 2.1.1) $\frac{200}{100} = 2.00$.

Using this factor, the safety factor is computed as follows:

For the inner shell at 500 degree F fire temperature per Table 2.1.1421, the allowable membrane stress intensity under the fire condition is compared to the amplified mean stress and the safety factor computed as

$$SF = \frac{42.5 \text{ ksi}}{(5.664 + 0.200) \text{ ksi}} = 7.25$$

2.7.3.3.3 Closure Bolts

Under the fire transient, it is required to demonstrate that the stresses in the closure bolts do not exceed allowable limits and the bolted joint does not unload to the extent that the pressure boundary is breached. To that end, an analysis of the fire condition is carried out with the purpose of determining the bolt stresses under the applied loading. The methodology employed for this analysis is that presented in the report, "Stress Analysis for Closure Bolts for Shipping Casks" [2.6.3]. The loadings applied are fire temperature, bolt preload, and accident internal pressure. The following result for closure lid bolting for the hypothetical fire accident is obtained.

Overpack Closure Bolt - Safety Factor (Load Case 19 in Table 2.1.9)	
Combined Load Case	Safety Factor on Bolt Tension
Average Tensile Stress	1.69

The average bolt tensile stress under the conditions of pressure, preload, and thermal effects appropriate to the hypothetical fire accident condition of transport is 8.5% greater than the average bolt tensile stress computed under the normal heat condition of transport. Therefore, it is concluded that there will be only minor unloading of the bolted joint and no breach of containment.

2.7.3.3.4 Bounding Thermal Stresses During the Fire Transient

Regulatory Guide 7.6, Section C.7 states that the extreme total stress intensity range between the initial state and accident conditions should be less than twice the adjusted value of the alternating stress intensity at 10 cycles given by the appropriate fatigue curves. It is demonstrated here that under very conservative assumptions on the calculation of thermal stresses, this regulatory requirement is met by the HI-STAR 100 System.

Under the fire transient, thermal gradients can lead to secondary or peak stresses due to local constraint by adjacent material that is at a lower temperature. The ASME Code does not require that secondary stresses be held to any limit for Level D Service Conditions. Nevertheless, bounding calculations are performed here to estimate the magnitude of the thermal stress. The most limiting secondary stress intensity state arises by conservatively assuming complete restraint of material by surrounding cooler material and has the solution:

$$|\sigma| = E \alpha \Delta T$$

where

- E = Young's Modulus at temperature
- α = coefficient of linear thermal expansion
- ΔT = temperature change from 70 degrees F, the assumed assembly temperature

For the fuel basket, $\Delta T = 775 - 70 = 705$ degrees F. The use of 775 degrees F is justified as follows:

The peak temperature of the fuel basket is 950 degrees F during the fire per Table 2.1.2. For a conservative estimate of the temperature between *two adjacent points* on the fuel basket, use the bounding hypothetical accident temperature limit for the enclosure vessel lid or baseplate from Table 2.1.2 as representative of the change between *two adjacent points* on the fuel basket. Therefore, no extrapolation of data is required for the calculations to follow.

From the material property table for Alloy X,

$$E = 24.282 \times 10^6 \text{ psi}$$

$$\alpha = 9.853 \times 10^{-6} \text{ inch/inch-degree F}$$

Therefore,

$$\sigma = 24.282 \times 9.853 \times 705 = 168,672 \text{ psi}$$

The conservative assumption is made that the maximum peak stress intensity due to mechanical loading plus thermal constraint occur at the same point at the same instant in time and reaches the value of S_u at room temperature. Thus, the total stress intensity range from assembly to this hypothetical conservative state is

$$S_R = 168,672 + 75,000 = 243,672 \text{ psi}$$

The alternating stress intensity range, after accounting for temperature effects of Young's Modulus, is

$$S_a = \frac{S_R}{2} \times \frac{\text{Young's Modulus (70° F)}}{\text{Young's Modulus (775° F)}}$$

$$= 121,836 \text{ psi} \times \frac{28.14}{24.282} = 141,194 \text{ psi}$$

For the overpack, the most severely constrained material is at the bottom plate. Material properties for this calculation are the values available at 700 degrees F and the peak temperature is conservatively set at 700 degrees F.

$$\text{Young's Modulus} = E = 24.9 \times 10^6 \text{ psi (at 700 degrees F)}$$

$$\text{Coefficient of linear thermal expansion} = \alpha = 7.52 \times 10^{-6} \text{ inch/inch-degrees F (Estimated)}$$

Therefore, the secondary stress intensity due to fully constrained thermal growth is

$$\sigma = 24.9 \times 7.52 \times (700-70) = 117,966 \text{ psi}$$

Conservatively, assuming that the membrane plus primary bending stress intensity achieves the ultimate strength at room temperature, at the same location in space and at the same instant in time, gives the total stress intensity range at this hypothetical location as

$$S_R = 117,966 + 75,000 = 192,966 \text{ psi}$$

The alternating stress intensity range, after accounting for temperature effects of Young's Modulus, is

$$S_a = \frac{192,966}{2} \times \frac{28.14}{24.9} = 109,037 \text{ psi}$$

These computed values for bounding alternating stress intensities are used in the next subsection for comparisons with allowable values.

2.7.3.4 Comparison of Fire Accident Results with Allowable Stresses

Stress

The safety factors for the MPC and overpack during a fire are addressed in Section 2.7.3.3. The lowest safety factors are 1.18 and 7.74 for the MPC and overpack, respectively.

Bounding Fire Transient

In accordance with Regulatory Position C.7 of the Regulatory Guide 7.6, Figure I-9.2.1 of ASME, Section III, Appendix I, gives the 10-cycle alternating stress intensity range as

$$S_{ALT} (\text{Alloy X}) = 700,000 \text{ psi}$$

Using the calculated stress intensity range from Subsection 2.7.3.3, the safety factor for the MPC basket is

$$SF = \frac{700,000}{141,194} = 4.96$$

Figure I-9.1 of ASME Section III, Appendix I is used for the overpack even though the temperature is limited to below 700 degrees F. It is conservative to use this curve for this short time event since increased temperatures will improve the material ductility. From that table, the 10-cycle alternating stress intensity range is given as 400,000 psi. Therefore using the aforementioned calculated results for stress intensity range from Subsection 2.7.3.3, the safety factor is computed as:

$$SF = \frac{400,000}{109,037} = 3.67$$

An analysis of the threaded holes in the top closure has been performed to assess the length of

engagement and stress requirements imposed on the connection by the transport loads. The methodology used to evaluate the connection is that set forth in Machinery's Handbook and uses the specific characteristics of the threaded joint. As part of the calculation, it is demonstrated that the bolt force required to maintain the seal (seal seating load plus pressure force) is only 27% of the total bolt preload force that must be applied to ensure bolt performance under the various drop scenarios. That is, there is 73% excess capacity. Therefore, the momentary joint decompression due to the hypothetical fire accident is not sufficient to unload the seal.

The above calculations demonstrate that the requirements of Paragraph C.7 of Regulatory Guide 7.6 are satisfied.

2.7.4 Immersion - Fissile Material

In order for the spent nuclear fuel in the HI-STAR 100 System to become flooded with water, a leak must develop in both the overpack containment structure and the MPC enclosure vessel. The analysis provided demonstrates that both the overpack containment boundary and the MPC enclosure vessel meet the applicable stress and stress intensity allowables for normal conditions of transport and hypothetical accident conditions. Therefore, no leak will develop.

10CFR71.73(c)(5) specifies that fissile material packages, in those cases where water inleakage has not been assumed for criticality analysis, must be evaluated for immersion under a head of water of at least 0.9 m (3 ft.) in the attitude for which maximum leakage is expected. The criticality analyses presented in Chapter 6 conservatively assumes flooding with water at optimum moderation. Therefore, this paragraph is not applicable. However, analysis is presented to demonstrate that there is no water inleakage and verify that the flooded assumption made in the criticality analysis is conservative.

A head of water at a depth of 0.9 m (3 ft.) is equal to 1.3 psi. This pressure is bounded by the MPC enclosure vessel normal condition of transport and hypothetical accident condition external pressures listed in Table 2.1.1. The head of water (1.3 psi) is also bounded by the hypothetical accident condition external pressure for the overpack. Analysis provided in this chapter demonstrates that both the overpack containment boundary and the MPC enclosure vessel meet the applicable stress and stress intensity allowables for normal conditions of transport and hypothetical accident conditions. Therefore, there is no in-leakage of water into the overpack or MPC under a head of water at a depth of 0.9 m (3 ft.).

2.7.5 Immersion - All Packages

Deep submergence of the HI-STAR 100 System in 200 meters (656 ft.) of water creates an external pressure load equal to 284 psi, which is less than the external design pressure of 300 psi. This condition is established as Load Case 18 in Table 2.1.9. Since the containment boundary is not punctured, stability of the package can be evaluated considering an undamaged package. The results for an external pressure of 300 psi bound the results for 21.7 psi gauge pressure that is established in 10CFR71.73(c)(6) as the applicable external pressure for this evaluation. The elastic/plastic stability of the overpack has been examined using the methodology of ASME Code Case N-284. In the analysis, all structural resistance to the external pressure is conservatively concentrated in the inner

containment shell. No credit is given to any structural support by the intermediate shells. The external pressure is assumed to act directly on the outer surface of the inner containment shell and the secondary fabrication stress is assumed to add to the stress due to the deep submergence pressure. The results for this case are summarized below:

Overpack Stability using ASME Code Case N-284 - Load Case 18 in Table 2.1.9			
Item	Value from Interaction Curve	Allowable Interaction Curve Value	Safety Factor
Yield Stress Limit	0.577*	1.34	2.32*
Elastic Stability	0.253	1.0	3.95

* *Applicable to inner shell fabricated from SA203-E material. Safety factor must be multiplied by 0.93 if inner shell is fabricated from optional SA350-LF3 material.*

It is noted that Code Case N-284 imposes limits on both stress and stability and includes a built-in safety factor of 1.34 for the Level D Service Limit. Therefore, the first row in the table above reports the true safety factor existing against exceeding the yield stress in the inner containment shell; the second row in the table provides the safety factor against elastic instability of the inner shell. The large values for the safety factors that are obtained, even with the conservative assumptions, attests to the ruggedness of the inner containment shell.

The analysis performed above for a 300 psi external pressure also confirms that the package meets the requirements of 10CFR71.61 that a 290 psi external pressure can be supported without any instability.

2.7.6 Summary of Damage

The results presented in Subsections 2.7.1 through 2.7.5 show that the HI-STAR 100 System meets the requirements of 10CFR71.61 and 10CFR71.73. All safety factors are greater than 1.0 for the hypothetical accident conditions of transport. Therefore, the HI-STAR 100 package, under the hypothetical accident conditions of transport, has adequate structural integrity to satisfy the subcriticality, containment, shielding, and temperature requirements of 10CFR71.

Table 2.7.1

MINIMUM SAFETY FACTORS FOR THE MPC FUEL BASKET UNDER HYPOTHETICAL ACCIDENT CONDITIONS OF TRANSPORT

Load Case Number	Load Combination [†]	Safety Factor	Location in SAR where Calculations or Results are Presented
F3			
F3.a	D + H', end drop	4.19	Subsection 2.7.1.1; Table 2.7.7
F3.b	D + H', 0° side drop	1.16	Table 2.7.4
F3.c	D + H', 45° side drop	1.28	Table 2.7.4

[†] The symbols used for loads are defined in Subsection 2.1.2.1.

Table 2.7.2

MINIMUM SAFETY FACTORS FOR THE MPC ENCLOSURE VESSEL
FOR HYPOTHETICAL CONDITIONS OF TRANSPORT

Load Case Number	Load Combination [†]	Safety Factor	Location in SAR where Calculations or Results are Presented
E3			
E3.a	D + H' + P _o , end drop	1.4 3.04 1.92	Lid Table 2.7.7 Baseplate Table 2.7.7 Shell Table 2.7.7
E3.b	D + H' + P _i , 0 deg. side drop	2.14 1.16	Shell Table 2.7.4 Supports Table 2.7.4
E3.c	D + H' + P _i , 45 deg. side drop	2.74 1.51	Shell Table 2.7.4 Supports Table 2.7.4
E5	P _i [*] or P _o [*]	8.59 1.17 1.18 (buckling) 4.16 (mean stress)	Lid Table 2.7.7 Baseplate Table 2.7.7 Shell Table 2.7.7 Subsection 2.7.3.3.1

[†] The symbols used for loads are defined in Subsection 2.1.2.1.

Table 2.7.3

**MINIMUM SAFETY FACTORS FOR THE OVERPACK
FOR HYPOTHETICAL ACCIDENT CONDITIONS OF TRANSPORT**

Load Case Number	Load Combination [†]	Safety Factor	Location in SAR where Calculations or Results are Presented
1	$T_h + D_{ba} + P_i + F + W_s$	2.16	Table 2.7.8
2	$T_h + D_{ta} + P_i + F + W_s$	1.75	Table 2.7.5
3	$T_h + D_{sa} + P_i + F + W_s$	2.19 (see note 2)	Table 2.7.5
4	$T_h + D_{ca} + P_i + F + W_s$	1.49	Table 2.7.5
5	$T_h + D_{ga} + P_i + F + W_s$	2.60 (see note 2)	Table 2.7.5
6	$T_h + P_s + P_i + F + W_s$	2.80 (see note 2)	Table 2.7.5
7	$T_h + P_t + P_i + F + W_s$	2.03 (see note 1)	Table 2.7.5
8	$T_h + P_b + P_i + F + W_s$	1.46	Table 2.7.5
9	$T_c + D_{ba} + P_o + F + W_s$	4.17	Table 2.7.6
10	$T_c + D_{ta} + P_o + F + W_s$	1.87	Table 2.7.6
11	$T_c + D_{sa} + P_o + F + W_s$	2.19	Table 2.7.6
12	$T_c + D_{ca} + P_o + F + W_s$	1.73	Table 2.7.6
13	$T_c + D_{ga} + P_o + F + W_s$	2.65	Table 2.7.6
14	$T_c + P_s + P_o + F + W_s$	3.05	Table 2.7.6
15	$T_c + P_t + P_o + F + W_s$	2.09 (see note 1)	Table 2.7.6
16	$T_c + P_b + P_o + F + W_s$	1.46	Table 2.7.6
17	$T_f + P_i + F + W_s$	pre-load maintained	Subsection 2.7.3.4
18	P_o^*	2.32	Table 2.7.8
19	$P_i^* + T_f + F + W_s$	7.2574	Subsection 2.7.3.3.2
20	$T_h + D_{ga} + P_i + F + W_s$	1.77	Table 2.7.5
21	$T_c + D_{ga} + P_i + F + W_s$	1.84	Table 2.7.6
22	$T_c + D_{ga} + P_i + F + W_s$	2.14 (see note 2)	Table 2.7.5

- Note: 1. This reported stress is directly under the point of impact. Therefore, the calculated value does not represent a primary stress; however, primary stress levels are met by this peak stress intensity.
2. *Applicable to inner shell fabricated from SA203-E material. Safety factor must be multiplied by 0.93 if inner shell is fabricated from optional SA350-LF3 material.*

[†] The symbols used here are defined in Subsection 2.1.2.1.

**Table 2.7.4 - FINITE ELEMENT ANALYSIS RESULTS
MINIMUM SAFETY FACTORS FOR MPC COMPONENTS UNDER ACCIDENT CONDITIONS**

Component - Stress Result	MPC-24		MPC-32		MPC-68	
	30 Ft. Side Drop, 0° Orientation Load Case F3.b or E3.b	30 Ft. Side Drop, 45° Orientation Load Case F3.c or E3.c	30 Ft. Side Drop, 0° Orientation Load Case F3.b or E3.b	30 Ft. Side Drop, 45° Orientation Load Case F3.c or E3.c	30 Ft. Side Drop, 0° Orientation Load Case F3.b or E3.b	30 Ft. Side Drop, 45° Orientation Load Case F3.c or E3.c
Fuel Basket - Primary Membrane (P_m)	2.80	3.85	2.78	3.90	3.07	4.30
Fuel Basket - Local Membrane Plus Primary Bending ($P_L + P_b$)	1.19	1.29	1.19	1.28	2.64	1.56
Enclosure Vessel - Primary Membrane (P_m)	6.43	6.88	5.77	6.95	5.65	7.13
Enclosure Vessel - Local Membrane Plus Primary Bending ($P_L + P_b$)	4.24	4.28	2.14	3.56	3.07	2.74
Basket Supports - Primary Membrane (P_m)	N/A	N/A	2.72	3.83	6.68	8.68
Basket Supports - Local Membrane Plus Primary Bending ($P_L + P_b$)	N/A	N/A	3.89	4.75	1.16	1.51

Table 2.7.4 (Continued) - FINITE ELEMENT ANALYSIS RESULTS
 MINIMUM SAFETY FACTORS FOR MPC COMPONENTS UNDER ACCIDENT CONDITIONS

Component - Stress Result	MPC-24E/EF	
	30 Ft. Side Drop, 0 deg Orientation Load Case F3.b or E3.b	30 Ft. Side Drop, 45 deg Orientation Load Case F3.c or E3.c
Fuel Basket - Primary Membrane (P_m)	2.75	3.80
Fuel Basket - Local Membrane Plus Primary Bending ($P_L + P_b$)	1.16	1.28
Enclosure Vessel - Primary Membrane (P_m)	6.41	6.88
Enclosure Vessel - Local Membrane Plus Primary Bending ($P_L + P_b$)	3.15	4.14

Table 2.7.5 - FINITE ELEMENT ANALYSIS RESULTS
MINIMUM SAFETY FACTORS FOR OVERPACK COMPONENTS UNDER ACCIDENT CONDITIONS (Hot Environment)

Component – Stress Result	30 Ft. Bottom End Drop Load Case 1	30 Ft. Top End Drop Load Case 2	30 Ft. Side Drop Load Case 3	30 Ft. C.G. Over-the- Bottom-Corner Drop Load Case 4
Lid – Local Membrane Plus Primary Bending ($P_L + P_b$)	34.04	1.75	2.60	7.76
Inner Shell – Local Membrane Plus Primary Bending ($P_L + P_b$)	4.35 (Note 2)	10.02 (Note 2)	2.19 (Note 2)	2.93 (Note 2)
Inner Shell – Primary Membrane (P_m)	4.48 (Note 2)	7.39 (Note 2)	2.45 (Note 2)	2.33 (Note 2)
Intermediate Shells - Local Membrane Plus Primary Bending ($P_L + P_b$)	6.63	7.95	2.33	1.49
Baseplate - Local Membrane Plus Primary Bending ($P_L + P_b$)	7.05	21.6	4.71	2.78
Enclosure Shell - Primary Membrane (P_m)	16.44	12.23	2.19	5.48

Notes:

1. Load cases are defined in Table 2.1.9.
2. *Applicable to inner shell fabricated from SA203-E material. Safety factor must be multiplied by 0.93 if inner shell is fabricated from optional SA350-LF3 material.*

Table 2.7.5 (Continued) - FINITE ELEMENT ANALYSIS RESULTS
 MINIMUM SAFETY FACTORS FOR OVERPACK COMPONENTS UNDER ACCIDENT CONDITIONS (Hot Environment)

Component - Stress Result	30 Ft. C.G. Over- the-Top-Corner Drop Load Case 5	Side Puncture Load Case 6	Top End Puncture Load Case 7	Bottom End Puncture Load Case 8	30 Ft. - 30 degree Drop Load Case 20	30 Ft. - Slapdown Load Case 22
Lid - Local Membrane Plus Primary Bending ($P_L + P_b$)	3.69	5.70	2.03 (See Note 2)	6.29	1.77	2.22
Inner Shell - Local Membrane Plus Primary Bending ($P_L + P_b$)	3.16 (Note 3)	2.80 (Note 3)	29.29 (Note 3)	9.52 (Note 3)	2.78 (Note 3)	2.73 (Note 3)
Inner Shell - Primary Membrane (P_m)	2.60 (Note 3)	5.95 (Note 3)	26.5 (Note 3)	10.61 (Note 3)	2.45 (Note 3)	2.14 (Note 3)
Intermediate Shells - Local Membrane Plus Primary Bending ($P_L + P_b$)	3.52	6.19	32.52	15.12	3.28	2.88
Baseplate - Local Membrane Plus Primary Bending ($P_L + P_b$)	6.95	21.62	28.62	1.46	27.32	17.9
Enclosure Shell - Primary Membrane (P_m)	3.56	4.53	51.32	29.9	8.02	2.40

- Notes: 1. Load cases are defined in Table 2.1.9.
2. Stress Intensity computed just outboard of the loaded area since surface stress is not a primary stress component.
3. *Applicable to inner shell fabricated from SA203-E material. Safety factor must be multiplied by 0.93 if inner shell is fabricated from optional SA350-LF3 material.*

Table 2.7.6 - FINITE ELEMENT ANALYSIS RESULTS
 MINIMUM SAFETY FACTORS FOR OVERPACK COMPONENTS UNDER ACCIDENT CONDITIONS (Cold Environment)

Component – Stress Result	30 Ft. Bottom End Drop Load Case 9	30 Ft. Top End Drop Load Case 10	30 Ft. Side Drop Load Case 11	30 Ft. C.G. Over-the- Bottom-Corner Drop Load Case 12
Lid – Local Membrane Plus Primary Bending ($P_L + P_b$)	30.29	1.87	2.73	8.00
Inner Shell – Local Membrane Plus Primary Bending ($P_L + P_b$)	4.17	9.69	2.19	2.94
Inner Shell – Primary Membrane (P_m)	4.37	7.33	2.47	2.36
Intermediate Shells - Local Membrane Plus Primary Bending ($P_L + P_b$)	4.95	8.66	2.61	1.73
Baseplate - Local Membrane Plus Primary Bending ($P_L + P_b$)	7.73	17.07	4.80	2.73
Enclosure Shell - Primary Membrane (P_m)	20.08	18.4	2.45	5.71

Notes: 1. Load cases are defined in Table 2.1.9.

Table 2.7.6 (Continued) - FINITE ELEMENT ANALYSIS RESULTS
 MINIMUM SAFETY FACTORS FOR OVERPACK COMPONENTS UNDER ACCIDENT CONDITIONS (Cold Environment)

Component – Stress Result	30 Ft. C.G. Over- the-Top-Corner Drop Load Case 13	Side Puncture Load Case 14	Top End Puncture Load Case 15	Bottom End Puncture Load Case 16	30 Ft. – 30 degree Drop Load Case 21
Lid – Local Membrane Plus Primary Bending ($P_L + P_b$)	3.91	5.91	2.09 (See Note 2)	6.64	1.84
Inner Shell – Local Membrane Plus Primary Bending ($P_L + P_b$)	3.21	3.05	24.97	8.54	2.78
Inner Shell – Primary Membrane (P_m)	2.65	7.60	17.03	9.59	2.48
Intermediate Shells - Local Membrane Plus Primary Bending ($P_L + P_b$)	4.10	7.06	27.55	14.9	3.81
Baseplate - Local Membrane Plus Primary Bending ($P_L + P_b$)	7.08	29.69	47.25	1.46	21.91
Enclosure Shell - Primary Membrane (P_m)	4.13	5.17	57.21	76.5	9.64

- Notes: 1. Load cases are defined in Table 2.1.9.
 2. Surface pressure not included in safety factor evaluation since it is not a primary stress.

Table 2.7.7

MINIMUM SAFETY FACTORS FOR MISCELLANEOUS ITEMS - MPC FUEL BASKET/CANISTER - HYPOTHETICAL
ACCIDENT CONDITIONS OF TRANSFER

Item	Loading	Safety Factor	Location in SAR Where Calculations or Results are Presented
Fuel Basket Axial Stress	End Drop	4.19	Subsection 2.7.1.1
Fuel Basket Axial Stress	Fire Transient (Regulatory Position C.7 of Regulatory Guide 7.6)	4.96	Subsection 2.7.3.4
MPC Canister Stability	30' End Drop (Load Case E3.a, Table 2.1.7)	1.92	Subsection 2.7.1.1
MPC Top Closure Lid Bending Stress	30' End Drop (Load Case E3.a in Table 2.1.7)	2.8 (single lid) 1.4 (dual lid)	Subsection 2.7.1.1
MPC Top Closure Lid – Loading in Peripheral Weld	30' End Drop (Load Case E3.a in Table 2.1.7)	2.37	Subsection 2.7.1.1
MPC Baseplate Bending Stress	30' End Drop (Load Case E3.a in Table 2.1.7)	3.04	Subsection 2.7.1.1
MPC Canister at Connection to Baseplate	30' End Drop (Load Case E3.a in Table 2.1.7)	2.14	Subsection 2.7.1.1
MPC Top Closure Lid Bending Stress	Fire accident (Load Case E5 in Table 2.1.7)	8.59	Subsection 2.7.3.3.1
MPC Baseplate Bending Stress	Fire accident (Load Case E5 in Table 2.1.7)	1.17	Subsection 2.7.3.3.1
MPC Canister Stability	Fire accident (Load Case E5 in Table 2.1.7)	1.18	Subsection 2.7.3.3.1
MPC Shell Mean Stress	Fire accident (Load Case E5 in Table 2.1.7)	4.16	Subsection 2.7.3.3.1

Table 2.7.8

MINIMUM SAFETY FACTORS FOR MISCELLANEOUS ITEMS - OVERPACK -
HYPOTHETICAL ACCIDENT CONDITIONS OF TRANSPORT

Item	Loading	Safety Factor	Location in SAR Where Calculations or Results are Presented
Overpack Stability	30' End Drop (Load Cases 1 and 2 in Table 2.1.9)	2.16*	Subsection 2.7.1.1
Closure Bolts	30' End Drop (Load Case 2 in Table 2.1.9)	1.30	Subsection 2.7.1.1
Closure Bolts	Top End Puncture	1.86	Subsection 2.7.2
Overpack Inner Shell Mean Stress	Fire Transient	7.2574	Subsection 2.7.3.3.2
Closure Bolts	Fire Transient	1.69	Subsection 2.7.3.3.3
Overpack Stress	Fire Transient (Regulatory Position C.7 of Regulatory Guide 7.6)	3.67	Subsection 2.7.3.4
Overpack Stability (Yield Stress Criteria)	Immersion (Load Case 18 in Table 2.1.9)	2.32*	Subsection 2.7.5
Overpack Stability (Stability Criteria)	Immersion (Load Case 18 in Table 2.1.9)	3.95	Subsection 2.7.5

* *Applicable to inner shell fabricated from SA203-E material. Safety factor must be multiplied by 0.93 if inner shell is fabricated from optional SA350-LF3 material.*

APPENDIX 2.A:
DESIGN, TESTING, AND COMPUTER SIMULATION OF THE AL-STAR™
IMPACT LIMITER

2.A.1 INTRODUCTION

As stated in Subsection 2.7, the central purpose of the AL-STAR™ impact limiter is to limit the package maximum deceleration, α_{\max} , under a postulated drop event to a specified design value. For the regulatory 9-meter hypothetical free drop event, the AL-STAR design is engineered to limit the maximum rigid body deceleration to 60 times the acceleration due to gravity (Table 2.1.10). The HI-STAR packaging, consisting of the loaded overpack and top and bottom impact limiters (illustrated in Figure 2.A.1.1) is essentially a cylindrical body with a rigid interior (namely, the overpack) surrounded by a pair of relatively soft crushable structures. The crushable structure (impact limiter) must deform and absorb the kinetic energy of impact without detaching itself from the overpack, disintegrating, or otherwise malfunctioning. A falling cylindrical body may theoretically impact the target surface in an infinite number of orientations; the impact limiter must limit the HI-STAR 100 decelerations to below 60g's and preserve the limiter-to-overpack connection regardless of the impact orientation. Figure 2.A.1.2 presents the side drop event. In general, a drop event orientation is defined by the angle of the HI-STAR 100 longitudinal axis, θ , with the impact surface. In this notation, $\theta = 0$ means a side drop and $\theta = 90^\circ$ implies a vertical or end drop scenario. Inasmuch as the top and bottom impact limiter are made of identical crush material, the top or bottom vertical drop events are mathematically and physically equivalent as far as the impact limiter design is concerned. In any orientation, the drop height is measured from the lowest point on the package.

An intermediate value of θ , $\theta = 67.5^\circ$, warrants special mention. At $\theta = 67.5$ degrees, the point of impact is directly below the center of gravity (C.G.) of the HI-STAR 100 package. This drop orientation is traditionally called the C.G.-over-corner (CGOC) configuration. The CGOC orientation is the demarcation line between single and dual impact events. At $90^\circ > \theta > 67.5^\circ$, the leading end of the packaging (denoted as the "primary" impact limiter) is the sole participant in absorbing the incident kinetic energy. At $\theta < 67.5^\circ$ drop orientations, the initial impact and crush of the leading (primary) impact limiter is followed by the downward rotation of the system with the initial impact surface acting as the pivot, culminating in the impact of the opposite (secondary) impact limiter on the target surface. In the dual impact scenarios, the first and second impact limiter crush events are referred to as the "primary" and "secondary" impacts, respectively. It is reasonable to speculate that for certain values of θ , the secondary impact may be the more severe of the two. As stated earlier, the design of AL-STAR must ensure that $\alpha_{\max} \leq 60$, regardless of the value of θ .

The AL-STAR attachment design must ensure that both impact limiters remain attached to the cask during and after the impact event. The impact limiters are also required to prevent cask body-to-unyielding target contact.

Finally, the package design must satisfy all criteria in ambient temperature conditions ranging from -20° to 100°F, and with humidity ranging from 0 to 100%. Therefore, the impact limiter design must be functionally insensitive to temperature and environmental conditions.

An aluminum honeycomb-based impact limiter design was selected as the preferred material for development. The detailed design of the AL-STAR impact limiters is presented in Holtec Drawing C1765 located in Section 1.4. A pictorial view of AL-STAR is presented in Figure 2.A.1.3.

Figure 2.A.1.3 indicates that in addition to the crushable honeycomb, the AL-STAR contains two internal cylindrical shells (also denoted as “rings”), which are stiffened with radial gussets. These carbon steel shells are sized to behave as undeformable surfaces during impact events. They are essentially the “backbone” of the impact limiter, lending a predictability to the impact limiter crush behavior and forcing the energy absorption to occur in the honeycomb metal mass. The design of this backbone structure was a subject of in-depth computer and experimental 1/8 scale static testing, as documented in Holtec Report HI-962501 [2.A.4] and summarized in Section 2.A.4 herein.

Another noteworthy aspect of the AL-STAR impact limiter design is the arrangement of uniaxial and cross core (biaxial) honeycombs. Regions of the honeycomb space that experience impact loading in only one direction are equipped with unidirectional honeycomb sectors. The regions where the direction of the impact loads can vary have cross-core (bi-directional) honeycomb material, as detailed in Subsection 2.3.1.5.

To summarize, the design objectives of the AL-STAR impact limiter are set down as five discrete items, namely:

- i. Limit peak deceleration (α_{max}) to 60g's under all potential drop orientations.
- ii. Impact limiter must not detach from the cask under a 9-meter drop event, under any impact orientation.
- iii. The impact limiters must bring the cask body to a complete stop, such that the overpack does not come in physical contact with the target surface.
- iv. Crush material must be equally effective at -20° and 100°F, with humidity ranging from 0 to 100%.
- v. All external surfaces must be corrosion-resistant.

The last two objectives are realized by utilizing aluminum honeycomb (Type 5052) as crush material and stainless steel (Type 304), for the external skin enclosure. As shown in the ASME Code (Section II, Part D, Table Y-1), the essential property of the constituent material for the honeycomb and the external skin, namely the yield strength remains constant in the -20° F to

100° F range. The surface of the carbon steel impact limiter backbone is painted to limit corrosion.

The remaining design objectives, namely, limiting of the maximum rigid body deceleration, α_{\max} , to 60 g's under a 9-meter drop event, maintaining positive attachment of the AL-STAR impact limiters to the overpack, and preventing contact of the overpack with the unyielding surface, are demonstrated by a combination of numerical simulations and scale model static and dynamic testing. This was accomplished through a research and development effort that is broadly subdivided into six phases, as follows:

- Phase 1: Characterize the honeycomb pressure-deflection relationship.
- Phase 2: Propose a force (static) vs. crush (F vs. d) model for AL-STAR.
- Phase 3: Perform 1/8 scale model static compression tests to validate the force-crush model and to establish the adequacy of the AL-STAR backbone structure.
- Phase 4: Conduct 9-meter quarter-scale model dynamic drop tests in selected limiting drop configurations and obtain test data.
- Phase 5: Simulate the experimental drop tests with a suitable "dynamic model" and establish that the dynamic model predictions of deceleration, crush and event time duration reasonably match the experimentally measured values. A reasonable prediction of the peak decelerations of each drop event is the minimum for the dynamic model to be acceptable.
- Phase 6: Utilize the experimentally confirmed dynamic model to evaluate the effects of tolerances on crush properties and on package weight, and to confirm the adequacy of the full-scale impact limiter design.

It is of crucial importance that the dynamic model benchmarked in Phase 5 be of high reliability, since it becomes the analytical model for the accident-event response prediction of the packaging when tolerances on material behavior and package mass are considered (Phase 6).

In this appendix, a description of the overall program and results for each of the six phases is presented.

2.A.2 Phase 1: Material Pressure-Crush Relationship

The extent of deflection, Δ , sustained by a honeycomb material when subjected to a uniform pressure, p , is an essential element of information in the impact limiter design. Towards this end, coupon specimens of uniaxial and cross-core honeycomb of various nominal crush strengths and densities were compression-tested by the material manufacturer. The results showed that all honeycomb coupons shared some common load-deflection characteristics, namely:

The initial pressure-deflection curve resembled an elastic material (pressure roughly proportional to deflection).

Upon reaching a limiting pressure, the material crushed at near constant pressure until the crush reached approximately 60-70 percent of the initial thickness. The required crush force had to increase rapidly to achieve small incremental crushing for strains beyond approximately 60-70 percent.

Figure 2.A.2.1 shows a typical static pressure-deflection curve for a 1"-thick honeycomb specimen. The curve with the initial peak is that of an un-precrushed honeycomb specimen; the curve without the peak (shown as a dashed line only where a difference occurs) corresponds to a pre-crushed specimen. Dynamic testing subsequently showed that removal of the initial peak by pre-crushing the material was a desired feature whenever a large flat area of honeycomb material experienced a crush force (such as in a 90 degree end drop).

Curve fitting of data from all tested coupons indicated that a single mathematical relationship between the applied pressure and compression strain could be developed. The mathematical relationship can provide a reasonable fit for coupons of all crush strengths (crush strength defined as the pressure corresponding to the flat portion of the curve in Figure 2.A.2.1; i.e., it is the constant pressure at which the honeycomb undergoes near-perfect plastic deformation). In other words, the pressure, p , for a given strain, ϵ , is represented by a unique function of the crush pressure, p_c , i.e.

$$p = f(p_c, \epsilon)$$

The relationship between p and compression strain was used in the subsequent mathematical efforts to simulate AL-STAR crush behavior. The above mathematical relation was developed to simulate material behavior for a honeycomb material under both non-pre-crushed and pre-crushed conditions.

2.A.3 Phase 2: Static Force-Crush Prediction Model

An essential step towards the development of a reliable dynamic model to simulate the impact of a dropped HI-STAR 100 package is to develop a static force-crush model that can subsequently be validated by scale model tests. The force-crush model should reliably duplicate the resistance provided by an impact limiter for a range of crush orientations for the full range of crush depths.

The required force-crush model for AL-STAR is developed using the concept of interpenetration, which is explained using the case of the side drop ($\theta = 0$) as an example (Figure 2.A.3.1(a)).

The condition existing in all impact limiter drop scenarios is that the relatively soft honeycomb material lies between two "hard" surfaces that are advancing towards each other during the impact. One of these two rigid surfaces is the essentially unyielding target (Rigid Body 1) and

the other is the structural backbone of the impact limiter (Rigid Body 2). While the target surface is flat, the backbone structure is cylindrical in profile. When squeezed between the two surfaces, the honeycomb material (at each instant in time) will crush at one or both interface locations. To determine which interface surface will undergo crushing at a given point during the impact event, the concept of interpenetration area is utilized as explained below.

In this concept, two separate crush scenarios, one assuming that the crush occurs at the external interface (target-to-impact limiter), and the other assuming that the crushing is at the internal interface (structural backbone/overpack-to-impact limiter), are compared at each instant during a simulated compression of the impact limiter. A metal honeycomb impact limiter, in general, may have multiple honeycomb material sections crushing at each interface. For simplicity in explaining the concept of interpenetration, we assume that each of the interfaces is characterized by a uniform distribution of honeycomb having crush pressures p_1 and p_2 , respectively. To determine the resistive force developed to crush the impact limiter by a small amount, d , against the external target, the impact limiter is assumed to penetrate the target by the amount "d" without deformation. The resulting area A_1 for the case of side drop, illustrated in Figure 2.A.3.1(b), can be computed as an algebraic expression in the amount of approach, d . (For oblique drop events, ANSYS [2.A.1] or CADKEY [2.A.2] are used to compute interpenetration area as a function of incremental interpenetration.) The pressure-compression relationship for the honeycomb stock at the external interface provides the crush pressure p_1 that develops due to deformation "d". The total force required for crush "d", at the external interface, is therefore equal to p_1A_1 .

In the second (independent) scenario, the impact limiter external surface is assumed to undergo no movement; rather, the backbone structure (along with the overpack) advances towards the target by an amount d (Figure 2.A.3.1(c)). Once again, assuming that the cylindrical rigid body moves through an amount "d", the resistance pressure developed in the honeycomb material lying in the path of penetration is available from the appropriate material pressure-compression curve. If the pressure corresponding to the deformation is p_2 and the projected area at the internal interface is A_2 , then the total resistive force encountered in realizing an approach equal to "d" between the overpack-backbone assemblage and the target under this latter scenario is p_2A_2 . In an actual drop event, at each instant during the event, incremental crush occurs at one of the two interfaces. If $p_1A_1 < p_2A_2$ at a given instant then crushing will occur at the external interface. Likewise, $p_1A_1 > p_2A_2$ will imply that crushing will occur internal to the impact limiter. The smaller of p_1A_1 and p_2A_2 is the required crush force and the corresponding location of crush is where the honeycomb material will compress to realize the approach equal to d . This "inequality test" to determine where crushing occurs is performed at every increment of crush during the simulation of the event. The appropriate value of the crush force is used in the equilibrium equations at that instant. The concept of interpenetration at two interfaces has been confirmed during testing of the impact limiters; the total crush is observed to be a sum of compression at each of the two interfaces.

To construct a mathematical force-deformation relationship for AL-STAR in any given orientation, the above process is repeated as the crush "d" is increased in small increments starting with the beginning of compression ($d = 0$). It is quite clear that the development of the

force-deflection model (F-d model) for AL-STAR in any orientation is a straightforward analysis in 3-D geometry. The F-d curve for AL-STAR for any given value of θ can be developed where, other than the geometry of the impact limiter, the crush strengths p of the honeycomb materials utilized in the impact limiter are the only other required inputs.

The force (F) vs. crush (d) relationship developed using the foregoing method is referred to as the F-d model that is subject to validation by appropriate 1/8 scale model compression tests described in the following section.

2.A.4 Phase 3: One-Eighth Scale Model Static Compression Tests

The 1/8 scale model tests consist of subjecting scaled replicas of the full-size AL-STAR to static compression tests in an engineered fixture such that the force-compression curve for the scaled model can be obtained in various orientations of compression. The scale model is made by making the diameters and length of the model one-eighth of the full-size AL-STAR. The thicknesses of the backbone components (i.e., the inner and outer shells and gussets), and the external skin (see Figure 2.A.1.3) are also scaled to one-eighth times the corresponding dimensions (to the nearest sheet metal gage, where applicable) in the full-size AL-STAR. In the one-eighth model, the performance of the attachment system is not assessed nor is the cask body modeled. However, the interface between overpack and impact limiter where the compression load is resisted is properly simulated. The crush pressure is a material property of the energy absorbing material; therefore, the material (and its density) is not scaled. The 1/8 scale model, therefore, has approximately $(1/8)^3$ or 1/512 the volume and weight of the full-size unit. Holtec documents [2.A.3, 2.A.4] provide complete details on the 1/8 scale model geometry and fabrication. The static compression behavior of such a 1/8-scale model is correlated with that of a full-size unit using the geometric scaling information. For example, under an axial compression test the area under crush in the scale model will be 1/64 of the full-size AL-STAR (recall that the diameter is scaled down by a factor of 8). Therefore, the crush force (which is crush force pressure times the area under crush) will be 1/64 of the full-size unit. On the other hand, the crush stroke (extent of deformation before "lock up") will be 1/8 of the full-size AL-STAR because the axial length of the scale model (which corresponds to the height of the crush column in axial compression) is one-eighth of the full-size hardware. Thus, the total energy absorbed (force times compression) will be $(1/8)^3$ of the full-size unit. The same scaling factor can be shown to apply in all directions of crush.

In summary, the 1/8 scale model scales the geometric dimensions of AL-STAR. The previously discussed F-d model is required to translate the force-crush relationship from the 1/8 scale replica to the full-size unit. In order to use the analytical F-d model as a valid vehicle for predicting the force-crush of the full-size (or quarter-scale) AL-STAR, it is necessary to check its prediction ability against actual test data from 1/8-scale model static compression tests.

The objectives of static scale model tests are twofold:

- i. Determine whether the static force-crush relationship predicted by the F-d model appropriately simulates the actual relationship determined by test;
- ii. Determine whether the backbone structure of the AL-STAR impact limiter is sufficiently rigid to withstand and transmit the large loads associated with the postulated accident scenarios.

2.A.4.1 Static Compression Tests on Initial Candidate Crush Material

To assess compression performance, a QA validated AL-STAR static test procedure was prepared [2.A.3] for the one-eighth scale model static compression tests and a series of cold and hot static compression tests performed on an impact limiter configuration with the initial candidate crush material. Holtec calculation package HI-961501 [2.A.4] contains a comprehensive documentation of the 1/8 scale static test program and results for the impact limiter configuration. A summary of the complete test program and test results is presented below.

Four 1/8-scale models were fabricated with details of the impact limiter carefully scaled, including the stiffening cylinders and the stainless steel skin. No impact limiter attachment bolts were incorporated in the model.

Aluminum honeycomb segments provided for the 1/8-scale models were manufactured utilizing the same procedures and processes as for the full-scale impact limiter. As stated earlier, the crush strengths were not scaled because they are considered as material properties.

An adjustable 1/8 scale static test fixture was designed, analyzed, and fabricated. The test fixture interfaced with the impact limiter and simulated the overpack hard surface. The test fixture could be adjusted to simulate any crush orientation. Figure 2.A.4.1 shows the test fixture and the 1/8 scale impact limiter being loaded in the heavy-load testing machine.

The following static one-eighth scale test series were carried out:

Test No.	Orientation, degrees	Temperature
1	0 (side)	+120°F
2	30 (oblique)	Ambient
3	60 (oblique)	Ambient
4	90 (end)	-30°F

For all tests except the end compression (where the orientation is immaterial), the circumferential orientation of the impact limiter was selected so that the initial point of contact between the impact limiter and the test machine was at the interface of two aluminum honeycomb sections. After each test, the impact limiters were cut open and examined.

Observations Based on 1/8 Scale Model Testing

- Effect of Ambient Temperature:

The end compression test was performed with the impact limiter cold (-30°F), the side compression test was performed with the impact limiter hot (+120°F), and the two oblique tests performed at ambient temperature. The material behavior showed no influence of test temperature. This confirms the expected result since the aluminum honeycomb and stainless steel skin yield strengths are insensitive to temperature in the range of interest (-20° F to 100° F) as prescribed in Table Y-1 of the ASME Code.

- Side compression orientation - 0 degree:

The inner stiffening cylinder experienced considerable permanent deformation. The gussets which buttress the inner cylinder buckled. The outer stiffening cylinder performed elastically.

- Oblique compression orientation:

Two oblique orientation static tests were performed. The 30-degree oblique test again showed the need to thicken the inner stiffening cylinder and to rearrange the stiffening gussets.

The 60-degree oblique test was a complete success; no plastic deformation of the backbone structure was indicated.

As would be expected, in those cases where the hard region (backbone structure) of the impact limiter sustained deformations, the scale model exhibited greater flexibility in the physical testing than the analytical prediction (the flexibility of the backbone structure added to the crush of the honeycomb resulting in a greater total measured deflection).

- End compression orientation - 90 degree:

The end-compression orientation is, structurally speaking, the least complicated of the four test configurations. The loading of the AL-STAR scale model in this test is purely axisymmetric. The initial peak in the pressure/deformation curve seen in the coupon tests (Figure 2.A.2.1) was clearly evident in the axial (end) compression test (Figure 2.A.4.3). The backbone structure performed without sustaining plastic deformation.

- Comparison of experimental and analytical predictions

Out of the four static 1/8-scale model tests, two tests (side compression and 30-degree oblique) were unsatisfactory because the backbone structure of the impact limiter did not remain elastic. These tests served to identify the need to reinforce the AL-STAR backbone structure. The other tests, namely end-compression (90 degree) and 60-degree oblique, wherein the backbone structure performed as designed, showed close agreement with the numerical model. Figures 2.A.4.3 and 2.A.4.4, respectively, show the static test results for 90-degree (end-compression) and 60 degree (oblique) cases, along with the prediction of the F-d model. There is good agreement between the computer model and the test data.

In summary, the 1/8 scale model static test program identified the required design changes to the internal structure of the impact limiters. The 1/8 scale model tests showed that the load-compliance characteristics of AL-STAR are insensitive to the changes in the ambient environment. A comparison of the test results with the mathematical model predictions from the F-d model indicated that the mathematical model was in good agreement with 1/8-scale static crush tests whenever the backbone structure performed as required (i.e. remained elastic). Since the crush geometry of the scale model was *not altered* by the strengthening of the backbone, any subsequent reinforcing of the backbone did not alter the F-d relationship for the impact limiter. The two successful static tests that showed excellent agreement with the computer F-d model, therefore, continued to serve as a valid benchmark of the numerical model after the backbone is stiffened. The reinforced backbone structure is incorporated into the final design drawings for the AL-STAR, and was confirmed as acceptable during the dynamic (1/4-scale) model drop tests. Subsequent to the one-quarter scale dynamic tests and the analytical correlation (Phases 4-6), three additional 1/8th scale confirmatory static tests were performed on impact limiters that included the internal backbone structure and the final crush material orientations used in the quarter-scale drop tests and in the analytical correlation. These additional confirmatory static tests were performed at room temperature. The tests simulated the crush orientation corresponding to the side drop, the "center-of-gravity-over corner" drop, and the end drop, respectively. Force-deflection results from the static test are compared with the predictions from the theory for the 1/8th-scale impact limiters. Subsection 2.A.10 discusses the results obtained from these three additional static tests.

2.A.5 Phase 4: 9 Meter Quarter-Scale Model Drop Tests

The one-quarter scale model dynamic tests provide physical confirmation of the HI-STAR impact limiter design and the performance of the attachment system. The quarter-scale and full-scale design of the impact limiter is presented in drawings in ~~Section 1.4~~[2.1.7.4].

In the 1/4 scale model drop test program, an instrumented scale model of the HI-STAR 100 dual-purpose cask was assembled with the top and bottom AL-STAR impact limiters, raised to a height of 9 meters (measured from the lowest point on the package), and then released to free fall onto an unyielding concrete and steel armor target (unyielding target). The impact limiter attachment system is reproduced in the model using the appropriate scale for bolt diameters, etc.

A detailed description of the quarter-scale model, instrumentation, data acquisition, and data processing is presented in a proprietary Holtec document [2.A.7]; a concise self-contained summary is provided in the following.

2.A.5.1 Test Plan:

The drop test program was performed at the drop testing facilities at the Oak Ridge National Laboratory. The target at the ORNL facility complies with guidance of IAEA Safety Series 37, Article A-618.

The quarter-scale model testing of the package required the design and fabrication of scale models of AL-STAR, the HI-STAR overpack, and the multi-purpose canister. The quarter-scale replicas of AL-STAR were prepared using the scaling procedure described previously in the context of the 1/8 scale model. In the scale model for the MPC and the overpack, the emphasis is in scaling the weight and moment of inertia, because it is these properties (translational as well as rotational) which are key to the response in the drop event. A schematic of the MPC design used in the scale model is shown in Figure 2.A.5.1. The weight of the MPC replica was set at 1,380 lbs (to simulate an 88,320 lb loaded multi-purpose canister).

The overpack scale model likewise is a cylindrical body whose length and outside diameter are 1/4, whose weight is 1/64, and whose mass moment of inertia is 1/1024 of the respective design parameters in the full-size hardware, as summarized below:

Key Quarter Scale HI-STAR Overpack Model Data			
Length (inch)	O.D. (nominal) (inch)	Overpack Plus MPC Weight (lb.)	Mass Moment of Inertia About a Transverse Centroidal Axis (Overpack Plus MPC) (lb.-in ²)
50.7813	21	3,733	1.351E+06

Figures 2.A.5.2 through 2.A.5.4 illustrate the principal geometric data of the quarter-scale overpack model. These figures are adapted from the design drawing 1546 (proprietary) provided in Section 1.4 of this report [2.1.7.4]. It is evident from the above description that the quarter-scale model is, from a geometrical and inertia standpoint, a quarter-scale emulation of a 84" diameter x 203.125" long, 238,900 lb. (approximate) HI-STAR system (overpack and loaded MPC). Finally, the attachment bolts which join the impact limiter to the overpack are also scaled down to 25% of their size in the full-size hardware (in both diameter and thread engagement length), as can be seen from Figures 2.A.5.3 and 2.A.5.4 or the applicable drawing in Section 1.4.

The one-quarter scale drop tests were performed with four discrete orientations of the cask longitudinal axis with respect to the impact surface, as defined below.

Test A – Vertical Drop (Top End): The cask is dropped such that the deceleration of the cask upon impact is essentially vertical.

Test B: Center of Gravity-Over-Corner (CGOC): For HI-STAR 100, C.G.-over-corner means an orientation wherein the axis of the cask is at 67.5° from the horizontal at the instant of release at the 9-meter height. This test seeks to establish the adequacy of the impact limiter under non-symmetric impact loading.

Test C – Side Drop: The cask is held horizontal with the lowest point on the package 9 meters above the target surface when released for free fall. In this test, both impact limiters participate, and the impact impulse is essentially equally divided between them.

Test D – Slapdown: In this test, the cask axis is held at 15° from the horizontal with the lowest point of the cask assembly at 9 meters from the impact surface. The orientation is such that the top end impact limiter impacts the surface first and the bottom end impact limiter experiences the secondary impact.

Each of the four tests has distinct impact characteristics. For example, in the “side drop” test both impact limiters will strike the target simultaneously; only one impact limiter sustains impact in the “end drop” test. The CGOC test involves a primary impact on one impact limiter at an angle such that the gravity vector is oriented with a line passing through the cask center of gravity and the lowest corner of the limiter. Finally, the slapdown test involves impact at both impact limiters with a very slight time separation. These four tests are deemed to adequately represent the limiting impact scenarios under the hypothetical accident conditions of 10CFR71.73.

The torque values used to secure the attachment bolts in the scale model package warrant special mention. The impact limiter attachment bolts serve two major functions during transportation:

1. During normal transport, the attachment bolts ensure that the impact limiters remain attached to the HI-STAR 100 overpack during a 10g axial deceleration as mandated by 10CFR71.45, and during exposure to normal vibratory loading that may reasonably be expected during the course of a normal transport operation. To ensure against loss of attachment due to vibratory loading during normal transport, an initial bolt pre-stress of 30,000 psi has been set, based on common engineering practice. For the bolt diameters specified for the HI-STAR 100 package, the pre-load torque is 245 ft-lb and 1,500 ft-lb for the top and bottom impact limiter attachment bolts, respectively.
2. During the hypothetical accident, the attachment bolts ensure that the impact limiters remain attached to the HI-STAR 100 overpack during and after the impact with the unyielding surface.

The bottom impact limiter is attached to the overpack by 16 bolts aligned with the longitudinal axis of the overpack and arranged in a circular pattern (Figure 2.A.5.4 shows the bottom view of

the one-quarter scale replica). These bolts perform their function by developing tensile stress to resist loading during the hypothetical accident. Because of close clearances with the overpack shielding, the bottom impact limiter also has a set of eight circumferentially arranged alignment pins that fit into mating holes in the overpack bottom plate. These mating holes are plugged when the impact limiter is not in place.

The top impact limiter is attached to the overpack using twenty radial bolts that are designed to resist relative motion and transfer loads by shear (Figure 2.A.5.3 shows the top view of the one-quarter scale replica).

Although the attachment analyses do not require pre-load (by application of an initial bolt torque) to demonstrate that the required performance during normal transport conditions is achieved, the presence of pre-load serves only to enhance the performance of bolting which resists loads by developing tensile bolt forces (bottom impact limiter attachment bolts). Pre-stress in the bottom impact limiter attachment bolts serves to develop an interfacial pressure between the two components being joined together. This interfacial pressure acts as a reserve against separation at the interface of the impact limiter and the overpack when the external force or moment act to separate them during the drop event. The actual tensile stress bolt will rise significantly over the initial pre-stress if and only if the external load acting to break apart the interface is large enough to cancel out the interfacial pressure.

The effect of pre-load on the performance of bolting that resists loads by shear (top impact limiter attachment bolts) is different. The presence of both tensile stress (due to bolt pre-load) and shear stress in the bolt (due to the impact loads in a drop event) will increase the maximum principal stress in the bolt, which will consequently reduce the shear capacity of the bolts. Applying a pre-load in excess of the required amount in the 1/4 scale HI-STAR 100 drop tests will therefore result in a conservative evaluation of the top impact limiter attachment bolts.

Based on the initial torque values set in the full-scale package, the appropriate bolt pre-load torque for the 1/4-scale impact limiter attachment bolts is (to the nearest foot-pound):

Top impact limiter (radial) bolts: 4 ft-lb. (full scale equivalent = 245 ft.-lb)
Bottom impact limiter (axial) bolts: 23 ft-lb. (full scale equivalent =1500 ft.-lb.)

Since a bolt pre-load will enhance the performance of bolts (located at the bottom impact limiter interface) that resist loading by developing tensile stress, the bolt torque was conservatively set at 20 ft-lb. or below for the bottom impact limiter bolts. Since a bolt pre-load will degrade the performance of bolts (located at the top impact limiter interface) that resist loading by developing shear stress, the bolt torque was conservatively set at 4 ft-lb. or above for the top impact limiter bolts.

The end drop onto the top impact limiter tests the resistance of the twenty radial attachment bolts against failure from shear. The use of an initial torque value (15 ft-lb.), in excess of 4 ft-lb., is conservative for evaluation of the performance of the bolts to resist shearing strains (i.e., as

noted earlier, due to an interaction relation between tension and shear, the presence of any tensile strain will reduce the allowable shear strain prior to failure).

The C.G. over corner drop used an initial torque of 15 ft-lb., a value below the mandated value of 20 ft-lb. on the bottom impact limiter. This is again conservative for the evaluation of the performance of the bottom impact limiter attachment bolts, since the presence of additional prestress would enhance the ability of the bolts to retain the impact limiter in position.

The slapdown test was performed using low initial bolt torque values for both impact limiters that simulated "hand-tight" values. Thus, there is almost no contribution from pre-load on the bolts on either impact limiter. In the slapdown drop, the bottom impact limiter experienced the largest deceleration. This test demonstrated that the use of a lower pre-load on the most highly loaded attachment bolt does not affect the ability of the bolts to perform their required function.

Finally, the final side drop used the bolt pre-loads that correlate with the final bolt pre-loads specified (top impact limiter - 4 ft-lb.; bottom impact limiter - 20 ft-lb.) for the one-quarter scale tests.

A minimum of five calibrated unidirectional accelerometers was installed on the test package for each test. Schematics of the accelerometer locations and numbering system for all four tests are presented in Figures 2.A.5.5 and 2.A.5.6.

The accelerometers are placed at three axial locations along the height of the overpack model and at different circumferential locations at each axial location. The placement of the accelerometers axially reflects locations consistent with the detailed 2-D finite element analyses of the MPC that conservatively neglected the effect of stiffening provided to the MPC shell by the MPC baseplate. Figure 2.A.5.2 shows the three cutouts of the outer 5/8" thick cylinder that are machined flat to position the accelerometers. The following table provides the locations of the accelerometers.

ACCELEROMETER LOCATIONS FOR ONE-QUARTER SCALE DROP TESTS								
NUMBER	TOP END DROP		SIDE DROP		SLAPDOWN		CG-OVER-CORNER	
	Axial (inch)	Peripheral (degrees)	Axial (inch)	Peripheral (degrees)	Axial (inch)	Peripheral (degrees)	Axial (inch)	Peripheral (degrees)
1	44.781	0	5	0	44.781 25	0	5	0
2	25	0	25	0	25	0	5	+120
3	5	0	44.781	0	5	0	5	-120
4	44.781	+120	25	+90	44.781	+120	44.781	0
5	44.781	-120	25	-90	44.781	-120	44.781	+120
6	5	+120	--	--	5	+120	44.781	-120

Notes:

1. All accelerometer axial distances measured from top end surface of overpack model (without impact limiters in place).
2. Peripheral locations measured from plane containing accelerometer #1; clockwise direction, viewed from Section A-A in Figures 2.A.5.5 and 2.A.5.6, is positive.

In addition to recording the deceleration during impact, a high-speed camera and a video camera were used to record the test events. The high-speed camera was used to confirm orientation angles just prior to impact and to aid in the evaluation of extent of crush subsequent to the test. The tests were conducted by attaching the ¼ scale package to a 15-ton mobile crane through appropriate rigging and lifting the package to the required height. An electronically activated guillotine-type cable cutter device was used for releasing the package for free fall. An array of photographs labelled Figures 2.A.5.7 through 2.A.5.13 provide pre-test and post-test visuals of the package. These photographs show quite clearly that the post-crush impact limiters maintained their own physical integrity and the attachments to the overpack scale model suffered no failures.

The following acceptance criteria for the scale model dynamic drop tests were identified in the Test Plan [2.A.11]:

- Filtered decelerations limited to a maximum of 60g's (after scaling to full-scale geometry) for all drop orientations.
- No impact of the cask body on the target surface.
- No separation of impact limiters from the cask body through the entire drop event.

2.A.5.2 Results of First Series of Drop Tests

The first series of three one-quarter scale drop tests (types A, B, and C denoted above) were performed in August 1997 and produced significant information [2.A.5]. Table 2.A.1 shows the maximum filtered decelerations registered in the three one-quarter scale tests after the test results are scaled up to the full-scale AL-STAR (by dividing test results by four).

Table 2.A.1: Peak Decelerations from August 1997 Tests

Test I.D.	Orientation	Deceleration (g)
A.	End Drop	134
B.	C.G.-Over-Corner	37.84
C.	Side Drop	51.3

The peak filtered deceleration in the first end-drop test was clearly above the 60g-design limit established for the HI-STAR 100 design. The reasons for this discrepancy were determined to be the use of a low value of the dynamic multiplier assumed in designing the impact limiter, and the lack of pre-crush of the honeycomb material. Numerical analyses also indicated that the honeycomb compression modulus was dependent on the impact limiter velocity during the drops. This confirms laboratory data available in the historical literature [2.A.9]. The velocity and deceleration information obtained from the first round dynamic drop tests enabled development of a simple dynamic correlation multiplier to be applied to the honeycomb material's static F-d behavior. This multiplier is an additional "experimentally based" input term in the computer prediction model for simulation of dynamic drop events [2.A.6]. Data from the initial test series shows that this multiplier is independent of test orientation and is a function of the ratio of crush velocity during the crushing process divided by the impact velocity at the initiation of crush. Based on the numerical analysis of the August 1997 tests, the honeycomb material was appropriately revised with new crush strengths and new sets of ¼ scale model impact limiters were manufactured. The correlation of the August 1997 quarter-scale tests with the numerical results from the computer model is presented in section 2.A.6.

In summary, the chief contribution of the August tests, therefore, lay in providing the database to quantify the crushing characteristic of the honeycomb material under dynamic conditions [2.A.6]. Since none of these tests is ascribed to confirmation of the final performance of the AL-STAR impact limiters, no accelerometer raw or filtered results are included herein. The full set of acceleration data (both raw and filtered) is provided in [2.A.5].

2.A.5.3 Results of the Second Series of Drop Tests

The second round of one-quarter scale dynamic drop tests, conducted in December 1997 and February 1998, using the new (lower crush strength) impact limiter materials, occurred in three phases. The first phase consisted of the top end drop, CGOC drop, and side drop tests. While the decelerations in all cases were within the design limit, the attachment system for the bottom impact limiter did not survive the side drop test. The attachment system was redesigned prior to the remaining (slapdown) test. The slapdown test is considered to be the most definitive test of the cask/impact limiter attachment integrity. The slapdown test was successfully completed, with the bottom impact limiter remaining in place during and after the secondary impact, on December 29, 1997 in Phase 2 of the second test series. In order to confirm the adequacy of the attachment system under side drop conditions, the side drop test was repeated in February 1998 during Phase 3. This test reconfirmed the attachment system integrity.

The results from the second round test series demonstrates that the HI-STAR 100 package meets all test acceptance criteria, namely:

- Appropriately filtered decelerations of less than 60g's (after appropriate scaling to reflect the full-size mass and geometry) for all tested orientations;
- All attachment bolts remained intact, ensuring that the impact limiters do not separate from the cask body through and after the drop event;
- No impact of the cask body on the target surface.

Figures 2.A.5.14 through 2.A.5.21, drawn from reference 2.A.7, provide the raw (unfiltered) and filtered deceleration time-histories for each of the four drop scenarios for the key accelerometers used to assess package performance. The accelerometer station numbers indicated in these accelerograms are located by referring to Figures 2.A.5.5 or 2.A.5.6, as applicable. The test report [2.A.7] provides the necessary background to justify the use of this data to evaluate package performance. The following remarks are pertinent concerning the results presented in Figures 2.A.5.14 through 2.A.5.21.

End Drop Decelerations (Figures 2.A.5.14, 2.A.5.15, and 2.A.5.15a-c)

All accelerometers for this test recorded decelerations in the direction of crush. Two accelerometers were subsequently determined to be defective (documented in [2.A.7]). The figures show the raw, the filtered response at 450Hz cut-off frequency, and a combined plot of the raw and filtered data covering a reduced time period. All of these results are obtained from the records from the working accelerometers. All working accelerometers gave essentially identical response; the final evaluation of performance presented herein is the average of the response from the accelerometers deemed to be recording correctly. Figures 2.A.5.15b and 2.A.5.15c demonstrate that the sensitivity to cut-off filter frequency is small even up to 1250Hz.

Center of Gravity Over Corner Decelerations (Figures 2.A.5.16, 2.A.5.17, and 2.A.5.17a)

The CGOC test was performed immediately after the end drop using the same set of accelerometers. The evaluation of the data after this test clearly determined that the same two accelerometers deemed suspect in the end drop test was also providing erroneous data here. Subsequent independent plate impact tests that definitively showed that these accelerometers were indeed faulty are documented in [2.A.7]. The acceleration data in the figures represents the vertical acceleration obtained by appropriate combination of the raw time data from the longitudinal and lateral mounted accelerometers on the inclined scale model cask. The raw vertical accelerations were then subject to filtering to remove non-rigid body behavior. Raw, filtered, and combined raw and filtered data over the strong response time period are presented.

Slap Down Decelerations (Figures 2.A.5.18, 2.A.5.19, and 2.A.5.19a)

Although the initial release of the package was at an angle of 15 degrees from the horizontal, the high-speed camera showed that impact occurred with the overpack longitudinal axis at an angle of 7.2 degrees from the horizontal. The numerical simulation of this test reflected the actual angle of impact rather than the initial setting at nine meters. The results for all accelerometers (raw data and filtered) are provided in [2.A.7]. The raw and filtered data presented in the figures here represent the deceleration at the bottom end of the package that experiences the larger magnitude secondary impact. Numerical analysis demonstrated that the peak deceleration from secondary impact is insensitive to impact angles between 5 and 12 degrees from the horizontal and decreases as the angle increases above 12 degrees. Raw, filtered, and combined raw and filtered data over the strong response time period are presented.

Side Drop Decelerations (Figures 2.A.5.20, 2.A.5.21, and 2.A.5.21a)

Both impact limiters are supposed to impact the target simultaneously in this test. An evaluation of the individual accelerometer data and an examination of the high-speed camera film clearly indicated that there was a small angle existing between the overpack longitudinal axis and the target horizontal surface at the moment of impact. This caused the expected result that accelerometer readings at one end of the package were slightly higher than readings at the other end. The results for raw and filtered data represent results obtained by averaging the data from the accelerometers at the ends of the package. Raw, filtered, and combined raw and filtered data over the strong response time period are presented.

The filter frequency used for the End Drop and CGOC Drop is 450 Hz. The filter frequency used for the Slap Down and Side Drops was 350 Hz. These filter frequencies were established by examination of the power spectral density function for each raw data trace that clearly showed that the majority of the energy occurred at frequencies well below the cut-off frequency. Independent confirmation of the appropriateness of the cut-off frequencies was made by determining the lowest frequency of elastic vibration of the package acting as either a bar or a simply supported beam. As described above, the sensitivity to cut-off frequency was examined for the end drop case by re-analyzing the data for three cut-off frequencies.

Table 2.A.2 provides the peak deceleration data culled from the above-mentioned accelograms for the four drop scenarios after filtering to remove high frequency effects. The table contains the results from the actual 1/4-scale experiments scaled up to the full-size packaging. The test report [2.A.7] provides the detailed information on this final one-quarter scale dynamic drop test series with raw and filtered outputs from all accelerometers. The test report also includes details on the filtering methodology, on the data reduction, and on the evaluation of the performance of the various accelerometers used in each of the tests.

In all of the four final one-quarter scale dynamic drop tests, the impact limiter attachments successfully performed without a single attachment bolt failure (ensuring that the impact limiters did not separate from the overpack), rigid body decelerations were below 60 g's, and the cask body did not contact the unyielding target surface. Also, additional crush margin remained in the aluminum honeycomb material.

Table 2.A.2: Peak Decelerations from AL-STAR™ Drop Tests (Second Series)

Test Case	Orientation	Peak Decelerations (g)
A	End-Drop	53.9
B	C.G.-over-Corner	38.8
C	Side Drop	45.7
D	Slap-Down	59

2.A.6 Phase 5: Numerical Prediction Model for Dynamic Analysis

The numerical prediction model for dynamic drop events utilizes the previously discussed force-crush (F-d) model and incorporates the information into the dynamic equations of equilibrium. Using the procedure discussed previously, the static F-d curves for the AL-STAR impact limiter under the four drop scenarios are readily constructed. Figures 2.A.6.1 to 2.A.6.4, respectively, provide the static force vs. crush plots for the full scale impact limiter with test orientations for drop cases A, B, C, and D (primary impact). An appropriate analytical fit for each curve is developed using the commercial graphing package Deltagraph [2.A.8]. Figures 2.A.6.1 through 2.A.6.4 also provide curves for upper and lower bound material strengths.

We now discuss the application of the F-d model to the prediction of impact limiter performance in a dynamic drop environment. In symbolic form, we can write the static resistive (crush) force, F , as a function of the crush depth, Δ , where a zero value for Δ represents an uncrushed condition.

$$F = f(\Delta)$$

The above symbolic formula represents the data on Figures 2.A.6.1 to 2.A.6.4 in analytical form. We have previously explicitly discussed the mathematical concepts underlying the above formulation by referencing the particular case of a side drop. In general, the static F-d curve can be expressed as a sum of local crush pressures multiplied by interface areas where the interface areas may be a function of the current crush. That is, the mathematical relation for static compression (which is validated by comparison to static testing) is also expressible in the form

$$f(\Delta) = \sum_i p_i A_i$$

where p_i are the crush pressures of the materials participating in the crush and A_i are the interface areas associated with the different crush strengths. The determination of the areas A_i as a function of crush depth, Δ , has previously been discussed within the context of interpenetration.

The dynamic model for simulating a packaging drop event consists of solving the classical Newtonian equations of motion. In the case of a unidirectional impact such as an end drop ($\theta=90^\circ$), side drop ($\theta=0$), or CGOC drop, the equation of motion simply reduces to:

$$M \frac{d^2 \Delta}{dt^2} = \text{Force} + Mg$$

where: M = mass of system undergoing deceleration

$d^2\Delta/dt^2$ = second derivative of package movement (which is equal to the impact limiter crush because the target is immovable and rigid).

The resistive "Force" opposes the downward movement and is given by the static force-crush functional relationship (appropriate for the drop orientation) multiplied by a dynamic multiplier Z . As noted earlier, there is historical evidence that metal honeycomb crush pressure is a linear function of velocity [2.A.9]. The Holtec correlation of the August 1997 test data by numerical simulation [2.A.6] also confirmed that the best correlation is achieved if the dynamic multiplier is represented by a linear function of local crush velocity ($d\Delta/dt$). Introducing the dynamic multiplier, the dynamic equation of force equilibrium for a case involving only primary impacts becomes

$$M \frac{d^2 \Delta}{dt^2} = ZF + Mg = Zf(\Delta) + Mg$$

The above equation is a second order non-linear differential equation in the time coordinate t , which can be solved for the post-contact event using any standard equation solver package. The initial condition is: @ $t = 0$, $\Delta = 0$, $d\Delta/dt = V_o$ (approach velocity at impact). We note that since the acceleration is an explicit function of both deformation and velocity, maximum acceleration will not, in general, occur at the instant when the velocity of the package is zero.

If the impact event involves both primary and secondary impacts, as is the case for the slapdown event (indeed any event wherein $\theta < 67.5^\circ$), then both the mass M and rotational moment of inertia I are involved. The modeling of a dual impact event is only slightly more involved than

the single variable modeling of the single impact case discussed above. Figure 2.A.6.5 pictorially illustrates the sequence of events leading to an appropriate mathematical model. Figure 2.A.6.6 provides the appropriate free-body diagrams associated with each portion of the event.

In the first step, the inertia force of the falling package is resisted by the crush force developed at the primary impact location. While the downward momentum of the package is dissipated by the resistive force, the package also experiences the overturning couple produced by the non-collinearity of the inertia force (which acts at the centroid) and the resistive force which acts at the primary impact zone (Figure 2.A.6.5(a)). The dynamic equation of force equilibrium is given above in terms of the downward movement of the package centroid and the resistive force static compression curve, modified by the dynamic factor Z , appropriate to the initial orientation at primary impact. The package decelerates and then begins to overturn, in effect pivoting about the initial point of contact in the primary impact region, gathering angular momentum as the second impact limiter (mounted at the far end) approaches the target surface. Referring to Figure 2.A.6.5(b), the dynamic equation insuring moment equilibrium during the overturning (before the initiation of the secondary impact) phase can be written as

$$I_p \frac{d^2\phi}{dt^2} = -MgR \cos(\phi)$$

where I_p : moment of inertia of the package about the pivot point
 ϕ : angular acceleration with respect to the horizontal plane
 R : radial distance of the package C.G. with respect to the pivot point.

The initial conditions for this phase are: $t = 0$, $\phi = \theta$, $d\phi/dt = 0$ where t is now redefined at the initiation of rotational motion.

Finally, the secondary impact commences wherein the angular momentum of the package plus any linear momentum not dissipated by the primary impact is dissipated by the crushing of the second impact limiter. During the secondary impact phase, the equation of dynamic moment equilibrium can be written by inspection of Figure 2.A.6.5(c):

$$I_p \frac{d^2\phi}{dt^2} = -MgR \cos(\phi) + Zf(D\phi)D$$

where $f(D\phi)$ is the static resistive force at the secondary impact location under compression $D\phi$, Z is the current dynamic multiplier appropriate to the secondary impact location, D is the moment arm, and I_p is the moment of inertia of the package about the pivot point. During this phase of the motion, the equation of dynamic force equilibrium is modified to reflect dynamic resistive forces from both impact limiters since the entire package may continue to move toward

the target surface with both impact limiters providing a dynamic resistive force. Therefore, during the final phase of the impact event, the dynamic force equilibrium equation can be written as

$$M \frac{d^2 \Delta}{dt^2} = Z_1 F_1 + Z_2 F_2 + Mg$$

where Z_i and F_i ($i=1,2$) represent the dynamic multiplier and static compression force appropriate to the primary and secondary impact limiter behavior during the final phase of the event. The dynamic multipliers Z_i ($i=1,2$) reflect the current value of the local crush velocities at each of the limiters.

The above formulation assumes, for simplicity, that the pivot point does not slide during the overturning or secondary impact phases.

It is evident from the foregoing that the impact limiter is essentially simulated by a non-linear spring whose static force-deformation curve is known a priori (from the F-d model) as a function of the drop orientation. The solution of this rigid body dynamics problem featuring up to two non-linear springs can be determined using any one of several standard software packages available in the public domain. Holtec International utilizes the commercial package WORKING MODEL [2.A.10], which has been validated in the company's QA system for this purpose.

The dynamic simulation model, constructed in the manner of the foregoing, was utilized to simulate all seven one-quarter scale drop events (three in the first series, four in the second series). In order to develop a high level of confidence, it was decided that the model should be validated at all three levels, namely, a comparison of acceleration, crush, and duration of impact. In other words, to be acceptable, the numerical prediction model must predict α_{max} , maximum crush sustained d_{max} , and the duration of impact, with reasonable accuracy. Since the actual crush d_{max} could be measured, and the duration of impact and α_{max} were available from accelerometer data, comparison between theory and experiment with respect to all three key indicators was possible. Tables 2.A.3 and 2.A.4 provide the results in a concise form for all of the one-quarter scale dynamic drop tests for the first and second series, respectively.

Note that in the tables, the comparison is made after scaling up the model results to reflect a full-scale package.

Table 2.A.3: Comparison Between Test Data and Prediction Model Results (First Test Series)

Case I.D.	Deceleration (g's)		Total Crush Depth (inch)		Impact Duration (milli-seconds)	
	Predicted	Measured	Predicted	Measured	Predicted	Measured
A. End-Drop	134.2	134.0	2.42	2.42	3.5	Not measured
B. C.G.O.C.	37.8	37.84	16	16	13.25	16.6
C. Side Drop	50.5	51.3	9.1	9.51	8.25	10.74

Table 2.A.4: Comparison Between Test Data and Prediction Model Results (Second Test Series)

Case I.D.	Deceleration (g's)		Total Crush Depth (inch)			Impact Duration (milli-seconds)	
	Predicted	Measured	Predicted	Measured	Max. Available	Predicted	Measured
A. End Drop	53.0	53.9	11.3	10.6	17.659	38.8	37.2
B. C.G.-Over-Corner	38.7	38.8	12*	9.82*	25.06	51.0	61/45.2
C. Side Drop	43.5	45.7	10.9	12.5	16	38.5	53.1 (averaged value)
D. Slap-Down							
Primary	46.4	49.0	9.50	10.7	16	48.5	44.4
Secondary	59.9	59.0	12.8	13.5	16	35.8	41.2

* For C.G.-Over-Corner, only crush at the external interface is measured.

It is evident from both Tables 2.A.3 and 2.A.4 that the numerical prediction model is robust in predicting all seven impact tests. Not only are peak values of α_{max} for each test predicted with good agreement, but also the crush depth and impact duration is also reliably simulated.

A perusal of the numerical results in Table 2.A.4 yields two additional insights into the behavior of AL-STAR which are most helpful in the "fine tuning" of the full-scale AL-STAR design:

- i. The maximum deceleration, α_{max} , predicted as well as measured, under the most limiting scenario (slapdown), is close to the permissible limit of 60g's.
- ii. The maximum crush, predicted as well as measured, in all drop scenarios, is well below the available limit (i.e., the value at which the crush material will "lock up").

The state-of-the-art manufacturing technology for aluminum honeycombs permits the material to be manufactured within a total tolerance range of 12 to 13% (between the maximum and minimum values). The above observations suggest that the upper and lower bound range of crush pressures for the honeycomb material in the AL-STAR impact limiter should be set at 95% and 82% of the values of honeycomb material used in the second series quarter-scale tests.

Finally, the agreement between the predictions and measured data in the above correlation effort fosters a high level of confidence in the numerical model, which can now be used to conduct sensitivity studies.

2.A.7 Phase 6: Simulation of the Effects of Material Crush Strength Variation, Package Mass Tolerances, and Oblique Drop Orientations

Having ensured the technical reliability of the numerical prediction model, it is now necessary to evaluate the system behavior under all "limiting conditions". As noted earlier, the impact limiter materials are insensitive to environmental temperature changes within the limits of -20° F and 100° F. Therefore, limiting conditions are broadly defined here as arising from two sources:

- i. Variation in the impact limiter honeycomb crush strength due to material manufacturing tolerance.
- ii. Variation in the package weight (due to different MPC types that may be transported in the HI-STAR 100 overpack, and manufacturing tolerances in fabrication of the overpack and impact limiters).
- iii. Variation in package angle of impact with the target.

To examine all limiting scenarios, additional simulations using the mathematical model were performed. The crush strength of the honeycomb material was varied within the range permitted in the Holtec Drawing 1765. The packaging weight was set at its upper bound and lower bound value (upper bound weight is 280,000 lb., and lower bound weight is 270,000 lb. based on values listed in Table 2.2.1). Three additional drop orientations (30 degree, 45 degree, and 60 degree orientation angle, measured from the horizontal) that were not the subject of tests were also analyzed numerically using input crush strength data that would maximize the decelerations with an average weight. The purpose of these additional simulations with varied drop angle is to ascertain which, if any, oblique drop orientation merits detailed finite element stress analysis to meet the requirements of the Regulatory Guide. Figures 2.A.7.1-2.A.7.3 provide the static crush force vs. crush depth information used in the dynamic simulation of these accident events. Table 2.A.5 provides key output data, peak decelerations and maximum crush, as obtained from these numerical simulations.

Table 2.A.5: Sensitivity of Package Response to Package Weight, Crush Material Strength Variations, and Package Orientation at Impact

Orientation	Case	Deceleration (g's)	Maximum Total Crush (2-interfaces) (inch)	Available Crush Stroke (inch)
End Drop	Max. Strength, Min. Weight	52.85	11.4	17.659
	Min. Strength, Max. Weight	46.3	12.8	17.659
C.G. Over Corner	Max. Strength, Min. Weight	38.25	17.0	25.06
	Min. Strength, Max. Weight	35.6	18.5	25.06
Side Drop	Max. Strength, Min. Weight	42.5	11.2	16
	Min. Strength, Max. Weight	37.5	12.7	16
Slap Down (secondary impact bounds)	Max. Strength, Min. Weight	58.5	13.2	16
	Min. Strength, Max. Weight	52.6	15.1	16
Oblique Drop – 30 degrees	Max. Strength, Min. Weight	36.44	19.57	24.1
Oblique Drop – 45 degrees	Max. Strength, Min. Weight	35.62	22.39	25.72
Oblique Drop – 60 degrees	Max. Strength, Min. Weight	38.01	19.2	25.65

The following conclusions are readily derived from Table 2.A.5 results:

- i. The maximum value of α_{max} is less than 60g's in all cases.
- ii. The total crush of the impact limiter is below the available "stroke", i.e., the overpack body will not contact the unyielding target surface nor will any "lock-up" of the crush material occur.
- iii. The three oblique drop simulations considered all produce approximately the same vertical deceleration from the primary impact. The decelerations resulting from the subsequent secondary impact, after rotation of the HI-STAR 100, are all below the value obtained from the simulation of the "slapdown" at low angles of

impact. If the "limiting" oblique drop is considered as the simulation providing maximum deceleration perpendicular to the longitudinal axis of the cask, then the drop most likely to develop the largest bending of the overpack in the oblique orientation is at 30 degree orientation (from the horizontal axis). Therefore, this case is subjected to detailed stress analysis in Section 2.7 with the applied impact loading (along and perpendicular to the cask axis) balanced solely by the cask inertia forces and moments.

In conclusion, the above work provides full confidence that the HI-STAR 100 packaging will perform in the manner set forth in the NRC regulations (10CFR71.73) under all conceivable hypothetical accident conditions of transport.

2.A.8 One-Foot Drop

Paragraph 2.6 of Reg. Guide 7.8 requires evaluation of the package response under a one-foot drop onto a flat unyielding surface in a position that is expected to inflict maximum damage.

Using the prediction model, the maximum deceleration sustained by the package under the one-foot end and side drop scenarios, the latter expected to produce maximum stress in the fuel basket, was computed. Table 2.A.6 provides summary results for the limiting case of minimum package weight and upper bound material crush strength (so as to maximize the decelerations).

Table 2.A.6: Peak Decelerations Under One-Foot Drop Event

Scenario	Max. Deceleration in g's	Crush (inch)	Duration of Impact (milli-seconds)
90° End Drop	17.25	0.85	20.0
0° Side Drop	11.45	1.33	26.0

2.A.9 Equivalent Dynamic Factor (EDF)

It is instructive to compute an effective equivalent dynamic factor on the predicted static crush force corresponding to the instant of maximum deceleration during the drop event. Table 2.A.7 presents the pseudo-deceleration (obtained by dividing the static force by the mass of the package) and the predicted deceleration; the ratio of the two is the "equivalent dynamic factor" (EDF). The EDF is also equal to the peak dynamic crush force divided by the static resistance force at the coincident instance of crush when the dynamic crush force is maximized. Note that the differences in package weight used in the table below reflect the actual weight of the impact limiters used in each one-quarter scale drop test (after increasing to full-scale equivalent values).

Table 2.A.7: Equivalent Dynamic Factor (EDF) for Different Drop Scenarios

Scenario	Predicted Force (lbs) $\times 10^{-7}$		Participating Package Weight (lbs)	Predicted Max. Deceleration		EDF
	Static	Dynamic		Pseudo- Accn (static)	Dynamic (from Table 2.A.4)	
End Drop	1.0785	1.454	274,336	39.313	53	1.348
CGOC Drop	0.8	1.059	273,680	29.231	38.7	1.324
Side Drop	0.4	0.597	137,270*	29.14	43.5	1.493
Slapdown	0.345	0.6607	†	†	59.9	1.915

* Only half of the total package weight participates at each impact limiter.

† Indeterminate for this drop configuration.

The last column of the above table demonstrates that the EDF, as defined above, is not a constant value independent of drop orientation.

2.A.10 Additional 1/8th Scale Static Tests

Three additional static crush tests on 1/8th scale impact limiters have been performed subsequent to the completion of all quarter-scale dynamic testing and theoretical correlation. The F-d test results for each of three impact limiter orientations are compared with the analytical F-d predictions in Figures 2.A.10.1-2.A.10.3. Figure 2.A.10.1 compares test results with theoretical prediction for the crush orientation corresponding to a side impact, Figure 2.A.10.2 presents the results for the Center-of-Gravity-Over-Corner impact orientation, and Figure 2.A.10.3 presents results for the end impact orientation. In all tests, the crush material orientation and location duplicated the final configurations subjected to quarter-scale tests. The internal backbone structure was also faithfully reproduced. The welds were also scaled to the extent practical given the thin material gages used for the one-eighth-scale model. In the three figures, the solid line without symbols represents the predictions of the theory developed for the F-d curves, while filled circles represent test results. Within the range tested for each orientation, good agreement is observed between theory and test for the side and CGOC crush orientation. For the end drop orientation, however, the tested results suggest that inclusion of some elastic behavior at the cask-impact limiter interface into the theory might improve the static correlation. The dynamic test results presented in Table 2.A.4, however, demonstrate conclusively that the prediction of peak deceleration, extent of crush, and impact duration would not be affected by these elastic effects that “smooth” the abrupt “staircase” shape of the F-d curve.

2.A.11 Conclusions

The AL-STAR impact limiter design was subjected to a series of static and dynamic tests to validate its functional performance. The 1/8 model static tests conducted under cold and hot, as well as ambient conditions, confirmed that AL-STAR's functional characteristics are independent of the environmental temperature conditions in the range specified in 10CFR71.73. The successful static tests on the 1/8 scale model (namely, end test and 60° oblique test) also correlated well with the theoretical force-crush model developed by Holtec. Subsequent static tests, performed after the final successful one-quarter scale dynamic tests, provided additional confirmation of the validity of the fundamental F-d model.

The static compression tests were followed by quarter-scale drop tests. The first series, in August 1997, consisting of three tests, provided the necessary test data to determine the dynamic multiplier applicable to the honeycomb materials. The numerical model for simulating the dynamic crushing of AL-STAR showed good agreement with the first test series data when the correct dynamic factor was incorporated in the computer model (Table 2.A.3).

While the prediction model for simulating AL-STAR crushing under 9-meter drop conditions was extremely well correlated, the peak deceleration under the end- drop condition in the August 1997 tests exceeded the acceptance criteria.

The second series of tests wherein the crush strength of the honeycomb was lowered (as selected by the prediction model), performed as expected. The agreement between the test data and the prediction model is high (Table 2.A.4).

The prediction model for AL-STAR therefore stands correlated with seven (7) quarter-scale drop events. The first three tests used different honeycomb crush strength materials than the last four, proving the ability of the prediction model to predict the AL-STAR crush performance for a wide range of crush material properties. The backbone structure of AL-STAR, enhanced after the 1/8-model static compression tests, performed as designed in all seven quarter-scale drop tests.

Finally, the AL-STAR-to-overpack attachment system remained intact and the cask did not contact the unyielding target during all four final dynamic tests.

2.A.12 References

- [2.A.1] ANSYS 5.3 Ansys Inc., 1996.
- [2.A.2] CADKEY, Version 7, 1996.
- [2.A.3] Project Procedure No. HPP-5014-5, HI-STAR Aluminum Honeycomb 1/8 Scale Impact Limiter Static Test Procedure.
- [2.A.4] HI-STAR 1/8 Scale Impact Limiter Test Report, HI-961501, Holtec International, June 1996.
- [2.A.5] Holtec Report HI-971774, *Revision 1*, "Impact Limiter Test Results – 30' Drop Tests" – August 1997
- [2.A.6] Holtec Report HI-971823783, *Revision 0*, "Improved Correlation of ORNL 30' Drop Tests" – August 1997
- [2.A.7] Holtec Report HI-981891, *Revision 2*, "Impact Limiter Test Report - Second Series", (~~Rev. 1~~), 1998.
- [2.A.8] Deltagraph Pro 3.5, Deltapoint Software, 1995.
- [2.A.9] J.M. Lewallen and E.A. Ripperger, Energy Dissipating Characteristics of Trussgrid Aluminum Honeycomb, SMRL RM-5, University of Texas Structural Mechanics Research Laboratory, 1962.
- [2.A.10] Working Model 3.0, Knowledge Revolution, 1995.
- [2.A.11] HI-STAR 100 Impact Limiter Test Program, Holtec Report No. HI-951278.

SUPPLEMENT 2.1: HI-STAR HB STRUCTURAL EVALUATION

2.1.0 OVERVIEW

In this supplement, the structural adequacy of the HI-STAR HB is evaluated pursuant to the guidelines of NUREG-1617 and the requirements of 10CFR71. The organization of this supplement mirrors the format and content of Chapter 2 except it only contains material directly pertinent to the HI-STAR HB.

The HI-STAR HB is a shortened version of the HI-STAR 100 that is evaluated in Chapter 2. All dimensions (radius, thickness) of the HI-STAR HB are identical to those of the HI-STAR 100 except for the overall length of the layered cylinders and the threaded diameter of the lifting trunnions. The impact limiters are identical in all respects except for the crush strengths of the internal aluminum honeycomb material, which are reduced to ensure that the deceleration limits are met with the lighter weight HI-STAR HB. The HI-STAR HB is configured to carry the MPC HB that has the appropriate length and fuel basket design to carry 80 spent fuel assemblies from the closed Humboldt Bay Nuclear Plant. The qualification of the MPC HB to withstand a 60g deceleration has been documented in the Part 72 license for Humboldt Bay (Humboldt Bay ISFSI, Pacific Gas and Electric Company, Final Safety Analysis Report Update, Revision 0 January 2006, NRC Docket No. 72-27). Therefore, no new analyses of the MPC HB are required in this Supplement 2.1 as long as the ~~design basis remains the same~~ maximum cask deceleration remains bounded by 60g.

The applicable design codes and standards, and the design criteria for the HI-STAR HB are identical to those applied to the HI-STAR 100. Therefore, since the differences between the HI-STAR HB and HI-STAR 100 are limited to:

- *Shorter overall length;*
- *Lower package weight;*
- *Reduced strength of impact limiter crush materials;*
- *Smaller diameter threads on lifting trunnions,*

the supplement is focused on documenting the results from new evaluations required because of the reported differences in length, weight, impact limiter crush strength, and thread diameter. The reduced length and weight of the HI-STAR HB ensures that all stress-based evaluations performed on the HI-STAR 100 produce safety factors that are lower bounds for the same evaluation on the HI-STAR HB, except for the trunnion analysis discussed below. Therefore, no stress-based calculations need to be performed, except ~~The only evaluations that are cask specific are~~ those that involve deceleration limits, because of the change in impact limiters, and those that involve the lifting trunnions, because of the smaller diameter threads; this supplement focuses only on providing summaries for the new evaluations performed for the HI-STAR HB, which are documented in Holtec calculation packages HI-2084158 [2.1.7.2] and HI-2033042 [2.1.7.3].

2.1.1 STRUCTURAL DESIGN

2.1.1.1 Discussion

The general discussion presented in Subsection 2.1.1 applies to the HI-STAR HB package. Drawings for the components of the HI-STAR HB package are provided in Section 1.1.4.

2.1.1.2 Design Criteria

The HI-STAR HB package meets the design criteria espoused in Section 2.1.2 in its entirety. For the HI-STAR HB overpack, however, the option to replace the SA203-E plate used for the 2.5" thick inner shell with comparable SA350 LF3 ring forgings, stacked to form the inner shell and welded together with full penetrant welds, has been added to the drawings. The Nil Ductility Transition Temperature is still required to be less than -70 degrees F when this option is used (per Subsection 2.1.2.3). Accordingly, Table 2.1.22 lists SA350 LF3 as an optional material for the inner shell. Similarly, Table 2.1.23 lists SA350 LF3 as an option for the port cover plates.

2.1.2 WEIGHTS AND CENTERS OF GRAVITY

Table 2.1.2.1 provides the weights of HI-STAR HB components as well as the total package weight. The weight of the impact limiter is also provided. Table 2.1.2.1 also provides the location of the calculated center of gravity for the HI-STAR HB package.

2.1.3 MECHANICAL PROPERTIES OF MATERIALS

Materials for the HI-STAR HB package are identical to those used for the HI-STAR 100 package.

2.1.4 GENERAL STANDARDS FOR ALL PACKAGES

The HI-STAR HB is a shorter and lighter version of the HI-STAR 100. Therefore, the features presented in Section 2.4 apply to the HI-STAR HB.

2.1.5 LIFTING AND TIE-DOWN STANDARDS

2.1.5.1 Lifting Devices

The lifting devices for the HI-STAR HB package are identical to those for the HI-STAR 100, except that the threaded portion of the lifting trunnions has a slightly smaller diameter. Therefore, even though the HI-STAR HB is lighter than the HI-STAR 100, the safety factors for the HI-STAR HB lifting trunnions and the top flange interface are recalculated based on the smaller trunnion diameter.

The embedded trunnion is analyzed as a cantilever beam in the same manner as described in Subsection 2.5.1.1. Calculations demonstrate that the stresses in the trunnions comply with NUREG-0612 provisions.

Specifically, the following results are obtained:

<i>Safety Factors from HI-STAR HB Lifting Trunnion Stress Analysis for a Bounding Lifted Load of 161,200 lb[†]</i>			
<i>Item</i>	<i>Value (ksi) or (lb) or (lb-in)</i>	<i>Allowable (ksi) or (lb) or (lb-in)</i>	<i>Safety Factor</i>
<i>Bending stress (Comparison with Yield Stress/6)</i>	11.2	24.5	2.19
<i>Shear stress (Comparison with Yield Stress/6)</i>	4.76	14.7	3.09
<i>Bending Moment (Comparison with Ultimate)</i>	208,600	574,400	2.75

<i>Moment/10)</i>			
<i>Shear Force (Comparison with Ultimate Force/10)</i>	92,690	282,500	3.05

* ~~The bounding lifted load is 161,200 lb. (per Table 2.1.2.1).~~

We note from the above that all safety factors are greater than 1.0. A factor of safety of exactly 1.0 means that the maximum stress, under apparent lift load D*, is equal to the yield stress in tension or shear divided by 6, or that the section moment or shear force is equal to the ultimate section moment capacity or section force capacity divided by 10.

It is also important to note that safety factors associated with satisfaction of 10CFR71.45(a) are double those reported in the table since 10CFR71.45 only requires a factor of safety of 3 on the yield strength.

The top flange interface with the trunnion under the lifted load is analyzed in the same manner as described in Subsection 2.5.1.2.2. The interface region is conservatively considered as subject to the provisions of NUREG-0612, and the thread shear stress and bearing stress are compared to 1/6 of the top forging yield stress in shear or compression. The following table summarizes the results:

<i>Top Flange B Minimum Safety Factors (Interface with Trunnion) for HI-STAR HB</i>			
<i>Item</i>	<i>Value (ksi)</i>	<i>Allowable (ksi)</i>	<i>Safety Factor</i>
<i>Bearing Stress (NUREG-0612 Comparison)</i>	2.555	5.975	2.34
<i>Thread Shear Stress (NUREG-0612 Comparison)</i>	2.466	3.585	1.45
<i>Stress Intensity (NB Comparison)</i>	5.655	34.6	6.12

It is noted from the above that all safety factors are greater than 1.0 and that the safety factors for bearing stress and thread shear stress represent the additional margin over the factor of safety inherent in the member by virtue of the load multiplier mandated in NUREG-0612.

2.1.5.2 Tie-Down Devices

Since the HI-STAR HB is shorter and lighter, but otherwise identical to the HI-STAR 100, the tie-down devices and the resulting tables of reaction loads in Section 2.5 bound those for the HI-STAR HB. The span between tie-down locations is less, reflecting the shorter overall length of the HI-STAR HB. The equilibrium equations presented in Subsection 2.5.2 also apply to the HI-STAR HB. No new analyses are performed.

2.1.5.3 Failure of Lifting and Tie-Down Devices

The discussion in Subsection 2.5.3 for the HI-STAR 100 also applies to the HI-STAR HB, except for the following. New calculations have been performed for the HI-STAR HB to demonstrate that the ultimate load carrying capacity of the lifting trunnions is governed by the cross section of the trunnion external to the overpack top forging rather than by any section within the top forging. It is concluded that the trunnion shank reaches ultimate load capacity limit prior to the top forging reaching its corresponding ultimate load capacity limit. Loss of the external shank of the lifting trunnion will not cause loss of any other structural or shielding function of the HI-STAR HB overpack; therefore, the requirement imposed by 10CFR71.45(a) is satisfied.

The following safety factors are established:

$$\frac{(\text{Ultimate Bearing Capacity at Trunnion/Top Forging Interface})}{(\text{Ultimate Trunnion Load})} = 1.04$$

$$\frac{(\text{Ultimate Moment Capacity at Trunnion/Top Forging Thread Interface})}{(\text{Ultimate Trunnion Moment Capacity})} = 1.51$$

2.1.6 NORMAL CONDITIONS OF TRANSPORT

The HI-STAR HB package, when subjected to the normal conditions of transport specified in 10CFR71.71, meets the design criteria in Subsection 2.1.2 (derived from the stipulations in 10CFR71.43 and 10CFR71.51). The HI-STAR HB is identical to the HI-STAR 100 in all respects except for the length of the overpack (and the MPC HB), the crush strength of the impact limiter material, and the lifting trunnion thread diameter; the total package weight is bounded by the

package weights listed for the HI-STAR 100. Component diameters and thicknesses for the HI-STAR HB overpack and its closures are identical to those of the HI-STAR 100. Therefore, with the exception of the lifting trunnions, all stress analysis results associated with the HI-STAR HB overpack are bounded by the available results for the HI-STAR 100. No new analyses are reported in this supplement except for those associated with the performance of the impact limiter and the lifting trunnions. Stress results for the MPC HB have been reported in detail in the ~~update to the~~ Humboldt Bay ISFSI FSAR [2.1.6.1]; the MPC HB analyses were performed using the design basis deceleration.

2.1.6.1 Heat

Consistent with Regulatory Guide 7.9, the thermal evaluation of the HI-STAR HB is performed in Supplement 3.1 and sets material temperatures, which are used in the structural evaluations discussed in this section and in Section 2.1.7. As the Humboldt Bay fuel is "old and cold", the operating temperatures are at or below comparable temperatures for the HI-STAR 100 analyses. This adds additional margins since the allowable strengths will generally be higher in a comparable strength analysis using the HI-STAR HB.

Design pressures and design temperatures for all conditions of transport are listed in Tables 2.1.1 and 2.1.2, respectively.

In summary, because of the lower weight and shorter length, all stress analyses performed for the HI-STAR 100 using the bounding deceleration inputs give stress results that are equal to or greater than results using the HI-STAR HB.

2.1.6.2 Cold

No new or modified calculations or discussions are required for this subsection.

2.1.6.3 Reduced External Pressure

No new or modified calculations or discussions are required for this subsection.

2.1.6.4 Increased External Pressure

No additional analyses need be performed here to demonstrate package performance of the HI-STAR HB.

2.1.6.5 Vibration

No new or modified calculations or discussions are required for this subsection.

2.1.6.6 Water Spray

The condition is not applicable to the HI-STAR HB System per Reg. Guide 7.8 [2.1.2].

2.1.6.7 Free Drop

The structural analysis of a 1-foot side drop ~~under heat and cold conditions~~ has been performed for the HI-STAR 100 in Subsections 2.6.1 and 2.6.2 for heat and cold conditions of normal transport. As demonstrated in Subsections 2.6.1 and 2.6.2, safety factors are well over 1.0. Since the HI-STAR HB is shorter and lighter than the HI-STAR 100, the safety factors determined in Subsections 2.6.1 and 2.6.2 are lower bounds for comparable safety factors for the HI-STAR HB. As final verification, the decelerations for the free drop for the HI-STAR HB are determined in Section 2.1.7 and shown to be less than the design basis limits for the 1-foot free drop. Results for the 1-foot drop simulations are presented in Table 2.1.7.2.

2.1.6.8 Corner Drop

This condition is not applicable to the HI-STAR HB System per [2.1.2].

2.1.6.9 Compression

The condition is not applicable to the HI-STAR HB System per [2.1.2].

2.I.7 HYPOTHETICAL ACCIDENT CONDITIONS

The hypothetical accident conditions, as defined in 10CFR71.73 and Regulatory Guide 7.9, have been applied to the HI-STAR 100 System in the required sequence in Subsection 2.7.

It is shown in the following subsections that the HI-STAR HB System also meets the standards set forth in 10CFR71, when it is subjected to the hypothetical accident conditions specified in 10CFR71.73.

2.I.7.1 Free Drop

In this subsection the performance and structural integrity of the HI-STAR HB System is evaluated for the most severe drop events. The drop events that are potentially most damaging are the end drops (top or bottom), the side drop, the orientation for which the center of gravity is directly over the point of impact, an oblique drop where the angle of impact is somewhere between center of gravity over corner and a near side drop, and an orientation where package rotation after an impact at one end induces a larger impact deceleration when the other end impacts the target (i.e., slapdown).

As has been noted, the HI-STAR HB is shorter and lighter than the HI-STAR 100, but is identical to the HI-STAR in all other aspects of geometry. The impact limiter crush strengths are adjusted from those used in the HI-STAR 100 in order to ensure that the design basis deceleration limits for the HI-STAR family continue to be met. In Section 2.7, the analysis was performed in two parts. Initially, 1/8 and 1/4 scale testing was performed to establish the characteristics of the impact limiter and to demonstrate that the experimentally obtained decelerations for all orientations of the cask were below the design basis. ~~Simplified~~ Analytical models were developed and demonstrated to be capable of predicting the observed responses from the experimental results. These ~~simplified~~ models were used to evaluate sensitivity to crush strength change and cask weight change. Once it was established that the impact limiter configuration and crush strengths successfully limited the rigid body decelerations of the cask to below the prescribed limits, various strength analyses were performed to assess the state of stress in the cask components and ensure that the proscribed stress limits were satisfied.

As the impact limiter for the HI-STAR HB has the same geometry as the HI-STAR 100 with the sole difference being the impact limiter crush material, no qualification testing is employed. In lieu of testing, the same analytical methodology (the differential equation method) ~~more sophisticated 3-D finite element code LS-DYNA [2.1.7.1]~~ is used to simulate the free drop tests and demonstrate the performance of the impact limiter for the HI-STAR HB. The key features of the differential equation method are presented in [2.1.7.1], which summarizes, in a single document, the general analysis method ~~all of the previous experimental and numerical analyses undertaken in support of~~ as it was first implemented for the HI-STAR 100 license under 10CFR71. ~~In order to employ LS-DYNA, it is first demonstrated that the finite element model of the cask structure and the impact limiters is benchmarked. That is, it is demonstrated that the LS-DYNA simulation model proposed for the HI-STAR HB adequately matches existing experimental results obtained for the HI-STAR 100 when the model is altered to match the geometry and the impact limiter crush strength used in the HI-STAR 100.~~

Figures ~~2.1.7.1-2.1.7.4~~ show details of the ~~LS-DYNA~~ model constructed for the ~~HI-STAR 100~~ and used here to reproduce the experimental results for the four free drop tests (~~end drop, side drop, center of gravity over corner (CGOC) drop at 67.5 degree orientation from the rigid target, and slapdown drop at 7.2 degree orientation from the rigid target~~). ~~Figure 2.1.7.1 shows the complete half model in the slapdown orientation. Figure 2.1.7.2 shows the details of the finite element grid for the overpack. Figure 2.1.7.3 shows the grid density employed to simulate the steel structure (skin and "backbone" stiffeners) of the top impact limiter, and Figure 2.1.7.4 shows the grid density used and the orientation of the different honeycomb blocks (with different material strengths) that make up the top impact limiter crush material volume. The MPC and its contents are modeled by a cylindrical body with appropriate dimensions and material density to replicate a loaded MPC. The HI-STAR 100 overpack density is adjusted so that the total weight of the overpack in LS-DYNA matches the weight of the one-quarter scale model of the HI-STAR 100 after sealing back to the full size cask. The half models of the HI-STAR 100 overpack and the MPC are modeled with adequate details to ensure correct representation of the geometry and mass distribution. The total weight of the modeled (full size) loaded HI-STAR 100 overpack is 244,412 lbs.~~

~~The HI STAR impact limiters are fabricated from carbon steel for the internal backbone structure, stainless steel for the thin enclosure, and aluminum honeycomb (with a specific crush strength for each honeycomb block). Of the impact limiter steel members, the stainless steel enclosure experiences the most significant deformation during the drop events, and its material behavior is characterized in LS-DYNA using an appropriate true stress true strain curve in MAT_024 (*MAT_PIECEWISE_LINEAR_PLASTICITY). Based on the engineering stress strain data obtained from the original tests of the honeycomb material for the HI STAR 100 impact limiters, the material characteristics of the honeycomb material are simulated by MAT_026 (*MAT_HONEYCOMB) in the LS-DYNA model, with the stress strain data for the material input to capture initial elastic behavior, a region of constant crush resistance, and a region where the material experiences "lock up". The total weight of the modeled HI STAR 100 top and bottom impact limiters is 36,553 lb., which matches well with the tabulated data in Section 2.2. The impact limiter to cask connection is modeled as a rigid connection, which conservatively neglects any energy absorption by the actual connection elements.~~

~~The free drop tests are performed using the HI STAR 100 LS-DYNA finite element model of the full size cask. Each test is performed by orienting the model appropriate to the rigid target, and imposing an initial velocity of 527 inch/second to every node; this simulates the 30 foot drop at the instant of initial impact with the target. Consistent with the locations of the embedded accelerometers on the tested 1/4 scale HI STAR 100 model, cask drop acceleration time histories are obtained at three locations on the finite element model (top flange, mid height, and cask bottom) so that comparisons could be made with the test data. Table 2.I.7.1 shows a comparison of key results from the finite element simulation with results from the tests (after scaling the test data back to the full size cask). It is clear that the simulation model is in excellent agreement with the test results in terms of prediction of peak acceleration, maximum impact limiter crush, and duration of impact. To also demonstrate that the LS-DYNA simulation matches test data throughout the entire event duration, filtered acceleration data from the test [2.I.7.2] is compared with similar filtered acceleration data from the LS-DYNA simulation at the same location; the comparison of results for all drop tests demonstrates that the HI STAR 100 Package response is appropriately captured by the LS-DYNA simulations through the entire strong response duration of the event.~~

~~Based on the tabular results and comparison of acceleration data vs. time, the benchmarking of the HI-STAR 100 LS DYNA model is complete, and the simulation model can be used to evaluate the performance of the HI-STAR HB. The drop analysis of the HI-STAR HB Package using the differential equation method differs from the drop analysis for the HI-STAR 100 only to the extent that:~~

- ~~• the axial length of the cylindrical body is reduced;~~
- ~~• the nominal strength of the energy absorbing honeycomb material is reduced;~~
- ~~• the mass of the package is reduced.~~

~~model is now obtained by reducing the axial length of the cylindrical body and reducing the nominal strength of the energy absorbing honeycomb material elements (making up the cylindrical body) without changing the numbering of nodes or elements, until the appropriate HI-STAR HB dimension is achieved. The final weight of the loaded HI-STAR HB (without impact limiters) is 156,611 lb, which compares well with the tabulated bounding weight in Table 2.1.2.1. The final weight of the impact limiters for the HI-STAR HB is calculated by LS DYNA as 24,774 lb. The drawings for the HI-STAR HB impact limiter, with specified crush strengths, are found in Section 1.4. Figure 2.1.7.5 shows the HI-STAR HB finite element model oriented for the end drop. Sheet 1 of Holtec drawing C1765 (Rev. 4) provides the reduced nominal crush strengths used in the impact limiters for the HI-STAR HB.~~

~~The results from the four free drop simulations of the HI-STAR HB are documented in Table 2.1.7.12 using the nominal strengths of the honeycomb energy absorbing material. (Because of the reduced length of the HI-STAR HB Package, the CGOC and slapdown angles are 58.6331.1 degrees and 6 or 10 degrees from the target plane, respectively). For the slapdown, the maximum deceleration of (The secondary impact limiter maximum deceleration (after filtering to eliminate oscillations exceeding a frequency of 350 Hz) was slightly larger at a 10 degree initial angle than it was at 6 degrees; the maximum crush, however, was larger at 6 degrees as the initial orientation angle of the cask. Therefore, simulations using nominal crush strength are~~

reported for both orientations, although sensitivity studies were performed only for the 6 degree initial orientation. -The results show that the HI-STAR HB impact limiters effectively protect the HI-STAR HB cask under the ~~Hypothetical Conditions of Transport~~ postulated 30-foot drop events by maintaining the peak cask rigid body deceleration ~~at the top and base of the cask~~ below the ~~cask~~ design basis limit of 60 g's. Since the peak decelerations are below the values computed for the HI-STAR 100, it is assured that the pin/bolt connections between the HI-STAR HB impact limiters and the HI-STAR HB body maintain their structural integrity.

Consistent with the requirements for 1-foot free drops as part of the Normal Conditions of Transport, two free drops (end drop and side drop) are also analyzed for the HI-STAR HB Package using the nominal strengths (plus 15%) specified for the honeycomb energy absorbing material.- The maximum decelerations sustained by the Ppackage, as well as the maximum impact limiter crush and impact durations, are summarized in Table 2.I.7.23. -Finally, Table 2.7.I.3 presents the results of some additional parametric simulations that ~~serve to fixset~~ upper and lower limits on permitted variation of the strength properties for the honeycomb material. Note that the peak end drop deceleration slightly exceeds the design basis value specified for the HI-STAR 100 (17g's per Table 2.I.10), but this has no adverse structural consequence on the package components. The analyses leading to the reported results are documented in a supporting calculation package [2.I.7.2].

2.I.7.2 Puncture

No new or modified calculations need be performed to qualify the HI-STAR HB, as the structure at the puncture locations is unchanged from the HI-STAR 100.

2.I.7.3 Thermal

Thermal evaluation of the fire accident is presented in Supplement 3.I. No new or modified structural calculations need be performed to qualify the HI-STAR HB for the fire accident.

2.I.7.4 Immersion - Fissile Material

No new or modified calculations need be performed to qualify the HI-STAR HB.

2.1.7.5 Immersion - All Packages

No new or modified calculations need be performed to qualify the HI-STAR HB.

2.1.7.6 Summary of Damage

The results presented in Subsections 2.1.7.1 through 2.1.7.5 show that the HI-STAR HB System meets the requirements of 10CFR71.61 and 10CFR71.73. The results from simulation of the hypothetical drop conditions produce deceleration levels that are below the design basis levels for the HI-STAR 100 for crush strength variations of plus or minus 15% of the nominal values specified for the HI-STAR HB impact limiters. Therefore, All-safety factors for the HI-STAR HB are greater than 1.0 by virtue of comparison with the corresponding calculations for the HI-STAR 100 for the Hypothetical Accident Conditions of Transport. Therefore, the HI-STAR 100 HB package, under the Hypothetical Accident Conditions of Transport, has adequate structural integrity to satisfy the subcriticality, containment, shielding, and temperature requirements of 10CFR71.

2.1.8 SPECIAL FORM

This section is not applicable to the HI-STAR HB+00 System. This application does not seek approval for transport of special form radioactive material as defined in 10CFR71.4.

2.1.9 FUEL RODS

The Humboldt Bay fuel is shorter than the design basis fuel carried by the HI-STAR 100; therefore, the computations and conclusions in Section 2.9 encompass the HI-STAR HB. The presence of "Undamaged Fuel Assemblies", which are defined in Table 1.0.1 Supplement 1.1 (Sub-section 1.1.2.3.2) will have ~~minimal~~no significant effect on the structural response of the HI-STAR HB. This is because ~~t~~he only fuel parameters that have an influence on the structural analyses are the fuel mass and center of gravity height. Therefore, since an undamaged fuel assembly has essentially the same mass as an intact fuel assembly, and ~~Since~~the exterior fuel rods serve to confine the interior fuel rods (with cladding in unknown condition) preventing them from dislocating and falling to the bottom of the fuel basket, the presence of undamaged fuel assemblies has no significant effect on the total amount of stored fuel mass or the center of gravity height used as input in the drop analysis for the HI-STAR HB.~~there could be a slight~~

~~lowering of the location of the package mass center. Since the fuel weight is less than 17% of the total package weight, the 60g design basis limit should remain unchallenged during a hypothetical bottom down slapdown event.~~

2.1.10 MISCELLANEOUS ITEMS

No new appendices are introduced in Supplement 2.I. Also, since the HI-STAR 100 Package meets applicable NUREG 1617/10CFR71 requirements, so does the HI-STAR HB.

2.1.11 REFERENCES

- [2.1.6.1] Pacific Gas and Electric Company, NRC Docket Number 72-27, Humboldt Bay ISFSI, Final Safety Analysis Report Update, Revision 0, January 2006.
- [2.1.7.1] A Classical Dynamics Based and Experimentally Benchmarked Impact Response Computation Methodology for AI-STAR Equipped Casks, HI-2084137, Rev. 0. ~~LS-DYNA 970, Livermore Software Technology, 2003.~~
- [2.1.7.2] Calculation Package for HI-STAR HB Drop Analyses, HI-2084158, Rev. 0.
- [2.1.7.3] Miscellaneous Calculations for the HI-STAR HB, HI-2033042, Rev. 3.
- ~~[2.1.7.2] Impact Limiter Drop Test Report - 2nd Series, Holtec Rpt. HI-981891, Rev. 2.~~

Table 2.I.2.1 Weights and Center of Gravity of HI-STAR HB Package			
<i>Item</i>	<i>Component Weight (lb.)</i>	<i>Total Weight (lb.)</i>	<i>Location of C.G. above base of cask (inch)</i>
<i>Impact Limiter</i>	<i>13,000</i>	<i>26000</i>	<i>-</i>
<i>MPC HB</i>	<i>59,000*</i>	<i>-</i>	<i>-</i>
<i>HI-STAR HB (with loaded MPC HB)</i>	<i>161,200</i>	<i>-</i>	<i>-</i>
<i>Total Package Weight</i>	<i>-</i>	<i>187,200</i>	<i>-</i>
<i>Loaded Package Center of Gravity</i>	<i>-</i>	<i>-</i>	<i>61.4</i>

** Includes approximately 32,000 lb of fuel*

Table 2.I.7.1 –HI-STAR HB 30’ DROP RESULTS

CONFIGURATION	MAXIMUM DECELERATION (G'S)†	MAXIMUM CRUSH (INCH)	DURATION OF IMPACT (SEC.)	COMMENTS
30' TOP END DROP	56.5	13.1	0.0425	Avg. strength=694 psi
30' BOTTOM END DROP	45.6	13.8	0.047	Strength=390 psi
30' SIDE DROP	34.8	13.4	0.0485	-
30' CGOC	33.75	22	0.0665	Bottom down
30' SLAPDOWN - 6 DEGREES	45.06*	15.08	0.0705	Secondary impact limiter
30' SLAPDOWN - 10 DEGREES	45.88*	14.93	0.0964	Secondary impact limiter
30' SLAPDOWN - 6 DEGREES	33.52*	11.43	-	Primary impact limiter
30' SLAPDOWN - 10 DEGREES	30.57*	13.82	-	Primary impact limiter

*Reported result is subsequent to filtering to remove high frequency effects above 350 Hz.

Table 2.I.7.2 –HI-STAR HB 1’ DROP RESULTS

COMMENTS	MAXIMUM DECELERATION (G'S)†	MAXIMUM CRUSH (INCH)	DURATION OF IMPACT (SEC.)	COMMENTS
1' TOP END DROP	14	1.07	0.02454	Crush strength increased by 15%
1' SIDE DROP	10	1.55	0.0305	Crush strength increased by 15%

Table 2.I.7.3 –HI-STAR HB 30’ DROP RESULTS – SENSITIVITY ANALYSES

CONFIGURATION	MAXIMUM DECELERATION (G'S)	MAXIMUM CRUSH (INCH)	DURATION OF IMPACT (SEC.)	COMMENTS
30' TOP END DROP	59	12.4	0.040	15% increase in crush strength
30' BOTTOM END DROP	44.3	14.8	0.050	15% decrease in crush strength
30' SIDE DROP	38.5	12.2	0.0435	15% increase in crush strength
30' SIDE DROP	43*	15.2*	0.053	15% decrease in crush strength
30' CGOC	36.75	20.75	0.0608	15% increase in crush strength
30' CGOC	30.55	23.75	0.0728	15% decrease in crush strength
30' SLAPDOWN -6 DEGREES	49.17**	13.6	0.0718	Secondary IL – 15% increase in crush strength
30' SLAPDOWN -6 DEGREES	34.9**	10.43	-	Primary IL – 15% increase in crush strength
30' SLAPDOWN -6 DEGREES	38.82**	17.08	0.0842	Secondary IL – 15% decrease in crush strength
30' SLAPDOWN -6 DEGREES	30.28**	12.88	-	Primary IL – 15% decrease in crush strength

* 1050 psi material experiences minimal lockup so peak deceleration value rises but remains below the design basis limit.

** No filtering performed on deceleration time histories.

Table 2.I.7.1, Comparison of HI-STAR 100 Test Results and LS-DYNA Simulation Results							
Drop Case		Deceleration (g's) ^A		Crush Depth (in)		Impact Duration (ms)	
		Measured	Predicted	Measured	Predicted	Measured	Predicted
1. End Drop		53.9	55.35	10.6	10.34	37.2/ 40.7 ^B	44
2. C.G. Over Corner		38.8	37.13	9.82/ 15.25 ^C	18.91	-61	62.5
3. Side Drop		45.7	49.18	12.5	12.65	53.1	47.5
4. Slap Down	Primary	49.0	48.04	10.7	9.77 ^D	44.4	45
	Secondary	59.0	62.74	13.5	14.63 ^E	41.2	42

Notes:

A. Averaged deceleration (except the slap-down case) from tracked locations consistent with the tests.

B. The impact duration would be 40.7 milli-seconds if the entire duration of positive deceleration were considered.

C. For CGOC impact the axis of the dropped cask is 22.5° off the vertical direction. Approximately half of the 10" thick small protruding ring (at the end of the φ128" impact limiter) is deformed, which indicates that the minimum vertical crush depth can be estimated as $d_{min} = [64" \times \tan(22.5^\circ) - 10"] \times \cos(22.5^\circ) = 15.25"$. For the reported value of 9.82", only crush at the external interface was reported in the final test report.

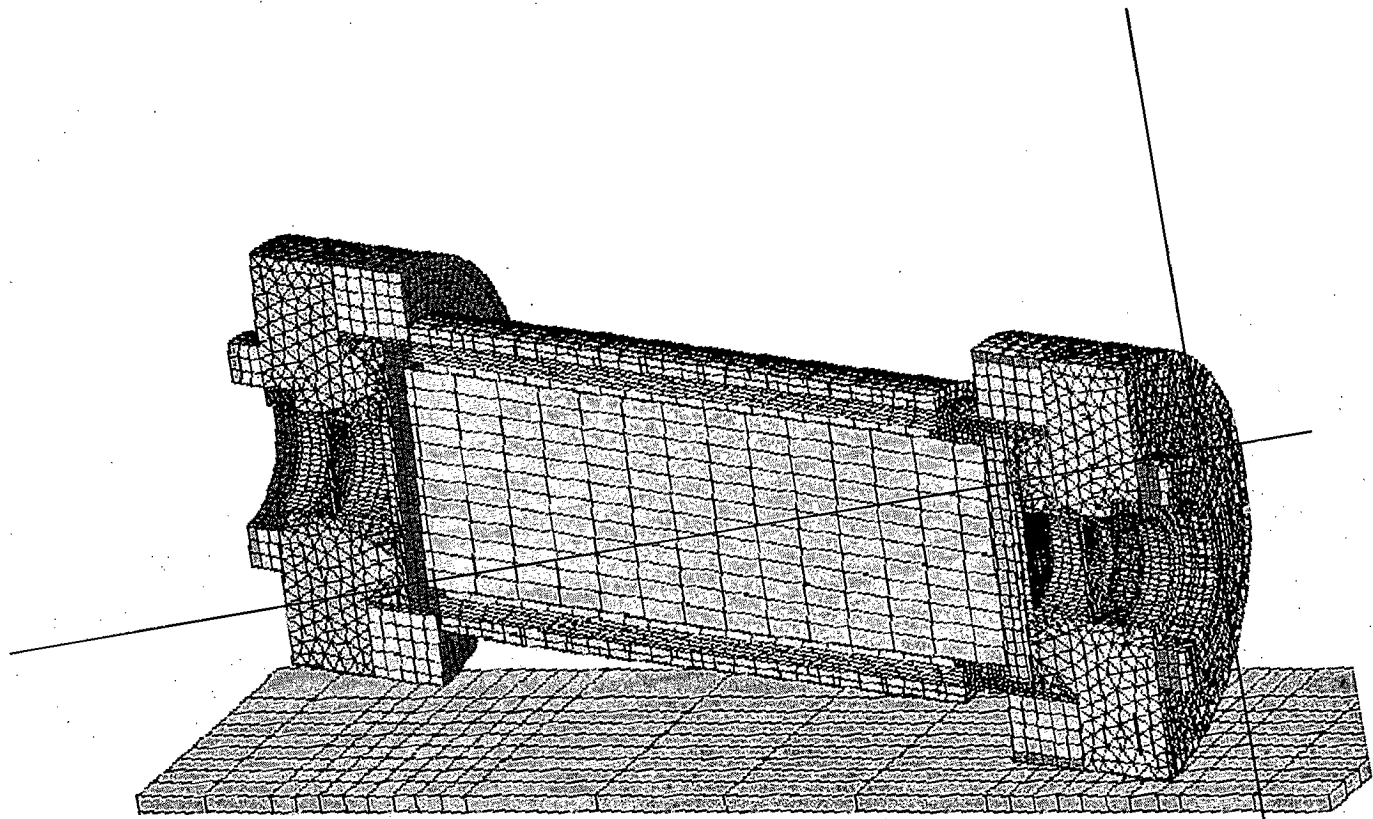
D. $9.77" = 64" - 83.25"/2$ (radius of HI-STAR top flange) $28.954"$ (initial vertical distance to ground) $+ 16.35"$ (cask top vertical displacement).

E. $14.63" = 64" - 83.25"/2$ (radius of HI-STAR bottom plate) $52.747"$ (initial vertical distance to ground) $+ 45.0"$ (cask bottom vertical displacement).

Table 2.I.7.2, LS-DYNA Analyses Results for HI-STAR HB Impact Limiters				
Drop Case		Deceleration (g ² s) ^A	Crush Depth (in)	Impact Duration (ms)
1. End Drop		45.95	11.18	52
2. C.G. Over Corner		31.16	23.83	80
3. Side Drop		45.13	13.32	54.5
4. Slap Down	Primary	36.26 (37.32 ^B)	11.72 ^C	93
	Secondary	47.48 (49.72 ^B)	14.37 ^D	54
Notes:				
A. Averaged deceleration (except the slap down case) from tracked locations.				
B. Deceleration results in the parenthesis are obtained for the additional case with upper bound honeycomb crush strengths (i.e., 10% greater than nominal values).				
C. $11.72'' = 64'' - 83.25''/2$ (radius of HI-STAR top flange) $- 27.903''$ (initial vertical distance to ground) $+ 17.27''$ (cask top vertical displacement).				
D. $14.37'' = 64'' - 83.25''/2$ (radius of HI-STAR bottom plate) $- 39.822''$ (initial vertical distance to ground) $+ 31.82''$ (cask bottom vertical displacement).				

Table 2.I.7.3, LS-DYNA Analysis Results of HI-STAR HB Package One-Foot Drop Events				
Drop Case		Deceleration (g ² s) ^A	Crush Depth (in)	Impact Duration (ms)
1. End Drop		17.96	0.90	41.7
2. Side Drop		10.31	1.95	57.5
Note:				
A. Averaged deceleration from tracked locations.				

2.I.12 ADDITIONAL FIGURES FOR SUPPLEMENT 2.I



Z
X
Y

Figure 2.I.7.1 LS DYNA Model of HI STAR 100 for Slapdown Simulation

Proposed Revision 13b

2.I-20

HI-STAR SAR
HI-951251

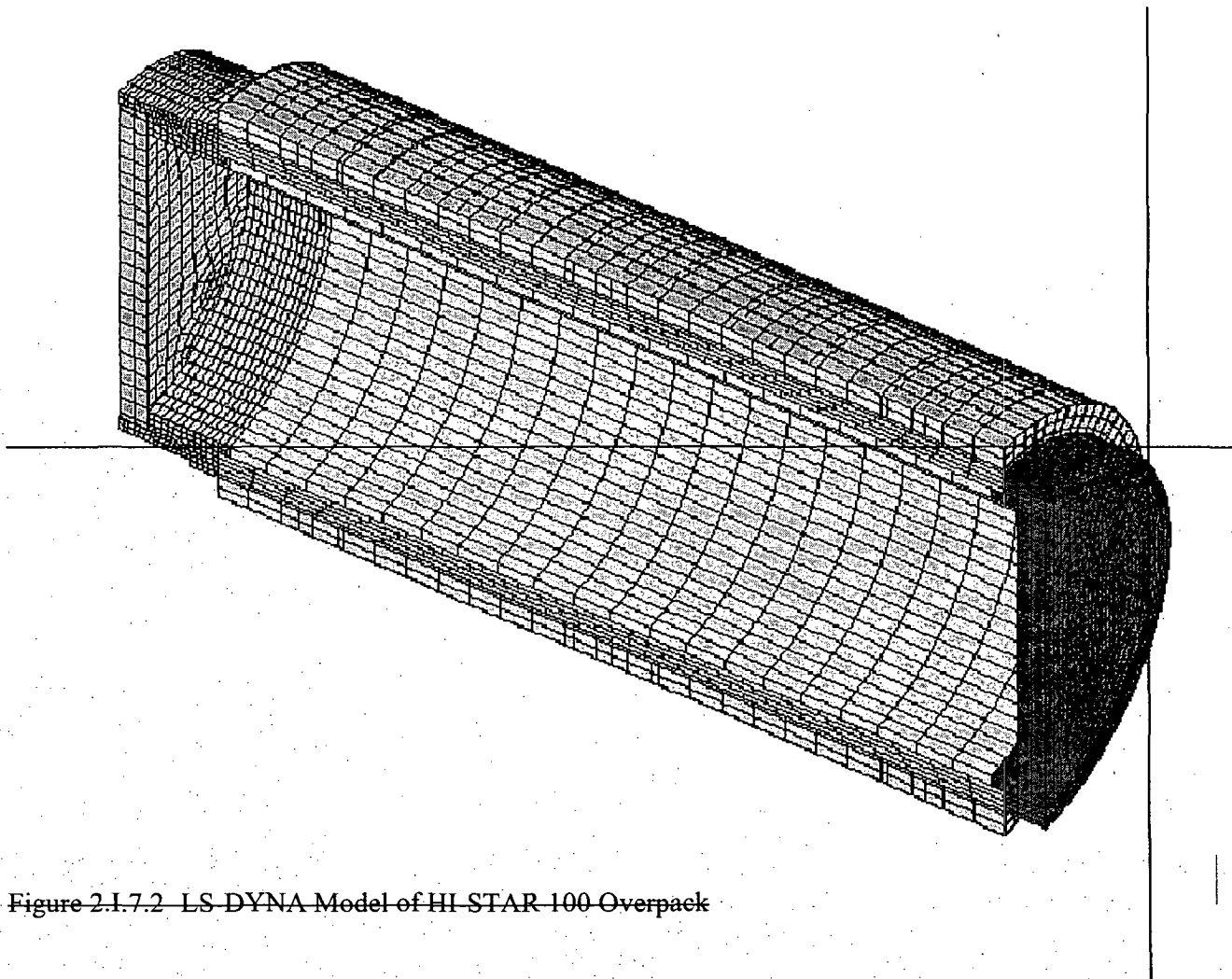


Figure 2.I.7.2 LS-DYNA Model of HI-STAR-100 Overpack

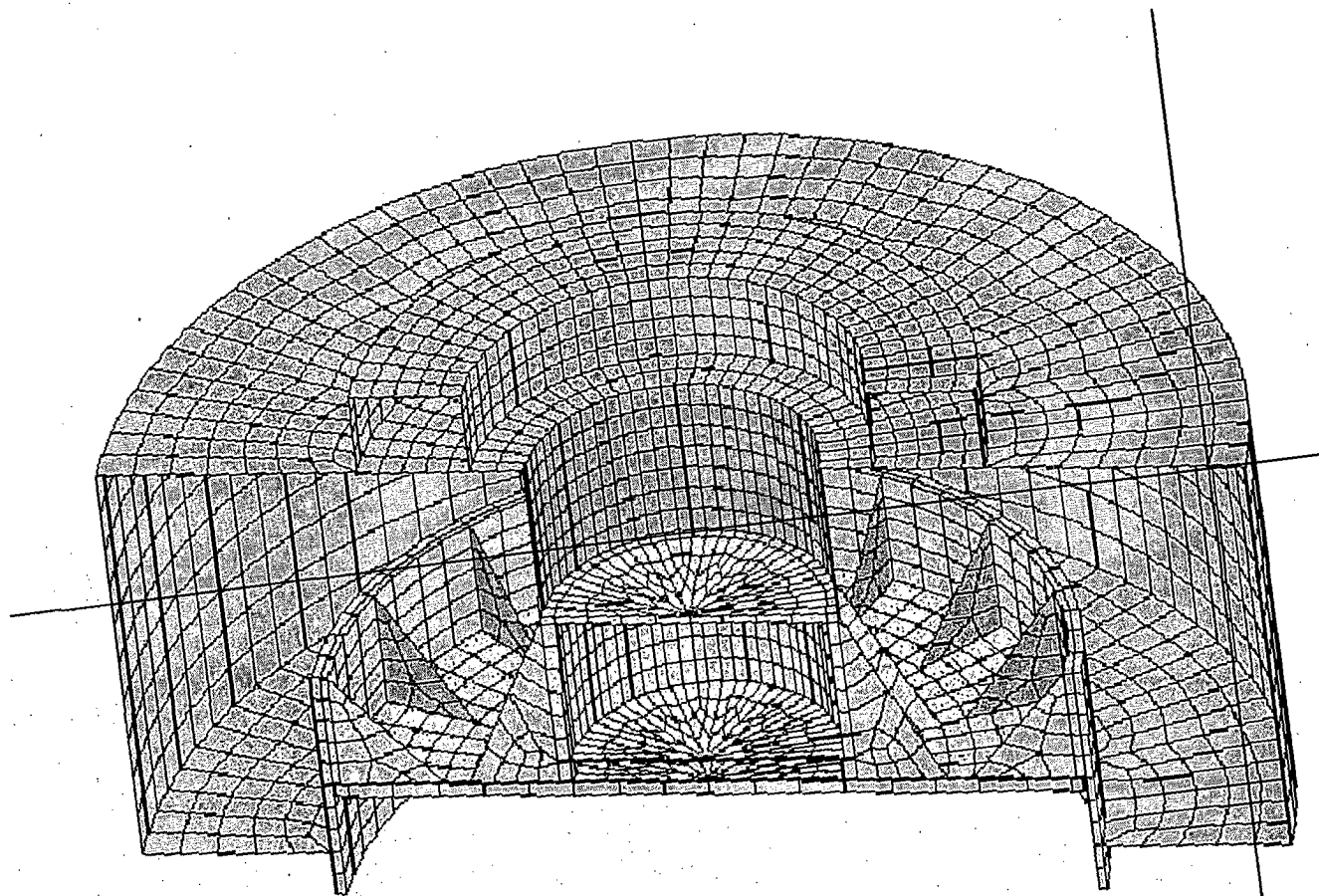
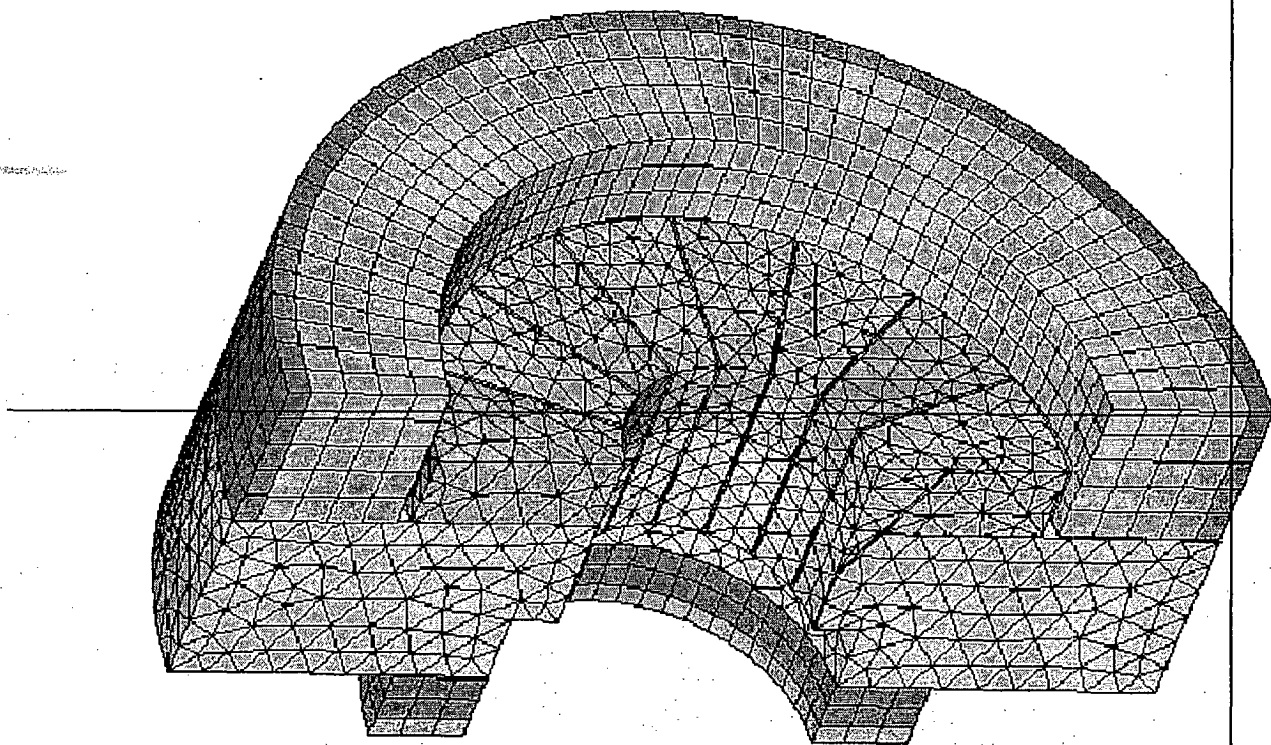


Figure 2.1.7.3 Top Impact Limiter Steel Structure



YZ
x

Figure 2.I.7.4 Top Impact Limiter Honeycomb Crush Material

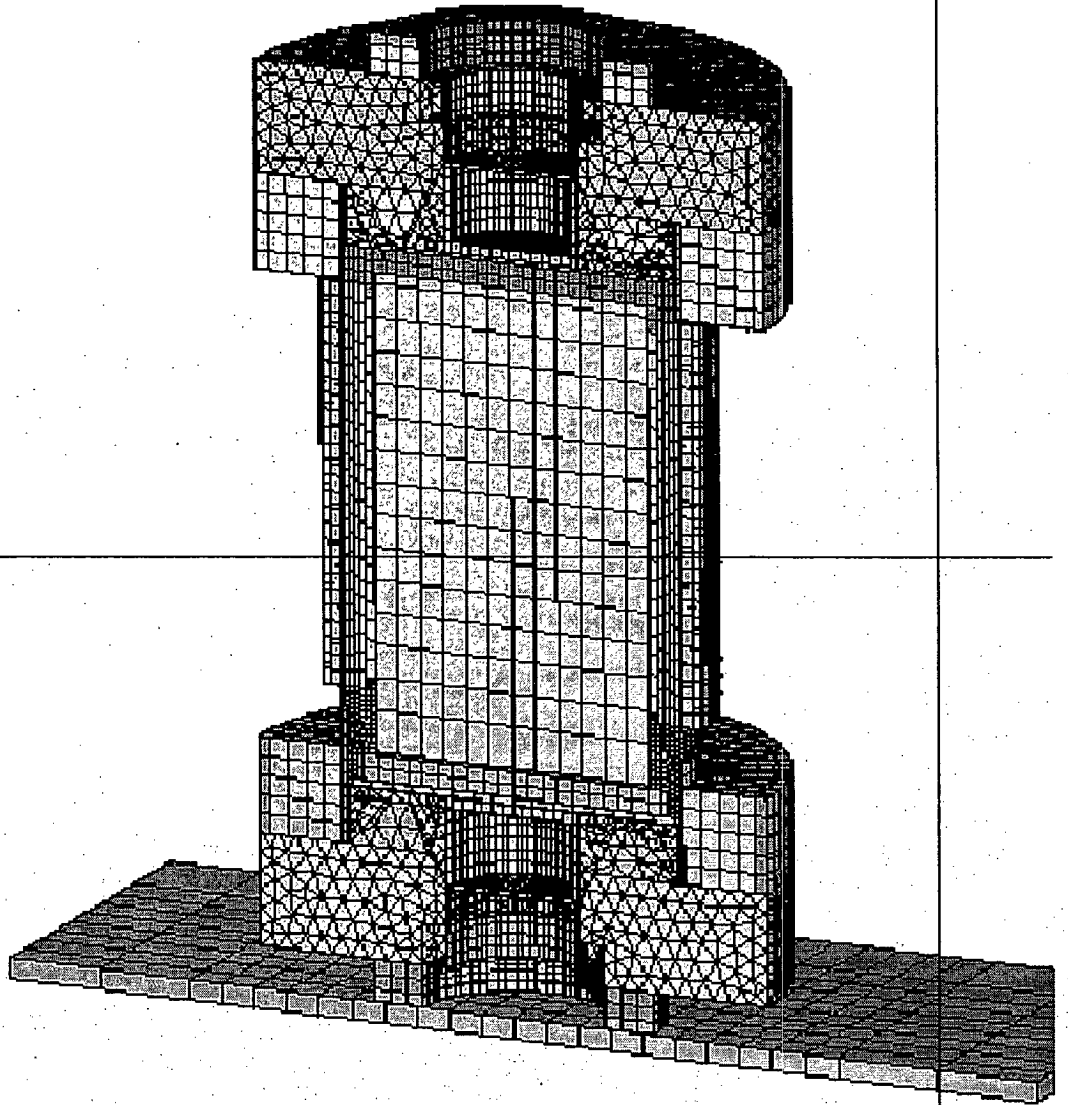


Figure 2.I.7.5 HI-STAR HB Finite Element Model in End Drop Orientation

3.1 DISCUSSION

Sectional views of the HI-STAR System have been presented earlier (see Figures 1.1.3 and 1.1.4). The system essentially consists of a loaded MPC situated inside an overpack equipped with a bolted closure. The fuel assemblies reside inside the MPC that has two redundant welded closures. The MPC contains a stainless steel honeycomb fuel basket that provides square-shaped fuel compartments of appropriate dimensions to facilitate insertion of fuel assemblies prior to welding of the MPC lid. Each fuel cell wall (except outer periphery MPC-32 and MPC-68 cell walls) is provided with ~~Boral~~ (thermal neutron absorber panels) (~~Boral or METAMIC~~) sandwiched between a stainless steel sheathing plate and the cell wall along the entire length of the active fuel region. Prior to sealing the MPC lid, the MPC is backfilled with helium to the levels specified in Table 1.2.3. This provides a stable and inert environment for the transport of the SNF. Additionally, the annular gap between the MPC and the overpack is backfilled with helium before the overpack vent and drain port plug plugs are installed. Heat is transferred from the SNF in the HI-STAR to the environment by passive heat transport mechanisms only.

The helium backfill gas is an integral part of the MPC and overpack thermal designs. The helium fills all the spaces between solid components and provides an improved conduction medium (compared to air) for dissipating decay heat in the MPC. Additionally, helium in the spaces between the fuel basket and the MPC shell is heated differentially and, therefore, subject to the "Rayleigh" effect which is discussed in detail later (Subsection 3.4.1.1.5). To ensure that the helium gas is retained and is not diluted by lower conductivity air, the MPC helium retention boundary is designed to comply with the provisions of the ASME B&PV Code Section III, Subsection NB, as an all-seal-welded pressure vessel with redundant closures. Similarly, the overpack containment boundary is designed as an ASME B&PV Code Section III, Subsection NB pressure vessel. Both the MPC helium retention boundary and the overpack containment boundary are required to meet maximum leakage rate requirements included in Section 7-4 8.1.4 of this SAR. These leakage rate criteria ensure the presence of helium during transport. The helium gas is therefore retained and undiluted, and may be credited in the thermal analyses.

An important thermal design criterion imposed on the HI-STAR System is to limit the maximum fuel cladding temperature during normal transport to below design basis limits (Table 1.2.3). An equally important design criterion is to reduce temperature gradients within the MPC to minimize thermal stresses. In order to meet these design objectives, the HI-STAR MPC basket is designed to possess certain distinctive characteristics, which are summarized in the following.

The MPC design minimizes resistance to heat transfer within the basket and basket periphery regions. This is ensured by a high structural integrity all-welded honeycomb structure. The MPC design incorporates top and bottom plenums with interconnected downcomer paths. The top plenum is formed between the MPC lid and the top of the honeycomb fuel basket with additional semicircular holes in the top of each fuel cell wall. The bottom plenum is formed by large elongated semicircular holes at the base of all cell walls. The MPC basket is designed to eliminate structural discontinuities (i.e., gaps) which introduce large thermal resistances to heat flow. Consequently, temperature gradients are minimized in this design, which results in lower thermal stresses within the basket. Low thermal stresses are also ensured by an MPC design that

permits unrestrained axial and radial growth of the basket to eliminate the possibility of thermally induced stresses due to restraint of free-end expansion.

The HI-STAR System is designed for transport of PWR and BWR spent fuel assemblies and features two distinct MPC fuel basket geometries. For intact PWR fuel a 24-assembly design (depicted in Figure 1.2.5) and a higher capacity canister (MPC-32) are available. A 68-assembly design for the transport of intact or specified damaged BWR fuel is shown in Figure 1.2.3. Damaged BWR fuel must be placed in a damaged fuel container for transport in the MPC-68. Extensively damaged BWR fuel assemblies (e.g. severed rods) classified as fuel debris shall be transported in the MPC-68F. The MPC-68F is identical to the MPC-68, except for the ^{10}B loading of the ~~Borax~~ *neutron absorber* panels for criticality control. Each basket design must comply with the required temperature limits under the imposed heat generation loads from the fuel assembly contents. For normal transport conditions, the maximum decay heat loads for the PWR and BWR MPCs are summarized in Table 1.2.3. The complete HI-STAR System consisting of the overpack and MPC under transport conditions is conservatively analyzed for the imposed design heat loads.

Thermal analysis of the HI-STAR System is based on including all three fundamental modes of heat transfer: conduction, natural convection and thermal radiation. Different combinations of these modes are active in different parts of the system. These modes are properly identified and conservatively analyzed within each region of the MPC and overpack, to enable bounding calculations of the temperature distribution within the HI-STAR System for both PWR and BWR MPC basket designs.

On the outside surface of the overpack, heat is dissipated to the environment by buoyancy induced convective air flow (natural convection) and thermal radiation. In the overpack internal metal structure, only conductive heat transport is possible. Between metal surfaces (e.g., between neighboring fuel rod surfaces) heat transport is due to a combination of conduction through a gaseous medium (helium) and thermal radiation. Finally, buoyancy-induced convective heat transport occurs within the open spaces of the MPC, aided by the MPC design which provides low pressure drop helium flow recirculation loops formed by the fuel cells, top plenum, downcomers, and bottom plenum. However, in the interest of conservatism, no credit for buoyancy-induced heat transport in the HI-STAR MPC basket is taken to satisfy either temperature or stress intensity limits. Heat transfer between the fuel basket external surface and MPC enclosure shell inside wall is further influenced by the so-called "Rayleigh" effect in differentially heated vertical cavities and "Rayleigh-Benard" effect in horizontal channels heated from below. A discussion on these effects is provided in Subsection 3.4.1.1.5.

The total heat generation in each assembly is non-uniformly distributed over the active fuel to account for design basis-fuel burnup distribution listed in Chapter 1 (Table 1.2.15 and Figures 1.2.13 and 1.2.14). As discussed later in this chapter (Subsection 3.4.6), an array of conservative assumptions bias the results of the thermal analysis towards much reduced computed margins than would be obtained by a rigorous analysis of the problem.

The complete thermal analysis is performed using the industry standard ANSYS finite element modeling package [3.1.1] and the finite volume Computational Fluid Dynamics (CFD) code FLUENT [3.1.2]. ANSYS has been previously used and accepted by the NRC on numerous dockets. The FLUENT CFD program is independently benchmarked and validated with a wide class of theoretical and experimental studies reported in the technical journals. Additionally, Holtec has confirmed the code's capability to reliably predict temperature fields in dry storage applications using independent full-scale test data from a loaded cask [3.1.3]. This study concluded that FLUENT can be used to model all modes of heat transfer, namely, conduction, convection, and radiation in dry cask systems.

3.2 SUMMARY OF THERMAL PROPERTIES OF MATERIALS

Materials present in the HI-STAR System include stainless steels, carbon steels, aluminum, neutron shield (*Holtite-A*), ~~Boral~~ neutron absorber and helium. In Table 3.2.1, a summary of references used to obtain cask material properties for performing all thermal analyses is presented.

Tables 3.2.2, 3.2.3 and 3.2.9 provide numerical thermal conductivity data for all materials at several representative temperatures. *The neutron absorber materials (~~BoralTM and MetamicTM~~) are both made of aluminum powder and boron carbide powder. Although their manufacturing processes differ, from a thermal standpoint, their ability to conduct heat is virtually identical. Therefore, the values of conductivity of the original neutron absorber (~~Boral~~) continue to be used in the thermal calculations. Table 3.2.8 lists the thermal properties of Boral are provided in Table 3.2.8. components (i.e., ~~B₄C core and aluminum cladding materials~~).*

Surface emissivity data for key materials of construction are provided in Table 3.2.4. The emissivity properties of painted surfaces are generally excellent. Kern [3.2.5] reports an emissivity range of 0.8 to 0.98 for a wide variety of paints. In the HI-STAR thermal analysis, an emissivity of 0.85[†] is applied to exterior painted surfaces. A conservative solar absorptivity coefficient of 1.0 is applied to all exposed cask surfaces.

In Table 3.2.5, the heat capacity and density data of different cask materials is presented. These properties are used in performing transient (hypothetical fire accident condition, for example) analyses. MPC Rayleigh effect calculations use helium density, heat capacity, and gas viscosity properties data, which are listed in Tables 3.2.5 and 3.2.6.

The HI-STAR System's outside surface heat transfer coefficient is calculated by accounting for both natural convection heat transfer and radiation. The natural convection coefficient of a heated horizontal cylinder depends upon the product of the Grashof (Gr) and Prandtl (Pr) numbers. Following the approach developed by Jakob and Hawkins [3.2.9], GrPr is expressed as $L^3 \Delta T Z$, where L is the diameter of the cask, ΔT is the HI-STAR System overpack surface-to-ambient temperature differential and Z is a parameter which depends upon air properties, which are known functions of temperature, evaluated at the average film temperature. The temperature dependence of Z for air is provided in Table 3.2.7.

The long-term thermal stability and radiation resistance of Holtite-A has been confirmed through qualification testing. The qualification test conditions exceed the Holtite-A thermal and radiation environment (gamma and neutron fluence) in the HI-STAR 100 cask. The Holtite-A thermal stability test temperature, 325°F, is well above the maximum operating temperature of Holtite-A (See Tables 3.4.10 and 3.4.11). The Holtite-A radiation test exposures exceed 50-year HI-STAR service neutron

[†] This is conservative with respect to prior cask industry practice, which has historically accepted higher emissivities. For example, the emissivity for painted surfaces ($\epsilon=0.95$) is used in the TN-32 cask TSAR (Docket 72-1021).

dose by a factor of 3.75 and gamma dose by a factor of 5.54 (See Table 3.2.10). The Holtite-A qualification test data is archived in the following reports:

- i) "Holtite A: Development history and thermal performance data", Holtec Report HI-2002396, Rev. 3.
- ii) "Holtite-A: Results of Pre-and-Post-Irradiation Tests and Measurements", Holtec Report HI-2002420, Rev. 1.

The testing referenced above confirms that Holtite-A does not degrade at elevated temperatures and Holtite-A is unaffected by high neutron fluence and megarad gamma doses. Even under very conservative assumptions (20-years of storage under the maximum temperature reached at the beginning of dry storage) only a 2% weight loss is computed (licensing basis commitment is 4%). Nevertheless, ~~Because of the excellent stability characteristics of Holtite A, the thermal properties remain essentially unchanged during the service life of the HI STAR overpack (40 years). P~~periodic thermal testing of HI-STAR 100 is ~~not~~ required.

Table 3.2.1

SUMMARY OF HI-STAR SYSTEM MATERIALS
THERMAL PROPERTY REFERENCES

Material	Emissivity	Conductivity	Density	Heat Capacity
Helium	NA	Handbook [3.2.2]	Ideal Gas Law	Handbook [3.2.2]
Air	NA	Handbook [3.2.2]	Ideal Gas Law	Handbook [3.2.2]
Zircaloy Cladding	EPRI [3.2.3]	NUREG [3.2.6], [3.2.7]	Rust [3.2.4]	Rust [3.2.4]
UO ₂	Not Used	NUREG [3.2.6], [3.2.7]	Rust [3.2.4]	Rust [3.2.4]
Stainless Steel (machined forgings)*	Kern [3.2.5]	ASME [3.2.8]	Marks [3.2.1]	Marks [3.2.1]
Stainless Steel Plates†	ORNL [3.2.12], [3.2.13]	ASME [3.2.8]	Marks [3.2.1]	Marks [3.2.1]
Carbon Steel	Kern [3.2.5]	ASME [3.2.8]	Marks [3.2.1]	Marks [3.2.1]
Aluminum Alloy 5052 (Impact Limiters)	Not Used	ASME [3.2.8]	ASME [3.2.8]	ASME [3.2.8]
Aluminum Alloy 1100 (Heat Conduction Elements)‡	Handbook [3.2.2]	ASME [3.2.8]	ASME [3.2.8]	ASME [3.2.8]
Boral†	Not Used Marks [3.2.1]	Test Data	Test Data	Test Data
Holtite-A**	Not Used	Test Data [3.2.14]	Test Data [3.2.14]	Test Data [3.2.13]
METAMIC§	Not Used	Test Data [3.2.10], [3.2.11]	Test Data [3.2.10], [3.2.11]	Test Data [3.2.10], [3.2.11]

* Used in the MPC lid.

† Used in the basket panels & sheathing, MPC shell & baseplate.

‡ Heat conduction elements used in certain early vintage MPCs

† AAR Structures' Boral thermophysical test data.

** From Holtite A test data (Appendix I.B).

§ Table lists all sources consulted for material properties.

Table 3.2.2

SUMMARY OF HI-STAR SYSTEM MATERIALS
THERMAL CONDUCTIVITY DATA

Material	@ 200°F (Btu/ft-hr-°F)	@ 450°F (Btu/ft-hr-°F)	@ 700°F (Btu/ft-hr-°F)
Helium	0.0976	0.1289	0.1575
Air	0.0173	0.0225	0.0272
Alloy X	8.4	9.8	11.0
Carbon Steel Radial Connectors	29.2	27.1	24.6
Carbon Steel Gamma Shield Layers	24.4	23.9	22.4
Impact Limiter Aluminum Alloy 5052	84.4	90.9	97.4
Holtite-A [†]	<i>See Footnote</i>		
Cryogenic Steel	23.8	23.7	22.3

[†] No credit taken for conduction through radial Holtite for the steady-state analysis, and before and after fire conditions for fire accident analysis. A conservative upper bound conductivity (1.0 Btu/ft-hr-°F) is applied during the fire condition to the radial neutron shield (between intermediate shells and overpack enclosure shell).

Table 3.2.3

SUMMARY OF FUEL ELEMENT COMPONENTS
THERMAL CONDUCTIVITY DATA

Fuel Cladding		Fuel (UO ₂)	
Temperature (°F)	Conductivity (Btu/ft-hr-°F)	Temperature (°F)	Conductivity (Btu/ft-hr-°F)
392	8.28 [†]	100	3.48
572	8.76	448	3.48
752	9.60	570	3.24
932	10.44	793	2.28 [†]

[†] Lowest value of conductivity is used in the thermal analysis for conservatism.

Table 3.2.4

SUMMARY OF MATERIALS SURFACE EMISSIVITY DATA

Material	Emissivity
Fuel cladding	0.80
Painted exterior surface	0.85
Rolled carbon steel	0.66
Stainless steel (<i>machined forgings</i>)	0.36
<i>Stainless Steel Plates</i>	0.587*
Sandblasted aluminum†	0.40

Note: The emissivities of package interior surfaces are understated to maximize normal operating temperatures of the package payload. As justified next, the lowerbound emissivities are used under hypothetical fire accident evaluations. The temperature elevation from the initial conditions, T_{fire} , of the HI-STAR package SNF under a hypothetical fire accident is principally a function of heat absorbed by the package during fire (Q_{fire}) and the thermal inertia (C) of the package. As Q_{fire} is unaffected by the emissivity of package internals (stainless steel basket panels and MPC pressure boundaries) and C is independent of emissivity, T_{fire} is unaffected by emissivity.

* Lowerbound value of stainless steel plates from cited references in Table 3.2.1. For conservatism, an even lower emissivity ($\epsilon = 0.36$) was used in the thermal calculations.

† Reported data covers the use of aluminum heat conduction elements in certain early vintage MPCs

Table 3.2.5

MATERIALS DENSITY AND HEAT CAPACITY PROPERTIES SUMMARY

Materials	Density (lbm/ft³)	Heat Capacity (Btu/lbm-°F)
Helium	(Ideal Gas Law)	1.24
Zircaloy Cladding	409	0.0728
Fuel (UO ₂)	684	0.056
Carbon Steel	489	0.1
Stainless Steel	501	0.12
Boral	154.7	0.13
Impact Limiter Alloy 5052	167.6	0.23
Aluminum Alloy 1100	169.3	0.23
Holtite-A [†]	105.0	0.39

† Conservatively postulated to underestimate thermal inertia for fire accident analysis.

Table 3.2.6

HELIUM GAS VISCOSITY[†] VARIATION WITH TEMPERATURE

Temperature (°F)	Viscosity (Micropoise)
167.4	220.5
200.3	228.2
297.4	250.6
346.9	261.8
463.0	288.7
537.8	299.8
737.6	338.8

[†] Obtained from Rohsenow and Hartnett [3.2.2].

Table 3.2.7

VARIATION OF NATURAL CONVECTION PROPERTIES
PARAMETER "Z" FOR AIR WITH TEMPERATURE

Temperature (°F)	Z (ft ⁻³ °F ⁻¹) [†]
40	2.1×10 ⁶
140	9.0×10 ⁵
240	4.6×10 ⁵
340	2.6×10 ⁵
440	1.5×10 ⁵

[†] Obtained from Jakob and Hawkins [3.2.9].

Table 3.2.8

BORAL COMPONENT MATERIALS[†]
THERMAL CONDUCTIVITY DATA

Temperature (°F)	B ₄ C Core Conductivity (Btu/ft-hr-°F)	Aluminum Cladding Conductivity (Btu/ft-hr-°F)
212	48.09	100.00
392	48.03	104.51
572	47.28	108.04
752	46.35	109.43

[†] Both B₄C and aluminum cladding conductivity values are obtained from AAR Structures Boral thermophysical test data.

Table 3.2.9

HEAT CONDUCTION ELEMENTS (ALUMINUM ALLOY 1100)
THERMAL CONDUCTIVITY DATA

Temperature (°F)	Conductivity (Btu/ft×hr×°F)
100	131.8
200	128.5
300	126.2
400	124.5

Table 3.2.10

*Holtite-A Radiation Exposure**

	<i>Under 50-Year Service Life</i>	<i>Test Exposure</i>
<i>Neutron Fluence (n/cm²)</i>	4×10^{14}	1.28×10^{15}
<i>Gamma Dose (rad)</i>	3.55×10^5	1.7×10^6
<i>Note: As tabulated above the Holtite-A qualification test exposures exceed 50-year service exposures by significant margins.</i>		

** Holtite-A: Results of Pre-and-Post-Irradiation Tests and Measurements", Holtec Report HI-2002420, Rev. 1.*

3.3 TECHNICAL SPECIFICATIONS FOR COMPONENTS

HI-STAR System materials and components which are required to be maintained within their safe operating temperature ranges to ensure their intended function are summarized in Table 3.3.1. Long-term stability and continued neutron shielding ability of the Holtite-A neutron shield material under normal transport conditions are ensured when material exposure temperatures are maintained below the maximum allowable limit. The overpack metallic seals will continue to ensure ~~leak tightness~~ sealing of the closure plate, and drain and vent ports if the manufacturer's recommended design temperature limits are not exceeded. Integrity of SNF during transport requires demonstration of HI-STAR System thermal performance to maintain fuel cladding temperatures to remain below regulatory design-basis limits. ~~Boral Neutron absorber materials used in MPC baskets for criticality control (a composite material composed of B₄C and aluminum) are~~ is stable in excess of up to 1000°F. ~~for short term and 850°F for long term dry storage~~ For conservatism temperature limits below the threshold of material integrity[†] are adopted (See Table 3.3.1). ~~However, for conservatism, a lower maximum temperature limit is imposed.~~

Compliance to 10CFR71 requires evaluation of hypothetical accident conditions. The inherent mechanical stability characteristics of the HI-STAR System materials and components ensure that no significant functional degradation is possible due to exposure to short-term temperature excursions outside the normal long-term temperature limits. For evaluation of the HI-STAR System's thermal performance under hypothetical accident conditions, material temperature limits for short-duration events are also provided in Table 3.3.1. In this Table, the cladding temperature limits of ISG-11, Rev. 32 [3.1.5] are adopted for Commercial Spent Fuel (CSF). These limits are applicable to all fuel types, burnup levels and cladding materials approved by the NRC for power generation. ~~Subsections 3.3.1 through 3.3.3 and their associated tables and figures are no longer needed and are deleted.~~

3.3.1 Evaluation of Moderate Burnup Fuel

It is recognized that hydrides present in irradiated fuel rods (predominantly circumferentially oriented) dissolve at cladding temperatures above 400 °C [3.3.8]. Upon cooling below a threshold temperature (T_p), the hydrides precipitate and reorient to an undesirable (radial) direction if cladding stresses at the hydride precipitation temperature T_p are excessive. For moderate burnup fuel, T_p is conservatively estimated as 350 °C [3.3.8].

Moderate Burnup Fuel (MBF) temperature limits for short term operations have been addressed in the PNNL report "Estimated Maximum Cladding Stresses for Bounding PWR Fuel Rods During Short Term Operations for Dry Cask Storage" published in Jan. 2004 [3.3.8]. In this report the potential for hydride re-orientation was evaluated in a simulated drying event in

[†] ~~AAR Structures Boral thermophysical test data.~~ Neutron absorber materials are manufactured using B₄C and aluminum. B₄C is a refractory material that is unaffected by high temperatures and aluminum is solid at temperatures in excess of 1000 °F.

which fuel was heated to the cladding temperature limit (570°C (1058°F)) and then cooled below the hydride precipitation temperature T_p . The study concluded that hydride re-orientation is not a concern in moderate burnup fuel because the coincident cladding stress at the hydride precipitation temperature is below the critical cladding stress. Accordingly, the 570°C (1058°F) temperature limit is justified for moderate burnup fuel and is adopted in the HI-STAR SAR for short-term operations with MBF fueled MPCs.

Table 3.3.1

HI-STAR SYSTEM MATERIAL TEMPERATURE LIMITS

Material	Normal Condition Temperature Limits	Short Term and Accident Condition Temperature Limits
CSF Cladding	752°F	1058°F
Neutron Absorber Boral [†]	800°F	950/1000°F
Overpack Closure Plate Mechanical Seals	See Table 4.1.1	See Table 4.1.1
Overpack Vent and Drain Port Plug Seals	See Table 4.1.1	See Table 4.1.1
Aluminum Alloy 5052	176°F ^{††}	1105°F ^{†††}
Holtite-A	300°F ^{††††}	N/A ^{†††††}
Aluminum Heat Conduction Elements (Alloy 1100) ¹	725°F	950°F

[†] Based on AAR Structures Boral thermophysical test data.

^{††} AL-STAR impact limiter aluminum honeycomb test data.

^{†††} Melting range of alloy is 1105°F-1200°F [3.3.1].

^{††††} Neutron shield manufacturer's test data (Appendix 1.B).

^{†††††} For shielding analysis (Chapter 5), Holtite-A is conservatively assumed to be lost during the fire accident.

¹ Temperature limits provided to cover the use of aluminum heat conduction elements in certain early vintage MPCs.

Tables 3.3.2 through 3.3.8

[INTENTIONALLY DELETED]

3.4 THERMAL EVALUATION FOR NORMAL CONDITIONS OF TRANSPORT

3.4.1 Thermal Model

The HI-STAR MPC basket designs consist of four distinct geometries engineered to hold 24 and 32 PWR (MPC-24, MPC-24E and MPC-32) or 68 BWR (MPC-68) fuel assemblies. The fuel basket forms a honeycomb matrix of square-shaped fuel compartments to retain the fuel assemblies during transport (refer to Figures 1.2.3 and 1.2.5 for an illustration of PWR and BWR baskets). The basket is formed by an interlocking honeycomb structure of steel plates and full-length edge welding of the cell corners to form an integral basket configuration. Individual cell walls (except outer periphery MPC-68 and MPC-32 cell walls) are provided with ~~Boral~~ or ~~METAMIC~~ neutron absorber panels, which consists of a ~~Boral~~ plate sandwiched between the cell wall and a stainless steel sheathing plate, for the full length of the active fuel region.

The design basis decay heat generation per PWR or BWR assembly for normal transport for each MPC type is specified in Table 1.2.13. The decay heat is considered to be non-uniformly distributed over the active fuel length based on the design basis axial burnup distribution specified in Chapter 1 (see Table 1.2.15 and Figures 1.2.13 and 1.2.14).

Transport of heat from the MPC basket interior to the basket periphery is accomplished by conduction through the MPC basket metal grid structure and the narrow helium gaps between the fuel assemblies and fuel cell walls. Heat dissipation in the MPC basket periphery-to-MPC shell gap is by a combination of helium conduction, natural convection (by means of the "Rayleigh" effect) and radiation across the gap. Between the MPC shell and the overpack inner shell is a small clearance, which is evacuated and backfilled with helium. Helium, besides being inert, is a better conductor of heat than air. Thus, heat conduction through the helium gap between the MPC and the overpack will minimize temperature differentials across this region.

The overpack, under normal transport conditions, passively rejects heat to the environment. Cooling of the exterior system surfaces is by natural convection and radiation. During transport, the HI-STAR System is placed in a horizontal position with stainless steel encased aluminum honeycomb impact limiters installed at both ends of the overpack. To conservatively maximize the calculated internal temperatures, the thermal conductivity of the impact limiters is set essentially equal to zero. Under normal transport conditions, the MPC shell rests on the overpack internal cavity surface forming an eccentric gap. Direct contact between the MPC and overpack surfaces is expected to minimize heat transfer resistance in this region of intimate contact. Significantly improved conductive heat transport due to reduction in the helium gap near the contact region is accounted for in the thermal analysis of the HI-STAR System. The HI-STAR System is conservatively analyzed assuming a minimum 0.02-inch gap at the line of metal-to-metal contact. Analytical modeling details of the various thermal transport mechanisms are provided in the following.

3.4.1.1 Analytical Model - General Remarks

Transport of heat from the heat generation region (fuel assemblies) to the outside environment is analyzed broadly in terms of three interdependent thermal models.

- i. The first model considers transport of heat from the fuel assembly to the basket cell walls. This model recognizes the combined effects of conduction (through helium) and radiation, and is essentially a finite element technology-based update of the classical Wooton & Epstein [3.4.1] formulation (which considers radiative heat exchange between fuel rod surfaces).
- ii. The second model considers heat transport within an MPC cross section by conduction and radiation. The effective cross sectional thermal conductivity of the basket region obtained from the combined fuel assembly/basket heat conduction radiation model is applied to an axisymmetric thermal model of the HI-STAR System on the FLUENT [3.1.2] code.
- iii. The third model deals with the transmission of heat from the MPC exterior surface to the external environment (heat sink). From the MPC shell to the cask exterior surface, heat is conducted through an array of concentric shells representing the MPC-to-overpack helium gap, the overpack inner shell, the intermediate shells, the Holtite-A neutron shielding and finally the overpack outer shell. Heat rejection from the outside cask surfaces to ambient air is considered by accounting for natural convection and thermal radiation heat transfer mechanisms from the exposed cask surfaces. Insolation on exposed cask surfaces is based on 12-hour levels prescribed in 10CFR71, averaged over a 24-hour period.

The following subsections contain a systematic description of the mathematical models devised to articulate the temperature field in the HI-STAR System. Table 3.4.2 shows the relationship between the mathematical models and the corresponding regions (i.e., fuel, MPC, overpack, etc.) of the HI-STAR System. The description begins with the method to characterize the heat transfer behavior of the prismatic (square) opening referred to as the "fuel space" containing a heat emitting fuel assembly. The methodology utilizes a finite-volume procedure to replace the heterogeneous SNF/fuel space region with an equivalent solid body having a well-defined temperature-dependent conductivity. In the following subsection, the method to replace the composite walls of the fuel basket cells with equivalent "solid" walls is presented. Having created the mathematical equivalents for the SNF/fuel spaces and the fuel basket walls, the method to represent the MPC cylinder containing the fuel basket by an equivalent cylinder whose thermal conductivity is a function of the spatial location and coincident temperature is presented.

Following the approach of presenting descriptions starting from the inside and moving to the outer region of a cask, the next subsections present the mathematical model to simulate the overpack. Subsection 3.4.1.1.12 concludes the presentation with a description of how the different models for the specific regions within the HI-STAR System are assembled into the final finite element model.

3.4.1.1.1 Overview of the Thermal Model

Thermal analysis of the HI-STAR System is performed by assuming that the system is subject to its maximum heat duty with each storage location occupied and with the heat generation rate in each stored fuel assembly equal to the design basis maximum value. While the assumption of equal heat generation imputes a certain symmetry to the cask thermal problem, the thermal model must incorporate three attributes of the physical problem to perform a rigorous analysis:

- i. While the rate of heat conduction through metals is a relatively weak function of temperature, radiation heat exchange is a nonlinear function of surface temperatures.
- ii. Heat generation in the MPC is axially non-uniform due to a non-uniform axial burnup profile in the fuel assemblies.
- iii. Inasmuch as the transfer of heat occurs from the inside of the basket region to the outside, the temperature field in the MPC is spatially distributed with the maximum values reached in the central region.

It is clearly impractical to explicitly model every fuel rod in every stored fuel assembly explicitly. Instead, the cross section bounded by the inside of the storage cell, which surrounds the assemblage of fuel rods and the interstitial helium gas, is replaced with an "equivalent" square (solid) section characterized by an effective thermal conductivity. Figure 3.4.1 pictorially illustrates the homogenization concept. Further details on this process for determining the effective conductivity is presented in Subsection 3.4.1.1.2. It suffices to state here that the effective conductivity of the cell space will be a function of temperature, because radiation heat transfer (a major component of the heat transport mechanism between the fuel rods to the basket metal square) is a strong function of the absolute temperatures of the participating bodies. Therefore, in effect, every storage cell location will have a different value of effective conductivity in the homogenized model. The process of determining the temperature-dependent effective conductivity is carried out using a finite volume procedure.

In the next step of homogenization, a planar section of MPC is considered. With each storage cell inside space replaced with an equivalent solid square, the MPC cross section consists of a metallic gridwork (basket cell walls with each cell space containing a solid fuel square with an effective thermal conductivity) circumscribed by a circular ring (MPC shell). There are four principal materials in this section that are included in all MPCs, namely the homogenized fuel cell squares, the Alloy X MPC structural materials in the MPC (including ~~Boral~~ sheathing material), *neutron absorber* (~~Boral or METAMIC~~) and helium gas. Aluminum heat conduction elements (AHCEs), included optionally in the MPC design, are appropriately ignored in the heat dissipation calculations. Each of the four constituent materials in this section has a different conductivity. As discussed earlier, the conductivity of the homogenized fuel cell is a strong function of temperature.

In order to replace this thermally heterogeneous MPC section with an equivalent conduction-only lamina, resort to the finite-element procedure is necessary. Because the rate of transport of heat within the MPC is influenced by radiation, which is a temperature-dependent effect, the equivalent conductivity of the MPC lamina must be computed as a function of temperature. Finally, it is recognized that the MPC section consists of two discrete regions, namely, the basket region and the periphery region. The periphery region is the space between the peripheral storage cells and the MPC enclosure shell. This space is essentially full of helium gas surrounded by Alloy X plates and optionally aluminum heat conduction elements. Accordingly, as illustrated in Figure 3.4.2 for MPC-68, the MPC cross section is replaced with two homogenized regions with temperature-dependent conductivities. In particular, the effective conductivity of the fuel cells is subsumed into the equivalent conductivity of the basket cross section using a finite element procedure. The ANSYS finite-element code is the vehicle for all modeling efforts described in the foregoing.

In summary, appropriate finite element models are used to replace the MPC cross section with an equivalent two-region homogeneous conduction lamina whose local conductivity is a known function of coincident absolute temperature. Thus, the MPC cylinder containing discrete fuel assemblies, helium, *neutron absorber* (~~Boral or METAMIC~~), Alloy X and optionally AHCEs* is replaced with a right circular cylinder whose material conductivity will vary with radial and axial position as a function of the coincident temperature.

The MPC-to-overpack gap is simply an annular space that is readily modeled with an equivalent conductivity that reflects the conduction and radiation modes of heat transfer. The overpack is a radially symmetric structure except for the neutron absorber region which is built from radial connectors and Holtite. Using the classical equivalence procedure as described in Section 3.4.1.1.9, this region is replaced with an equivalent radially symmetric annular cylinder.

The thermal analysis procedure described above makes frequent use of equivalent thermal properties to ease the geometric modeling of the cask components. These equivalent properties are rigorously calculated values based on detailed evaluations of actual cask system geometries. All these calculations are performed conservatively to ensure a bounding representation of the cask system. This process commonly referred to as submodeling, yields accurate (not approximate) results. Given the detailed nature of the submodeling process, experimental validation of the individual submodels is not necessary.

In this manner, a HI-STAR System overpack containing a loaded MPC is replaced with a right circular cylinder with spatially varying temperature-dependent conductivity. Heat is generated within the basket space in this cylinder in the manner of the prescribed axial distribution. In addition, heat is deposited from insolation on its external surface. Natural convection and thermal radiation to ambient air dissipate heat. Details of the elements of mathematical modeling are provided in the following sections.

3.4.1.1.2 Fuel Region Effective Thermal Conductivity Calculation

Thermal properties of a large number of PWR and BWR fuel assembly configurations manufactured by the major fuel suppliers (i.e., Westinghouse, CE, B&W, and GE) have been evaluated for inclusion in the HI-STAR System thermal analysis. Bounding PWR and BWR fuel assembly configurations are determined using the simplified procedure described below. This is followed by the determination of temperature-dependent properties of the bounding PWR and BWR fuel assembly configurations to be used for cask thermal analysis using a finite-volume (FLUENT) approach.

To determine which of the numerous PWR assembly types listed in Table 3.4.4 should be used in the thermal model for the PWR fuel baskets, we must establish which assembly has the maximum thermal resistance. The same determination must be made for the MPC-68, out of the menu of SNF types listed in Table 3.4.5. For this purpose, we utilize a simplified procedure that we describe below.

* In the thermal model, AHCEs are appropriately ignored.

Each fuel assembly consists of a large array of fuel rods typically arranged on a square layout. Every fuel rod in this array is generating heat due to radioactive decay in the enclosed fuel pellets. There is a finite temperature difference required to transport heat from the innermost fuel rods to the storage cell walls. Heat transport within the fuel assembly is based on principles of conduction heat transfer combined with the highly conservative analytical model proposed by Wooton and Epstein [3.4.1]. The Wooton-Epstein model considers radiative heat exchange between individual fuel rod surfaces as a means to bound the hottest fuel rod cladding temperature.

Transport of heat energy within any cross section of a fuel assembly is due to a combination of radiative energy exchange and conduction through the helium gas that fills the interstices between the fuel rods in the array. With the assumption of uniform heat generation within any given horizontal cross section of a fuel assembly, the combined radiation and conduction heat transport effects result in the following heat flow equation:

$$Q = \sigma C_o F_\epsilon A [T_C^4 - T_B^4] + 13.5740 L K_{cs} [T_C - T_B]$$

where,

$$F_\epsilon = \text{Emissivity Factor} = \frac{1}{\left(\frac{1}{\epsilon_C} + \frac{1}{\epsilon_B} - 1\right)}$$

ϵ_C, ϵ_B = emissivities of fuel cladding, fuel basket (see Table 3.2.4)

C_o = *Assembly Geometry Factor*

$$= \frac{4N}{(N+1)^2} \text{ (when } N \text{ is odd)}$$

$$= \frac{4}{N+2} \text{ (when } N \text{ is even)}$$

N = Number of rows or columns of rods arranged in a square array

A = fuel assembly "box" heat transfer area
= $4 \times \text{width} \times \text{length}$ (ft²)

L = fuel assembly length (ft)

K_{cs} = fuel assembly constituent materials volume fraction weighted mixture conductivity (Btu/ft-hr-°F)

T_C = hottest fuel cladding temperature (°R)

- T_B = box temperature ($^{\circ}R$)
- Q = net radial heat transport from the assembly interior (Btu/hr)
- σ = Stefan-Boltzman Constant (0.1714×10^{-8} Btu/ft²-hr- $^{\circ}R^4$)

In the above heat flow equation, the first term is the Wooten-Epstein radiative heat flow contribution while the second term is the conduction heat transport contribution based on the classical solution to the temperature distribution problem inside a square shaped block with uniform heat generation [3.4.3]. The 13.574 factor in the conduction term of the equation is the shape factor for two-dimensional heat transfer in a square section. Planar fuel assembly heat transport by conduction occurs through a series of resistances formed by the interstitial helium fill gas, fuel cladding and enclosed fuel. An effective planar mixture conductivity is determined by a volume fraction weighted sum of the individual constituent materials resistances. For BWR assemblies, this formulation is applied to the region inside the fuel channel. A second conduction and radiation model is applied between the channel and the fuel basket gap. These two models are combined, in series, to yield a total effective conductivity.

The effective thermal conductivities of several representative intact PWR and BWR assemblies are presented in Tables 3.4.4 and 3.4.5. At higher temperatures (greater than 450 $^{\circ}F$), the zircaloy clad fuel assemblies with the lowest effective thermal conductivities are the Westinghouse 17 \times 17 OFA (PWR) and the General Electric GE-11 9 \times 9 (BWR). A discussion of fuel assembly conductivities for some of the newer 10 \times 10 array and plant specific BWR fuel designs is presented near the end of this subsection. Based on this simplified analysis, the Westinghouse 17 \times 17 OFA PWR and GE-11 9 \times 9 BWR fuel assemblies are determined to be the bounding configurations for analysis at design basis maximum heat loads. As discussed in Section 3.3.2, stainless clad fuel assemblies with significantly lower decay heat emission characteristics are not deemed to be bounding.

Several of the assemblies listed in Tables 3.4.5 were excluded from consideration when determining the bounding assembly because of their extremely low decay heat loads. The excluded assemblies, which were each used at a single reactor only, are physically small and have extremely low burnups and long cooling times. These factors combine to result in decay heat loads that are much lower than the design basis maximum. The excluded assemblies are:

- Dresden Unit 1 8 \times 8
- Dresden Unit 1 6 \times 6
- Allis-Chalmers 10 \times 10 Stainless
- Exxon Nuclear 10 \times 10 Stainless
- Humboldt Bay 7 \times 7
- Quad⁺ 8 \times 8

The Allis-Chalmers and Exxon assemblies are used only in the LaCrosse reactor of the Dairyland Power Cooperative. The design basis assembly decay heat loads for Dresden Unit 1 and LaCrosse SNF (Tables 1.2.14 and 1.2.19) are approximately 58% lower and 69% lower, respectively, than the MPC-68 design basis assembly maximum heat load (Table 1.2.13). Examining Table 3.4.5, the

effective thermal conductivity of damaged Dresden Unit 1 fuel assemblies inside DFCs (the lowest of any Dresden Unit 1 assembly) and LaCrosse fuel assemblies are approximately 40% lower and 30% lower, respectively, than that of the bounding (GE-11 9×9) fuel assembly. Consequently, the fuel cladding temperatures in the HI-STAR System with Dresden Unit 1 and LaCrosse fuel assemblies (intact or damaged) will be bounded by design basis fuel cladding temperatures.

To accommodate Trojan Nuclear Plant (TNP) SNF in a HI-STAR System's MPC-24E canister*, the discharged fuel characteristics at this permanently shutdown site are evaluated herein. To permit TNP fuel in the HI-STAR System, it is necessary to confirm that certain key fuel parameters, viz. burnup (B) and cask decay heat (D) are bounded by the thermal design limits (42,500 MWD/MTU and 20 kW for PWR MPCs). The TNP SNF is a member of the 17x17 class of fuel types. The bulk of the fuel inventory is from Westinghouse and balance from B&W. The B&W SNF configuration and cladding dimensions are same as that of the Westinghouse 17x17 SNF. The fuel is more than nine years old and the burnups are in the range of 5073 MWD/MTU to 41889 MWD/MTU. The TNP SNF burnups are bounded by the design maximum for PWR class of fuel (i.e. $B < 42500$ MWD/MTU). Because the fuel decay heat is exponentially attenuating with time, it is conservative to evaluate decay heat on a date that precedes fuel loading. For this purpose, a reference date (RD) of 11/9/2001 is employed herein. The decay heat from the most emissive Trojan fuel is bounded by 725 W on RD. Postulating every cell location in an MPC-24E is occupied by this most heat emissive fuel assembly, a conservatively bounding $D = 17.4$ kW† is computed. The Trojan MPC-24E heat loads are below the HI-STAR System design heat load (i.e. $D < 20$ kW) by a significant margin.

A limited number of Trojan assemblies have poison inserts (RCCAs and BPRAs) and other non-fuel hardware (Thimble Plugs). The inclusion of PWR non-fuel hardware influences the MPC thermal response in two ways: (i) The presence of non-fuel hardware increases the effective basket conductivity, thus enhancing heat dissipation and lowering fuel temperatures and (ii) Volume displaced by the mass of non-fuel hardware lowers the available cavity free volume for accommodating gas released in hypothetical rod rupture scenarios. For a conservatively bounding evaluation, the thermal modeling ignores the presence of non-fuel hardware and the MPC cavity volume is computed based on volume displacement by the heaviest fuel (bounding weight) with non-fuel hardware included.

Having established the governing (most resistive) PWR and BWR SNF types, a finite-volume code is used to determine the effective conductivities in a conservative manner. Detailed conduction-radiation finite-volume models of the bounding PWR and BWR fuel assemblies are developed in the FLUENT code as shown in Figures 3.4.7 and 3.4.8, respectively. The PWR model was originally developed on the ANSYS code which enables individual rod-to-rod and rod-to-basket wall view factor calculations to be performed using that code's AUX12 processor. Limitations of radiation modeling techniques implemented in ANSYS make it difficult to take advantage of the symmetry of the fuel assembly geometry. Unacceptably long CPU time and large workspace requirements necessary for performing gray body radiation calculations for a complete fuel assembly geometry on ANSYS prompted the development of an alternate simplified model on the FLUENT code. The FLUENT model was benchmarked with the ANSYS model results for a Westinghouse 17×17 OFA

* The height of MPC-24E for Trojan SNF is shorter than the height of generic HI-STAR MPCs.

† Projected MPC heat loads are much lower (in the range of 6 kW to 14.5 kW in circa 2003).

fuel assembly geometry for the case of black body radiation (emissivities = 1). The FLUENT model was found to yield conservative results in comparison to the ANSYS model for the “black” surface case. The FLUENT model benchmarked in this manner is used to solve the gray body radiation problem to provide the necessary results for determining the effective thermal conductivity of the governing PWR fuel assembly. The same modeling approach using FLUENT is then applied to the governing BWR fuel assembly and the effective conductivity of GE-11 9×9 fuel is determined.

An equivalent homogeneous material that fills the basket opening replaces the combined fuel rods-helium matrix by the following two-step procedure. In the first step, the FLUENT-based fuel assembly model is solved by applying equal heat generation per unit length to the individual fuel rods and a uniform boundary temperature along the basket cell opening inside periphery. The temperature difference between the peak cladding and boundary temperatures is used to determine an effective conductivity as described in the next step. For this purpose, we consider a two-dimensional cross section of a square shaped block of size equal to 2L and a uniform volumetric heat source (q_g) cooled at the periphery with a uniform boundary temperature. Under the assumption of constant material thermal conductivity (K), the temperature difference (ΔT) from the center of the cross section to the periphery is analytically given by [3.4.3]:

$$\Delta T = 0.29468 \frac{q_g L^2}{K}$$

This analytical formula is applied to determine the effective material conductivity from a known quantity of heat generation applied in the FLUENT model (smeared as a uniform heat source, q_g), basket opening size and ΔT calculated in the first step.

As discussed earlier, the effective fuel space conductivity is a function of the temperature coordinate. The above two step analysis is carried out for a number of reference temperatures. In this manner, the effective conductivity as a function of temperature is established.

In Table 3.4.25, 10×10 array type BWR fuel assembly effective thermal conductivity results from a simplified analysis are presented to determine the most resistive fuel assembly in this class. Using the simplified analysis procedure discussed earlier, the Atrium-10 fuel type is determined to be the most resistive in this class of fuel assemblies. A detailed finite-element model of this assembly type was developed to rigorously quantify the heat dissipation characteristics. The results of this study are presented in Table 3.4.26 and compared to the bounding BWR fuel assembly effective thermal conductivity depicted in Figure 3.4.13. The results of this study demonstrate that the bounding BWR fuel assembly effective thermal conductivity is conservative with respect to the 10×10 class of BWR assemblies. Table 3.4.34 summarizes plant specific fuel types’ effective conductivities. From these analytical results, the SPC-5 is determined to be the most resistive fuel assembly in this group of fuel types. A rigorous finite element model of SPC-5 fuel assembly was developed to confirm that its in-plane heat dissipation characteristics are bounded from below by the design basis BWR fuel conductivities used in the HI-STAR thermal analysis.

Temperature-dependent effective conductivities of PWR and BWR design basis fuel assemblies (most resistive SNF types) are shown in Figure 3.4.13. The finite-volume results are also compared

to results reported from independent technical sources. From this comparison, it is readily apparent that FLUENT-based fuel assembly conductivities are conservative. The FLUENT computed values (not the published literature data) are used in the MPC thermal analysis presented in this document.

3.4.1.1.3 Effective Thermal Conductivity of Sheathing/~~Boral~~Neutron Absorber/Cell Wall Sandwich

Each MPC basket cell wall (except outer periphery MPC-68 & MPC-32 cell walls) is manufactured with a ~~Boral~~neutron absorbing plate for criticality control. Each ~~Boral~~ neutron absorbing plate is sandwiched in a sheathing-to-basket wall pocket. A schematic of the “Box Wall-~~Boral~~Neutron Absorber-Sheathing” sandwich geometry of an MPC basket is illustrated in Figure 3.4.5. During fabrication, a uniformly applied normal pressure on each sheathing-~~Boral~~Neutron Absorber-cell wall sandwich prior to stitch welding of the sheathing periphery to the box wall ensures adequate surface-to-surface contact for elimination of any macroscopic gaps. The mean coefficient of linear expansion of ~~Boral~~neutron absorber is higher than the basket materials thermal expansion coefficients. Consequently, basket heat-up from the contained SNF will further ensure a tight fit of the ~~Boral~~ neutron absorber plate in the sheathing-to-cell wall pocket. The presence of small microscopic gaps due to less than perfect surface finish characteristics requires consideration of an interfacial contact resistance between the ~~Boral~~neutron absorber and the box and sheathing surfaces. A conservative contact resistance resulting from a 2 mils ~~Boral~~neutron absorber-to-pocket gap is applied to the analysis. Note that this gap would actually be filled with helium. In other words, no credit is taken for the interfacial pressure between ~~neutron absorber~~~~Boral~~ and stainless plate/sheet stock produced by the fixturing and welding process.

Heat conduction properties of a composite “Box Wall-~~Boral~~Neutron Absorber-Sheathing” sandwich in the two principal basket cross sectional directions as illustrated in Figure 3.4.5 (i.e., lateral “out-of-plane” and longitudinal “in-plane”) are unequal. In the lateral direction, heat is transported across layers of sheathing, helium-gap, ~~Boral~~neutron absorber, (~~B₄C and cladding layers~~) helium-gap, and cell wall resistances that are in series (except for the small helium filled end regions shown in Figure 3.4.6). Heat conduction in the longitudinal direction, in contrast, is through an array of essentially parallel resistances comprised of these same layers. For the ANSYS based MPC basket thermal model, corresponding non-isotropic effective thermal conductivities in the two orthogonal directions are determined and applied in the analysis.

The non-isotropic conductivities are determined by constructing ANSYS models of the composite “Box Wall-~~Boral~~Neutron Absorber-Sheathing” sandwich for the “in-plane” and “out-of-plane” directions. For determining the effective conductivity (K_{eff}), a heat flux is applied to the to one end of the sandwich and an ANSYS numerical solution to the sandwich temperature differential obtained. From Fourier equation for one-dimensional conduction heat transfer, the following equation for K_{eff} is obtained:

$$K_{eff} = \frac{qL}{\Delta T}$$

where:

q = Sandwich heat flux
 L = Sandwich length in the direction of heat transfer
 ΔT = Sandwich temperature differential (obtained from ANSYS solution)

In the equation above, L is the width or thickness of the sandwich, respectively, for in-plane or out-of-plane heat transfer directions.

3.4.1.1.4 Modeling of Basket Conductive Heat Transport

Conduction of heat in a fuel basket is a combination of planar and axial contributions. These component contributions are individually calculated for each MPC basket design and combined (as described later in this subsection) to obtain an equivalent isotropic thermal conductivity. The heat rejection capability of each MPC design (i.e., MPC-24, MPC-24E, MPC-32 and MPC-68) is evaluated by developing a thermal model of the combined fuel assemblies and composite basket walls geometry on the ANSYS finite element code. The ANSYS model includes a geometric layout of the basket structure in which the "Box Wall-Boral Neutron Absorber-Sheathing" sandwich is replaced by a "homogeneous wall" with an equivalent thermal conductivity. Since the thermal conductivity of the Alloy X material is a weakly varying function of temperature, the equivalent "homogeneous wall" must have a temperature-dependent effective conductivity. Similarly, as illustrated in Figure 3.4.6, the conductivities in the in-plane and through-thickness direction of the equivalent "homogeneous wall" are different. Finally, as discussed earlier, the fuel assemblies occupying the basket cell openings are modeled as homogeneous heat generating regions with effective temperature dependent in-plane conductivities. The methodology used to reduce the heterogeneous MPC basket - fuel assemblage to an equivalent homogeneous region with effective thermal properties is discussed in the following.

Consider a cylinder of height L and radius r_o with a uniform volumetric heat source term q_g , with insulated top and bottom faces and its cylindrical boundary maintained at a uniform temperature T_c . The maximum centerline temperature (T_h) to boundary temperature difference is readily obtained from classical one-dimensional conduction relationships (for the case of a conducting region with constant thermal conductivity K_s):

$$(T_h - T_c) = q_g r_o^2 / (4 K_s)$$

Noting that the total heat generated in the cylinder (Q_t) is $\pi r_o^2 L q_g$, the above temperature rise formula can be reduced to the following simplified form in terms of the total heat generation per unit length (Q/L):

$$(T_h - T_c) = (Q_t / L) / (4 \pi K_s)$$

This simple analytical approach is employed to determine an effective basket cross-sectional conductivity by applying an equivalence between the ANSYS finite element model of the basket and the analytical case. The equivalence principle employed in the HI-STAR System thermal analysis is depicted in Figure 3.4.2. The 2-dimensional ANSYS finite element model of the MPC basket is solved by applying a uniform heat generation per unit length in each basket cell region and a constant basket periphery boundary temperature, T_c' . Noting that the basket region with uniformly

distributed heat sources and a constant boundary temperature is equivalent to the analytical case of a cylinder with uniform volumetric heat source discussed earlier, an effective MPC basket conductivity (K_{eff}) is readily derived from the analytical formula and the ANSYS solution leading to the following relationship:

$$K_{eff} = N (Q_f'/L) / (4 \pi [T_h' - T_c'])$$

where:

N = number of fuel assemblies

(Q_f'/L) = each fuel assembly heat generation per unit length applied in ANSYS model

T_h' = peak basket cross-section temperature from ANSYS model

Cross sectional views of MPC basket ANSYS models are illustrated in Figures 3.4.10 and 3.4.11 for a PWR and BWR MPC. Notice that many of the basket supports and all shims have been conservatively neglected in the models. This conservative geometry simplification, coupled with the conservative neglect of thermal expansion which would minimize the gaps, yields conservative gap thermal resistances. Temperature dependent equivalent thermal conductivities of the fuel region and composite basket walls, as determined from analysis procedures described earlier, are applied to the ANSYS model. The planar ANSYS conduction model is solved by applying a constant basket periphery temperature with uniform heat generation in the fuel region. Table 3.4.6 summarizes effective thermal conductivity results of each basket design obtained from the ANSYS models. It is recalled that the equivalent thermal conductivity values presented in Table 3.4.6 are lower bound values because, among other elements of conservatism, the effective conductivity of the most resistive SNF type (Tables 3.4.4 and 3.4.5) is used in the MPC finite-element simulations.

The axial conductivity of a fuel basket is determined by calculating a cross-sectional area-weighted sum of the component conductivities (Helium, Alloy-X, ~~Boron~~ neutron absorber and fuel cladding). In accordance with NUREG-1536 guidelines, credit for fuel rod axial heat conduction is conservatively limited to cladding.

Having obtained planar and axial thermal conductivities as described above, an equivalent isotropic conductivity (defined as the Square Root of the Mean Sum of Squares (SRMSS[†])) is obtained as shown below:

$$k_{iso} = \sqrt{\frac{k_{rad}^2 + k_{ax}^2}{2}}$$

where:

k_{iso} = equivalent isotropic thermal conductivity

k_{rad} = equivalent planar thermal conductivity

k_{ax} = equivalent axial thermal conductivity

[†] This formulation has been benchmarked for specific application to the MPC basket designs and confirmed to yield conservative results.

The equivalent isotropic conductivities are employed in the HI-STAR thermal modeling as discussed in Subsection 3.4.2.

3.4.1.1.5 Heat Transfer in MPC Basket Peripheral Regions

Each of the MPC designs for storing PWR or BWR fuel are provided with relatively large helium filled regions formed between the relatively cooler MPC shell and hot basket peripheral panels. For a horizontally oriented cask under normal transport conditions, heat transfer in these helium-filled regions is similar to heat transfer in closed cavities under three cases listed below:

- i. differentially heated short vertical cavity
- ii. horizontal channel heated from below
- iii. horizontal channel heated from above

In a closed cavity (case i scenario), an exchange of hot and cold fluids occurs near the top and bottom ends of the cavity, resulting in a net transport of heat across the gap.

The case (ii) scenario is similar to the classical Rayleigh-Benard instability of a layer of fluid heated from below [3.4.6]. If the condition for onset of fluid motion is satisfied, then a multi-cellular natural convection pattern is formed. The flow pattern results in upward motion of heated fluid and downward motion of relatively cooler fluid from the top plate, resulting in a net transport of heat across the heated fluid channel.

The case (iii) is a special form of case (ii) with an inverted (stably stratified) temperature profile. No fluid motion is possible in this circumstance and heat transfer is thus limited to fluid (helium) conduction only.

The three possible cases of closed cavity natural convection are illustrated in Figure 3.4.3 for an MPC-68 basket geometry. Peripheral spaces labeled B and B' illustrate the case (i) scenario, the space labeled D illustrates the case (ii) scenario, and the space labeled D' illustrates the case (iii) scenario. The basket is oriented to conservatively maximize the number of peripheral spaces having *no* fluid motion. A small alteration in the basket orientation will result in a non-zero gravity component in the x-direction which will induce case (i) type fluid motion in the D' space. The rate of natural convection heat transfer is characterized by a Rayleigh number for the cavity defined as follows:

$$Ra_L = \frac{C_p \rho^2 g \beta \Delta T L^3}{\mu K}$$

where:

C_p = fluid heat capacity

ρ	=	average fluid density
g	=	acceleration due to gravity
β	=	coefficient of thermal expansion (equal to reciprocal of absolute temperature for gases)
ΔT	=	temperature difference between hot and cold surfaces
L	=	spacing between hot and cold surfaces
μ	=	fluid viscosity
K	=	fluid conductivity

Hewitt et al. [3.4.5] report Nusselt number correlations for the closed cavity natural convection cases discussed earlier. A Nusselt number equal to unity implies heat transfer by fluid conduction only. A higher than unity Nusselt number is due to the so-called "Rayleigh" effect, which monotonically rises with increasing Rayleigh number. Nusselt numbers applicable to helium filled PWR and BWR MPCs in the peripheral voids are provided in Table 3.4.1. For conservatism, the heat dissipation enhancement due to Rayleigh effect is ignored.

3.4.1.1.6 Effective Conductivity of Multi-Layered Intermediate Shell Region

Fabrication of the layered overpack intermediate shells is discussed in Section 1.2 of this SAR. In the thermal analysis, each intermediate shell metal-to-metal interface presents an additional resistance to heat transport. The contact resistance arises from microscopic pockets of air trapped between surface irregularities of the contacting surfaces. Since air is a relatively poor conductor of heat, this results in a reduction in the ability to transport heat across the interface compared to that of the base metal. Interfacial contact conductance depends upon three principal factors, namely: (i) base material conductivity, (ii) interfacial contact pressure, and (iii) surface finish.

Rohsenow and Hartnett [3.2.2] have reported results from experimental studies of contact conductance across air entrapped stainless steel surfaces with a typical 100 μ -inch surface finish. A minimum contact conductance of 350 Btu/ft-hr- $^{\circ}$ F is determined from extrapolation of results to zero contact pressure.

The thermal conductivity of carbon steel is about three times that of stainless steel. Thus the choice of carbon steel as the base material in a multi-layered construction significantly improves heat transport across interfaces. The fabrication process guarantees interfacial contact. Contact conductance values extrapolated to zero contact pressures are therefore conservative. The surface finish of hot-rolled carbon steel plate stock is generally in the range of 250-1000 μ -inch [3.2.1]. The process of forming hot-rolled flat plate stock to cylindrical shapes to form the intermediate shells by rolling will result in a smoother surface finish. This results from the large surface pressures exerted by the hardened roller faces that flatten out any surface irregularities.

In the HI-STAR thermal analysis, a conservatively bounding interfacial contact conductance value is determined based on the following assumptions:

1. No credit is taken for high base metal conductivity.
2. No credit is taken for interfacial contact pressure.
3. No credit is taken for a smooth surface finish resulting from rolling of hot-rolled plate stock to cylindrical shapes.
4. Contact conductance is based on a uniform 2000 μ -inch (1000 μ -inch for each surface condition) interfacial air gap at all interfaces.
5. No credit for radiation heat exchange across this hypothetical inter-surface air gap.
6. Bounding low thermal conductivity at 200°F.

These assumptions guarantee a conservative assessment of heat dissipation characteristics of the multi-layered intermediate shell region. The resistances of the five carbon steel layers along with the associated interfacial resistances are combined as resistances in series to determine an effective conductivity of this region leading to the following relationship:

$$K_{gs} = r_o \ell n \left[\frac{r_5}{r_o} \right] \left[\sum_{i=1}^5 \frac{\delta}{K_{air} r_i} + \frac{r_o \ell n \left[\frac{r_5}{r_o} \right]}{K_{cst}} \right]^{-1}$$

where (in conventional U.S. units):

K_{gs}	=	effective intermediate shell region thermal conductivity
r_o	=	inside radius of inner gamma shield layer
r_i	=	outer radius of i^{th} intermediate shell layer
δ	=	interfacial air gap (2000 μ -inch)
K_{air}	=	air thermal conductivity
K_{cst}	=	carbon steel thermal conductivity

3.4.1.1.7 Heat Rejection from Overpack and Impact Limiter Outside Surfaces

Jakob and Hawkins [3.2.9] recommend the following correlations for natural convection heat transfer to air from heated vertical surfaces (flat impact limiter ends) and from single horizontal cylinders (overpack and impact limiter curved surfaces):

Turbulent range:

$$h = 0.19 (\Delta T)^{1/3} \text{ (Vertical, GrPr} > 10^9 \text{)}$$

$$h = 0.18 (\Delta T)^{1/3} \text{ (Horizontal Cylinder, GrPr} > 10^9 \text{)}$$

(in conventional U.S. units)

Laminar range:

$$h = 0.29 \left(\frac{\Delta T}{L} \right)^{1/4} \text{ (Vertical, GrPr} < 10^9 \text{)}$$

$$h = 0.27 \left(\frac{\Delta T}{D} \right)^{1/4} \text{ (Horizontal Cylinder, GrPr} < 10^9 \text{)}$$

(in conventional U.S. units)

where ΔT is the temperature differential between the system exterior surface and ambient air. During normal transport conditions, the surfaces to be cooled are the impact limiter and overpack cylindrical surfaces, and the flat vertical faces of the impact limiters. The corresponding length scales for these surfaces are the impact limiter diameter, overpack diameter, and impact limiter diameter, respectively. Noting that $Gr \times Pr$ is expressed as $L^3 \Delta T Z$, where Z (from Table 3.2.7) is at least 2.6×10^5 at a conservatively high upper bound system exterior surface temperature of $340^\circ F$, it is apparent that the turbulent condition is always satisfied for ΔT in excess of a few degrees Fahrenheit. Under turbulent conditions, the more conservative heat transfer correlation for horizontal cylinders (i.e., $h = 0.18 \Delta T^{1/3}$) is utilized for thermal analyses on all exposed system surfaces.

Including both convective and radiative heat loss from the system exterior surfaces, the following relationship for surface heat flux is developed:

$$q_s = 0.18 (T_s - T_A)^{4/3} + \sigma \times \varepsilon \times [(T_s + 460)^4 - (T_A + 460)^4]$$

where:

- T_s, T_A = surface, ambient temperatures ($^\circ F$)
- q_s = surface heat flux (Btu/ft²-hr)
- ε = surface emissivity (see Table 3.2.4)
- σ = Stefan-Boltzman Constant (0.1714×10^{-8} Btu/ft²-hr- $^\circ R^4$)

3.4.1.1.8 Determination of Solar Heat Input

The intensity of solar radiation incident on an exposed surface depends on a number of time varying parameters. The solar heat flux strongly depends upon the time of the day as well as on latitude and day of the year. Also, the presence of clouds and other atmospheric conditions (dust, haze, etc.) can significantly attenuate solar intensity levels. Rapp [3.4.2] has discussed the influence of such factors in considerable detail.

The HI-STAR System thermal analysis is based upon insolation levels specified in 10CFR71, Subpart F, which are for a 12-hour daytime period. During normal transport conditions, the HI-STAR System is cyclically subjected to solar heating during the 12-hour daytime period followed by cooling during the 12-hour nighttime. However, due to the large mass of metal and the size of the system, the inherent dynamic time lag in the temperature response is substantially larger than the 24-hour heating-cooling time period. Accordingly, the HI-STAR System cask model includes insolation at exposed surfaces averaged over a 24-hour time period. A bounding solar absorption coefficient of 1.0 is applied to cask exterior surfaces. The 10CFR71 mandated 12-hour average incident solar

radiation levels are summarized in Table 3.4.7. The combined incident insolation heat flux absorbed by exposed cask surfaces and decay heat load from the MPC is rejected by natural convection and radiation to ambient air.

3.4.1.1.9 Effective Thermal Conductivity of Radial Channels - Holtite Region

In order to minimize heat transfer resistance limitations due to the poor thermal conductivity of the Holtite-A neutron shield material, a large number of thick radial channels formed from high strength and conductivity carbon steel material are embedded in the neutron shield region. These radial channels form highly conductive heat transfer paths for efficient heat removal. Each channel is welded to the outside surface of the outermost intermediate shell and at the overpack enclosure shell, thereby providing a continuous path for heat removal to the ambient environment.

The effective thermal conductivity of the composite neutron shielding and radial channels region is determined by combining the heat transfer resistance of individual components in a parallel network. In determining the heat transfer capability of this region to the outside ambient environment for normal transport conditions, no credit is taken for conduction through the neutron shielding material. Thus, heat transport from the outer intermediate shell surface to the overpack outer shell is conservatively based on heat transfer through the carbon steel radial channel legs alone. Thermal conductivity of the parallel neutron shield and radial channel leg region is given by the following formula:

$$K_{ne} = \frac{K_R N_R t_R \ln \left[\frac{r_B}{r_A} \right]}{2 \pi L_R} + \frac{K_{ns} N_R t_{ns} \ln \left[\frac{r_B}{r_A} \right]}{2 \pi L_R}$$

where (in consistent U.S. units):

K_{ne}	=	effective thermal conductivity of neutron shield region
r_A	=	inner radius of neutron shielding
r_B	=	outer radius of neutron shielding
K_R	=	effective thermal conductivity of carbon steel radial channel leg
N_R	=	total number of radial channel legs (also equal number of neutron shield sections)
t_R	=	minimum (nominal) thickness of each radial channel leg
L_R	=	effective radial heat transport length through radial channel leg
K_{ns}	=	neutron shield thermal conductivity
t_{ns}	=	neutron shield circumferential thickness (between two radial channel legs)

The radial channel leg to outer intermediate shell surface weld thickness is equal to half the plate thickness. The additional weld resistance is accounted for by reducing the plate thickness in the weld region for a short radial span equal to the weld size. Conductivity of the radial carbon steel channel legs based on the full thickness for the entire radial span is correspondingly reduced. Figure 3.4.4 depicts a resistance network developed to combine the neutron shield and radial channel legs resistances to determine an effective conductivity of the neutron shield region. Note that in the resistance network analogy only the annulus region between overpack outer enclosure inner surface

and intermediate shells outer surface is considered in this analysis. The effective thermal conductivity of neutron shield region is provided in Table 3.4.8.

3.4.1.1.10 Effective Thermal Conductivity of the Eccentric MPC to Overpack Gap

During horizontal shipment of the HI-STAR System under normal transport conditions, the MPC will rest on the inside surface of the overpack. In the region of line contact, the resistance to heat transfer across the gap will be negligibly small due to a vanishingly small gap thickness. The resistance to heat transfer at other regions along the periphery of the MPC will, however, increase in direct proportion to the thickness of the local gap. This variation in gap thickness can be accounted for in the thermal model by developing a relation for the total heat transferred across the gap as given below:

$$Q_E = 2 \int_0^\pi \frac{K_{He}}{g(\theta)} L R_o \Delta T d\theta$$

where:

Q_E	=	total heat transfer across the gap (Btu/hr)
K_{He}	=	helium conductivity Btu/ft-hr-°F
L	=	length of MPC (ft.)
R_o	=	MPC radius (ft.)
θ	=	angle from point of line contact
$g(\theta)$	=	variation of gap thickness with angle (ft.)
ΔT	=	temperature difference across the gap (°F)

A corresponding relationship for heat transferred across a uniform gap is given by:

$$Q_c = \frac{K_{eff}}{(R_i - R_o)} 2\pi R_o L \Delta T$$

where R_i is the inside radius of the overpack and K_{eff} is the effective thermal conductivity of an equivalent concentric MPC/overpack gap configuration. From these two relationships, the ratio of effective gap conductivity to helium thermal conductivity in the MPC/overpack region is shown below:

$$\frac{K_{eff}}{K_{He}} = \frac{R_i - R_o}{\pi} \int_0^\pi \frac{1}{g(\theta)} d\theta$$

Based on an analysis of the geometry of a thin gap between two eccentrically positioned cylinders, the following relationship is developed for variation of the gap thickness with position:

$$g(\theta) = (R_i - R_o)(1 - \cos \theta) + \epsilon \cos \theta$$

The above equation conservatively accounts for imperfect contact by postulating a minimum gap ϵ at the point where the two surfaces would ideally form a line of perfect contact. The relatively thin MPC shell is far more flexible than the much thicker overpack inner shell, and will ovalize to yield

greater than line contact. The substantial weight of the fuel basket and contained fuel assemblies will also cause the MPC shell to conform to the overpack inner shell. An evaluation based on contact along a line would therefore be reasonable and conservative. However, a minimum gap is assumed to further increase conservatism in this calculation.

Based on an applied gap of 0.02-inch, which is conservative compared to contact along a line, the effective gap thermal conductivity determined from analytical integration [3.4.7] is in excess of 200% of the conductivity of helium gas. In the HI-STAR analysis, a conservative effective gap conductivity equal to twice the helium gas conductivity is applied to the performance evaluation.

3.4.1.1.11 Effective Thermal Conductivity of MPC Basket-to-Shell Aluminum Heat Conduction Elements

The HI-STAR MPCs feature an option to install full-length heat conduction elements fabricated from aluminum alloy 1100 in the large MPC basket-to-shell gaps. Due to the high aluminum alloy 1100 thermal conductivity (about 15 times that of Alloy X), a significant rate of net heat transfer is possible along the thin plates. For conservatism, heat dissipation by the Aluminum Heat Conduction Elements (AHCEs) is ignored in normal transport analyses. This overstates the initial fuel temperature for hypothetical fire accident evaluation. To conservatively compute heating of MPC contents in a hypothetical fire condition, the presence of heat conduction elements in AHCE equipped MPCs is duly recognized.

Figure 3.4.12 shows a mathematical idealization of a heat conduction element inserted between basket periphery panels and the MPC shell. The aluminum insert is shown to cover the MPC basket Alloy X peripheral panel and MPC shell surfaces (Regions I and III depicted in Figure 3.4.12) along the full-length of the basket. Heat transport to and from the aluminum insert is conservatively postulated to occur across a thin helium gap as shown in the figure (i.e., no credit is considered for aluminum insert to Alloy X metal-to-metal contact). Aluminum surfaces inside the hollow region are sandblasted prior to fabrication to result in a rough surface finish which has a significantly higher emissivity compared to smooth surfaces of rolled aluminum. The untreated aluminum surfaces directly facing Alloy X panels have a smooth finish to minimize contact resistance.

Net heat transfer resistance from the hot basket periphery panel to the relatively cooler MPC shell along the aluminum heat conduction element pathway is a sum of three individual resistances in regions labeled I, II, and III. In Region I, heat is transported from the basket to the aluminum insert surface directly facing the basket panel across a thin helium resistance gap. Longitudinal transport of heat (in the z direction) in the aluminum plate (in Region I) will result in an axially non-uniform temperature distribution. Longitudinal one-dimensional heat transfer in the Region I aluminum plate is analytically formulated to result in the following ordinary differential equation for the non-uniform temperature distribution:

$$t K_{Al} \frac{\partial^2 T}{\partial z^2} = - \frac{K_{He}}{h} (T_h - T) \quad \text{(Equation a)}$$

Boundary Conditions

$$\begin{aligned}\frac{\partial T}{\partial z} &= 0 \text{ at } z = 0 \\ T &= T_h' \text{ at } z = P\end{aligned}\tag{Equation b}$$

where (see Figure 3.4.12):

$T(z)$	=	non-uniform aluminum metal temperature distribution
t	=	conduction element thickness
K_{Al}	=	conduction element conductivity
K_{He}	=	helium conductivity
h	=	helium gap thickness
T_h	=	hot basket temperature
T_h'	=	conduction element Region I boundary temperature at $z = P$
P	=	conduction element Region I length

Solution of this ordinary differential equation subject to the imposed boundary condition is:

$$(T_h - T) = (T_h - T_h') \left[\frac{e^{\frac{z}{\sqrt{\alpha}}} + e^{-\frac{z}{\sqrt{\alpha}}}}{e^{\frac{P}{\sqrt{\alpha}}} + e^{-\frac{P}{\sqrt{\alpha}}}} \right]\tag{Equation c}$$

where α is a dimensional parameter equal to htK_{Al}/K_{He} . The net heat transfer (Q_1) across the Region I helium gap can be determined by the following integrated heat flux to a conduction element of length L as:

$$Q_1 = \int_0^P \frac{K_{He}}{h} (T_h - T)(L) dz\tag{Equation d}$$

Substituting the analytical temperature distribution result obtained in Equation c into Equation d and then integrating, the following expression for net heat transfer is obtained:

$$Q_1 = \frac{K_{He} L \sqrt{\alpha}}{h} \left(1 - \frac{1}{e^{\frac{P}{\sqrt{\alpha}}} + e^{-\frac{P}{\sqrt{\alpha}}}} \right) (T_h - T_h')\tag{Equation e}$$

Based on this result, an expression for Region I resistance is obtained as shown below:

$$R_I = \frac{T_h - T_{h'}}{Q_I} = \frac{h}{K_{He} L \sqrt{\alpha}} \left(1 - \frac{1}{e^{\frac{P}{\sqrt{\alpha}}} + e^{-\frac{P}{\sqrt{\alpha}}}} \right)^{-1} \quad (\text{Equation f})$$

Similarly, a Region III resistance expression can be analytically determined as shown below:

$$R_{III} = \frac{(T_c' - T_c)}{Q_{III}} = \frac{h}{K_{He} L \sqrt{\alpha}} \left(1 - \frac{1}{e^{\frac{P}{\sqrt{\alpha}}} + e^{-\frac{P}{\sqrt{\alpha}}}} \right)^{-1} \quad (\text{Equation g})$$

A Region II resistance expression can be developed from the following net heat transfer equation in the vertical leg of the conduction element as shown below:

$$Q_{II} = \frac{K_{Al} L t}{W} (T_h' - T_c') \quad (\text{Equation h})$$

Hence,

$$R_{II} = \frac{T_h' - T_c'}{Q_{II}} = \frac{W}{K_{Al} L t} \quad (\text{Equation i})$$

This completes the analysis for the total thermal resistance attributable to the heat conduction elements equal to sum of the three individual resistances. The total resistance is smeared across the basket-to-MPC shell region as an effective uniform annular gap conductivity (see Figure 3.4.2). Note that heat transport along the conduction elements is an independent conduction path in parallel with conduction and radiation mechanisms in the large helium gaps. Helium conduction and radiation between the MPC basket and the MPC shell is accounted for separately in the ANSYS MPC models described earlier in this section. Therefore, the total MPC basket-to-MPC shell peripheral gaps conductivity will be the sum of the conduction elements effective conductivity and the helium conduction-radiation gap effective conductivity.

3.4.1.1.12 FLUENT Model for HI-STAR Temperature Field Computation

In the preceding subsections, the series of analytical and numerical models to define the thermal characteristics of the various elements of the HI-STAR System are presented. The thermal modeling begins with the replacement of the SNF cross section and surrounding fuel cell space by a solid lamina with an equivalent conductivity. Since radiation is an important constituent of the heat

transfer process in the SNF/storage cell space and the rate of radiation heat transfer is a strong function of the surface temperatures, it is necessary to treat the equivalent lamina conductivity as a function of temperature. In fact, because of the relatively large range of temperatures which will exist in a loaded HI-STAR System under the design basis heat loads, it is necessary to include the effect of variation in the thermal conductivity of materials with temperature throughout the system finite volume model. The presence of significant radiation effect in the storage cell spaces adds to the imperative to treat the equivalent lamina conductivity as temperature-dependent.

FLUENT finite volume simulations have been performed to establish the equivalent thermal conductivity as a function of temperature for the limiting (thermally most resistive) BWR and PWR spent fuel types. By utilizing the most limiting SNF (established through a simplified analytical process for comparing conductivities) the numerical idealization for the fuel space conductivity is ensured to be conservative for all non-limiting fuel types.

Having replaced the interior of the cell spaces by solid prismatic (square) columns possessing a temperature-dependent conductivity essentially renders the basket into a non-homogeneous three-dimensional solid where the non-homogeneity is introduced by the honeycomb basket structure. The basket panels themselves are a composite of Alloy X cell wall, Boraf-neutron absorber, and Alloy X sheathing metal. A conservative approach to replace this composite section with an equivalent "solid wall" is described in a preceding subsection.

In the next step, a planar section of the MPC is considered. The MPC, externally radially symmetric, contains a non-symmetric basket lamina wherein the equivalent fuel space solid squares are separated by the "equivalent" solid metal walls. The space between the basket and the MPC, called the peripheral gap, is filled with helium gas and optionally aluminum heat conduction elements. The equivalent thermal conductivity of this MPC section is computed using a finite element procedure on ANSYS, as described previously. For hypothetical fire conditions the "helium-conduction-radiation" based peripheral gap conductivity and the effective conductivity of aluminum conduction elements are added to obtain a combined effective conductivity. At this stage in the thermal analysis, the SNF/basket/MPC assemblage has been replaced with a two-zone (Figure 3.4.2) cylindrical solid whose thermal conductivity is a strong function of temperature.

The idealization for the overpack is considerably more straightforward. The overpack is radially symmetric except for the Holtite region (discussed in Subsection 3.4.1.1.9). The procedure to replace the multiple shell layers, Holtite-A and radial connectors with an equivalent solid utilizes classical heat conduction analogies, as described in the preceding subsections.

In the final step of the analysis, the equivalent two-zone MPC cylinder, the equivalent overpack shell, the top and bottom plates, and the impact limiters are assembled into a comprehensive finite volume model. A cross section of this axisymmetric model implemented on FLUENT is shown in Figure 3.4.14. A summary of the essential features of this model is presented in the following:

- The overpack shell is represented by 840×9 elements. The effective thermal conductivity of the overpack shell elements is set down as a function of temperature based on the analyses described earlier.

- The overpack bottom plate and bolted closure plate are modeled by 312×9 axisymmetric elements.
- The two-zone MPC “solid” is represented by 1,144×9 axisymmetric elements.
- The space between the MPC “solid” and the overpack interior space is assumed to contain helium.
- Heat input due to insolation is applied to the impact limiter surfaces and the cylindrical surface of the overpack.
- The heat generation in the MPC solid basket region is assumed to be uniform in each horizontal plane, but to vary in the axial direction to correspond to the axial burnup distribution in the active fuel region postulated in Chapter 1.

The finite volume model constructed in this manner will produce an axisymmetric temperature distribution. The peak temperature will occur near the centerline and is expected to correspond to the axial location of peak heat generation. As is shown later, the results from the finite element solution bear out these observations.

3.4.1.1.13 Effect of Fuel Cladding Crud Resistance

In this subsection, a conservatively bounding estimate of the temperature drop across a crud film adhering to a fuel rod during dry storage conditions is determined. The evaluation is performed for a BWR fuel assembly based on an upper bound crud thickness obtained from PNL-4835 report ([3.3.5], Table 3). The crud present on fuel assemblies is predominantly iron oxide mixed, with small quantities of other metals such as cobalt, nickel, chromium, etc. Consequently, the effective conductivity of the crud mixture is expected to be in the range of typical metal alloys. Metals have thermal conductivities several orders of magnitude larger than that of helium. In the interest of extreme conservatism, however, a film of helium with the same thickness replaces the crud layer. The calculation is performed in two steps. In the first step, a crud film resistance is determined based on bounding maximum crud layer thickness replaced as a helium film on the fuel rod surfaces. This is followed by a peak local cladding heat flux calculation for the smaller GE 7×7 fuel assembly postulated to emit a conservatively bounding decay heat equal to 0.5kW. The temperature drop across the crud film obtained as a product of the heat flux and crud resistance terms is determined to be less than 0.1°F. The calculations are presented below:

$$\text{Bounding Crud Thickness } (\delta) = 130\mu\text{m } (4.26 \times 10^{-4} \text{ ft})$$

(PNL-4835)

$$\text{Crud Conductivity } (K) = 0.1 \text{ Btu/ft-hr-}^\circ\text{F (conservatively assumed as helium)}$$

GE 7x7 Fuel Assembly:

Rod O.D.	=	0.563"
Active Fuel Length	=	150"
Heat Transfer Area	=	$(7 \times 7) (\pi \times 0.563) \times 150 / 144$
	=	90.3 ft ²
Axial Peaking Factor	=	1.195 (Burnup distribution Table 1.2.15)
Decay Heat	=	500W (conservative assumption)

$$\text{Crud Resistance} = \frac{\delta}{K} = \frac{4.26 \times 10^{-4}}{0.1} = 4.26 \times 10^{-3} \frac{\text{ft}^2 \cdot \text{hr} \cdot ^\circ\text{F}}{\text{Btu}}$$

$$\begin{aligned} \text{Peak Heat Flux} &= \frac{(500 \times 3.417) \text{ Btu/hr}}{90.3 \text{ ft}^2} \times 1.195 \\ &= 18.92 \times 1.195 = 22.6 \frac{\text{Btu}}{\text{ft}^2 \cdot \text{hr}} \end{aligned}$$

Temperature drop (ΔT_c) across crud film:

$$\begin{aligned} &= 4.26 \times 10^{-3} \frac{\text{ft}^2 \cdot \text{hr} \cdot ^\circ\text{F}}{\text{Btu}} \times 22.6 \frac{\text{Btu}}{\text{ft}^2 \cdot \text{hr}} \\ &= 0.096^\circ\text{F} \\ &\text{(i.e., less than } 0.1^\circ\text{F)} \end{aligned}$$

Therefore, it is concluded that deposition of crud does not materially change the SNF cladding temperature.

3.4.1.1.14 Maximum Time Limit During Wet Transfer

While loading an empty HI-STAR System for transport directly from a spent fuel pool, water inside the MPC cavity is not permitted to boil. Consequently, uncontrolled pressures in the de-watering, purging, and recharging system that may result from two-phase condition are completely avoided. This requirement is accomplished by imposing a limit on the maximum allowable time duration for fuel to be submerged in water after a loaded HI-STAR cask is removed from the pool and prior to the start of vacuum drying operations.

When the HI-STAR overpack and the loaded MPC under water-flooded conditions are removed from the pool, the combined mass of the water, the fuel, the MPC, and the overpack will absorb the decay heat emitted by the fuel assemblies. This results in a slow temperature rise of the entire system with time, starting from an initial temperature of the contents. The rate of temperature rise is limited by the thermal inertia of the HI-STAR system. To enable a bounding heat-up rate determination for the HI-STAR system, the following conservative assumptions are imposed:

- i. Heat loss by natural convection and radiation from the exposed HI-STAR surfaces to the pool building ambient air is neglected (i.e., an adiabatic temperature rise calculation is performed).
- ii. Design Basis maximum decay heat input from the loaded fuel assemblies is imposed on the HI-STAR system.
- iii. The smallest of the *minimum* MPC cavity-free volumes between the two MPC types is considered for flooded water mass determination.
- iv. Fifty percent of the water mass in the MPC cavity is credited towards water thermal inertia evaluation.

Table 3.4.19 summarizes the weights and thermal inertias of several components in the loaded HI-STAR system. The rate of temperature rise of the HI-STAR and its contents during an adiabatic heat-up is governed by the following equation:

$$\frac{dT}{d\tau} = \frac{Q}{C_h}$$

where:

Q = decay heat load (Btu/hr) [equal to Design Basis maximum (between the two MPC types) 20.0 kW (i.e., 68,260 Btu/hr)]

C_h = combined thermal inertia of the loaded HI-STAR system (Btu/°F)

T = temperature of the contents (°F)

τ = time after HI-STAR system is removed from the pool (hr)

A bounding heat-up rate for the HI-STAR system contents is determined to be equal to 2.19°F/hr. From this adiabatic rate of temperature rise estimate, the maximum allowable time duration (t_{max}) for fuel to be submerged in water is determined as follows:

$$t_{\max} = \frac{T_{\text{boil}} - T_{\text{initial}}}{dT/d\tau}$$

where:

T_{boil} = boiling temperature of water (equal to 212°F at the water surface in the MPC cavity)

T_{initial} = initial temperature of the HI-STAR contents when removed from the pool

Table 3.4.20 provides a summary of t_{max} at several initial HI-STAR contents temperatures.

As set forth in Section 7.4, in the unlikely event where the maximum allowable time provided in Table 3.4.20 is found to be insufficient to complete all wet transfer operations, a forced water circulation shall be initiated and maintained to remove the decay heat from the MPC cavity. In this case, relatively cooler water will enter via the MPC lid drain port connection and heated water will exit from the vent port. The minimum water flow rate required to maintain the MPC cavity water temperature below boiling with an adequate subcooling margin is determined as follows:

$$M_w = \frac{Q}{C_{pw}(T_{max} - T_{in})}$$

where:

M_w = minimum water flow rate (lb/hr)

C_{pw} = water heat capacity (Btu/lb-°F)

T_{max} = maximum MPC cavity water mass temperature

T_{in} = temperature of water supply to MPC

With the MPC cavity water temperature limited to 150°F, MPC inlet water maximum temperature equal to 125°F and at the design basis maximum heat load, the water flow rate is determined to be 2,731 lb/hr (5.5 gpm).

3.4.1.1.15 Cask Cooldown and Reflood Analysis During Fuel Unloading Operation

Before a loaded HI-STAR System can be unloaded (i.e., fuel removed from the MPC) the cask must be cooled from the operating temperatures and reflooded with water[†]. Past industry experience generally supports cooldown of cask internals and fuel from hot storage conditions by direct water quenching. However, the extremely rapid cooldown rates that are typical during water injection, to which the hot cask internals and fuel cladding are subjected to, may result in uncontrolled thermal stresses and failure in the structural members. Moreover, water injection results in large amounts of steam generation and unpredictable transient two-phase flow conditions inside the MPC cavity, which may result in over-pressurization of the MPC helium retention boundary and a potentially unacceptable reduction in the safety margins to prevent criticality. To avoid potential safety concerns related to rapid cask cooldown by direct water quenching, the HI-STAR MPCs are designed to be cooled in a gradual manner, thereby eliminating thermal shock loads on the cask internals and fuel cladding.

In the unlikely event that a HI-STAR system is required to be unloaded, it will be transported back to the fuel handling building. Prior to reflooding the MPC cavity with water, a forced flow helium recirculation system with adequate flow capacity shall be operated to remove the decay heat and initiate a slow cask cooldown lasting for several days. The operating procedures in Section 7.2

[†] Certain fuel configurations in PWR MPCs require Borated water for criticality control (Chapter 6). Such MPCs are reflooded with Borated water.

provide a detailed description of the steps involved in the cask unloading. In this section, an analytical evaluation is presented to provide the basis for helium flow rates and time of forced cooling to meet the objective of eliminating thermal shock when the MPC cavity is eventually flooded with water.

Under a closed loop forced helium circulation condition, the helium gas is cooled via an external chiller, down to 100°F, and then introduced inside the MPC cavity from the drain line near the bottom baseplate. The helium gas enters the MPC basket from the bottom oversized flow holes and moves upward through the hot fuel assemblies, removing heat and cooling the MPC internals. The heated helium gas exits from the basket top and collects in the top plenum, from where it is expelled through the MPC lid vent connection to the helium recirculation and cooling system. The bulk average temperature reduction of the MPC contents as a function of time is principally dependent upon the rate of helium circulation. The temperature transient is governed by the following heat balance equation:

$$C_h \frac{dT}{d\tau} = Q_D - m C_p (T - T_i) - Q_c$$

Initial Condition: $T = T_o$ at $\tau = 0$

where:

T = MPC bulk average temperature (°F)

T_o = initial MPC bulk average temperature in the HI-STAR system (483°F[†])

τ = time after start of forced circulation (hr)

Q_D = decay heat load (Btu/hr)
(equal to Design Basis maximum 20.0 kW (i.e., 68,260 Btu/hr))

m = helium circulation rate (lb/hr)

C_p = helium heat capacity (Btu/lb-°F)
(equal to 1.24 Btu/lb-°F)

Q_c = heat rejection from cask exposed surfaces to ambient (Btu/hr)
(conservatively neglected)

C_h = thermal capacity of the loaded MPC (Btu/°F)
(For a bounding upper bound 100,000 lb loaded MPC weight, and heat capacity of Alloy X equal to 0.12 Btu/lb-°F, the heat capacity is equal to 12,000 Btu/°F)

[†] Bounding for HI-STAR normal transport.

T_i = MPC helium inlet temperature (°F)

The differential equation is analytically solved, yielding the following expression for time-dependent MPC bulk temperature:

$$T(t) = \left(T_i + \frac{Q_D}{m C_p}\right) \left(1 - e^{-\frac{m C_p t}{c_h}}\right) + T_o e^{-\frac{m C_p t}{c_h}}$$

This equation is used to determine the minimum helium mass flow rate that would cool the MPC cavity down from initially hot conditions to less than 200°F. For example, to cool the MPC to less than 200°F in 72 hours would require a helium mass flow rate of 574 lb/hr (i.e., 859 SCFM).

Once the helium gas circulation has cooled the MPC internals to less than 200°F, water can be injected to the MPC without risk of boiling and the associated thermal stress concerns. Because of the relatively long cooldown period, the thermal stress contribution to the total cladding stress would be negligible, and the total stress would therefore be bounded by the normal (dry) condition. The elimination of boiling eliminates any concern of over-pressurization due to steam production.

3.4.1.1.16 MPC Evaluation Under Drying Conditions

The initial loading of SNF in the MPC requires that the water within the MPC be drained, residual moisture removed and MPC filled with helium. This operation on the HI-STAR MPCs will be carried out using a Forced Helium Dehydrator (FHD) for a "load-and-go" operation. A "load-and-go" operation is defined as an activity wherein an MPC is loaded for direct off-site shipment in a HI-STAR transport cask. MPCs prepared via other competent methods for MPC drying as approved by the NRC on other dockets (1008 and 1014) are duly recognized for transport under this docket.

To reduce moisture to trace levels in the MPC using a Forced Helium Dehydration (FHD) system, a closed loop system consisting of a condenser, a demister, a compressor, and a pre-heater is utilized to extract moisture from the MPC cavity through repeated displacement of its contained helium, accompanied by vigorous flow turbulence. Appendix 3.B contains detailed discussion of the design and operation criteria for the FHD system.

The FHD system provides concurrent fuel cooling during the moisture removal process through forced convective heat transfer. The attendant forced convection-aided heat transfer occurring during operation of the FHD system ensures that the fuel cladding temperature will remain below the applicable peak cladding temperature limit for normal conditions of transport (752°F) for all combinations of SNF type, burnup, decay heat, and cooling time. Because the FHD operation induces a state of forced convection heat transfer in the MPC, (in contrast to the quiescent mode of natural convection in transport), it is readily concluded that the peak fuel cladding temperature under the latter condition will be greater than that during the FHD operation phase. In the event that the FHD system malfunctions, the forced convection state will degenerate to natural convection, which corresponds to the conditions of normal transport. As a result, the peak fuel cladding temperatures will approximate the values reached during normal transport as described elsewhere in this chapter.

3.4.1.1.17 Effects of Helium Dilution from Fuel Rod Gases

In this subsection, the generic cask transportation accident issue raised in a USNRC Spent Fuel Project Office (SFPO) staff guidance letter[†] is addressed. This issue directs cask designers to evaluate the impact of fission gas release into the canister, from a 100% fuel rods rupture accident, on the cask component temperatures and pressures when the MNOP^{††} is within 10% of the design pressure. To determine whether the HI-STAR System falls within the stipulated criteria, the MNOP results from Table 3.4.15 are provided below:

Canister	MNOP (psig)	Threshold Criteria ^{†††} for Accident Evaluation (psig)
MPC-24	88.8	90
MPC-68	86.9	90
MPC-24E	88.9	90
MPC-32	89.3	90

As shown above the MNOPs are below the threshold and an accident evaluation is not required. Nevertheless, for illustrative purposes, a 100% rods rupture accident for a HI-STAR package with an MPC-24 canister is evaluated.

Under a severe hypothetical accident scenario 100% of the fuel rods may rupture, releasing the rod fill gas (helium) and a portion of the gaseous fission products (³H, ⁸⁵Kr, ¹²⁹I and ¹³¹Xe). The gaseous fission products release fractions are stipulated in NUREG-1536. The released gases will mix with the MPC backfill gas and reduce its thermal conductivity. This reduction in conductivity will result in a small increase in MPC temperatures and pressures.

Appendix C of NUREG/CR-0497 [3.4.13] describes a method for calculating the effective thermal conductivity of a mixture of gases. The same method is also described by Rohsenow and Hartnett [3.2.2]. The following expression is provided by both references:

$$k_{mix} = \sum_{i=1}^n \left(\frac{k_i x_i}{x_i + \sum_{\substack{j=1 \\ j \neq i}}^n \phi_{ij} x_j} \right)$$

[†] SFPO Director's Interim Staff Guidance Letter(s), W.F. Kane, (Interim Staff-Guidance-7), October 8, 1998.

^{††} MNOP is a regulatory term defined in NUREG-1617 as the maximum gauge pressure that would develop in the containment in a period of 1 year under the heat condition specified in 10 CFR 71.71(c)(1) in the absence of venting, external ancillary cooling or operational controls.

^{†††} Accident evaluation required when MNOP is within 10% of the design pressure. This translates to a pressure that is between 100 psig (HI-STAR design pressure (Table 2.1.1)) and 90 psig.

where:

- k_{mix} = thermal conductivity of the gas mixture (Btu/hr-ft-°F)
- n = number of gases
- k_i = thermal conductivity of gas component i (Btu/hr-ft-°F)
- x_i = mole fraction of gas component i

In the preceding equation, the term ϕ_{ij} is given by the following:

$$\phi_{ij} = \phi_{ij} \left[1 + 2.41 \frac{(M_i - M_j)(M_i - 0.142 \cdot M_j)}{(M_i + M_j)^2} \right]$$

where M_i and M_j are the molecular weights of gas components i and j , and ϕ_{ij} is:

$$\phi_{ij} = \frac{\left[1 + \left(\frac{k_i}{k_j} \right)^{\frac{1}{2}} \left(\frac{M_i}{M_j} \right)^{\frac{1}{4}} \right]^2}{2^{\frac{3}{2}} \left(1 + \frac{M_i}{M_j} \right)^{\frac{1}{2}}}$$

Table 3.4.30 presents a summary of the gas mixture thermal conductivity calculations for MPC-24 containing design basis PWR fuel assemblies.

Having calculated the gas mixture thermal conductivity, the effective thermal conductivity of the design basis PWR fuel assembly is calculated using the finite-volume model described in Subsection 3.4.1.1.2. Only the helium gas conductivity is changed, all other modeling assumptions are the same. The fuel assembly effective thermal conductivity with diluted helium is compared to that with undiluted helium in Table 3.4.31.

Next, the effective thermal conductivities of the MPC fuel basket and basket periphery regions are determined as described in Subsections 3.4.1.1.3 and 3.4.1.1.4. This calculation incorporates both the diluted helium thermal conductivity and the effective thermal conductivity of the fuel assembly with diluted helium. The Rayleigh effect thermal conductivity multipliers are unchanged in this analysis. This is conservative because the released rod gases will increase the average fluid density and decrease the gas thermal conductivity, consequently increasing the Rayleigh number. The effective thermal conductivities with diluted helium are compared to those with undiluted helium in Table 3.4.31.

The MPC fuel basket effective thermal conductivities are input to a finite-volume model of the HI-STAR System arranged for transport. The cask system temperature distribution with diluted MPC helium is determined using the finite-volume model, as described in Subsection 3.4.1.1.12. Design basis normal environmental conditions are applied to the model and a temperature field solution obtained. Cask system temperatures with diluted MPC helium are summarized in Table 3.4.32.

The slightly higher MPC cavity temperature with MPC helium dilution will result in a small perturbation in MPC internal pressure. Based on the temperature field obtained with helium dilution, the MPC internal pressure is determined using the Ideal Gas Law. The calculated MPC internal pressure with helium dilution is presented in Table 3.4.33.

The results of analyses presented in this subsection are performed to illustrate the effect of a hypothetical 100% rods rupture on a HI-STAR package with an MPC-24. Even under the extreme postulated conditions, the MPC component temperatures and pressures remain substantially below the design limits.

3.4.1.1.18 HI-STAR Temperature Field With Low Heat Emitting Fuel

The HI-STAR 100 thermal evaluations for BWR fuel are divided in two groups of fuel assemblies proposed for storage in MPC-68. These groups are classified as Low Heat Emitting (LHE) fuel assemblies and Design Basis (DB) fuel assemblies. The LHE group of fuel assemblies are characterized by low burnup, long cooling time, and short active fuel lengths. Consequently, their heat loads are dwarfed by the DB group of fuel assemblies. The Dresden-1 (6x6 and 8x8), QUAD+, and Humboldt Bay (7x7 and 6x6) fuel characteristics warrant their classification as LHE fuel. These characteristics, including burnup and cooling time limits imposed on this class of fuel, are presented in Table 2.1.6. This fuel (except Quad+) is permitted to be loaded when encased in Damaged Fuel Containers (DFCs). As a result of interruption of radiation heat exchange between the fuel assembly and the fuel basket by the DFC boundary, this loading configuration is bounding for thermal evaluation. In Subsection 3.4.1.1.2, two canister designs for encasing LHE fuel are evaluated – a previously approved Holtec Design (Figure 1.2.10) and an existing canister in which some of the Dresden-1 fuel is currently stored (Transnuclear D-1 Canister). The most resistive fuel assembly determined by analytical evaluation is considered for thermal evaluation (see Table 4.4.6). The MPC-68 basket effective conductivity, loaded with the most resistive fuel assembly from the LHE group of fuel (encased in a canister) is provided in Table 4.4.7. To this basket, LHE fuel decay heat load, is applied and a HI-STAR 100 System temperature field obtained. The low heat load burden limits the initial peak cladding temperature to less than 579°F which is substantially below the cladding temperature limit (Table 3.3.1).

A thorium rod canister designed to hold a maximum of 20 fuel rods arrayed in a 5x4 configuration is currently stored at the Dresden-1 spent fuel pool. The fuel rods contain a mixture of enriched UO₂ and Thorium Oxide in the fuel pellets. The fuel rods were originally constituted as part of an 8x8 fuel assembly and used in the second and third cycle of Dresden-1 operation. The maximum fuel burnup of these rods is quite low (~13,100 MWD/MTU). The thorium rod canister internal design is a honeycomb structure formed from 12 gage stainless steel plates. The rods are loaded in individual square cells and are isolated from each other by the cell walls. The few number of rods (18 per assembly) and very low burnup of fuel stored in these Dresden-1 canisters render them as miniscule sources of decay heat. The canister all-metal internal honeycomb construction serves as an additional means of heat dissipation in the fuel cell space. In accordance with preferential fuel loading requirements, low burnup fuel shall be loaded toward the basket periphery (i.e., away from the hot central core of the fuel basket). All these considerations provide ample assurance that these

fuel rods will be stored in a benign thermal environment and therefore remain protected during transport.

3.4.1.2 Test Model

A detailed analytical model for evaluating the thermal design of the HI-STAR System was developed using the FLUENT CFD code and the industry standard ANSYS modeling system as discussed in Subsection 3.4.1.1. Furthermore, the analysis incorporates many conservative assumptions in order to demonstrate compliance with specified temperature limits for operation with adequate margins. In view of these considerations, the HI-STAR thermal design complies with the thermal criteria set forth in the design basis for normal transport conditions. Additional experimental verification of the thermal design is therefore not required. Acceptance and periodic thermal testing for the HI-STAR System is discussed in Sections 8.1 and 8.2.

3.4.2 Maximum Temperatures Under Normal Transport Conditions

Both MPC-basket designs developed for the HI-STAR System have been analyzed to determine temperature distributions under normal transport conditions. In the HI-STAR System thermal analysis models developed on FLUENT, the overpack impact limiters are included in the finite volume geometry. However, no credit is considered for the presence of heat conducting aluminum honeycomb material. In other words, heat transmission through the ends is conservatively neglected in the analysis. The thermal results are therefore bounding with respect to impact limiter design. The MPC baskets are considered to be loaded at design-basis maximum heat load with PWR or BWR fuel assemblies, as appropriate.

As discussed in Subsection 3.4.1.1.1, the thermal analysis is performed using a submodeling process where the results of an analysis on an individual component are incorporated into the analysis of a larger set of components. Specifically, the submodeling process yields directly computed fuel temperatures from which fuel basket temperatures are indirectly calculated. This modeling process differs from previous analytical approaches wherein the basket temperatures were evaluated first and then a basket-to-cladding temperature difference calculation by Wooten-Epstein or other means provided a basis for cladding temperatures. Subsection 3.4.1.1.2 describes the calculation of an effective fuel assembly thermal conductivity for an equivalent homogenous region. It is important to note that the result of this analysis is a function for thermal conductivity versus temperature. This function for fuel thermal conductivity is then input to the fuel basket effective thermal conductivity calculation described in Subsection 3.4.1.1.4. This calculation uses a finite-element methodology, wherein each fuel cell region containing multiple finite-elements has temperature varying thermal conductivity properties. The resultant temperature varying fuel basket thermal conductivity computed by this basket-fuel composite model is then input to the fuel basket region of the FLUENT cask model.

Because the FLUENT cask model incorporates the results of the fuel basket submodel, which in turn incorporates the fuel assembly submodel, the peak temperature reported from the FLUENT model is the peak temperature in any component. In a dry storage cask, the hottest components are the fuel assemblies. It should be noted that, because the fuel assembly models described in Subsection 3.4.1.1.2 include the fuel pellets, the FLUENT calculated peak temperatures reported in Tables

3.4.10 and 3.4.11 are actually peak pellet centerline temperatures which bound the peak cladding temperatures. We conservatively assume that the peak clad temperature is equal to the peak pellet centerline temperature.

From a thermal/hydraulic standpoint, the HI-STAR transport cask must cover two scenarios:

- i. MPCs equipped with AHCEs
- ii. MPCs without AHCEs

In the thermal analysis submitted in support of HI-STAR's original transport certification, which we now refer to as the Baseline Thermal Model (BTM), the AHCEs are included in the thermal models and the basket thermal model is constructed in an exceedingly conservative manner. In particular, the axial conductance of the basket fuel assemblage is assumed to be equal to the in-plane conductance (in reality, the in-plane conductance is much smaller than the axial conductance due to the presence of physical gaps between the fuel and the cell and within the fuel assemblies). For the Scenario (ii) analysis, such an overarching conservatism is removed while certain other less sweeping conservatisms are retained. The revised model, which we refer to as the Refined Thermal Model (RTM), forms the licensing basis for thermal evaluation. The conservatisms germane to the RTM are summarized in Appendix 3.A. To summarize, the principal difference between the BTM and RTM are as follows:

<i>Item</i>	<i>Description</i>	<i>BTM Assumption</i>	<i>RTM Assumption</i>
1	AHCE heat dissipation	Included	Excluded
2	Rayleigh effect	Included	Excluded
3	Basket Axial Conductivity	Grossly Understated	Realistic modeling of axial conductivity (See discussion in Subsection 3.4.1.1.4)

For representative PWR (MPC-24) and BWR (MPC-68) MPC-basket configurations with AHCEs installed, the temperature contours obtained with the Baseline Thermal Model (BTM) corresponding to steady-state hot conditions (100°F ambient, maximum design basis maximum decay heat and full insolation) are shown in Figures 3.4.16 and 3.4.17. Figures 3.4.19 and 3.4.20 show the axial temperature variation of the hottest fuel rod in the MPC-24 and MPC-68 basket designs, respectively. Figures 3.4.22 and 3.4.23 show the radial temperature profile in the MPC-24 and MPC-68 basket designs, respectively, in the horizontal plane where maximum fuel cladding temperature is indicated. Tables 3.4.10 and 3.4.11 summarize maximum calculated temperatures in different parts of the HI-STAR System at design-basis maximum decay heat loads. Tables 3.4.28 and 3.4.29 summarize the peak fuel cladding temperatures with heat loads lower than the design basis maximum. In Tables 3.4.22 and 3.4.23, maximum calculated temperatures in different parts of the HI-STAR System under steady-state cold conditions (-40°F ambient, maximum design basis maximum decay heat and no insolation) are summarized. To confirm the BTM fuel temperatures provided herein are bounding for all MPCs without the AHCEs option (MPC-24, MPC-24E, MPC-32 and MPC-68) a Refined Thermal Model (RTM) is articulated as discussed in the preceding

paragraph. As shown next, the results of the refined calculations confirm the BTM results are bounding.

Maximum Cladding Temperatures		
MPC Type	BTM [°F]	RTM [°F]
PWR	701	671 (MPC-24) 668 (MPC-24E) 699 (MPC-32)
BWR	713	642 (MPC-68)

The following additional observations can be derived by inspecting the temperature field obtained from the finite element analysis:

- The maximum fuel cladding temperature is well within the PNL recommended temperature limit.
- The maximum temperature of basket structural material is well within the stipulated design temperatures.
- The maximum temperature of the ~~Boral~~ neutron absorber is below the material ~~supplier's recommended~~ *supplier's recommended* temperature limit.
- The maximum temperatures of the MPC helium retention boundary materials are well below their respective ASME Code limits.
- The maximum temperatures of the aluminum heat conduction elements are well below the stipulated design temperature limits.
- The maximum temperature of the HI-STAR containment boundary materials is well below their respective ASME Code limits.
- The neutron shielding material (Holtite-A) will not experience temperatures in excess of its qualified limit.

The above observations lead us to conclude that the temperature field in the HI-STAR System with a fully loaded MPC containing design-basis heat emitting SNF complies with all regulatory and industry thermal requirements for normal conditions of transport. In other words, the thermal environment in the HI-STAR System will be conducive to safe transport of spent nuclear fuel.

3.4.2.1 Maximum Accessible Surface Temperatures

Access to the HI-STAR overpack cylindrical surface is restricted by the use of a personnel barrier (See Holtec Drawing 1809 in Chapter 1). Therefore, the HI-STAR System surfaces accessible during normal transport are the exposed impact limiter surfaces outside the personnel barrier. In this subsection, the exposed impact limiter surface temperatures are computed by including heat

transmission from the hot overpack ends through the impact limiters. A conservatively bounding analysis is performed by applying the thermal conductivity of aluminum to the encased aluminum-honeycomb material in the impact limiter shells to the normal condition thermal model discussed earlier in this chapter. In this manner heat transport to the exposed surfaces from the hot overpack is maximized and accessible surface temperatures over estimated. The maximum exposed cask surface temperatures for a PWR MPC (MPC-24) and a BWR MPC (MPC-68) at design maximum heat loads are 142°F and 139°F respectively. In Figure 3.4.28, a color contour map of the regions of HI-STAR System less than 185°F (358°K) is depicted for the hotter MPC-24 basket design. From this map, it is apparent that the accessible (impact limiter) surface temperatures are below the 10CFR71.43(g) mandated limit by a significant margin.

3.4.3 Minimum Temperatures

As specified in 10CFR71, the minimum ambient temperature conditions for the HI-STAR System are -20°F and a cold environment at -40°F. The HI-STAR System design does not have any minimum decay heat load restrictions for transport. Therefore, under zero decay heat load in combination with no solar input conditions, the temperature distribution will be uniformly equal to the imposed minimum ambient conditions. All HI-STAR System materials of construction would satisfactorily perform their intended function in the transport mode at this minimum postulated temperature condition. Evaluations in Chapter 2 demonstrate the acceptable structural performance of the overpack and MPC steel materials at low temperature. Shielding and criticality functions of the HI-STAR System materials (Chapters 5 and 6) are unaffected by exposure to this minimum temperature.

3.4.3.1 Post Rapid Ambient Temperature Drop Overpack Cooldown Event

In this section, the thermal response of the HI-STAR overpack to a rapid ambient temperature drop is analyzed and evaluated. The ambient temperature is postulated to drop from the maximum to minimum temperature under normal condition of transport in a very short time (100°F to -40°F during a 1 hour period) and is assumed to hold steady at -40°F thereafter. The initial overpack condition prior to this rapid temperature drop corresponds to normal steady state transport with maximum design basis heat load. During this postulated cooldown event, the outer surface of the overpack will initially cool more rapidly than the bulk of metal away from the exposed surfaces. Consequently, it is expected that the through-thickness temperature gradients will increase for a period of time, reach a maximum and follow an asymptotic return to the initial steady condition through thickness temperature gradients as the overpack temperature field approaches the -40°F ambient steady condition. The results of the transient analysis reported in this sub-section verify these observations.

Noting that the state of thermal stress is influenced by changes in the overpack temperature field during the cooldown transient, a number of critical locations in the containment boundary depicted in Figure 3.4.24 are identified as pertinent to a structural integrity evaluation discussed in Subsection 2.6.2.3 of this SAR. Locations (1) and (2) are chosen to track the through-thickness temperature gradients in the overpack top forging which is directly exposed to the ambient. Locations (3) and (4) are chosen to track the overpack inner containment shell through-thickness temperature gradient in a plane of maximum heat generation (i.e. active fuel mid-height) where the heat fluxes and

corresponding temperature gradients are highest. Locations (A) and (B) are similarly chosen to track the temperature differential in the multi-layered shells (outer-to-inner shells).

The normal transport condition thermal model discussed previously in this chapter is employed in the overpack cooldown transient analysis. This analysis is carried out by applying time-dependent thermal boundary conditions to the model and starting the transient solution in the FLUENT program. In the cooldown event, the ambient temperature is decreased from 100°F to -40°F in 10°F steps every 4 minutes (i.e. a total of 14 steps lasting 56 minutes). The ambient temperature is held constant thereafter. The maximum design basis heat load cask (i.e. the MPC-24 design) was selected to maximize the thermal gradients (by Fourier's Law, thermal gradient is proportional to heat flow). The overpack cooldown event is tracked by the thermal model for a period of 24 hours and results are reported in Figures 3.4.25 through 3.4.27 as discussed below.

In Figure 3.2.25, the overpack containment through-thickness temperature gradient responses are plotted. From this figure, it is evident that the exposed surface of the overpack forging (location (2)) initially cools at a faster rate than the recessed location (1). A similar but less pronounced result is observed in the multi-layered shells temperature changes depicted in Figure 3.4.26. This out-of-phase rate of cooling results in an increasing temperature gradient through the overpack metal layers. The thermal response of deeply recessed locations (3) and (4) show gradual temperature changes that follow each other closely. In other words, while through-thickness temperature gradients in the forging are somewhat altered the overpack inner shell gradients are essentially unchanged during the cooldown period. A closer examination of the forging temperature gradient is therefore warranted.

In Figure 3.4.27, the time dependent forging through thickness temperature differential is depicted. The gradient increases to a maximum in a short time period followed by a slow return towards the starting state. In absolute terms, both the steady state and transient temperature gradients in the forging are quite modest. In the steady state the forging through thickness temperature gradient is approximately 3°F. This value reaches a maximum plateau of 7°F during the transient event (Figure 3.4.27). The incremental thermal stress arising from this short-term gradient elevation is computed and discussed in Subsection 2.6.2.3 of this SAR.

3.4.4 Maximum Internal Pressures

The MPC is initially filled with dry helium after fuel loading and prior to sealing the MPC lid port cover plates and closure ring. During normal transport conditions, the gas temperature within the MPC rises to its maximum operating temperature as determined by the thermal analysis methodology described earlier (see Subsection 3.4.1). The gas pressure inside the MPC will increase with rising temperature. The pressure rise is determined using the Ideal Gas Law which states that the absolute pressure of a fixed volume of entombed gas is proportional to its absolute temperature.

The HI-STAR Maximum Normal Operating Pressure (MNOP) is calculated for 10 CFR 71.71(c)(1) heat condition (100°F ambient & insolation) and the HI-STAR Overpack passively cooled at design maximum heat load. For other lower than design maximum heat load scenarios, (e.g. transport with Trojan fuel) the MNOP results are confirmed to be bounding. In Tables 3.4.13 and 3.4.14, summary calculations for determining net free volume in the PWR and BWR canisters are presented.

Based on a 30% release of the significant radioactive gases, a 100% release of the rod fill gas from postulated cladding breaches, the net free volume and the initial fill gas pressure (see Table 3.3.2), the MNOP results are given in Table 3.4.15. The overpack containment boundary MNOP for a hypothetical MPC breach condition is bounded by the MPC pressure results reported in this table.

3.4.5 Maximum Thermal Stresses

Thermal expansion induced mechanical stresses due to imposed non-uniform temperature distributions have been determined and reported in Chapter 2. Tables 3.4.17 and 3.4.18 summarize the HI-STAR System components temperatures, under steady-state hot conditions, for structural evaluation.

Additionally, Table 3.4.24 provides a summary of MPC helium retention boundary temperatures during normal transport conditions (steady state hot). Structural evaluations in Section 2.6 reference these temperature results to demonstrate the MPC helium retention boundary integrity.

3.4.6 Evaluation of System Performance for Normal Conditions of Transport

The HI-STAR System thermal analysis is based on detailed and complete heat transfer models that properly account for radiation, conduction and natural convection modes of heat transfer. The thermal models incorporate many conservative assumptions that are listed below. A quantitative evaluation of HI-STAR conservatisms is provided in Appendix 3.A.

1. No credit for gap reduction between the MPC and overpack due to differential thermal expansion under hot condition is considered.
2. No credit is considered for MPC basket internal thermosiphon heat transfer. Under a perfectly horizontal transport condition, axial temperature gradients with peaking at active fuel mid-height induces buoyancy flows from both ends of the basket in each MPC cell. Buoyancy flow in shallow horizontal channels has been widely researched and reported in the technical literature [3.4.10 to 3.4.12]. An additional mode of heat transport due to thermosiphon flow within the basket cells is initiated for any cask orientation other than a perfectly horizontal condition. In practice this is a highly likely scenario. However, in the interest of conservatism, no credit is considered for this mode of heat transfer.
3. An upper bound solar absorptivity of unity is applied to all exposed surfaces.
4. No credit considered for radiative heat transfer between the ~~Boral~~ neutron absorber panels and the ~~Boral neutron absorber~~ pocket walls, ~~or for the presence of helium in the pocket gaps.~~
5. No credit is considered for conduction through the neutron shielding materials.
6. No credit is considered for contact between fuel assemblies and the MPC basket wall or between the MPC basket and the MPC basket supports. The fuel assemblies and MPC basket are conservatively considered to be in concentric alignment.

7. No credit considered for presence of highly conducting aluminum honeycomb material inside impact limiters.
8. The fuel assembly contribution to MPC basket axial conductivity is conservatively limited to the fuel cladding only (i.e. axial heat transfer through fuel pellets is neglected).
9. The MPC is assumed to be loaded with the SNF type which has the maximum equivalent thermal resistance of all fuel types in its category (BWR or PWR), as applicable.
10. The design basis maximum decay heat loads are used for all thermal-hydraulic analyses. For casks loaded with fuel assemblies having decay heat generation rates less than design basis, additional thermal margins of safety will exist.
11. Interfacial contact conductance of multi-layered intermediate shell contacting layers was conservatively determined to bound surface finish, contact pressure, and base metal conductivity conditions.
12. Flow turbulence in the MPC space neglected.

Temperature distribution results obtained from a conservatively developed thermal model show that maximum fuel cladding temperature limits are met with adequate margins. Margins during actual normal transport conditions are expected to be greater due to the many conservative assumptions incorporated in the analysis. The maximum local temperatures in the neutron shield and overpack seals are lower than design limits. The maximum local MPC basket temperature level is below the recommended limits for structural materials in terms of susceptibility to stress, corrosion and creep induced degradation. Furthermore, structural evaluation (Chapter 2) has demonstrated that stresses (including those induced due to imposed temperature gradients) are within ASME B&PV Code limits. Section 3.6 provides a discussion of compliance with the regulatory requirements and acceptance criteria listed in Section 3.0. As a result of the above-mentioned considerations, it is concluded that the HI-STAR thermal design is in compliance with 10CFR71 requirements for normal conditions of transport.

Table 3.4.1

CLOSED CAVITY NUSSOLT NUMBER[†]
 RESULTS FOR HELIUM FILLED MPC PERIPHERAL VOIDS

Temperature (°F)	Case (i) Nusselt Number		Case (ii) Nusselt Number	
	MPC-24, MPC-24E, MPC-32	MPC-68	MPC-24, MPC-24E, MPC-32	MPC-68
200	6.93	4.72	5.45	3.46
450	5.44	3.71	4.09	2.58
700	4.60	3.13	3.36	2.12

[†] For conservatism, the heat dissipation enhancement due to Rayleigh effect discussed in Sub-section 3.4.1.1.5 is ignored

Table 3.4.2

RELATIONSHIP BETWEEN HI-STAR SYSTEM REGIONS
AND MATHEMATICAL MODEL DESCRIPTIONS

<u>HI-STAR System Region</u>	<u>Mathematical Model</u>	<u>Subsections</u>
Fuel Assembly	Fuel Region Effective Thermal Conductivity	3.4.1.1.2
MPC	Effective Thermal Conductivity of Boral <i>Neutron Absorber/Sheathing/Box Wall Sandwich</i>	3.4.1.1.3
	Basket In-Plane Conductive Heat Transport	3.4.1.1.4
	Heat Transfer in MPC Basket Peripheral Region	3.4.1.1.5
	Effective Thermal Conductivity of MPC Basket-to-Shell Aluminum Heat Conduction Elements	3.4.1.1.11
Overpack	Effective Conductivity of Multi-Layered Intermediate Shell Region	3.4.1.1.6
	Effective Thermal Conductivity of Holtite Neutron Shielding Region	3.4.1.1.9
Ambient Environment	Heat Rejection from Overpack Exterior Surfaces	3.4.1.1.7
	Solar Heat Input	3.4.1.1.8
Assembled Cask Model	Overview of the Thermal Model	3.4.1.1.1
	Effective Conductivity of MPC to Overpack Gap	3.4.1.1.10
	FLUENT Model for HI-STAR	3.4.1.1.12

Table 3.4.3.

THIS TABLE IS INTENTIONALLY DELETED.

Table 3.4.4

SUMMARY OF PWR FUEL ASSEMBLIES
EFFECTIVE THERMAL CONDUCTIVITIES

No.	Fuel	@ 200°F (Btu/ft-hr-°F)	@ 450°F (Btu/ft-hr-°F)	@ 700°F (Btu/ft-hr-°F)
1	W 17×17 OFA	0.182	0.277	0.402
2	W 17×17 Std	0.189	0.286	0.413
3	W 17×17 Vantage-5H	0.182	0.277	0.402
4	W 15×15 Std	0.191	0.294	0.430
5	W 14×14 Std	0.182	0.284	0.424
6	W 14×14 OFA	0.175	0.275	0.413
7	B&W 17×17	0.191	0.289	0.416
8	B&W 15×15	0.195	0.298	0.436
9	CE 16×16	0.183	0.281	0.411
10	CE 14×14	0.189	0.293	0.435
11	HN [†] 15×15 SS	0.180	0.265	0.370
12	W 14×14 SS	0.170	0.254	0.361
13	B&W 15x15 Mark B-11	0.187	0.289	0.424
14	CE 14x14 (MP2)	0.188	0.293	0.434

Note: Boldface values denote the lowest thermal conductivity in each column (excluding stainless steel clad fuel assemblies).

[†] Haddam Neck B&W or Westinghouse stainless steel clad fuel assemblies.

Table 3.4.5

SUMMARY OF BWR FUEL ASSEMBLIES EFFECTIVE THERMAL CONDUCTIVITIES

No.	Fuel	@ 200°F (Btu/ft-hr-°F)	@ 450°F (Btu/ft-hr-°F)	@ 700°F (Btu/ft-hr-°F)
1	Dresden 1 8×8 [†]	0.119	0.201	0.319
2	Dresden 1 6×6	0.126	0.215	0.345
3	GE 7×7	0.171	0.286	0.449
4	GE 7×7R	0.171	0.286	0.449
5	GE 8×8	0.168	0.278	0.433
6	GE 8×8R	0.166	0.275	0.430
7	GE-10 8×8	0.168	0.280	0.437
8	GE-11 9×9	0.167	0.273	0.422
9	AC ^{††} 10×10 SS	0.152	0.222	0.309
10	Exxon 10×10 SS	0.151	0.221	0.308
11	Damaged Dresden 1 8×8 in a DFC [†]	0.107	0.169	0.254
12	Dresden-1 Thin Clad 6×6 [†]	0.124	0.212	0.343
13	Humboldt Bay-7×7 [†]	0.127	0.215	0.343
14	Damaged Dresden-1 8×8 (in TND-1 canister) [†]	0.107	0.168	0.252
15	8×8 QUAD+ Westinghouse [†]	0.164	0.278	0.435

Note: Boldface values denote the lowest thermal conductivity in each column (excluding Dresden and LaCrosse clad fuel assemblies).

† Low heat emitting fuel assemblies excluded from list of fuel assemblies (zircaloy clad) evaluated to determine the most resistive SNF type

†† Allis-Chalmers stainless steel clad fuel assemblies

Table 3.4.6

**MPC BASKET EFFECTIVE THERMAL CONDUCTIVITY RESULTS
FROM ANSYS MODELS**

Basket	@200°F (Btu/ft-hr-°F)	@450°F (Btu/ft-hr-°F)	@700°F (Btu/ft-hr-°F)
MPC-24 (Zircaloy Clad Fuel)	1.127	1.535	2.026
MPC-68 (Zircaloy Clad Fuel)	1.025	1.257	1.500
MPC-24 (Stainless Steel Clad Fuel) (Note 1)	0.901	1.230	1.615
MPC-68 (Stainless Steel Clad Fuel) (Note 1)	0.987	1.180	1.360
MPC-68 (Dresden-1 8x8 in canisters)	0.921	1.118	1.306
MPC-32 (Zircaloy Clad Fuel)	0.964	1.214	1.486
MPC-32 (Stainless Steel Clad Fuel) (Note 1)	0.762	0.936	1.104
MPC-24E (Zircaloy Clad Fuel)	1.211	1.635	2.137
MPC-24E (Stainless Steel Clad Fuel) (Note 1)	0.988	1.348	1.766

Note-1: Evaluated for a conservatively bounding configuration (fuel in a damaged fuel canister)

Table 3.4.7

INSOLATION DATA SPECIFIED BY 10CFR71, SUBPART F

Surface Type	12-Hour Total Insolation Basis	
	(g-cal/cm ²)	(Watts/m ²)
Horizontally Transported Flat Surfaces		
- Base	None	None
- Other Surfaces	800	774.0
Non-Horizontal Flat Surfaces	200	193.5
Curved Surfaces	400	387.0

Table 3.4.8

EFFECTIVE THERMAL CONDUCTIVITY OF THE NEUTRON SHIELD/RADIAL CHANNELS REGION

Condition/Temperature (°F)	Thermal Conductivity (Btu/ft-hr-°F)
Normal Condition: 200 450 700	 1.953 1.812 1.645
Fire Condition: 200 450 700	 3.012 2.865 2.689

Table 3.4.9

THIS TABLE IS INTENTIONALLY DELETED.

Table 3.4.10

HI-STAR SYSTEM NORMAL TRANSPORT[†] MAXIMUM TEMPERATURES
(PWR MPCs)

	Bounding Temperature [°F]	Normal Condition Temperature Limit [°F]
Fuel Cladding	701	752
MPC Basket Centerline	667	725
MPC Basket Periphery	430	725
MPC Outer Shell Surface	315	450
MPC/Overpack Helium Gap Outer Surface	291	400
Radial Neutron Shield Inner Surface	271	300
Overpack Enclosure Shell Surface	222	350
Axial Neutron Shield	292	300
Impact Limiter Exposed Surface	121	176
Overpack Closure Plate ^{††}	163	400
Overpack Bottom Plate ^{††}	295	350

[†] Steady-state hot (100°F ambient) with maximum decay heat and insolation.

^{††} Overpack closure plate and vent/drain port plug seals normal condition design temperature is 400°F. The maximum seals temperatures are bounded by the reported closure plate and bottom plate maximum temperatures. Consequently, a large margin of safety exists to permit safe operation of seals in the overpack helium retention boundary.

Table 3.4.11

HI-STAR SYSTEM NORMAL TRANSPORT[†] MAXIMUM TEMPERATURES
(MPC-68)

	Bounding Temperature [°F]	Normal Condition Temperature Limit [°F]
Fuel Cladding	713	752
MPC Basket Centerline	697	725
MPC Basket Periphery	365	725
MPC Outer Shell Surface	306	450
MPC/Overpack Gap Outer Surface	282	400
Radial Neutron Shield Inner Surface	264	300
Overpack Enclosure Shell Surface	217	350
Axial Neutron Shield	255	300
Impact Limiter Exposed Surface	121	176
Overpack Closure Plate ^{††}	162	400
Overpack Bottom Plate ^{††}	256	350

† Steady-state hot (100°F ambient) with maximum decay heat and insolation.

†† Overpack closure plate and vent/drain port plug seals normal condition design temperature is 400°F. The maximum seals temperatures are bounded by the reported closure plate and bottom plate maximum temperatures. Consequently, a large margin of safety exists to permit safe operation of seals in the overpack helium retention boundary.

Table 3.4.12

THIS TABLE IS INTENTIONALLY DELETED.

Table 3.4.13

SUMMARY OF BOUNDING MINIMUM
FREE VOLUME CALCULATIONS (PWR MPCs)

Item	MPC-24 Volume (ft ³)	MPC-24E Volume (ft ³)	MPC-32 Volume (ft ³)
Cavity Volume	367	367	367
Basket Metal Volume	45	52	25
Bounding Fuel Assemblies Volume	79	79	106
Basket Supports and Fuel Spacers Volume	7	7	9
Aluminum Conduction Elements [†]	6	6	6
Net Free Volume	230 (6512 liters)	223 (6314 liters)	221 (6258 liters)

[†] Bounding 1,000 lbs aluminum weight.

Table 3.4.14

SUMMARY OF BOUNDING MINIMUM
MPC-68 FREE VOLUME CALCULATIONS

Item	Volume (ft ³)
Cavity Volume	367
Basket Metal Volume	35
Bounding Fuel Assemblies Volume	93
Basket Supports and Fuel Spacers Volume	12
Aluminum Conduction Elements [†]	6
Net Free Volume	221 (6258 liters)

[†] Bounding 1,000 lbs aluminum weight.

Table 3.4.15

SUMMARY OF MAXIMUM NORMAL OPERATING PRESSURE (MNOP)[†]
FOR HORIZONTAL TRANSPORT CONDITIONS

Condition	Pressure (psig)	Bounding MPC Cavity Bulk Temperature (°F)
MPC-24: Initial Backfill (at 70°F) Normal Condition With 3% Rods Rupture ^(Note 1)	42.8 87.7 88.8	483
MPC-68: Initial Backfill (at 70°F) Normal Condition With 3% Rods Rupture ^(Note 1)	42.8 86.0 86.9	468
MPC-24E: Initial Backfill (at 70°F) Normal Condition With 3% Rods Rupture ^(Note 1)	42.8 87.7 88.9	483
MPC-32: Initial Backfill (at 70°F) Normal Condition With 3% Rods Rupture ^(Note 1)	42.8 87.7 89.3	483

Note 1: NUREG-1617 requires an assumption for normal transport that 3% of the rods are breached with release of 100% fill gas and 30% fission gas to containment.

[†] Pressure analysis in accordance with heat condition specified in 10 CFR 71.71(c)(1) in the absence of venting, external ancillary cooling or operational controls.

Table 3.4.16

THIS TABLE IS INTENTIONALLY DELETED.

Table 3.4.17

PWR MPCs NORMAL HORIZONTAL TRANSPORT CONDITION
 HI-STAR SYSTEM COMPONENTS BOUNDING TEMPERATURE SUMMARY

	MPC Basket Axial Mid-Length [°F]	MPC Basket Axial Ends [°F]
Overpack enclosure shell	222	147
Overpack inner shell	291	163
MPC shell	315	164
Basket periphery	430	166
Basket center	667	177

Table 3.4.18

MPC-68 NORMAL HORIZONTAL TRANSPORT CONDITION
 HI-STAR SYSTEM COMPONENTS TEMPERATURE [°F] SUMMARY

	MPC Basket Axial Mid-Length	MPC Basket Axial Ends
Overpack enclosure shell	217	146
Overpack inner shell	282	161
MPC shell	306	163
Basket periphery	365	164
Basket center	697	175

Table 3.4.19

SUMMARY OF LOADED HI-STAR SYSTEM
 BOUNDING COMPONENT WEIGHTS AND THERMAL INERTIAS

Component	Weight (lbs)	Heat Capacity (Btu/lb-°F)	Thermal Inertia (Btu/°F)
Holtite-A	11,000	0.39	4,290
Carbon Steel	140,000	0.1	14,000
Alloy-X MPC (empty)	35,000	0.12	4,200
Fuel	40,000	0.056	2,240
MPC Cavity Water [†]	6,500	1.0	6,500
			31,230 (Total)

[†] Based on smallest MPC-68 cavity net free volume with 50% credit for flooded water mass.

Table 3.4.20

MAXIMUM ALLOWABLE TIME DURATION
FOR WET TRANSFER OPERATIONS

Initial Temperature (°F)	Time Duration (hr)
115	44.3
120	42.0
125	39.7
130	37.4
135	35.2
140	32.9
145	30.6
150	28.3

Table 3.4.21

THIS TABLE IS INTENTIONALLY DELETED.

Table 3.4.22

HI-STAR SYSTEM BOUNDING TEMPERATURES [°F]
 UNDER STEADY-STATE COLD[†] CONDITIONS (PWR MPCs)

Fuel Cladding	620
MPC Basket Centerline	586
MPC Basket Periphery	329
MPC Outer Shell Surface	190
MPC/Overpack Gap Outer Surface	165
Radial Neutron Shield Inner Surface	141
Overpack Enclosure Shell Surface	96
Axial Neutron Shield	165
Impact Limiter Exposed Surface	-40

[†] -40°F ambient temperature with maximum decay heat and no insolation.

Table 3.4.23

HI-STAR SYSTEM MAXIMUM TEMPERATURES [°F]
 UNDER STEADY-STATE COLD[†] CONDITIONS (MPC-68)

Fuel Cladding	621
MPC Basket Centerline	605
MPC Basket Periphery	254
MPC Outer Shell Surface	178
MPC/Overpack Gap Outer Surface	153
Radial Neutron Shield Inner Surface	130
Overpack Enclosure Shell Surface	88
Axial Neutron Shield	123
Impact Limiter Exposed Surface	-40

[†] -40°F ambient temperature with maximum decay heat and no insolation.

Table 3.4.24

SUMMARY OF MPC HELIUM RETENTION BOUNDARY BOUNDING
TEMPERATURE DISTRIBUTION DURING NORMAL STORAGE CONDITIONS

Location	Figure 2.6.20 Designation	PWR MPCs [°F]	MPC-68 [°F]
MPC Lid Inside Surface at Centerline	A	176	173
MPC Lid Outside Surface at Centerline	B	171	169
MPC Lid Inside Surface at Periphery	C	164	163
MPC Lid Outside Surface at Periphery	D	162	161
MPC Baseplate Inside Surface at Centerline	E	301	260
MPC Baseplate Outside Surface at Centerline	F	295	256
MPC Baseplate Inside Surface at Periphery	G	267	239
MPC Baseplate Outside Surface at Periphery	H	267	239
MPC Shell Maximum	I	315	306

Table 3.4.25

SUMMARY OF 10×10 ARRAY BWR FUEL ASSEMBLY TYPES
EFFECTIVE THERMAL CONDUCTIVITIES[†]

Fuel	k_{eff} at 200°F [Btu/(ft-hr-°F)]	k_{eff} at 450°F [Btu/(ft-hr-°F)]	k_{eff} at 700°F [Btu/(ft-hr-°F)]
GE-12/14	0.166	0.269	0.412
Atrium-10	0.164	0.266	0.409
SVEA-96	0.164	0.269	0.416

[†] The conductivities reported in this table are obtained by the simplified method described in the beginning of Subsection 3.4.1.1.2.

Table 3.4.26

COMPARISON OF ATRIUM-10[†] AND BOUNDING^{††} BWR FUEL ASSEMBLY
EFFECTIVE THERMAL CONDUCTIVITIES

Temperature	Atrium-10 Assembly		Bounding BWR Assembly		
	°F	Btu/(ft-hr-°F)	W/m-K	Btu/(ft-hr-°F)	W/m-K
200		0.225	0.389	0.171	0.296
450		0.345	0.597	0.271	0.469
700		0.504	0.872	0.410	0.710

[†] The reported effective thermal conductivity has been obtained from a rigorous finite-element modeling of the Atrium-10 assembly.

^{††} The bounding BWR fuel assembly effective thermal conductivity applied in the MPC-68 basket thermal analysis.

Table 3.4.27

THIS TABLE IS INTENTIONALLY DELETED.

Table 3.4.28

PWR MPCs BOUNDING PEAK FUEL CLADDING TEMPERATURE
AS A FUNCTION OF TOTAL HEAT LOAD

Total MPC Decay Heat Load (kW)	Peak Fuel Cladding Temperature (°F)
20.0 [†]	700.6
19.0	678.9
17.0	633.9
15.5	598.8

[†] Design Basis Maximum.

Table 3.4.29

MPC-68 PEAK FUEL CLADDING TEMPERATURE
AS A FUNCTION OF TOTAL HEAT LOAD

Total MPC Decay Heat Load (kW)	Peak Fuel Cladding Temperature (°F)
18.5 [†]	712.7
17.0	674.0
15.5	634.1

[†] Design Basis Maximum.

Table 3.4.30

SUMMARY OF THERMAL CONDUCTIVITY CALCULATIONS
FOR MPC HELIUM DILUTED BY RELEASED ROD GASES

Component Gas	Molecular Weight (g/mole)	Mole Fraction	Thermal Conductivity* (Btu/hr-ft-°F)
MPC and Fuel Rod Backfill Helium	4	0.817	0.098 @ 200°F 0.129 @ 450 °F 0.158 @ 700°F
Rod Tritium	3	8.007×10^{-5}	0.119 @ 200 0.148 @ 450°F 0.177 @ 700°F
Rod Krypton	85	0.016	6.76×10^{-3} @ 200°F 8.782×10^{-3} @ 450°F 0.011 @ 700°F
Rod Xenon	131	0.160	3.987×10^{-3} @ 200°F 5.258×10^{-3} @ 450°F 6.471×10^{-3} @ 700°F
Rod Iodine	129	6.846×10^{-3}	2.496×10^{-3} @ 200°F 3.351×10^{-3} @ 450°F 4.201×10^{-3} @ 700°F
Mixture of Gases (diluted helium)	N/A	1.000	0.053 @ 200°F 0.069 @ 450°F 0.085 @ 700°F

* References [3.2.2], [3.4.18] & [3.4.19] consulted for fission gases (Tritium, Krypton, Xenon and Iodine) conductivities.

Table 3.4.31

COMPARISON OF COMPONENT EFFECTIVE THERMAL CONDUCTIVITIES
WITH AND WITHOUT MPC HELIUM DILUTION

	Effective Thermal Conductivity (Btu/hr-ft-°F)		
	Value at 200°F	Value at 450°F	Value at 700°F
Fuel Assembly with Undiluted Helium	0.257	0.406	0.604
Fuel Assembly with Diluted Helium	0.160	0.278	0.458
MPC Fuel Basket with Undiluted Helium	1.127	1.535	2.026
MPC Fuel Basket with Diluted Helium	0.948	1.338	1.829

Table 3.4.32

MPC-24 HYPOTHETICAL 100% RODS RUPTURE ACCIDENT
 MAXIMUM TEMPERATURES*

	Calculated Maximum Temperature (°F)	Accident Condition Temperature Limit (°F)
Fuel Cladding	743	1058
MPC Basket Centerline	709	950
MPC Basket Periphery	444	950
MPC Outer Shell Surface	314	775
MPC/Overpack Helium Gap Outer Surface	291	500
Radial Neutron Shield Inner Surface	271	N/A
Overpack Enclosure Shell Surface	222	1350
Overpack Closure Plate	176	700
Overpack Bottom Plate	296	700

* The results reported herein are obtained from thermal models employing grossly understated fuel basket conductivities.

Table 3.4.33

MPC-24 HYPOTHETICAL 100% RODS RUPTURE ACCIDENT PRESSURES

Calculated Accident Pressure (psig)	Accident Condition Design Pressure (psig)
134	200

Table 3.4.34

PLANT SPECIFIC BWR FUEL TYPES EFFECTIVE THERMAL CONDUCTIVITY*

Fuel	@200°F [Btu/ft-hr-°F]	@450°F [Btu/ft-hr-°F]	@700°F^o [Btu/ft-hr-°F]
Oyster Creek (7x7)	0.165	0.273	0.427
Oyster Creek (8x8)	0.162	0.266	0.413
TVA Browns Ferry (8x8)	0.160	0.264	0.411
SPC-5 (9x9)	0.149	0.245	0.380

* The conductivities reported in this table are obtained by a simplified analytical method described in Subsection 3.4.1.1.2.

3.6 REGULATORY COMPLIANCE

Section 3.1 defines the requirements of 10CFR71 and ISG-11, Rev. 32 [3.1.5]) that must be met by the HI-STAR cask thermal design. The cask thermal evaluations in support of these requirements are provided in Sections 3.1 through 3.5. In this Section, a summary of the requirements and results of the evaluations are provided.

1. The applicant must include a description of the proposed package in sufficient detail to identify the package accurately and provide a sufficient basis for the evaluation of the package. The description must include, with respect to the packaging: specific materials of construction, weights, dimensions, and fabrication methods of materials specifically used as non-fissile neutron absorbers or moderators; and structural and mechanical means for the transfer and dissipation of heat. The description must include, with respect to the contents of the package: chemical and physical form; maximum normal operating pressure; maximum amount of decay heat; and identification and volumes of any coolants.

A general description of the HI-STAR System is included in Chapter 1. Descriptions of cask materials are presented in Subsection 1.2.1, Section 1.4 and Appendices 1.A, 1.B and 1.C. Shielding materials are specifically addressed in Subsection 1.2.1.4. Cask component weights are presented in Subsections 1.2.1.1 and 2.2. Cask component dimensions are presented in Subsection 1.2.1.2 and in engineering drawings included in Section 1.4. The transfer and dissipation of heat are discussed generally in Subsection 1.2.1.6, and in detail in this chapter.

General descriptions of and requirements for fuel assemblies for transport are presented in Subsection 1.2.3, including design basis maximum decay heat load specifications in Subsection 1.2.3.5. Maximum normal operating pressures are reported in Subsection 3.4.4. As stated in Subsection 1.2.1.7, there are no coolant volumes (reservoirs) in the HI-STAR System.

2. A package must be designed, constructed, and prepared for shipment so that under normal conditions of transport there would be no substantial reduction in the effectiveness of the packaging.

The results of thermal evaluations presented in Section 3.4 demonstrate that the HI-STAR System performs as designed under all normal conditions of transport.

3. A package must be designed, constructed, and prepared for shipment so that in still air at 100°F and in the shade, no accessible surface of the package would have a temperature exceeding 185°F in an exclusive use shipment.

Maximum exposed surface temperatures for the HI-STAR System are reported in Subsection 3.4.2. All impact limiter surface temperatures are shown to be below 185°F. The personnel

barrier, described in Chapter 7, renders the hot overpack enclosure shell surfaces inaccessible.

4. Compliance with the permitted activity release limits for a Type B package may not depend on filters or on a mechanical cooling system.

As stated in Section 3.1, all cooling mechanisms in the HI-STAR System are completely passive.

5. With respect to the initial conditions for the events of normal conditions of transport and hypothetical accident conditions, the demonstration of compliance with the requirements of 10CFR71 must be based on the ambient temperature preceding and following the event remaining constant at that value between -20°F and 100°F, which is most unfavorable for the feature under consideration. The initial internal pressure within the containment system must be considered to be the maximum normal operating pressure (MNOP), unless a lower internal pressure consistent with the ambient temperature considered to precede and follow the event is more unfavorable.

Hypothetical fire accident transient calculations for the HI-STAR System are described in Section 3.5. The initial condition for this event corresponds to the most severe steady-state solution for normal conditions of transport, which correspond to a 100°F ambient temperature with full insolation. These same environmental conditions are applied during the post-accident phase of the evaluation as well. All calculated temperatures for this event are below the specified design temperature limits.

Maximum calculated normal condition internal pressures (MNOPs) are reported in Subsection 3.4.4. Maximum calculated hypothetical accident condition internal pressures are reported in Subsection 3.5.4. All calculated MNOPs are below the design pressure limits for the MPC helium retention boundary and the overpack containment boundary.

6. For normal conditions of transport, a heat event consisting of an ambient temperature of 100°F in still air and prescribed insolation must be evaluated.

The maximum temperatures in the HI-STAR System reported in Subsection 3.4.2 correspond to the heat event. All calculated temperatures for this event are below the appropriate design temperature limits. As stated in Subsection 3.4.5, thermal stresses are determined and reported in Chapter 2.

7. For normal conditions of transport, a cold event consisting of an ambient temperature of -40°F in still air and shade must be evaluated.

The minimum temperatures in the HI-STAR System reported in Subsection 3.4.3 correspond to the cold event. All calculated temperatures for this event are below the appropriate design

temperature limits. As stated in Subsection 3.4.5, thermal stresses are determined and reported in Chapter 2.

8. Evaluation for hypothetical accident conditions is to be based on sequential application of the specified events, in the prescribed order, to determine their cumulative effect on a package.

As described in Section 3.5, the HI-STAR System hypothetical accident thermal condition (hydrocarbon fuel/air fire) evaluation incorporates bounding representations of the results of the preceding accident conditions. Specifically, the impact limiters are assumed to be completely crushed (drop event) and the heat transfer effectiveness of the radial channels region is reduced (puncture event). All calculated temperatures for this event are below the appropriate design temperature limits.

9. For hypothetical accident conditions, a thermal event consisting of a fully engulfing hydrocarbon fuel/air fire with an average emissivity coefficient of at least 0.9, with an average flame temperature of at least 1475°F for a period of 30 minutes.

The description of the HI-STAR System hypothetical accident thermal event model (Subsection 3.5.1.1) specifies the fire condition input parameters. All input parameters are in accordance with the requirements of 10CFR71.73(c)(4). All calculated temperatures for this event are below the appropriate design temperature limits.

The thermal evaluations in Sections 3.4, 3.5, 3.I.4 and 3.I.5 demonstrate compliance with ISG-11, Rev. 32 [3.1.5] temperature limits. Specifically, the maximum cladding temperatures for normal transport and accident conditions are below the prescribed limits (normal (752°F) and accident (1058°F)). The thermal evaluations provided in this SAR demonstrate that the HI-STAR and HI-STAR HB System description and evaluation satisfy the thermal requirements of 10 CFR Part 71. Specifically:

- The material properties and component specifications used in the thermal evaluation are sufficient to provide a basis for evaluation of the HI-STAR System against the thermal requirements of 10 CFR Part 71.
- The methods used in the thermal evaluation are described in sufficient detail to permit an independent review, with confirmatory calculations, of the HI-STAR System thermal design.
- The accessible surface temperatures of the HI-STAR System as it will be prepared for shipment satisfy 10 CFR 71.43(g) for exclusive use shipments.
- The HI-STAR System design, construction, and preparations for shipment ensure that the material and component temperatures will not extend beyond the specified allowable limits during normal conditions of transport consistent with 10 CFR 71.71.

- The HI-STAR System design, construction, and preparations for shipment ensure that the material and component temperatures will not exceed the specified allowable temperature limits during hypothetical accident conditions consistent with 10 CFR 71.73.

It is therefore concluded that the thermal design of the HI-STAR System is in compliance with 10 CFR Part 71, and that the applicable design and acceptance criteria have been satisfied. The evaluation of the thermal design provides reasonable assurance that the HI-STAR System will allow safe transport of spent fuel. This conclusion is based on the technical data and analyses presented in this chapter in conjunction with provisions of 10 CFR Part 71, appropriate regulatory guides, applicable codes and standards, and accepted engineering practices.

3.7 REFERENCES

- [3.1.1] ANSYS Finite Element Modeling Package, Swanson Analysis Systems, Inc., Houston, PA, 1993.
- [3.1.2] FLUENT Computational Fluid Dynamics Software (Fluent, Inc., Centerra Resource Park, 10 Cavendish Court, Lebanon, NH 03766).
- [3.1.3] Greer et al., "The TN-24P PWR Spent Fuel Storage Cask: Testing and Analyses," EPRI NP-5128, PNL-6054, UC-85, (April 1987).
- [3.1.4] Deleted.
- [3.1.5] "Cladding Considerations for the Transportation and Storage of Spent Fuel", Interim Staff Guidance – 11, Revision 32, (11/17/037/30/02).
- [3.2.1] Baumeister, T., Avallone, E.A. and Baumeister III, T., "Marks' Standard Handbook for Mechanical Engineers", 8th Edition, McGraw Hill Book Company, 1978.
- [3.2.2] Rohsenow, W.M. and Hartnett, J.P., "Handbook of Heat Transfer," McGraw Hill Book Company, New York, 1973.
- [3.2.3] Greer et al., "The TN-24P Spent Fuel Storage Cask: Testing and Analyses," EPRI NP-5128, PNL-6054, UC-85, (April 1987).
- [3.2.4] Rust, J.H., "Nuclear Power Plant Engineering," Haralson Publishing Company, (1979).
- [3.2.5] Kern, D.Q., "Process Heat Transfer," McGraw Hill Kogakusha, (1950).
- [3.2.6] "A Handbook of Materials Properties for Use in the Analysis of Light Water Reactor Fuel Rod Behavior", NUREG/CR-0497, (August 1981).
- [3.2.7] "Safety Analysis Report for the NAC Storable Transport Cask," Docket No. 71-9235.
- [3.2.8] ASME Boiler and Pressure Vessel Code, Section II, Part D, (1995).
- [3.2.9] Jakob, M. and Hawkins, G.A., "Elements of Heat Transfer," John Wiley & Sons, New York, 1957.
- [3.2.10] "*Qualification of METAMIC for Spent-Fuel Storage Application*", EPRI Report 1003137, (October 2001), EPRI, Palo Alto, CA.

- [3.2.11] *"Sourcebook for METAMIC Performance Assessment", Holtec Report HI-2043215, Holtec International, Marlton, NJ, 08053.*
- [3.2.12] *"Nuclear Systems Materials Handbook, Vol. 1, Design Data", ORNL TID 26666.*
- [3.2.13] *"Scoping Design Analyses for Optimized Shipping Casks Containing 1-, 2-, 3-, 5-, 7-, or 10-Year-Old PWR Spent Fuel", ORNL/CSD/TM-149 TTC-0316, (1983).*
- [3.2.14] *"Holtite A: Development History and Thermal Performance Data", Holtec Report HI-2002396, Rev. 3., Holtec International, Marlton, NJ, 08053.*
- [3.3.1] "Handbook of Aluminum," Alcan Aluminum Corporation, 3rd Edition, page 170, (1970).
- [3.3.2] Levy, I.S. et al., "Recommended Temperature Limits for Dry Storage of Spent Light Water Reactor Zircaloy Clad Fuel Rods in Inert Gas," PNL-6189, (May 1987).
- [3.3.3] Deleted.
- [3.3.4] "Characteristics of Spent Fuel, High-Level Waste, and Other Radioactive Wastes Which May Require Long-Term Isolation," DOE/RW-0184, (December 1987).
- [3.3.5] Johnson, Jr., A.B. and Gilbert, E.R., "Technical Basis for Storage of Zircaloy-Clad Spent Fuel in Inert Gases," PNL-4835, (September 1983).
- [3.3.6] Cunningham et. al., "Evaluation of Expected Behavior of LWR Stainless Steel-Clad Fuel in Long-Term Dry Storage," EPRI TR-106440, (April 1996).
- [3.3.7] "Temperature Limit Determination for the Inert Dry Storage of Spent Nuclear Fuel," EPRI TR-103949, (May 1994).
- [3.3.8] *Lanning and Beyer, "Estimated Maximum Cladding Stresses for Bounding PWR Fuel Rod During Short Term Operations for Dry Cask Storage," PNNL White Paper, (January 2004).*
- [3.4.1] Wooton, R.O. and Epstein, H.M., "Heat Transfer from a Parallel Rod Fuel Element in a Shipping Container," Battelle Memorial Institute, 1963.
- [3.4.2] Rapp, D., "Solar Energy," Prentice-Hall, Inc., Englewood Cliffs, NJ, 1981.
- [3.4.3] Sanders et al., "A Method for Determining the Spent-Fuel Contribution to Transport Cask Containment Requirements," Sandia Report SAND90-2406-TTC-

1019UC-820, page II-127, (November 1992).

- [3.4.4] Holman, J.P., "Heat Transfer," 6th ed., McGraw Hill Book Company, 1986.
- [3.4.5] Hewitt, G.F., Shires, G.L., and Bott, T.R., "Process Heat Transfer," CRC Press, (1994).
- [3.4.6] Chandrasekhar, S., "Hydrodynamic and Hydromagnetic Stability," Dover, (1961).
- [3.4.7] Gradshteyn, I.S. and Ryzhik, I.M., "Table of Integrals Series and Products," Academic Press, Fourth Edition, page 366, (1965).
- [3.4.8] Deleted.
- [3.4.9] Deleted.
- [3.4.10] Cormack, D.E., L.G. Leal and J. Imberger, "Natural Convection in a Shallow Cavity With Differentially Heated End Walls. Part 1 Asymptotic Theory," J. Fluid Mechanics, 65, 209-229, (1974).
- [3.4.11] Cormack, D.E., L.G. Leal and J.H. Seinfeld, "Natural Convection in a Shallow Cavity With Differentially Heated End Walls. Part 2 Numerical Solutions," J. Fluid Mechanics, 65, 231-246, (1974).
- [3.4.12] Imberger, J., "Natural Convection in a Shallow Cavity with Differentially Heated End Walls. Part 3 Experimental Results," J. Fluid Mechanics, 65, 247-260, (1974).
- [3.4.13] Hagrman, Reymann and Mason, "MATPRO-Version 11 (Revision 2) A Handbook of Materials Properties for Use in the Analysis of Light Water Reactor Fuel Rod Behavior," NUREG/CR-0497, Tree 1280, Rev. 2, EG&G Idaho, August 1981.
- [3.4.14] Deleted.
- [3.4.15] Deleted.
- [3.4.16] Deleted.
- [3.4.17] Deleted.
- [3.4.18] Perry and Green, "Perry's Chemical Engineers' Handbook", 6th Edition, McGraw-Hill, 1984.

- [3.4.19] Reid, Prauznitz and Poling, "The Properties of Gases and Liquids", Fourth Edition, McGraw-Hill, 1987.
- [3.5.1] 10CFR Part 71, Paragraph 71.73, (January 1, 1998).
- [3.5.2] Jakob, M., "Heat Transfer," John Wiley & Sons, Inc., page 555, (1967).

SUPPLEMENT 3.1

THERMAL EVALUATION OF HI-STAR HB

3.1.0 INTRODUCTION

The Humboldt Bay HI-STAR HB cask is licensed to store permanently shutdown Unit 3 BWR spent nuclear fuel (SNF) at the Humboldt Bay ISFSI. In this supplement compliance of the HI-STAR HB cask to 10CFR71 and ISG-11, Rev. 3 thermal requirements are evaluated for transport. The analysis considers passive rejection of decay heat from the spent nuclear fuel to an environment under the 10CFR71 mandated ambient conditions for normal and accident scenarios. The regulatory requirements and acceptance criteria for transport evaluation are listed in Section 3.0.

3.1.1 DISCUSSION

The HI-STAR HB, with the exception noted below, is an essentially shortened version of the HI-STAR 100 cask. The HI-STAR 100 cask thermal design features discussed in Section 3.1 are applicable to the HI-STAR HB design. Prior to sealing the HI-STAR HB MPC lid, the MPC-HB is backfilled with helium to Table 1.1.2 specifications.

The HI-STAR HB overpack design features a neutron shield placed in the annulus region between the multi-layered shells and enclosure shell without connecting ribs. (See HI-STAR HB overpack dwg. 4082, Sht. 6 included in the Chapter 1 Supplement, Section 1.1.4). This feature is unique to the "HB" version of the generic HI-STAR 100 overpack design. As the annular shield is a thick layer of a low conductivity material, Holtite A, it retards the lateral transmission of fire heat during hypothetical accidents, thus minimizing the heating of HI-STAR HB package internals and the stored fuel during fires.

3.1.2 THERMAL PROPERTIES OF MATERIALS

The thermophysical data compiled in Section 3.2 of the SAR provides the required materials information except for Holtite thermal conductivity. Holtite conductivity data [3.1.1] is provided in Table 3.1.1.

Holtite-A is qualified to withstand the effects of much elevated temperatures and high radiation exposures reached in the generic HI-STAR 100 Cask (heat loads upto 20 kW). As the HI-STAR HB package heat loads (2 kW) are dwarfed by the generic design, much larger margins against thermal and radiation degradation are realized. The Holtite-A thermal characterization and qualification testing for use in dry storage casks are archived in references [3.1.1] and [3.1.2].

3.1.3 TECHNICAL SPECIFICATIONS OF COMPONENTS

The HI-STAR materials and components required to be maintained within safe operating limits are listed in Section 3.3. The temperature limits specified in this section are adopted for transport evaluation.

3.1.4 NORMAL TRANSPORT THERMAL EVALUATION

The HI-STAR HB cask features an all-welded multi-purpose canister (MPC) containing spent nuclear fuel emplaced in a bolted steel overpack. From a thermal standpoint the HI-STAR HB cask is identical to the generic HI-STAR cask except for the following differences:

- a) The height of the cask is reduced to be compatible with the short-length Humboldt Bay fuel.
- b) To accommodate the narrow width Humboldt Bay fuel the fuel storage cells count is increased to 80.
- c) Radial connectors in the neutron shield region are replaced with a continuous neutron shield ring to minimize streaming.

The thermal payload of the HI-STAR HB transport package is given in Table 3.1.2.

3.1.4.1 Thermal Model

Thermal modeling of the HI-STAR HB adopts the same methodology used for HI-STAR thermal evaluation. An overview of the thermal methodology is given in the following.

Transport of heat from the HI-STAR HB to the ambient is analyzed broadly using three connected thermal models.

- i. The first model considers transport of heat from the fuel assembly to the basket cell walls. This model recognizes the combined effects of conduction (through helium) and radiation using finite element methods.
- ii. The second model considers heat transport within an MPC cross section by conduction and radiation. This model computes an effective cross sectional conductivity of the fuel basket.
- iii. The third model deals with the transmission of heat from the MPC exterior surface to the external environment (heat sink). From the MPC shell to the cask exterior surface, heat is conducted through an array of concentric shells representing the MPC-to-overpack helium gap, the overpack inner shell, the intermediate shells, the Holtite-A neutron shielding and finally the overpack outer shell. Heat rejection from the outside cask surfaces to ambient air is considered by accounting for natural convection and thermal radiation heat transfer from the cask external surfaces. Insolation on exposed cask surfaces is based on 12-hour

levels prescribed in 10CFR71, averaged over a 24-hour period.

Detailed descriptions of the above models are provided in Section 3.4. Using these steps, effective properties of the fuel, MPC and HI-STAR HB overpack are obtained and used in an axi-symmetric rendering of the cask geometry. For a conservative portrayal of cask temperatures the thermal evaluation incorporates the following assumptions:

- a) Fuel basket conductivity is understated.
- b) Neutron shield conductivity is understated.
- c) A theoretical bounding absorptivity of 1.0 assumed for insulation.
- d) Heat dissipation by internal helium motion is ignored.
- e) The ends of the overpack are assumed to be insulated.
- f) To conservatively bound the hottest fuel the cask decay heat is non-uniformly distributed with a robust peaking in the interior.

Thermal analysis results are provided in the next section.

3.I.4.1.1 Evaluation of Damaged and Undamaged Fuel Assemblies

The HI-STAR HB cask is designed to store damaged and undamaged fuel assemblies ("Damaged" and "Undamaged Fuel Assemblies" are defined in Table 1.0.1). From a thermal perspective, damaged fuel assemblies storage is limiting because damaged fuel must be placed in a Damaged Fuel Container (DFC) which blocks radiation heat dissipation from the fuel assemblies. To bound the HI-STAR HB thermal condition in a conservative manner all fuel assemblies placed in the HI-STAR HB cask are assumed to be "Damaged" and in DFCs.

3.I.4.2 Maximum Temperatures

As discussed in the previous section, an axi-symmetric model of the HI-STAR HB is constructed for thermal evaluation. This model adopts the same methodology used in the generic HI-STAR cask thermal analysis. To this model design basis heat loads (Table 3.I.2) and 10CFR71 inputs (100°F ambient temperature and Table 3.4.7 insolation) are imposed and steady state cask temperatures obtained. The results are provided in Table 3.I.3.

3.I.4.3 Minimum Temperatures

As specified in 10CFR71, the minimum ambient temperature conditions for the HI-STAR System are -20°F and a cold environment at -40°F. The HI-STAR System design does not have any minimum decay heat load restrictions for transport. Therefore, under bounding cold conditions (zero decay heat and no insolation), the cask temperatures will approach ambient conditions. All HI-STAR System materials of construction satisfactorily perform their intended function at these cold temperatures. Evaluations in Chapter 2 demonstrate the acceptable structural performance of the overpack and MPC steel materials at low temperature. Shielding and criticality functions of the cask materials are unaffected by cold.

3.1.4.4 Maximum Internal Pressures

The Humboldt Bay multi-purpose canisters (MPC HB) are pressurized with helium prior to sealing the lid ports. In Table 3.1.4 the initial backfill pressures are listed. In response to higher than ambient transport temperatures the helium pressure rises above the initial backfill pressures. In accordance with NUREG-1617 the maximum normal operating pressure (MNOP) is computed assuming normal operating temperatures and 3% fuel rods are ruptured. For conservatism, the MPC HB is assumed to be backfilled at the maximum backfill pressure (See Table 3.1.4). The normal transport pressures are provided in Table 3.1.5.

3.1.4.5 Maximum Thermal Stresses

Thermal expansion induced mechanical stresses are evaluated, using bounding temperature distributions, in Chapter 2.

3.1.4.6 Evaluation of Normal Transport

Based on a comparison of HI-STAR HB normal transport conditions (Tables 3.1.3 and 3.1.5) with generic HI-STAR temperatures and pressures (Tables 3.4.10, 3.4.11 and 3.4.15) we conclude the following:

- a) Fuel temperatures are bounded by generic HI-STAR.
- b) Containment boundary temperatures are bounded by generic HI-STAR.
- c) Surface temperatures are bounded by generic HI-STAR.
- d) MNOP is bounded by generic HI-STAR.

As the HI-STAR HB temperatures and pressures are bounded by the generic HI-STAR package transport evaluation and the HI-STAR complies with 10CFR Part 71 and ISG 11, Rev. 3 requirements (See Section 3.6) we conclude that the HI-STAR HB package is in compliance with the 10CFR Part 71 and ISG 11, Rev. 3 requirements for normal transport.

3.1.5 HYPOTHETICAL ACCIDENT THERMAL EVALUATION

In compliance with 10CFR71 requirements, the HI-STAR System is evaluated for hypothetical accident conditions. The accident scenarios are: (1) a 30 foot free drop onto an unyielding surface; (2) a 40-inch drop onto a mild steel bar; and (3) exposure to a 30-minute fire at 1475 °F. The effects of the drop accidents (items (1) and (2)) are evaluated in Chapter 2. In this section the effect of a 30-minute fire are evaluated.

The HI-STAR HB is a short height version of the generic HI-STAR overpack. This version includes a solid shell of a low conductivity material (Holtite-A) in the neutron shield region. The HI-STAR HB initial conditions (normal transport) are bounded by HI-STAR generic temperatures and pressures. Based on the above information the following observations apply to HI-STAR HB fire evaluation:

<i>Observation</i>	<i>Basis</i>
<i>Fire heat input to HI-STAR HB overpack is bounded by the generic HI-STAR</i>	<i>Exposed area of overpack is bounded by generic design</i>
<i>Rate of through-overpack fire heat transmission is bounded by generic HI-STAR</i>	<i>HI-STAR HB overpack design features a neutron shield ring without ribs (See discussion in Section 3.I.1)</i>
<i>Start of fire conditions are bounded by generic HI-STAR</i>	<i>See 3.I.4.6</i>

Based on the observations above we conclude that the generic HI-STAR fire evaluation is bounding and the HI-STAR HB package complies with the 10CFR Part 71 requirements for hypothetical accidents.

3.I.6 REGULATORY COMPLIANCE

The Humboldt Bay cask evaluations for normal transport and hypothetical accident conditions show that the HI-STAR HB is bounded by the generic HI-STAR (See Sections 3.I.4.6 and 3.I.5). Accordingly, the regulatory compliance evaluated in Section 3.6 for HI-STAR cask applies to HI-STAR HB.

3.I.7 REFERENCES

- [3.I.1] "Holtite A: Development History and Thermal Performance Data", Holtec Report HI-2002396, Rev. 3., Holtec International, Marlton, NJ, 08053.*
- [3.I.2] "Holtite-A: Results of Pre-and-Post-Irradiation Tests and Measurements", Holtec Report HI-2002420, Rev. 1.*

Table 3.I.1: Holtite A Thermal Conductivity Data [3.I.1]

<i>Temperature</i>	<i>Conductivity (Btu/ft-hr-°F)</i>
106	0.543
154	0.537
208	0.509
252	0.488
306	0.480

Table 3.I.2: HI-STAR HB Thermal Payload

<i>Fuel Decay Heat</i>	<i>2 kW</i>
------------------------	-------------

Table 3.I.3: Maximum Normal Transport Temperatures

<i>Component</i>	<i>Temperature (°F)</i>
<i>Fuel Cladding</i>	<i>419</i>
<i>MPC Shell</i>	<i>162</i>
<i>Overpack Inner Shell</i>	<i>156</i>
<i>Overpack Top Plate</i>	<i>129</i>
<i>Overpack Bottom Plate</i>	<i>154</i>
<i>Overpack Outer Shell</i>	<i>147</i>

Table 3.I.4: Helium Backfill Pressures

<i>Minimum Pressure¹</i>	<i>45.2 psig @ 70°F</i>
<i>Maximum Pressure</i>	<i>48.8 psig @ 70°F</i>

¹ As MPC internal convection is conservatively neglected in transport evaluations the minimum required helium backfill pressure is 0 psig. This value is adopted in the transport CoC requirements for HI-STAR HB.

Table 3.1.5: HI-STAR HB Normal Operating Pressures

<i>Condition</i>	<i>Pressure (psig)</i>
<i>Initial Backfill</i>	<i>48.8</i>
<i>Normal Transport</i>	<i>68.82</i>
<i>MNOP (with 3% rods rupture)</i>	<i>69.72²</i>

² According to ISG-7, a 100% rods rupture evaluation is required for casks within 10% of the vessel design pressure (See Section 3.4.1.1.17). As the HI-STAR HB maximum normal operating pressure is below the regulatory threshold (90 psig) a 100% rods rupture evaluation is not required.

CHAPTER 4: CONTAINMENT

4.0 INTRODUCTION

This chapter demonstrates the HI-STAR 100 containment boundary compliance with the permitted activity release limits specified in 10CFR71, 71.51(a)(1) and 71.51(a)(2) for both normal and hypothetical accident conditions of transport [4.0.1]. Satisfaction of the containment criteria, expressed as the leakage rate acceptance criterion ($\text{atm}\cdot\text{cm}^3/\text{sec}$, Helium), ensures that the HI-STAR 100 package will not exceed the specified allowable radionuclide release rates. Leakage rates are determined in accordance with the recommendations of ANSI N14.5 [4.0.2], and utilizing NUREG/CR-6487, *Containment Analysis for Type B Packages Used to Transport Various Contents* [4.0.3], Regulatory Guide 7.4, *Leakage Tests on Packages for Shipment of Radioactive Materials* [4.0.4] as content guides, and Draft NUREG-1617, *Standard Review Plan for Transportation Packages for Spent Nuclear Fuel* [4.0.5].

The HI-STAR 100 packaging allowable leakage rates established herein ensures that the requirements of 10CFR71.51 and ~~10CFR71.63(b)~~ are met. The ~~primary~~ containment system boundary for the HI-STAR 100 packaging consists of the overpack inner shell, the bottom plate, the top flange, the top closure plate, closure bolts, the overpack vent and drain port plugs, and their respective mechanical seals. ~~The secondary containment system boundary for a HI-STAR 100 packaging containing BWR fuel debris in the MPC 68F or Trojan PWR fuel debris in the MPC 24EF consists of the MPC enclosure vessel including the MPC shell, the MPC bottom plate, the MPC lid, closure ring, and vent and drain port cover plates. The MPC 24EF and MPC 68F each provide the separate inner container per 10CFR71.63(b) for the HI-STAR 100 System transporting fuel classified as fuel debris. The other MPC designs (MPC 24, MPC 24E, MPC 32 and MPC 68) are not currently evaluated for secondary containment requirements.~~

Chapter 2 of this SAR shows that all ~~primary and secondary~~ containment boundary components are maintained within their code-allowable stress limits during all normal and hypothetical accident conditions of transport as defined in 10CFR71.71 and 10CFR71.73. Chapter 3 of this SAR shows that the peak containment component temperatures and pressures are within the design basis limits for all normal and hypothetical accident conditions of transport as defined in 10CFR71.71 and 10CFR71.73. Since both the ~~primary and secondary~~ containment boundaries ~~are~~ is shown to remain intact, and the temperature and pressure design bases are not exceeded, the design basis leakage rates are not exceeded during normal or hypothetical accident conditions of transport.

The HI-STAR overpack is subjected to a containment system fabrication verification test before the first use as described in Chapter 8. The containment system fabrication verification test is performed at the factory as part of the HI-STAR 100 acceptance testing. The welds of the ~~primary~~ containment boundary, the closure plate inner seal, and the vent and drain port plug seals are helium leakage tested in accordance with ANSI N14.5. A containment system periodic verification test as described in Chapter 8, will be performed prior to each loaded transport. The mechanical seals of the HI-STAR 100 overpack will be replaced and retested each time the HI-STAR 100 is loaded. ~~The~~

~~secondary containment boundary system (MPC 24EF or MPC 68F) will be subjected to the fabrication verification leakage testing at the fabrication facility as described in Chapter 8 of this SAR. Prior to transport of an MPC containing fuel debris, a secondary containment boundary periodic verification leakage test will be performed as described in Chapter 8 to ensure that the measured leakage rates are below the limit specified in this chapter.~~

As the containment system periodic verification leakage test shall be performed on each the containment boundary ~~separately~~ prior to each loaded transport, this test takes the place of and is performed in lieu of the assembly verification.

4.1 CONTAINMENT BOUNDARIES

The ~~primary~~-containment system boundary for the HI-STAR 100 packaging consists of the overpack inner shell, the bottom plate, the top flange, the top closure plate, closure bolts, the overpack vent and drain port plugs, and their respective mechanical seals. The ~~primary~~-containment boundary system components for the HI-STAR 100 system are designed and fabricated in accordance with the requirements of ASME Code, Section III, Subsection NB [4.1.1], to the maximum extent practicable. Chapter 1 provides design criteria for the containment design. Section 1.3 provides applicable Code requirements. Exceptions to specific Code requirements with complete justifications are presented in Table 1.3.2. The ~~primary~~-containment boundary components are shown on Figure 4.1.1 with additional details provided in Figures 4.1.2 and 4.1.3.

~~The secondary containment system boundary for a HI-STAR 100 packaging containing fuel debris in the MPC 24EF or the MPC 68F consists of the enclosure vessel including the MPC shell, the MPC bottom plate, the MPC lid, vent and drain port cover plates and MPC closure ring. The secondary containment boundary system components for the HI-STAR 100 system are designed and fabricated in accordance with the requirements of ASME Code, Section III, Subsection NB, to the maximum extent practicable. Chapter 2 provides design criteria for the containment design. Section 1.3 provides applicable Code requirements. Alternatives to specific Code requirements with complete justifications are presented in Table 1.3.2. The secondary containment boundary components are shown in Figure 4.1.4. The use of two independent and testable containment boundaries provides the capability to load and transport the specified fuel debris in accordance with the requirements of 10CFR71.63(b) [4.0.1]. The MPC 24EF or MPC 68F each provide the separate inner container per 10CFR71.63(b) for the HI-STAR 100 System transporting fuel classified as fuel debris. The other MPC designs (MPC 24, MPC 24E, MPC 32 and MPC 68) are not currently evaluated for secondary containment requirements.~~

4.1.1 Containment Vessel

The ~~primary~~-containment vessel for the HI-STAR 100 packaging consists of the overpack components which form the inner cavity volume used to house any of the MPC designs which contain spent nuclear fuel. The ~~primary~~-containment vessel is represented by the overpack inner shell, bottom plate, the top flange, and the closure plate. These components create an enclosed cylindrical cavity sufficient for insertion and enclosure of an MPC. The materials of construction for the packaging ~~primary~~-containment vessel are specified in the drawings in Section 1.4.

~~The secondary containment vessel for the HI-STAR 100 packaging consists of either the MPC 24EF or the MPC 68F enclosure vessel complete with field installed MPC lid, closure ring, vent and drain port cover plates. The enclosure vessel components create an enclosed cylindrical cavity sufficient for insertion and enclosure of fuel debris. The materials of construction for the secondary containment vessel are specified in the drawings in Section 1.4.~~

Table 4.1.1 provides a summary of the containment boundary design specifications.

4.1.2 Containment Penetrations

The ~~primary~~ containment system boundary penetrations for the HI-STAR 100 package include the closure plate test port plug, the vent port plug, the drain port plug, and their respective mechanical seals. Each penetration has redundant mechanical seals. The vent port is located in the closure plate and the drain port is located in the bottom plate. The closure configuration of the vent and drain ports is essentially identical (See Figure 4.1.3). The ~~primary~~ containment penetrations are designed and tested to ensure that the radionuclide release rates specified in 10CFR71.51 will not be exceeded.

~~The secondary containment boundary for the HI-STAR 100 packaging is the either the MPC 24EF or the MPC 68F. The penetrations on the MPC include the MPC vent and drain port cover plates. The MPC penetrations are designed to prevent the release of radionuclides. Two penetrations (the MPC vent and drain ports) are provided in the MPC lid for MPC draining, vacuum drying and backfilling during MPC loading operations, and for fuel cool down and MPC flooding during unloading operations. No other confinement penetrations exist in the MPC. The MPC vent and drain ports are equipped with metal to metal seals to minimize leakage and withstand the long term effects of temperature and radiation. No containment credit is taken for the vent and drain mechanical seals. The vent and drain connectors allow the vent and drain ports to be operated like valves and prevent the need to hot tap into the penetrations during unloading operations. The vent and drain port covers are sealed with the fully welded vent and drain port cover plates. The MPC closure ring covers the vent and drain port cover plate welds, and the MPC lid to shell weld providing redundant closure of the MPC vessel. Both the MPC 24EF and MPC 68F are designed and tested to ensure that the radionuclide release rates specified in 10CFR71.63(b) will not be exceeded.~~

4.1.3 Seals and Welds

The HI-STAR 100 ~~primary~~ containment vessel uses a combination of seals and welds designed and tested during normal transport conditions, and during and after the hypothetical transport accident conditions. ~~The secondary containment boundary utilizes a fully welded vessel to prevent the release of radioactive materials.~~ Seals and welds are individually discussed below.

The seals and welds discussed below provides a containment systems which ~~are~~ is securely closed and ~~cannot~~ be opened unintentionally or by an internal pressure within the package as required in 10CFR71.43(c).

4.1.3.1 Containment Seals

The HI-STAR 100 closure plate uses two concentric metallic seals to form the closure between the top flange surface and the closure plate. To protect the sealing surfaces against corrosion, a stainless steel weld inlay is provided during manufacturing on both the closure plate and mating overpack surfaces. The closure plate inner seal is tested for leakage through a small test port in the overpack closure plate (See Figure 4.1.2). The test port provides access to the volume between the two mechanical lid seals for leakage testing of the closure plate inner seal. Following leakage testing, a threaded plug with a metallic seal is installed in the test port hole to provide redundant closure.

~~Primary~~ Closure of the vent and drain ports is achieved via a threaded plug with a single metallic seal. The metallic seal is compressed between the underside of the threaded plug head and the overpack body to form the seal. The sealing surfaces are not subject to corrosion due to the presence of the cover plates and their seals preventing exposure of the seal surfaces to the elements. Each port plug seal is independently tested for leakage to verify containment performance. A bolted cover plate, with a machined seal groove, is installed over the vent and drain ports. A metallic seal, installed in the cover plate groove, is compressed between the cover plate and the overpack body during cover plate bolt torquing. These cover plates provide redundant closure of the drain and vent port penetrations.

Details on the seals are provided in the drawings in Section 1.4 and in Appendix 4.B. Table 4.1.1 contains reference information for the seals from the selected supplier. Note that the seals selected are designed and fabricated to meet the design requirements of the HI-STAR 100 System. The Chapter 7 procedures require replacement of any used seal after closure opening except for transportation of an empty overpack.

~~There are no seals on the secondary containment boundary.~~

4.1.3.2 Containment Welds

The ~~primary~~ containment boundary welds of the HI-STAR 100 overpack body include the welds forming the inner closure shell, the weld connecting the inner shell to the top flange, and the weld connecting the bottom plate to the inner shell. All ~~primary~~ containment boundary welds are fabricated and inspected in accordance with ASME Code Section III, Subsection NB (no stamp required). Full-penetration welds are specified for the plates that form the overpack inner shell. Full-penetration welds are also specified for the inner shell to the top flange and bottom plate welds. The weld details are shown in the drawings in Section 1.4. The containment boundary welds are volumetrically examined by radiography (RT) as described in Chapter 8.

~~The secondary containment boundary welds of the MPC 24EF and MPC 68F include the welds forming the MPC shell, the weld connecting the shell to the MPC baseplate, and the final field closure welds described in Section 4.1.4.2. All secondary containment welds are fabricated and inspected in accordance with ASME Code Section III, Subsection NB, except for the field installed closure welds. The alternatives to the ASME Code for the secondary containment are detailed in Table 1.3.2. The weld details are shown on the MPC 24EF and MPC 68F drawings in Section 1.4. The secondary containment boundary welds are volumetrically examined by radiography (RT) or ultrasonic (UT) inspection methods as described in Chapter 8.~~

4.1.4 Closure

4.1.4.1 Primary Closure

The HI-STAR 100 packaging closure plate is secured using multiple closure bolts around the perimeter. Torquing of the closure plate bolts compresses the closure plate concentric mechanical seals between the closure plate and the overpack flange forming the closure plate seal.

Closure of the overpack vent and drain ports is provided by a single threaded plug installed in each penetration (see Figure 4.1.3). The mechanical seal is compressed between the underside of the port plug head and the overpack body forming the primary port closure. A cover plate, containing a single metallic seal, is installed over each of the ports forming the redundant closure of the vent and drain port penetrations. The cover plate is secured by bolts. The closure plate test port is sealed using a port plug and mechanical seal in the same manner as the vent and drain port penetrations (see Figure 4.1.2).

The installation procedures, bolt torquing patterns, required lubrication, and torque values are provided in Table 7.1.13. The torque values are established to maintain containment during normal and accident conditions of transport. Torque values for the closure plate bolts were determined to preclude separation of the closure plate from the overpack flange. Appendix 4.A contains the calculations for the test, vent and drain port plugs and the vent and drain port cover plates bolt torques.

Table 4.1.2 provides a summary of the containment closure bolting for the HI-STAR 100 overpack penetrations.

4.1.4.2 Secondary Closure

~~The secondary closure of the HI-STAR 100 packaging is provided by the MPC lid which is welded to the MPC shell. Following fuel loading and MPC lid welding, the MPC lid to shell weld may be examined by either volumetric or multi-layer liquid penetrant examination. If volumetric examination is used, it shall be the ultrasonic method and shall include a PT of the root and final weld layers. If PT alone is used, at a minimum, it must include the root and final weld layers and sufficient intermediate layers to detect critical weld flaws.~~

~~Then the MPC lid to shell weld is helium leakage tested and hydrostatic tested. If the MPC lid weld is acceptable, the vent and drain port cover plates are welded in place, examined by the liquid penetrant method (root and final), and a leakage rate test is performed. Finally, the MPC closure ring (with no closure ring penetrations) is installed, welded and inspected by the liquid penetrant method (root and final).~~

~~Alternatively, the MPC lid to shell weld is only hydrostatic tested. If the MPC lid weld is acceptable, the vent and drain port cover plates are welded in place, examined by liquid penetrant method (root and final). The MPC closure ring, with the closure ring penetrations, is installed, welded and inspected by the liquid penetrant method (root and final) and a leakage rate test is performed on the MPC lid to shell weld and vent and drain port cover plates. The closure ring penetrations are welded and inspected by the liquid penetrant method (final).~~

4.1.5 Damaged Fuel Container

Fuel assemblies classified as damaged fuel or fuel debris (assembly array/class 6x6A, 6x6B, 6x6C, 7x7A, and 8x8A for BWR fuel as specified in Table 1.2.11 and Trojan damaged fuel and fuel debris for PWR fuel as specified in Table 1.2.10) have been evaluated.

The MPC is designed to transport damaged fuel, fuel debris, or intact fuel. ~~The sole additional requirement imposed on an MPC to load fuel debris is an additional leakage rate criteria test just prior to shipment. Therefore, an MPC which is to transport fuel debris will be designated to ensure the proper leakage rate test criteria is applied. To distinguish an MPC which is fabricated to transport fuel debris, the MPC will be designated with an "F" after the MPC designation (i.e. MPC-68F or MPC-24EF)~~

To aid in loading and unloading, damaged fuel assemblies and fuel debris will be loaded into stainless steel DFCs ~~prior to placement in the HI-STAR 100 System~~. The damaged fuel container (DFC) is shown in the drawings in Section 1.4. The DFC is designed to provide SNF loose component retention and handling capabilities. The DFC consists of a smooth-walled, welded stainless steel square canister with a removable lid. The canister lid provides the means of DFC closure and handling. The DFC is provided with stainless steel wire mesh screens in the top and bottom for draining, ~~vacuum~~ drying and helium backfill operations. The screens are specified as a 250-by-250-mesh with an effective opening of 0.0024 inches. There are no other openings in the DFC. Chapter 1 specifies the fuel assembly characteristics for damaged fuel acceptable for loading in the MPC-68, MPC-68F, or MPC-24EF and for fuel debris acceptable for loading in the MPC-68F or MPC-24EF.

Up to four (4) DFCs containing specified fuel debris may be placed in a custom-designed Trojan MPC-24EF (Trojan PWR fuel debris) or an MPC-68F (BWR fuel debris). Up to 4 PWR damaged fuel assemblies in DFCs may be transported in a custom-designed Trojan MPC-24EF or up to 68 BWR damaged fuel assemblies in DFCs may be transported in an MPC-68 or MPC-68F, respectively. The quantity of fuel debris is limited to meet the off-site transportation requirements of 10CFR71, specifically, 10CFR71.51~~63~~(a)(1). Analyses provided in this chapter conservatively assume 100% of the rods of the fuel debris are breached under normal conditions of transport. Therefore, 100% of the contents of the DFCs are available for release.

Table 4.1.1

SUMMARY OF CONTAINMENT BOUNDARY DESIGN SPECIFICATIONS

Design Attribute	Design Rating	
	Primary (Overpack) 10CFR71.51	Secondary (MPC) 10CFR71.63(b)
Closure Plate Mechanical Seals: ^{††} Design Temperature Pressure Rating Design Leakage Rate	1200°F 1,000 psig 1×10^{-6} cm ³ /s, Helium	N/A
Overpack Vent and Drain Port Cover Plate Mechanical Seals: ^{†,††} Design Temperature Pressure Rating Design Leakage Rate	1200°F 1,000 psig 1×10^{-6} cm ³ /sec, Helium	N/A
Overpack Vent and Drain Port Plug Mechanical Seals: ^{††} Design Temperature Pressure Rating Design Leakage Rate	1200°F 1,000 psig 1×10^{-6} cm ³ /sec, Helium	N/A
Leakage Rate Acceptance Criterion	4.3×10^{-6} atm cm ³ /s, He	5.0×10^{-6} atm cm ³ /s, He
Leakage Rate Test Sensitivity	2.15×10^{-6} atm cm ³ /s, He	2.5×10^{-6} atm cm ³ /s, He

[†] No credit is taken for the overpack vent and drain port cover plate seals as part of the containment boundary. Specifications are provided for information.

^{††} Per manufacturer's recommended operating limits.

Table 4.1.2

CONTAINMENT CLOSURE BOLTING SUMMARY

Item	Qty	Type	Material
Closure Plate Bolt (Long)	52	1-5/8"-8 UNC x 7-3/8" LG Cap Screw	SB-637-N07718
Closure Plate Bolt (Short)	2	1-5/8"-8 UNC x 7-1/8" LG Cap Screw	SB-637-N07718
Vent/Drain Port Cover Plate Bolt	4 ea	3/8 -16 UNC x 5/8" LG Cap Screw	SA-193 GRADE B7
Vent/Drain/Closure Plate Test Port Plugs	1 ea	7/8" diameter Fabricated Plug	SA-193 GRADE B8

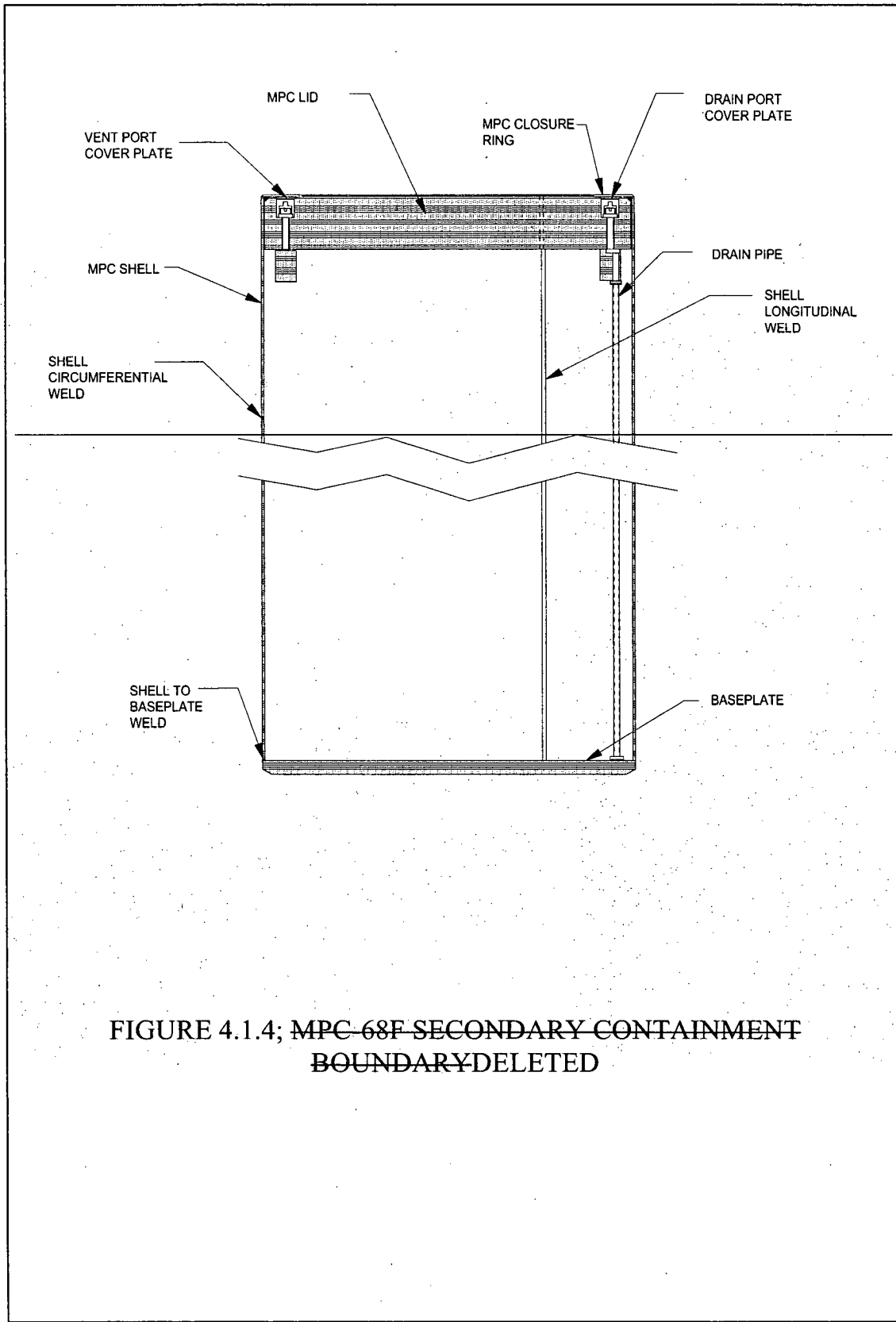


**FIGURE 4.1.4; MPC-68F SECONDARY CONTAINMENT
BOUNDARY DELETED**

4.2 REQUIREMENTS FOR NORMAL AND HYPOTHETICAL ACCIDENT CONDITIONS OF TRANSPORT

Chapter 2 shows that all ~~primary and secondary~~ containment components are maintained within their code-allowable stress limits during all normal and hypothetical accident conditions of transport as defined in 10CFR71.71 and 10CFR71.73 [4.0.1]. Chapter 3 shows that the peak containment component temperatures and pressure are within the design basis limits for all normal and hypothetical accident conditions of transport as defined in 10CFR71.71 and 10CFR71.73. Since the ~~primary and secondary~~ containment vessels remains intact, and the temperature and pressure design bases are not exceeded, the design basis leakage rate (see Table 4.1.1) will not be exceeded during normal or hypothetical accident conditions of transport.

4.2.1 Containment Criteria

The allowable leakage rates presented in this chapter were determined in accordance with ANSI N14.5-1997 [4.0.2] and shall be used for containment system fabrication verification and containment system periodic verification tests of the HI-STAR 100 containment boundaries. Measured leakage rates shall not exceed the values presented in Table 4.1.1. Compliance with these leakage rates ensures that the radionuclide release rates specified in 10CFR71.51 and ~~10CFR71.63(b)~~ will not be exceeded during normal or hypothetical accident conditions of transport.

4.2.2 Containment of Radioactive Material

The HI-STAR 100 packaging allowable leakage rate (See Table 4.1.1) ensures that the requirements of 10CFR71.51 and ~~10CFR71.63(b)~~ are met. Section 4.2.5 determines the maximum leakage rate for normal and hypothetical accident conditions of transport and the allowable leakage rate criterion for the HI-STAR 100 packaging containing each of the MPC types. The maximum calculated leakage rates for normal transport conditions assume a full complement of design-basis fuel assembly types with bounding radiological source terms. The calculations also assume 3% fuel rod rupture for normal conditions. This bounds all possible MPC fuel loading configurations. For calculating the maximum leakage rates for normal conditions of transport, the internal pressure is conservatively assumed to be greater than the MPC internal pressure for the most limiting MPC type determined in Chapter 3. Following testing, no credit is taken for the MPC as a containment boundary ~~for the transport of intact fuel. The MPC enclosure vessel is identified as the secondary containment boundary for the transport of the specified fuel debris in accordance with the 10CFR71.63(b) requirements for a separate inner container.~~

The allowable leakage rate is then conservatively chosen to be less than the calculated maximum leakage rates from all MPC types for normal conditions of transport. This ensures that the 10CFR71.51(a)(1) and ~~71.63(b)~~ limits for radionuclide release are not exceeded.

4.2.3 Pressurization of Containment Vessel

The HI-STAR 100 overpack contains a sealed MPC during normal conditions of transport. Except for the small space between the MPC and overpack, the overpack internal cavity is essentially filled. This space (annulus) is drained, dried, evacuated and backfilled with helium gas prior to final

closure of the overpack; therefore, no vapors or gases are present which could cause a reaction or explosion inside the overpack. Procedural steps (Chapter 7) prevent overpack over-pressurization during closure operations. The enclosed MPC is also drained, dried, and backfilled with helium gas prior to final closure; therefore, any MPC leak would not introduce any explosive gases into the overpack cavity. Since the exterior of the MPC is entirely composed of stainless steel, there is no possibility of chemical reaction that would produce gas or vapor. The overpack accident condition design basis internal pressure analysis assumes a non-mechanistic event resulting in the loss of MPC closure welds, a full-complement of design basis fuel with 100% fill gas and 30% of significant fission gas release, and the hypothetical 10CFR71.73(c)(4) fire condition. Even in this event, structural integrity and containment of the HI-STAR 100 packaging are maintained.

As the MPC is drained, dried, evacuated and backfilled with helium gas, no vapors or gases are present which could cause a reaction or explosion inside the MPC. Procedural steps (Chapter 7) prevent MPC over-pressurization during closure operations. The interior of the MPC contains stainless steel, ~~Boron~~ *neutron absorber*, and optional aluminum heat conductive inserts. There is no possibility of chemical reaction that would produce gas or vapor.

4.2.4 Assumptions

The HI-STAR 100 System is designed to meet the radioactive release limit requirements of 10CFR71.51 and ~~10CFR71.63(b)~~. Allowable leakage rates are determined in accordance with the requirements of ANSI N14.5, and utilizing NUREG/CR-6487, *Containment Analysis for Type B Packages Used to Transport Various Contents* [4.0.3] and Regulatory Guide 7.4, *Leakage Tests on Packages for Shipment of Radioactive Materials* [4.0.4] as guides.

The following assumptions have been used in determining the allowable leakage rates:

1. For MPCs other than the MPC-24EF with Trojan fuel debris and MPC-68F, three percent of the fuel rods are assumed to have failed during normal conditions of transportation. One-hundred percent of the fuel rods are assumed to have failed during hypothetical accident conditions.
2. Thirty percent of the radioactive gases are assumed to escape each failed fuel rod.
3. Fifteen percent of the ^{60}Co from the crud on the surface of the fuel rods is released as an aerosol in normal conditions of transport. One-hundred percent of the ^{60}Co is released as an aerosol from the surfaces of the fuel assemblies during accident conditions.
4. Since the overpack internals are never exposed to contaminants, the residual activity on the overpack interior surface and the MPC exterior surface is negligible compared to crud deposits on the fuel and is neglected as a source term.
5. Up to four (4) DFCs containing specified fuel debris may be placed in an MPC-24EF (only the custom-designed Trojan MPC-24EF) or an MPC-68F.
6. Crud spallation and cladding breaches occur instantaneously after fuel loading and container

closure operations.

7. The calculation for normal transport conditions of an MPC containing fuel debris assumes 100% of the rods of the fuel debris are breached.
8. For containment analysis purposes, the MPC-24, MPC-24E or MPC-24EF contain up to 24 PWR assemblies, of which 4 of these in the custom-designed Trojan MPC-24EF may be DFCs with Trojan fuel debris, the MPC-32 contains up to 32 PWR assemblies, the MPC-68 contains up to 68 BWR assemblies, and the MPC-68F contains up to 68 intact BWR fuel assemblies, of which 4 of those may be specified BWR fuel debris in damaged fuel containers.
9. 0.003% of the total fuel mass contained in a rod is assumed to be released as fines if the cladding on the rod ruptures (i.e., $f_r=3 \times 10^{-5}$).
10. Bounding values for the crud surface activity for PWR rods is 140×10^{-6} Ci/cm² and for BWR rods is 1254×10^{-6} Ci/cm².
11. The rod surface area per assembly is 3×10^5 cm² for PWR and 1×10^5 cm² for BWR fuel assemblies. These surface areas are also conservatively used for the surface area of damaged fuel or fuel debris..
12. The release fractions for volatiles (⁸⁹Sr, ⁹⁰Sr, ¹⁰³Ru, ¹⁰⁶Ru, ¹³⁴Cs, ¹³⁵Cs, and ¹³⁷Cs) are all assumed to be 2×10^{-4} ($f_v=2 \times 10^{-4}$).
13. In the analysis of the ~~primary~~ containment boundary, *no credit is taken for the presence of the seal welded MPC. the MPC is assumed to rupture. In the analysis of the secondary containment boundary, the primary containment is assumed to fail.*
14. In calculating the leakage rates of the ~~primary~~ containment system for normal conditions of transport, the internal pressure of the overpack is conservatively assumed to be *equal to or larger than the maximum internal pressure of all MPC types determined in Chapter 3.*
15. The average cavity temperature for all *accident* analyses is conservatively assumed to be the design basis peak cladding temperature.
16. All of the activity associated with crud is assumed to be Cobalt-60.
17. It is assumed that the flow is unchoked for all leakage analyses.
18. ~~Deleted In the evaluation to demonstrate compliance with 10CFR71.63(b), the source activity due to Plutonium was determined by conservatively assuming that all of the rods develop cladding breaches during normal transportation and hypothetical accident conditions (i.e., $f_B=1.0$).~~
19. ~~Deleted In the evaluation to demonstrate compliance with 10CFR71.63(b), the assumption~~

was also made that roughly 0.003% of the plutonium is released from a fuel rod (i.e., $f_{pu}=3 \times 10^{-5}$).

4.2.5 Analysis and Results

The allowable leakage rates for the ~~primary and secondary~~ containment boundaries under normal and hypothetical accident conditions of transport at operating conditions for the HI-STAR 100 packaging containing each of the MPC types were determined and are presented in this chapter. To calculate the leakage rates for a particular contents type and transportation condition, the following were determined: the source term concentration for the releasable material; the effective A_2 of the individual contributors; the releasable activity; the effective A_2 for the total source term; the allowable radionuclide release rates; and the allowable leakage rates at transport (operating) conditions. Using the equations for continuum and molecular flow, the corresponding leakage hole diameters were calculated. Then, using these leak hole diameters, the corresponding allowable leakage rates at test conditions were calculated. Parameters were utilized in a way that ensured conservatism in the final leakage rates for the conditions, contents, and package arrangements considered.

The methodology and analysis results are summarized below.

4.2.5.1 Volume in the Containment Vessel

As discussed above, the ~~primary~~ containment system boundary for the HI-STAR 100 packaging consists of the overpack inner shell and associated components ~~and the secondary containment system boundary consists of the MPC enclosure vessel and associated components~~. The MPC provides the separate inner container per 10CFR71.63(b) for the HI-STAR 100 System transporting fuel classified as fuel debris.

Except for a small volume between the MPC and the overpack (the annulus), the overpack internal cavity is essentially filled. Therefore, the free gas volume for the ~~primary~~ containment boundary includes the free gas volume for the MPC plus the overpack annulus volume. The free gas volume in each of the MPC types is presented in Chapter 3. The free gas volumes of the ~~primary and secondary~~ containment system are repeated in Table 4.2.1 for completeness. The MPC-24E and MPC-24EF basket designed for Trojan are shorter to allow for storage in their overpacks. These shorter baskets are designated as the Trojan MPC-24E and Trojan MPC-24EF, respectively, where necessary. For calculating the free volume in the ~~primary~~ containment system (overpack) with either of the Trojan MPCs, the annulus space is assumed to be the same as that for the larger generic MPCs (i.e. the larger annulus space between the Trojan MPC and HI-STAR overpack is neglected). This will conservatively underestimate the free volume inside the ~~primary~~ containment boundary.

4.2.5.2 Source Terms For Spent Nuclear Fuel Assemblies

In accordance with NUREG/CR-6487 [4.0.3], the following contributions are considered in determining the releasable source term for packages designed to transport irradiated fuel rods: (1) the radionuclides comprising the fuel rods, (2) the radionuclides on the surface of the fuel rods, and

(3) the residual contamination on the inside surfaces of the vessel. NUREG/CR-6487 goes on to state that a radioactive aerosol can be generated inside a vessel when radioactive material from the fuel rods or from the inside surfaces of the container become airborne. The sources for the airborne material are (1) residual activity on the cask interior, (2) fission and activation-product activity associated with corrosion-deposited material (crud) on the fuel assembly surface, and (3) the radionuclides within the individual fuel rods. In accordance with NUREG/CR-6487, contamination due to residual activity on the cask interior surfaces is negligible as compared to crud deposits on the fuel rods themselves and therefore may be neglected. The source term considered for this calculation results from the spallation of crud from the fuel rods and from the fines, gases and volatiles which result from cladding breaches.

The inventory for isotopes other than ^{60}Co is calculated with the SAS2H and ORIGEN-S modules of the SCALE 4.3 system as described in Chapter 5. The inventory for the MPC-24, MPC-24E, MPC-24EF, and MPC-32 was conservatively based on the B&W 15x15 fuel assembly with a burnup of 45,000 MWD/MTU, 5 years of cooling time, and an enrichment of 3.6%. The inventory for the Trojan MPCs (Trojan MPC-24E, Trojan MPC-24EF) was based on the Westinghouse 17x17 fuel assembly with a burnup of 42,000 MWD/MTU, 9 years cooling time, and an enrichment of 3.09%. The inventory for the MPC-68 was based the GE 7x7 fuel assembly with a burnup of 45,000 MWD/MTU, 5 years of cooling time, and 3.2% enrichment. The inventory for the MPC-68F was based on the GE 6x6 fuel assembly with a burnup of 30,000 MWD/MTU, 18 years of cooling time, and 1.8% enrichment. Additionally, an MPC-68F was analyzed containing 67 GE 6x6 assemblies and a DFC containing 18 thorium rods. Finally, an Sb-Be source stored in one fuel rod in one assembly with 67 GE 6x6 assemblies was analyzed. The isotopes which contribute greater than 0.01% to the total curie inventory for the fuel assembly are considered in the evaluation as fines. Additionally, isotopes with A_2 values less than 1.0 in Table A-1, Appendix A, 10CFR71 are included as fines. Isotopes which contribute greater than 0.01% but which do not have an assigned A_2 value in Table A-1 are assigned an A_2 value based on the guidance in Table A-32, Appendix A, 10CFR71. Isotopes which contribute greater than 0.01% but have a radiological half life less than 10 days are neglected. Table 4.2.2 presents the isotope inventory used in the calculation.

A. Source Activity Due to Crud Spallation from Fuel Rods

The majority of the activity associated with crud is due to ^{60}Co [4.0.3]. The inventory for ^{60}Co was determined by using the crud surface activity for PWR rods ($140 \times 10^{-6} \text{ Ci/cm}^2$) and for BWR rods ($1254 \times 10^{-6} \text{ Ci/cm}^2$) provided in NUREG/CR-6487 [4.0.3] multiplied by the surface area per assembly ($3 \times 10^5 \text{ cm}^2$ and $1 \times 10^5 \text{ cm}^2$ for PWR and BWR, respectively, also provided in NUREG/CR-6487).

The source terms were then decay corrected (5 years for the MPC-24, MPC-24E, MPC-24EF, MPC-32 and the MPC-68; 18 years for the MPC-68F; 9 years for the Trojan MPCs) using the basic radioactive decay equation:

$$A(t) = A_0 e^{-\lambda t} \quad (4-1)$$

where:

- A(t) is activity at time t [Ci]
A_o is the initial activity [Ci]
λ is the ln2/t_{1/2} (where t_{1/2} = 5.272 years for ⁶⁰Co)
t is the time in years (5 years for the MPC-24, MPC-24E, MPC-24EF, MPC-32 and the MPC-68; 18 years for the MPC-68F; 9 years for the Trojan MPCs)

The inventory for ⁶⁰Co was determined using the methodology described above with the following results:

PWR

Surface area per Assy = 3.0E+05 cm²
140 μCi/cm² x 3.0E+05 cm² = 42.0 Ci/assy

BWR

Surface area per Assy = 1.0E+05 cm²
1254 μCi/cm² x 1.0E+05 cm² = 125.4 Ci/assy

⁶⁰Co(t) = ⁶⁰Co₀ e^{-(λt)}, where λ = ln2/t_{1/2}, t = 5 years (for the MPC-24, MPC-24E, MPC-24EF, MPC-32 and MPC-68), t = 18 years (MPC-68F), t = 9 years (Trojan MPCs), t_{1/2} = 5.272 years for ⁶⁰Co [4.2.4]

MPC-24, MPC-24E, MPC-24EF, MPC-32

⁶⁰Co(5) = 42.0 Ci e^{-(ln 2/5.272)(5)}
⁶⁰Co(5) = 21.77 Ci/assy

MPC-68

⁶⁰Co(5) = 125.4 Ci e^{-(ln 2/5.272)(5)}
⁶⁰Co(5) = 64.98 Ci/assy

Trojan MPC-24E, Trojan MPC-24EF

⁶⁰Co(5) = 42.0 Ci e^{-(ln 2/5.272)(9)}
⁶⁰Co(5) = 12.86 Ci/assy

MPC-68F

⁶⁰Co(18) = 125.4 Ci e^{-(ln 2/5.272)(18)}
⁶⁰Co(18) = 11.76 Ci/assy

A summary of the ⁶⁰Co inventory available for release is provided in Table 4.2.2.

The activity density that results inside the containment vessel as a result of crud spallation from spent fuel rods can be formulated as:

$$C_{\text{crud}} = \frac{f_C M_A N_A}{V} \quad (4-2)$$

where:

- C_{crud} is the activity density inside the containment vessel as a result of crud spallation [Ci/cm³],
M_A is the total crud activity inventory per assembly [Ci/assy],
f_C is the crud spallation fraction,
N_A is the number of assemblies, and
V is the free volume inside the containment vessel [cm³].

NUREG/CR-6487 states that measurements have shown 15% to be a reasonable value for the percent of crud spallation for both PWR and BWR fuel rods under normal transportation conditions. For hypothetical accident conditions, it is assumed that there is 100% crud spallation [4.0.3].

B. Source Activity Due to Releases of Fines from Cladding Breaches

A breach in the cladding of a fuel rod may allow radionuclides to be released from the resulting cladding defect into the interior of the MPC. If there is a leak in the ~~primary or secondary~~ containment vessels, then the radioisotopes emitted from a cladding breach that were aerosolized may be entrained in the gases escaping from the package and result in a radioactive release to the environment.

NUREG/CR-6487 suggests that a bounding value of 3% of the rods develop cladding breaches during normal transportation (i.e., $f_B=0.03$). For hypothetical accident conditions, it is assumed that all of the rods develop a cladding breach (i.e., $f_B=1.0$). These values were used for both PWR and BWR fuel rods. As described in NUREG/CR-6487, roughly 0.003% of the fuel mass contained in a rod is released as fines if the cladding on the rod ruptures (i.e., $f_f=3 \times 10^{-5}$).

The calculation for normal transport conditions of either a Trojan MPC-24EF or an MPC-68F containing four (4) DFCs containing fuel debris assumes that for the four DFCs, 100% of the rods of the fuel debris are breached. The remaining 20 or 64 assemblies in either the Trojan MPC-24EF or the MPC-68F, respectively, were assumed to have a 3% cladding rupture. Therefore, f_B for a Trojan MPC-24EF or an MPC-68F containing fuel debris is:

$$f_B = (0.03) \frac{20}{24} + (1.0) \frac{4}{20} \quad (4-3a)$$

$$f_B = 0.192$$

$$f_B = (0.03) \frac{64}{68} + (1.0) \frac{4}{68} \quad (4-3b)$$

$$f_B = 0.087$$

The activity concentration inside the containment vessel due to fines being released from cladding breaches is given by:

$$C_{fines} = \frac{f_f I_{fines} N_A f_B}{V} \quad (4-4)$$

where:

- C_{fines} is the activity concentration inside the containment vessel as a result of fines released from cladding breaches [Ci/cm^3],
- f_f is the fraction of a fuel rod's mass released as fines as a result of a cladding breach ($f_f=3 \times 10^{-5}$),
- I_{fines} is the total activity inventory [Ci/assy],
- N_A is the number of assemblies,
- f_B is the fraction of rods that develop cladding breaches, and
- V is the free volume inside the containment vessel [cm^3].

C. Source Activity from Gases due to Cladding Breaches

If a cladding failure occurs in a fuel rod, a large fraction of the gap fission gases will be introduced into the free volume of the system. Tritium and Krypton-85 are typically the major sources of radioactivity among the gases present [4.0.3]. NUREG/CR-6487 suggests that a bounding value of 30% of the fission product gases escape from a fuel rod as a result of a cladding breach (i.e., $f_g=0.3$).

The activity concentration due to the release of gases from a cladding breach is given by:

$$C_{\text{gases}} = \frac{f_g I_{\text{gases}} N_A f_B}{V} \quad (4-5)$$

where:

- C_{gases} is the releasable activity concentration inside the containment vessel due to gases released from cladding breaches [Ci/cm^3],
- f_g is the fraction of gas that would escape from a fuel rod that developed a cladding breach,
- I_{gases} is the gas activity inventory [^3H , ^{129}I , ^{85}Kr , ^{81}Kr , ^{127}Xe] [Ci/assy],
- N_A is the number of assemblies,
- f_B is the fraction of rods that develop cladding breaches, and
- V is the free volume inside the containment vessel [cm^3].

D. Source Activity from Volatiles due to Cladding Breaches

Volatiles such as cesium, strontium, and ruthenium, can also be released from a fuel rod as a result of a cladding breach. NUREG/CR-6487 estimates that 2×10^{-4} is a conservative bounding value for the fraction of the volatiles released from a fuel rod (i.e., $f_v=2 \times 10^{-4}$).

The activity concentration due to the release of volatiles is given by:

$$C_{\text{vol}} = \frac{f_v I_{\text{vol}} N_A f_B}{V} \quad (4-6)$$

where:

- C_{vol} is the releasable activity concentration inside the containment vessel due to volatiles released from cladding breaches [Ci/cm^3],
- f_v is the fraction of volatiles that would escape from a fuel rod that developed a cladding breach,
- I_{vol} is the volatile activity inventory [^{89}Sr , ^{90}Sr , ^{134}Cs , ^{135}Cs , ^{137}Cs , ^{134}Cs , ^{103}Ru , ^{106}Ru] [Ci/assy],
- N_A is the number of assemblies,
- f_B is the fraction of rods that develop cladding breaches, and
- V is the free volume inside the containment vessel [cm^3].

E. Total Source Term for the HI-STAR 100 System

The total source term was determined by combining Equations 4-2, 4-4, 4-5, and 4-6:

$$C_{\text{total}} = C_{\text{crud}} + C_{\text{fines}} + C_{\text{gases}} + C_{\text{vol}} \quad (4-7)$$

where C_{total} has units of Ci/cm³.

Table 4.2.3 presents the total source term determined using the above methodology. Table 4.2.4 summarizes the parameters from NUREG/CR-6487 used in this analysis.

4.2.5.3 Effective A₂ of Individual Contributors (Crud, Fines, Gases, and Volatiles)

The A₂ of the individual contributions (i.e., crud, fines, gases, and volatiles) were determined in accordance with NUREG/CR-6487. As previously described, the majority of the activity due to crud is from Cobalt-60. Therefore, the A₂ value of 10.8 Ci used for crud for both PWR and BWR fuel is the same as that for Cobalt-60 found in 10CFR71, Appendix A.

In accordance with 10CFR71.51(b) the methodology presented in 10CFR71, Appendix A for mixtures of different radionuclides was used to determine the A₂ values for the gases, fines and volatiles.

$$A_2 \text{ for a mixture} = \frac{1}{\sum_{i=1}^I \frac{f_i}{(A_2)_i}} \quad (4-8)$$

Where f(i) is the fraction of activity of nuclide I in the mixture and A₂(i) is the appropriate A₂ value for the nuclide I.

10CFR71.51(b) also states that for Krypton-85, an effective A₂ value equal to 10 A₂ may be used. Table 4.2.5 summarizes the effective A₂ for all individual contributors.

4.2.5.4 Releasable Activity

The releasable activity is the product of the respective activity concentrations (C_{fines}, C_{gas}, C_{crud}, and C_{vol}) and the respective MPC volume. The releasable activity of fines, volatiles, gases, and crud were determined using this methodology.

$$\text{Releasable Activity [Ci]} = \text{Activity Concentration} \left[\frac{\text{Ci}}{\text{cm}^3} \right] \times \text{Volume [cm}^3] \quad (4-9)$$

4.2.5.5 Effective A₂ for the Total Source Term

Using the releasable activity and the effective A₂ values from the individual contributors (i.e., crud, fines, gases, and volatiles), the effective A₂ for the total source term was calculated for each MPC

type, for normal transportation and hypothetical accident conditions. The methodology used to determine the effective A_2 is the same as that used for a mixture, which is provided in Equation 4-8.

The results are summarized in Table 4.2.6. As stated in 4.2.5.3, the effective A_2 used for Krypton-85 is $10 A_2$ (2700 Ci).

4.2.5.6 Allowable Radionuclide Release Rates

The containment criterion for the HI-STAR 100 System under normal conditions of transport is given in 10CFR71.51(a)(1). This criterion requires that a package have a radioactive release rate less than $A_2 \times 10^{-6}$ in one hour, where A_2 is the effective A_2 for the total source term in the packaging determined in 4.2.5.5. Additionally, 10CFR71.51(b)(2) specifies that for hypothetical accident conditions, the quantity that may be released in one week is A_2 (effective A_2 for the total source term determined in 4.2.5.5).

NUREG/CR-6487 and ANSIN14.5 provides the following equations for the allowable release rates.

Release rate for normal conditions of transport:

$$R_N = L_N C_N \leq A_2 \times 2.78 \times 10^{-10} / \text{second} \quad (4-10)$$

where:

- R_N is the release rate for normal transport [Ci/s]
- L_N is the volumetric gas leakage rate [cm^3/s]
- C_N is the total source term activity concentration [Ci/cm^3]
- A_2 is the appropriate effective A_2 value [Ci].

Release rate for hypothetical accident conditions:

$$R_A = L_A C_A \leq A_2 \times 1.65 \times 10^{-6} / \text{second} \quad (4-11)$$

where:

- R_A is the release rate for hypothetical accident conditions [Ci/s]
- L_A is the volumetric gas leakage rate [cm^3/s]
- C_A is the total source term activity concentration [Ci/cm^3]
- A_2 is the appropriate effective A_2 value [Ci].

Equations 4-10 and 4-11 were used to determine the allowable radionuclide release rates for each MPC type and transport condition. The release rates are summarized in Table 4.2.7.

4.2.5.7 Allowable Leakage Rates at Operating Conditions

The allowable leakage rates at operating conditions were determined by dividing the allowable release rates by the appropriate source term activity concentration (modifying Equations 4-10 and 4-

11).

$$L_N = \frac{R_N}{C_N} \quad \text{or} \quad L_A = \frac{R_A}{C_A} \quad (4-12)$$

where,

L_N or L_A is the allowable leakage rate at the upstream pressure for normal (N) or accident (A) conditions [cm^3/s],

R_N or R_A is the allowable release rate for normal (N) or accident (A) conditions [Ci/s], and

C_N or C_A is the allowable release rate for normal (N) or accident (A) conditions [Ci/cm^3].

The allowable leakage rates determined using Equation 4-12 are the allowable leakage rates at the upstream pressure. Table 4.2.9 summarizes the allowable leakage rates at the upstream pressures. The most limiting allowable leakage rate presented in Table 4.2.9 was conservatively selected and used to determine the leakage rate acceptance criterion-

Equation deleted (4-13)

4.2.5.8 Leakage Rate Acceptance Criteria for Test Conditions

The leakage rates discussed thus far were determined at operating conditions (see normal and accident conditions in Table 4.2.12). The following provides details of the methodology used to convert the allowable leakage rate at operating conditions to a leakage rate acceptance criterion at reference test conditions.

For conservatism, unchoked flow correlations were used as the unchoked flow correlations better approximate the true measured flow rate for the leakage rates associated with transportation packages. Using the equations for molecular and continuum flow provided in NUREG/CR-6487, the corresponding leak hole diameter was calculated by solving Equation 4-14a for D , the leak hole diameter. The capillary length required for Equation 4-14a for the ~~primary~~ containment was conservatively chosen as the closure plate inner seal seating width which is 0.25 cm; ~~for the secondary containment, the capillary length was conservatively chosen to be the MPC lid closure weld thickness which is 1.25 inches thick (3.175 cm).~~

$$L_{@P_u} = \left[\frac{2.49 \times 10^6 D^4}{a u} + \frac{3.81 \times 10^3 D^3 \sqrt{\frac{T}{M}}}{a P_a} \right] [P_u - P_d] \frac{P_a}{P_u} \quad (4-14a)$$

where:

$L_{@P_u}$ is the allowable leakage rate at the upstream pressure for normal and accident conditions [cm^3/s],

a is the capillary length [cm],

T is the temperature for normal and accident conditions [K],

M is the gas molecular weight [g/mole] = 4.0 from ANSI N14.5, Table B1 [4.0.2],

- u is the fluid viscosity for helium [cP] from Rosenhow and Hartnett [4.2.3]
- P_u is the upstream pressure [ATM],
- D leak hole diameter [cm],
- P_d is the downstream pressure for normal and accident conditions [ATM], and
- P_a is the average pressure; P_a = (P_u + P_d)/2 for normal and accident conditions [ATM].

The actual leakage tests performed on the ~~primary and secondary confinement containment boundary welds~~ are typically not performed under exactly the same conditions every time. Therefore, reference test conditions are specified to provide a consistent comparison of the measured leakage rate to the leakage rate acceptance criterion. ~~For example, the MPC Lid to Shell weld is performed with either an elevated pressure (85 psig min) inside the MPC cavity to magnify the leakage rate in the event of a leak or with a vacuum pulled on the area between the MPC lid and the cover ring and the helium backfill pressure inside the MPC cavity.~~ The reference test conditions, and approximate actual test conditions are specified in Table 4.2.12.

The corresponding leak hole diameter at operating conditions was determined by solving Equation 4-14a for 'D' where L_{@P_u} is equal to 1.03x10⁻⁵ cm³/s the most restrictive allowable leakage rate at the upstream pressure from Table 4.2.9 and using the parameters for normal conditions of transport presented in Table 4.2.12.

Using this leak hole diameter and the temperature and pressure specified for reference test conditions provided in Table 4.2.12, Equation 4-14a was solved for the volumetric leakage rate at reference test conditions.

Equation B-1 of ANSI N14.5-1997 [4.0.2] is used to express this volumetric leakage rate into a mass-like helium flow rate (Q_u) as follows:

$$Q_u = L_u * P_u \text{ (atm-cm}^3\text{/sec)} \quad (4-14b)$$

where:

- L_u is the upstream volumetric leakage rate [cm³/sec],
- Q_u is the mass-like helium leak rate [atm-cm³/sec], and
- P_u is the upstream pressure [atm].

Using Equation 4-14b to convert the volumetric flow rate into a mass-like flow, the leakage rate acceptance criteria is calculated to be 5.41x10⁻⁶ atm-cm³/sec, which has been and conservatively reduced and is presented in to the value presented in Table 4.1.1.

Table 4.2.12 provides additional parameters used in the analysis.

4.2.5.9 ~~10CFR71.63(b) Plutonium Leakage Verification~~

~~The HI-STAR 100 System configured to transport fuel debris must meet the criteria of~~

10CFR71.63(b) for plutonium shipments. This criteria specifies that for normal conditions of transport, the separate inner container must not release plutonium as demonstrated to a sensitivity of $A_2 \times 10^{-6}$ in one hour, where A_2 is the effective A_2 for the plutonium inventory in the damaged fuel (up to four DFCs containing specified fuel debris). Additionally, 10CFR71.63(b) specifies that for hypothetical accident conditions, the separate inner container must restrict the loss of plutonium to not more than A_2 in one week (effective A_2 for the plutonium inventory determined using the methodology described in Section 4.2.5.3).

To demonstrate compliance with this requirement, the leakage rate acceptance criterion was determined following the basic methodology described above. To determine this leakage rate, the plutonium inventory for the GE 6x6 MOX fuel assembly and the plutonium inventories for the assemblies described in Section 4.2.5.2 was analyzed. Table 4.2.11 contains the plutonium inventory for the MOX fuel used in this evaluation.

As discussed in 4.2.5.2, Equation 4-3a and Equation 4-3b presents the methodology to determine f_B for a Trojan MPC 24EF and an MPC 68F containing fuel debris, respectively. This f_B was applied in determining the source activity due to Plutonium. The calculation for normal transport conditions of an MPC containing four (4) DFCs containing fuel debris assumes that for the four DFCs, 100% of the rods of the fuel debris are breached. The remaining assemblies in the MPC were assumed to have a 3% cladding rupture. The source activity due to Plutonium was determined by conservatively assuming that all of the rods develop cladding breaches during hypothetical accident conditions (i.e., $f_B=1.0$). The assumption was also made that roughly 0.003% of the plutonium is released from a fuel rod (i.e., $f_{Pu}=3 \times 10^{-5}$). Therefore, the activity concentration inside the containment vessel due to plutonium is given by:

$$C_{Pu} = \frac{f_{Pu} I_{Pu} N_A f_B}{V} \quad (4-15)$$

where:

- C_{Pu} is the activity concentration inside the containment vessel from Plutonium [Ci/cm^3],
- f_{Pu} is the fraction of a fuel rod's mass released as Plutonium ($f_{Pu}=3 \times 10^{-5}$),
- I_{Pu} is the total Plutonium inventory of one assembly [$Ci/assy$],
- N_A is the number of assemblies,
- f_B is the fraction of rods that develop cladding breaches ($f_B=0.087$ for BWR fuel and $f_B=0.192$ for PWR fuel under normal conditions of transport and $f_B=1.0$ for accident conditions), and
- V is the free volume inside the containment vessel [cm^3] from Table 4.2.1.

The methodology described in 4.2.5.3 for mixtures was used to calculate the effective A_2 for Plutonium. The methodology in 4.2.5.4 was used to determine the releasable activity. The allowable radionuclide release rates were determined using the methodology presented in 4.2.5.6 and are summarized in Table 4.2.13. The allowable leakage rates at the upstream pressure were determined as discussed in 4.2.5.7 (using Equation 4-12). The allowable leakage rates are presented in Table 4.2.14. As in 4.2.5.7, the most limiting allowable leakage rate presented in Table 4.2.14

was conservatively selected and used to determine the leakage rate acceptance criterion for the MPC.

As discussed in 4.2.5.8, the allowable leakage rate was then converted to a leakage rate acceptance criterion at test conditions using the equations for molecular and continuum flow provided in NUREG/CR-6487 (Equation 4-14a). The capillary length required for Equation 4-14a for the secondary containment was conservatively chosen to be the MPC lid closure weld thickness which is assumed to be 1.25 inches thick (3.175 cm). Equation 4-14a was solved for D , the leak hole diameter and then using this leak hole diameter, and the temperature and pressures for test conditions (Table 4.1.12), Equation 4-14a was solved for the volumetric leakage rate acceptance criterion at test conditions. Equation 4-14b is used to convert the volumetric flow rate into the mass-like flow rate, resulting in an acceptance criterion leakage rate of 8.94×10^{-6} atm cm³/sec. For additional conservatism to ensure compliance with 10CFR71.63(b), this leakage rate acceptance criterion was conservatively reduced and is presented in Table 4.1.1.

4.2.5.910 Leak Test Sensitivity

The sensitivity for the overpack leakage test procedures is equal to one-half of the allowable leakage rate. The HI-STAR 100 containment packaging tests in Chapter 8 incorporate the appropriate leakage test procedure sensitivity. The leakage rates for the HI-STAR 100 containment packaging with its corresponding sensitivity are presented in Table 4.1.1.

Table 4.2.1

FREE GAS VOLUME OF THE ~~PRIMARY~~
AND ~~SECONDARY~~ CONTAINMENT SYSTEM

MPC Type	Primary Containment Volume (overpack) (cm ³)
MPC-24	6.70 x 10 ⁶
MPC-24E MPC-24EF	6.55 x 10 ⁶
Trojan MPC-24E Trojan MPC-24EF	6.12 x 10 ⁶
MPC-32	6.35 x 10 ⁶
MPC-68	6.15 x 10 ⁶
MPC-68F	6.15 x 10 ⁶

Table 4.2.2

ISOTOPE INVENTORY
Ci/Assembly

Nuclide	PWR MPCs Ci/Assembly	MPC-68 Ci/Assembly	MPC-68F Ci/Assembly	Trojan MPCs Ci/Assembly
Gases				
³ H	2.76E+02	1.09E+02	1.78E+01	1.75E+02
¹²⁹ I	2.17E-02	8.66E-03	3.49E-03	1.93E-02
⁸⁵ Kr	4.69E+03	1.79E+03	2.37E+02	2.76E+03
⁸¹ Kr	7.97E-08	3.50E-08	1.19E-08	6.80E-08
¹²⁷ Xe	5.95E-11	2.05E-11	0.00E+001.62 E-17	3.39E-29
Crud				
⁶⁰ Co	2.18E+01	6.50E+01	1.18E+01	1.29E+01
Volatiles				
⁹⁰ Sr	4.53E+04	1.76E+04	4.29E+03	3.36E+04
¹⁰⁶ Ru	4.97E+04	1.74E+04	2.30E-01	7.99E+02
¹³⁴ Cs	4.43E+04	1.66E+04	3.16E+01	5.14E+03
¹³⁷ Cs	6.76E+04	2.68E+04	7.21E+03	5.20E+04
⁸⁹ Sr	1.25E-01	3.47E-02	2.41E-35	1.01E-14
¹⁰³ Ru	3.65E-03	1.13E-03	0.00E+00	5.47E-20
¹³⁵ Cs	2.79E-01	1.11E-01	4.54E-02	2.16E-01
Fines				
²²⁵ Ac*	3.05E-08	2.14E-08	9.69E-09	4.02E-089.89E- 13
²²⁷ Ac*	2.36E-06	1.18E-06	1.45E-06	2.0856E-068
^{110m} Ag	1.73E+02	6.58E+01	4.97E-06	3.322.04E-017

²⁴¹ Am*	4.76E+02	1.61E+02	2.52E+02	9.50147E+020
Table 4.2.2 (continued) ISOTOPE INVENTORY				
	MPC-24PWR MPCs Ci/Assembly	MPC-68 Ci/Assembly	MPC-68F Ci/Assembly	Trojan MPCs Ci/Assembly
^{242M} Am*	5.60E+00	1.94E+00	9.35E-01	4.12506E+00-03
²⁴³ Am*	2.23E+01	9.42E+00	3.30E+00	2.0653E+01-02
^{137m} Ba	6.39E+04	2.53E+04	6.81E+03	0.00E+00
^{210M} Bi*	0.00E+00	0.00E+00	0.00E+00	8.62E-191.38E-10
²⁴⁷ Bk*	0.00E+002.82E-08	0.00E+001.32E-08	5.94E-080.00E+00	0.00E+007.06E-24
¹⁴⁴ Ce	4.77E+04	1.45E+04	7.33E-03	2.1362E+02-04
²⁴⁸ Cf*	0.00E+00	0.00E+00	0.00E+00	0.00E+00
²⁴⁹ Cf*	8.01E-05	4.47E-05	3.62E-06	5.86720E-058
²⁵⁰ Cf*	2.92E-04	1.86E-04	6.69E-06	1.57773E-048
²⁵¹ Cf*	3.40E-06	2.06E-06	1.36E-07	2.3184E-069
²⁵² Cf*	4.11E-04	3.14E-04	3.64E-07	6.17152E-058
²⁵⁴ Cf*	1.19E-13	1.05E-13	0.00E+00	1.28532E-248
²⁴⁰ Cm*	0.00E+00	0.00E+00	0.00E+00	0.00E+00
²⁴² Cm*	3.21E+02	1.26E+02	7.71E-01	38.42E+-005
²⁴³ Cm*	1.61E+01	6.51E+00	1.54E+00	1.16951E+01-03
²⁴⁴ Cm*	3.26E+03	1.453E+03	2.17E+02	2.30142E+030
²⁴⁵ Cm*	3.25E-01	1.23E-01	2.48E-02	2.61321E-014
²⁴⁶ Cm*	1.06E-01	5.40E-02	1.01E-02	9.26114E-024

$^{247}\text{Cm}^*$	7.07E-07	3.72E-07	5.26E-08	5.717-04E-0740
$^{248}\text{Cm}^*$	4.20E-06	2.43E-06	2.53E-07	3.174.56E-068

Table 4.2.2 (continued)
ISOTOPE INVENTORY

Ci/Assembly

	MPC-24PWR MPCs Ci/Assembly	MPC-68 Ci/Assembly	MPC-68F Ci/Assembly	Trojan MPCs Ci/Assembly
²⁵³ Es*	6.35E-20	4.62E-20	0.00E+00	0.00E+00
²⁵⁴ Es*	1.93E-08	1.96E-08	8.05E-16	5.24E-15
¹⁵⁴ Eu	4.03E+03	1.47E+03	1.44E+02	2.061.01E+-03
¹⁵⁵ Eu	1.34E+03	5.46E+02	2.23E+01	4.936.06E+-025
⁵⁵ Fe	6.98E+01	3.23E+01	2.94E-01	1.8011E+-017
²⁵⁷ Fm*	4.26E-07	1.69E-07	0.00E+00	2.35E-26
¹⁴⁸ Gd*	0.00E+00	0.00E+00	0.00E+00	0.00E+00
¹⁸² Hf*	0.00E+00	0.00E+00	0.00E+00	0.00E+00
²³⁶ Np*	9.77E-06	3.29E-06	7.30E-07	7.231.78E-069
²³⁷ Np*	2.33E-01	8.07E-02	2.55E-02	1.902.33E-014
²³⁹ Np	2.23E+01	9.42E+00	3.30E+00	2.061.01E+01-05
²³¹ Pa*	1.82E-05	8.17E-06	3.16E-06	7.943.26E-068
²¹⁰ Pb*	4.30E-09	2.17E-09	1.17E-08	3.77E-13
¹⁴⁷ Pm	4.28E+04	1.52E+04	1.18E+02	7.932.17E+-03
²⁰⁸ Po*	0.00E+00	0.00E+00	0.00E+00	0.00E+00
²⁰⁹ Po*	0.00E+00	0.00E+00	0.00E+00	0.00E+00
²¹⁰ Po*	3.92E-09	1.98E-09	1.08E-08	1.2149E-0813
¹⁴⁴ Pf	4.77E+04	1.45E+04	7.33E-03	0.00E+00
^{144m} Pf	6.68E+02	2.04E+02	1.03E-04	0.00E+00

$^{236}\text{Pu}^*$	2.04E-01	6.32E-02	3.66E-04	3.59126E-025
---------------------	----------	----------	----------	--------------

Table 4.2.2 (continued)
ISOTOPE INVENTORY

Ci/Assembly

	MPC-24PWR MPCs Ci/Assembly	MPC-68 Ci/Assembly	MPC-68F Ci/Assembly	Trojan MPCs Ci/Assembly
²³⁸ Pu*	2.56E+03	9.55E+02	2.50E+02	1.932.37E+030
²³⁹ Pu*	1.91E+02	6.24E+01	2.95E+01	1.632.00E+02-01
²⁴⁰ Pu*	3.27E+02	1.34E+02	6.81E+01	3.01.70E+02-01
²⁴¹ Pu	7.55E+04	2.47E+04	5.16E+03	4.921.21E+0400
²⁴² Pu*	1.65E+00	7.05E-01	3.06E-01	1.6097E+00-03
²⁴⁴ Pu*	1.11E-13	6.58E-14	3.73E-14	2.3487E-136
²²³ Ra*	2.37E-06	1.18E-06	1.45E-06	2.081.70E-0611
²²⁴ Ra*	8.57E-03	3.40E-03	1.72E-03	1.31E-02
²²⁵ Ra*	3.05E-08	2.14E-08	9.69E-09	4.0294E-0813
²²⁶ Ra*	2.82E-08	1.32E-08	5.94E-08	1.1238E-0712
²²⁸ Ra*	9.87E-12	4.63E-12	1.24E-11	3.07E-11
¹⁰⁶ Rh	4.97E+04	1.74E+04	2.30E-01	0.00E+00
²²² Rn*	2.82E-08	1.32E-08	5.94E-08	1.12E-076.89E-12
¹²⁵ Sb	2.87E+03	1.15E+03	9.468.02E+00	5.82E+021.59E-04
¹⁵¹ Sm	2.60E+02	7.92E+01	2.53E+01	2.01E+021.24E-05
^{119m} Sn	5.46E+02	3.08E+02	1.9807E-046	3.18E+004.23E-05
^{125m} Te	6.99E+02	2.82E+02	2.311.96E+00	1.42E+021.89E-

				03
²²⁷ Th*	2.33E-06	1.16E-06	1.43E-06	2.05E-06 11
²²⁸ Th*	8.56E-03	3.40E-03	1.71E-03	1.31E-02 06
²²⁹ Th*	3.05E-08	2.14E-08	9.69E-09	4.02E-08 10
²³⁰ Th*	2.16E-05	8.26E-06	1.29E-05	4.40E-05 08
²³⁰ U*	1.33E-23	4.74E-24	0.00E+00	0.00E+00

Table 4.2.2 (continued)
ISOTOPE INVENTORY
Ci/Assembly

	<i>PWR MPCs Ci/Assembly</i> C-24 Ci/Assembly	<i>MPC-68 Ci/Assembly</i> MPC-68 Ci/Assembly	MPC-68F Ci/Assembly	Trojan MPCs Ci/Assembly
²³¹ Th*	7.11E-03	1.67E-03	5.43E-04	5.07E-03
²³⁰ U*	1.33E-23	4.74E-24	0.00E+00	0.00E+00
²³² U*	1.51E-02	5.58E-03	1.69E-03	1.4824E-025
²³³ U*	1.41E-05	4.20E-06	3.03E-06	1.60394E-059
²³⁴ U*	4.97E-01	1.70E-01	7.26E-02	4.37108E-014
²³⁶ U*	1.60E-01	5.85E-02	1.84E-02	1.29318E-015
⁹⁰ Y	4.53E+04	1.76E+04	4.29E+03	3.36413E+04- 02

Note: The isotopes which contribute greater than 0.01% to the total curie inventory for the fuel assembly are considered in the evaluation as fines. Additionally, isotopes with A₂ values less than 1.0 in Table A-1, Appendix A, 10CFR71 are included as fines and are designated in the table by an "*".

Table 4.2.3

TOTAL SOURCE TERM FOR THE HI-STAR 100 SYSTEM (Ci/cm³)

	C _{crud} (Ci/cm ³)	C _{finest} (Ci/cm ³)	C _{vol} (Ci/cm ³)	C _{gas} (Ci/cm ³)	Total (Ci/cm ³)
Normal Transport Conditions					
MPC-24	1.17E-05	7.37126E-07	4.45E-06	1.60E-04	1.77E-04
MPC-24E, MPC-24EF	1.20E-05	7.53129E-07	4.55E-06	1.64E-04	1.812E-04
Trojan MPC-24E	7.56E-06	3.53531E-07	2.15E-06	1.04E-04	1.14E-04
Trojan MPC-24EF Secondary	7.77E-06	3.49E-06	1.42E-05	6.81E-04	7.06E-04
Trojan MPC-24EF-Primary	7.56E-06	2.26340E-06	1.38E-05	6.63E-04	6.878E-04
MPC-32	1.64E-05	1.0477E-07	6.26E-06	2.25E-04	2.4950E-04
MPC-68	1.08E-04	7.85136E-07	5.20E-06	1.89E-04	3.03E-04
MPC-68F-Secondary	2.00E-05	5.16E-07	2.28E-06	7.55E-05	9.83E-05
MPC-68F-Primary	1.95E-05	3.06502E-078	2.22E-06	7.35E-05	9.568E-05
Accident Conditions					
MPC-24	7.79E-05	2.46420E-05	1.48E-04	5.34E-03	5.5960E-03
MPC-24E, MPC-24EF	7.97E-05	2.51429E-05	1.52E-04	5.46E-03	5.723E-03
Trojan MPC-24E	5.04E-05	1.18177E-05	7.18E-05	3.45E-03	3.59E-03
Trojan MPC-24EF Secondary	5.18E-05	1.82E-05	7.37E-05	3.55E-03	3.69E-03
Trojan MPC-24EF-Primary	5.04E-05	1.18177E-05	7.18E-05	3.45E-03	3.59E-03
MPC-32	1.10E-04	3.45590E-05	2.09E-04	7.51E-03	7.868E-03

MPC-68	7.18E-04	2.624.52E-05	1.73E-04	6.30E-03	7.223E-03
MPC-68F-Secondary	1.34E-04	5.93E-06	2.62E-05	8.68E-04	1.03E-03
MPC-68F-Primary	1.30E-04	3.525.77E-06	2.55E-05	8.45E-04	1.004E-03

Table 4.2.4

VARIABLES FOUND IN NUREG/CR-6487 USED IN THE
LEAKAGE RATE ANALYSIS

Variable	PWR		BWR	
	Normal	Accident	Normal	Accident
Fraction of crud that spalls, f_C	0.15	1.0	0.15	1.0
Crud surface activity (Ci/cm^2)	140×10^{-06}	140×10^{-06}	1254×10^{-06}	1254×10^{-06}
Surface area per assembly, cm^2	3×10^5	3×10^5	1×10^5	1×10^5
Fraction of rods that develop cladding breach, f_B^\dagger	0.03	1.0	0.03	1.0
Fraction of fines that are released, f_f	3×10^{-5}	3×10^{-5}	3×10^{-5}	3×10^{-5}
Fraction of gases that are released, f_G	0.3	0.3	0.3	0.3
Fraction of volatiles that are released, f_v	2×10^{-04}	2×10^{-04}	2×10^{-04}	2×10^{-04}

[†] The calculation for normal transport conditions of the Trojan MPC-24EF and MPC-68F each containing four (4) DFCs with fuel debris assumes that for the four DFCs, 100% of the rods of the fuel debris are breached. The remaining 20 or 64 assemblies in the Trojan MPC-24EF and MPC-68F, respectively, were assumed to have a 3% cladding rupture. Therefore, f_B for the Trojan MPC-24EF and the MPC-68F containing fuel debris is 0.192 and 0.087, respectively.

Table 4.2.5

INDIVIDUAL CONTRIBUTOR EFFECTIVE A₂
FOR GASES, CRUD, FINES, AND VOLATILES

MPC Type	A ₂ (Ci)
Gases	
PWR MPCs	282
MPC-68	282
MPC-68F	285
Trojan MPCs	4798
Crud	
All MPCs	10.8
Fines	
PWR MPCs	0.889308
MPC-68	0.812284
MPC-68F	0.351415
Trojan MPCs	0.494147
Volatiles	
PWR MPCs	9.726.04
MPC-68	9.906.05
MPC-68F	11.85.43
Trojan MPCs	11.85.44

Table 4.2.6

TOTAL SOURCE TERM EFFECTIVE A₂ FOR
NORMAL AND HYPOTHETICAL
ACCIDENT CONDITIONS

Normal Transport Conditions	
	Effective A ₂ (Ci)
MPC-24	60.327.4
MPC-24E MPC-24EF	60.327.4
Trojan MPC-24E	62.623.1
Trojan MPC-24EF	87.724.7
MPC-32	60.327.4
MPC-68	24.918.6
MPC-68F	14.030.6
Accident Conditions	
MPC-24	81.030.0
MPC-24E MPC-24EF	81.030.0
Trojan MPC-24E	85.824.6
Trojan MPC-24EF	85.824.6
MPC-32	81.030.0
MPC-68	52.126.2
MPC-68F	37.014.4

Table 4.2.7

RADIONUCLIDE RELEASE RATES

	Allowable Release Rate (R _N or R _A) (Ci/s)
Normal Conditions	
MPC-24	1.687.62E-089
MPC-24E, MPC-24EF	1.687.62E-089
Trojan MPC-24E	1.746.41E-089
Trojan MPC-24EF	2.446.87E-089
MPC-32	1.687.62E-089
MPC-68	6.935.18E-09
MPC-68F	8.513.88E-09
Accident Conditions	
MPC-24	1.344.94E-045
MPC-24E, MPC-24EF	1.344.94E-045
Trojan MPC-24E	1.424.06E-045
Trojan MPC-24EF	1.424.06E-045
MPC-32	1.344.94E-045
MPC-68	8.594.32E-055
MPC-68F	6.102.37E-05

Table 4.2.8

Table Deleted

Table 4.2.9

ALLOWABLE LEAKAGE RATES AT UPSTREAM PRESSURE

	C_{total} (Ci/cm ³)	Allowable Leakage Rate at P _u L _N or L _A (cm ³ /s)
Normal Transport Conditions		
MPC-24	1.77E-04	9.474.29E- 055
MPC-24E, MPC-24EF	1.812E-04	9.264.20E- 05
Trojan MPC-24E	1.14E-04	1.535.63E- 045
Trojan MPC-24EF Secondary	7.06E-04	9.73E- 06
Trojan MPC-24EF Primary	6.878E-04	3.551.00E- 05
MPC-32	2.4950E-04	6.733.05E- 05
MPC-68	3.03E-04	2.291.71E- 05
MPC-68F Secondary	9.83E-05	3.95E- 05
MPC-68F Primary	9.568E-05	8.914.05E- 05
Accident Conditions		
MPC-24	5.5960E-03	2.398.82E- 023
MPC-24E, MPC-24EF	5.723E-03	2.348.62E- 023
Trojan MPC-24E	3.59E-03	3.951.13E- 02
Trojan MPC-24EF Secondary	3.69E-03	1.10E- 02

Trojan MPC-24EF Primary	3.59E-03	3.951.13E- 02
MPC-32	7.868E-03	1.706.27E- 023
MPC-68	7.223E-03	1.195.96E- 023
MPC-68F Secondary	1.03E-03	2.29E-02
MPC-68F Primary	1.004E-03	6.072.35E- 02

Table 4.2.10

Table Deleted

Table 4.2.11

DELETED
PLUTONIUM INVENTORY
 (Ci/assembly)

Nuclide	MPC 68F MOX fuel Ci/Assy	MPC 68F UO ₂ fuel Ci/Assy	Trojan MPC 24EF UO ₂ fuel Ci/Assy
Pu 236	4.92E-04	3.66E-04	2.04E-01
Pu 237	0.00E+00	0.00E+00	3.04E-07
Pu 238	1.11E+03	2.50E+02	2.56E+03
Pu 239	3.29E+01	2.95E+01	1.91E+02
Pu 240	7.83E+01	6.81E+01	3.27E+02
Pu 241	6.15E+03	5.16E+03	7.55E+04
Pu 242	3.44E-01	3.06E-01	1.65E+00
Pu 244	0.0	3.73E-14	1.11E-13
Total	7.37E+03	5.51E+03	7.86E+04

Table 4.2.12

PARAMETERS FOR NORMAL, HYPOTHETICAL ACCIDENT
AND TEST CONDITIONS

Parameter	Normal Conditions	Hypothetical Accident Conditions	Reference Test Conditions	Actual Test Conditions [†]
P_u	104 psia ² (7.07 ATM)	214.7 psia (14.61 ATM)	Primary: 1.68 ATM Secondary: 2.0 ATM	Primary: 1.68 ATM (min) Secondary: 6.78 ATM (min)
P_d	14.7 psia (1 ATM)	14.7 psia (1 ATM)	14.7 psia (1 ATM)	14.7 psia (1 ATM)
T	495°F (530 K)	1058°F (843 K)	373 K	373 K (max)
M	4 g/mol	4 g/mol	4 g/mol	4 g/mol
μ	0.0293 cP	0.0397 cP	0.0231 cP	0.0231 cP
a	Primary: 0.25 cm Secondary: 3.175 cm	Primary: 0.25 cm Secondary: 3.175 cm	Primary: 0.25 cm Secondary: 3.175 cm	Primary: 0.25 cm Secondary: 3.175 cm

[†] For the leakage rate test performed by drawing a vacuum between the MPC lid and the cover ring, P_u is 2.0 ATM (min) and P_d is 0.01 ATM.

² The maximum upstream pressure for normal operating conditions in the Trojan MPCs is 83.2 psia (5.66 ATM). This value has been used to determine the maximum allowable leakage rate from the Trojan MPCs.

Table 4.2.13
~~DELETED~~
RADIONUCLIDE RELEASE RATES
FOR PLUTONIUM (SECONDARY CONTAINMENT)

	Effective A_2 (Ci)	Allowable Release Rate (R_N or R_A) (Ci/s)
Normal Transport Conditions		
MPC-68F MOX Fuel	0.0297	8.24E-12
MPC-68F UO₂ Fuel	0.0660	1.84E-11
Trojan MPC-24EF UO₂ Fuel	0.0926	2.57E-11
Accident Conditions		
MPC-68F	0.0297	4.89E-08
MPC-68F UO₂ Fuel	0.0660	1.09E-07
Trojan MPC-24EF UO₂ Fuel	0.0926	1.53E-07

Table 4.2.14
~~DELETED~~
~~ALLOWABLE LEAKAGE RATES AT UPSTREAM PRESSURE~~
~~FOR PLUTONIUM (SECONDARY CONTAINMENT)~~

	C_{Pu} (Ci/cm ³)	Allowable Leakage Rate at P_u L_N or L_A (cm ³ /s)
Normal Transport Conditions		
MPC 68F MOX Fuel	2.18E-07	3.77E-05
MPC 68F UO ₂ Fuel	1.63E-07	1.12E-04
Trojan MPC 24EF UO ₂ Fuel	1.82E-06	1.41E-05
Accident Conditions		
MPC 68F	2.51E-06	1.95E-02
MPC 68F UO ₂ Fuel	1.88E-06	5.81E-02
Trojan MPC 24EF UO ₂ Fuel	9.49E-06	1.61E-02

4.3 REGULATORY COMPLIANCE

Chapter 4 of this SAR has been prepared to summarize the containment features and capabilities of the HI-STAR 100 packaging. The containment boundaries of the HI-STAR 100 packaging are designed and tested to ensure that the radionuclide release rates specified in 10CFR71.51 and ~~10CFR71.63(b)~~ [4.0.1] will not be exceeded.

Leakage rates presented in Chapter 4 are determined in accordance with the requirements of ANSI N14.5 [4.0.2], and utilizing NUREG/CR-6487, *Containment Analysis for Type B Packages Used to Transport Various Contents* [4.0.3], Regulatory Guide 7.4, *Leakage Tests on Packages for Shipment of Radioactive Materials* [4.0.4] as content guides, and NUREG-1617, Standard Review Plan for Transportation Packages for Spent Nuclear Fuel [4.0.5].

The containment features and capabilities of the HI-STAR 100 packaging can be summarized in the following evaluation statements:

1. The HI-STAR 100 packaging, as presented in Chapter 4, complies with all applicable codes and standards for the containment system as identified in the chapter.
2. The ~~primary~~ containment boundary is securely closed by using multiple bolts and plugs. ~~The secondary containment boundary is closed using multi-pass welds.~~ The closure of both the containment boundaries is sufficient to prevent unintentional opening or opening by pressure that may arise in the package as required by 10CFR71.43(c).
3. The materials of construction for the packaging ~~primary and secondary~~ containment are specified in the Bills-of-Material in Section 1.4. All materials and construction assure that there will be no significant chemical, galvanic, or other reaction as required by 10CFR71.43(d).
4. The overpack and MPC penetrations are designed to prevent leakage and protect against unauthorized operation by using cover plates to provide redundant closure as required by 10CFR71.43(e).
5. The ~~primary~~ containment system boundary for the HI-STAR 100 packaging consists of the overpack inner shell, the bottom plate, the top flange, the top closure plate, closure bolts, the overpack vent and drain port plugs, and their respective mechanical seals. ~~The secondary containment system boundary for a HI-STAR 100 packaging containing fuel debris consists of the MPC enclosure vessel including the MPC shell, the MPC bottom plate, the MPC lid, closure ring, and vent and drain port cover plates. The use of two independent containment boundaries provides the capability to load and transport specified fuel debris in accordance with the requirements of 10CFR71.63(b).~~

6. The HI-STAR 100 packaging is design, constructed, and prepared for shipment so that under the tests specified in 10CFR71.71 (normal conditions of transport), the package satisfies the containment requirement of 10CFR71.43(f) and 10CFR71.51(a)(1) for normal conditions of transport and 10CFR71.51(a)(2) for hypothetical accident conditions with no dependence on filters or a mechanical cooling system as required by 10CFR71.51(c).
- ~~7. The HI-STAR 100 packaging satisfies the requirements of 10CFR71.63(b) for transport related to fuel debris with plutonium in excess of 20 Ci per package.~~
- 8-7. The HI-STAR 100 packaging satisfies the containment requirements of 10CFR71, and the packaging meets the containment criteria of ANSI N14.5.

4.4 REFERENCES

- [4.0.1] 10CFR71. "Packaging and Transportation of Radioactive Material." 2006
- [4.0.2] ANSI N14.5-1997. "American National Standard for Radioactive Materials-Leakage Tests on Packages for Shipment."
- [4.0.3] B.L. Anderson et al. *Containment Analysis for Type B Packages Used to Transport Various Contents*. NUREG/CR-6487, UCRL-ID-124822. Lawrence Livermore National Laboratory, November 1996.
- [4.0.4] U.S. Nuclear Regulatory Commission, Regulatory Guide 7.4, *Leakage Tests on Packages for Shipment of Radioactive Materials*, June 1975.
- [4.0.5] NUREG-1617, "Standard Review Plan for Transportation Packages for Spent Nuclear Fuel", Draft Report for Comment, March 1998.
- [4.1.1] American Society of Mechanical Engineers (ASME), Boiler and Pressure Vessel Code, Section III, Division 1, Subsection NB, Class 1 Components, 1995 Edition.
- [4.2.1] Deleted.
- [4.2.2] Deleted.
- [4.2.3] Rosenhow, W.M. and Hartnett, J.P., *Handbook of Heat Transfer*, Hemisphere Publishing Corporation, New York, 1973.
- [4.2.4] Shleien, B., *The Health Physics and Radiological Health Handbook*, Scinta, Inc. Silver Spring, MD, 1992.

SUPPLEMENT 4.I

CONTAINMENT EVALUATION OF HUMBOLDT BAY FUEL IN THE HI-STAR HB

4.I.0 INTRODUCTION

This supplement is focused on providing containment evaluations for fuel from the Humboldt Bay Power Plant (HBPP) in the HI-STAR HB. The evaluation presented herein supplements those evaluations contained in the main body of Chapter 4 of this FSAR, and information in the main body of Chapter 4 is not repeated in this supplement. To aid the reader, the sections in this supplement are numbered in the same fashion as the corresponding sections in the main body of this chapter, i.e., Sections 4.I.1 through 4.I.3 correspond to Sections 4.1 through 4.3. Tables and figures in this supplement are labeled sequentially. The results of the evaluations in this supplement demonstrates the HI-STAR HB containment boundary compliance with the permitted activity release limits specified in 10 CFR 71, 71.51(a)(1) and 71.51(a)(2) for both normal and hypothetical accident conditions of transport.

4.I.1 CONTAINMENT BOUNDARIES

The containment system boundary for the HI-STAR HB is identical to that of the HI-STAR 100 System described in Section 4.1. Therefore, the discussion provided in the main part of the chapter on the containment vessel, penetrations, seals, welds, closure and damaged fuel containers for the HI-STAR 100 System are directly applicable to the HI-STAR HB.

4.I.2 REQUIREMENTS FOR NORMAL AND HYPOTHETICAL ACCIDENT CONDITIONS OF TRANSPORT

Supplement 2.I shows that all containment components for the HI-STAR HB are maintained within their code-allowable stress limits during all normal and hypothetical accident conditions of transport as defined in 10CFR71.71 and 10CFR71.73 [4.0.1]. Supplement 3.I shows that the peak containment component temperatures and pressure are within the design basis limits for all normal and hypothetical accident conditions of transport as defined in 10CFR71.71 and 10CFR71.73. Since the containment vessels remain intact, and the temperature and pressure design bases are not exceeded, the design basis leakage rate will not be exceeded during normal or hypothetical accident conditions of transport.

4.I.2.1 Containment Criteria

The containment criteria are identical to those identified in Section 4.2.1 of the main part of the chapter.

4.I.2.2 Containment of Radioactive Material

The HI-STAR HB packaging allowable leakage rate ensures that the requirements of 10CFR71.51 are met. Section 4.I.2.5 determines the maximum leakage rate for normal and hypothetical accident conditions of transport and the allowable leakage rate criterion for the HI-STAR HB packaging containing the MPC-HB. Following testing, no credit is taken for the MPC as a containment boundary for the transport of spent fuel.

4.I.2.3 Pressurization of Containment Vessel

The HI-STAR HB is drained, dried, evacuated and backfilled with helium gas prior to final closure of the overpack in an identical way as the HI-STAR 100 System described in the main part of the chapter.

4.I.2.4 Assumptions

The following assumptions have been used in determining the allowable leakage rates in addition to those already listed in Section 4.2.4:

- 1. The MPC-HB contains 80 Humboldt Bay fuel assemblies of which up to forty (40) may be DFCs containing specified fuel debris or damaged fuel and the remaining forty (40) are undamaged fuel assemblies.*
- 2. In calculating the leakage rates of the containment system for normal conditions of transport, the internal pressure of the overpack is assumed to be equal to the maximum internal pressure determined in Supplement 3.I with 3% rod rupture.*
- 3. The average cavity temperature for normal conditions is conservatively assumed to be the maximum cladding temperature from Supplement 3.I.*
- 4. The average cavity temperature for hypothetical accident conditions is conservatively assumed to be the design basis peak cladding temperature.*
- 5. 100% of the fuel rods in undamaged fuel, damaged fuel and fuel debris are assumed to develop cladding breaches during normal transport.*

4.I.2.5 Analysis and Results

The methodology to determine the allowable leakage rates from the HI-STAR HB for normal and hypothetical accident conditions is identical to the methodology employed in the main part of the chapter for the HI-STAR 100 System. The only differences are in the input information, which is detailed in the following sections.

4.I.2.5.1 Volume in the Containment Vessel

The free gas volume in the MPC-HB is presented in Table 4.I.2.1. For calculating the free volume in the containment system (overpack) the volume of the annulus space is added to the free volume of the MPC-HB. This will conservatively underestimate the free volume inside the containment boundary.

4.I.2.5.2 Source Terms for Spent Nuclear Fuel Assemblies

The inventory for isotopes other than ^{60}Co is calculated with the SAS2H and ORIGEN-S modules of the SCALE 4.3 system as described in Chapter 5. The inventory for the MPC-HB was based the Humboldt Bay 6x6 fuel assembly with a burnup of 23,000 MWD/MTU, 29 years of cooling time, and 2.09 wt% enrichment. The isotopes which contribute greater than 0.01% to the total curie inventory for the fuel assembly are considered in the evaluation as fines. Additionally, isotopes with A_2 values less than 1.0 in Table A-1, Appendix A, 10CFR71 are included as fines. Isotopes which contribute greater than 0.01% but which do not have an assigned A_2 value in Table A-1 are assigned an A_2 value based on the guidance in Table A-3, Appendix A, 10CFR71. Isotopes which contribute greater than 0.01% but have a radiological half life less than 10 days are neglected. Table 4.I.2.2 presents the isotope inventory used in the calculation.

A. Source Activity Due to Crud Spallation from Fuel Rods

The source term activity associated with crud for the Humboldt Bay fuel was calculated in the same way as in the main part of the chapter. The inventory for ^{60}Co was determined by using the crud surface activity for BWR rods ($1254 \times 10^{-6} \text{ Ci/cm}^2$) provided in NUREG/CR-6487 [4.0.3] multiplied by the surface area per assembly ($1 \times 10^5 \text{ cm}^2$ for BWR fuel, also provided in NUREG/CR-6487). The source terms were then decay corrected 29 years using equation 4-1.

BWR

$$\begin{aligned} \text{Surface area per Assy} &= 1.0\text{E}+05 \text{ cm}^2 \\ 1254 \mu\text{Ci/cm}^2 \times 1.0\text{E}+05 \text{ cm}^2 &= 125.4 \text{ Ci/assy} \end{aligned}$$

MPC-HB

$$\begin{aligned} {}^{60}\text{Co}(29) &= 125.4 \text{ Ci } e^{-(\ln 2/5.272)(29)} \\ {}^{60}\text{Co}(29) &= 2.769 \text{ Ci/assy} \end{aligned}$$

A summary of the ^{60}Co inventory available for release is provided in Table 4.I.2.2.

The activity density that results inside the HI-STAR HB containment vessel as a result of crud spallation from spent fuel rods is calculated using Equation 4-2.

B. Source Activity Due to Releases of Fines from Cladding Breaches

The source term activity associated with fines for the Humboldt Bay fuel was calculated in the same way as in the main part of the chapter.

The calculation for normal transport conditions of a MPC-HB containing forty (40) DFCs containing fuel debris assumes that for the forty DFCs, 100% of the rods of the fuel debris are breached. The remaining 40 undamaged fuel assemblies in the MPC-HB were also assumed to have ~~a~~ 3%-100% cladding rupture. Therefore, f_B for an MPC-HB containing fuel debris is:

$$f_B = (1.0)\frac{40}{80} + (1.0)\frac{40}{80} \quad (4.I-1)$$
$$f_B = 1.0$$

The activity concentration inside the containment vessel due to fines being released from cladding breaches is given by Equation 4-4.

C. Source Activity from Gases due to Cladding Breaches

The source term activity associated with gases for the Humboldt Bay fuel was calculated in the same way as in the main part of the chapter.

The activity concentration due to the release of gases from a cladding breach is given by Equation 4-5.

D. Source Activity from Volatiles due to Cladding Breaches

The source term activity associated with volatiles for the Humboldt Bay fuel was calculated in the same way as in the main part of the chapter.

The activity concentration due to the release of volatiles from a cladding breach is given by Equation 4-6.

E. Total Source Term for the HI-STAR HB System

The total source term was determined using Equation 4-7. Table 4.I.2.3 presents the total source term determined using the above methodology.

4.I.2.5.3 Effective A_2 of Individual Contributors (Crud, Fines, Gases, and Volatiles)

Table 4.I.2.3 presents the total source term determined using the above methodology. Table 4.2.4 in the main part of the chapter summarizes the parameters from NUREG/CR-6487 used in this analysis, with the exception of the fraction of rods that develop cladding breaches, which is explained in the previous section. Table 4.I.2.4 summarizes the effective A_2 for all individual contributors.

4.I.2.5.4 Releasable Activity

The release activity of fines, volatiles, gases, and crud were determined using Equation 4-9.

4.1.2.5.5 Effective A_2 for the Total Source Term

The total source term effective A_2 was calculated in the same way as in the main chapter. The results are summarized in Table 4.1.2.5

4.1.2.5.6 Allowable Radionuclide Release Rates

The HI-STAR HB containment system is designed to the same containment criteria as the HI-STAR 100 System. These criterion are given in 10CFR71.51(a)(1) for normal conditions and 10CFR71.51(b)(2) for hypothetical accident conditions.

Equations 4-10 and 4-11 were used to determine the allowable radionuclide release rate for the MPC-HB under normal and hypothetical accident conditions. The release rates for the MPC-HB are summarized in Table 4.1.2.6.

4.1.2.5.7 Allowable Leakage Rates at Operating Conditions

The allowable leakage rates at operating conditions were determined using Equation 4-12. Table 4.1.2.7 summarizes the allowable leakage rates at the upstream pressures. The most limiting allowable leakage rate presented in Table 4.1.2.7 was conservatively selected and used to determine the leakage rate acceptance criterion for the MPC-HB.

4.1.2.5.8 Leakage Rate Acceptance Criteria for Test Conditions

The leakage rate acceptance criteria for test conditions was determined using the same methodology presented in Section 4.2.5.8 of the main part of the chapter. The reference test conditions, and approximate actual test conditions for the MPC-HB are specified in Table 4.1.2.8.

4.1.2.5.9 Leak Test Sensitivity

The sensitivity for the overpack leakage test procedures is equal to one-half of the allowable leakage rate. The HI-STAR HB containment packaging tests in Chapter 8 incorporate the appropriate leakage test procedure sensitivity. The leakage rates for the HI-STAR 100 containment packaging with its corresponding sensitivity are presented in Table 4.1.1.

4.1.3 REGULATORY COMPLIANCE

The HI-STAR HB is identical to the HI-STAR 100 System in that it is designed and tested to ensure compliance with the radionuclide release rates specified in 10CFR71.51 [4.0.1] for normal and hypothetical accident transport conditions.

Table 4.I.2.1

FREE GAS VOLUME OF THE HI-STAR HB CONTAINMENT SYSTEM

<i>Containment Volume [cm³]</i>	<i>3.40 x 10⁶</i>
--	------------------------------

Table 4.1.2.2

Isotopic Inventory for the HI-STAR HB

Nuclide	Ci/Assembly
<i>Gases</i>	
³ H	5.09E+00
¹²⁹ I	1.77E-03
⁸⁵ Kr	7.26E+01
⁸¹ Kr	3.76E-09
¹²⁷ Xe	0.00E+00
<i>Crud</i>	
⁶⁰ Co	2.77E+00
<i>Volatiles</i>	
⁹⁰ Sr	2.02E+03
¹⁰⁶ Ru	6.97E-05
¹³⁴ Cs	3.39E-01
¹³⁷ Cs	3.00E+03
⁸⁹ Sr	0.00E+00
¹⁰³ Ru	0.00E+00
¹³⁵ Cs	2.39E-02
<i>Fines</i>	
²²⁵ Ac*	6.21E-09
²²⁷ Ac*	6.72E-07
^{110m} Ag	2.36E-11
²⁴¹ Am	1.61E+02

Table 4.I.2.2 (continued)
ISOTOPE INVENTORY

$^{242M}\text{Am}^*$	3.55E-01
$^{243}\text{Am}^*$	8.13E-01
$^{210M}\text{Bi}^*$	4.04E-20
$^{247}\text{Bk}^*$	1.27E-07
^{144}Ce	3.26E-07
$^{248}\text{Cf}^*$	0.00E+00
$^{249}\text{Cf}^*$	7.07E-08
$^{250}\text{Cf}^*$	6.71E-08
$^{251}\text{Cf}^*$	1.98E-09
$^{252}\text{Cf}^*$	1.99E-10
$^{254}\text{Cf}^*$	0.00E+00
$^{240}\text{Cm}^*$	0.00E+00
$^{242}\text{Cm}^*$	2.93E-01
$^{243}\text{Cm}^*$	2.95E-01
^{244}Cm	2.20E+01
$^{245}\text{Cm}^*$	2.95E-03
$^{246}\text{Cm}^*$	7.58E-04
$^{247}\text{Cm}^*$	2.54E-09
$^{248}\text{Cm}^*$	7.32E-09

Table 4.I.2.2 (continued)
ISOTOPE INVENTORY

^{154}Eu	2.41E+01
^{155}Eu	1.92E+00
$^{148}\text{Gd}^*$	0.00E+00
$^{236}\text{Np}^*$	2.29E-07
$^{237}\text{Np}^*$	1.36E-02
^{239}Np	8.13E-01
$^{231}\text{Pa}^*$	1.31E-06
^{147}Pm	4.68E+00
$^{210}\text{Po}^*$	3.17E-08
$^{236}\text{Pu}^*$	9.26E-06
^{238}Pu	7.91E+01
^{239}Pu	1.87E+01
^{240}Pu	3.53E+01
^{241}Pu	1.55E+03

Table 4.1.2.2 (continued)
ISOTOPE INVENTORY

$^{242}\text{Pu}^*$	1.06E-01
$^{244}\text{Pu}^*$	1.71E-15
$^{223}\text{Ra}^*$	6.73E-07
$^{224}\text{Ra}^*$	5.29E-04
$^{225}\text{Ra}^*$	6.21E-09
$^{226}\text{Ra}^*$	1.27E-07
$^{222}\text{Rn}^*$	1.27E-07
^{151}Sm	1.42E+01
$^{227}\text{Th}^*$	6.64E-07
$^{228}\text{Th}^*$	5.27E-04
$^{229}\text{Th}^*$	6.21E-09
$^{230}\text{Th}^*$	1.84E-05
$^{231}\text{Th}^*$	8.36E-04
$^{230}\text{U}^*$	0.00E+00
$^{232}\text{U}^*$	5.13E-04
$^{233}\text{U}^*$	2.47E-06
$^{234}\text{U}^*$	6.53E-02
$^{236}\text{U}^*$	1.35E-02
^{90}Y	2.02E+03

Table 4.I.2.3

TOTAL SOURCE TERM FOR THE HI-STAR HB (Ci/cm³)

	C_{crud} (Ci/cm ³)	C_{fines} (Ci/cm ³)	C_{gas} (Ci/cm ³)	C_{vol} (Ci/cm ³)	Total (Ci/cm ³)
<i>Normal Transport Conditions</i>					
<i>HI-STAR HB</i>	9.77E-06	1.43E-06 2.78E-06	2.82E-04 5.48E-04	1.22E-05 2.36E-05	3.06E-04 5.85E-04
<i>Accident Conditions</i>					
<i>HI-STAR HB</i>	6.52E-05	2.78E-06	5.48E-04	2.36E-05	6.40E-04

Table 4.I.2.4

INDIVIDUAL CONTRIBUTOR EFFECTIVE A₂ FOR GASES, CRUD, FINES, AND VOLATILES FOR THE HI-STAR HB

<i>HI-STAR HB</i>	<i>A₂ (Ci)</i>
<i>Gases</i>	<i>2.46E+03</i>
<i>Crud</i>	<i>10.8</i>
<i>Fines</i>	<i>3.13E-01</i>
<i>Volatiles</i>	<i>1.16E+01</i>

Table 4.I.2.5

*TOTAL SOURCE TERM EFFECTIVE A_2 FOR NORMAL
AND HYPOTHETICAL ACCIDENT CONDITIONS FOR THE HI-STAR HB*

	<i>Effective A_2 (Ci)</i>
<i>Normal Transport Conditions</i>	
<i>HI-STAR HB</i>	46.1 48.6
<i>Accident Conditions</i>	
<i>HI-STAR HB</i>	37.3

Table 4.I.2.6

RADIONUCLIDE RELEASE RATES FOR THE HI-STAR HB

	<i>Allowable Release Rate (R_N or R_A) (Ci/s)</i>
<i>Normal Conditions</i>	
<i>HI-STAR HB</i>	<i>1.28E-08 1.35E-08</i>
<i>Accident Conditions</i>	
<i>HI-STAR HB</i>	<i>6.15E-05</i>

Table 4.I.2.7

ALLOWABLE LEAKAGE RATES AT UPSTREAM PRESSURE FOR THE HI-STAR HB

	<i>Allowable Leakage Rate at $P_u L_N$ or L_A (cm^3/s)</i>
<i>Normal Transport Conditions</i>	
<i>HI-STAR HB</i>	<i>4.19E-05 2.31E-05</i>
<i>Accident Conditions</i>	
<i>HI-STAR HB</i>	<i>9.61E-02</i>

Table 4.I.2.8

PARAMETERS FOR NORMAL, HYPOTHETICAL ACCIDENT
AND TEST CONDITIONS FOR THE HI-STAR HB

<i>Parameter</i>	<i>Normal Conditions</i>	<i>Hypothetical Accident Conditions</i>	<i>Reference Test Conditions</i>	<i>Actual Test Conditions</i>
P_u	84.4 psia (5.74 ATM)	214.7 psia (14.61 ATM)	1.68 ATM	1.68 ATM (min)
P_d	14.7 psia (1 ATM)	14.7 psia (1 ATM)	14.7 psia (1 ATM)	14.7 psia (1 ATM)
T	419°F (488 K)	1058°F (843 K)	373 K	373 K (max)
M	4 g/mol	4 g/mol	4 g/mol	4 g/mol
u	0.0276 cP	0.0397 cP	0.0231 cP	0.0231 cP
a	0.25 cm	0.25 cm	0.25 cm	0.25 cm

5.1 DISCUSSION AND RESULTS

The principal sources of radiation in the HI-STAR 100 System are:

- Gamma radiation originating from the following sources
 1. Decay of radioactive fission products
 2. Hardware activation products generated during core operations
 3. Secondary photons from neutron capture in fissile and non-fissile nuclides

- Neutron radiation originating from the following sources
 1. Spontaneous fission
 2. α, n reactions in fuel materials
 3. Secondary neutrons produced by fission from subcritical multiplication
 4. γ, n reactions (this source is negligible)
 5. Dresden Unit 1 and Trojan neutron sources

Shielding from gamma radiation is provided by the steel structure of the MPC and overpack. In order for the neutron shielding to be effective, the neutrons must be thermalized and then absorbed in a material of high neutron cross section. In the HI-STAR 100 System design, a neutron shielding material, Holtite-A, is used to thermalize the neutrons. Boron carbide, dispersed in the neutron shield, utilizes the high neutron absorption cross section of ^{10}B to absorb the thermalized neutrons.

The shielding analyses were performed with MCNP-4A [5.1.1] from Los Alamos National Laboratory. The source terms for the design basis fuels were calculated with the SAS2H and ORIGEN-S sequences from the SCALE 4.3 system [5.1.2, 5.1.3] from Oak Ridge National Laboratory. The source terms for the Trojan specific inventory were calculated with the SAS2H and ORIGEN-S sequences from the SCALE 4.4 system [5.1.4, 5.1.5] as described in the Trojan FSAR [5.1.6]. A detailed description of the MCNP models and the source term calculations are presented in Sections 5.3 and 5.2, respectively.

The design basis intact zircaloy clad fuels used in calculating the dose rates presented in this chapter are the B&W 15x15 (with zircaloy and non-zircaloy incore spacers) and the GE 7x7, for PWR and BWR fuel types, respectively. The design basis intact 6x6, damaged, and mixed oxide (MOX) fuel assemblies are the GE 6x6. Tables 1.2.22 through 1.2.27 specify the acceptable intact zircaloy clad fuel characteristics for transport. Tables 1.2.23 and 1.2.24 specify the acceptable damaged and MOX zircaloy clad fuel characteristics for transport.

The design bases intact stainless steel clad fuels are the WE 15x15 and the AC 10x10, for PWR and BWR fuel types, respectively. Tables 1.2.22, 1.2.23, 1.2.25, and 1.2.26 specify the acceptable fuel characteristics of stainless steel clad fuel for transport.

The Trojan spent fuel contents were analyzed separately, as discussed in later sections, and therefore are not covered by the design basis fuel assemblies mentioned above.

Tables 1.2.28 through 1.2.33 specify, in tabular form, the minimum enrichment, burnup and cooling time combinations for spent nuclear fuel that were analyzed for transport in the MPC-24, MPC-32, and MPC-68. Each combination provides a dose rate equal to or below the maximum values reported in this section. These tables represent the fuel assembly acceptance criteria.

The burnup, cooling time, and minimum enrichment combinations specified in Tables 1.2.28 through 1.2.33 were determined strictly based on the shielding analysis in this chapter. Each combination was specifically analyzed and it was verified that the calculated dose rates were less than the regulatory limits. Detailed results (e.g. dose from gammas, neutrons, co-60, etc...) are not presented in this chapter for each burnup, cooling time, and minimum enrichment combination analyzed. Rather, the detailed results for the combination that produced the highest dose rate for each of the three regulatory acceptance criteria and locations (i.e. surface normal condition, 2 meter normal condition, 1 meter accident condition) in a specific MPC are presented in this section. However, the total dose rates for all approved burnup and cooling time combinations are presented in Section 5.4. The choice of burnup and cooling time combinations for which detailed (i.e. individual dose components in addition to total) results are provided is discussed further in the following subsections.

Unless otherwise stated, all dose rates reported in this chapter are average surface dose rates. The effect of radiation peaking due to azimuthal variations in the fuel loading pattern and the steel radial channels is specifically addressed in Subsection 5.4.1.

5.1.1 Normal Operations

The 10CFR71.47 external radiation requirements during normal transport operations for an exclusive use shipment are:

1. 200 mrem/hr (2 mSv/hr) on the external surface of the package, unless the following conditions are met, in which case the limit is 1000 mrem/hr (10 mSv/hr).
 - i. The shipment is made in a closed transport vehicle;
 - ii. The package is secured within the vehicle so that its position remains fixed during transportation; and
 - iii. There are no loading and unloading operations between the beginning and end of the transportation.
2. 200 mrem/hr (2 mSv/hr) at any point on the outer surface of the vehicle, including the top and underside of the vehicle; or in the case of a flat-bed style vehicle, at any point on the vertical planes projected from the outer edges of the vehicle, on the upper surface of the load or enclosure, if used, and on the lower external surface of the vehicle.

3. 10 mrem/hr (0.1 mSv/hr) at any point 2 meters (80 in) from the outer lateral surfaces of the vehicle (excluding the top and underside of the vehicle); or in the case of a flat-bed style vehicle, at any point 2 meters (6.6 feet) from the vertical planes projected by the outer edges of the vehicle (excluding the top and underside of the vehicle).
4. 2 mrem/h (0.02 mSv/hr) in any normally occupied space, except that this provision does not apply to private carriers, if exposed personnel under their control wear radiation dosimetry devices in conformance with 10CFR20.1502.

The Standard Review Plan for Transportation Packages of Spent Nuclear Fuel, NUREG-1617 [5.2.1] states that "Personnel barriers and similar devices that are attached to the conveyance, rather than the package, can, however, qualify the vehicle as a closed vehicle (NUREG/CR-5569A and NUREG/CR-5569B) as defined in 49 CFR 173.403."

When the HI-STAR is transported, a personnel barrier will be placed over the HI-STAR as depicted in Figure 1.2.8. This personnel barrier spans the distance between the impact limiters. The outer radial location of the personnel barrier is equal to the outer radial surface of the impact limiters and the personnel barrier is attached to the saddle on the rail car rather than the HI-STAR overpack. Therefore, the personnel barrier acts as an enclosure for the main body of the HI-STAR overpack. Consequently, the 1000 mrem/hr limit for the enclosed package is applicable for the outer radial surface of the overpack in the region between the impact limiters. Since the impact limiters are not enclosed, the surface of the impact limiters is required to meet the lower 200 mrem/hr limit for the package.

The HI-STAR 100 System will be transported on either a flat-bed rail car, heavy haul vehicle, or a barge. The smallest width of a transport vehicle is equivalent to the width of the impact limiters. Therefore, the vertical planes projected by the outer side edges of the transport vehicle are equivalent to the outer edge of the impact limiters. The minimum length of any transport vehicle will be 12 feet longer than the length of the overpack, with impact limiters attached. The bottom impact limiter of the HI-STAR 100 System will be conservatively positioned a minimum of 9 feet from the end of the transport vehicle. Therefore, the vertical planes projected from the outer edge of the ends of the vehicle will be taken as the end of the top impact limiter and 9 feet from the end of the bottom impact limiter.

Figure 5.1.1 shows the HI-STAR 100 System during normal transport conditions. The impact limiters and personnel barrier are outlined on the figure and various dose point locations are shown on the surface of the enclosure (personnel barrier) and the HI-STAR 100 System. The dose values reported at the locations shown on Figure 5.1.1 are averaged over a region that is approximately 1 foot in width. Each of the dose locations in Figure 5.1.1 (with the exception of 2a and 3a) has a corresponding location at 2 meters from the surface of the transport vehicle as defined above.

Dose locations 2a, 3a, and 2 shown in Figure 5.1.1 and Figure 5.1.2 (discussed below) do not correspond to single dose locations. Rather the dose rate for multiple axial segments of approximately 1 foot or less were calculated and the highest value was chosen for the corresponding dose location. Dose locations 2a and 2 encompass 14 axial segments that range from the pocket trunnion to the top of the Holtite. The highest dose rate of these 14 axial segments was chosen as the value for dose locations 2a and 2. Dose location 3a corresponds to two axial segments while dose locations 1, 3, and 4 correspond to a single axial segment. Dose locations 5 and 6 correspond to either the center radial segment of the overpack along the axis or the adjacent location radial segment.

Tables 5.1.1 through 5.1.3, 5.1.10, and 5.1.11 provide the maximum dose rates on the surface of the system during normal transport conditions for the MPC-24, MPC-32, and MPC-68 with design basis intact zircaloy clad fuel. Tables 5.1.4 through 5.1.6, 5.1.12, and 5.1.13 list the maximum dose rates two meters from the edge of the transport vehicle during normal conditions. Section 5.4 provides a detailed list of the total dose rates at several cask locations for all burnup and cooling times analyzed. The burnup and cooling time combinations chosen for the tables mentioned above was the combination that resulted in the absolute highest dose rate for the normal condition regulatory locations (i.e. surface and 2 meter). For example, Table 5.1.1 presents the burnup and cooling time combination that results in the highest dose rate from a review of the dose rates, in Table 5.4.8, for locations 2a, 3a, and 1-6 for all allowable burnup and cooling time combinations. This combination may not result in the highest dose rate at each individual dose location (e.g. 2a, 3a, 1-6) but it is the combination that results in the absolute highest dose rate for the surface or 2 meter locations.

Subsections 5.2.1 and 5.2.2 list the gamma and neutron sources for the design basis zircaloy clad intact, zircaloy clad damaged and MOX fuel assemblies. Since the source strengths of the damaged and MOX fuel are significantly smaller in all energy groups than the intact design basis fuel source strengths, the damaged and MOX fuel dose rates for normal conditions are bounded by the MPC-68 analysis with design basis intact fuel. Therefore, no explicit analysis of the MPC-68 with either damaged or MOX fuel for normal conditions is required to demonstrate that the MPC-68 with damaged fuel or MOX fuel will meet the normal condition regulatory requirements.

Subsection 5.2.6 lists the gamma and neutron sources from the Dresden Unit 1 Thoria rod canister and demonstrates that the Thoria rod canister is bounded by the design basis 6x6 intact fuel.

Subsection 5.4.5 demonstrates that the Dresden Unit 1 fuel assemblies containing antimony-beryllium neutron sources are bounded by the shielding analysis presented in this section.

Subsections 5.4.7 and 5.4.8 present the results for the Trojan contents in the MPC-24E/EF and demonstrate that these contents are acceptable for transportation.

Subsection 5.2.3 lists the gamma and neutron sources for the design basis intact stainless steel clad fuels. The dose rates from these fuels are provided in Subsection 5.4.4.

Tables 5.1.4 through 5.1.6, 5.1.12, and 5.1.13 show that the dose rate at Dose Location #5 (the top of the HI-STAR 100 System, see Figure 5.1.1) at 2 meters from the edge of the transport vehicle is less than 2 mrem/hr. It is, therefore, recommended that the HI-STAR 100 System be positioned such that the top impact limiter is facing the normally occupied space. If this is the orientation, radiation dosimetry will not be required as long as the normally occupied space is a minimum of 2 meters from the impact limiter on the top of the HI-STAR 100 System. If a different orientation is chosen for the HI-STAR 100 System, the dose rate in the normally occupied space will have to be evaluated against the dose requirement for the normally occupied space to determine if radiation dosimetry is required.

The analyses summarized in this section demonstrate the HI-STAR 100 System's compliance with the 10CFR71.47 limits.

5.1.2 Hypothetical Accident Conditions

The 10CFR71.51 external radiation dose limit for design basis accidents is:

- The external radiation dose rate shall not exceed 1 rem/hr (10 mSv/hr) at 1 m (40 in.) from the external surface of the package.

The hypothetical accident conditions of transport have two bounding consequences which affect the shielding materials. They are the damage to the neutron shield as a result of the design basis fire and damage of the impact limiters as a result of the 30 foot drop. In a conservative fashion, the dose analysis assumes that as a result of the fire, the neutron shield is completely destroyed and replaced by a void. Additionally, the impact limiters are assumed to have been lost. These are highly conservative assumptions since some portion of the neutron shield would be expected to remain after the fire as the neutron shield material is fire retardant, and the impact limiters have been shown by 1/4-scale testing to remain attached following impact.

Throughout the hypothetical accident condition the axial location of the fuel will remain fixed within the MPC because of the fuel spacers or by the MPC lid and baseplate if spacers are not used. Chapter 2 provides an analysis to show that the fuel spacers do not fail under all normal and hypothetical accident conditions. Chapter 2 also shows that the inner shell, intermediate shell, radial channels, and outer enclosure shell of the overpack remain unaltered throughout the hypothetical accident conditions. Localized damage of the overpack outer enclosure shell could be experienced during the pin puncture. However, the localized deformations will have only a negligible impact on the dose rate at 1 meter from the surface.

Figure 5.1.2 shows the HI-STAR 100 System after the postulated accident. The various dose point locations at 1 meter from the HI-STAR 100 System are shown on the figure. Tables 5.1.7

through 5.1.9, 5.1.14 and 5.1.15 provide the maximum dose rates at 1 meter for the accident conditions. The burnup and cooling time combinations chosen for the aforementioned tables were the combinations that resulted in the absolute highest dose rate for the accident condition regulatory location (i.e. 1 meter).

The consequences of the hypothetical accident conditions for the MPC-68F storing either damaged or MOX (which can also be considered damaged) fuel differ slightly from those with intact fuel. For this accident condition, it is conservatively assumed that during a drop accident the damaged fuel collapses and the pellets rest in the bottom of the damaged fuel container. The analysis presented in Subsections 5.4.2 and 5.4.3 demonstrate that the damaged fuel in the post-accident condition has lower source terms (both gamma and neutron) per inch than the intact BWR design basis fuel. Therefore, the damaged fuel post-accident dose rates are bounded by the BWR intact fuel post-accident dose rates.

Subsections 5.4.7 and 5.4.8 present the results for the Trojan contents in the MPC-24E/EF and demonstrate that these contents are acceptable for transportation.

Analyses summarized in this section demonstrate the HI-STAR 100 System's compliance with the 10CFR71.51 radiation dose limit.

Table 5.1.1

DOSE RATES ON THE SURFACE OF THE HI-STAR 100 SYSTEM FOR NORMAL CONDITIONS
MPC-24 WITH DESIGN BASIS ZIRCALOY CLAD FUEL WITH ZIRCALOY INCORE SPACERS
AT WORST CASE BURNUP AND COOLING TIME
44,500 MWD/MTU AND 14-YEAR COOLING

Dose Point [†] Location	Fuel Gammas ^{††} (mrem/hr)	Gammas from Incore Spacers (mrem/hr)	⁶⁰ Co Gammas (mrem/hr)	Neutrons (mrem/hr)	Totals (mrem/hr)	10 CFR 71.47 Limit
2a	23.91	0.00	0.01	22.27	46.19	1000
3a	0.96	0.00	28.52	108.98	138.47	1000
1	1.92	0.00	13.98	18.95	34.85	200
2	15.33	0.00	0.09	12.82	28.24	200
3	1.11	0.00	10.45	18.63	30.19	200
4	0.62	0.00	9.21	18.22	28.05	200
5	0.500.49	0.00	0.020.02	3.633.82	4.154.33	200
6	4.744.60	0.00	55.8553.31	29.4231.63	90.0289.54	200

[†] Refer to Figure 5.1.1.

^{††} Gammas generated by neutron capture are included with fuel gammas.

Table 5.1.2

DOSE RATES ON THE SURFACE OF THE HI-STAR 100 SYSTEM FOR NORMAL CONDITIONS
MPC-24 WITH DESIGN BASIS ZIRCALOY CLAD FUEL WITH NON-ZIRCALOY INCORE SPACERS
AT WORST CASE BURNUP AND COOLING TIME
44,500 MWD/MTU AND 18-YEAR COOLING

Dose Point [†] Location	Fuel Gammas ^{††} (mrem/hr)	Gammas from Incore Spacers (mrem/hr)	⁶⁰ Co Gammas (mrem/hr)	Neutrons (mrem/hr)	Totals (mrem/hr)	10 CFR 71.47 Limit
2a	18.10	8.92	0.01	19.22	46.24	1000
3a	0.78	0.14	16.91	94.04	111.87	1000
1	1.48	0.63	8.29	16.35	26.75	200
2	11.56	5.93	0.05	11.07	28.62	200
3	0.85	0.35	6.19	16.08	23.47	200
4	0.49	0.19	5.46	15.72	21.85	200
5	0.442 ^{†††}	-	0.010-01	3.133-30	3.583-73	200
6	4.8569 ^{†††}	-	33.1031-60	25.3927-29	63.3563-58	200

[†] Refer to Figure 5.1.1.

^{††} Gammas generated by neutron capture are included with fuel gammas.

^{†††} Gammas from incore spacers are included with fuel gammas.

Table 5.1.3

DOSE RATES ON THE SURFACE OF THE HI-STAR 100 SYSTEM FOR NORMAL CONDITIONS
MPC-68 WITH DESIGN BASIS ZIRCALOY CLAD FUEL AT
WORST CASE BURNUP AND COOLING TIME
3420,5000 MWD/MTU AND 17-YEAR COOLING

Dose Point [†] Location	Fuel Gammas ^{††} (mrem/hr)	Gammas from Incore Spacers (mrem/hr)	⁶⁰ Co Gammas (mrem/hr)	Neutrons (mrem/hr)	Totals (mrem/hr)	10 CFR 71.47 Limit
2a	0.5027.04	0.104.53	49.980.01	2.1018.53	52.6950.12	1000
3a	0.330.43	0.120.08	140.6694.78	13.3036.91	154.42132.20	1000
1	2.032.15	0.540.36	31.6321.32	5.0914.13	39.2937.96	200
2	1.2117.55	0.313.08	24.280.08	1.7310.40	27.5331.12	200
3	0.590.67	0.140.10	34.1723.02	2.857.90	37.7531.69	200
4	0.310.36	0.080.06	32.6722.01	2.697.48	35.7629.91	200
5	0.0720 ^{†††}	-	0.040.03	0.491.56	0.601.78	200
6	2.523.17 ^{†††}	-	111.6972.37	7.0019.73	121.2195.27	200

[†] Refer to Figure 5.1.1.

^{††} Gammas generated by neutron capture are included with fuel gammas.

^{†††} Gammas from incore spacers are included with fuel gammas.

Table 5.1.4

DOSE RATES AT TWO METERS FOR NORMAL CONDITIONS
MPC-24 WITH DESIGN BASIS ZIRCALOY CLAD FUEL WITH ZIRCALOY INCORE SPACERS
AT WORST CASE BURNUP AND COOLING TIME
24,500 MWD/MTU AND 6-YEAR COOLING

Dose Point [†] Location	Fuel Gammas ^{††} (mrem/hr)	Gammas from Incore Spacers (mrem/hr)	⁶⁰ Co Gammas (mrem/hr)	Neutrons (mrem/hr)	Totals (mrem/hr)
1	3.06	0.00	3.56	0.78	7.41
2	7.52	0.00	1.16	0.88	9.57
3	2.57	0.00	3.41	0.74	6.72
4	2.03	0.00	3.43	0.70	6.16
5	0.010.01	0.00	0.010.01	0.070.09	0.090.10
6	0.280.32	0.00	7.857.60	0.260.19	8.398.11
10CFR71.47 Limit					10.00

[†] Refer to Figure 5.1.1.

^{††} Gammas generated by neutron capture are included with fuel gammas.

Table 5.1.5

DOSE RATES AT TWO METERS FOR NORMAL CONDITIONS
MPC-24 WITH DESIGN BASIS ZIRCALOY CLAD FUEL WITH NON-ZIRCALOY INCORE SPACERS
AT WORST CASE BURNUP AND COOLING TIME
24,500 MWD/MTU AND 9-YEAR COOLING

Dose Point [†] Location	Fuel Gammas ^{††} (mrem/hr)	Gammas from Incore Spacers (mrem/hr)	⁶⁰ Co Gammas (mrem/hr)	Neutrons (mrem/hr)	Totals (mrem/hr)
1	1.42	1.90	2.40	0.70	6.42
2	3.38	4.56	0.80	0.77	9.51
3	1.18	1.54	2.30	0.66	5.68
4	0.94	1.21	2.31	0.63	5.08
5	0.01 ^{†††}	-	0.010.01	0.070.08	0.080.09
6	0.328 ^{†††}	-	5.295.12	0.230.17	5.845.67
10CFR71.47 Limit					10.00

[†] Refer to Figure 5.1.1.

^{††} Gammas generated by neutron capture are included with fuel gammas.

^{†††} Gammas from incore spacers are included with fuel gammas.

Table 5.1.6

DOSE RATES AT TWO METERS FOR NORMAL CONDITIONS
MPC-68 WITH DESIGN BASIS ZIRCALOY CLAD FUEL
AT WORST CASE BURNUP AND COOLING TIME
34,500 MWD/MTU AND 11-YEAR COOLING

Dose Point [†] Location	Fuel Gammas ^{††} (mrem/hr)	Gammas from Incore Spacers (mrem/hr)	⁶⁰ Co Gammas (mrem/hr)	Neutrons (mrem/hr)	Totals (mrem/hr)
1	2.38	0.43	2.33	2.45	7.59
2	5.19	0.95	0.65	2.83	9.62
3	1.56	0.28	3.14	1.64	6.62
4	1.21	0.21	3.33	1.57	6.32
5	0.02 ^{†††}	-	0.010.01	0.130.18	0.150.20
6	0.175 ^{†††}	-	4.394.31	0.450.48	5.014.94
10CFR71.47 Limit					10.00

[†] Refer to Figure 5.1.1.

^{††} Gammas generated by neutron capture are included with fuel gammas.

^{†††} Gammas from incore spacers are included with fuel gammas.

Table 5.1.7

DOSE RATES AT ONE METER FOR ACCIDENT CONDITIONS
MPC-24 WITH DESIGN BASIS ZIRCALOY CLAD FUEL WITH ZIRCALOY INCORE SPACERS
AT WORST CASE BURNUP AND COOLING TIME
29,500 MWD/MTU AND 7-YEAR COOLING

Dose Point [†] Location	Fuel Gammas ^{††} (mrem/hr)	⁶⁰ Co Gammas (mrem/hr)	Neutrons (mrem/hr)	Totals (mrem/hr)
1	7.11	34.28	56.17	97.55
2	37.07	1.19	185.96	224.23
3	4.67	19.87	39.87	64.41
4	2.70	15.08	29.35	47.12
5	0.03	0.24	6.32	6.59
6	20.66	618.44	47.99	687.08
10CFR71.51 Limit				1000.00

[†] Refer to Figure 5.1.2.

^{††} Gammas generated by neutron capture and gammas from incore spacers are included with fuel gammas.

Table 5.1.8

DOSE RATES AT ONE METER FOR ACCIDENT CONDITIONS
MPC-24 WITH DESIGN BASIS ZIRCALOY CLAD FUEL WITH NON-ZIRCALOY INCORE SPACERS
AT WORST CASE BURNUP AND COOLING TIME
24,500 MWD/MTU AND 9-YEAR COOLING

Dose Point [†] Location	Fuel Gammas ^{††} (mrem/hr)	⁶⁰ Co Gammas (mrem/hr)	Neutrons (mrem/hr)	Totals (mrem/hr)
1	8.40	23.69	30.24	62.33
2	44.07	0.82	100.11	145.00
3	5.51	13.73	21.46	40.70
4	3.17	10.42	15.80	29.39
5	0.02	0.17	3.40	3.59
6	25.07	427.37	25.84	478.28
10CFR71.51 Limit				1000.00

[†] Refer to Figure 5.1.2.

^{††} Gammas generated by neutron capture and gammas from incore spacers are included with fuel gammas.

Table 5.1.9

DOSE RATES AT ONE METER FOR ACCIDENT CONDITIONS
MPC-68 WITH DESIGN BASIS ZIRCALOY CLAD FUEL
AT WORST CASE BURNUP AND COOLING TIME
4420,5000 MWD/MTU AND 497-YEAR COOLING

Dose Point [†] Location	Fuel Gammas ^{††} (mrem/hr)	⁶⁰ Co Gammas (mrem/hr)	Neutrons (mrem/hr)	Totals (mrem/hr)
1	7.904.47	37.5410.20	40.74183.86	86.18198.52
2	38.8421.94	0.800.22	133.11600.71	172.74622.86
3	3.071.81	25.516.93	20.8193.91	49.39102.65
4	1.711.02	22.736.18	14.8867.17	39.3374.36
5	0.020.04	0.260.07	2.4210.93	2.7011.04
6	9.725.76	631.00171.42	27.37123.53	668.09300.71
10CFR71.51 Limit				1000.00

[†] Refer to Figure 5.1.2.

^{††} Gammas generated by neutron capture and gammas from incore spacers are included with fuel gammas.

Table 5.1.10

DOSE RATES ON THE SURFACE OF THE HI-STAR 100 SYSTEM FOR NORMAL CONDITIONS
MPC-32 WITH DESIGN BASIS ZIRCALOY CLAD FUEL WITH ZIRCALOY INCORE SPACERS
AT WORST CASE BURNUP AND COOLING TIME
44,500 MWD/MTU AND 19-YEAR COOLING

Dose Point [†] Location	Fuel Gammas ^{††} (mrem/hr)	Gammas from Incore Spacers (mrem/hr)	⁶⁰ Co Gammas (mrem/hr)	Neutrons (mrem/hr)	Totals (mrem/hr)	10 CFR 71.47 Limit
2a	2.77	0.00	17.29	30.84	50.90	1000
3a	2.01	0.00	27.39	234.56	263.95	1000
1	1.90	0.00	11.60	29.02	42.51	200
2	2.80	0.00	8.42	24.26	35.48	200
3	1.45	0.00	9.60	38.62	49.68	200
4	0.74	0.00	8.99	37.58	47.31	200
5	0.930 0.89	0.00	0.020 0.01	7.528 2.1	8.469 1.1	200
6	5.695 5.3	0.00	44.214 2.31	45.554 9.50	95.459 7.35	200

[†] Refer to Figure 5.1.1.

^{††} Gammas generated by neutron capture are included with fuel gammas.

Table 5.1.11

DOSE RATES ON THE SURFACE OF THE HI-STAR 100 SYSTEM FOR NORMAL CONDITIONS
MPC-32 WITH DESIGN BASIS ZIRCALOY CLAD FUEL WITH NON-ZIRCALOY INCORE SPACERS
AT WORST CASE BURNUP AND COOLING TIME
42,500 MWD/MTU AND 20-YEAR COOLING

Dose Point [†] Location	Fuel Gammas ^{††} (mrem/hr)	Gammas from Incore Spacers (mrem/hr)	⁶⁰ Co Gammas (mrem/hr)	Neutrons (mrem/hr)	Totals (mrem/hr)	10 CFR 71.47 Limit
2a	18.92	9.15	0.01	16.46	44.54	1000
3a	1.65	0.29	22.98	188.28	213.21	1000
1	1.61	0.70	9.73	23.29	35.33	200
2	2.38	1.01	7.06	19.48	29.93	200
3	1.22	0.46	8.06	31.01	40.74	200
4	0.63	0.24	7.54	30.17	38.57	200
5	0.754 ^{†††}	-	0.010.01	6.046.59	6.797.32	200
6	5.9778 ^{†††}	-	37.1035.51	36.5639.74	79.6481.03	200

[†] Refer to Figure 5.1.1.

^{††} Gammas generated by neutron capture are included with fuel gammas.

^{†††} Gammas from incore spacers are included with fuel gammas.

Table 5.1.12

DOSE RATES AT TWO METERS FOR NORMAL CONDITIONS
MPC-32 WITH DESIGN BASIS ZIRCALOY CLAD FUEL WITH ZIRCALOY INCORE SPACERS
AT WORST CASE BURNUP AND COOLING TIME
39,500 MWD/MTU AND 14-YEAR COOLING

Dose Point [†] Location	Fuel Gammas ^{††} (mrem/hr)	Gammas from Incore Spacers (mrem/hr)	⁶⁰ Co Gammas (mrem/hr)	Neutrons (mrem/hr)	Totals (mrem/hr)
1	2.29	0.00	2.59	3.56	8.43
2	5.25	0.00	0.82	3.58	9.65
3	1.92	0.00	2.66	4.52	9.10
4	1.57	0.00	2.67	4.56	8.79
5	0.060.05	0.00	0.010.01	0.490.64	0.550.70
6	0.190.23	0.00	4.554.41	0.920.96	5.665.60
10CFR71.47 Limit					10.00

[†] Refer to Figure 5.1.1.

^{††} Gammas generated by neutron capture are included with fuel gammas.

Table 5.1.13

DOSE RATES AT TWO METERS FOR NORMAL CONDITIONS
MPC-32 WITH DESIGN BASIS ZIRCALOY CLAD FUEL WITH NON-ZIRCALOY INCORE SPACERS
AT WORST CASE BURNUP AND COOLING TIME
42,500 MWD/MTU AND 20-YEAR COOLING

Dose Point [†] Location	Fuel Gammas ^{††} (mrem/hr)	Gammas from Incore Spacers (mrem/hr)	⁶⁰ Co Gammas (mrem/hr)	Neutrons (mrem/hr)	Totals (mrem/hr)
1	1.68	0.80	1.22	3.43	7.13
2	3.81	1.96	0.38	3.46	9.61
3	1.43	0.67	1.25	4.36	7.71
4	1.16	0.54	1.26	4.40	7.36
5	0.056 ^{†††}	-	0.000.00	0.470.62	0.530.67
6	0.214 ^{†††}	-	2.142.08	0.890.92	3.243.24
10CFR71.47 Limit					10.00

[†] Refer to Figure 5.1.1.

^{††} Gammas generated by neutron capture are included with fuel gammas.

^{†††} Gammas from incore spacers are included with fuel gammas.

Table 5.1.14

DOSE RATES AT ONE METER FOR ACCIDENT CONDITIONS
MPC-32 WITH DESIGN BASIS ZIRCALOY CLAD FUEL WITH ZIRCALOY INCORE SPACERS
AT WORST CASE BURNUP AND COOLING TIME
29,500 MWD/MTU AND 9-YEAR COOLING

Dose Point [†] Location	Fuel Gammas ^{††} (mrem/hr)	⁶⁰ Co Gammas (mrem/hr)	Neutrons (mrem/hr)	Totals (mrem/hr)
1	6.51	43.30	68.18	117.99
2	32.65	1.42	196.89	230.95
3	4.37	25.54	60.00	89.91
4	2.64	20.54	43.37	66.55
5	0.06	0.27	14.76	15.09
6	18.89	720.63	77.64	817.16
10CFR71.51 Limit				1000.00

[†] Refer to Figure 5.1.2.

^{††} Gammas generated by neutron capture and gammas from incore spacers are included with fuel gammas.

Table 5.1.15

DOSE RATES AT ONE METER FOR ACCIDENT CONDITIONS
MPC-32 WITH DESIGN BASIS ZIRCALOY CLAD FUEL WITH NON-ZIRCALOY INCORE SPACERS
AT WORST CASE BURNUP AND COOLING TIME
24,500 MWD/MTU AND 12-YEAR COOLING

Dose Point [†] Location	Fuel Gammas ^{††} (mrem/hr)	⁶⁰ Co Gammas (mrem/hr)	Neutrons (mrem/hr)	Totals (mrem/hr)
1	8.07	26.23	35.50	69.80
2	40.10	0.86	102.53	143.48
3	5.43	15.47	31.25	52.15
4	3.29	12.44	22.58	38.31
5	0.04	0.16	7.69	7.89
6	23.63	436.48	40.43	500.54
10CFR71.51 Limit				1000.00

† Refer to Figure 5.1.2.

†† Gammas generated by neutron capture and gammas from incore spacers are included with fuel gammas.

5.2 SOURCE SPECIFICATION

The neutron and gamma source terms, decay heat values, and quantities of radionuclides available for release were calculated with the SAS2H and ORIGEN-S modules of the SCALE 4.3 system [5.1.2, 5.1.3]. The source terms for the Trojan specific inventory were calculated with the SAS2H and ORIGEN-S sequences from the SCALE 4.4 system [5.1.4, 5.1.5] as described in the Trojan FSAR [5.1.6]. Sample input files for SAS2H and ORIGEN-S are provided in Appendices 5.A and 5.B, respectively. The gamma source term is actually comprised of three distinct sources. The first is a gamma source term from the active fuel region due to decay of fission products. The second source term is from ^{60}Co activity of the steel structural material in the fuel assembly above and below the active fuel region. The third source is from (n,γ) reactions described below.

A description of the design basis intact zircaloy clad fuel for the source term calculations is provided in Table 5.2.1. The PWR fuel assembly described is the assembly that produces the highest neutron and gamma sources and the highest decay heat load from the following fuel assembly classes listed in Table 1.2.8: B&W 15x15, B&W 17x17, CE 14x14, CE 16x16, WE 14x14, WE 15x15, WE 17x17, St. Lucie, and Ft. Calhoun. The BWR fuel assembly described is the assembly that produces the highest neutron and gamma sources and the highest decay heat load from the following fuel assembly classes listed in Table 1.2.9: GE BWR/2-3, GE BWR/4-6, Humboldt Bay 7x7, and Dresden 1 8x8. Multiple SAS2H and ORIGEN-S calculations were performed to confirm that the B&W 15x15 and the GE 7x7, which have the highest UO_2 mass, bound all other PWR and BWR fuel assemblies, respectively. Subsection 5.2.5 discusses, in detail, the determination of the design basis fuel assemblies.

The design basis Humboldt Bay and Dresden 1 6x6 fuel assembly, which is also the design basis damaged fuel assembly for the Humboldt Bay and Dresden 1 damaged fuel or fuel debris, is described in Table 5.2.2. The design basis damaged fuel assembly is also the design basis fuel assembly for fuel debris. The fuel assembly type listed produces the highest total neutron and gamma sources from the fuel assemblies at Dresden 1 and Humboldt Bay. Table 5.2.15 provides a description of the design basis Dresden 1 MOX fuel assembly used in this analysis. The design basis 6x6, damaged, and MOX fuel assemblies which are smaller than the GE 7x7, are assumed to have the same hardware characteristics as the GE 7x7. This is conservative because the larger hardware mass of the GE 7x7 results in a larger ^{60}Co activity.

The design basis stainless steel clad fuel assembly for the Indian Point 1, Haddam Neck and San Onofre 1 assembly classes is described in Table 5.2.18. This table also describes the design basis stainless steel clad LaCrosse fuel assembly.

Since the MPC-24E being used for Trojan fuel is slightly different than the standard MPC-24E, the Trojan contents were specifically analyzed and are not covered by the design basis PWR fuel assembly described above. The design basis Trojan WE 17x17 fuel assembly is described in Table 5.2.32 and was taken from the site specific Trojan FSAR analysis [5.1.6].

In performing the SAS2H and ORIGEN-S calculations, a single full power cycle was used to achieve the desired burnup. This assumption, in conjunction with the above-average specific powers listed in Tables 5.2.1, 5.2.2, 5.2.15, 5.2.18, and 5.2.32 resulted in conservative source term calculations.

Subsections 5.2.1 and 5.2.2 describe the calculation of the gamma and neutron source terms for zircaloy clad fuel while Subsection 5.2.3 discusses the calculation of the gamma and neutron source terms for the stainless steel clad fuel.

5.2.1 Gamma Source

Tables 5.2.3 through 5.2.6, 5.2.33, 5.2.40, and 5.2.41 provide the gamma source in MeV/s and photons/s as calculated with SAS2H and ORIGEN-S for the design bases intact fuels for the MPC-24, MPC-32, MPC-68, the design basis damaged fuel, and the Trojan fuel. Table 5.2.16 provides the gamma source in MeV/s and photons/s for the design basis MOX fuel. NUREG-1617 [5.2.1] states that "In general, only gammas from approximately 0.8 MeV-2.5 MeV will contribute significantly to the external radiation levels." However, specific analysis for the HI-STAR 100 system has revealed that, due to the magnitude of the gamma source in the energy range just below 0.8 MeV, gammas with energies as low as 0.45 MeV must be included in the shielding analysis. The effect of gammas with energies above 3.0 MeV, on the other hand, was found to be insignificant (less than 1% of the total gamma dose). This is due to the fact that the source of gammas in this range (i.e., above 3.0 MeV) is extremely low (less than 1% of the total source). Therefore, all gammas with energies in the range of 0.45 to 3.0 MeV are included in the shielding calculations. Photons with energies below 0.45 MeV are too weak to penetrate the steel of the overpack, and photons with energies above 3.0 MeV are too few to contribute significantly to the external dose. As discussed earlier, the MPC-24, MPC-32, and the MPC-68 are analyzed for transportation of spent nuclear fuel with varying minimum enrichments, burnup levels and cooling times. This section provides the radiation source for each of the burnup levels and cooling times evaluated.

The primary source of activity in the non-fuel regions of an assembly arise from the activation of ^{59}Co to ^{60}Co . The primary source of ^{59}Co in a fuel element is the steel and inconel structural material. The zircaloy in these regions is neglected since it does not have a significant ^{59}Co impurity level. Reference [5.2.3] indicates that the ^{59}Co impurity level in steel is 800 ppm or 0.8 gm/kg and in inconel is approximately 4700 ppm or 4.7 gm/kg. In the early to mid 1980s, the fuel vendors reduced the ^{59}Co impurity level in both inconel and steel to less than 500 ppm or 0.5 gm/kg. Prior to that, the impurity level in inconel in fuel assemblies was typically less than 1200 ppm or 1.2 gm/kg. Nevertheless, a conservative ^{59}Co impurity level of 1.0 gm/kg was used for the stainless steel end fittings and a highly conservative impurity level of 4.7 gm/kg was used for the inconel.

PWR fuel assemblies are currently manufactured with zircaloy incore grid spacers (the plenum spacer and the lower spacer are still inconel in some cases). However, earlier assemblies were manufactured with inconel incore grid spacers. Since the mass of the spacers is significant and since the cobalt impurity level assumed for inconel is very conservative, the Cobalt-60 activity from the incore spacers contributes significantly to the external dose rate. As a result, separate burnup and cooling times were developed for PWR assemblies that utilize zircaloy and non-zircaloy incore spacers. Since steel has a lower cobalt impurity level than inconel, any zircaloy clad PWR assemblies with stainless steel grid spacers are bounded by the analysis performed in this chapter utilizing inconel grid spacers. The BWR assembly grid spacers are zircaloy, however, some assembly designs have inconel springs in conjunction with the grid spacers. The gamma source for the BWR fuel assembly includes the activation of these springs associated with the grid spacers.

The non-fuel data listed in Table 5.2.1 was taken from References [5.2.3], [5.2.4], and [5.2.5] while the non-fuel data listed in Table 5.2.32 was taken from References [5.2.5] and [5.2.8]. The BWR masses are for an 8x8 fuel assembly. These masses are also appropriate for the 7x7 assembly since the masses of the non-fuel hardware from a 7x7 and an 8x8 are approximately the same. The masses listed are those of the steel components. The zircaloy in these regions was not included because zircaloy does not produce significant activation. These masses are larger than most other fuel assemblies from other manufacturers. This, in combination with the conservative ^{59}Co impurity level, results in a conservative estimate of the ^{60}Co activity.

The masses in Table 5.2.1 and 5.2.32 were used to calculate a ^{59}Co impurity level in the fuel material. The grams of impurity were then used in ORIGEN-S to calculate a ^{60}Co activity level for the desired burnup and decay time. The methodology used to determine the activation level was developed from Reference [5.2.2] and is described here:

1. The activity of the ^{60}Co is calculated using ORIGEN-S. The flux used in the calculation was the in-core fuel region flux at full power.
2. The activity calculated in Step 1 for the region of interest was modified by the appropriate scaling factors listed in Table 5.2.7. These scaling factors were taken from Reference [5.2.2]. In the case of the Trojan fuel, the higher value of 0.2 was used for both the gas plenum springs and spacer consistent with the Trojan FSAR [5.1.6].

Tables 5.2.8 through 5.2.10, 5.2.34, 5.2.42, and 5.2.43 provide the ^{60}Co activity utilized in the shielding calculations in the non-fuel regions of the assemblies for the MPC-24, MPC-32, MPC-68, and Trojan fuel. The design basis damaged and MOX fuel assemblies are conservatively assumed to have the same ^{60}Co source strength as the BWR intact design basis fuel. This is a conservative assumption as the design basis damaged fuel and MOX fuel are limited to a significantly lower burnup and longer cooling time than the intact design basis zircaloy clad fuel.

In addition to the two sources already mentioned, a third source arises from (n,γ) reactions in the material of the MPC and the overpack. This source of photons is properly accounted for in MCNP when a neutron calculation is performed in a coupled neutron-gamma mode.

5.2.2 Neutron Source

It is well known that the neutron source strength increases as enrichment decreases, for a constant burnup and decay time. This is due to the increase in Pu content in the fuel which increases the inventory of other transuranium nuclides such as Cm. The gamma source also varies with enrichment, although only slightly. Because of this effect and in order to obtain conservative source terms, low initial fuel enrichments were chosen for the BWR and PWR design basis fuel assemblies as a function of burnup and cooling time. Conservatively, the minimum enrichments used to develop the source terms and dose rates presented in this chapter are specified in Tables 1.2.28 through 1.2.33 as fuel assembly acceptance criteria. The minimum enrichments for the design basis PWR and BWR assemblies are also listed in Table 5.2.23 for convenience.

The neutron source calculated for the design basis intact fuel assemblies for the MPC-24, MPC-32, MPC-68, Trojan fuel, and the design basis damaged fuel are listed in Tables 5.2.11 through 5.2.14, 5.2.35, 5.2.44, and 5.2.45 in neutrons/s. Table 5.2.17 provides the neutron source in neutrons/sec for the design basis MOX fuel assembly. ^{244}Cm accounts for approximately 96% of the total number of neutrons produced, with slightly over 2% originating from (α,n) reactions within the UO_2 fuel. The remaining 2% derive from spontaneous fission in various Pu and Cm radionuclides. In addition, any neutrons generated from subcritical multiplication, $(n,2n)$ or similar reactions are properly accounted for in the MCNP calculation.

5.2.3 Stainless Steel Clad Fuel Source

Table 5.2.18 lists the characteristics of the design basis stainless steel clad fuel. The fuel characteristics listed in this table are the input parameters that were used in the shielding calculations described in this chapter. The active fuel length listed in the table is actually longer than the true active fuel length of 122 inches for the W15x15 and 83 inches for the A/C 10x10. Since the true active fuel length is shorter than the design basis zircaloy clad active fuel length, it would be incorrect to calculate source terms for the stainless steel fuel using the actual fuel length and compare them directly to the source terms from the zircaloy clad fuel with a longer active fuel length.

In order to eliminate the potential confusion when comparing source terms, the stainless steel clad fuel source terms were calculated with the same active fuel length as the design basis zircaloy clad fuel. Reference [5.2.3] indicates that the Cobalt-59 impurity level in steel is 800 ppm or 0.8 gm/kg and in inconel is approximately 4700 ppm or 4.7 gm/kg. In the early to mid 1980s, the fuel vendors reduced the Cobalt-59 impurity level in both inconel and steel to less than 500 ppm or 0.5 gm/kg. Prior to that, the impurity level in inconel in fuel assemblies was

typically less than 1200 ppm or 1.2 gm/kg. Nevertheless, a conservative Cobalt-59 impurity level of 0.8 gm/kg was used for the stainless steel cladding and a highly conservative impurity level of 4.7 gm/kg was used for the inconel incore spacers. It is assumed that the end fitting masses of the stainless steel clad fuel are the same as the end fittings masses of the zircaloy clad fuel. Therefore, separate source terms are not provided for the end fittings of the stainless steel fuel.

Tables 5.2.19 through 5.2.22 list the neutron and gamma source strengths for the design basis stainless steel clad fuel. The gamma source strengths include the contribution from the cobalt activation in the incore spacers. Subsection 5.4.4 presents the dose rates around the HI-STAR 100 for the normal and hypothetical accident conditions for the stainless steel fuel. In the calculation of these dose rates the length of the active fuel was conservatively assumed to be 144 inches. In addition, the fuel assembly configuration used in the MCNP calculations was identical to the configuration used for the design basis fuel assemblies as described in Table 5.3.1.

5.2.4 Non-fuel Hardware

Generic PWR non-fuel hardware is not permitted for transport in the HI-STAR 100 system. However, certain non-fuel hardware from the Trojan Nuclear plant has been analyzed and is approved for transportation. These components include rod cluster control assemblies (RCCAs), burnable poison rod assemblies (BPRAs) and thimble plug devices (TPDs). The methodology for analyzing the non-fuel hardware authorized for transportation is described below and has been previously approved in the HI-STORM 100 FSAR [5.2.9].

5.2.4.1 BPRAs and TPDs

Burnable poison rod assemblies (BPRAs) and thimble plug devices (TPD) are an integral, yet removable, part of a large portion of PWR fuel. The TPDs are not used in all assemblies in a reactor core but are reused from cycle to cycle. Therefore, these devices can achieve very high burnups. In contrast, BPRAs are burned with a fuel assembly in core and are not reused. In fact, many BPRAs are removed after one or two cycles before the fuel assembly is discharged. Therefore, the achieved burnup for BPRAs is not significantly different than fuel assemblies.

TPDs are made of stainless steel and may contain a small amount of inconel. These devices extend down into the plenum region of the fuel assembly but do not extend into the active fuel region. Since these devices are made of stainless steel, there is a significant amount of cobalt-60 produced during irradiation. This is the only significant radiation source from the activation of steel and inconel.

BPRAs are made of stainless steel in the region above the active fuel zone and may contain a small amount of inconel in this region. Within the active fuel zone the BPRAs may contain 2-24 rodlets which are burnable absorbers clad in either zircaloy or stainless steel. The stainless steel clad BPRAs create a significant radiation source (Co-60) while the zircaloy clad BPRAs create a negligible radiation source. Therefore the stainless steel clad BPRAs are bounding.

SAS2H and ORIGEN-S were used to calculate a radiation source term for the Trojan TPDs and BPRAs. In the ORIGEN-S calculations the cobalt-59 impurity level was conservatively assumed to be 0.8 gm/kg for stainless steel and 4.7 gm/kg for inconel. These calculations were performed by irradiating the appropriate mass of steel and inconel using the flux calculated for the design basis Trojan 17x17 fuel assembly. The mass of material in the regions above the active fuel zone was scaled by the appropriate scaling factors listed in Table 5.2.7 in order to account for the reduced flux levels above the fuel assembly. The total curies of cobalt were calculated for the Trojan TPDs and BPRAs for the actual burnups and cooling times (the BPRAs were only used in the first cycle whereas the TPDs were used in all but the last cycle). The accumulated burnup and cooling time for the BPRAs and TPDs are 15,998 MWD/MTU and 24 years cooling and 118,674 MWD/MTU and 11 years cooling, respectively. Since the operating history of the shutdown Trojan reactor is well known the actual cycle lengths and conservatively short downtimes between cycles were used in the calculation of the source terms. In the ORIGEN-S calculations it was assumed that the burned fuel assembly was replaced with a fresh fuel assembly after every cycle. This was achieved in ORIGEN-S by resetting the flux levels and cross sections to the 0 MWD/MTU condition after every cycle.

Currently only the Trojan non-fuel hardware is permitted for transportation in the HI-STAR 100 System. The masses of the Trojan TPD and BPA are listed in Table 5.2.36. This information was taken from references [5.2.5] and [5.2.7] and is the same information used in the Trojan FSAR [5.1.6].

Table 5.2.37 shows the curies of Co-60 that were calculated for BPRAs and TPDs in each region of the fuel assembly (e.g. incore, plenum, top). An allowable cooling time, separate from the fuel assemblies, of 24 years and 11 years is used for the Trojan BPRAs and TPDs, respectively.

Subsection 5.4.7 discusses the analysis of cask dose rates from Trojan fuel including the effect of the insertion of BPRAs or TPDs into Trojan fuel assemblies.

5.2.4.2 RCCAs

Rod cluster control assemblies (RCCAs) are an integral, yet reusable, portion of a PWR fuel assembly. These devices are utilized for many years (upwards of 20 years) prior to discharge into the spent fuel pool. The manner in which the RCCAs are utilized varies from plant to plant. Some utilities maintain the RCCAs fully withdrawn during normal operation while others may operate with a bank of rods partially inserted (approximately 10%) during normal operation. Even when fully withdrawn, the ends of the RCCAs are present in the upper portion of the fuel assembly since they are never fully removed from the fuel assembly during operation. The result of the different operating styles is a variation in the source term for the RCCAs. In all cases, however, only the lower portion of the RCCAs will be significantly activated. Therefore, when the RCCAs are stored with the PWR fuel assembly, the activated portion of the RCCAs will be in the lower portion of the cask. RCCAs are fabricated of various materials. The cladding is

typically stainless steel, although inconel has been used. The absorber can be a single material or a combination of materials. AgInCd is possibly the most common absorber although B₄C in aluminum is used, and hafnium has also been used. AgInCd produces a noticeable source term in the 0.3-1.0 MeV range due to the activation of Ag. The Trojan RCCAs, the only RCCAs currently authorized for transport, were made of AgInCd clad in stainless steel.

In order to determine the impact on the dose rates around the HI-STAR 100 System, source terms for the Trojan RCCAs were calculated using SAS2H and ORIGEN-S. In the ORIGEN-S calculations the cobalt-59 impurity level was conservatively assumed to be 0.8 gm/kg for stainless steel and 4.7 gm/kg for inconel. These calculations were performed by irradiating 1 kg of steel, inconel, and AgInCd using the flux calculated for the Trojan W 17x17 fuel assembly. The total curies of cobalt for the steel and inconel and the 0.3-1.0 MeV source for the AgInCd were calculated for a single burnup, 125,515 MWD/MTU, and cooling time, 9 years, corresponding to the lifetime operation of the Trojan reactor. Since the operating history of the shutdown Trojan reactor is well known the actual cycle lengths and conservatively short downtimes between cycles were used in the calculation of the source terms. In the ORIGEN-S calculations it was assumed that the burned fuel assembly was replaced with a fresh fuel assembly after every cycle. This was achieved in ORIGEN-S by resetting the flux levels and cross sections to the 0 MWD/MTU condition after every cycle. The sources were then scaled by the appropriate mass using the flux weighting factors for the different regions of the assembly to determine the final source term. Since the Trojan reactor normally operated with all RCCA rods fully withdrawn only one configuration was analyzed for the RCCAs. The configuration, which is summarized below, is described in Table 5.2.38 for the RCCAs. The masses of the materials listed in these tables were determined from reference [5.2.5]. The masses listed in Table 5.2.38 do not match exact values from [5.2.5] because the values in the reference were adjusted to the lengths shown in the tables.

RCCA Configuration

This configuration represents a fully removed RCCA during normal core operations. The activated portion corresponds to the upper portion of a fuel assembly above the active fuel length with the appropriate flux weighting factors used.

Table 5.2.38 presents the source terms that were calculated for the Trojan RCCAs. The only significant source from the activation of inconel or steel is Co-60 and the only significant source from the activation of AgInCd is from 0.3-1.0 MeV.

Subsection 5.4.7 discusses the analysis of cask dose rates from Trojan fuel including the effect of the insertion of RCCAs into Trojan fuel assemblies.

5.2.5 Choice of Design Basis Assembly

The analysis presented in this chapter was performed to bound the fuel assembly classes listed in Tables 1.2.8 and 1.2.9. In order to perform a bounding analysis, a design basis fuel assembly

must be chosen. Therefore, a fuel assembly from each fuel class was analyzed and a comparison of the neutrons/sec, photons/sec, and thermal power (watts) was performed. The fuel assembly which produced the highest source for a specified burnup, cooling time, and enrichment was chosen as the design basis fuel assembly. A separate design basis assembly was chosen for the PWR baskets (MPC-24 and MPC-32) and the BWR basket (MPC-68).

5.2.5.1 PWR Design Basis Assembly

Table 1.2.8 lists the PWR fuel assembly classes that were evaluated to determine the design basis PWR fuel assembly. Within each class, the fuel assembly with the highest UO_2 mass was analyzed. Since the variations of fuel assemblies within a class are very minor (pellet diameter, clad thickness, etc.), it is conservative to choose the assembly with the highest UO_2 mass. For a given class of assemblies, the one with the highest UO_2 mass will produce the highest radiation source because, for a given burnup (MWD/MTU) and enrichment, the highest UO_2 mass will have produced the most energy and therefore the most fission products.

Table 5.2.24 presents the characteristics of the fuel assemblies analyzed to determine the design basis zircaloy clad PWR fuel assembly. The fuel assembly listed for each class is the assembly with the highest UO_2 mass. The St. Lucie and Ft. Calhoun classes are not present in Table 5.2.24. These assemblies are shorter versions of the CE 16x16 and CE 14x14 assembly classes, respectively. Therefore, these assemblies are bounded by the CE 16x16 and CE 14x14 classes and were not explicitly analyzed. Since the Haddam Neck and San Onofre 1 classes are stainless steel clad fuel, these classes were analyzed separately and are discussed below. All fuel assemblies in Table 5.2.24 were analyzed at the same burnup and cooling time. The results of the comparison are provided in Table 5.2.26. These results indicate that the B&W 15x15 fuel assembly has the highest radiation source term of the zircaloy clad fuel assembly classes considered in Table 1.2.8. This fuel assembly also has the highest UO_2 mass (see Table 5.2.24) which confirms that, for a given initial enrichment, burnup, and cooling time, the assembly with the highest UO_2 mass produces the highest radiation source term.

The Haddam Neck and San Onofre 1 classes are shorter stainless steel clad versions of the WE 15x15 and WE 14x14 classes, respectively. Since these assemblies have stainless steel clad, they were analyzed separately as discussed in Subsection 5.2.3. Based on the results in Table 5.2.26, which show that the WE 15x15 assembly class has a higher source term than the WE 14x14 assembly class, the Haddam Neck, WE 15x15, fuel assembly was analyzed as the bounding PWR stainless steel clad fuel assembly.

5.2.5.2 BWR Design Basis Assembly

Table 1.2.9 lists the BWR fuel assembly classes that were evaluated to determine the design basis BWR fuel assembly. Since there are minor differences between the array types in the GE BWR/2-3 and GE BWR/4-6 assembly classes, these assembly classes were not considered individually but rather as a single class. Within that class, the array types, 7x7, 8x8, 9x9, and

10x10 were analyzed to determine the bounding BWR fuel assembly. Since the Humboldt Bay 7x7 and Dresden 1 8x8 are smaller versions of the 7x7 and 8x8 assemblies they are bounded by the 7x7 and 8x8 assemblies in the GE BWR/2-3 and GE BWR/4-6 classes. Within each array type, the fuel assembly with the highest UO₂ mass was analyzed. Since the variations of fuel assemblies within an array type are very minor, it is conservative to choose the assembly with the highest UO₂ mass. For a given array type of assemblies, the one with the highest UO₂ mass will produce the highest radiation source because, for a given burnup (MWD/MTU) and enrichment, it will have produced the most energy and therefore the most fission products. The Humboldt Bay 6x6, Dresden 1 6x6, and LaCrosse assembly classes were not considered in the determination of the bounding fuel assembly. However, these assemblies were analyzed explicitly as discussed below.

Table 5.2.25 presents the characteristics of the fuel assemblies analyzed to determine the design basis zircaloy clad BWR fuel assembly. The fuel assembly listed for each array type is the assembly that has the highest UO₂ mass. All fuel assemblies in Table 5.2.25 were analyzed at the same burnup and cooling time. The results of the comparison are provided in Table 5.2.27. These results indicate that the 7x7 fuel assembly has the highest radiation source term of the zircaloy clad fuel assembly classes considered in Table 1.2.9. This fuel assembly also has the highest UO₂ mass which confirms that, for a given initial enrichment, burnup, and cooling time, the assembly with the highest UO₂ mass produces the highest radiation source term. According to Reference [5.2.6], the last discharge of a 7x7 assembly was in 1985 and the maximum average burnup for a 7x7 during their operation was 29,000 MWD/MTU. This clearly indicates that the existing 7x7 assemblies have an average burnup and minimum cooling time that is well within the burnup and cooling time limits in Table 1.2.20. Therefore, the 7x7 assembly has never reached the burnup level analyzed in this chapter. However, in the interest of conservatism the 7x7 was chosen as the bounding fuel assembly array type.

Since the LaCrosse fuel assembly type is a stainless steel clad 10x10 assembly, it was analyzed separately. The maximum burnup and minimum cooling times for this assembly are limited to 22,500 MWD/MTU and 15-year cooling as specified in Table 1.2.19. This assembly type is discussed further in Subsection 5.2.3.

The Humboldt Bay 6x6 and Dresden 1 6x6 fuel are older and shorter than the other array types analyzed and therefore are considered separately. The Dresden 1 6x6 was chosen as the design basis fuel assembly for the Humboldt Bay 6x6 and Dresden 1 6x6 fuel assembly classes because it has the higher UO₂ mass. Dresden 1 also contains a few 6x6 MOX fuel assemblies which were explicitly analyzed as well.

Reference [5.2.6] indicates that the Dresden 1 6x6 fuel assembly has a higher UO₂ mass than the Dresden 1 8x8 or the Humboldt Bay fuel (6x6 and 7x7). Therefore, the Dresden 1 6x6 fuel assembly was also chosen as the bounding assembly for damaged fuel and fuel debris for the Humboldt Bay and Dresden 1 fuel assembly classes.

Since the design basis damaged fuel assembly and the design basis intact 6x6 fuel assembly are identical, the analysis presented in Subsection 5.4.2 for the damaged fuel assembly also demonstrates the acceptability of transporting intact 6x6 fuel assemblies from the Dresden 1 and Humboldt Bay fuel assembly classes.

5.2.5.3 Decay Heat Loads

The decay heat values per assembly were calculated using the methodology described in Section 5.2. As demonstrated in Tables 5.2.26 and 5.2.27, the design basis fuel assembly produces a higher decay heat value than the other assembly types considered. This is due to the higher heavy metal mass in the design basis fuel assemblies. Conservatively, Tables 1.2.10 and 1.2.11 limit the heavy metal mass of the design basis fuel assembly classes to a value less than the design basis value utilized in this chapter. This provides additional assurance that the radiation source terms are bounding values.

As further demonstration that the decay heat values (calculated using the design basis fuel assemblies) are conservative, a comparison between these calculated decay heats and the decay heats reported in Reference [5.2.7] are presented in Table 5.2.28. This comparison is made for a burnup of 30,000 MWD/MTU and a cooling time of 5 years. The burnup was chosen based on the limited burnup data available in Reference [5.2.7].

The heavy metal mass of the non-design basis fuel assembly classes in Tables 1.2.10 and 1.2.11 are limited to the masses used in Tables 5.2.24 and 5.2.25. No margin is applied between the allowable mass and the analyzed mass of heavy metal for the non-design basis fuel assemblies. This is acceptable because additional assurance that the radiation source terms for the non-design basis fuel assemblies are bounding values is obtained by using the radiation source terms for the design basis fuel assemblies in determining the acceptable loading criteria for all fuel assemblies.

5.2.6 Thoria Rod Canister

Dresden Unit 1 has a single DFC containing 18 thoria rods which have obtained a relatively low burnup, 16,000 MWD/MTU. These rods were removed from two 8x8 fuel assemblies which contained 9 rods each. The irradiation of thorium produces an isotope which is not commonly found in depleted uranium fuel. Th-232 when irradiated produces U-233. The U-233 can undergo an (n,2n) reaction which produces U-232. The U-232 decays to produce Tl-208 which produces a 2.6 MeV gamma during Beta decay. This results in a significant source in the 2.5-3.0 MeV range which is not commonly present in depleted uranium fuel. Therefore, this single DFC container was analyzed to determine if it was bounded by the current shielding analysis.

A radiation source term was calculated for the 18 thoria rods using SAS2H and ORIGEN-S for a burnup of 16,000 MWD/MTU and a cooling time of 18 years. Table 5.2.29 describes the 8x8 fuel assembly that contains the thoria rods. Table 5.2.30 and 5.2.31 show the gamma and neutron source terms, respectively, that were calculated for the 18 thoria rods in the thoria rod canister.

Comparing these source terms to the design basis 6x6 source terms for Dresden Unit 1 fuel in Tables 5.2.6 and 5.2.14 clearly indicates that the design basis source terms bound the thoria rods source terms in all neutron groups and in all gamma groups except the 2.5-3.0 MeV group. As mentioned above, the thoria rods have a significant source in this energy range due to the decay of Tl-208.

Subsection 5.4.6 provides a further discussion of the thoria rod canister and its acceptability for transport in the HI-STAR 100 System.

5.2.7 Fuel Assembly Neutron Sources

Neutron sources are used in reactors during initial startup of reactor cores. There are different types of neutron sources (e.g. californium, americium-beryllium, plutonium-beryllium, antimony-beryllium). These neutron sources are typically inserted into the water rod of a fuel assembly and are usually removable.

Currently the only neutron source permitted for transport in the HI-STAR 100 System are from Dresden Unit 1 and Trojan Nuclear Plant as discussed below.

5.2.7.1 Dresden Unit 1 Neutron Source Assemblies

Dresden Unit 1 has a few antimony-beryllium neutron sources. These sources have been analyzed in Subsection 5.4.5 to demonstrate that they are acceptable for transport in the HI-STAR 100 System.

5.2.7.2 Trojan Nuclear Plant Neutron Source Assemblies

Trojan Nuclear Power has two primary (californium) neutron source assemblies and four secondary (antimony-beryllium) neutron source assemblies. The neutron source assemblies are basically BPRAs with the source material placed in a few of the rods instead of burnable absorber. In the case of the californium source, a single rod contained a nominally 1.5 inch long californium capsule while the remaining locations consisted of 19 burnable poison rods and 4 thimble plug rods. The initial source strength of the primary sources were approximately $6.0E+8$ neutrons/sec. Since these devices were delivered prior to startup, they have realized more than 24 years of decay time. Based on the half-life of Cf-252 (2.65 years), the neutron source strength of these devices would be less than $1.2E+6$ neutrons/sec after 24 years of decay time. Therefore, the neutron contribution from these devices is negligible and is not considered in the analysis in this chapter. Since these devices are clad in stainless steel, there is the potential for significant Co-60 activation from in-core activation of the cladding material. The primary sources were only operated during the first cycle of the Trojan nuclear plant and as a result achieved a burnup of 15,998 MWD/MTU and have a cooling time of more than 24 years. This burnup and cooling time is identical to the burnup and cooling time for the Trojan BPRAs as discussed in Subsection

5.2.4.1. Therefore, the primary sources are not explicitly considered in this analysis but are bounded by the analysis of the BPRAs.

The Trojan Nuclear Plant secondary neutron source assemblies used 4 rods for the antimony-beryllium source and the remaining rods were either burnable poison rods or thimble plug rods. The 4 source rods in a secondary neutron source assembly each contained 88 inches of antimony-beryllium. Since the antimony-beryllium neutron sources are regenerative sources they will be producing a steady state level of neutrons while in the MPC. This production of neutrons has been explicitly analyzed in Subsection 5.4.8. In addition to the neutron source from the secondary sources, there will be a substantial Co-60 source from the activation of the stainless steel cladding. There are two different levels of activation since the first two source assemblies were used in-core for cycles 1-4 and the latter two source assemblies were used in-core for cycles 4-14. The operating history for these devices results in a burnup of 45,361 MWD/MTU and a cooling time of 19 years for the source assemblies that operated in the first four cycles. The burnup and cooling time for the other two source assemblies is 88,547 MWD/MTU and 9 years. In addition to the difference in the burnup and cooling times between the two sets of secondary source assemblies, the number of burnable poison rods and thimble plug rods is different. The two source assemblies used in Cycles 1-4 each contained 4 source rods, 16 burnable poison rods and 4 thimble plug rods. The two source assemblies used in Cycles 4-14 each contained 4 source rods and 20 thimble plug rods. Table 5.2.39 shows the physical description of these devices that was used in the source term calculation and the resultant Co-60 source term in each region. Subsection 5.4.8 discusses the effect of the secondary source assemblies on the calculated dose rates and demonstrates that these devices are acceptable for transport.

5.2.8 Trojan Non-Fuel Bearing Components, Damaged Fuel and Fuel Debris

Trojan Nuclear Power has failed fuel cans containing fuel process can capsules and fuel debris. The fuel process can capsules contain only a limited amount of fuel in the form of fuel debris (metal fragments). The source term from the fuel process can capsules is therefore bounded by the source from a fuel assembly.

The fuel assemblies classified as fuel debris consist of a few assemblies with each containing a maximum of 17 rods. There is also a single damaged fuel container that has 23 individual rods not bound in a fuel assembly configuration. If it is assumed that the 23 individual rods are from a design basis Trojan fuel assembly and have not collapsed, then the source strength per inch of active fuel is a small fraction (23 rods/264 rods in an intact assembly) of the source in an intact assembly. If it is assumed that the source strength per rod is "A" then the source per inch in an intact assembly is $264A/144=1.833A$. The damaged fuel assembly with 23 rods would have to collapse from 144 inches in height to 12.5 inches (height = $23A/1.833A$) in order for the source strength per unit inch in the collapsed assembly to be equivalent to the source strength per unit

inch in an intact assembly. Further collapse would increase the source strength per inch beyond that of a design basis assembly but it is not considered likely that this would occur. Therefore, even in a collapsed state which might exist after a transport accident, this fuel debris is bounded by an intact fuel assembly and therefore is not explicitly considered in the analysis in this chapter.

There are also a couple of fuel assemblies classified as damaged fuel because of missing rods. These assemblies are also bounded by an intact assembly and during the transport accident it is expected that these damaged assemblies would react the same as intact assemblies. Therefore, the Trojan damaged fuel assemblies were not explicitly considered in the analysis in this chapter.

Trojan fuel assembly hardware, non-fuel bearing components and one fuel skeleton will also be transported. These components are made of stainless steel, zircaloy and inconel. The source term from these additional components were not explicitly considered but are bounded by intact fuel assemblies. Therefore, the source term from these components were not explicitly considered.

Table 5.2.1

DESCRIPTION OF DESIGN BASIS INTACT ZIRCALOY CLAD FUEL

	PWR	BWR
Assembly type/class	B&W 15x15	GE 7x7
Active fuel length (in.)	144	144
No. of fuel rods	208	49
Rod pitch (in.)	0.568	0.738
Cladding material	zircaloy-4	zircaloy-2
Rod diameter (in.)	0.428	0.570
Cladding thickness (in.)	0.0230	0.0355
Pellet diameter (in.)	0.3742	0.488
Pellet material	UO ₂	UO ₂
Pellet density (gm/cc)	10.412 (95% of theoretical)	10.412 (95% of theoretical)
Enrichment (w/o ²³⁵ U)	See Tables 1.2.28, 1.2.29, 1.2.32, 1.2.33	See Table 1.2.31
Burnup (MWD/MTU)	See Table 1.2.28, 1.2.29, 1.2.32, 1.2.33	See Table 1.2.31
Cooling Time (years)	See Table 1.2.28, 1.2.29, 1.2.32, 1.2.33	See Table 1.2.31
Specific power (MW/MTU)	40	30
Weight of UO ₂ (kg) [†]	562.029	225.177
Weight of U (kg) [†]	495.485	198.516

Notes:

1. The B&W 15x15 is the design basis assembly for the following fuel assembly classes listed in Table 1.2.8: B&W 15x15, B&W 17x17, CE 14x14, CE 16x16, WE 14x14, WE 15x15, WE 17x17, St. Lucie, and Ft. Calhoun.
2. The GE 7x7 is the design basis assembly for the following fuel assembly classes listed in Table 1.2.9: GE BWR/2-3, GE BWR/4-6, Humboldt Bay 7x7, and Dresden 1 8x8.

[†] Derived from parameters in this table.

Table 5.2.1 (continued)

DESCRIPTION OF DESIGN BASIS INTACT ZIRCALOY CLAD FUEL

	PWR	BWR
No. of Water Rods/Guide Tubes	17	0
Water Rod O.D. (in.)	0.53	N/A
Water Rod Thickness (in.)	0.0160	N/A
Lower End Fitting (kg)	8.16 (steel) 1.3 (inconel)	4.8 (steel)
Gas Plenum Springs (kg)	0.48428 (inconel) 0.23748 (steel)	1.1 (steel)
Gas Plenum Spacer (kg)	0.55572 (inconel) 0.27252 (steel)	N/A
Expansion Springs (kg)	N/A	0.4 (steel)
Upper End Fitting (kg)	9.28 (steel)	2.0 (steel)
Handle (kg)	N/A	0.5 (steel)
Incore Grid Spacers (kg)	4.9 (inconel) [†]	0.33 (inconel springs)

[†] This mass of inconel was used for fuel assemblies with non-zircaloy grid spacers. For fuel assemblies with zircaloy grid spacers the mass was 0.0. However, the mass of the inconel and steel in the other assembly components are identical for assemblies with zircaloy and non-zircaloy incore grid spacers.

Table 5.2.2

DESCRIPTION OF DESIGN BASIS DAMAGED ZIRCALOY CLAD FUEL

	BWR
Fuel type	GE 6x6
Active fuel length (in.)	110
No. of fuel rods	36
Rod pitch (in.)	0.694
Cladding material	zircaloy-2
Rod diameter (in.)	0.5645
Cladding thickness (in.)	0.035
Pellet diameter (in.)	0.494
Pellet material	UO ₂
Pellet density (gm/cc)	10.412 (95% of theoretical)
Enrichment (w/o ²³⁵ U)	4.8145
Burnup (MWD/MTU)	30,000
Cooling Time (years)	18
Specific power (MW/MTU)	16.5
Weight of UO ₂ (kg) [†]	129.5
Weight of U (kg) [†]	114.2
Incore spacers (kg inconel)	1.07

Notes:

1. The 6x6 is the design basis damaged fuel assembly for the Humboldt Bay (all array types) and the Dresden 1 (all array types) damaged fuel assembly classes. It is also the design basis fuel assembly for the intact Humboldt Bay 6x6 and Dresden 1 6x6 fuel assembly classes.
2. This design basis damaged fuel assembly is also the design basis fuel assembly for fuel debris.

[†] Derived from parameters in this table.

Table 5.2.3

CALCULATED MPC-24 PWR FUEL GAMMA SOURCE PER ASSEMBLY FOR DESIGN BASIS ZIRCALOY CLAD FUEL WITH NON-ZIRCALOY INCORE SPACERS FOR VARYING BURNUPS AND COOLING TIMES

Lower Energy	Upper Energy	24,500 MWD/MTU 9 Year Cooling		29,500 MWD/MTU 11 Year Cooling		34,500 MWD/MTU 13 Year Cooling	
(MeV)	(MeV)	(MeV/s)	(Photons/s)	(MeV/s)	(Photons/s)	(MeV/s)	(Photons/s)
0.45	0.7	7.61E+14	1.32E+15	8.35E+14	1.45E+15	9.05E+14	1.57E+15
0.7	1.0	8.94E+13	1.05E+14	6.95E+13	8.18E+13	5.54E+13	6.52E+13
1.0	1.5	3.29E+13	2.63E+13	3.33E+13	2.67E+13	3.41E+13	2.73E+13
1.5	2.0	1.70E+12	9.74E+11	1.73E+12	9.91E+11	1.84E+12	1.05E+12
2.0	2.5	2.19E+11	9.71E+10	5.49E+10	2.44E+10	1.89E+10	8.40E+09
2.5	3.0	1.32E+10	4.81E+09	4.06E+09	1.47E+09	1.49E+09	5.42E+08
Totals		8.85E+14	1.46E+15	9.39E+14	1.56E+15	9.96E+14	1.67E+15
Lower Energy	Upper Energy	39,500 MWD/MTU 15 Year Cooling		44,500 MWD/MTU 18 Year Cooling			
(MeV)	(MeV)	(MeV/s)	(Photons/s)	(MeV/s)	(Photons/s)		
0.45	0.7	9.70E+14	1.69E+15	1.00E+15	1.74E+15		
0.7	1.0	4.49E+13	5.28E+13	3.32E+13	3.90E+13		
1.0	1.5	3.39E+13	2.71E+13	3.07E+13	2.46E+13		
1.5	2.0	1.89E+12	1.08E+12	1.78E+12	1.02E+12		
2.0	2.5	1.11E+10	4.92E+09	9.00E+09	4.00E+09		
2.5	3.0	8.82E+08	3.21E+08	8.14E+08	2.96E+08		
Totals		1.05E+15	1.77E+15	1.07E+15	1.81E+15		

Table 5.2.4

CALCULATED MPC-24 PWR FUEL GAMMA SOURCE PER ASSEMBLY FOR DESIGN BASIS ZIRCALOY CLAD FUEL WITH ZIRCALOY INCORE SPACERS FOR VARYING BURNUPS AND COOLING TIMES

Lower Energy	Upper Energy	24,500 MWD/MTU 6 Year Cooling		29,500 MWD/MTU 7 Year Cooling		34,500 MWD/MTU 9 Year Cooling	
		(MeV/s)	(Photons/s)	(MeV/s)	(Photons/s)	(MeV/s)	(Photons/s)
0.45	0.7	9.60E+14	1.67E+15	1.06E+15	1.85E+15	1.08E+15	1.88E+15
0.7	1.0	2.17E+14	2.55E+14	2.09E+14	2.46E+14	1.48E+14	1.74E+14
1.0	1.5	5.67E+13	4.54E+13	5.96E+13	4.77E+13	5.44E+13	4.35E+13
1.5	2.0	3.71E+12	2.12E+12	3.24E+12	1.85E+12	2.70E+12	1.54E+12
2.0	2.5	2.48E+12	1.10E+12	1.19E+12	5.27E+11	2.57E+11	1.14E+11
2.5	3.0	1.02E+11	3.70E+10	5.83E+10	2.12E+10	1.67E+10	6.08E+09
Totals		1.24E+15	1.97E+15	1.33E+15	2.14E+15	1.29E+15	2.10E+15
Lower Energy	Upper Energy	39,500 MWD/MTU 11 Year Cooling		44,500 MWD/MTU 14 Year Cooling			
		(MeV/s)	(Photons/s)	(MeV/s)	(Photons/s)		
0.45	0.7	1.12E+15	1.94E+15	1.12E+15	1.95E+15		
0.7	1.0	1.05E+14	1.24E+14	6.36E+13	7.48E+13		
1.0	1.5	5.06E+13	4.05E+13	4.35E+13	3.48E+13		
1.5	2.0	2.58E+12	1.47E+12	2.37E+12	1.35E+12		
2.0	2.5	6.36E+10	2.83E+10	1.55E+10	6.89E+09		
2.5	3.0	5.07E+09	1.84E+09	1.41E+09	5.12E+08		
Totals		1.28E+15	2.11E+15	1.23E+15	2.06E+15		

Table 5.2.5
 CALCULATED MPC-68 BWR FUEL GAMMA SOURCE PER ASSEMBLY FOR DESIGN BASIS ZIRCALOY CLAD
 FUEL FOR VARYING BURNUPS AND COOLING TIMES

Lower Energy (MeV)	Upper Energy (MeV)	10,000 MWD/MTU 5 Year Cooling		20,000 MWD/MTU 7 Year Cooling		24,500 MWD/MTU 8 Year Cooling		29,500 MWD/MTU 9 Year Cooling	
		(MeV/s)	(Photons/s)	(MeV/s)	(Photons/s)	(MeV/s)	(Photons/s)	(MeV/s)	(Photons/s)
0.45	0.7	1.68E+14	2.93E+14	2.83E+14	4.92E+14	3.21E+14	5.57E+14	3.64E+14	6.34E+14
0.7	1.0	3.28E+13	3.86E+13	4.89E+13	5.75E+13	4.54E+13	5.34E+13	4.46E+13	5.25E+13
1.0	1.5	9.61E+12	7.69E+12	1.42E+13	1.13E+13	1.46E+13	1.17E+13	1.63E+13	1.30E+13
1.5	2.0	1.11E+12	6.34E+11	8.42E+11	4.81E+11	7.68E+11	4.39E+11	8.20E+11	4.69E+11
2.0	2.5	1.22E+12	5.40E+11	3.47E+11	1.54E+11	1.65E+11	7.34E+10	8.09E+10	3.60E+10
2.5	3.0	4.73E+10	1.72E+10	1.87E+10	6.82E+09	9.32E+09	3.39E+09	5.31E+09	1.93E+09
Total		2.13E+14	3.40E+14	3.47E+14	5.62E+14	3.82E+14	6.23E+14	4.26E+14	7.00E+14
Lower Energy (MeV)	Upper Energy (MeV)	34,500 MWD/MTU 11 Year Cooling		39,500 MWD/MTU 14 Year Cooling		44,500 MWD/MTU 19 Year Cooling			
		(MeV/s)	(Photons/s)	(MeV/s)	(Photons/s)	(MeV/s)	(Photons/s)		
0.45	0.7	3.87E+14	6.73E+14	3.96E+14	6.89E+14	3.87E+14	6.73E+14		
0.7	1.0	3.31E+13	3.89E+13	2.03E+13	2.39E+13	1.09E+13	1.28E+13		
1.0	1.5	1.57E+13	1.26E+13	1.38E+13	1.10E+13	1.05E+13	8.38E+12		
1.5	2.0	8.10E+11	4.63E+11	7.59E+11	4.34E+11	6.17E+11	3.53E+11		
2.0	2.5	2.05E+10	9.10E+09	5.27E+09	2.34E+09	3.33E+09	1.48E+09		
2.5	3.0	1.62E+09	5.91E+08	4.16E+08	1.51E+08	2.84E+08	1.03E+08		
Total		4.36E+14	7.25E+14	4.31E+14	7.24E+14	4.09E+14	6.95E+14		

Table 5.2.6

CALCULATED MPC-68 and MPC-68F BWR FUEL GAMMA
SOURCE PER ASSEMBLY FOR DESIGN BASIS
ZIRCALOY CLAD DAMAGED FUEL

Lower Energy (MeV)	Upper Energy (MeV)	30,000 MWD/MTU 18 Year Cooling	
		(MeV/s)	(Photons/s)
0.45	0.7	1.52E+14	2.65E+14
0.7	1.0	4.14E+12	4.87E+12
1.0	1.5	3.91E+12	3.13E+12
1.5	2.0	2.28E+11	1.30E+11
2.0	2.5	1.17E+09	5.21E+08
2.5	3.0	7.48E+07	2.72E+07
Totals		1.60E+14	2.73E+14

Table 5.2.7

SCALING FACTORS USED IN CALCULATING THE ⁶⁰Co SOURCE

Region	PWR	BWR
Handle	N/A	0.05
Top end fitting	0.1	0.1
Gas plenum spacer	0.1	N/A
Expansion springs	N/A	0.1
Gas plenum springs	0.2	0.2
Grid spacer spring	N/A	1.0
Bottom end fitting	0.2	0.15

Table 5.2.8

CALCULATED MPC-24 ⁶⁰Co SOURCE PER ASSEMBLY FOR DESIGN BASIS ZIRCALOY CLAD FUEL
WITH NON-ZIRCALOY INCORE SPACERS AT VARYING BURNUPS AND COOLING TIMES

Location	24,500 MWD/MTU 9 Year Cooling (curies)	29,500 MWD/MTU 11 Year Cooling (curies)	34,500 MWD/MTU 13 Year Cooling (curies)	39,500 MWD/MTU 15 Year Cooling (curies)	44,500 MWD/MTU 18 Year Cooling (curies)
Lower end fitting	95.83	81.89	68.71	56.79	41.33
Gas plenum springs	18.64	15.93	13.37	11.05	8.04
Gas plenum spacer	10.70	9.14	7.67	6.34	4.61
Expansion springs	N/A	N/A	N/A	N/A	N/A
Grid spacers	870.53	743.87	624.11	515.87	375.39
Upper end fitting	35.08	29.97	25.15	20.79	15.13
Handle	N/A	N/A	N/A	N/A	N/A

Table 5.2.9

CALCULATED MPC-24 ⁶⁰Co SOURCE PER ASSEMBLY FOR DESIGN BASIS ZIRCALOY CLAD FUEL
WITH ZIRCALOY INCORE SPACERS AT VARYING BURNUPS AND COOLING TIMES

Location	24,500 MWD/MTU 6 Year Cooling (curies)	29,500 MWD/MTU 7 Year Cooling (curies)	34,500 MWD/MTU 9 Year Cooling (curies)	39,500 MWD/MTU 11 Year Cooling (curies)	44,500 MWD/MTU 14 Year Cooling (curies)
Lower end fitting	142.23	138.68	116.12	96.09	69.72
Gas plenum springs	27.67	26.98	22.59	18.69	13.56
Gas plenum spacer	15.88	15.48	12.96	10.73	7.78
Expansion springs	N/A	N/A	N/A	N/A	N/A
Grid spacers [†]	N/A	N/A	N/A	N/A	N/A
Upper end fitting	52.06	50.76	42.50	35.17	25.52
Handle	N/A	N/A	N/A	N/A	N/A

[†] These burnup and cooling times represent fuel with zircaloy grid spacers. Therefore, the cobalt activation is negligible.

Table 5.2.10

CALCULATED MPC-68 ⁶⁰CO SOURCE PER ASSEMBLY FOR DESIGN BASIS ZIRCALOY CLAD FUEL
AT VARYING BURNUPS AND COOLING TIMES

Location	10,000 MWD/MTU 5 Year Cooling (curies)	20,000 MWD/MTU 7 Year Cooling (curies)	24,500 MWD/MTU 8 Year Cooling (curies)	29,500 MWD/MTU 9 Year Cooling (curies)	34,500 MWD/MTU 11 Year Cooling (curies)	39,500 MWD/MTU 14 Year Cooling (curies)	44,500 MWD/MTU 19 Year Cooling (curies)
Lower end fitting	39.71	40.80	34.04	30.55	27.49	19.64	11.08
Gas plenum springs	12.13	12.47	10.40	9.33	8.40	6.00	3.39
Gas plenum spacer	N/A	N/A	N/A	N/A	N/A	N/A	N/A
Expansion springs	2.21	2.27	1.89	1.70	1.53	1.09	0.62
Grid spacers	85.54	87.89	73.32	65.80	59.22	42.30	23.88
Upper end fitting	11.03	11.33	9.45	8.48	7.64	5.45	3.08
Handle	1.38	1.42	1.18	1.06	0.95	0.68	0.38

Table 5.2.11

CALCULATED MPC-24 PWR NEUTRON SOURCE PER ASSEMBLY
 FOR DESIGN BASIS ZIRCALOY CLAD FUEL WITH NON-ZIRCALOY
 INCORE SPACERS FOR VARYING BURNUPS AND COOLING TIMES

Lower Energy (MeV)	Upper Energy (MeV)	24,500 MWD/MTU 9 Year Cooling (Neutrons/s)	29,500 MWD/MTU 11 Year Cooling (Neutrons/s)	34,500 MWD/MTU 13 Year Cooling (Neutrons/s)	39,500 MWD/MTU 15 Year Cooling (Neutrons/s)	44,500 MWD/MTU 18 Year Cooling (Neutrons/s)
1.0E-01	4.0E-01	2.50E+06	4.04E+06	6.01E+06	8.09E+06	1.05E+07
4.0E-01	9.0E-01	1.28E+07	2.06E+07	3.07E+07	4.13E+07	5.35E+07
9.0E-01	1.4	1.18E+07	1.90E+07	2.82E+07	3.79E+07	4.91E+07
1.4	1.85	8.77E+06	1.41E+07	2.09E+07	2.81E+07	3.63E+07
1.85	3.0	1.58E+07	2.52E+07	3.73E+07	5.00E+07	6.47E+07
3.0	6.43	1.40E+07	2.25E+07	3.35E+07	4.50E+07	5.82E+07
6.43	20.0	1.23E+06	1.98E+06	2.94E+06	3.96E+06	5.13E+06
TOTALS		6.69E+07	1.07E+08	1.60E+08	2.14E+08	2.77E+08

Table 5.2.12

CALCULATED MPC-24 PWR NEUTRON SOURCE PER ASSEMBLY
 FOR DESIGN BASIS ZIRCALOY CLAD FUEL WITH ZIRCALOY
 INCORE SPACERS FOR VARYING BURNUPS AND COOLING TIMES

Lower Energy (MeV)	Upper Energy (MeV)	24,500 MWD/MTU 6 Year Cooling (Neutrons/s)	29,500 MWD/MTU 7 Year Cooling (Neutrons/s)	34,500 MWD/MTU 9 Year Cooling (Neutrons/s)	39,500 MWD/MTU 11 Year Cooling (Neutrons/s)	44,500 MWD/MTU 14 Year Cooling (Neutrons/s)
1.0E-01	4.0E-01	2.80E+06	4.69E+06	6.98E+06	9.40E+06	1.22E+07
4.0E-01	9.0E-01	1.43E+07	2.40E+07	3.57E+07	4.80E+07	6.22E+07
9.0E-01	1.4	1.32E+07	2.20E+07	3.27E+07	4.40E+07	5.70E+07
1.4	1.85	9.76E+06	1.63E+07	2.42E+07	3.26E+07	4.21E+07
1.85	3.0	1.75E+07	2.90E+07	4.30E+07	5.78E+07	7.47E+07
3.0	6.43	1.56E+07	2.61E+07	3.88E+07	5.22E+07	6.75E+07
6.43	20.0	1.37E+06	2.29E+06	3.42E+06	4.60E+06	5.96E+06
TOTALS		7.45E+07	1.24E+08	1.85E+08	2.49E+08	3.22E+08

Table 5.2.13

CALCULATED MPC-68 BWR NEUTRON SOURCE PER ASSEMBLY
 FOR DESIGN BASIS ZIRCALOY CLAD FUEL
 FOR VARYING BURNUPS AND COOLING TIMES

Lower Energy (MeV)	Upper Energy (MeV)	10,000 MWD/MTU 5 Year Cooling (Neutrons/s)	20,000 MWD/MTU 7 Year Cooling (Neutrons/s)	24,500 MWD/MTU 8 Year Cooling (Neutrons/s)	29,500 MWD/MTU 9 Year Cooling (Neutrons/s)	34,500 MWD/MTU 11 Year Cooling (Neutrons/s)	39,500 MWD/MTU 14 Year Cooling (Neutrons/s)	44,500 MWD/MTU 19 Year Cooling (Neutrons/s)
1.0E-01	4.0E-01	1.62E+05	1.01E+06	1.08E+06	1.81E+06	2.80E+06	3.61E+06	4.57E+06
4.0E-01	9.0E-01	8.29E+05	5.15E+06	5.52E+06	9.23E+06	1.43E+07	1.84E+07	2.33E+07
9.0E-01	1.4	7.68E+05	4.72E+06	5.08E+06	8.47E+06	1.31E+07	1.69E+07	2.14E+07
1.4	1.85	5.79E+05	3.50E+06	3.77E+06	6.27E+06	9.71E+06	1.25E+07	1.58E+07
1.85	3.0	1.07E+06	6.25E+06	6.75E+06	1.12E+07	1.73E+07	2.22E+07	2.80E+07
3.0	6.43	9.26E+05	5.61E+06	6.04E+06	1.01E+07	1.56E+07	2.00E+07	2.53E+07
6.43	20.0	7.91E+04	4.93E+05	5.29E+05	8.84E+05	1.37E+06	1.77E+06	2.24E+06
TOTALS		4.41E+06	2.67E+07	2.88E+07	4.79E+07	7.42E+07	9.54E+07	1.21E+08

Table 5.2.14

CALCULATED MPC-68 and MPC-68F BWR NEUTRON
SOURCE PER ASSEMBLY FOR DESIGN BASIS
DAMAGED ZIRCALOY CLAD FUEL

Lower Energy (MeV)	Upper Energy (MeV)	30,000 MWD/MTU 18 Year Cooling (Neutrons/s)
1.0E-01	4.0E-01	1.18E59E+6
4.0E-01	9.0E-01	6.058.10E+6
9.0E-01	1.4	5.557.43E+6
1.4	1.85	4.115.49E+6
1.85	3.0	7.349.76E+6
3.0	6.43	6.598.80E+6
6.43	20.0	5.797.76E+5
Totals		3.144.19E+7

Table 5.2.15

DESCRIPTION OF DESIGN BASIS ZIRCALOY CLAD MIXED OXIDE FUEL

	BWR
Fuel type	GE 6x6
Active fuel length (in.)	110
No. of fuel rods	36
Rod pitch (in.)	0.696
Cladding material	zircaloy-2
Rod diameter (in.)	0.5645
Cladding thickness (in.)	0.036
Pellet diameter (in.)	0.482
Pellet material	UO ₂ and PuUO ₂
No. of UO ₂ Rods	27
No. of PuUO ₂ Rods	9
Pellet density (gm/cc)	10.412 (95% of theoretical)
Enrichment (w/o ²³⁵ U) [†]	1.8 (UO ₂ rods) 0.711 (PuUO ₂ rods)
Burnup (MWD/MTU)	30,000
Cooling Time (years)	18
Specific power (MW/MTU)	16.5
Weight of UO ₂ , PuUO ₂ (kg) ^{††}	123.3
Weight of U,Pu (kg) ^{††}	108.7
Incore spacers (kg inconel)	1.07

[†] See Table 5.3.3 for detailed composition of PuUO₂ rods.

^{††} Derived from parameters in this table.

Table 5.2.16

CALCULATED MPC-68 BWR FUEL GAMMA SOURCE PER ASSEMBLY
FOR DESIGN BASIS ZIRCALOY CLAD MIXED OXIDE FUEL

Lower Energy (MeV)	Upper Energy (MeV)	30,000 MWD/MTU 18-Year Cooling	
		(MeV/s)	(Photons/s)
0.45	0.7	1.45E+14	2.52E+14
0.7	1.0	3.95E+12	4.65E+12
1.0	1.5	3.82E+12	3.06E+12
1.5	2.0	2.22E+11	1.27E+11
2.0	2.5	1.11E+9	4.93E+8
2.5	3.0	9.31E+7	3.39E+7
Totals		1.53E+14	2.60E+14

Table 5.2.17

CALCULATED MPC-68 BWR NEUTRON SOURCE PER ASSEMBLY
FOR DESIGN BASIS ZIRCALOY CLAD MIXED OXIDE FUEL

Lower Energy (MeV)	Upper Energy (MeV)	30,000 MWD/MTU 18-Year Cooling (Neutrons/s)
1.0E-01	4.0E-01	1.50E+6
4.0E-01	9.0E-01	7.67E+6
9.0E-01	1.4	7.09E+6
1.4	1.85	5.31E+6
1.85	3.0	9.67E+6
3.0	6.43	8.47E+6
6.43	20.0	7.33E+5
Totals		4.04E+7

Table 5.2.18
DESCRIPTION OF DESIGN BASIS INTACT STAINLESS STEEL CLAD FUEL

	PWR	BWR
Fuel type	WE 15x15	A/C 10x10
Active fuel length (in.)	144	144
No. of fuel rods	204	100
Rod pitch (in.)	0.563	0.565
Cladding material	304 SS	348H SS
Rod diameter (in.)	0.422	0.396
Cladding thickness (in.)	0.0165	0.02
Pellet diameter (in.)	0.3825	0.35
Pellet material	UO ₂	UO ₂
Pellet density (gm/cc)	10.412 (95% of theoretical)	10.412 (95% of theoretical)
Enrichment (w/o ²³⁵ U)	3.1	3.5
Burnup (MWD/MTU)	30,000 @ 19 yr (MPC-24) 40,000 @ 24 yr (MPC-24)	22,500 (MPC-68)
Cooling Time (years)	19 (MPC-24) 24 (MPC-24)	16 (MPC-68)
Specific power (MW/MTU)	37.96	29.17
No. of Water Rods	21	0
Water Rod O.D. (in.)	0.546	N/A
Water Rod Thickness (in.)	0.017	N/A
Incore spacers (kg inconel)	5.1	0.83

Notes:

1. The WE 15x15 is the design basis assembly for the following fuel assembly classes listed in Table 1.2.8: Indian Point, Haddam Neck and San Onofre 1.
2. The A/C 10x10 is the design basis assembly for the following fuel assembly class listed in Table 1.2.9: LaCrosse.

Table 5.2.19

CALCULATED BWR FUEL GAMMA SOURCE PER ASSEMBLY
FOR STAINLESS STEEL CLAD FUEL

Lower Energy (MeV)	Upper Energy (MeV)	22,500 MWD/MTU 16-Year Cooling	
		(MeV/s)	(Photons/s)
0.45	0.7	2.26E+14	3.94E+14
0.7	1.0	6.02E+12	7.08E+12
1.0	1.5	4.04E+13	3.23E+13
1.5	2.0	2.90E+11	1.66E+11
2.0	2.5	2.94E+9	1.31E+9
2.5	3.0	7.77E+7	2.83E+7
Totals		2.73E+14	4.33E+14

Note:

1. These source terms were calculated for a 144 inch active fuel length. The actual active fuel length is 83 inches.
2. The ⁶⁰Co activation from incore spacers is included in the 1.0-1.5 MeV energy group.

Table 5.2.20

CALCULATED PWR FUEL GAMMA SOURCE PER ASSEMBLY
FOR STAINLESS STEEL CLAD FUEL

Lower Energy (MeV)	Upper Energy (MeV)	30,000 MWD/MTU 19-Year Cooling		40,000 MWD/MTU 24-Year Cooling	
		(MeV/s)	(Photons/s)	(MeV/s)	(Photons/s)
0.45	0.7	6.81E+14	1.18E+15	7.97E+14	1.39E+15
0.7	1.0	1.83E+13	2.16E+13	1.70E+13	2.01E+13
1.0	1.5	1.13E+14	9.06E+13	8.24E+13	6.60E+13
1.5	2.0	1.06E+12	6.04E+11	1.12E+12	6.42E+11
2.0	2.5	7.25E+9	3.22E+9	7.42E+9	3.30E+9
2.5	3.0	3.52E+8	1.28E+8	6.43E+8	2.34E+8
Totals		8.14E+14	1.30E+15	8.98E+14	1.47E+15

Note:

1. These source terms were calculated for a 144 inch active fuel length. The actual active fuel length is 122 inches.
2. The ⁶⁰Co activation from incore spacers is included in the 1.0-1.5 MeV energy group.

Table 5.2.21

CALCULATED BWR NEUTRON SOURCE PER ASSEMBLY
FOR STAINLESS STEEL CLAD FUEL

Lower Energy (MeV)	Upper Energy (MeV)	22,500 MWD/MTU 16-Year Cooling (Neutrons/s)
1.0E-01	4.0E-01	1.81E+5
4.0E-01	9.0E-01	9.26E+5
9.0E-01	1.4	8.75E+5
1.4	1.85	6.85E+5
1.85	3.0	1.34E+6
3.0	6.43	1.08E+6
6.43	20.0	8.77E+4
Total		5.18E+6

Note:

These source terms were calculated for a 144 inch active fuel length. The actual active fuel length is 83 inches.

Table 5.2.22

CALCULATED PWR NEUTRON SOURCE PER ASSEMBLY
FOR STAINLESS STEEL CLAD FUEL

Lower Energy (MeV)	Upper Energy (MeV)	30,000 MWD/MTU 19-Year Cooling (Neutrons/s)	40,000 MWD/MTU 24-Year Cooling (Neutrons/s)
1.0E-01	4.0E-01	2.68E+6	7.07E+6
4.0E-01	9.0E-01	1.37E+7	3.61E+7
9.0E-01	1.4	1.27E+7	3.32E+7
1.4	1.85	9.50E+6	2.47E+7
1.85	3.0	1.74E+7	4.43E+7
3.0	6.43	1.52E+7	3.95E+7
6.43	20.0	1.31E+6	3.46E+6
Totals		7.24E+7	1.88E+8

Note:

These source terms were calculated for a 144 inch active fuel length. The actual active fuel length is 122 inches.

Table 5.2.23

MINIMUM ENRICHMENTS AS A FUNCTION OF BURNUP
FOR THE SHIELDING ANALYSIS

Minimum Enrichment (wt.% ²³⁵ U)	Maximum Burnup Analyzed (MWD/MTU)	
	MPC-24	MPC-32
PWR assemblies with non-zircaloy incore spacers		
2.3	24,500	24,500
2.6	29,500	29,500
2.9	34,500	34,500
3.2	39,500	39,500
3.4	44,500	42,500
PWR assemblies with zircaloy incore spacers		
2.3	24,500	24,500
2.6	29,500	29,500
2.9	34,500	34,500
3.2	39,500	39,500
3.4	44,500	44,500
MPC-68		
0.7	10,000	
1.35	20,000	
2.1	24,500	
2.4	29,500	
2.6	34,500	
2.9	39,500	
3.0	44,500	

Table 5.2.24

DESCRIPTION OF EVALUATED INTACT ZIRCALOY CLAD PWR FUEL

Assembly class	WE 14×14	WE 15×15	WE 17×17	CE 14×14	CE 16×16	B&W 15×15	B&W 17×17
Active fuel length (in.)	144	144	144	144	150	144	144
No. of fuel rods	179	204	264	176	236	208	264
Rod pitch (in.)	0.556	0.563	0.496	0.580	0.5063	0.568	0.502
Cladding material	Zr-4						
Rod diameter (in.)	0.422	0.422	0.374	0.440	0.382	0.428	0.377
Cladding thickness (in.)	0.0243	0.0245	0.0225	0.0280	0.0250	0.0230	0.0220
Pellet diameter (in.)	0.3659	0.366	0.3225	0.377	0.3255	0.3742	0.3252
Pellet material	UO ₂						
Pellet density (gm/cc) (95% of theoretical)	10.412	10.412	10.412	10.412	10.412	10.412	10.412
Enrichment (wt.% ²³⁵ U)	3.4	3.4	3.4	3.4	3.4	3.4	3.4
Burnup (MWD/MTU)	40,000	40,000	40,000	40,000	40,000	40,000	40,000
Cooling time (years)	5	5	5	5	5	5	5
Specific power (MW/MTU)	40	40	40	40	40	40	40
Weight of UO ₂ (kg) [†]	462.451	527.327	529.848	482.706	502.609	562.029	538.757
Weight of U (kg) [†]	407.697	464.891	467.114	425.554	443.100	495.485	474.968
No. of Guide Tubes	17	21	25	5	5	17	25
Guide Tube O.D. (in.)	0.539	0.546	0.474	1.115	0.98	0.53	0.564
Guide Tube Thickness (in.)	0.0170	0.0170	0.0160	0.0400	0.0400	0.0160	0.0175

[†] Derived from parameters in this table.

Table 5.2.25

DESCRIPTION OF EVALUATED INTACT ZIRCALOY CLAD BWR FUEL

Array Type	7×7	8×8	9×9	10×10
Active fuel length (in.)	144	144	144	144
No. of fuel rods	49	63	74	92
Rod pitch (in.)	0.738	0.640	0.566	0.510
Cladding material	Zr-2	Zr-2	Zr-2	Zr-2
Rod diameter (in.)	0.570	0.493	0.440	0.404
Cladding thickness (in.)	0.0355	0.0340	0.0280	0.0260
Pellet diameter (in.)	0.488	0.416	0.376	0.345
Pellet material	UO ₂	UO ₂	UO ₂	UO ₂
Pellet density (gm/cc) (95% of theoretical)	10.412	10.412	10.412	10.412
Enrichment (wt.% ²³⁵ U)	3.0	3.0	3.0	3.0
Burnup (MWD/MTU)	40,000	40,000	40,000	40,000
Cooling time (years)	5	5	5	5
Specific power (MW/MTU)	30	30	30	30
Weight of UO ₂ (kg) [†]	225.177	210.385	201.881	211.307
Weight of U (kg) [†]	198.516	185.475	177.978	186.288
No. of Water Rods	0	1	2	2
Water Rod O.D. (in.)	n/a	0.493	0.980	0.980
Water Rod Thickness (in.)	n/a	0.0340	0.0300	0.0300

[†] Derived from parameters in this table.

Table 5.2.26

COMPARISON OF SOURCE TERMS FOR INTACT ZIRCALOY CLAD PWR FUEL
 3.4 wt.% ²³⁵U - 40,000 MWD/MTU - 5 years cooling

Assembly class	WE 14x14	WE 15x15	WE 17x17	CE 14x14	CE 16x16	B&W 15x15	B&W 17x17
Neutrons/sec	2.29E+8 / 2.31E+8	2.63E+8 / 2.65E+8	2.62E+8	2.31E+8	2.34E+8	2.94E+8	2.64E+8
Photons/sec (0.45-3.0 MeV)	3.28E+15/ 3.33E+15	3.74E+15/ 3.79E+15	3.76E+15	3.39E+15	3.54E+15	4.01E+15	3.82E+15
Thermal power (watts)	926.6 / 936.8	1056 / 1068	1062	956.6	995.7	1137	1077

Note:

The WE 14x14 and WE 15x15 have both zircaloy and stainless steel guide tubes. The first value presented is for the assembly with zircaloy guide tubes and the second value is for the assembly with stainless steel guide tubes.

Table 5.2.27

COMPARISON OF SOURCE TERMS FOR INTACT ZIRCALOY CLAD BWR FUEL
 3.0 wt.% ²³⁵U - 40,000 MWD/MTU - 5 years cooling

Assembly class	7×7	8×8	9×9	10×10
Neutrons/sec	1.33E+8	1.17E+8	1.11E+8	1.22E+8
Photons/sec (0.45-3.0 MeV)	1.55E+15	1.44E+15	1.38E+15	1.46E+15
Thermal power (watts)	435.5	402.3	385.3	407.4

Table 5.2.28

COMPARISON OF CALCULATED DECAY HEATS FOR DESIGN BASIS FUEL
AND VALUES REPORTED IN THE
DOE CHARACTERISTICS DATABASE [†] FOR
30,000 MWD/MTU AND 5-YEAR COOLING

Fuel Assembly Class	Decay Heat from the DOE Database (watts/assembly)	Decay Heat from Design Basis Fuel (watts/assembly)
PWR Fuel		
B&W 15x15	752.0	827.5
B&W 17x17	732.9	827.5
CE 16x16	653.7	827.5
CE 14x14	601.3	827.5
WE 17x17	742.5	827.5
WE 15x15	762.2	827.5
WE 14x14	649.6	827.5
BWR Fuel		
7x7	310.9	315.7
8x8	296.6	315.7
9x9	275.0	315.7

Notes:

1. The PWR and BWR design basis fuels are the B&W 15x15 and the GE 7x7, respectively.
2. The decay heat values from the database include contributions from in-core material (e.g. spacer grids).
3. Information on the 10x10 was not available in the DOE database. However, based on the results in Table 5.2.27, the actual decay heat values from the 10x10 would be very similar to the values shown above for the 8x8.

[†] Reference [5.2.7].

Table 5.2.29
DESCRIPTION OF FUEL ASSEMBLY USED TO ANNALYZE
THORIA RODS IN THE THORIA ROD CANISTER

	BWR
Fuel type	8x8
Active fuel length (in.)	110.5
No. of UO ₂ fuel rods	55
No. of UO ₂ /ThO ₂ fuel rods	9
Rod pitch (in.)	0.523
Cladding material	zircaloy
Rod diameter (in.)	0.412
Cladding thickness (in.)	0.025
Pellet diameter (in.)	0.358
Pellet material	98.2% ThO ₂ and 1.8% UO ₂ for UO ₂ /ThO ₂ rods
Pellet density (gm/cc)	10.412
Enrichment (w/o ²³⁵ U)	93.5 in UO ₂ for UO ₂ /ThO ₂ rods and 1.8 for UO ₂ rods
Burnup (MWD/MTIHM)	16,000
Cooling Time (years)	18
Specific power (MW/MTIHM)	16.5
Weight of ThO ₂ and UO ₂ (kg) [†]	121.46
Weight of U (kg) [†]	92.29
Weight of Th (kg) [†]	14.74

[†] Derived from parameters in this table.

Table 5.2.30

CALCULATED FUEL GAMMA SOURCE FOR THORIA ROD
CANISTER CONTAINING EIGHTEEN THORIA RODS

Lower Energy (MeV)	Upper Energy (MeV)	16,000 MWD/MTIHM 18-Year Cooling	
		(MeV/s)	(Photons/s)
7.0E-01	1.0	5.79E+11	6.81E+11
1.0	1.5	3.79E+11	3.03E+11
1.5	2.0	4.25E+10	2.43E+10
2.0	2.5	4.16E+8	1.85E+8
2.5	3.0	2.31E+11	8.39E+10
Totals		1.23E+12	1.09E+12

Table 5.2.31

CALCULATED FUEL NEUTRON SOURCE FOR THORIA ROD
CANISTER CONTAINING EIGHTEEN THORIA RODS

Lower Energy (MeV)	Upper Energy (MeV)	16,000 MWD/MTIHM 18-Year Cooling (Neutrons/s)
1.0E-01	4.0E-01	5.65E+2
4.0E-01	9.0E-01	3.19E+3
9.0E-01	1.4	6.79E+3
1.4	1.85	1.05E+4
1.85	3.0	3.68E+4
3.0	6.43	1.41E+4
6.43	20.0	1.60E+2
Totals		7.21E+4

Table 5.2.32

DESCRIPTION OF DESIGN BASIS TROJAN FUEL

	PWR
Assembly type/class	WE 17×17
Active fuel length (in.)	144
No. of fuel rods	264
Rod pitch (in.)	0.496
Cladding material	zircaloy-4
Rod diameter (in.)	0.374
Cladding thickness (in.)	0.0225
Pellet diameter (in.)	0.3225
Pellet material	UO ₂
Pellet density (gm/cc)	10.412 (95% of theoretical)
Enrichment (w/o ²³⁵ U) ^{††}	2.1, 2.6, 3.09
Burnup (MWD/MTU)	30,000, 37,500, 42,000
Cooling Time (years)	16
Specific power (MW/MTU)	40
Weight of UO ₂ (kg) [†]	529.85
Weight of U (kg) [†]	467.11
No. of Water Rods/Guide Tubes	25
Water Rod O.D. (in.)	0.482
Water Rod Thickness (in.)	0.016
Lower End Fitting (kg)	5.9 (steel)
Gas Plenum Springs (kg)	1.15 (steel)
Gas Plenum Spacer (kg)	0.84 (steel) 0.79 (inconel)
Upper End Fitting (kg)	6.89 (steel) 0.96 (inconel)
Incore Grid Spacers (kg)	4.9 (inconel)

^{††} The enrichments correspond directly to the burnups (e.g. 2.1 for 30,000 MWD/MTU)

[†] Derived from parameters in this table.

Table 5.2.33
CALCULATED TROJAN PWR FUEL GAMMA SOURCE PER ASSEMBLY

Lower Energy	Upper Energy	30,000 MWD/MTU 16 Year Cooling		37,500 MWD/MTU 16 Year Cooling		42,000 MWD/MTU 16 Year Cooling	
		(MeV/s)	(Photons/s)	(MeV/s)	(Photons/s)	(MeV/s)	(Photons/s)
0.45	0.7	6.80E+14	1.18E+15	8.46E+14	1.47E+15	9.44E+14	1.64E+15
0.7	1.0	2.52E+13	2.96E+13	3.35E+13	3.94E+13	3.82E+13	4.50E+13
1.0	1.5	2.04E+13	1.64E+13	2.71E+13	2.17E+13	3.09E+13	2.47E+13
1.5	2.0	1.16E+12	6.65E+11	1.53E+12	8.77E+11	1.75E+12	9.99E+11
2.0	2.5	6.72E+09	2.99E+09	8.28E+09	3.68E+09	9.33E+09	4.15E+09
2.5	3.0	4.10E+08	1.49E+08	6.13E+08	2.23E+08	7.47E+08	2.72E+08
Totals		7.26E+14	1.23E+15	9.08E+14	1.53E+15	1.01E+15	1.71E+15

Table 5.2.34
 CALCULATED TROJAN FUEL ⁶⁰Co SOURCE PER ASSEMBLY

Location	30,000 MWD/MTU 16 Year Cooling (curies)	37,500 MWD/MTU 16 Year Cooling (curies)	42,000 MWD/MTU 16 Year Cooling (curies)
Lower End Fitting	21.48	23.72	24.19
Gas Plenum Springs	4.19	4.62	4.72
Gas Plenum Spacer	15.99	17.66	18.02
Grid Spacers	419.15	462.90	472.12
Upper End Fitting	18.29	20.20	20.60

Table 5.2.35
 CALCULATED TROJAN FUEL NEUTRON SOURCE PER ASSEMBLY

Lower Energy (MeV)	Upper Energy (MeV)	30,000 MWD/MTU 16 Year Cooling (Neutrons/s)	37,500 MWD/MTU 16 Year Cooling (Neutrons/s)	42,000 MWD/MTU 16 Year Cooling (Neutrons/s)
1.0E-01	4.0E-01	4.71E+06	8.11E+06	9.55E+06
4.0E-01	9.0E-01	2.41E+07	4.15E+07	4.88E+07
9.0E-01	1.4	2.21E+07	3.80E+07	4.47E+07
1.4	1.85	1.64E+07	2.81E+07	3.31E+07
1.85	3.0	2.93E+07	5.00E+07	5.88E+07
3.0	6.43	2.63E+07	4.51E+07	5.30E+07
6.43	20.0	2.30E+06	3.97E+06	4.67E+06
Total		1.25E+08	2.15E+08	2.53E+08

Table 5.2.36

DESCRIPTION OF TROJAN BURNABLE POISON ROD ASSEMBLY
AND THIMBLE PLUG DEVICE

Region	BPRA	TPD
Upper End Fitting (kg of steel)	2.62	2.31
Upper End Fitting (kg of inconel)	0.42	0.42
Gas Plenum Spacer (kg of steel)	0.72	1.6
Gas Plenum Springs (kg of steel)	0.73	1.6
In-core (kg of steel)	12.10	N/A

Table 5.2.37

COBALT-60 ACTIVITIES FOR TROJAN BURNABLE POISON ROD
ASSEMBLIES AND THIMBLE PLUG DEVICES

Region	BPRA	TPD
Burnup (MWD/MTU)	15,998	118,674
Cooling Time (years)	24	11
Upper End Fitting (curies Co-60)	1.20	18.86
Gas Plenum Spacer (curies Co-60)	0.34	12.80
Gas Plenum Springs (curies Co-60)	0.34	12.80
In-core (curies Co-60)	28.68	N/A

Table 5.2.38

DESCRIPTION OF TROJAN ROD CLUSTER CONTROL ASSEMBLY
FOR SOURCE TERM CALCULATIONS

Physical Description

Axial Dimensions Relative to Bottom of Active Fuel			Flux Weighting Factor	Mass of cladding (kg Steel)	Mass of absorber (kg AgInCd)
Start (in)	Finish (in)	Length (in)			
Configuration - Fully Removed					
0.0	8.358	8.358	0.2	0.76	3.18
8.358	12.028	3.67	0.1	0.34	1.40

Radiological Description
125,515 MWD/MTU
9 Year Cooling

Axial Dimensions Relative to Bottom of Active Fuel			Photons/sec from AgInCd			Curies Co-60 from Steel
Start (in)	Finish (in)	Length (in)	0.3-0.45 MeV	0.45-0.7 MeV	0.7-1.0 MeV	
Configuration - Fully Removed						
0.0	8.358	8.358	7.66E+12	7.12E+12	5.66E+12	7.34
8.358	12.028	3.67	1.68E+12	1.56E+13	1.24E+12	1.61

Table 5.2.39

DESCRIPTION OF TROJAN SECONDARY SOURCE ASSEMBLIES

Physical Description

Region	Source in Cycles 1-4	Sources in Cycles 4-14
Upper End Fitting (kg of steel)	2.62	2.62
Upper End Fitting (kg of inconel)	0.42	0.42
Gas Plenum Spacer (kg of steel)	1.6	1.6
Gas Plenum Springs (kg of steel)	1.6	1.6
In-core (kg of steel)	10.08	2.02

Radiological Description

Region	Source in Cycles 1-4	Sources in Cycles 4-14
Burnup (MWD/MTU)	45,361	88,547
Cooling Time (years)	19	9
Upper End Fitting (curies Co-60)	10.08	45.09
Gas Plenum Spacer (curies Co-60)	3.18	14.30
Gas Plenum Springs (curies Co-60)	3.18	14.30
In-core (curies Co-60)	100.20	90.29

Table 5.2.40

CALCULATED MPC-32 PWR FUEL GAMMA SOURCE PER ASSEMBLY FOR DESIGN BASIS ZIRCALOY CLAD FUEL WITH NON-ZIRCALOY INCORE SPACERS FOR VARYING BURNUPS AND COOLING TIMES

Lower Energy	Upper Energy	24,500 MWD/MTU 12 Year Cooling		29,500 MWD/MTU 14 Year Cooling		34,500 MWD/MTU 16 Year Cooling	
		(MeV/s)	(Photons/s)	(MeV/s)	(Photons/s)	(MeV/s)	(Photons/s)
0.45	0.7	6.67E+14	1.16E+15	7.51E+14	1.31E+15	8.26E+14	1.44E+15
0.7	1.0	4.19E+13	4.94E+13	3.59E+13	4.23E+13	3.18E+13	3.74E+13
1.0	1.5	2.29E+13	1.83E+13	2.45E+13	1.96E+13	2.59E+13	2.07E+13
1.5	2.0	1.23E+12	7.05E+11	1.36E+12	7.80E+11	1.48E+12	8.47E+11
2.0	2.5	2.57E+10	1.14E+10	1.14E+10	5.06E+09	8.42E+09	3.74E+09
2.5	3.0	1.87E+09	6.78E+08	7.75E+08	2.82E+08	5.66E+08	2.06E+08
Totals		7.33E+14	1.23E+15	8.13E+14	1.37E+15	8.85E+14	1.50E+15
Lower Energy	Upper Energy	39,500 MWD/MTU 19 Year Cooling		42,500 MWD/MTU 20 Year Cooling			
		(MeV/s)	(Photons/s)	(MeV/s)	(Photons/s)		
0.45	0.7	8.72E+14	1.52E+15	9.13E+14	1.59E+15		
0.7	1.0	2.51E+13	2.95E+13	2.46E+13	2.89E+13		
1.0	1.5	2.42E+13	1.94E+13	2.46E+13	1.97E+13		
1.5	2.0	1.43E+12	8.17E+11	1.46E+12	8.35E+11		
2.0	2.5	7.78E+09	3.46E+09	8.08E+09	3.59E+09		
2.5	3.0	5.98E+08	2.17E+08	6.89E+08	2.51E+08		
Totals		9.22E+14	1.57E+15	9.63E+14	1.64E+15		

Table 5.2.41
 CALCULATED MPC-32 PWR FUEL GAMMA SOURCE PER ASSEMBLY FOR DESIGN BASIS ZIRCALOY CLAD
 FUEL WITH ZIRCALOY INCORE SPACERS FOR VARYING BURNUPS AND COOLING TIMES

Lower Energy	Upper Energy	24,500 MWD/MTU 8 Year Cooling		29,500 MWD/MTU 9 Year Cooling		34,500 MWD/MTU 12 Year Cooling	
		(MeV/s)	(Photons/s)	(MeV/s)	(Photons/s)	(MeV/s)	(Photons/s)
0.45	0.7	8.09E+14	1.41E+15	9.20E+14	1.60E+15	9.38E+14	1.63E+15
0.7	1.0	1.19E+14	1.40E+14	1.17E+14	1.38E+14	6.91E+13	8.13E+13
1.0	1.5	3.84E+13	3.07E+13	4.30E+13	3.44E+13	3.78E+13	3.02E+13
1.5	2.0	2.04E+12	1.17E+12	2.17E+12	1.24E+12	1.99E+12	1.14E+12
2.0	2.5	4.83E+11	2.15E+11	2.40E+11	1.07E+11	3.18E+10	1.41E+10
2.5	3.0	2.60E+10	9.46E+09	1.51E+10	5.48E+09	2.53E+09	9.20E+08
Totals		9.69E+14	1.58E+15	1.08E+15	1.77E+15	1.05E+15	1.74E+15
Lower Energy	Upper Energy	39,500 MWD/MTU 14 Year Cooling		44,500 MWD/MTU 19 Year Cooling			
		(MeV/s)	(Photons/s)	(MeV/s)	(Photons/s)		
0.45	0.7	1.00E+15	1.74E+15	9.78E+14	1.70E+15		
0.7	1.0	5.41E+13	6.37E+13	2.92E+13	3.44E+13		
1.0	1.5	3.71E+13	2.97E+13	2.84E+13	2.27E+13		
1.5	2.0	2.03E+12	1.16E+12	1.66E+12	9.50E+11		
2.0	2.5	1.42E+10	6.32E+09	8.63E+09	3.84E+09		
2.5	3.0	1.17E+09	4.25E+08	7.88E+08	2.87E+08		
Totals		1.09E+15	1.83E+15	1.04E+15	1.76E+15		

Table 5.2.42

CALCULATED MPC-32 ⁶⁰Co SOURCE PER ASSEMBLY FOR DESIGN BASIS ZIRCALOY CLAD FUEL WITH NON-ZIRCALOY INCORE SPACERS AT VARYING BURNUPS AND COOLING TIMES

Location	24,500 MWD/MTU 12 Year Cooling (curies)	29,500 MWD/MTU 14 Year Cooling (curies)	34,500 MWD/MTU 16 Year Cooling (curies)	39,500 MWD/MTU 19 Year Cooling (curies)	42,500 MWD/MTU 20 Year Cooling (curies)
Lower end fitting	64.65	55.27	46.40	33.47	30.42
Gas plenum springs	12.58	10.75	9.03	6.51	5.92
Gas plenum spacer	7.22	6.17	5.18	3.74	3.40
Expansion springs	N/A	N/A	N/A	N/A	N/A
Grid spacers	587.27	502.05	421.45	304.00	276.36
Upper end fitting	23.66	20.23	16.98	12.25	11.14
Handle	N/A	N/A	N/A	N/A	N/A

Table 5.2.43

CALCULATED MPC-32 ⁶⁰Co SOURCE PER ASSEMBLY FOR DESIGN BASIS ZIRCALOY CLAD FUEL
WITH ZIRCALOY INCORE SPACERS AT VARYING BURNUPS AND COOLING TIMES

Location	24,500 MWD/MTU 8 Year Cooling (curies)	29,500 MWD/MTU 9 Year Cooling (curies)	34,500 MWD/MTU 12 Year Cooling (curies)	39,500 MWD/MTU 14 Year Cooling (curies)	44,500 MWD/MTU 19 Year Cooling (curies)
Lower end fitting	109.27	106.74	78.34	64.65	36.25
Gas plenum springs	21.26	20.77	15.24	12.58	7.05
Gas plenum spacer	12.20	11.91	8.74	7.22	4.05
Expansion springs	N/A	N/A	N/A	N/A	N/A
Grid spacers [†]	N/A	N/A	N/A	N/A	N/A
Upper end fitting	40.00	39.07	28.68	23.66	13.27
Handle	N/A	N/A	N/A	N/A	N/A

[†] These burnup and cooling times represent fuel with zircaloy grid spacers. Therefore, the cobalt activation is negligible.

Table 5.2.44

CALCULATED MPC-32 PWR NEUTRON SOURCE PER ASSEMBLY
 FOR DESIGN BASIS ZIRCALOY CLAD FUEL WITH NON-ZIRCALOY
 INCORE SPACERS FOR VARYING BURNUPS AND COOLING TIMES

Lower Energy (MeV)	Upper Energy (MeV)	24,500 MWD/MTU 12 Year Cooling (Neutrons/s)	29,500 MWD/MTU 14 Year Cooling (Neutrons/s)	34,500 MWD/MTU 16 Year Cooling (Neutrons/s)	39,500 MWD/MTU 19 Year Cooling (Neutrons/s)	42,500 MWD/MTU 20 Year Cooling (Neutrons/s)
1.0E-01	4.0E-01	2.24E+06	3.61E+06	5.37E+06	6.97E+06	8.08E+06
4.0E-01	9.0E-01	1.15E+07	1.84E+07	2.74E+07	3.56E+07	4.13E+07
9.0E-01	1.4	1.06E+07	1.70E+07	2.52E+07	3.27E+07	3.79E+07
1.4	1.85	7.88E+06	1.26E+07	1.87E+07	2.43E+07	2.81E+07
1.85	3.0	1.43E+07	2.27E+07	3.35E+07	4.34E+07	5.02E+07
3.0	6.43	1.26E+07	2.02E+07	3.00E+07	3.89E+07	4.50E+07
6.43	20.0	1.10E+06	1.76E+06	2.63E+06	3.41E+06	3.95E+06
TOTALS		6.01E+07	9.63E+07	1.43E+08	1.85E+08	2.15E+08

Table 5.2.45

CALCULATED MPC-32 PWR NEUTRON SOURCE PER ASSEMBLY
 FOR DESIGN BASIS ZIRCALOY CLAD FUEL WITH ZIRCALOY
 INCORE SPACERS FOR VARYING BURNUPS AND COOLING TIMES

Lower Energy (MeV)	Upper Energy (MeV)	24,500 MWD/MTU 8 Year Cooling (Neutrons/s)	29,500 MWD/MTU 9 Year Cooling (Neutrons/s)	34,500 MWD/MTU 12 Year Cooling (Neutrons/s)	39,500 MWD/MTU 14 Year Cooling (Neutrons/s)	44,500 MWD/MTU 19 Year Cooling (Neutrons/s)
1.0E-01	4.0E-01	2.60E+06	4.35E+06	6.24E+06	8.40E+06	1.01E+07
4.0E-01	9.0E-01	1.33E+07	2.22E+07	3.19E+07	4.29E+07	5.16E+07
9.0E-01	1.4	1.22E+07	2.04E+07	2.92E+07	3.94E+07	4.73E+07
1.4	1.85	9.08E+06	1.51E+07	2.17E+07	2.91E+07	3.50E+07
1.85	3.0	1.63E+07	2.70E+07	3.86E+07	5.19E+07	6.24E+07
3.0	6.43	1.45E+07	2.42E+07	3.47E+07	4.67E+07	5.61E+07
6.43	20.0	1.27E+06	2.13E+06	3.05E+06	4.11E+06	4.94E+06
TOTALS		6.93E+07	1.16E+08	1.65E+08	2.23E+08	2.67E+08

5.4 SHIELDING EVALUATION

The MCNP-4A code[5.1.1] was used for all of the shielding analyses. MCNP is a continuous energy, three-dimensional, coupled neutron-photon-electron Monte Carlo transport code. Continuous energy cross section data is represented with sufficient energy points to permit linear-linear interpolation between these points. The individual cross section libraries used for each nuclide are those recommended by the MCNP manual. All of these data are based on ENDF/B-V data. MCNP has been extensively benchmarked against experimental data by the large user community. References [5.4.2], [5.4.3], and [5.4.4] are three examples of the benchmarking that has been performed.

The energy distribution of the source term, as described earlier, is used explicitly in the MCNP model. A different MCNP calculation is performed for each of the three source terms (neutron, decay gamma, and ^{60}Co). The axial distribution of the fuel source term is described in Table 1.2.15 and Figures 1.2.13 and 1.2.14. The PWR and BWR axial burnup distributions were obtained from References [5.4.5] and [5.4.6] respectively. These axial distributions were obtained from operating plants and are representative of PWR and BWR fuel with burnups greater than 30,000 MWD/MTU. The ^{60}Co source in the hardware was assumed to be uniformly distributed over the appropriate regions. The axial distribution used for the Trojan Plant fuel was similar but not identical to the generic PWR distribution. Table 1.2.15 and Figure 1.2.13a present the axial burnup distribution used for the Trojan Plant fuel taken from the Trojan FSAR [5.1.6].

It has been shown that the neutron source strength varies as the burnup level raised by the power of 4.2. Since this relationship is non-linear and since the burnup in the axial center of a fuel assembly is greater than the average burnup, the neutron source strength in the axial center of the assembly is greater than the relative burnup times the average neutron source strength. In order to account for this effect, the neutron source strength in each of the 10 axial nodes listed in Table 1.2.15 was determined by multiplying the average source strength by the relative burnup level raised to the power of 4.2. The peak relative burnups listed in Table 1.2.15 for the generic PWR and BWR fuels are 1.105 and 1.195 respectively. Using the power of 4.2 relationship results in a 37.6% ($1.105^{4.2}/1.105$) and 76.8% ($1.195^{4.2}/1.195$) increase in the neutron source strength in the peak nodes for the PWR and BWR fuel respectively. The total neutron source strength increases by 15.6% for the PWR fuel assemblies and 36.9% for the BWR fuel assemblies.

MCNP was used to calculate dose at the various desired locations. MCNP calculates neutron or photon flux and these values can be converted into dose by the use of dose response functions. This is done internally in MCNP and the dose response functions are listed in the input file. The response functions used in these calculations are listed in Table 5.4.1 and were taken from ANSI/ANS 6.1.1, 1977 [5.4.1].

The dose rate at the various locations were calculated with MCNP using a two step process. The first step was to calculate the dose rate for each dose location per starting particle for each neutron and gamma group and each axial location in the end fittings. The second and last step was to multiply the dose rate per starting particle for each group by the source strength (i.e. particles/sec) in that group and sum the resulting dose rates for all groups in each dose location. The standard deviations of the various results were statistically combined to determine the standard deviation of the total dose in each dose location.

Figures 5.1.1 and 5.1.2 depict the dose point locations during normal and hypothetical accident conditions of transport. Dose point location 3a in Figure 5.1.1 covers two regions of different radii. The outermost region is 5.75 inches in height and the innermost region is 6.875 inches in height. The dose rate was calculated over both segments and the highest value was reported for dose location 3a. Dose point locations 1 through 4 in Figure 5.1.2 are conservatively located at a radial position that is approximately 1 meter from the outer radial surface of the bottom plate.

Tables 5.4.8, 5.4.9, 5.4.19, 5.4.29, and 5.4.32 provide the total dose rate on the surface of the HI-STAR 100 System for each burnup level and cooling time. Tables 5.4.10 through 5.4.13, 5.4.20, 5.4.21, 5.4.30, 5.4.31, 5.4.33, and 5.4.34 provide the total dose rate at 2 meters for normal conditions and at 1 meter for accident conditions for each burnup level and cooling time for the MPC-24, MPC-68 and the MPC-32. This information was used to determine the worst case burnup level and cooling time and corresponding maximum dose rates reported in Section 5.1.

Since MCNP is a statistical code, there is an uncertainty associated with the calculated values. In MCNP the uncertainty is expressed as the relative error which is defined as the standard deviation of the mean divided by the mean. Therefore, the standard deviation is represented as a percentage of the mean. The relative error for the total dose rates presented in this chapter were typically less than 2% and the relative error for the individual dose components was typically less than 5%.

5.4.1 Streaming Through Radial Steel Fins and Pocket Trunnions

The HI-STAR 100 overpack utilizes 0.5 inch thick radial channels for structural support and cooling. The attenuation of neutrons through steel is substantially less than the attenuation of neutrons through the neutron shield. Therefore, it is possible to have neutron streaming through the channels which could result in a localized dose peak. The reverse is true for photons which would result in a localized reduction in the photon dose. Analyses were performed to determine the magnitude of the dose peaks and depressions and the impact on localized dose as compared to average total dose. This effect was evaluated at the radial surface of the HI-STAR 100 System and a distance of two meters.

In addition to the radial channels, the pocket trunnions are essentially blocks of steel that are approximately 12 inches wide and 12 inches high. The effect of the pocket trunnion on neutron

streaming and photon transmission will be more substantial than the effect of a single fin. Therefore, analyses were performed to quantify this effect. Figures 5.3.7 and 5.3.8 illustrate the location of the pocket trunnion and its axial position relative to the active fuel.

The fuel loading pattern in the MPC-32, MPC-24 and the MPC-68, as depicted in Figures 5.3.1 through 5.3.3, is not cylindrical. Therefore, there is a potential to experience peaking as a result of azimuthal variations in the fuel loading. Since the MCNP models represent the fuel in the correct positions (i.e., cylindrical homogenization is not performed) the effect of azimuthal variations in the loading pattern is automatically accounted for in the calculations that are discussed below.

The effect of streaming through the pocket trunnion and the radial channels was analyzed using the full three-dimensional MCNP models of the MPC-24 and the MPC-68. The effect of peaking was calculated on the surface of the overpack adjacent to the pocket trunnion and dose locations 2a and 3a in Figures 5.1.1. The effect of peaking was also analyzed at 2 meters from the overpack at dose location 2 and at the axial height of the impact limiter. Dose location 3 was not analyzed at two meters because the dose at that point is less than the dose at location 2 as demonstrated in the tables at the end of this section. Figure 5.4.1 shows a quarter of the HI-STAR 100 overpack with 41 azimuthal bins drawn. There is one bin per steel fin and 3 bins in each neutron shield region. This azimuthal binning structure was used over the axial height of the overpack. The dose was calculated in each of these bins and then compared to the average dose calculated over the surface to determine a peak-to-average ratio for the dose in that bin. The azimuthal location of the pocket trunnion is shown in Figure 5.4.1. The pocket trunnion was modeled as solid steel. During shipping, a steel rotation trunnion or plug shall be placed in the pocket trunnion recess. To conservatively evaluate the peak to average ratio, the pocket trunnion is assumed to be solid steel.

Table 5.4.14 provides representative peak-to-average ratios that were calculated for the various dose components and locations. Table 5.4.15 presents the dose rates at the dose locations analyzed including the effect of peaking. These results can be compared with the surface average results in Tables 5.1.1, 5.1.3, 5.1.4, and 5.1.6. The peak dose on the surface of the overpack at dose location 2a occurs at a steel channel (fin). This is evident by the high neutron peaking at dose location 2a on the surface of the overpack. The dose rate at the pocket trunnion, in those overpacks containing pocket trunnions, is higher than the dose rate at dose location 2 on the surface of the overpack. However, these results clearly indicate that, at two meters, the peaking associated with the pocket trunnion is not present and that the peak dose location is #2.

The MPC-32 was not explicitly analyzed for azimuthal peaking. It is expected that the peaking in the MPC-32 will be similar if not smaller than in the MPC-24 due to the fact that the fuel assemblies in the MPC-24 are not as closely positioned to each other as in the MPC-32.

5.4.2 Damaged Fuel Post-Accident Shielding Evaluation

As discussed in Subsection 5.2.5.2, the analysis presented below, even though it is for damaged fuel, demonstrates the acceptability of transporting intact Humboldt Bay 6x6 and intact Dresden 1 6x6 fuel assemblies. As discussed in Subsection 5.2.8, the Trojan damaged fuel and fuel debris were not explicitly analyzed because they are bounded by the intact fuel assemblies.

For the damaged fuel and fuel debris accident condition, it is conservatively assumed the damaged fuel cladding ruptures and all the fuel pellets fall and collect at the bottom of the damaged fuel container. The inner dimension of the damaged fuel container, specified in the Design Drawings of Section 1.4, and the design basis damaged fuel and fuel debris assembly dimensions in Table 5.2.2 are used to calculate the axial height of the rubble in the damaged fuel container assuming 50% compaction. Neglecting the fuel pellet to cladding inner diameter gap, the volume of cladding and fuel pellets available for deposit is calculated assuming the fuel rods are solid. Using the volume in conjunction with the damaged fuel container, the axial height of rubble is calculated to be 80 inches.

Some of the 6x6 assemblies described in Table 5.2.2 were manufactured with Inconel grid spacers (the mass of inconel is listed in Table 5.2.2). The calculated ^{60}Co activity from these spacers was 66.7 curies for a burnup of 30,000 MWD/MTU and a cooling time of 18 years. Including this source with the total fuel gamma source for damaged fuel in Table 5.2.6 and dividing by the 80 inch rubble height provides a gamma source per inch of $3.47\text{E}+12$ photon/s. Dividing the total neutron source for damaged fuel in Table 5.2.14 by 80 inches provides a neutron source per inch of $3.935.24\text{E}+5$ neutron/s. These values are both bounded by the BWR design basis fuel gamma source per inch and neutron source per inch values of $5.03\text{E}+12$ photon/s and $6.63\text{E}+5$ neutron/s. These BWR design basis values were calculated by dividing the total source strengths as calculated from Tables 5.2.5 and 5.2.13 (39,500 MWD/MTU and 14 year cooling values) by the active fuel length of 144 inches. *Additionally, a separate analysis added the calculated ^{60}Co activity from the Inconel grid spacers to the 1.0 to 1.5 MeV energy range of the gamma source rather than to the total of the fuel gamma source. While the gamma source in the 1.0 to 1.5 MeV range is not bounded, the resulting dose rate is still below the limit, since the contribution from the other energy ranges are lower.*

The resulting side dose rates from the damaged fuel assemblies are approximately 20 to 25% lower than the side dose rates from the design basis BWR intact fuel assemblies. MPC-68 with Therefore, the design basis damaged fuel assembly is bounded by the design basis intact BWR fuel assembly for accident conditions. No explicit analysis of the damaged fuel dose rates are provided as they are bounded by the intact fuel analysis.

5.4.3 Mixed Oxide Fuel Evaluation

The source terms calculated for the Dresden Unit 1 GE 6x6 MOX fuel assemblies can be compared to the design basis source terms for the BWR assemblies which demonstrates that the

MOX fuel source terms are bounded by the design basis source terms and no additional shielding analysis is needed.

Since the active fuel length of the MOX fuel assemblies is shorter than the active fuel length of the design basis fuel, the source terms must be compared on a per inch basis. Including the ^{60}Co source from grid spacers as calculated in the previous subsection (66.7 curies) with the total fuel gamma source for the MOX fuel in Table 5.2.16 and dividing by the 110 inch active fuel height provides a gamma source per inch of $2.41\text{E}+12$ photons/s. Dividing the total neutron source for the MOX fuel assemblies in Table 5.2.17 by 110 inches provides a neutron source strength per inch of $3.67\text{E}+5$ neutrons/s. These values are both bounded by the BWR design basis fuel gamma source per inch and neutron source per inch values of $5.03\text{E}+12$ photons/s and $6.63\text{E}+5$ neutrons/s. These BWR design basis values were calculated by dividing the total source strengths as calculated from Tables 5.2.5 and 5.2.13 (39,500 MWD/MTU and 14 year cooling values) by the active fuel length of 144 inches. This comparison shows that the MOX fuel source terms are bound by the design basis source terms. Therefore, no explicit analysis of dose rates is provided for MOX fuel.

Since the MOX fuel assemblies are Dresden Unit 1 6x6 assemblies, they can also be considered as damaged fuel. Using the same methodology as described in Subsection 5.4.2, the source term for the MOX fuel is calculated on a per inch basis assuming a post-accident rubble height of 80 inches. The resulting gamma and neutron source strengths are $3.31\text{E}+12$ photons/s and $5.05\text{E}+5$ neutrons/s. These values are also bounded by the design basis fuel gamma source per inch and neutron source per inch. Therefore, no explicit analysis of dose rates is provided for MOX fuel in a post-accident configuration.

5.4.4 Stainless Steel Clad Fuel Evaluation

Tables 5.4.22 through 5.4.24 present the dose rates from the stainless steel clad fuel at various dose locations around the HI-STAR 100 overpack for the MPC-24 and the MPC-68 for normal and hypothetical accident conditions. These dose rates are below the regulatory limits indicating that these fuel assemblies are acceptable for transport.

As described in Subsection 5.2.3, the source term for the stainless steel fuel was calculated conservatively with an artificial active fuel length of 144 inches. The end fitting masses of the stainless steel clad fuel are also assumed to be identical to the end fitting masses of the zircaloy clad fuel. In addition, the fuel assembly configuration used in the MCNP calculations was identical to the configuration used for the design basis fuel assemblies as described in Table 5.3.1.

5.4.5 Dresden Unit 1 Antimony-Beryllium Neutron Sources

Dresden Unit 1 has antimony-beryllium neutron sources which are placed in the water rod location of their fuel assemblies. These sources are steel rods which contain a cylindrical antimony-beryllium source which is 77.25 inches in length. The steel rod is approximately 95 inches in length. Information obtained from Dresden Unit 1 characterizes these sources in the following manner: "About one-quarter pound of beryllium will be employed as a special neutron source material. The beryllium produces neutrons upon gamma irradiation. The gamma rays for the source at initial start-up will be provided by neutron-activated antimony (about 865 curies). The source strength is approximately $1E+8$ neutrons/second."

As stated above, beryllium produces neutrons through gamma irradiation and in this particular case antimony is used as the gamma source. The threshold gamma energy for producing neutrons from beryllium is 1.666 MeV. The outgoing neutron energy increases as the incident gamma energy increases. Sb-124, which decays by Beta decay with a half life of 60.2 days, produces a gamma of energy 1.69 MeV which is just energetic enough to produce a neutron from beryllium. Approximately 54% of the Beta decays for Sb-124 produce gammas with energies greater than or equal to 1.69 MeV. Therefore, the neutron production rate in the neutron source can be specified as $5.8E-6$ neutrons per gamma ($1E+8/865/3.7E+10/0.54$) with energy greater than 1.666 MeV or $1.16E+5$ neutrons/curie ($1E+8/865$) of Sb-124.

With the short half life of 60.2 days all of the initial Sb-124 is decayed and any Sb-124 that was produced while the neutron source was in the reactor is also decayed since these neutron sources are assumed to have the same minimum cooling time as the Dresden 1 fuel assemblies (array classes 6x6A, 6x6B, 6x6C, and 8x8A) of 18 years. Therefore, there are only two possible gamma sources which can produce neutrons from this antimony-beryllium source. The first is the gammas from the decay of fission products in the fuel assemblies in the MPC. The second gamma source is from Sb-124 which is being produced in the MPC from neutron activation from neutrons from the decay of fission products.

MCNP calculations were performed to determine the gamma source as a result of decay gammas from fuel assemblies and Sb-124 activation. The calculations explicitly modeled the 6x6 fuel assembly described in Table 5.2.2. A single fuel rod was removed and replaced by a guide tube. In order to determine the amount of Sb-124 that is being activated from neutrons in the MPC it was necessary to estimate the amount of antimony in the neutron source. The O.D. of the source was assumed to be the I.D. of the steel rod encasing the source (0.345 in.). The length of the source is 77.25 inches. The beryllium is assumed to be annular in shape encompassing the antimony. Using the assumed O.D. of the beryllium and the mass and length, the I.D. of the beryllium was calculated to be 0.24 inches. The antimony is assumed to be a solid cylinder with an O.D. equal to the I.D. of the beryllium. These assumptions are conservative since the antimony and beryllium are probably encased in another material which would reduce the mass of antimony. A larger mass of antimony is conservative since the calculated activity of Sb-124 is directly proportional to the initial mass of antimony.

The number of gammas from fuel assemblies with energies greater than 1.666 MeV entering the 77.25 inch long neutron source was calculated to be $1.04\text{E}+8$ gammas/sec which would produce a neutron source of 603.2 neutrons/sec ($1.04\text{E}+8 * 5.8\text{E}-6$). The steady state amount of Sb-124 activated in the antimony was calculated to be 39.9 curies. This activity level would produce a neutron source of $4.63\text{E}+6$ neutrons/sec ($39.9 * 1.16\text{E}+5$) or $6.0\text{E}+4$ neutrons/sec/inch ($4.63\text{E}+6/77.25$). These calculations conservatively neglect the reduction in antimony and beryllium which would have occurred while the neutron sources were in the core and being irradiated at full reactor power.

Since this is a localized source (77.25 inches in length) it is appropriate to compare the neutron source per inch from the design basis Dresden Unit 1 fuel assembly, 6x6, containing an Sb-Be neutron source to the design basis fuel neutron source per inch. This comparison, presented in Table 5.4.25, demonstrates that a Dresden Unit 1 fuel assembly containing an Sb-Be neutron source is bounded by the design basis fuel.

As stated above, the Sb-Be source is encased in a steel rod. Therefore, the gamma source from the activation of the steel was considered assuming a burnup of 120,000 MWD/MTU which is the maximum burnup assuming the Sb-Be source was in the reactor for the entire 18 year life of Dresden Unit 1. The cooling time assumed was 18 years which is the minimum cooling time for Dresden Unit 1 fuel. The source from the steel was bounded by the design basis fuel assembly. In conclusion, transport of a Dresden Unit 1 Sb-Be neutron source in a Dresden Unit 1 fuel assembly is acceptable and bounded by the current analysis.

5.4.6 Thoria Rod Canister

Based on a comparison of the gamma spectra from Tables 5.2.30 and 5.2.6 for the thoria rod canister and design basis 6x6 fuel assembly, respectively, it is difficult to determine if the thoria rods will be bounded by the 6x6 fuel assemblies. However, it is obvious that the neutron spectra from the 6x6, Table 5.2.14, bounds the thoria rod neutron spectra, Table 5.2.31, with a significant margin. In order to demonstrate that the gamma spectrum from the single thoria rod canister is bounded by the gamma spectrum from the design basis 6x6 fuel assembly, the gamma dose rate on the outer radial surface of the overpack was estimated conservatively assuming an MPC full of thoria rod canisters. This gamma dose rate was compared to an estimate of the dose rate from an MPC full of design basis 6x6 fuel assemblies. The gamma dose rate from the 6x6 fuel was higher than the dose rate from an MPC full of thoria rod canisters. This in conjunction with the significant margin in neutron spectrum and the fact that there is only one thoria rod canister clearly demonstrates that the thoria rod canister is acceptable for transport in the MPC-68 or the MPC-68F.

5.4.7 Trojan Fuel Contents

Tables 5.4.26 through 5.4.28 present the results for the Trojan MPC-24E for normal surface and

2 meter as well as accident results. These results are presented for a single burnup and cooling time of 42,000 MWD/MTU and 16 year cooling. This burnup and cooling time combination is shown in Tables 5.2.33 through 5.2.35 to bound the other allowable burnup and cooling time combinations for Trojan fuel. Since the Trojan MPCs will contain BPRAs, RCCAs, and TPDs, the source from these devices was considered in the analysis. The source from BPRAs and TPDs were added to the fuel source in the appropriate location. The mass from these devices was conservatively neglected. Separate calculations were performed for the BPRAs and the TPDs since both devices can not be present in the same fuel assembly. The results presented in Tables 5.4.26 through 5.4.28 represent the configuration (fuel plus non-fuel hardware: BPRAs or TPD) that produces the highest dose rate at that location. Separate results for the different non-fuel hardware are not provided. Separate MCNP calculations were performed for the consideration of the RCCAs since this source is localized at the bottom of the MPC. The results for the RCCAs indicate that the presence of RCCAs will increase the dose rate on the surface of the overpack by a maximum of 1.3 mrem/hr and the dose rate at 2 meters will increase by a maximum of 0.08-09 mrem/hr for normal conditions. During accident conditions the dose rate will increase by a maximum of 6 mrem/hr with the presence of RCCAs.

These dose rates are less than the regulatory limits and therefore the Trojan contents are approved for transportation.

5.4.8 Trojan Antimony-Beryllium Neutron Sources

The analysis of the Trojan secondary antimony-beryllium neutron sources was performed in a manner very similar to that described above in Subsection 5.4.5. The secondary sources are basically BPRAs with four rods containing the antimony-beryllium with a length of 88 inches in each rod. As mentioned in Subsection 5.4.5, the antimony-beryllium source is a regenerative source in which the antimony is activated and the gammas released from the antimony induce a gamma,n reaction in the beryllium.

The steady state production of neutrons from this antimony-beryllium source was conservatively calculated in the MPC using an approach very similar to that described in Subsection 5.4.5. The depletion of antimony from the operation in the reactor core was conservatively neglected in the analysis. MCNP calculations were performed with explicitly modeled fuel assemblies in a Trojan MPC model to calculate the steady state activity of Sb-124 in the antimony-beryllium source due to the neutrons from the spent fuel. This activity level was used in a subsequent MCNP calculation to determine the gamma,n reaction rate in the beryllium. The gamma,n cross section for beryllium, which exhibits peaks at 1.5E-3 with lows at approximately 0.3E-3 barns, was used in MCNP as a reaction rate multiplier for the flux tallies. Additionally, the gamma,n reaction rate due to gammas from the spent fuel was determined. In the latter case, gammas from the spent fuel with energies up to 11 MeV were considered in the analysis compared to an upper limit of 3 MeV for the cask dose rate analysis. Finally, the gamma,n reaction rate was converted to neutrons/sec to yield the neutron source per secondary source assembly. In this conversion

process the spectrum of neutrons emitted from the Sb-Be source was determined based on the energy spectrum of the gammas reacting in the beryllium [5.4.7]. The neutron source strength per secondary source assembly was calculated to be $9.9E+5$ neutrons/sec with more than 99% of these having an upper energy of 0.03 MeV. The remaining 1% of the secondary source neutrons had energies up to 0.74 MeV. This is a conservative estimate of the neutrons/sec from the secondary source because it neglects depletion of the antimony that has occurred during core operation and it assumes that all assemblies in the MPC are design basis Trojan fuel assemblies.

In order to determine the impact of the secondary neutron sources on the dose rates, MCNP calculations were performed. Since the dose rate that is closest to the regulatory limit is at 2 meters from the overpack, this was the only location considered in the analysis. Rather than calculate the average dose rate around the overpack at the 2 meter location, the dose rate was calculated for a specific location. Figure 5.4.2 shows the location where the dose rate was calculated. This location (an 8.2 inch diameter cylinder) is at 2 meters from the transport vehicle on a line drawn from the center of the MPC through the center of a corner assembly. The dose rate in this cylinder was calculated using the same axial segmentation as in the design basis calculations. In this analysis, the corner assembly was the only assembly considered to have the secondary source assembly. This choice of assembly position and dose location bounds all other possible locations for the single Trojan secondary source assembly permitted in any MPC.

The dose rates were calculated for the following combinations of fuel assemblies and non-fuel hardware inserts. In all dose rate calculations, both the neutron and gamma source from the secondary sources was considered.

1. One fuel assembly with secondary source assembly from cycles 1-4 and the remaining 23 fuel assemblies with BPRAs.
2. One fuel assembly with secondary source assembly from cycles 1-4 and the remaining 23 fuel assemblies with TPDs.
3. One fuel assembly with secondary source assembly from cycles 4-14 and the remaining 23 fuel assemblies with BPRAs.
4. One fuel assembly with secondary source assembly from cycles 4-14 and the remaining 23 fuel assemblies with TPDs.

The worst case dose rate from the configurations listed above was less than 9.8 mrem/hr from configuration 4. This value was conservatively calculated assuming all fuel assemblies were identical design basis Trojan fuel assemblies with design basis Trojan non-fuel hardware. This dose rate is slightly higher than the design basis dose rates for the Trojan fuel. However, this value is still below the regulatory limit of 10.0 mrem/hr. Therefore, the insertion of a single secondary source assembly into a Trojan MPC is acceptable for transport.

Table 5.4.1

FLUX-TO-DOSE CONVERSION FACTORS
(FROM [5.4.1])

Gamma Energy (MeV)	(rem/hr)/(photon/cm²-s)
0.01	3.96E-06
0.03	5.82E-07
0.05	2.90E-07
0.07	2.58E-07
0.1	2.83E-07
0.15	3.79E-07
0.2	5.01E-07
0.25	6.31E-07
0.3	7.59E-07
0.35	8.78E-07
0.4	9.85E-07
0.45	1.08E-06
0.5	1.17E-06
0.55	1.27E-06
0.6	1.36E-06
0.65	1.44E-06
0.7	1.52E-06
0.8	1.68E-06
1.0	1.98E-06
1.4	2.51E-06
1.8	2.99E-06
2.2	3.42E-06

Table 5.4.1 (continued)

FLUX-TO-DOSE CONVERSION FACTORS
(FROM [5.4.1])

Gamma Energy (MeV)	(rem/hr)/(photon/cm²-s)
2.6	3.82E-06
2.8	4.01E-06
3.25	4.41E-06
3.75	4.83E-06
4.25	5.23E-06
4.75	5.60E-06
5.0	5.80E-06
5.25	6.01E-06
5.75	6.37E-06
6.25	6.74E-06
6.75	7.11E-06
7.5	7.66E-06
9.0	8.77E-06
11.0	1.03E-05
13.0	1.18E-05
15.0	1.33E-05

Table 5.4.1 (continued)

FLUX-TO-DOSE CONVERSION FACTORS
(FROM [5.4.1])

Neutron Energy (MeV)	Quality Factor	(rem/hr)/(n/cm ² -s) [†]
2.5E-8	2.0	3.67E-6
1.0E-7	2.0	3.67E-6
1.0E-6	2.0	4.46E-6
1.0E-5	2.0	4.54E-6
1.0E-4	2.0	4.18E-6
1.0E-3	2.0	3.76E-6
1.0E-2	2.5	3.56E-6
0.1	7.5	2.17E-5
0.5	11.0	9.26E-5
1.0	11.0	1.32E-4
2.5	9.0	1.25E-4
5.0	8.0	1.56E-4
7.0	7.0	1.47E-4
10.0	6.5	1.47E-4
14.0	7.5	2.08E-4
20.0	8.0	2.27E-4

[†] Includes the Quality Factor.

Table 5.4.2

DELETED

Table 5.4.3

DELETED

Table 5.4.4

DELETED

Table 5.4.5

DELETED

Table 5.4.6

DELETED

Table 5.4.7

DELETED

Table 5.4.8

TOTAL DOSE RATES
DOSE LOCATION ON THE SURFACE OF THE HI-STAR 100 SYSTEM FOR NORMAL CONDITIONS
MPC-24 DESIGN BASIS ZIRCALOY CLAD FUEL WITH ZIRCALOY INCORE SPACERS
AT VARYING BURNUPS AND COOLING TIMES

Dose Point [†] Location	24,500 MWD/MTU 6 Year Cooling (mrem/hr)	29,500 MWD/MTU 7 Year Cooling (mrem/hr)	34,500 MWD/MTU 9 Year Cooling (mrem/hr)	39,500 MWD/MTU 11 Year Cooling (mrem/hr)	44,500 MWD/MTU 14 Year Cooling (mrem/hr)
2a	49.81	50.88	46.38	43.02	46.19
3a	95.80	108.16	113.72	124.43	138.47
1	35.33	37.42	36.18	35.89	34.85
2	29.01	28.87	26.11	26.57	28.24
3	27.02	29.30	29.26	29.94	30.19
4	23.73	26.05	26.43	27.40	28.05
5	1.001.04	1.641.70	2.412.51	3.223.36	4.154.33
6	125.44120.60	127.01122.66	114.18111.08	104.20102.27	90.0289.54
10CFR71.47 Limit	1000.00 (2a,3a) 200.00 (1-6)	1000.00 (2a,3a) 200.00 (1-6)	1000.00 (2a,3a) 200.00 (1-6)	1000.00 (2a,3a) 200.00 (1-6)	1000.00 (2a,3a) 200.00 (1-6)

[†] Refer to Figure 5.1.1.

Table 5.4.9

TOTAL DOSE RATES
DOSE LOCATION ON THE SURFACE OF THE HI-STAR 100 SYSTEM FOR NORMAL CONDITIONS
MPC-68 DESIGN BASIS ZIRCALOY CLAD FUEL AT VARYING BURNUPS AND COOLING TIMES

Dose Point [†] Location	10,000 MWD/MTU 5 Year Cooling (mrem/hr)	20,000 MWD/MTU 7 Year Cooling (mrem/hr)	24,500 MWD/MTU 8 Year Cooling (mrem/hr)	29,500 MWD/MTU 9 Year Cooling (mrem/hr)	34,500 MWD/MTU 11 Year Cooling (mrem/hr)	39,500 MWD/MTU 14 Year Cooling (mrem/hr)	44,500 MWD/MTU 19 Year Cooling (mrem/hr)
2a	49.51	52.69	44.53	44.60	50.12	52.65	55.25
3a	139.50	154.42	132.09	129.62	132.20	115.66	103.70
1	34.25	39.29	34.23	35.33	37.96	35.72	33.64
2	25.50	27.53	24.21	27.97	31.12	32.05	33.07
3	34.44	37.75	32.25	31.43	31.69	27.33	22.81
4	32.63	35.76	30.52	29.69	29.91	25.74	21.42
5	0.14	0.60	0.640.71	1.031.16	1.581.78	2.012.28	2.532.86
6	112.26	121.21	103.0699.53	98.9795.87	97.9695.27	82.2680.46	65.7364.92
10CFR71.47 Limit	1000.00 (2a,3a) 200.00 (1-6)	1000.00 (2a,3a) 200.00 (1-6)	1000.00 (2a,3a) 200.00 (1-6)				

[†] Refer to Figure 5.1.1.

Table 5.4.10

TOTAL DOSE RATES
DOSE LOCATION AT TWO METERS FOR NORMAL CONDITIONS
MPC-24 DESIGN BASIS ZIRCALOY CLAD FUEL WITH ZIRCALOY INCORE SPACERS
AT VARYING BURNUPS AND COOLING TIMES

Dose Point [†] Location	24,500 MWD/MTU 6 Year Cooling (mrem/hr)	29,500 MWD/MTU 7 Year Cooling (mrem/hr)	34,500 MWD/MTU 9 Year Cooling (mrem/hr)	39,500 MWD/MTU 11 Year Cooling (mrem/hr)	44,500 MWD/MTU 14 Year Cooling (mrem/hr)
1	7.41	7.61	7.26	7.31	7.27
2	9.57	9.45	8.77	8.95	9.10
3	6.72	6.93	6.61	6.64	6.59
4	6.16	6.39	6.13	6.16	6.11
5	0.090.10	0.150.17	0.210.24	0.280.32	0.350.41
6	8.398.11	8.348.01	7.266.91	6.365.99	5.154.75
10CFR71.47 Limit	10.00	10.00	10.00	10.00	10.00

[†] Refer to Figure 5.1.1.

Table 5.4.11

TOTAL DOSE RATES
DOSE LOCATION AT TWO METERS FOR NORMAL CONDITIONS
MPC-68 DESIGN BASIS ZIRCALOY CLAD FUEL AT VARYING BURNUPS AND COOLING TIMES

Dose Point [†] Location	10,000 MWD/MTU 5 Year Cooling (mrem/hr)	20,000 MWD/MTU 7 Year Cooling (mrem/hr)	24,500 MWD/MTU 8 Year Cooling (mrem/hr)	29,500 MWD/MTU 9 Year Cooling (mrem/hr)	34,500 MWD/MTU 11 Year Cooling (mrem/hr)	39,500 MWD/MTU 14 Year Cooling (mrem/hr)	44,500 MWD/MTU 19 Year Cooling (mrem/hr)
1	6.67	7.33	6.58	7.05	7.59	7.34	7.07
2	8.32	8.71	8.03	8.94	9.62	9.55	9.39
3	6.66	7.20	6.31	6.44	6.62	6.02	5.36
4	6.43	6.98	6.09	6.15	6.32	5.70	5.03
5	0.02	0.06	0.070-08	0.100-13	0.150-20	0.190-26	0.240-32
6	6.55	6.85	5.775-67	5.345-25	5.014-94	3.873-84	2.652-65
10CFR71.47 Limit	10.00	10.00	10.00	10.00	10.00	10.00	10.00

[†] Refer to Figure 5.1.1.

Table 5.4.12

TOTAL DOSE RATES
DOSE LOCATION AT ONE METER FOR ACCIDENT CONDITIONS
MPC-24 DESIGN BASIS ZIRCALOY CLAD FUEL WITH ZIRCALOY INCORE SPACERS
AT VARYING BURNUPS AND COOLING TIMES

Dose Point [†] Location	24,500 MWD/MTU 6 Year Cooling (mrem/hr)	29,500 MWD/MTU 7 Year Cooling (mrem/hr)	34,500 MWD/MTU 9 Year Cooling (mrem/hr)	39,500 MWD/MTU 11 Year Cooling (mrem/hr)	44,500 MWD/MTU 14 Year Cooling (mrem/hr)
1	76.55	97.55	117.95	141.21	166.93
2	153.26	224.23	307.31	399.33	504.35
3	49.37	64.41	79.67	96.85	116.00
4	35.97	47.12	58.44	71.10	85.20
5	4.06	6.59	9.62	12.83	16.51
6	685.36	687.08	605.96	539.45	447.78
10CFR71.51 Limit	1000.00	1000.00	1000.00	1000.00	1000.00

[†] Refer to Figure 5.1.2.

Table 5.4.13

TOTAL DOSE RATES
DOSE LOCATION AT ONE METER FOR ACCIDENT CONDITIONS
MPC-68 DESIGN BASIS ZIRCALOY CLAD FUEL AT VARYING BURNUPS AND COOLING TIMES

Dose Point[†] Location	10,000 MWD/MTU 5 Year Cooling (mrem/hr)	20,000 MWD/MTU 7 Year Cooling (mrem/hr)	24,500 MWD/MTU 8 Year Cooling (mrem/hr)	29,500 MWD/MTU 9 Year Cooling (mrem/hr)	34,500 MWD/MTU 11 Year Cooling (mrem/hr)	39,500 MWD/MTU 14 Year Cooling (mrem/hr)	44,500 MWD/MTU 19 Year Cooling (mrem/hr)
1	51.38	86.18	82.43	108.56	145.23	169.25	198.52
2	62.71	172.74	179.75	275.87	403.87	504.00	622.86
3	31.39	49.39	46.51	59.30	77.64	88.84	102.65
4	26.31	39.33	36.57	45.32	58.13	65.34	74.36
5	0.66	2.70	2.84	4.55	6.92	8.80	11.04
6	629.12	668.09	564.75	530.59	509.65	408.69	300.71
10CFR71.51 Limit	1000.00	1000.00	1000.00	1000.00	1000.00	1000.00	1000.00

[†] Refer to Figure 5.1.2.

Table 5.4.14

PEAK-TO-AVERAGE RATIOS FOR THE DOSE COMPONENTS
AT VARIOUS LOCATIONS

Location	Fuel Gammas	Gammas from Neutrons	⁶⁰ Co Gammas	Neutron
MPC-24				
Surface				
Pocket Trunnion	0.081	0.262	0.075	6.695
2a	0.713	0.955	0.407	2.362
3a	1.317	1.011	1.005	1.177
2 meter				
Pocket Trunnion	1.109	1.232	1.059	0.809
2	1.034	0.974	1.086	0.990
MPC-68				
Surface				
Pocket Trunnion	0.070	0.432	0.074	7.340
2a	0.737	0.977	1.123	2.284
3a	0.908	0.816	1.217	0.940
2 meter				
Pocket Trunnion	1.121	0.982	1.144	1.171
2	1.070	0.939	1.146	0.950

Table 5.4.15

DOSE RATES FOR NORMAL CONDITIONS SHOWING THE
EFFECT OF PEAKING

Dose Point [†] Location	Fuel Gammas (mrem/hr)	Gammas from Neutrons (mrem/hr)	⁶⁰ Co Gammas (mrem/hr)	Neutrons (mrem/hr)	Total (mrem/hr)
MPC-24					
Surface 44,500 MWD/MTU 14-Year Cooling					
Pocket Trunnion	0.15	0.37	1.98	97.92	100.42
2a	12.30	6.35	0.00	52.60	71.26
3a	0.40	0.67	28.67	128.27	158.01
2 meter 24,500 MWD/MTU 6-Year Cooling					
Pocket Trunnion	4.03	0.17	3.50	0.64	8.34
2	7.55	0.21	1.26	0.87	9.90
MPC-68					
Surface 34,500 MWD/MTU 11-Year Cooling					
Pocket Trunnion	0.25	0.45	1.97	77.42	80.09
2a	19.24	5.35	0.02	42.33	66.93
3a	0.33	0.12	115.34	34.69	150.49
2 meter 34,500 MWD/MTU 11-Year Cooling					
Pocket Trunnion	3.23	0.46	2.06	3.03	8.77
2	5.80	0.68	0.74	2.69	9.91

[†] Refer to Figure 5.1.1.

Table 5.4.16

DELETED

Table 5.4.17

DELETED

Table 5.4.18

DELETED

Table 5.4.19

TOTAL DOSE RATES
DOSE LOCATION ON THE SURFACE OF THE HI-STAR 100 SYSTEM FOR NORMAL CONDITIONS
MPC-24 DESIGN BASIS ZIRCALOY CLAD FUEL WITH NON-ZIRCALOY INCORE SPACERS
AT VARYING BURNUPS AND COOLING TIMES

Dose Point [†] Location	24,500 MWD/MTU 9 Year Cooling (mrem/hr)	29,500 MWD/MTU 11 Year Cooling (mrem/hr)	34,500 MWD/MTU 13 Year Cooling (mrem/hr)	39,500 MWD/MTU 15 Year Cooling (mrem/hr)	44,500 MWD/MTU 18 Year Cooling (mrem/hr)
2a	42.91	42.11	43.11	45.08	46.24
3a	69.70	74.06	83.00	96.79	111.87
1	25.77	25.19	25.54	26.31	26.75
2	26.97	26.54	27.34	28.35	28.62
3	19.70	19.86	20.87	22.23	23.47
4	17.23	17.64	18.84	20.37	21.85
5	0.890.92	1.401.46	2.072.16	2.772.89	3.583.73
6	87.6084.38	80.0377.61	74.3572.77	69.9769.20	63.3563.58
10CFR71.47 Limit	1000.00 (2a,3a) 200.00 (1-6)	1000.00 (2a,3a) 200.00 (1-6)	1000.00 (2a,3a) 200.00 (1-6)	1000.00 (2a,3a) 200.00 (1-6)	1000.00 (2a,3a) 200.00 (1-6)

[†] Refer to Figure 5.1.1.

Table 5.4.20

TOTAL DOSE RATES
DOSE LOCATION AT TWO METERS FOR NORMAL CONDITIONS
MPC-24 DESIGN BASIS ZIRCALOY CLAD FUEL WITH NON-ZIRCALOY INCORE SPACERS
AT VARYING BURNUPS AND COOLING TIMES

Dose Point [†] Location	24,500 MWD/MTU 9 Year Cooling (mrem/hr)	29,500 MWD/MTU 11 Year Cooling (mrem/hr)	34,500 MWD/MTU 13 Year Cooling (mrem/hr)	39,500 MWD/MTU 15 Year Cooling (mrem/hr)	44,500 MWD/MTU 18 Year Cooling (mrem/hr)
1	6.42	6.24	6.29	6.42	6.40
2	9.51	9.16	9.18	9.27	9.09
3	5.68	5.52	5.58	5.70	5.71
4	5.08	4.96	5.03	5.16	5.19
5	0.080-09	0.120-14	0.180-21	0.240-28	0.300-35
6	5.845-67	5.195-00	4.624-40	4.133-88	3.473-17
10CFR71.47 Limit	10.00	10.00	10.00	10.00	10.00

[†] Refer to Figure 5.1.1.

Table 5.4.21

TOTAL DOSE RATES
DOSE LOCATION AT ONE METER FOR ACCIDENT CONDITIONS
MPC-24 DESIGN BASIS ZIRCALOY CLAD FUEL WITH NON-ZIRCALOY INCORE SPACERS
AT VARYING BURNUPS AND COOLING TIMES

Dose Point[†] Location	24,500 MWD/MTU 9 Year Cooling (mrem/hr)	29,500 MWD/MTU 11 Year Cooling (mrem/hr)	34,500 MWD/MTU 13 Year Cooling (mrem/hr)	39,500 MWD/MTU 15 Year Cooling (mrem/hr)	44,500 MWD/MTU 18 Year Cooling (mrem/hr)
1	62.33	76.36	95.99	117.23	140.85
2	145.00	201.06	275.44	354.15	442.83
3	40.70	51.15	65.54	81.04	98.36
4	29.39	37.13	47.76	59.20	72.01
5	3.59	5.63	8.26	11.03	14.21
6	478.28	429.22	388.56	354.69	306.90
10CFR71.51 Limit	1000.00	1000.00	1000.00	1000.00	1000.00

[†] Refer to Figure 5.1.2.

Table 5.4.22

DOSE RATES FOR
MPC-68 DESIGN BASIS STAINLESS STEEL CLAD FUEL
22,500 MWD/MTU AND 16-YEAR COOLING

Dose Point [†] Location	Fuel Gammas ^{††} (mrem/hr)	⁶⁰ Co Gammas (mrem/hr)	Neutrons (mrem/hr)	Totals (mrem/hr)
Dose Location at Surface for Normal Condition				
1	2.91	9.19	1.00	13.09
2a	39.68	0.00	1.20	40.88
3a	0.62	40.84	2.60	44.07
4	0.45	9.49	0.53	10.47
5	0.020-01	0.010-01	0.100-11	0.120-14
6	2.372-35	32.433-19	1.371-40	36.183-93
10CFR71.47 Limit				200.00
Dose Location at Two Meters for Normal Condition				
1	3.45	1.00	0.17	4.63
2	7.71	0.27	0.19	8.18
3	2.26	1.35	0.12	3.73
4	1.67	1.43	0.11	3.21
5	0.00	0.000-00	0.010-01	0.010-02
6	0.20	1.891-82	0.030-03	2.122-05
10CFR71.47 Limit				10.00
Dose Location at One Meter for Accident Condition				
1	9.43	10.90	7.95	28.29
2	46.22	0.23	25.97	72.42
3	3.58	7.41	4.06	15.05
4	2.00	6.60	2.91	11.51
5	0.01	0.07	0.48	0.57
6	11.14	183.23	5.34	199.71
10CFR71.51 Limit				1000.00

Note: The more conservative limit of 200 mrem/hr was applied for dose locations 2a and 3a while dose locations 2 and 3 were not analyzed.

[†] Refer to Figures 5.1.1 and 5.1.2.

^{††} Gammas generated by neutron capture and gammas from incore spacers are included with fuel gammas.

Table 5.4.23

DOSE RATES FOR
MPC-24 DESIGN BASIS STAINLESS STEEL CLAD FUEL
30,000 MWD/MTU AND 19-YEAR COOLING

Dose Point [†] Location	Fuel Gammas ^{††} (mrem/hr)	⁶⁰ Co Gammas (mrem/hr)	Neutrons (mrem/hr)	Totals (mrem/hr)
Dose Location at Surface for Normal Condition				
1	2.40	5.54	4.27	12.22
2a	35.54	0.01	4.41	39.96
3a	0.66	11.31	24.60	36.57
4	0.73	3.65	4.11	8.49
5	0.120.11	0.010.01	0.820.86	0.940.98
6	4.364.19	22.1421.13	6.657.14	33.1532.46
10CFR71.47 Limit				200.00
Dose Location at Two Meters for Normal Condition				
1	3.05	0.69	0.76	4.50
2	7.23	0.23	0.83	8.29
3	2.47	0.66	0.72	3.85
4	1.95	0.67	0.69	3.30
5	0.010.01	0.000.00	0.070.08	0.080.09
6	0.300.36	1.531.48	0.250.18	2.082.02
10CFR71.47 Limit				10.00
Dose Location at One Meter for Accident Condition				
1	7.57	6.83	32.78	47.18
2	39.78	0.24	108.52	148.54
3	4.96	3.96	23.27	32.19
4	2.85	3.00	17.13	22.99
5	0.02	0.05	3.69	3.76
6	22.73	123.24	28.03	174.00
10CFR71.51 Limit				1000.00

Note: The more conservative limit of 200 mrem/hr was applied for dose locations 2a and 3a while dose locations 2 and 3 were not analyzed.

[†] Refer to Figures 5.1.1 and 5.1.2.

^{††} Gammas generated by neutron capture and gammas from incore spacers are included with fuel gammas.

Table 5.4.24

DOSE RATES FOR
MPC-24 DESIGN BASIS STAINLESS STEEL CLAD FUEL
40,000 MWD/MTU AND 24-YEAR COOLING

Dose Point [†] Location	Fuel Gammas ^{††} (mrem/hr)	⁶⁰ Co Gammas (mrem/hr)	Neutrons (mrem/hr)	Totals (mrem/hr)
Dose Location at Surface for Normal Condition				
1	2.12	5.80	11.10	19.02
2a	28.04	0.00	13.06	41.10
3a	0.78	11.82	63.88	76.48
4	0.66	3.82	10.68	15.16
5	0.300.29	0.010.01	2.132.24	2.432.53
6	4.444.28	23.1522.10	17.2518.54	44.8444.92
10CFR71.47 Limit				200.00
Dose Location at Two Meters for Normal Condition				
1	2.55	0.72	1.98	5.26
2	5.82	0.24	2.23	8.29
3	2.06	0.69	1.86	4.62
4	1.64	0.70	1.78	4.11
5	0.020.02	0.000.00	0.190.22	0.210.24
6	0.250.29	1.601.55	0.650.47	2.492.31
10CFR71.47 Limit				10.00
Dose Location at One Meter for Accident Condition				
1	5.88	7.14	85.12	98.14
2	30.69	0.25	281.83	312.76
3	3.85	4.14	60.42	68.41
4	2.24	3.14	44.48	49.86
5	0.04	0.05	9.57	9.66
6	17.44	128.89	72.74	219.07
10CFR71.51 Limit				1000.00

Note: The more conservative limit of 200 mrem/hr was applied for dose locations 2a and 3a while dose locations 2 and 3 were not analyzed.

[†] Refer to Figures 5.1.1 and 5.1.2.

^{††} Gammas generated by neutron capture and gammas from incore spacers are included with fuel gammas.

Table 5.4.25

COMPARISON OF NEUTRON SOURCE PER INCH PER SECOND FOR
DESIGN BASIS 7X7 FUEL AND DESIGN BASIS DRESDEN UNIT 1 FUEL

Assembly	Active fuel length (inch)	Neutrons per sec per inch	Neutrons per sec per inch with Sb-Be source	Reference for neutrons per sec per inch
7x7 design basis	144	6.63E+5	N/A	Table 5.2.13 39.5 GWD/MTU and 14 year cooling
6x6 design basis	110	2.85E+5 3.81E+5	3.45E+5 4.41E+5	Table 5.2.14
6x6 design basis MOX	110	3.67E+5	4.27E+5	Table 5.2.17

Table 5.4.26

DOSE RATES AT THE SURFACE OF THE HI-STAR 100 SYSTEM FOR NORMAL CONDITIONS
MPC-24 WITH TROJAN ZIRCALOY CLAD FUEL WITH NON-ZIRCALOY INCORE SPACERS
42,000 MWD/MTU AND 16-YEAR COOLING

Dose Point [†] Location	Fuel Gammas ^{††} (mrem/hr)	Gammas from Incore Spacers (mrem/hr)	⁶⁰ Co Gammas (mrem/hr)	Neutrons (mrem/hr)	Totals (mrem/hr)	10 CFR 71.47 Limit
2a	3.72	2.48	38.39	2.25	46.84	1000
3a	0.39	0.07	14.34	49.81	64.61	1000
1	1.62	1.09	4.54	14.43	21.68	200
2	10.94	7.72	0.05	9.69	28.40	200
3	0.62	0.32	10.66	8.00	19.60	200
4	0.36	0.16	5.01	7.80	13.34	200
5	0.340.36 ^{†††}	-	0.060.08	3.172.88	3.583.32	200
6	6.997.35 ^{†††}	-	21.4522.44	23.2621.29	51.7051.08	200

[†] Refer to Figure 5.1.1.

^{††} Gammas generated by neutron capture are included with fuel gammas.

^{†††} Gammas from incore spacers are included with fuel gammas.

Table 5.4.27

DOSE RATES AT TWO METERS FROM THE HI-STAR 100 SYSTEM FOR NORMAL CONDITIONS
MPC-24 WITH TROJAN ZIRCALOY CLAD FUEL WITH NON-ZIRCALOY INCORE SPACERS
42,000 MWD/MTU AND 16-YEAR COOLING

Dose Point [†] Location	Fuel Gammas ^{††} (mrem/hr)	Gammas from Incore Spacers (mrem/hr)	⁶⁰ Co Gammas (mrem/hr)	Neutrons (mrem/hr)	Totals (mrem/hr)
1	1.52	1.11	0.55	2.52	5.69
2	3.41	2.53	0.64	2.67	9.24
3	1.20	0.82	2.31	1.71	6.05
4	0.97	0.62	2.13	1.50	5.21
5	0.02 ^{†††}	-	0.050.07	0.270.22	0.340.31
6	0.560.62 ^{†††}	-	2.052.25	0.870.80	3.493.68
10CFR71.47 Limit					10.00

[†] Refer to Figure 5.1.1.

^{††} Gammas generated by neutron capture are included with fuel gammas.

^{†††} Gammas from incore spacers are included with fuel gammas.

Table 5.4.28

DOSE RATES AT ONE METER FOR ACCIDENT CONDITIONS
 MPC-24 WITH TROJAN ZIRCALOY CLAD FUEL WITH NON- ZIRCALOY INCORE SPACERS
 42,000 MWD/MTU AND 16-YEAR COOLING

Dose Point [†] Location	Fuel Gammas ^{††} (mrem/hr)	⁶⁰ Co Gammas (mrem/hr)	Neutrons (mrem/hr)	Totals (mrem/hr)
1	7.01	5.69	106.18	118.88
2	31.31	0.30	356.39	387.99
3	3.27	15.94	69.43	88.64
4	1.86	8.65	49.17	59.68
5	0.11	0.25	12.42	12.78
6	34.74	128.20	82.48	245.42
10CFR71.51 Limit				1000.00

[†] Refer to Figure 5.1.2.

^{††} Gammas generated by neutron capture and gammas from incore spacers are included with fuel gammas.

Table 5.4.29

TOTAL DOSE RATES
DOSE LOCATION ON THE SURFACE OF THE HI-STAR 100 SYSTEM FOR NORMAL CONDITIONS
MPC-32 DESIGN BASIS ZIRCALOY CLAD FUEL WITH ZIRCALOY INCORE SPACERS
AT VARYING BURNUPS AND COOLING TIMES

Dose Point [†] Location	24,500 MWD/MTU 8 Year Cooling (mrem/hr)	29,500 MWD/MTU 9 Year Cooling (mrem/hr)	34,500 MWD/MTU 12 Year Cooling (mrem/hr)	39,500 MWD/MTU 14 Year Cooling (mrem/hr)	44,500 MWD/MTU 19 Year Cooling (mrem/hr)
2a	62.31	66.79	58.99	59.34	50.90
3a	162.02	192.08	205.87	245.88	263.95
1	44.46	48.87	45.01	46.94	42.51
2	34.63	38.55	36.17	38.33	35.48
3	40.30	46.47	46.08	50.81	49.68
4	37.52	43.47	43.40	48.09	47.31
5	2.242.40	3.703.97	5.265.66	7.067.60	8.469.11
6	149.23144.35	154.74150.66	128.70126.87	122.42122.14	95.4597.35
10CFR71.47 Limit	1000.00 (2a,3a) 200.00 (1-6)	1000.00 (2a,3a) 200.00 (1-6)	1000.00 (2a,3a) 200.00 (1-6)	1000.00 (2a,3a) 200.00 (1-6)	1000.00 (2a,3a) 200.00 (1-6)

[†] Refer to Figure 5.1.1.

Table 5.4.30

TOTAL DOSE RATES
DOSE LOCATION AT TWO METERS FOR NORMAL CONDITIONS
MPC-32 DESIGN BASIS ZIRCALOY CLAD FUEL WITH ZIRCALOY INCORE SPACERS
AT VARYING BURNUPS AND COOLING TIMES

Dose Point [†] Location	24,500 MWD/MTU 8 Year Cooling (mrem/hr)	29,500 MWD/MTU 9 Year Cooling (mrem/hr)	34,500 MWD/MTU 12 Year Cooling (mrem/hr)	39,500 MWD/MTU 14 Year Cooling (mrem/hr)	44,500 MWD/MTU 19 Year Cooling (mrem/hr)
1	7.85	8.67	8.01	8.43	7.69
2	8.22	9.28	8.86	9.65	9.19
3	7.83	8.83	8.44	9.10	8.59
4	7.50	8.48	8.14	8.79	8.34
5	0.180.22	0.290.37	0.410.52	0.550.70	0.660.83
6	8.227.98	8.218.02	6.376.27	5.665.60	3.833.82
10CFR71.47 Limit	10.00	10.00	10.00	10.00	10.00

[†] Refer to Figure 5.1.1.

Table 5.4.31

TOTAL DOSE RATES
DOSE LOCATION AT ONE METER FOR ACCIDENT CONDITIONS
MPC-32 DESIGN BASIS ZIRCALOY CLAD FUEL WITH ZIRCALOY INCORE SPACERS
AT VARYING BURNUPS AND COOLING TIMES

Dose Point [†] Location	24,500 MWD/MTU 8 Year Cooling (mrem/hr)	29,500 MWD/MTU 9 Year Cooling (mrem/hr)	34,500 MWD/MTU 12 Year Cooling (mrem/hr)	39,500 MWD/MTU 14 Year Cooling (mrem/hr)	44,500 MWD/MTU 19 Year Cooling (mrem/hr)
1	91.38	117.99	134.85	162.88	176.78
2	150.55	230.95	310.10	406.55	477.18
3	66.27	89.91	108.35	134.66	150.49
4	49.53	66.55	79.40	98.17	109.14
5	9.17	15.09	21.41	28.69	34.38
6	802.16	817.16	656.05	601.72	437.06
10CFR71.51 Limit	1000.00	1000.00	1000.00	1000.00	1000.00

[†] Refer to Figure 5.1.2.

Table 5.4.32

TOTAL DOSE RATES
DOSE LOCATION ON THE SURFACE OF THE HI-STAR 100 SYSTEM FOR NORMAL CONDITIONS
MPC-32 DESIGN BASIS ZIRCALOY CLAD FUEL WITH NON-ZIRCALOY INCORE SPACERS
AT VARYING BURNUPS AND COOLING TIMES

Dose Point [†] Location	24,500 MWD/MTU 12 Year Cooling (mrem/hr)	29,500 MWD/MTU 14 Year Cooling (mrem/hr)	34,500 MWD/MTU 16 Year Cooling (mrem/hr)	39,500 MWD/MTU 19 Year Cooling (mrem/hr)	42,500 MWD/MTU 20 Year Cooling (mrem/hr)
2a	40.66	40.41	42.78	42.27	44.54
3a	110.58	127.81	162.16	189.57	213.21
1	29.82	30.69	32.88	33.09	35.33
2	24.88	25.46	27.44	27.93	29.93
3	27.57	30.30	34.70	37.26	40.74
4	25.39	28.15	32.50	35.17	38.57
5	1.932.07	3.073.30	4.544.88	5.876.32	6.797.32
6	94.2691.55	89.2087.51	86.6786.14	78.0478.83	79.6481.03
10CFR71.47 Limit	1000.00 (2a,3a) 200.00 (1-6)				

[†] Refer to Figure 5.1.1.

Table 5.4.33

TOTAL DOSE RATES
DOSE LOCATION AT TWO METERS FOR NORMAL CONDITIONS
MPC-32 DESIGN BASIS ZIRCALOY CLAD FUEL WITH NON-ZIRCALOY INCORE SPACERS
AT VARYING BURNUPS AND COOLING TIMES

Dose Point [†] Location	24,500 MWD/MTU 12 Year Cooling (mrem/hr)	29,500 MWD/MTU 14 Year Cooling (mrem/hr)	34,500 MWD/MTU 16 Year Cooling (mrem/hr)	39,500 MWD/MTU 19 Year Cooling (mrem/hr)	42,500 MWD/MTU 20 Year Cooling (mrem/hr)
1	6.55	6.64	6.95	6.78	7.13
2	8.99	9.14	9.54	9.21	9.61
3	6.38	6.65	7.17	7.23	7.71
4	5.93	6.21	6.76	6.88	7.36
5	0.150.19	0.240.30	0.350.45	0.460.58	0.530.67
6	5.104.95	4.554.46	4.084.05	3.323.32	3.243.24
10CFR71.47 Limit	10.00	10.00	10.00	10.00	10.00

[†] Refer to Figure 5.1.1.

Table 5.4.34

TOTAL DOSE RATES
DOSE LOCATION AT ONE METER FOR ACCIDENT CONDITIONS
MPC-32 DESIGN BASIS ZIRCALOY CLAD FUEL WITH NON-ZIRCALOY INCORE SPACERS
AT VARYING BURNUPS AND COOLING TIMES

Dose Point[†] Location	24,500 MWD/MTU 12 Year Cooling (mrem/hr)	29,500 MWD/MTU 14 Year Cooling (mrem/hr)	34,500 MWD/MTU 16 Year Cooling (mrem/hr)	39,500 MWD/MTU 19 Year Cooling (mrem/hr)	42,500 MWD/MTU 20 Year Cooling (mrem/hr)
1	69.80	86.91	110.36	128.98	144.97
2	143.48	202.73	279.80	346.19	395.59
3	52.15	68.42	90.21	108.35	122.82
4	38.31	49.93	65.54	78.49	88.90
5	7.89	12.51	18.46	23.84	27.60
6	500.54	460.23	430.39	368.33	367.17
10CFR71.51 Limit	1000.00	1000.00	1000.00	1000.00	1000.00

[†] Refer to Figure 5.1.2.

5.5 REGULATORY COMPLIANCE

The analysis presented in this chapter has shown that the external radiation levels will not increase during normal conditions of transport consistent with the tests specified in 10CFR71.71. This chapter also confirms that the external dose rates from HI-STAR 100 System, when fully loaded with fuel assemblies that meet the acceptance criteria specified in Chapter 1, are less than the regulatory limits specified in 10CFR71.47.

This chapter also demonstrates that the maximum external radiation level at one meter from the external surface of the package does not exceed 1 Rem/hr (10 mSv/hr) during the hypothetical accident conditions consistent with the tests specified in 10CFR71.73.

Tables 5.5.1 through 5.5.3 summarize the maximum dose rates, including the effect of radiation peaking as discussed in Subsection 5.4.1, and demonstrate the HI-STAR 100 System's compliance with the regulatory requirements of 10CFR71.47 and 10CFR71.51. Since these dose rates include the effect of peaking, they may not be equivalent to values reported earlier in this chapter which were surface average dose rates. In these tables "Side" refers to the dose point location that has the maximum dose rate from locations 1-4 (including the pocket trunnion) on Figures 5.1.1 and 5.1.2; "Top" and "Bottom" refer to locations 5 and 6, respectively, on Figures 5.1.1 and 5.1.2. Dose location 2a and 3a from Figure 5.1.1 are not used in Tables 5.5.1 through 5.5.3. Since the maximum dose rate at each location is provided, the corresponding burnup and cooling time may be different between locations and therefore is not listed in the tables. Some of the dose rates in these tables are very close to the regulatory limit. These high dose rates are acceptable because the analysis has been demonstrated to be conservative. In addition, it is extremely unlikely that the casks would be loaded with all fuel assemblies containing the same identical burnup and cooling time analyzed. Finally, the ultimate demonstration of compliance with the 10 CFR 71 regulations will be the measurements that are taken before shipment of the fuel.

Table 5.5.1
 MAXIMUM EXTERNAL DOSE RATES FOR THE
 HI-STAR 100 SYSTEM CONTAINING THE MPC-24

Normal Conditions of Transport			
	External Surface of Package		
Radiation (mrem/hr)	Top	Side	Bottom
Gamma [†]	0.524	1.35	110.43/115.63
Neutron	3.6382	78.65	12.23/11.38
Total	4.1533	80.00	122.66/127.01
10 CFR 71.47(b)(1) Limit	200	200	200
	2 Meters from Vehicle Outer Surface^{††}		
Radiation (mrem/hr)	Top	Side	Bottom
Gamma [†]	0.034	9.04	7.92/8.13
Neutron	0.37/0.32	0.87	0.19/0.26
Total	0.41/0.35	9.91	8.11/8.39
10 CFR 71.47(b)(3) Limit	10	10	10
Hypothetical Accident Conditions			
	1 Meter from Surface of Package^{†††}		
Radiation (mrem/hr)	Top	Side	Bottom
Gamma [†]	0.18	23.43	639.09
Neutron	16.33	480.92	47.99
Total	16.51	504.35	687.08
10 CFR 71.51(a)(2) Limit	1000	1000	1000

[†] This includes fuel gammas, gammas from hardware activation including incore spacers, and gammas generated by neutron capture.

^{††} The vehicle outer surface is the outer radial surface of the impact limiters, the end of the top impact limiter, and 9 feet from the end of the bottom impact limiter.

^{†††} The impact limiters are not present.

Table 5.5.2

MAXIMUM EXTERNAL DOSE RATES FOR THE
HI-STAR 100 SYSTEM CONTAINING THE MPC-32

Normal Conditions of Transport			
	External Surface of Package		
Radiation (mrem/hr)	Top	Side	Bottom
Gamma [†]	0.900.95	1.19	129.27135.06
Neutron	8.217.52	112.38	21.3919.68
Total	9.118.46	113.57	150.66154.74
10 CFR 71.47(b)(1) Limit	200	200	200
	2 Meters from Vehicle Outer Surface^{††}		
Radiation (mrem/hr)	Top	Side	Bottom
Gamma [†]	0.060.08	5.89	7.527.98
Neutron	0.770.58	4.09	0.590.23
Total	0.830.66	9.98	8.028.22
10 CFR 71.47(b)(3) Limit	10	10	10
Hypothetical Accident Conditions			
	1 Meter from Surface of Package^{†††}		
Radiation (mrem/hr)	Top	Side	Bottom
Gamma [†]	0.22	21.45	739.52
Neutron	34.16	455.73	77.64
Total	34.38	477.18	817.16
10 CFR 71.51(a)(2) Limit	1000	1000	1000

[†] This includes fuel gammas, gammas from hardware activation including incore spacers, and gammas generated by neutron capture.

^{††} The vehicle outer surface is the outer radial surface of the impact limiters, the end of the top impact limiter, and 9 feet from the end of the bottom impact limiter.

^{†††} The impact limiters are not present.

Table 5.5.3
 MAXIMUM EXTERNAL DOSE RATES FOR THE
 HI-STAR 100 SYSTEM CONTAINING THE MPC-68

Normal Conditions of Transport			
	External Surface of Package		
Radiation (mrem/hr)	Top	Side	Bottom
Gamma [†]	0.330.34	1.15	91.87114.21
Neutron	2.532.19	99.04	7.667.00
Total	2.862.53	100.19	99.53121.21
10 CFR 71.47(b)(1) Limit	200	200	200
2 Meters from Vehicle Outer Surface ^{††}			
Radiation (mrem/hr)	Top	Side	Bottom
Gamma [†]	0.03	5.92	5.486.69
Neutron	0.290.21	4.05	0.190.16
Total	0.320.24	9.97	5.676.85
10 CFR 71.47(b)(3) Limit	10	10	10
Hypothetical Accident Conditions			
	1 Meter from Surface of Package ^{†††}		
Radiation (mrem/hr)	Top	Side	Bottom
Gamma [†]	0.11	22.15	535.29640.72
Neutron	10.93	600.71	29.4627.37
Total	11.04	622.86	564.75668.09
10 CFR 71.51(a)(2) Limit	1000	1000	1000

[†] This includes fuel gammas, gammas from hardware activation including incore spacers, and gammas generated by neutron capture.

^{††} The vehicle outer surface is the outer radial surface of the impact limiters, the end of the top impact limiter, and 9 feet from the end of the bottom impact limiter.

^{†††} The impact limiters are not present.

SUPPLEMENT 5.I

SHIELDING EVALUATION OF THE MPC-HB

5.I.0 INTRODUCTION

This supplement is focused on providing a shielding evaluation of the HI-STAR 100 System with the MPC-HB. The evaluation presented herein supplements those evaluations of the HI-STAR System contained in the main body of Chapter 5 of this SAR and information in the main body of Chapter 5 that remains applicable to the HI-STAR 100 System with the MPC-HB is not repeated in this supplement. To aid the reader, the sections in this supplement are numbered in the same fashion as the corresponding sections in the main body of this chapter, i.e., Sections 5.I.1 through 5.I.5 correspond to Sections 5.1 through 5.5. Tables and figures in this supplement are labeled sequentially.

5.I.1 DISCUSSION AND RESULTS

The MPC-HB is designed to accommodate 80 Humboldt Bay fuel assemblies. The maximum burnup of these assemblies is 23,000 MWD/MTU with a minimum cooling time of 29 years. The minimum enrichment is 2.09 wt% ²³⁵U. Since the burnup of these assemblies is very low and the cooling time is long, an explicit evaluation of the dose rate outside a HI-STAR 100 overpack is not performed. Rather, the neutron and gamma source and assembly hardware activation inside an MPC-HB is compared to the ~~neutron and gamma source~~ corresponding values from an MPC-68 with design basis fuel to demonstrate that the MPC-HB is bounded by the analysis of the MPC-68. This comparison is performed in Section 5.I.4.

5.I.2 SOURCE SPECIFICATION

The neutron and gamma source term for the Humboldt Bay fuel assemblies were calculated using the same techniques described in Section 5.2. Table 5.I.1 provides the fuel characteristics for the Humboldt Bay fuel assemblies as analyzed in this supplement. These fuel characteristics are the same as those used in reference [5.I.1], except for an additional amount of 1.5 kg of stainless steel cladding that has been added for the DFCs. This is to allow for loading of stainless steel clad fuel rod fragments, should this be necessary. The value of 1.5 kg is a conservative upper bound value of the expected amount, based on the expected total amount of fuel fragments to be loaded, and the assumption that all those fragments have stainless steel clad.

Table 5.I.2 and 5.I.3 provide the neutron and gamma source term for Humboldt Bay fuel. Table 5.I.4 shows the fuel hardware activation. The activity of the stainless steel cladding fragments is directly derived from the activity of the lower tie plate by adjustment for the difference in steel weight (5.73 vs 1.5) and the flux factor (0.2 vs 1). Note that the source for the stainless steel clad is for the entire amount of steel, while all other values are per assembly. Note that the stainless steel clad source is smaller than the total source from steel from a single assembly, and therefore negligible compared to the total source from steel activation in an entire MPC with 80 assemblies.

5.1.3 MODEL SPECIFICATIONS

Generally, the same as in Section 5.3. However, the HOLTITE thickness in the HI-STAR HB is only 4.0 inches, compared to 4.3 inches in the HI-STAR 100. A study shows that this could result in an increase in neutron dose rates of up to 30%. This increase is considered in the source term comparison in Section 5.1.4 below. The MPC-HB is manufactured with Metamic neutron absorbing materials, while the MPCs discussed in the main part of this chapter are manufactured with Boral neutron absorber material. Both materials are made of aluminum and B₄C powder. The Boral contains an aluminum and B₄C powder mixture sandwiched between two aluminum plates while the Metamic is a single plate of aluminum and B₄C. The materials are therefore essentially equivalent and there is no distinction between the two materials from a shielding perspective.

5.1.4 SHIELDING EVALUATION

5.1.4.1 Normal Condition

The acceptability of transporting the MPC-HB was determined by comparing the source terms for the MPC-HB to the source terms for an MPC-68 containing BWR fuel with a burnup and cooling time of 24,500 MWD/MTU and 8 years. The neutron and gamma source terms for this burnup and cooling time can be found in Tables 5.2.5 and 5.2.13 in the main portion of this chapter, respectively. The source term in each energy group was multiplied by the number of assemblies in the basket (68 or 80) and then divided by the active fuel length (144 inches for the MPC-68 and 77.5 inches for the MPC-HB) to determine the source strength per unit length. For neutrons, the total number of assemblies in the basket (68 or 80) is used for the comparison. For gammas, where the dose rates are dominated by the contributions of the assemblies on the periphery of the basket, the number of assemblies in the outer rows of the basket is used. These are 36 for the MPC-68, and 48 for the MPC-HB. Additionally, for neutrons in the HI-STAR HB, an increase of 30% (factor of 1.3) is applied as discussed in 5.1.3. In all neutron and gamma energy group cases, the design basis source term for the MPC-68 bounds the source term for the MPC-HB, and in most cases by a substantial margin. Therefore, the dose rates from a HI-STAR containing the MPC-HB will be bounded by the dose rates from a HI-STAR containing the MPC-68 under normal conditions.

5.1.4.2 Accident Condition

The accident condition was evaluated in the same manner as the normal condition. However, similar to the analysis in Section 5.4.2, it was assumed that the fuel assemblies that are not intact in the damaged fuel containers are compacted by 50%. The effect of this compaction is discussed below for damaged and undamaged assemblies.

- For damaged fuel in DFCs, it is assumed that ~~With~~ 50% of the volume in the DFC cross-section is filled with fuel rods and cladding. Given, the amount of fuel and cladding in a

HB assembly, this corresponds ~~amounts~~ to an active fuel height of 55 inches inside the DFC, i.e. an increase in the source per unit of active length by a factor of $77.5/55 \doteq 1.41$.

- For the undamaged assemblies, fuel relocation would be limited by the intact peripheral rods, so the compaction, if any, would also be limited. For a 6x6 assembly it is reasonable to assume that the 4x4 rods inside of the periphery could at most be replaced by a 5x5 rod array, resulting in a maximum number of rods in a cross section of $6x6 - 4x4 + 5x5 = 45$ rods. This represents an increase by factor 1.25 compared to the intact assembly. Correspondingly, for a 7x7 assembly the maximum number would be $7x7 - 5x5 + 6x6 = 60$, or an increase by factor 1.22.*

As a bounding approach, an increase in source term per unit of active length of 1.41, corresponding to an active length reduced to 55 inch, was assumed for all assemblies in the basket, i.e. for both damaged and undamaged assemblies. The source term for the MPC-68, assuming an active height of 144 inches, was then compared, on a per inch basis, to the source term from the MPC-HB for an active height of 55 inches. In all neutron and gamma energy groups, the design basis source term for the MPC-68 bounds the source term for the MPC-HB, in most cases by a substantial margin. Therefore, the dose rates from a HI-STAR containing the MPC-HB will be bounded by the dose rates from a HI-STAR containing the MPC-68 during the design basis accident for all assembly conditions.

5.1.5 REGULATORY COMPLIANCE

In summary it can be concluded that dose rates from the HI-STAR 100 System with the MPC-HB are bounded by the dose rates for the MPCs analyzed in the main body of the report. The shielding system of the HI-STAR 100 System is therefore in compliance with 10CFR71.

5.1.6 REFERENCES

- [5.1.1] "Humboldt Bay Independent Spent Fuel Storage Installation Safety Analysis Report", Pacific Gas and Electric Company, Docket No. 72-27.*

Table 5.I.1

DESCRIPTION OF HUMBOLDT BAY FUEL

Description	Value
<i>Fuel type</i>	6x6
<i>Active fuel length (in.)</i>	77.5
<i>No. of fuel rods</i>	36
<i>Rod pitch (in.)</i>	0.740
<i>Cladding material</i>	Zircaloy-2
<i>Rod diameter (in.)</i>	0.563
<i>Cladding thickness (in.)</i>	0.032
<i>Pellet diameter (in.)</i>	0.488
<i>Pellet material</i>	UO ₂
<i>Pellet density (gm/cc)</i>	10.412 (945% of theoretical)
<i>Enrichment (w/o ²³⁵U)</i>	2.09
<i>Burnup (MWD/MTU)</i>	23,000
<i>Cooling Time (years)</i>	29
<i>Specific power (MW/MTU)</i>	17.836
<i>Lower tie plate mass (kg)</i>	5.73 Steel
<i>Grid spacer mass (kg)</i>	0.16 Inconel 0.84 Steel
<i>Plenum springs mass (kg)</i>	0.027 Inconel
<i>Compression / expansion springs mass (kg)</i>	0.11 Inconel
<i>Upper tie plate mass (kg)</i>	1.55 Steel
<i>Stainless Steel Cladding on Fuel Fragments in DFC (kg)</i>	1.5

Table 5.I.2

*CALCULATED NEUTRON SOURCE PER ASSEMBLY
FOR HUMBOLDT BAY FUEL*

<i>Lower Energy (MeV)</i>	<i>Upper Energy (MeV)</i>	<i>23,000 MWD/MTU 29-Year Cooling (Neutrons/sec)</i>
<i>1.0E-01</i>	<i>4.0E-01</i>	<i>1.27E+05</i>
<i>4.0E-01</i>	<i>9.0E-01</i>	<i>6.48E+05</i>
<i>9.0E-01</i>	<i>1.4</i>	<i>6.06E+05</i>
<i>1.4</i>	<i>1.85</i>	<i>4.66E+05</i>
<i>1.85</i>	<i>3.0</i>	<i>8.85E+05</i>
<i>3.0</i>	<i>6.43</i>	<i>7.41E+05</i>
<i>6.43</i>	<i>20.0</i>	<i>6.17E+04</i>
<i>Total</i>		<i>3.53E+06</i>

Table 5.I.3

CALCULATED FUEL GAMMA SOURCE PER ASSEMBLY
FOR HUMBOLDT BAY FUEL

Lower Energy	Upper Energy	23,000 MWD/MTU 29-Year Cooling	
<i>(MeV)</i>	<i>(MeV)</i>	<i>(MeV/s)</i>	<i>(Photons/s)</i>
0.45	0.7	6.31E+13	1.10E+14
0.7	1.0	7.96E+11	9.37E+11
1.0	1.5	7.47E+11	5.98E+11
1.5	2.0	5.26E+10	3.01E+10
2.0	2.5	5.67E+08	2.52E+08
2.5	3.0	1.94E+07	7.04E+06
<i>Totals</i>		6.47E+13	1.12E+14

Table 5.I.4
Non Fuel Hardware Sources
(23,000 MWD/MTU Burnup)

Location	29-Year Cooling (curies)
<i>Lower Tie Plate</i>	2.218
<i>Active Fuel Zone (grid spacers)</i>	4.107
<i>Plenum Springs</i>	0.065
<i>Compression / Expansion Springs</i>	0.133
<i>Upper Tie Plate</i>	0.400
<i>Stainless Steel Cladding Fragments</i>	1.932.9

CHAPTER 6: CRITICALITY EVALUATION

This chapter documents the criticality evaluation of the HI-STAR 100 System for the packaging and transportation of radioactive materials (spent nuclear fuel) in accordance with 10CFR71. The results of this evaluation demonstrate that, for the designated fuel assembly classes and basket configurations, an infinite number of HI-STAR 100 Systems with variations in internal and external moderation remain subcritical with a margin of subcriticality greater than $0.05\Delta k$. This corresponds to a ~~transport~~ *Criticality Safety Index (CSI)* of zero (0) and demonstrates compliance with 10CFR71 criticality requirements for normal and hypothetical accident conditions of transport.

The criticality design is based on favorable geometry, fixed neutron poisons (~~Boral~~), an administrative limit on the maximum allowable enrichment, and an administrative limit on the minimum average assembly burnup for the MPC-32. Criticality safety of the HI-STAR 100 System does *not* rely on credit for: (1) fuel burnup except for the MPC-32; (2) fuel-related burnable absorbers; or (3) more than 75% of the manufacturer's minimum B-10 content for the ~~Boral~~ *fixed neutron absorber when subject to standard acceptance tests*[†].

In addition to demonstrating that the criticality safety acceptance criteria are satisfied, this chapter describes the HI-STAR 100 System design structures and components important to criticality safety and limiting fuel characteristics in sufficient detail to identify the package accurately and provide a sufficient basis for the evaluation of the package.

Note:

The MPC-32 requires burnup credit. Methodology and results for burnup credit are not yet presented in this chapter, and will be added as Appendix 6.E in a later revision of this SAR. However, general discussions regarding the MPC-32, tables for burnup credit results and references to Appendix 6.E have already been added throughout this chapter.

[†] *For greater credit allowance, fabrication tests capable of verifying the presence and uniformity of the neutron absorber are needed.*

In conformance with the principles established in 10CFR71 [6.1.1], NUREG-1617 [6.1.2], and NUREG-0800 Section 9.1.2 [6.1.3], the results in this chapter demonstrate that the effective multiplication factor (k_{eff}) of the HI-STAR 100 System, including all biases and uncertainties evaluated with a 95% probability at the 95% confidence level, does not exceed 0.95 under all credible normal and hypothetical accident conditions of transport. This criterion provides a large subcritical margin, sufficient to assure the criticality safety of the HI-STAR 100 System when fully loaded with fuel of the highest permissible reactivity. In addition, the results of this evaluation demonstrate that the HI-STAR 100 System is in full compliance with the requirements outlined in the Standard Review Plan for Dry Cask Storage Systems, NUREG-1536.

Criticality safety of the HI-STAR 100 System depends on the following four principal design parameters:

1. The inherent geometry of the fuel basket designs within the MPC (and the flux-trap water gaps in the MPC-24),
2. The incorporation of permanent fixed neutron-absorbing panels (~~Boral~~) in the fuel basket structure, and
3. An administrative limit on the maximum average enrichment for PWR fuel and maximum planar-average enrichment for BWR fuel, and
4. An administrative limit on the minimum average assembly burnup for PWR fuel in the MPC-32.

The HI-STAR 100 System is designed such that the fixed neutron absorber (~~Boral~~) will remain effective for a period greater than 20 years, and there are no credible means to lose it. Therefore, there is no need to provide a surveillance or monitoring program to verify the continued efficacy of the neutron absorber.

Criticality safety of the HI-STAR 100 System does not rely on the use of any of the following credits:

- burnup of fuel, except for the MPC-32
- fuel-related burnable neutron absorbers

- more than 75 percent of the B-10 content for the *Boral* fixed neutron absorber (~~Boral~~).
- *more than 90 percent of the B-10 content for the Metamic fixed neutron absorber, with comprehensive fabrication tests as described in Chapter 8.*

The following ~~interchangeable~~ basket designs are available for use in the HI-STAR 100 System:

- a 24-cell basket (MPC-24), designed for intact PWR fuel assemblies with a specified maximum enrichment.
- a 24-cell basket (MPC-24E/EF), designed for intact and damaged PWR fuel assemblies, and fuel debris (~~MPC-24EF only~~). This is a variation of the MPC-24, with increased ^{10}B content in the ~~Boral-fixed neutron absorber~~ and with four cells capable of accommodating either intact fuel or a damaged fuel container (DFC). The MPC-24E and MPC-24EF is designed for fuel assemblies with a specified maximum enrichment. Although the MPC-24E/EF is designed and analyzed for damaged fuel and fuel debris, it is only certified for intact fuel assemblies.
- a 24-cell basket (MPC-24E/EF Trojan), design for intact and damaged PWR fuel assemblies, and fuel debris (~~MPC-24EF Trojan only~~) from the Trojan Nuclear Plant (TNP). This is a variation of the MPC-24E/EF, with a slightly reduced height, and increased cell sizes for the cells designated for damaged fuel and fuel debris. This increased cell size is required to accommodate the Trojan specific Failed Fuel Cans and DFCs.
- a 32-cell basket (MPC-32), designed for intact PWR fuel assemblies of a specified minimum burnup, and
- a 68-cell basket (MPC-68), designed for both intact and damaged BWR fuel assemblies with a specified maximum planar-average enrichment. Additionally, a variation in the MPC-68, designated MPC-68F, is designed for damaged BWR fuel assemblies and BWR fuel debris with a specified maximum planar-average enrichment.
- *a 80-cell basket (MPC-HB), designed for Humboldt Bay fuel. See Supplement 6.1 for details and evaluations for this basket version.*

Two ~~interchangeable~~ neutron absorber materials are used in these baskets, Boral and Metamic. Metamic is used for the MPC-HB, while Boral is used in all other MPCs. For Boral, 75 percent of the minimum B-10 content is credited in the criticality analysis, while for Metamic, up to 90 percent of the minimum B-10 content ~~is~~ may be credited, based on the neutron absorber tests specified in Chapter 8. However, the B-10 content in Metamic is chosen to be lower than the B-10 content in Boral, and is chosen so that the absolute B-10 content credited in the criticality

~~analysis is the same for the two materials. This makes the two materials identical from a criticality perspective. This is confirmed by comparing results for a selected number of cases that were performed with both materials (see Section 6.4.12). Calculations in this chapter are therefore only performed for the Boral neutron absorber, with results directly applicable to Metamic.~~

During the normal conditions of transport, the HI-STAR 100 System is dry (no moderator), and thus, the reactivity is very low ($k_{\text{eff}} < 0.50$). However, the HI-STAR 100 System for loading and unloading operations, as well as for the hypothetical accident conditions, is flooded, and thus, represents the limiting case in terms of reactivity. The calculational models for these conditions conservatively include: full flooding with ordinary water, corresponding to the highest reactivity, and the worst case (most conservative) combination of manufacturing and fabrication tolerances.

The MPC-24EF contains the same basket as the MPC-24E. More specifically, all dimensions relevant to the criticality analyses are identical between the MPC-24E and MPC-24EF. Therefore, all criticality results obtained for the MPC-24E are valid for the MPC-24EF and no separate analyses for the MPC-24EF are necessary.

Confirmation of the criticality safety of the HI-STAR 100 Systems under flooded conditions, when filled with fuel of the maximum permissible reactivity for which they are designed, was accomplished with the three-dimensional Monte Carlo code MCNP4a [6.1.4]. Independent confirmatory calculations were made with NITAWL-KENO5a from the SCALE-4.3 package. KENO5a [6.1.5] calculations used the 238-group SCALE cross-section library in association with the NITAWL-II program [6.1.6], which adjusts the uranium-238 cross sections to compensate for resonance self-shielding effects. The Dancoff factors required by NITAWL-II were calculated with the CELLDAN code [6.1.13], which includes the SUPERDAN code [6.1.7] as a subroutine. K-factors for one-sided statistical tolerance limits with 95% probability at the 95% confidence level were obtained from the National Bureau of Standards (now NIST) Handbook 91 [6.1.8].

For the burnup credit calculations, CASMO-4, a two-dimensional transport theory code [6.1.10-6.1.12] for fuel assemblies, was used to calculate the isotopic composition of the spent fuel. The criticality evaluations for burnup credit were performed with MCNP4a [6.1.4].

To assess the incremental reactivity effects due to manufacturing tolerances, CASMO and MCNP4a [6.1.4] were used. The CASMO and MCNP4a calculations identify those tolerances that cause a positive reactivity effect, enabling the Monte Carlo code input to define the worst case (most conservative) conditions. CASMO was not used for quantitative criticality evaluations, but only to qualitatively indicate the direction and approximate magnitude of the reactivity effects of the manufacturing tolerances.

Benchmark calculations were made to compare the primary code packages (MCNP4a, CASMO and KENO5a) with experimental data, using experiments selected to encompass, insofar as practical, the design parameters of the HI-STAR 100 System. The most important parameters are (1) the enrichment, (2) the water-gap size (MPC-24) or cell spacing (MPC-32 and MPC-68), (3) the ^{10}B loading of the neutron absorber panels, and (4) the assembly burnup (MPC-32 only). Benchmark calculations are presented in Appendix 6.A and Appendix 6.E.

Applicable codes, standards, and regulations, or pertinent sections thereof, include the following:

- U.S. Code of Federal Regulations, "Packaging and Transportation of Radioactive Materials," Title 10, Part 71.
- NUREG-1617, "Standard Review Plan for Transportation Packages for Spent Nuclear Fuel" USNRC, Washington D.C., March 2000.
- U.S. Code of Federal Regulations, "Prevention of Criticality in Fuel Storage and Handling," Title 10, Part 50, Appendix A, General Design Criterion 62.
- USNRC Standard Review Plan, NUREG-0800, Section 9.1.2, Spent Fuel Storage, Rev. 3, July 1981.
- USNRC Interim Staff Guidance 8 (ISG-8), Revision 2, "Burnup Credit in the Criticality Safety Analyses of PWR Spent Fuel in Transport and Storage Casks".

To assure the true reactivity will always be less than the calculated reactivity, the following conservative assumptions were made:

- The MPCs are assumed to contain the most reactive fuel authorized to be loaded into a specific basket design.
- No credit for fuel burnup is assumed, either in depleting the quantity of fissile nuclides or in producing fission product poisons, except for fuel in the MPC-32.
- The criticality analyses assume 75% of the manufacturer's minimum Boron-10 content for the ~~Boral~~ all neutron absorbers ~~and 90% of the manufacturer's minimum Boron-10 content for the Metamic neutron absorber.~~
- The fuel stack density is assumed to be 96% of theoretical (10.522 g/cm^3) for all criticality analyses. The fuel stack density is approximately equal to 98% of the pellet density. Therefore, while the pellet density of some fuels might be slightly greater than 96% of theoretical, the actual stack density will still be less.

- For fresh fuel, no credit is taken for the ^{234}U and ^{236}U in the fuel.
- When flooded, the moderator is assumed to be water at a temperature corresponding to the highest reactivity within the expected operating range (i.e., water density of 1.000 g/cc).
- Neutron absorption in minor structural members and optional heat conduction elements is neglected, i.e., spacer grids, basket supports, and optional aluminum heat conduction elements are replaced by water.
- The worst hypothetical combination of tolerances (most conservative values within the range of acceptable values), as identified in Section 6.3, is assumed.
- When flooded, the fuel rod pellet-to-clad gap regions are assumed to be flooded.
- Planar-averaged enrichments are assumed for BWR fuel. (Analyses are presented in Appendix 6.B to demonstrate that the use of planar-average enrichments produces conservative results.)
- Fuel-related burnable neutron absorbers, such as the Gadolinia normally used in BWR fuel and IFBA normally used in PWR fuel, are neglected.
- For evaluation of the reactivity bias, all benchmark calculations that result in a k_{eff} greater than 1.0 are conservatively truncated to 1.0000.
- For fuel assemblies that contain low-enriched axial blankets, the governing enrichment is that of the highest planar average, and the blankets are not included in determining the average enrichment.
- Regarding the position of assemblies in the basket, configurations with centered and eccentric positioning of assemblies in the fuel storage locations are considered. For further discussions see Section 6.3.3.
- For intact fuel assemblies, as defined in Chapter 1, missing fuel rods must be replaced with dummy rods that displace a volume of water that is equal to, or larger than, that displaced by the original rods.
- The burnup credit methodology for the MPC-32 contains significant additional conservative assumptions specific to burnup credit, as discussed in Appendix 6.E.

The principal calculational results, which address the following conditions:

- A single package, under the conditions of 10 CFR 71.55(b), (d), and (e);
- An array of undamaged packages, under the conditions of 10 CFR 71.59(a)(1); and
- An array of damaged packages, under the conditions of 10 CFR 71.59(a)(2)

are summarized in Table 6.1.4 for all MPCs and for the most reactive configuration and fuel condition in each MPC. These results demonstrate that the HI-STAR 100 System is in full compliance with 10CFR71 (71.55(b), (d), and (e) and 71.59(a)(1) and (a)(2)). The calculations for package arrays are performed for infinite arrays of HI-STAR 100 Systems under flooded conditions. Therefore, the ~~transportation~~ *Criticality Safety Index (CSI)* ~~based on criticality control~~ is zero (0). It is noted that the results for the internally flooded single package and package arrays are statistically equivalent for each basket. This shows that the physical separation between overpacks and the steel radiation shielding are each adequate to preclude any significant neutronic coupling between casks in an array configuration. In addition, the table shows the result for an unreflected, internally flooded cask for each MPC. This configuration is used in many calculations and studies throughout this chapter, and is shown to yield results that are statistically equivalent to the results for the corresponding reflected package. Further analyses for the various conditions of flooding that support the conclusion that the fully flooded condition corresponds to the highest reactivity, and thus is most limiting, are presented in Section 6.4. These analyses also include cases with various internal and external moderator densities and various cask-to-cask spacings.

Additional results of the design basis criticality safety calculations for single unreflected, internally flooded casks (limiting cases) are listed in Tables 6.1.1 through 6.1.3 and 6.1.5 through 6.1.7, conservatively evaluated for the worst combination of manufacturing tolerances (as identified in Section 6.3), and including the calculational bias, uncertainties, and calculational statistics. For each of the MPC designs and fuel assembly classes[†], Tables 6.1.1 through 6.1.3 and 6.1.5 through 6.1.7 list the bounding maximum k_{eff} value, the associated maximum allowable enrichment, and the minimum required assembly average burnup (if applicable), as required by 10CFR71.33(b)(2). The maximum enrichment and minimum burnup acceptance criteria are defined in Chapter 1. Additional results for each of the candidate fuel assemblies, that are bounded by those listed in Tables 6.1.1 through 6.1.3, are given in Section 6.2 for the MPC-24, MPC-68 and MPC-68F. The tables in Section 6.2 list the maximum k_{eff} (including bias, uncertainties, and calculational statistics), calculated k_{eff} , standard deviation, and energy of the average lethargy causing fission (EALF) for each of the candidate fuel assemblies

[†] For each array size (e.g., 6x6, 7x7, 14x14, etc.), the fuel assemblies have been subdivided into a number of assembly classes, where an assembly class is defined in terms of the (1) number of fuel rods; (2) pitch; (3) number and location of guide tubes (PWR) or water rods (BWR); and (4) cladding material. The assembly classes for BWR and PWR fuel are defined in Section 6.2.

and basket configurations analyzed. The capability of the MPC-68F to safely accommodate Dresden-1 and Humboldt Bay damaged fuel (fuel assembly classes 6x6A, 6x6B, 6x6C, 7x7A, and 8x8A) is demonstrated in Subsection 6.4.4.

In Summary, these results confirm that the maximum k_{eff} values for the HI-STAR 100 System are below the limiting design criteria ($k_{eff} < 0.95$) when fully flooded and loaded with any of the candidate fuel assemblies and basket configurations. The ~~transportation~~ *Criticality Safety Index* based on criticality control is zero (0).

Table 6.1.1

BOUNDED MAXIMUM k_{eff} VALUES FOR EACH ASSEMBLY CLASS IN THE MPC-24

Fuel Assembly Class	Maximum Allowable Enrichment (wt% ^{235}U)	Maximum [†] k_{eff}
14x14A	4.6	0.9296
14x14B	4.6	0.9228
14x14C	4.6	0.9307
14x14D	4.0	0.8507
14x14E	5.0	0.7627
15x15A	4.1	0.9227
15x15B	4.1	0.9388
15x15C	4.1	0.9361
15x15D	4.1	0.9367
15x15E	4.1	0.9392
15x15F	4.1	0.9410
15x15G	4.0	0.8907
15x15H	3.8	0.9337
16x16A	4.6	0.9287
17x17A	4.0	0.9368
17x17B	4.0	0.9355
17x17C	4.0	0.9349

Note: These calculations are for single unreflected, fully flooded casks. However, comparable reactivities were obtained for fully reflected casks and for arrays of casks.

† The term "maximum k_{eff} " as used here, and elsewhere in this document, means the highest possible k-effective, including bias, uncertainties, and calculational statistics, evaluated for the worst case combination of manufacturing tolerances.

Table 6.1.2

BOUNDED MAXIMUM k_{eff} VALUES FOR EACH ASSEMBLY CLASS IN THE MPC-68

Fuel Assembly Class	Maximum Allowable Planar-Average Enrichment (wt% ^{235}U)	Maximum [†] k_{eff}
6x6A	2.7 ^{††}	0.7888 ^{†††}
6x6B [‡]	2.7 ^{††}	0.7824 ^{†††}
6x6C	2.7 ^{††}	0.8021 ^{†††}
7x7A	2.7 ^{††}	0.7974 ^{†††}
7x7B	4.2	0.9386
8x8A	2.7 ^{††}	0.7697 ^{†††}
8x8B	4.2	0.9416
8x8C	4.2	0.9425
8x8D	4.2	0.9403
8x8E	4.2	0.9312
8x8F	4.0	0.9459

Note: These calculations are for single unreflected, fully flooded casks. However, comparable reactivities were obtained for fully reflected casks and for arrays of casks.

- † The term "maximum k_{eff} " as used here, and elsewhere in this document, means the highest possible k-effective, including bias, uncertainties, and calculational statistics, evaluated for the worst case combination of manufacturing tolerances.
- †† This calculation was performed for 3.0% planar-average enrichment, however, the authorized contents are limited to maximum planar-average enrichment of 2.7%. Therefore, the listed maximum k_{eff} value is conservative.
- ††† This calculation was performed for a ^{10}B loading of 0.0067 g/cm², which is 75% of a minimum ^{10}B loading of 0.0089 g/cm². The minimum ^{10}B loading in the MPC-68 is ~~at least~~ 0.031072 g/cm². Therefore, the listed maximum k_{eff} value is conservative.
- ‡ Assemblies in this class contain both MOX and UO₂ pins. The composition of the MOX fuel pins is given in Table 6.3.4. The maximum allowable planar-average enrichment for the MOX pins is given in the specification of authorized contents, Chapter 1.

Table 6.1.2 (continued)

BOUNDED MAXIMUM k_{eff} VALUES FOR EACH ASSEMBLY CLASS IN THE MPC-68

Fuel Assembly Class	Maximum Allowable Planar-Average Enrichment (wt% ^{235}U)	Maximum [†] k_{eff}
9x9A	4.2	0.9417
9x9B	4.2	0.9436
9x9C	4.2	0.9395
9x9D	4.2	0.9394
9x9E	4.0	0.9486
9x9F	4.0	0.9486
9x9G	4.2	0.9383
10x10A	4.2	0.9457 ^{††}
10x10B	4.2	0.9436
10x10C	4.2	0.9433
10x10D	4.0	0.9376
10x10E	4.0	0.9185

Note: These calculations are for single unreflected, fully flooded casks. However, comparable reactivities were obtained for fully reflected casks and for arrays of casks.

† The term "maximum k_{eff} " as used here, and elsewhere in this document, means the highest possible k-effective, including bias, uncertainties, and calculational statistics, evaluated for the worst case combination of manufacturing tolerances.

†† KENO5a verification calculation resulted in a maximum k_{eff} of 0.9453.

Table 6.1.3

BOUNDING MAXIMUM k_{eff} VALUES FOR EACH ASSEMBLY CLASS IN THE MPC-68F

Fuel Assembly Class	Maximum Allowable Planar-Average Enrichment (wt% ^{235}U)	Maximum [†] k_{eff}
6x6A	2.7 ^{††}	0.7888
6x6B ^{†††}	2.7	0.7824
6x6C	2.7	0.8021
7x7A	2.7	0.7974
8x8A	2.7	0.7697

Note:

1. These calculations are for single unreflected, fully flooded casks. However, comparable reactivities were obtained for fully reflected casks and for arrays of casks.
2. These calculations were performed for a ^{10}B loading of 0.0067 g/cm², which is 75% of a minimum ^{10}B loading of 0.0089 g/cm². The minimum ^{10}B loading in the MPC-68F is 0.010 g/cm². Therefore, the listed maximum k_{eff} values are conservative.

† The term "maximum k_{eff} " as used here, and elsewhere in this document, means the highest possible k-effective, including bias, uncertainties, and calculational statistics, evaluated for the worst case combination of manufacturing tolerances.

†† These calculations were performed for 3.0% planar-average enrichment, however, the authorized contents are limited to a maximum planar-average enrichment of 2.7%. Therefore, the listed maximum k_{eff} values are conservative.

††† Assemblies in this class contain both MOX and UO₂ pins. The composition of the MOX fuel pins is given in Table 6.3.4. The maximum allowable planar-average enrichment for the MOX pins is given in the specification of authorized contents, Chapter 1.

Table 6.1.4
SUMMARY OF THE CRITICALITY RESULTS FOR THE MOST REACTIVE ASSEMBLY FROM
THE ASSEMBLY CLASSES IN EACH MPC[†]
TO DEMONSTRATE COMPLIANCE WITH 10CFR71.55 AND 10CFR71.59

MPC-24, Assembly Class 15x15F, 4.1 wt% ²³⁵U				
Configuration	% Internal Moderation	% External Moderation	Applicable Requirement	Maximum k_{eff} [‡]
Single Package, unreflected	100%	0%	n/a	0.9410
Single Package, fully reflected	100%	100%	10CFR71.55 (b), (d), and (e)	0.9397
Containment, fully reflected	100%	100%		0.9397
Infinite Array of Damaged Packages	100%	100%	10CFR71.59 (a)(2)	0.9436
Infinite Array of Undamaged Packages	0%	0%	10CFR71.59 (a)(1)	0.3950
MPC-68, Assembly Class 9x9E/F, 4.0 wt% ²³⁵U				
Configuration	% Internal Moderation	% External Moderation	Applicable Requirement	Maximum k_{eff}
Single Package, unreflected	100%	0%	n/a	0.9486
Single Package, fully reflected	100%	100%	10CFR71.55 (b), (d), and (e)	0.9470
Containment, fully reflected	100%	100%		0.9461
Infinite Array of Damaged Packages	100%	100%	10CFR71.59 (a)(2)	0.9468
Infinite Array of Undamaged Packages	0%	0%	10CFR71.59 (a)(1)	0.3808
MPC-68F, Assembly Class 6x6C, 2.7 wt% ²³⁵U				
Configuration	% Internal Moderation	% External Moderation	Applicable Requirement	Maximum k_{eff}
Single Package, unreflected	100%	0%	n/a	0.8021
Single Package, fully reflected	100%	100%	10CFR71.55 (b), (d), and (e)	0.8033
Containment, fully reflected	100%	100%		0.8033
Infinite Array of Damaged Packages	100%	100%	10CFR71.59 (a)(2)	0.8026
Infinite Array of Undamaged Packages	0%	0%	10CFR71.59 (a)(1)	0.3034

[†] See Supplement 6.1, Table 6.1.1 for results for the MPC-HB.

[‡] The maximum k_{eff} is equal to the sum of the calculated k_{eff} , two standard deviations, the code bias, and the uncertainty in the code bias. For cases with 100% internal moderation, the standard deviation is between 0.0007 and 0.0009, for cases with 0% internal moderation, the standard deviation is between 0.0002 and 0.0004.

Table 6.1.4 (continued)
SUMMARY OF THE CRITICALITY RESULTS FOR THE MOST REACTIVE ASSEMBLY FROM
THE ASSEMBLY CLASSES IN EACH MPC[†]
TO DEMONSTRATE COMPLIANCE WITH 10CFR71.55 AND 10CFR71.59

MPC-24E/EF, Assembly Class 15x15F, 4.5 wt% ²³⁵U				
Configuration	% Internal Moderation	% External Moderation	Applicable Requirement	Maximum k_{eff} [‡]
Single Package, unreflected	100%	0%	n/a	0.9495
Single Package, fully reflected	100%	100%	10CFR71.55 (b), (d), and (e)	0.9485
Containment, fully reflected	100%	100%		0.9486
Infinite Array of Damaged Packages	100%	100%	10CFR71.59 (a)(2)	0.9495
Infinite Array of Undamaged Packages	0%	0%	10CFR71.59 (a)(1)	0.4026
MPC-24E/EF TROJAN, Trojan Intact and Damaged Fuel, 3.7 wt% ²³⁵U				
Configuration	% Internal Moderation	% External Moderation	Applicable Requirement	Maximum k_{eff}
Single Package, unreflected	100%	0%	n/a	0.9377
Single Package, fully reflected	100%	100%	10CFR71.55 (b), (d), and (e)	0.9366
Containment, fully reflected	100%	100%		0.9377
Infinite Array of Damaged Packages	100%	100%	10CFR71.59 (a)(2)	0.9383
Infinite Array of Undamaged Packages	0%	0%	10CFR71.59 (a)(1)	0.3518
MPC-32, Assembly Class 15x15F, 4.0 wt% ²³⁵U				
Configuration	% Internal Moderation	% External Moderation	Applicable Requirement	Maximum k_{eff}
Single Package, unreflected	100%	0%	n/a	later
Single Package, fully reflected	100%	100%	10CFR71.55 (b), (d), and (e)	later
Containment, fully reflected	100%	100%		later
Infinite Array of Damaged Packages	100%	100%	10CFR71.59 (a)(2)	later
Infinite Array of Undamaged Packages	0%	0%	10CFR71.59 (a)(1)	later

[†] See Supplement 6.I, Table 6.I.1 for results for the MPC-HB.

[‡] The maximum k_{eff} is equal to the sum of the calculated k_{eff} , two standard deviations, the code bias, and the uncertainty in the code bias. For cases with 100% internal moderation, the standard deviation is between 0.0007 and 0.0009, for cases with 0% internal moderation, the standard deviation is between 0.0002 and 0.0004.

Table 6.1.5

BOUNDING MAXIMUM k_{eff} VALUES FOR EACH ASSEMBLY CLASS IN THE MPC-24E/EF

Fuel Assembly Class	Maximum Allowable Enrichment (wt% ^{235}U)	Maximum [†] k_{eff}
14x14A	5.0	0.9380
14x14B	5.0	0.9312
14x14C	5.0	0.9365
14x14D	5.0	0.8875
14x14E	5.0	0.7651
15x15A	4.5	0.9336
15x15B	4.5	0.9487
15x15C	4.5	0.9462
15x15D	4.5	0.9445
15x15E	4.5	0.9471
15x15F	4.5	0.9495
15x15G	4.5	0.9062
15x15H	4.2	0.9455
16x16A	5.0	0.9358
17x17A	4.4	0.9447
17x17B	4.4	0.9438
17x17C	4.4	0.9433

† The term "maximum k_{eff} " as used here, and elsewhere in this document, means the highest possible k-effective, including bias, uncertainties, and calculational statistics, evaluated for the worst case combination of manufacturing tolerances.

Table 6.1.6

BOUNDING MAXIMUM k_{eff} VALUES IN THE MPC-24E/EF TROJAN

Fuel Assembly Class	Maximum Allowable Enrichment (wt% ^{235}U)	Content	Maximum [†] k_{eff}
17x17B	3.7	Intact Fuel	0.9187
17x17B	3.7	Intact Fuel, Damaged Fuel and Fuel Debris	0.9377

† The term "maximum k_{eff} " as used here, and elsewhere in this document, means the highest possible k-effective, including bias, uncertainties, and calculational statistics, evaluated for the worst case combination of manufacturing tolerances.

Table 6.1.7

BOUNDED MAXIMUM k_{eff} VALUES IN THE MPC-32

Fuel Assembly Class	Maximum Allowable Enrichment ^{††} (wt% ²³⁵ U)	Minimum Required Assembly Average Burnup ^{††} (GWd/MTU)	Maximum [†] k_{eff}
15x15D, E, F, H	2.0	later	later
	3.0	later	later
	4.0	later	later
	5.0	later	later
17x17A, B, C	2.0	later	later
	3.0	later	later
	4.0	later	later
	5.0	later	later

†† Other combinations of maximum enrichment and minimum burnup have been evaluated which result in the same maximum k_{eff} . See Appendix 6.E for a bounding polynomial function.

† The term "maximum k_{eff} " as used here, and elsewhere in this document, means the highest possible k-effective, including bias, uncertainties, and calculational statistics, evaluated for the worst case combination of manufacturing tolerances.

Specifications for the BWR and PWR fuel assemblies that were analyzed in this criticality evaluation are given in Tables 6.2.1 and 6.2.2, respectively. For the BWR fuel characteristics, the number and dimensions for the water rods are the actual number and dimensions. For the PWR fuel characteristics, the actual number and dimensions of the control rod guide tubes and thimbles are used. Table 6.2.1 lists 72 unique BWR assemblies while Table 6.2.2 lists 46 unique PWR assemblies, all of which were explicitly analyzed for this evaluation. Examination of Tables 6.2.1 and 6.2.2 reveals that there are a large number of minor variations in fuel assembly dimensions.

Due to the large number of minor variations in fuel assembly dimensions, the use of explicit dimensions in defining the authorized contents could limit the applicability of the HI-STAR 100 System. To resolve this limitation, bounding criticality analyses are presented in this section for a number of defined fuel assembly classes for both fuel types (PWR and BWR). The results of the bounding criticality analyses justify using bounding fuel dimensions for defining the authorized contents.

6.2.1 Definition of Assembly Classes

For each array size (e.g., 6x6, 7x7, 15x15, etc.), the fuel assemblies have been subdivided into a number of defined classes, where a class is defined in terms of the (1) number of fuel rods; (2) pitch; (3) number and locations of guide tubes (PWR) or water rods (BWR); and (4) cladding material. The assembly classes for BWR and PWR fuel are defined in Tables 6.2.1 and 6.2.2, respectively. It should be noted that these assembly classes are unique to this evaluation and are not known to be consistent with any class designations in the open literature.

For each assembly class, calculations have been performed for all of the dimensional variations for which data is available (i.e., all data in Tables 6.2.1 and 6.2.2). These calculations demonstrate that the maximum reactivity corresponds to:

- maximum active fuel length,
- maximum fuel pellet diameter,
- minimum cladding outside diameter (OD),
- maximum cladding inside diameter (ID),
- minimum guide tube/water rod thickness, and
- maximum channel thickness (for BWR assemblies only).

Therefore, for each assembly class, a bounding assembly was defined based on the above characteristics and a calculation for the bounding assembly was performed to demonstrate compliance with the regulatory requirement of $k_{\text{eff}} < 0.95$. In some assembly classes this bounding assembly corresponds directly to one of the actual (real) assemblies; while in most

assembly classes, the bounding assembly is artificial (i.e., based on bounding dimensions from more than one of the actual assemblies). In classes where the bounding assembly is artificial, the reactivity of the actual (real) assemblies is typically much less than that of the bounding assembly; thereby providing additional conservatism. As a result of these analyses, the authorized contents (Chapter 1) are defined in terms of the bounding assembly parameters for each class.

To demonstrate that the aforementioned characteristics are bounding, a parametric study was performed for a reference BWR assembly, designated herein as 8x8C04 (identified generally as a GE8x8R). The results of this study are shown in Table 6.2.3, and verify the positive reactivity effect associated with (1) increasing the pellet diameter, (2) maximizing the cladding ID (while maintaining a constant cladding OD), (3) minimizing the cladding OD (while maintaining a constant cladding ID), (4) decreasing the water rod thickness, (5) artificially replacing the Zircaloy water rod tubes with water, (6) maximizing the channel thickness, and (7) increasing the active length. These results, and the many that follow, justify the approach for using bounding dimensions for defining the authorized contents. Where margins permit, the Zircaloy water rod tubes (BWR assemblies) are artificially replaced by water in the bounding cases to remove the requirement for water rod thickness from the specification of authorized contents.

As mentioned, the bounding approach used in these analyses often results in a maximum k_{eff} value for a given class of assemblies that is much greater than the reactivity of any of the actual (real) assemblies within the class, and yet, is still below the 0.95 regulatory limit.

6.2.2 PWR Fuel Assemblies in the MPC-24

For PWR fuel assemblies (specifications listed in Table 6.2.2) the 15x15F01 fuel assembly at 4.1% enrichment has the highest reactivity (see Table 6.2.13). The 17x17A01 assembly (otherwise known as a Westinghouse 17x17 OFA) has a similar reactivity (see Table 6.2.17) and was used throughout this criticality evaluation as a reference PWR assembly. The 17x17A01 assembly is a representative PWR fuel assembly in terms of design and reactivity and is useful for the reactivity studies presented in Sections 6.3 and 6.4. Calculations for the various PWR fuel assemblies in the MPC-24 are summarized in Tables 6.2.4 through 6.2.19 and 6.2.43 for the fully flooded condition with the fuel centered in each fuel storage location.

Tables 6.2.4 through 6.2.19 and 6.2.43 show the maximum k_{eff} values for the assembly classes that are acceptable for storage in the MPC-24. All maximum k_{eff} values include the bias, uncertainties, and calculational statistics, evaluated for the worst combination of manufacturing tolerances. All calculations for the MPC-24 were performed for a ^{10}B loading of 0.020 g/cm^2 , which is 75% of the minimum loading, ~~of 0.0267 g/cm^2 for Boral, or 90% of the minimum loading of 0.0223 g/cm^2 for Metamic,~~ specified for the MPC-24 in Section 1.4. The maximum allowable enrichment in the MPC-24 varies from 3.8 to 5.0 wt% ^{235}U , depending on the assembly class, and is defined in Tables 6.2.4 through 6.2.19 and 6.2.43. It should be noted that

the maximum allowable enrichment does not vary within an assembly class. Table 6.1.1 summarizes the maximum allowable enrichments for each of the assembly classes that are acceptable for storage in the MPC-24.

Tables 6.2.4 through 6.2.19 and 6.2.43 are formatted with the assembly class information in the top row, the unique assembly designations, dimensions, and k_{eff} values in the following rows above the bold double lines, and the bounding dimensions selected to define the authorized contents and corresponding bounding k_{eff} values in the final rows. Where the bounding assembly corresponds directly to one of the actual assemblies, the fuel assembly designation is listed in the bottom row in parentheses (e.g., Table 6.2.4). Otherwise, the bounding assembly is given a unique designation. For an assembly class that contains only a single assembly (e.g., 14x14D, see Table 6.2.7), the authorized contents dimensions are based on the assembly dimensions from that single assembly. Generally, the maximum k_{eff} values corresponding to the selected bounding dimensions are greater than or equal to those for the actual assembly dimensions, and all maximum k_{eff} values are below the 0.95 regulatory limit.

The results of the analyses for the MPC-24, which were performed for all assemblies in each class, further confirm the validity of the bounding dimensions established in Subsection 6.2.1. Thus, for all following calculations, namely analyses of the MPC-24E, only the bounding assembly in a class is analyzed. For the MPC-32 with burnup credit, the validity of the bounding dimensions is verified in Appendix 6.E.

6.2.3 BWR Fuel Assemblies in the MPC-68

For BWR fuel assemblies (specifications listed in Table 6.2.1) the artificial bounding assembly for the 10x10A assembly class at 4.2% enrichment has the highest reactivity (see Table 6.2.32). Calculations for the various BWR fuel assemblies in the MPC-68 are summarized in Tables 6.2.20 through 6.2.36 and 6.2.44 for the fully flooded condition. In all cases, the gadolinia (Gd_2O_3) normally incorporated in BWR fuel was conservatively neglected and the fuel assembly was assumed to be centered in the fuel storage location.

For calculations involving BWR assemblies, the use of a uniform (planar-average) enrichment, as opposed to the distributed enrichments normally used in BWR fuel, produces conservative results. Calculations confirming this statement are presented in Appendix 6.B for several representative BWR fuel assembly designs. These calculations justify the specification of planar-average enrichments to define acceptability of BWR fuel for loading into the MPC-68.

Tables 6.2.20 through 6.2.36 and 6.2.44 show the maximum k_{eff} values for assembly classes that are acceptable for storage in the MPC-68. All maximum k_{eff} values include the bias, uncertainties, and calculational statistics, evaluated for the worst combination of manufacturing tolerances. With the exception of assembly classes 6x6A, 6x6B, 6x6C, 7x7A, and 8x8A, which will be discussed in Section 6.2.4, all calculations for the MPC-68 were performed with a ^{10}B loading of 0.0279 g/cm^2 , which is 75% of the minimum loading, of 0.0372 g/cm^2 for Boral, or

~~90% of the minimum loading of 0.031 g/cm² for Metamie~~, specified for the MPC-68 in Section 1.4. Calculations for assembly classes 6x6A, 6x6B, 6x6C, 7x7A, and 8x8A were conservatively performed with a ¹⁰B loading of 0.0067 g/cm². The maximum allowable enrichment in the MPC-68 varies from 2.7 to 4.2 wt% ²³⁵U, depending on the assembly class. It should be noted that the maximum allowable enrichment does not vary within an assembly class. Table 6.1.2 summarizes the maximum allowable enrichments for all assembly classes that are acceptable for storage in the MPC-68.

Tables 6.2.20 through 6.2.36 and 6.2.44 are formatted with the assembly class information in the top row, the unique assembly designations, dimensions, and k_{eff} values in the following rows above the bold double lines, and the bounding dimensions selected to define the authorized contents and corresponding bounding k_{eff} values in the final rows. Where an assembly class contains only a single assembly (e.g., 8x8E, see Table 6.2.24), the authorized contents dimensions are based on the assembly dimensions from that single assembly. For assembly classes that are suspected to contain assemblies with thicker channels (e.g., 120 mils), bounding calculations are also performed to qualify the thicker channels (e.g., 7x7B, see Table 6.2.20). All of the maximum k_{eff} values corresponding to the selected bounding dimensions are shown to be greater than or equal to those for the actual assembly dimensions and are below the 0.95 regulatory limit.

For assembly classes that contain partial length rods (i.e., 9x9A, 10x10A, and 10x10B), calculations were performed for the actual (real) assembly configuration and for the axial segments (assumed to be full length) with and without the partial length rods. In all cases, the axial segment with only the full length rods present (where the partial length rods are absent) is bounding. Therefore, the bounding maximum k_{eff} values reported for assembly classes that contain partial length rods bound the reactivity regardless of the active fuel length of the partial length rods. As a result, the specification of authorized contents has no minimum requirement for the active fuel length of the partial length rods.

For BWR fuel assembly classes where margins permit, the Zircaloy water rod tubes are artificially replaced by water in the bounding cases to remove the requirement for water rod thickness from the specification of authorized contents. For these cases, the bounding water rod thickness is listed as zero.

As mentioned, the highest observed maximum k_{eff} value[†] corresponds to the artificial bounding assembly in the 10x10A assembly class. This assembly has the following bounding characteristics: (1) the partial length rods are assumed to be zero length (most reactive configuration); (2) the channel is assumed to be 120 mils thick; and (3) the active fuel length of the full length rods is 155 inches.

[†] Assuming assemblies are centered in their basket position. For cases with eccentric positioning see Section 6.3.3.

In addition to storing intact PWR and BWR fuel assemblies, the HI-STAR 100 System is designed to store damaged BWR fuel assemblies and BWR fuel debris. Damaged fuel assemblies and fuel debris are defined in Chapter 1. Both damaged BWR fuel assemblies and BWR fuel debris are required to be loaded into Damaged Fuel Containers (DFCs). Two different DFC types with slightly different cross sections are considered. DFCs containing fuel debris ~~must be stored~~ *are only analyzed* in the MPC-68F. DFCs containing damaged fuel assemblies may be stored in either the MPC-68 or MPC-68F. The criticality evaluation of various possible damaged conditions of the fuel is presented in Subsection 6.4.4 for both DFC types.

Tables 6.2.37 through 6.2.41 show the maximum k_{eff} values for the six assembly classes that may be stored as damaged fuel or fuel debris. All maximum k_{eff} values include the bias, uncertainties, and calculational statistics, evaluated for the worst combination of manufacturing tolerances. All calculations were performed for a ^{10}B loading of 0.0067 g/cm^2 , which is 75% of a minimum loading, 0.0089 g/cm^2 . However, because the practical manufacturing lower limit for minimum ^{10}B loading is 0.01 g/cm^2 , the minimum ^{10}B loading of 0.01 g/cm^2 is specified in Section 1.4, for the MPC-68F. As an additional level of conservatism in the analyses, the calculations were performed for an enrichment of 3.0 wt% ^{235}U , while the maximum allowable enrichment for these assembly classes is limited to 2.7 wt% ^{235}U in the specification of authorized contents. Therefore, the maximum k_{eff} values for damaged BWR fuel assemblies and fuel debris are conservative. Calculations for the various BWR fuel assemblies in the MPC-68F are summarized in Tables 6.2.37 through 6.2.41 for the fully flooded condition.

For the assemblies that may be stored as damaged fuel or fuel debris, the 6x6C01 assembly at 3.0 wt% ^{235}U enrichment has the highest reactivity (see Table 6.2.39). Considering all of the conservatism built into this analysis (e.g., higher than allowed enrichment and lower than actual ^{10}B loading), the actual reactivity will be lower.

Because the analysis for the damaged BWR fuel assemblies and fuel debris was performed for a minimum ^{10}B loading of 0.0089 g/cm^2 , which conservatively bounds damaged BWR fuel assemblies in a standard MPC-68 with a minimum ^{10}B loading of ~~at least~~ 0.031072 g/cm^2 , damaged BWR fuel assemblies may also be stored in the standard MPC-68. However, fuel debris is limited to the MPC-68F by the specification of authorized contents in Chapter 1.

Tables 6.2.37 through 6.2.41 are formatted with the assembly class information in the top row, the unique assembly designations, dimensions, and k_{eff} values in the following rows above the bold double lines, and the bounding dimensions selected to define the authorized contents and corresponding bounding k_{eff} values in the final rows. Where an assembly class contains only a single assembly (e.g., 6x6C, see Table 6.2.39), the authorized contents dimensions are based on the assembly dimensions from that single assembly. All of the maximum k_{eff} values corresponding to the selected bounding dimensions are greater than or equal to those for the actual assembly dimensions and are well below the 0.95 regulatory limit.

6.2.5 Thoria Rod Canister

Additionally, the HI-STAR 100 System is designed to store a Thoria Rod Canister in the MPC68 or MPC68F. The canister is similar to a DFC and contains 18 intact Thoria Rods placed in a separator assembly. The reactivity of the canister in the MPC68 or MPC68F is very low compared to the reactivity of the approved fuel assemblies (The ^{235}U content of these rods corresponds to UO_2 rods with an initial enrichment of approximately 1.7 wt% ^{235}U). It is therefore permissible to store the Thoria Rod Canister together with any other approved content in a MPC68 or MPC68F. Specifications of the canister and the Thoria Rods that are used in the criticality evaluation are given in Table 6.2.42. The criticality evaluation is presented in Subsection 6.4.6.

6.2.6 PWR Assemblies in the MPC-24E and MPC-24EF

The MPC-24E and MPC-24EF are variations of the MPC-24, which provide for transportation of higher enriched fuel than the MPC-24 through an increased ^{10}B loading in the ~~Boral~~-neutron absorber. The maximum allowable fuel enrichment varies between 4.2 and 5.0 wt% ^{235}U , depending on the assembly class. The maximum allowable enrichment for each assembly class is listed in Table 6.1.5, together with the maximum k_{eff} for the bounding assembly in the assembly class. All maximum k_{eff} values are below the 0.95 regulatory limit. The 15x15F assembly class at 4.5% enrichment has the highest reactivity.

6.2.7 PWR Intact Fuel, Damaged Fuel and Fuel Debris in the Trojan MPC-24E/EF

The Trojan MPC-24E and MPC-24EF are variations of the MPC-24E/EF, designed to transport Trojan intact and damaged PWR fuel assemblies (~~MPC-24E and MPC-24EF~~) and fuel debris (~~MPC-24EF only~~). Damaged PWR fuel assemblies and fuel debris are required to be loaded into PWR Damaged Fuel Containers (DFCs) or Failed Fuel Cans. Up to four DFCs may be loaded in the MPC-24E or MPC-24EF. The maximum enrichment for intact fuel, damaged fuel and fuel debris is 3.7 wt% ^{235}U . Only the assembly class 17x17B is certified for the Trojan MPC-24E/EF. The maximum k_{eff} is listed in Table 6.1.6. The criticality evaluation of the damaged fuel is presented in Subsection 6.4.9.

6.2.8 PWR Assemblies in the MPC-32

Burnup credit is necessary to store PWR assemblies in the MPC-32, i.e. a required minimum average assembly burnup is specified as a function of the assembly initial enrichment. Only the assembly classes 15x15D, E, F, H and 17x17A, B, C are certified for transportation in the MPC-32. The maximum initial enrichment is 5.0 wt% ^{235}U . The criticality evaluations for burnup credit are presented in Appendix 6.E.

Table 6.2.1 (page 1 of 6)
 BWR FUEL CHARACTERISTICS AND ASSEMBLY CLASS DEFINITIONS
 (all dimensions are in inches)

Fuel Assembly Designation	Clad Material	Pitch	Number of Fuel Rods	Cladding OD	Cladding Thickness	Pellet Diameter	Active Fuel Length	Number of Water Rods	Water Rod OD	Water Rod ID	Channel Thickness	Channel ID
6x6A Assembly Class												
6x6A01	Zr	0.694	36	0.5645	0.0350	0.4940	110.0	0	n/a	n/a	0.060	4.290
6x6A02	Zr	0.694	36	0.5645	0.0360	0.4820	110.0	0	n/a	n/a	0.060	4.290
6x6A03	Zr	0.694	36	0.5645	0.0350	0.4820	110.0	0	n/a	n/a	0.060	4.290
6x6A04	Zr	0.694	36	0.5550	0.0350	0.4820	110.0	0	n/a	n/a	0.060	4.290
6x6A05	Zr	0.696	36	0.5625	0.0350	0.4820	110.0	0	n/a	n/a	0.060	4.290
6x6A06	Zr	0.696	35	0.5625	0.0350	0.4820	110.0	1	0.0	0.0	0.060	4.290
6x6A07	Zr	0.700	36	0.5555	0.03525	0.4780	110.0	0	n/a	n/a	0.060	4.290
6x6A08	Zr	0.710	36	0.5625	0.0260	0.4980	110.0	0	n/a	n/a	0.060	4.290
6x6B (MOX) Assembly Class												
6x6B01	Zr	0.694	36	0.5645	0.0350	0.4820	110.0	0	n/a	n/a	0.060	4.290
6x6B02	Zr	0.694	36	0.5625	0.0350	0.4820	110.0	0	n/a	n/a	0.060	4.290
6x6B03	Zr	0.696	36	0.5625	0.0350	0.4820	110.0	0	n/a	n/a	0.060	4.290
6x6B04	Zr	0.696	35	0.5625	0.0350	0.4820	110.0	1	0.0	0.0	0.060	4.290
6x6B05	Zr	0.710	35	0.5625	0.0350	0.4820	110.0	1	0.0	0.0	0.060	4.290
6x6C Assembly Class												
6x6C01	Zr	0.740	36	0.5630	0.0320	0.4880	77.5	0	n/a	n/a	0.060	4.542
7x7A Assembly Class												
7x7A01	Zr	0.631	49	0.4860	0.0328	0.4110	80	0	n/a	n/a	0.060	4.542

Table 6.2.1 (page 2 of 6)
 BWR FUEL CHARACTERISTICS AND ASSEMBLY CLASS DEFINITIONS
 (all dimensions are in inches)

Fuel Assembly Designation	Clad Material	Pitch	Number of Fuel Rods	Cladding OD	Cladding Thickness	Pellet Diameter	Active Fuel Length	Number of Water Rods	Water Rod OD	Water Rod ID	Channel Thickness	Channel ID
7x7B Assembly Class												
7x7B01	Zr	0.738	49	0.5630	0.0320	0.4870	150	0	n/a	n/a	0.080	5.278
7x7B02	Zr	0.738	49	0.5630	0.0370	0.4770	150	0	n/a	n/a	0.102	5.291
7x7B03	Zr	0.738	49	0.5630	0.0370	0.4770	150	0	n/a	n/a	0.080	5.278
7x7B04	Zr	0.738	49	0.5700	0.0355	0.4880	150	0	n/a	n/a	0.080	5.278
7x7B05	Zr	0.738	49	0.5630	0.0340	0.4775	150	0	n/a	n/a	0.080	5.278
7x7B06	Zr	0.738	49	0.5700	0.0355	0.4910	150	0	n/a	n/a	0.080	5.278
8x8A Assembly Class												
8x8A01	Zr	0.523	64	0.4120	0.0250	0.3580	110	0	n/a	n/a	0.100	4.290
8x8A02	Zr	0.523	63	0.4120	0.0250	0.3580	120	0	n/a	n/a	0.100	4.290

Table 6.2.1 (page 3 of 6)
 BWR FUEL CHARACTERISTICS AND ASSEMBLY CLASS DEFINITIONS
 (all dimensions are in inches)

Fuel Assembly Designation	Clad Material	Pitch	Number of Fuel Rods	Cladding OD	Cladding Thickness	Pellet Diameter	Active Fuel Length	Number of Water Rods	Water Rod OD	Water Rod ID	Channel Thickness	Channel ID
8x8B Assembly Class												
8x8B01	Zr	0.641	63	0.4840	0.0350	0.4050	150	1	0.484	0.414	0.100	5.278
8x8B02	Zr	0.636	63	0.4840	0.0350	0.4050	150	1	0.484	0.414	0.100	5.278
8x8B03	Zr	0.640	63	0.4930	0.0340	0.4160	150	1	0.493	0.425	0.100	5.278
8x8B04	Zr	0.642	64	0.5015	0.0360	0.4195	150	0	n/a	n/a	0.100	5.278
8x8C Assembly Class												
8x8C01	Zr	0.641	62	0.4840	0.0350	0.4050	150	2	0.484	0.414	0.100	5.278
8x8C02	Zr	0.640	62	0.4830	0.0320	0.4100	150	2	0.591	0.531	0.000	no channel
8x8C03	Zr	0.640	62	0.4830	0.0320	0.4100	150	2	0.591	0.531	0.080	5.278
8x8C04	Zr	0.640	62	0.4830	0.0320	0.4100	150	2	0.591	0.531	0.100	5.278
8x8C05	Zr	0.640	62	0.4830	0.0320	0.4100	150	2	0.591	0.531	0.120	5.278
8x8C06	Zr	0.640	62	0.4830	0.0320	0.4110	150	2	0.591	0.531	0.100	5.278
8x8C07	Zr	0.640	62	0.4830	0.0340	0.4100	150	2	0.591	0.531	0.100	5.278
8x8C08	Zr	0.640	62	0.4830	0.0320	0.4100	150	2	0.493	0.425	0.100	5.278
8x8C09	Zr	0.640	62	0.4930	0.0340	0.4160	150	2	0.493	0.425	0.100	5.278
8x8C10	Zr	0.640	62	0.4830	0.0340	0.4100	150	2	0.591	0.531	0.120	5.278
8x8C11	Zr	0.640	62	0.4830	0.0340	0.4100	150	2	0.591	0.531	0.120	5.215
8x8C12	Zr	0.636	62	0.4830	0.0320	0.4110	150	2	0.591	0.531	0.120	5.215

Table 6.2.1 (page 4 of 6)
 BWR FUEL CHARACTERISTICS AND ASSEMBLY CLASS DEFINITIONS
 (all dimensions are in inches)

Fuel Assembly Designation	Clad Material	Pitch	Number of Fuel Rods	Cladding OD	Cladding Thickness	Pellet Diameter	Active Fuel Length	Number of Water Rods	Water Rod OD	Water Rod ID	Channel Thickness	Channel ID
8x8D Assembly Class												
8x8D01	Zr	0.640	60	0.4830	0.0320	0.4110	150	2 large/ 2 small	0.591/ 0.483	0.531/ 0.433	0.100	5.278
8x8D02	Zr	0.640	60	0.4830	0.0320	0.4110	150	4	0.591	0.531	0.100	5.278
8x8D03	Zr	0.640	60	0.4830	0.0320	0.4110	150	4	0.483	0.433	0.100	5.278
8x8D04	Zr	0.640	60	0.4830	0.0320	0.4110	150	1	1.34	1.26	0.100	5.278
8x8D05	Zr	0.640	60	0.4830	0.0320	0.4100	150	1	1.34	1.26	0.100	5.278
8x8D06	Zr	0.640	60	0.4830	0.0320	0.4110	150	1	1.34	1.26	0.120	5.278
8x8D07	Zr	0.640	60	0.4830	0.0320	0.4110	150	1	1.34	1.26	0.080	5.278
8x8D08	Zr	0.640	61	0.4830	0.0300	0.4140	150	3	0.591	0.531	0.080	5.278
8x8E Assembly Class												
8x8E01	Zr	0.640	59	0.4930	0.0340	0.4160	150	5	0.493	0.425	0.100	5.278
8x8F Assembly Class												
8x8F01	Zr	0.609	64	0.4576	0.0290	0.3913	150	4 [†]	0.291 [†]	0.228 [†]	0.055	5.390
9x9A Assembly Class												
9x9A01	Zr	0.566	74	0.4400	0.0280	0.3760	150	2	0.98	0.92	0.100	5.278
9x9A02	Zr	0.566	66	0.4400	0.0280	0.3760	150	2	0.98	0.92	0.100	5.278
9x9A03	Zr	0.566	74/66	0.4400	0.0280	0.3760	150/90	2	0.98	0.92	0.100	5.278
9x9A04	Zr	0.566	66	0.4400	0.0280	0.3760	150	2	0.98	0.92	0.120	5.278

[†] Four rectangular water cross segments dividing the assembly into four quadrants

Table 6.2.1 (page 5 of 6)
 BWR FUEL CHARACTERISTICS AND ASSEMBLY CLASS DEFINITIONS
 (all dimensions are in inches)

Fuel Assembly Designation	Clad Material	Pitch	Number of Fuel Rods	Cladding OD	Cladding Thickness	Pellet Diameter	Active Fuel Length	Number of Water Rods	Water Rod OD	Water Rod ID	Channel Thickness	Channel ID
9x9B Assembly Class												
9x9B01	Zr	0.569	72	0.4330	0.0262	0.3737	150	1	1.516	1.459	0.100	5.278
9x9B02	Zr	0.569	72	0.4330	0.0260	0.3737	150	1	1.516	1.459	0.100	5.278
9x9B03	Zr	0.572	72	0.4330	0.0260	0.3737	150	1	1.516	1.459	0.100	5.278
9x9C Assembly Class												
9x9C01	Zr	0.572	80	0.4230	0.0295	0.3565	150	1	0.512	0.472	0.100	5.278
9x9D Assembly Class												
9x9D01	Zr	0.572	79	0.4240	0.0300	0.3565	150	2	0.424	0.364	0.100	5.278
9x9E Assembly Class [†]												
9x9E01	Zr	0.572	76	0.4170	0.0265	0.3530	150	5	0.546	0.522	0.120	5.215
9x9E02	Zr	0.572	48 28	0.4170 0.4430	0.0265 0.0285	0.3530 0.3745	150	5	0.546	0.522	0.120	5.215
9x9F Assembly Class [†]												
9x9F01	Zr	0.572	76	0.4430	0.0285	0.3745	150	5	0.546	0.522	0.120	5.215
9x9F02	Zr	0.572	48 28	0.4170 0.4430	0.0265 0.0285	0.3530 0.3745	150	5	0.546	0.522	0.120	5.215
9x9G Assembly Class												
9x9G01	Zr	0.572	72	0.4240	0.0300	0.3565	150	1	1.668	1.604	0.120	5.278

[†] The 9x9E and 9x9F fuel assembly classes represent a single fuel type containing fuel rods with different dimensions (SPC 9x9-5). In addition to the actual configuration (9x9E02 and 9x9F02), the 9x9E class contains a hypothetical assembly with only small fuel rods (9x9E01), and the 9x9F class contains a hypothetical assembly with only large rods (9x9F01). This was done in order to simplify the specification of this assembly for the authorized contents.

Table 6.2.1 (page 6 of 6)
 BWR FUEL CHARACTERISTICS AND ASSEMBLY CLASS DEFINITIONS
 (all dimensions are in inches)

Fuel Assembly Designation	Clad Material	Pitch	Number of Fuel Rods	Cladding OD	Cladding Thickness	Pellet Diameter	Active Fuel Length	Number of Water Rods	Water Rod OD	Water Rod ID	Channel Thickness	Channel ID
10x10A Assembly Class												
10x10A01	Zr	0.510	92	0.4040	0.0260	0.3450	155	2	0.980	0.920	0.100	5.278
10x10A02	Zr	0.510	78	0.4040	0.0260	0.3450	155	2	0.980	0.920	0.100	5.278
10x10A03	Zr	0.510	92/78	0.4040	0.0260	0.3450	155/90	2	0.980	0.920	0.100	5.278
10x10B Assembly Class												
10x10B01	Zr	0.510	91	0.3957	0.0239	0.3413	155	1	1.378	1.321	0.100	5.278
10x10B02	Zr	0.510	83	0.3957	0.0239	0.3413	155	1	1.378	1.321	0.100	5.278
10x10B03	Zr	0.510	91/83	0.3957	0.0239	0.3413	155/90	1	1.378	1.321	0.100	5.278
10x10C Assembly Class												
10x10C01	Zr	0.488	96	0.3780	0.0243	0.3224	150	5	1.227	1.165	0.055	5.457
10x10D Assembly Class												
10x10D01	SS	0.565	100	0.3960	0.0200	0.3500	83	0	n/a	n/a	0.08	5.663
10x10E Assembly Class												
10x10E01	SS	0.557	96	0.3940	0.0220	0.3430	83	4	0.3940	0.3500	0.08	5.663

Table 6.2.2 (page 1 of 4)
PWR FUEL CHARACTERISTICS AND ASSEMBLY CLASS DEFINITIONS
(all dimensions are in inches)

Fuel Assembly Designation	Clad Material	Pitch	Number of Fuel Rods	Cladding OD	Cladding Thickness	Pellet Diameter	Active Fuel Length	Number of Guide Tubes	Guide Tube OD	Guide Tube ID	Guide Tube Thickness
14x14A Assembly Class											
14x14A01	Zr	0.556	179	0.400	0.0243	0.3444	150	17	0.527	0.493	0.0170
14x14A02	Zr	0.556	179	0.400	0.0243	0.3444	150	17	0.528	0.490	0.0190
14x14A03	Zr	0.556	179	0.400	0.0243	0.3444	150	17	0.526	0.492	0.0170
14x14B Assembly Class											
14x14B01	Zr	0.556	179	0.422	0.0243	0.3659	150	17	0.539	0.505	0.0170
14x14B02	Zr	0.556	179	0.417	0.0295	0.3505	150	17	0.541	0.507	0.0170
14x14B03	Zr	0.556	179	0.424	0.0300	0.3565	150	17	0.541	0.507	0.0170
14x14B04	Zr	0.556	179	0.426	0.0310	0.3565	150	17	0.541	0.507	0.0170
14x14C Assembly Class											
14x14C01	Zr	0.580	176	0.440	0.0280	0.3765	150	5	1.115	1.035	0.0400
14x14C02	Zr	0.580	176	0.440	0.0280	0.3770	150	5	1.115	1.035	0.0400
14x14C03	Zr	0.580	176	0.440	0.0260	0.3805	150	5	1.111	1.035	0.0380
14x14D Assembly Class											
14x14D01	SS	0.556	180	0.422	0.0165	0.3835	144	16	0.543	0.514	0.0145

Table 6.2.2 (page 2 of 4)
PWR FUEL CHARACTERISTICS AND ASSEMBLY CLASS DEFINITIONS
(all dimensions are in inches).

Fuel Assembly Designation	Clad Material	Pitch	Number of Fuel Rods	Cladding OD	Cladding Thickness	Pellet Diameter	Active Fuel Length	Number of Guide Tubes	Guide Tube OD	Guide Tube ID	Guide Tube Thickness
14x14E Assembly Class											
14x14E01 [†]	SS	0.453 and 0.441	162 3 8	0.3415 0.3415 0.3415	0.0120 0.0285 0.0200	0.313 0.280 0.297	102	0	n/a	n/a	n/a
14x14E02 [†]	SS	0.453 and 0.441	173	0.3415	0.0120	0.313	102	0	n/a	n/a	n/a
14x14E03 [†]	SS	0.453 and 0.441	173	0.3415	0.0285	0.280	102	0	n/a	n/a	n/a
15x15A Assembly Class											
15x15A01	Zr	0.550	204	0.418	0.0260	0.3580	150	21	0.533	0.500	0.0165

[†] This is the fuel assembly used at Indian Point 1 (IP-1). This assembly is a 14x14 assembly with 23 fuel rods omitted to allow passage of control rods between assemblies. It has a different pitch in different sections of the assembly, and different fuel rod dimensions in some rods.

Table 6.2.2 (page 3 of 4)
PWR FUEL CHARACTERISTICS AND ASSEMBLY CLASS DEFINITIONS
(all dimensions are in inches)

Fuel Assembly Designation	Clad Material	Pitch	Number of Fuel Rods	Cladding OD	Cladding Thickness	Pellet Diameter	Active Fuel Length	Number of Guide Tubes	Guide Tube OD	Guide Tube ID	Guide Tube Thickness
15x15B Assembly Class											
15x15B01	Zr	0.563	204	0.422	0.0245	0.3660	150	21	0.533	0.499	0.0170
15x15B02	Zr	0.563	204	0.422	0.0245	0.3660	150	21	0.546	0.512	0.0170
15x15B03	Zr	0.563	204	0.422	0.0243	0.3660	150	21	0.533	0.499	0.0170
15x15B04	Zr	0.563	204	0.422	0.0243	0.3659	150	21	0.545	0.515	0.0150
15x15B05	Zr	0.563	204	0.422	0.0242	0.3659	150	21	0.545	0.515	0.0150
15x15B06	Zr	0.563	204	0.420	0.0240	0.3671	150	21	0.544	0.514	0.0150
15x15C Assembly Class											
15x15C01	Zr	0.563	204	0.424	0.0300	0.3570	150	21	0.544	0.493	0.0255
15x15C02	Zr	0.563	204	0.424	0.0300	0.3570	150	21	0.544	0.511	0.0165
15x15C03	Zr	0.563	204	0.424	0.0300	0.3565	150	21	0.544	0.511	0.0165
15x15C04	Zr	0.563	204	0.417	0.0300	0.3565	150	21	0.544	0.511	0.0165
15x15D Assembly Class											
15x15D01	Zr	0.568	208	0.430	0.0265	0.3690	150	17	0.530	0.498	0.0160
15x15D02	Zr	0.568	208	0.430	0.0265	0.3686	150	17	0.530	0.498	0.0160
15x15D03	Zr	0.568	208	0.430	0.0265	0.3700	150	17	0.530	0.499	0.0155
15x15D04	Zr	0.568	208	0.430	0.0250	0.3735	150	17	0.530	0.500	0.0150
15x15E Assembly Class											
15x15E01	Zr	0.568	208	0.428	0.0245	0.3707	150	17	0.528	0.500	0.0140
15x15F Assembly Class											
15x15F01	Zr	0.568	208	0.428	0.0230	0.3742	150	17	0.528	0.500	0.0140

Table 6.2.2 (page 4 of 4)
PWR FUEL CHARACTERISTICS AND ASSEMBLY CLASS DEFINITIONS
(all dimensions are in inches)

Fuel Assembly Designation	Clad Material	Pitch	Number of Fuel Rods	Cladding OD	Cladding Thickness	Pellet Diameter	Active Fuel Length	Number of Guide Tubes	Guide Tube OD	Guide Tube ID	Guide Tube Thickness
15x15G Assembly Class											
15x15G01	SS	0.563	204	0.422	0.0165	0.3825	144	21	0.543	0.514	0.0145
15x15H Assembly Class											
15x15H01	Zr	0.568	208	0.414	0.0220	0.3622	150	17	0.528	0.500	0.0140
16x16A Assembly Class											
16x16A01	Zr	0.506	236	0.382	0.0250	0.3255	150	5	0.980	0.900	0.0400
16x16A02	Zr	0.506	236	0.382	0.0250	0.3250	150	5	0.980	0.900	0.0400
17x17A Assembly Class											
17x17A01	Zr	0.496	264	0.360	0.0225	0.3088	150	25	0.474	0.442	0.0160
17x17A02	Zr	0.496	264	0.360	0.0250	0.3030	150	25	0.480	0.448	0.0160
17x17B Assembly Class											
17x17B01	Zr	0.496	264	0.374	0.0225	0.3225	150	25	0.482	0.450	0.0160
17x17B02	Zr	0.496	264	0.374	0.0225	0.3225	150	25	0.474	0.442	0.0160
17x17B03	Zr	0.496	264	0.376	0.0240	0.3215	150	25	0.480	0.448	0.0160
17x17B04	Zr	0.496	264	0.372	0.0205	0.3232	150	25	0.427	0.399	0.0140
17x17B05	Zr	0.496	264	0.374	0.0240	0.3195	150	25	0.482	0.450	0.0160
17x17B06	Zr	0.496	264	0.372	0.0205	0.3232	150	25	0.480	0.452	0.0140
17x17C Assembly Class											
17x17C01	Zr	0.502	264	0.379	0.0240	0.3232	150	25	0.472	0.432	0.0200
17x17C02	Zr	0.502	264	0.377	0.0220	0.3252	150	25	0.472	0.432	0.0200

Table 6.2.3
 REACTIVITY EFFECT OF ASSEMBLY PARAMETER VARIATIONS
 (all dimensions are in inches)

Fuel Assembly/ Parameter Variation	reactivity effect	calculated k_{eff}	standard deviation	cladding OD	cladding ID	cladding thickness	pellet OD	water rod thickness	channel thickness
8x8C04 (GE8x8R)	reference	0.9307	0.0007	0.483	0.419	0.032	0.410	0.030	0.100
increase pellet OD (+0.001)	+0.0005	0.9312	0.0007	0.483	0.419	0.032	0.411	0.030	0.100
decrease pellet OD (-0.001)	-0.0008	0.9299	0.0009	0.483	0.419	0.032	0.409	0.030	0.100
increase clad ID (+0.004)	+0.0027	0.9334	0.0007	0.483	0.423	0.030	0.410	0.030	0.100
decrease clad ID (-0.004)	-0.0034	0.9273	0.0007	0.483	0.415	0.034	0.410	0.030	0.100
increase clad OD (+0.004)	-0.0041	0.9266	0.0008	0.487	0.419	0.034	0.410	0.030	0.100
decrease clad OD (-0.004)	+0.0023	0.9330	0.0007	0.479	0.419	0.030	0.410	0.030	0.100
increase water rod thickness (+0.015)	-0.0019	0.9288	0.0008	0.483	0.419	0.032	0.410	0.045	0.100
decrease water rod thickness (-0.015)	+0.0001	0.9308	0.0008	0.483	0.419	0.032	0.410	0.015	0.100
remove water rods (i.e., replace the water rod tubes with water)	+0.0021	0.9328	0.0008	0.483	0.419	0.032	0.410	0.000	0.100
remove channel	-0.0039	0.9268	0.0009	0.483	0.419	0.032	0.410	0.030	0.000
increase channel thickness (+0.020)	+0.0005	0.9312	0.0007	0.483	0.419	0.032	0.410	0.030	0.120
reduced active length (120 Inches)	-0.0007	0.9300	0.0007	0.483	0.419	0.032	0.410	0.030	0.100
reduced active length (90 Inches)	-0.0043	0.9264	0.0007	0.483	0.419	0.032	0.410	0.030	0.100

Table 6.2.4
 MAXIMUM K_{EFF} VALUES FOR THE 14X14A ASSEMBLY CLASS IN THE MPC-24
 (all dimensions are in inches)

14x14A (4.6% Enrichment, Boral Fixed neutron absorber ^{10}B minimum loading of 0.02 g/cm ²)										
179 fuel rods, 17 guide tubes, pitch=0.556, Zr clad										
Fuel Assembly Designation	maximum k_{eff}	calculated k_{eff}	standard deviation	EALF	cladding OD	cladding ID	cladding thickness	pellet OD	fuel length	guide tube thickness
14x14A01	0.9295	0.9252	0.0008	0.2084	0.400	0.3514	0.0243	0.3444	150	0.017
14x14A02	0.9286	0.9242	0.0008	0.2096	0.400	0.3514	0.0243	0.3444	150	0.019
14x14A03	0.9296	0.9253	0.0008	0.2093	0.400	0.3514	0.0243	0.3444	150	0.017
Dimensions Listed for Authorized Contents					0.400 (min.)	0.3514 (max.)		0.3444 (max.)	150 (max.)	0.017 (min.)
bounding dimensions (14x14A03)	0.9296	0.9253	0.0008	0.2093	0.400	0.3514	0.0243	0.3444	150	0.017

Table 6.2.5
 MAXIMUM K_{EFF} VALUES FOR THE 14X14B ASSEMBLY CLASS IN THE MPC-24
 (all dimensions are in inches)

14x14B (4.6% Enrichment, Boral Fixed neutron absorber ^{10}B minimum loading of 0.02 g/cm ³)										
179 fuel rods, 17 guide tubes, pitch=0.556, Zr clad										
Fuel Assembly Designation	maximum k_{eff}	calculated k_{eff}	standard deviation	EALF	cladding OD	cladding ID	cladding thickness	pellet OD	fuel length	guide tube thickness
14x14B01	0.9159	0.9117	0.0007	0.2727	0.422	0.3734	0.0243	0.3659	150	0.017
14x14B02	0.9169	0.9126	0.0008	0.2345	0.417	0.3580	0.0295	0.3505	150	0.017
14x14B03	0.9110	0.9065	0.0009	0.2545	0.424	0.3640	0.0300	0.3565	150	0.017
14x14B04	0.9084	0.9039	0.0009	0.2563	0.426	0.3640	0.0310	0.3565	150	0.017
Dimensions Listed for Authorized Contents					0.417 (min.)	0.3734 (max.)		0.3659 (max.)	150 (max.)	0.017 (min.)
bounding dimensions (B14x14B01)	0.9228	0.9185	0.0008	0.2675	0.417	0.3734	0.0218	0.3659	150	0.017

Table 6.2.6
 MAXIMUM K_{EFF} VALUES FOR THE 14X14C ASSEMBLY CLASS IN THE MPC-24
 (all dimensions are in inches)

14x14C (4.6% Enrichment, Boral Fixed neutron absorber ^{10}B minimum loading of 0.02 g/cm ²)										
176 fuel rods, 5 guide tubes, pitch=0.580, Zr clad										
Fuel Assembly Designation	maximum k_{eff}	calculated k_{eff}	standard deviation	EALF	cladding OD	cladding ID	cladding thickness	pellet OD	fuel length	guide tube thickness
14x14C01	0.9258	0.9215	0.0008	0.2729	0.440	0.3840	0.0280	0.3765	150	0.040
14x14C02	0.9265	0.9222	0.0008	0.2765	0.440	0.3840	0.0280	0.3770	150	0.040
14x14C03	0.9287	0.9242	0.0009	0.2825	0.440	0.3880	0.0260	0.3805	150	0.038
Dimensions Listed for Authorized Contents					0.440 (min.)	0.3880 (max.)		0.3805 (max.)	150 (max.)	0.038 (min.)
bounding dimensions (14x14C03)	0.9287	0.9242	0.0009	0.2825	0.440	0.3880	0.0260	0.3805	150	0.038

Table 6.2.7
 MAXIMUM K_{EFF} VALUES FOR THE 14X14D ASSEMBLY CLASS IN THE MPC-24
 (all dimensions are in inches)

14x14D (4.0% Enrichment, Boral Fixed neutron absorber ^{10}B minimum loading of 0.02 g/cm ²)										
180 fuel rods, 16 guide tubes, pitch=0.556, SS clad										
Fuel Assembly Designation	maximum k_{eff}	calculated k_{eff}	standard deviation	EALF	cladding OD	cladding ID	cladding thickness	pellet OD	fuel length	guide tube thickness
14x14D01	0.8507	0.8464	0.0008	0.3308	0.422	0.3890	0.0165	0.3835	144	0.0145
Dimensions Listed for Authorized Contents					0.422 (min.)	0.3890 (max.)		0.3835 (max.)	144 (max.)	0.0145 (min.)

Table 6.2.8
 MAXIMUM K_{EFF} VALUES FOR THE 15X15A ASSEMBLY CLASS IN THE MPC-24
 (all dimensions are in inches)

15x15A (4.1% Enrichment, Boral Fixed neutron absorber ¹⁰ B minimum loading of 0.02 g/cm ²) 204 fuel rods, 21 guide tubes, pitch=0.550, Zr clad										
Fuel Assembly Designation	maximum k_{eff}	calculated k_{eff}	standard deviation	EALF	cladding OD	cladding ID	cladding thickness	pellet OD	fuel length	guide tube thickness
15x15A01	0.9204	0.9159	0.0009	0.2608	0.418	0.3660	0.0260	0.3580	150	0.0165
Dimensions Listed for Authorized Contents					0.418 (min.)	0.3660 (max.)		0.3580 (max.)	150 (max.)	0.0165 (min.)

Table 6.2.9
 MAXIMUM K_{EFF} VALUES FOR THE 15X15B ASSEMBLY CLASS IN THE MPC-24
 (all dimensions are in inches)

15x15B (4.1% Enrichment, Boral Fixed neutron absorber ^{10}B minimum loading of 0.02 g/cm ²)										
204 fuel rods, 21 guide tubes, pitch=0.563, Zr clad										
Fuel Assembly Designation	maximum k_{eff}	calculated k_{eff}	standard deviation	EALF	cladding OD	cladding ID	cladding thickness	pellet OD	fuel length	guide tube thickness
15x15B01	0.9369	0.9326	0.0008	0.2632	0.422	0.3730	0.0245	0.3660	150	0.017
15x15B02	0.9338	0.9295	0.0008	0.2640	0.422	0.3730	0.0245	0.3660	150	0.017
15x15B03	0.9362	0.9318	0.0008	0.2632	0.422	0.3734	0.0243	0.3660	150	0.017
15x15B04	0.9370	0.9327	0.0008	0.2612	0.422	0.3734	0.0243	0.3659	150	0.015
15x15B05	0.9356	0.9313	0.0008	0.2606	0.422	0.3736	0.0242	0.3659	150	0.015
15x15B06	0.9366	0.9324	0.0007	0.2638	0.420	0.3720	0.0240	0.3671	150	0.015
Dimensions Listed for Authorized Contents					0.420 (min.)	0.3736 (max.)		0.3671 (max.)	150 (max.)	0.015 (min.)
bounding dimensions (B15x15B01)	0.9388	0.9343	0.0009	0.2626	0.420	0.3736	0.0232	0.3671	150	0.015

Table 6.2.10
 MAXIMUM K_{EFF} VALUES FOR THE 15X15C ASSEMBLY CLASS IN THE MPC-24
 (all dimensions are in inches)

15x15C (4.1% Enrichment, Boral Fixed neutron absorber ^{10}B minimum loading of 0.02 g/cm ²)										
204 fuel rods, 21 guide tubes, pitch=0.563, Zr clad										
Fuel Assembly Designation	maximum k_{eff}	calculated k_{eff}	standard deviation	EALF	cladding OD	cladding ID	cladding thickness	pellet OD	fuel length	guide tube thickness
15x15C01	0.9255	0.9213	0.0007	0.2493	0.424	0.3640	0.0300	0.3570	150	0.0255
15x15C02	0.9297	0.9255	0.0007	0.2457	0.424	0.3640	0.0300	0.3570	150	0.0165
15x15C03	0.9297	0.9255	0.0007	0.2440	0.424	0.3640	0.0300	0.3565	150	0.0165
15x15C04	0.9311	0.9268	0.0008	0.2435	0.417	0.3570	0.0300	0.3565	150	0.0165
Dimensions Listed for Authorized Contents					0.417 (min.)	0.3640 (max.)		0.3570 (max.)	150 (max.)	0.0165 (min.)
bounding dimensions (B15x15C01)	0.9361	0.9316	0.0009	0.2385	0.417	0.3640	0.0265	0.3570	150	0.0165

Table 6.2:11
 MAXIMUM K_{EFF} VALUES FOR THE 15X15D ASSEMBLY CLASS IN THE MPC-24
 (all dimensions are in inches)

15x15D (4.1% Enrichment, Boral Fixed neutron absorber ^{10}B minimum loading of 0.02 g/cm ²)										
208 fuel rods, 17 guide tubes, pitch=0.568, Zr clad										
Fuel Assembly Designation	maximum k_{eff}	calculated k_{eff}	standard deviation	EALF	cladding OD	cladding ID	cladding thickness	pellet OD	fuel length	guide tube thickness
15x15D01	0.9341	0.9298	0.0008	0.2822	0.430	0.3770	0.0265	0.3690	150	0.0160
15x15D02	0.9367	0.9324	0.0008	0.2802	0.430	0.3770	0.0265	0.3686	150	0.0160
15x15D03	0.9354	0.9311	0.0008	0.2844	0.430	0.3770	0.0265	0.3700	150	0.0155
15x15D04	0.9339	0.9292	0.0010	0.2958	0.430	0.3800	0.0250	0.3735	150	0.0150
Dimensions Listed for Authorized Contents					0.430 (min.)	0.3800 (max.)		0.3735 (max.)	150 (max.)	0.0150 (min.)
bounding dimensions (15x15D04)	0.9339 [†]	0.9292	0.0010	0.2958	0.430	0.3800	0.0250	0.3735	150	0.0150

[†] The k_{eff} value listed for the 15x15D02 case is slightly higher than that for the case with the bounding dimensions. However, calculations with significantly increased number of particles show that the two cases are statistically equivalent, with a maximum k_{eff} value of 0.9339. Nevertheless, the 15x15D02 case is used in Table 6.3.5 for the eccentric positioning analysis.

Table 6.2.12.
 MAXIMUM K_{EFF} VALUES FOR THE 15X15E ASSEMBLY CLASS IN THE MPC-24
 (all dimensions are in inches)

15x15E (4.1% Enrichment, Boral Fixed neutron absorber ^{10}B minimum loading of 0.02 g/cm ²)										
208 fuel rods, 17 guide tubes, pitch=0.568, Zr clad										
Fuel Assembly Designation	maximum k_{eff}	calculated k_{eff}	standard deviation	EALF	cladding OD	cladding ID	cladding thickness	pellet OD	fuel length	guide tube thickness
15x15E01	0.9368	0.9325	0.0008	0.2826	0.428	0.3790	0.0245	0.3707	150	0.0140
Dimensions Listed for Authorized Contents					0.428 (min.)	0.3790 (max.)		0.3707 (max.)	150 (max.)	0.0140 (min.)

Table 6.2.13
 MAXIMUM K_{EFF} VALUES FOR THE 15X15F ASSEMBLY CLASS IN THE MPC-24
 (all dimensions are in inches)

15x15F (4.1% Enrichment, Boral Fixed neutron absorber ^{10}B minimum loading of 0.02 g/cm ²)										
208 fuel rods, 17 guide tubes, pitch=0.568, Zr clad										
Fuel Assembly Designation	maximum k_{eff}	calculated k_{eff}	standard deviation	EALF	cladding OD	cladding ID	cladding thickness	pellet OD	fuel length	guide tube thickness
15x15F01	0.9395 [†]	0.9350	0.0009	0.2903	0.428	0.3820	0.0230	0.3742	150	0.0140
Dimensions Listed for Authorized Contents					0.428 (min.)	0.3820 (max.)		0.3742 (max.)	150 (max.)	0.0140 (min.)

[†] KENO5a verification calculation resulted in a maximum k_{eff} of 0.9378.

Table 6.2.14
 MAXIMUM K_{EFF} VALUES FOR THE 15X15G ASSEMBLY CLASS IN THE MPC-24
 (all dimensions are in inches)

15x15G (4.0% Enrichment, Boral Fixed neutron absorber ^{10}B minimum loading of 0.02 g/cm ²)										
204 fuel rods, 21 guide tubes, pitch=0.563, SS clad										
Fuel Assembly Designation	maximum k_{eff}	calculated k_{eff}	standard deviation	EALF	cladding OD	cladding ID	cladding thickness	pellet OD	fuel [†] length	guide tube thickness
15x15G01	0.8876	0.8833	0.0008	0.3357	0.422	0.3890	0.0165	0.3825	144	0.0145
Dimensions Listed for Authorized Contents					0.422 (min.)	0.3890 (max.)		0.3825 (max.)	144 (max.)	0.0145 (min.)

[†] Calculations were conservatively performed for a fuel length of 150 inches.

Table 6.2.15
 MAXIMUM K_{EFF} VALUES FOR THE 15X15H ASSEMBLY CLASS IN THE MPC-24
 (all dimensions are in inches)

15x15H (3.8% Enrichment, Boral Fixed neutron absorber ^{10}B minimum loading of 0.02 g/cm ²)										
208 fuel rods, 17 guide tubes, pitch=0.568, Zr clad										
Fuel Assembly Designation	maximum k_{eff}	calculated k_{eff}	standard deviation	EALF	cladding OD	cladding ID	cladding thickness	pellet OD	fuel length	guide tube thickness
15x15H01	0.9337	0.9292	0.0009	0.2349	0.414	0.3700	0.0220	0.3622	150	0.0140
Dimensions Listed for Authorized Contents					0.414 (min.)	0.3700 (max.)		0.3622 (max.)	150 (max.)	0.0140 (min.)

Table 6.2.16.
 MAXIMUM K_{EFF} VALUES FOR THE 16X16A ASSEMBLY CLASS IN THE MPC-24
 (all dimensions are in inches)

16x16A (4.6% Enrichment, Boral Fixed neutron absorber ^{10}B minimum loading of 0.02 g/cm ²)										
236 fuel rods, 5 guide tubes, pitch=0.506, Zr clad										
Fuel Assembly Designation	maximum k_{eff}	calculated k_{eff}	standard deviation	EALF	cladding OD	cladding ID	cladding thickness	pellet OD	fuel length	guide tube thickness
16x16A01	0.9287	0.9244	0.0008	0.2704	0.382	0.3320	0.0250	0.3255	150	0.0400
16x16A02	0.9263	0.9221	0.0007	0.2702	0.382	0.3320	0.0250	0.3250	150	0.0400
Dimensions Listed for Authorized Contents					0.382 (min.)	0.3320 (max.)		0.3255 (max.)	150 (max.)	0.0400 (min.)
bounding dimensions (16x16A01)	0.9287	0.9244	0.0008	0.2704	0.382	0.3320	0.0250	0.3255	150	0.0400

Table 6.2.17
 MAXIMUM K_{EFF} VALUES FOR THE 17X17A ASSEMBLY CLASS IN THE MPC-24
 (all dimensions are in inches)

17x17A (4.0% Enrichment, Boral Fixed neutron absorber ^{10}B minimum loading of 0.02 g/cm ²)										
264 fuel rods, 25 guide tubes, pitch=0.496, Zr clad										
Fuel Assembly Designation	maximum k_{eff}	calculated k_{eff}	standard deviation	EALF	cladding OD	cladding ID	cladding thickness	pellet OD	fuel length	guide tube thickness
17x17A01	0.9368	0.9325	0.0008	0.2131	0.360	0.3150	0.0225	0.3088	150	0.016
17x17A02	0.9329	0.9286	0.0008	0.2018	0.360	0.3100	0.0250	0.3030	150	0.016
Dimensions Listed for Authorized Contents					0.360 (min.)	0.3150 (max.)		0.3088 (max.)	150 (max.)	0.016 (min.)
bounding dimensions (17x17A01)	0.9368	0.9325	0.0008	0.2131	0.360	0.3150	0.0225	0.3088	150	0.016

Table 6.2.18
 MAXIMUM K_{EFF} VALUES FOR THE 17X17B ASSEMBLY CLASS IN THE MPC-24
 (all dimensions are in inches)

17x17B (4.0% Enrichment, Boral Fixed neutron absorber ^{10}B minimum loading of 0.02 g/cm ²)										
264 fuel rods, 25 guide tubes, pitch=0.496, Zr clad										
Fuel Assembly Designation	maximum k_{eff}	calculated k_{eff}	standard deviation	EALF	cladding OD	cladding ID	cladding thickness	pellet OD	fuel length	guide tube thickness
17x17B01	0.9288	0.9243	0.0009	0.2607	0.374	0.3290	0.0225	0.3225	150	0.016
17x17B02	0.9290	0.9247	0.0008	0.2596	0.374	0.3290	0.0225	0.3225	150	0.016
17x17B03	0.9243	0.9199	0.0008	0.2625	0.376	0.3280	0.0240	0.3215	150	0.016
17x17B04	0.9324	0.9279	0.0009	0.2576	0.372	0.3310	0.0205	0.3232	150	0.014
17x17B05	0.9266	0.9222	0.0008	0.2539	0.374	0.3260	0.0240	0.3195	150	0.016
17x17B06	0.9311	0.9268	0.0008	0.2593	0.372	0.3310	0.0205	0.3232	150	0.014
Dimensions Listed for Authorized Contents					0.372 (min.)	0.3310 (max.)		0.3232 (max.)	150 (max.)	0.014 (min.)
bounding dimensions (17x17B06)	0.9311 [†]	0.9268	0.0008	0.2593	0.372	0.3310	0.0205	0.3232	150	0.014

[†] The k_{eff} value listed for the 17x17B04 case is slightly higher than that for the case with the bounding dimensions. However, the difference (0.0013) is well within the statistical uncertainties, and thus, the two values are statistically equivalent (within 2σ). Nevertheless, the 17x17B04 case is used in Table 6.3.5 for the eccentric analysis.

Table 6.2.19
 MAXIMUM K_{EFF} VALUES FOR THE 17X17C ASSEMBLY CLASS IN THE MPC-24
 (all dimensions are in inches)

17x17C (4.0% Enrichment, Boral Fixed neutron absorber ^{10}B minimum loading of 0.02 g/cm ²)										
264 fuel rods, 25 guide tubes, pitch=0.502, Zr clad										
Fuel Assembly Designation	maximum k_{eff}	calculated k_{eff}	standard deviation	EALF	cladding OD	cladding ID	cladding thickness	pellet OD	fuel length	guide tube thickness
17x17C01	0.9293	0.9250	0.0008	0.2595	0.379	0.3310	0.0240	0.3232	150	0.020
17x17C02	0.9336	0.9293	0.0008	0.2624	0.377	0.3330	0.0220	0.3252	150	0.020
Dimensions Listed for Authorized Contents					0.377 (min.)	0.3330 (max.)		0.3252 (max.)	150 (max.)	0.020 (min.)
bounding dimensions (17x17C02)	0.9336	0.9293	0.0008	0.2624	0.377	0.3330	0.0220	0.3252	150	0.020

Table 6.2.20
 MAXIMUM K_{EFF} VALUES FOR THE 7X7B ASSEMBLY CLASS IN THE MPC-68
 (all dimensions are in inches)

7x7B (4.2% Enrichment, Boral Fixed neutron absorber ^{10}B minimum loading of 0.0279 g/cm ²)											
49 fuel rods, 0 water rods, pitch=0.738, Zr clad											
Fuel Assembly Designation	maximum k_{eff}	calculated k_{eff}	standard deviation	EALF	cladding OD	cladding ID	cladding thickness	pellet OD	fuel length	water rod thickness	channel thickness
7x7B01	0.9372	0.9330	0.0007	0.3658	0.5630	0.4990	0.0320	0.4870	150	n/a	0.080
7x7B02	0.9301	0.9260	0.0007	0.3524	0.5630	0.4890	0.0370	0.4770	150	n/a	0.102
7x7B03	0.9313	0.9271	0.0008	0.3438	0.5630	0.4890	0.0370	0.4770	150	n/a	0.080
7x7B04	0.9311	0.9270	0.0007	0.3816	0.5700	0.4990	0.0355	0.4880	150	n/a	0.080
7x7B05	0.9350	0.9306	0.0008	0.3382	0.5630	0.4950	0.0340	0.4775	150	n/a	0.080
7x7B06	0.9298	0.9260	0.0006	0.3957	0.5700	0.4990	0.0355	0.4910	150	n/a	0.080
Dimensions Listed for Authorized Contents					0.5630 (min.)	0.4990 (max.)		0.4910 (max.)	150 (max.)	n/a	0.120 (max.)
bounding dimensions (B7x7B01)	0.9375	0.9332	0.0008	0.3887	0.5630	0.4990	0.0320	0.4910	150	n/a	0.102
bounding dimensions with 120 mil channel (B7x7B02)	0.9386	0.9344	0.0007	0.3983	0.5630	0.4990	0.0320	0.4910	150	n/a	0.120

Table 6.2.21
 MAXIMUM K_{EFF} VALUES FOR THE 8X8B ASSEMBLY CLASS IN THE MPC-68
 (all dimensions are in inches)

8x8B (4.2% Enrichment, Boral Fixed neutron absorber ^{10}B minimum loading of 0.0279 g/cm ²)													
63 or 64 fuel rods, 1 or 0 water rods, pitch [†] = 0.636-0.642, Zr clad													
Fuel Assembly Designation	maximum k_{eff}	calculated k_{eff}	standard deviation	EALF	Fuel rods	pitch	cladding OD	cladding ID	cladding thickness	pellet OD	fuel length	water rod thickness	channel thickness
8x8B01	0.9310	0.9265	0.0009	0.2935	63	0.641	0.4840	0.4140	0.0350	0.4050	150	0.035	0.100
8x8B02	0.9227	0.9185	0.0007	0.2993	63	0.636	0.4840	0.4140	0.0350	0.4050	150	0.035	0.100
8x8B03	0.9299	0.9257	0.0008	0.3319	63	0.640	0.4930	0.4250	0.0340	0.4160	150	0.034	0.100
8x8B04	0.9236	0.9194	0.0008	0.3700	64	0.642	0.5015	0.4295	0.0360	0.4195	150	n/a	0.100
Dimensions Listed for Authorized Contents					63 or 64	0.636-0.642	0.4840 (min.)	0.4295 (max.)		0.4195 (max.)	150 (max.)	0.034	0.120 (max.)
bounding (pitch=0.636) (B8x8B01)	0.9346	0.9301	0.0009	0.3389	63	0.636	0.4840	0.4295	0.02725	0.4195	150	0.034	0.120
bounding (pitch=0.640) (B8x8B02)	0.9385	0.9343	0.0008	0.3329	63	0.640	0.4840	0.4295	0.02725	0.4195	150	0.034	0.120
bounding (pitch=0.641) (B8x8B03)	0.9416	0.9375	0.0007	0.3293	63	0.642	0.4840	0.4295	0.02725	0.4195	150	0.034	0.120

[†] This assembly class was analyzed and qualified for a small variation in the pitch and a variation in the number of fuel and water rods.

Table 6.2.22
 MAXIMUM K_{EFF} VALUES FOR THE 8X8C ASSEMBLY CLASS IN THE MPC-68
 (all dimensions are in inches)

8x8C (4.2% Enrichment, Boral Fixed neutron absorber ^{10}B minimum loading of 0.0279 g/cm ²)												
62 fuel rods, 2 water rods, pitch [†] = 0.636-0.641, Zr clad												
Fuel Assembly Designation	maximum k_{eff}	calculated k_{eff}	standard deviation	EALF	pitch	cladding OD	cladding ID	cladding thickness	pellet OD	fuel length	water rod thickness	channel thickness
8x8C01	0.9315	0.9273	0.0007	0.2822	0.641	0.4840	0.4140	0.0350	0.4050	150	0.035	0.100
8x8C02	0.9313	0.9268	0.0009	0.2716	0.640	0.4830	0.4190	0.0320	0.4100	150	0.030	0.000
8x8C03	0.9329	0.9286	0.0008	0.2877	0.640	0.4830	0.4190	0.0320	0.4100	150	0.030	0.800
8x8C04	0.9348 ^{††}	0.9307	0.0007	0.2915	0.640	0.4830	0.4190	0.0320	0.4100	150	0.030	0.100
8x8C05	0.9353	0.9312	0.0007	0.2971	0.640	0.4830	0.4190	0.0320	0.4100	150	0.030	0.120
8x8C06	0.9353	0.9312	0.0007	0.2944	0.640	0.4830	0.4190	0.0320	0.4110	150	0.030	0.100
8x8C07	0.9314	0.9273	0.0007	0.2972	0.640	0.4830	0.4150	0.0340	0.4100	150	0.030	0.100
8x8C08	0.9339	0.9298	0.0007	0.2915	0.640	0.4830	0.4190	0.0320	0.4100	150	0.034	0.100
8x8C09	0.9301	0.9260	0.0007	0.3183	0.640	0.4930	0.4250	0.0340	0.4160	150	0.034	0.100
8x8C10	0.9317	0.9275	0.0008	0.3018	0.640	0.4830	0.4150	0.0340	0.4100	150	0.030	0.120
8x8C11	0.9328	0.9287	0.0007	0.3001	0.640	0.4830	0.4150	0.0340	0.4100	150	0.030	0.120
8x8C12	0.9285	0.9242	0.0008	0.3062	0.636	0.4830	0.4190	0.0320	0.4110	150	0.030	0.120
Dimensions Listed for Authorized Contents					0.636-0.641	0.4830 (min.)	0.4250 (max.)		0.4160 (max.)	150 (max.)	0.000 (min.)	0.120 (max.)
bounding (pitch=0.636) (B8x8C01)	0.9357	0.9313	0.0009	0.3141	0.636	0.4830	0.4250	0.0290	0.4160	150	0.000	0.120
bounding (pitch=0.640) (B8x8C02)	0.9425	0.9384	0.0007	0.3081	0.640	0.4830	0.4250	0.0290	0.4160	150	0.000	0.120
bounding (pitch=0.641) (B8x8C03)	0.9418	0.9375	0.0008	0.3056	0.641	0.4830	0.4250	0.0290	0.4160	150	0.000	0.120

[†] This assembly class was analyzed and qualified for a small variation in the pitch.

^{††} KENO5a verification calculation resulted in a maximum k_{eff} of 0.9343.

Table 6.2.23
 MAXIMUM K_{EFF} VALUES FOR THE 8X8D ASSEMBLY CLASS IN THE MPC-68
 (all dimensions are in inches)

8x8D (4.2% Enrichment, Boral Fixed neutron absorber ^{10}B minimum loading of 0.0279 g/cm ²)											
60 or 61 fuel rods, 1-4 water rods [†] , pitch=0.640, Zr clad											
Fuel Assembly Designation	maximum k_{eff}	calculated k_{eff}	standard deviation	EALF	cladding OD	cladding ID	cladding thickness	pellet OD	fuel length	water rod thickness	channel thickness
8x8D01	0.9342	0.9302	0.0006	0.2733	0.4830	0.4190	0.0320	0.4110	150	0.03/0.025	0.100
8x8D02	0.9325	0.9284	0.0007	0.2750	0.4830	0.4190	0.0320	0.4110	150	0.030	0.100
8x8D03	0.9351	0.9309	0.0008	0.2731	0.4830	0.4190	0.0320	0.4110	150	0.025	0.100
8x8D04	0.9338	0.9296	0.0007	0.2727	0.4830	0.4190	0.0320	0.4110	150	0.040	0.100
8x8D05	0.9339	0.9294	0.0009	0.2700	0.4830	0.4190	0.0320	0.4100	150	0.040	0.100
8x8D06	0.9365	0.9324	0.0007	0.2777	0.4830	0.4190	0.0320	0.4110	150	0.040	0.120
8x8D07	0.9341	0.9297	0.0009	0.2694	0.4830	0.4190	0.0320	0.4110	150	0.040	0.080
8x8D08	0.9376	0.9332	0.0009	0.2841	0.4830	0.4230	0.0300	0.4140	150	0.030	0.080
Dimensions Listed for Authorized Contents					0.4830 (min.)	0.4230 (max.)		0.4140 (max.)	150 (max.)	0.000 (min.)	0.120 (max.)
bounding dimensions (B8x8D01)	0.9403	0.9363	0.0007	0.2778	0.4830	0.4230	0.0300	0.4140	150	0.000	0.120

[†] Fuel assemblies 8x8D01 through 8x8D03 have 4 water rods that are similar in size to the fuel rods, while assemblies 8x8D04 through 8x8D07 have 1 large water rod that takes the place of the 4 water rods. Fuel assembly 8x8D08 contains 3 water rods that are similar in size to the fuel rods.

Table 6.2.24
 MAXIMUM K_{EFF} VALUES FOR THE 8X8E ASSEMBLY CLASS IN THE MPC-68
 (all dimensions are in inches)

8x8E (4.2% Enrichment, Boral Fixed neutron absorber ^{10}B minimum loading of 0.0279 g/cm ²)											
59 fuel rods, 5 water rods, pitch=0.640, Zr clad											
Fuel Assembly Designation	maximum k_{eff}	calculated k_{eff}	standard deviation	EALF	cladding OD	cladding ID	cladding thickness	pellet OD	fuel length	water rod thickness	channel thickness
8x8E01	0.9312	0.9270	0.0008	0.2831	0.4930	0.4250	0.0340	0.4160	150	0.034	0.100
Dimensions Listed for Authorized Contents					0.4930 (min.)	0.4250 (max.)		0.4160 (max.)	150 (max.)	0.034 (min.)	0.100 (max.)

Table 6.2.25
 MAXIMUM K_{EFF} VALUES FOR THE 8X8F ASSEMBLY CLASS IN THE MPC-68
 (all dimensions are in inches)

8x8F (4.0% Enrichment, Boral Fixed neutron absorber ^{10}B minimum loading of 0.0279 g/cm ²)											
64 fuel rods, 4 rectangular water cross segments dividing the assembly into four quadrants, pitch=0.609, Zr clad											
Fuel Assembly Designation	maximum k_{eff}	calculated k_{eff}	standard deviation	EALF	cladding OD	cladding ID	cladding thickness	pellet OD	fuel length	water rod thickness	channel thickness
8x8F01	0.9411	0.9366	0.0009	0.2264	0.4576	0.3996	0.0290	0.3913	150	0.0315	0.055
Dimensions Listed for Authorized Contents					0.4576 (min.)	0.3996 (max.)		0.3913 (max.)	150 (max.)	0.0315 (min.)	0.055 (max.)

Table 6.2.26
 MAXIMUM K_{EFF} VALUES FOR THE 9X9A ASSEMBLY CLASS IN THE MPC-68
 (all dimensions are in inches)

9x9A (4.2% Enrichment, Boral Fixed neutron absorber ^{10}B minimum loading of 0.0279 g/cm ²)											
74/66 fuel rods [†] , 2 water rods, pitch=0.566, Zr clad											
Fuel Assembly Designation	maximum k_{eff}	calculated k_{eff}	standard deviation	EALF	cladding OD	cladding ID	cladding thickness	pellet OD	fuel length	water rod thickness	channel thickness
9x9A01 (axial segment with all rods)	0.9353	0.9310	0.0008	0.2875	0.4400	0.3840	0.0280	0.3760	150	0.030	0.100
9x9A02 (axial segment with only the full length rods)	0.9388	0.9345	0.0008	0.2228	0.4400	0.3840	0.0280	0.3760	150	0.030	0.100
9x9A03 (actual three-dimensional representation of all rods)	0.9351	0.9310	0.0007	0.2837	0.4400	0.3840	0.0280	0.3760	150/90	0.030	0.100
9x9A04 (axial segment with only the full length rods)	0.9396	0.9355	0.0007	0.2262	0.4400	0.3840	0.0280	0.3760	150	0.030	0.120
Dimensions Listed for Authorized Contents					0.4400 (min.)	0.3840 (max.)		0.3760 (max.)	150 (max.)	0.000 (min.)	0.120 (max.)
bounding dimensions (axial segment with only the full length rods) (B9x9A01)	0.9417	0.9374	0.0008	0.2236	0.4400	0.3840	0.0280	0.3760	150	0.000	0.120

[†] This assembly class contains 66 full length rods and 8 partial length rods. In order to eliminate a requirement on the length of the partial length rods, separate calculations were performed for the axial segments with and without the partial length rods.

Table 6.2.27
 MAXIMUM K_{EFF} VALUES FOR THE 9X9B ASSEMBLY CLASS IN THE MPC-68
 (all dimensions are in inches)

9x9B (4.2% Enrichment, Boral Fixed neutron absorber ^{10}B minimum loading of 0.0279 g/cm ²)												
72 fuel rods, 1 water rod (square, replacing 9 fuel rods), pitch=0.569 to 0.572 [†] ; Zr clad												
Fuel Assembly Designation	maximum k_{eff}	calculated k_{eff}	standard deviation	EALF	pitch	cladding OD	cladding ID	cladding thickness	pellet OD	fuel length	water rod thickness	channel thickness
9x9B01	0.9380	0.9336	0.0008	0.2576	0.569	0.4330	0.3807	0.0262	0.3737	150	0.0285	0.100
9x9B02	0.9373	0.9329	0.0009	0.2578	0.569	0.4330	0.3810	0.0260	0.3737	150	0.0285	0.100
9x9B03	0.9417	0.9374	0.0008	0.2545	0.572	0.4330	0.3810	0.0260	0.3737	150	0.0285	0.100
Dimensions Listed for Authorized Contents					0.572	0.4330 (min.)	0.3810 (max.)		0.3740 (max.)	150 (max.)	0.000 (min.)	0.120 (max.)
bounding dimensions (B9x9B01)	0.9436	0.9394	0.0008	0.2506	0.572	0.4330	0.3810	0.0260	0.3740 ^{††}	150	0.000	0.120

[†] This assembly class was analyzed and qualified for a small variation in the pitch.

^{††} This value was conservatively defined to be larger than any of the actual pellet diameters.

Table 6.2.28
 MAXIMUM K_{EFF} VALUES FOR THE 9X9C ASSEMBLY CLASS IN THE MPC-68
 (all dimensions are in inches)

9x9C (4.2% Enrichment, Boral Fixed neutron absorber ^{10}B minimum loading of 0.0279 g/cm ²)											
80 fuel rods, 1 water rods, pitch=0.572, Zr clad											
Fuel Assembly Designation	maximum k_{eff}	calculated k_{eff}	standard deviation	EALF	cladding OD	cladding ID	cladding thickness	pellet OD	fuel length	water rod thickness	channel thickness
9x9C01	0.9395	0.9352	0.0008	0.2698	0.4230	0.3640	0.0295	0.3565	150	0.020	0.100
Dimensions Listed for Authorized Contents					0.4230 (min.)	0.3640 (max.)		0.3565 (max.)	150 (max.)	0.020 (min.)	0.100 (max.)

Table 6.2.29
 MAXIMUM K_{EFF} VALUES FOR THE 9X9D ASSEMBLY CLASS IN THE MPC-68
 (all dimensions are in inches)

9x9D (4.2% Enrichment, Boral Fixed neutron absorber ^{10}B minimum loading of 0.0279 g/cm ²)											
79 fuel rods, 2 water rods, pitch=0.572, Zr clad											
Fuel Assembly Designation	maximum k_{eff}	calculated k_{eff}	standard deviation	EALF	cladding OD	cladding ID	cladding thickness	pellet OD	fuel length	water rod thickness	channel thickness
9x9D01	0.9394	0.9350	0.0009	0.2625	0.4240	0.3640	0.0300	0.3565	150	0.0300	0.100
Dimensions Listed for Authorized Contents					0.4240 (min.)	0.3640 (max.)		0.3565 (max.)	150 (max.)	0.0300 (min.)	0.100 (max.)

Table 6.2.30
 MAXIMUM K_{EFF} VALUES FOR THE 9X9E ASSEMBLY CLASS IN THE MPC-68
 (all dimensions are in inches)

9x9E (4.0% Enrichment, Boral Fixed neutron absorber ^{10}B minimum loading of 0.0279 g/cm ²)											
76 fuel rods, 5 water rods, pitch=0.572, Zr clad											
Fuel Assembly Designation	maximum k_{eff}	calculated k_{eff}	standard deviation	EALF	cladding OD	cladding ID	cladding thickness	pellet OD	fuel length	water rod thickness	channel thickness
9x9E01	0.9334	0.9293	0.0007	0.2227	0.4170	0.3640	0.0265	0.3530	150	0.0120	0.120
9x9E02	0.9401	0.9359	0.0008	0.2065	0.4170 0.4430	0.3640 0.3860	0.0265 0.0285	0.3530 0.3745	150	0.0120	0.120
Dimensions Listed for Authorized Contents [†]					0.4170 (min.)	0.3640 (max.)		0.3530 (max.)	150 (max.)	0.0120 (min.)	0.120 (max.)
bounding dimensions (9x9E02)	0.9401	0.9359	0.0008	0.2065	0.4170 0.4430	0.3640 0.3860	0.0265 0.0285	0.3530 0.3745	150	0.0120	0.120

[†] This fuel assembly, also known as SPC 9x9-5, contains fuel rods with different cladding and pellet diameters which do not bound each other. To be consistent in the way fuel assemblies are listed for Authorized Contents, two assembly classes (9x9E and 9x9F) are required to specify this assembly. Each class contains the actual geometry (9x9E02 and 9x9F02), as well as a hypothetical geometry with either all small rods (9x9E01) or all large rods (9x9F01). The Authorized Content lists the small rod dimensions for class 9x9E and the large rod dimensions for class 9x9F, and a note that both classes are used to qualify the assembly. The analyses demonstrate that all configurations, including the actual geometry, are acceptable.

Table 6.2.31
 MAXIMUM K_{EFF} VALUES FOR THE 9X9F ASSEMBLY CLASS IN THE MPC-68
 (all dimensions are in inches)

9x9F (4.0% Enrichment, Boral Fixed neutron absorber ^{10}B minimum loading of 0.0279 g/cm ²)											
76 fuel rods, 5 water rods, pitch=0.572, Zr clad											
Fuel Assembly Designation	maximum k_{eff}	calculated k_{eff}	standard deviation	EALF	cladding OD	cladding ID	cladding thickness	pellet OD	fuel length	water rod thickness	channel thickness
9x9F01	0.9307	0.9265	0.0007	0.2899	0.4430	0.3860	0.0285	0.3745	150	0.0120	0.120
9x9F02	0.9401	0.9359	0.0008	0.2065	0.4170 0.4430	0.3640 0.3860	0.0265 0.0285	0.3530 0.3745	150	0.0120	0.120
Dimensions Listed for Authorized Contents [†]					0.4430 (min.)	0.3860 (max.)		0.3745 (max.)	150 (max.)	0.0120 (min.)	0.120 (max.)
bounding dimensions (9x9F02)	0.9401	0.9359	0.0008	0.2065	0.4170 0.4430	0.3640 0.3860	0.0265 0.0285	0.3530 0.3745	150	0.0120	0.120

[†] This fuel assembly, also known as SPC 9x9-5, contains fuel rods with different cladding and pellet diameters which do not bound each other. To be consistent in the way fuel assemblies are listed for Authorized Contents, two assembly classes (9x9E and 9x9F) are required to specify this assembly. Each class contains the actual geometry (9x9E02 and 9x9F02), as well as a hypothetical geometry with either all small rods (9x9E01) or all large rods (9x9F01). The Authorized Content lists the small rod dimensions for class 9x9E and the large rod dimensions for class 9x9F, and a note that both classes are used to qualify the assembly. The analyses demonstrate that all configurations, including the actual geometry, are acceptable.

Table 6.2.32
 MAXIMUM K_{EFF} VALUES FOR THE 10X10A ASSEMBLY CLASS IN THE MPC-68
 (all dimensions are in inches)

10x10A (4.2% Enrichment, Boral Fixed neutron absorber ¹⁰ B, minimum loading of 0.0279 g/cm ²)											
92/78 fuel rods [†] , 2 water rods, pitch=0.510, Zr clad											
Fuel Assembly Designation	maximum k_{eff}	calculated k_{eff}	standard deviation	EALF	cladding OD	cladding ID	cladding thickness	pellet OD	fuel length	water rod thickness	channel thickness
10x10A01 (axial segment with all rods)	0.9377	0.9335	0.0008	0.3170	0.4040	0.3520	0.0260	0.3450	155	0.030	0.100
10x10A02 (axial segment with only the full length rods)	0.9426	0.9386	0.0007	0.2159	0.4040	0.3520	0.0260	0.3450	155	0.030	0.100
10x10A03 (actual three-dimensional representation of all rods)	0.9396	0.9356	0.0007	0.3169	0.4040	0.3520	0.0260	0.3450	155/90	0.030	0.100
Dimensions Listed for Authorized Contents					0.4040 (min.)	0.3520 (max.)		0.3455 (max.)	150 ^{††} (max.)	0.030 (min.)	0.120 (max.)
bounding dimensions (axial segment with only the full length rods) (B10x10A01)	0.9457 ^{†††}	0.9414	0.0008	0.2212	0.4040	0.3520	0.0260	0.3455 [‡]	155	0.030	0.120

[†] This assembly class contains 78 full-length rods and 14 partial-length rods. In order to eliminate the requirement on the length of the partial length rods, separate calculations were performed for axial segments with and without the partial length rods.

^{††} Although the analysis qualifies this assembly for a maximum active fuel length of 155 inches, the specification for authorized contents limits the active fuel length to 150 inches. This is due to the fact that the Boral Fixed neutron absorber panels are 156 inches in length.

^{†††} KENO5a verification calculation resulted in a maximum k_{eff} of 0.9453.

[‡] This value was conservatively defined to be larger than any of the actual pellet diameters.

Table 6.2.33
 MAXIMUM K_{EFF} VALUES FOR THE 10X10B ASSEMBLY CLASS IN THE MPC-68
 (all dimensions are in inches)

10x10B (4.2% Enrichment, Boral Fixed neutron absorber ^{10}B minimum loading of 0.0279 g/cm ²)											
91/83 fuel rods [†] , 1 water rods (square, replacing 9 fuel rods), pitch=0.510, Zr clad											
Fuel Assembly Designation	maximum k_{eff}	calculated k_{eff}	standard deviation	EALF	cladding OD	cladding ID	cladding thickness	pellet OD	fuel length	water rod thickness	channel thickness
10x10B01 (axial segment with all rods)	0.9384	0.9341	0.0008	0.2881	0.3957	0.3480	0.0239	0.3413	155	0.0285	0.100
10x10B02 (axial segment with only the full length rods)	0.9416	0.9373	0.0008	0.2333	0.3957	0.3480	0.0239	0.3413	155	0.0285	0.100
10x10B03 (actual three-dimensional representation of all rods)	0.9375	0.9334	0.0007	0.2856	0.3957	0.3480	0.0239	0.3413	155/90	0.0285	0.100
Dimensions Listed for Authorized Contents					0.3957 (min.)	0.3480 (max.)		0.3420 (max.)	150 ^{††} (max.)	0.000 (min.)	0.120 (max.)
bounding dimensions (axial segment with only the full length rods) (B10x10B01)	0.9436	0.9395	0.0007	0.2366	0.3957	0.3480	0.0239	0.3420 ^{†††}	155	0.000	0.120

[†] This assembly class contains 83 full length rods and 8 partial length rods. In order to eliminate a requirement on the length of the partial length rods, separate calculations were performed for the axial segments with and without the partial length rods.

^{††} Although the analysis qualifies this assembly for a maximum active fuel length of 155 inches, the specification for authorized contents limits the active fuel length to 150 inches. This is due to the fact that the Boral Fixed neutron absorber panels are 156 inches in length.

^{†††} This value was conservatively defined to be larger than any of the actual pellet diameters.

Table 6.2.34
MAXIMUM K_{EFF} VALUES FOR THE 10X10C ASSEMBLY CLASS IN THE MPC-68
 (all dimensions are in inches)

10x10C (4.2% Enrichment, Boral Fixed neutron absorber ^{10}B minimum loading of 0.0279 g/cm ²)											
96 fuel rods, 5 water rods (1 center diamond and 4 rectangular), pitch=0.488, Zr clad											
Fuel Assembly Designation	maximum k_{eff}	calculated k_{eff}	standard deviation	EALF	cladding OD	cladding ID	cladding thickness	pellet OD	fuel length	water rod thickness	channel thickness
10x10C01	0.9433	0.9392	0.0007	0.2416	0.3780	0.3294	0.0243	0.3224	150	0.031	0.055
Dimensions Listed for Authorized Contents					0.3780 (min.)	0.3294 (max.)		0.3224 (max.)	150 (max.)	0.031 (min.)	0.055 (max.)

Table 6.2.35
 MAXIMUM K_{EFF} VALUES FOR THE 10X10D ASSEMBLY CLASS IN THE MPC-68
 (all dimensions are in inches)

10x10D (4.0% Enrichment, Boral Fixed neutron absorber ^{10}B minimum loading of 0.0279 g/cm ²)											
100 fuel rods, 0 water rods, pitch=0.565, SS clad											
Fuel Assembly Designation	maximum k_{eff}	calculated k_{eff}	standard deviation	EALF	cladding OD	cladding ID	cladding thickness	pellet OD	fuel length	water rod thickness	channel thickness
10x10D01	0.9376	0.9333	0.0008	0.3355	0.3960	0.3560	0.0200	0.350	83	n/a	0.080
Dimensions Listed for Authorized Contents					0.3960 (min.)	0.3560 (max.)		0.350 (max.)	83 (max.)	n/a	0.080 (max.)

Table 6.2.36
 MAXIMUM K_{EFF} VALUES FOR THE 10X10E ASSEMBLY CLASS IN THE MPC-68
 (all dimensions are in inches)

10x10E (4.0% Enrichment, Boral Fixed neutron absorber. ^{10}B minimum loading of 0.0279 g/cm ²)											
96 fuel rods, 4 water rods, pitch=0.557, SS clad											
Fuel Assembly Designation	maximum k_{eff}	calculated k_{eff}	standard deviation	EALF	cladding OD	cladding ID	cladding thickness	pellet OD	fuel length	water rod thickness	channel thickness
10x10E01	0.9185	0.9144	0.0007	0.2936	0.3940	0.3500	0.0220	0.3430	83	0.022	0.080
Dimensions Listed for Authorized Contents					0.3940 (min.)	0.3500 (max.)		0.3430 (max.)	83 (max.)	0.022 (min.)	0.080 (max.)

Table 6.2.37
 MAXIMUM K_{EFF} VALUES FOR THE 6X6A ASSEMBLY CLASS IN THE MPC-68F
 (all dimensions are in inches)

6x6A (3.0% Enrichment [†] , Boral Fixed neutron absorber ¹⁰ B minimum loading of 0.0067 g/cm ²)													
35 or 36 fuel rods ^{††} , 1 or 0 water rods ^{††} , pitch=0.694 to 0.710 ^{††} , Zr clad													
Fuel Assembly Designation	maximum k_{eff}	calculated k_{eff}	standard deviation	EALF	pitch	fuel rods	cladding OD	cladding ID	cladding thickness	pellet OD	fuel length	water rod thickness	channel thickness
6x6A01	0.7539	0.7498	0.0007	0.2754	0.694	36	0.5645	0.4945	0.0350	0.4940	110	n/a	0.060
6x6A02	0.7517	0.7476	0.0007	0.2510	0.694	36	0.5645	0.4925	0.0360	0.4820	110	n/a	0.060
6x6A03	0.7545	0.7501	0.0008	0.2494	0.694	36	0.5645	0.4945	0.0350	0.4820	110	n/a	0.060
6x6A04	0.7537	0.7494	0.0008	0.2494	0.694	36	0.5550	0.4850	0.0350	0.4820	110	n/a	0.060
6x6A05	0.7555	0.7512	0.0008	0.2470	0.696	36	0.5625	0.4925	0.0350	0.4820	110	n/a	0.060
6x6A06	0.7618	0.7576	0.0008	0.2298	0.696	35	0.5625	0.4925	0.0350	0.4820	110	0.0	0.060
6x6A07	0.7588	0.7550	0.0007	0.2360	0.700	36	0.5555	0.4850	0.03525	0.4780	110	n/a	0.060
6x6A08	0.7808	0.7766	0.0007	0.2527	0.710	36	0.5625	0.5105	0.0260	0.4980	110	n/a	0.060
Dimensions Listed for Authorized Contents					0.710 (max.)	35 or 36	0.5550 (min.)	0.5105 (max.)	0.02225	0.4980 (max.)	120 (max.)	0.0	0.060 (max.)
bounding dimensions (B6x6A01)	0.7727	0.7685	0.0007	0.2460	0.694	35	0.5550	0.5105	0.02225	0.4980	120	0.0	0.060
bounding dimensions (B6x6A02)	0.7782	0.7738	0.0008	0.2408	0.700	35	0.5550	0.5105	0.02225	0.4980	120	0.0	0.060
bounding dimensions (B6x6A03)	0.7888	0.7846	0.0007	0.2310	0.710	35	0.5550	0.5105	0.02225	0.4980	120	0.0	0.060

[†] Although the calculations were performed for 3.0%, the enrichment is limited in the specification for authorized contents to 2.7%.

^{††} This assembly class was analyzed and qualified for a small variation in the pitch and a variation in the number of fuel and water rods.

Table 6.2.38
 MAXIMUM K_{EFF} VALUES FOR THE 6X6B ASSEMBLY CLASS IN THE MPC-68F
 (all dimensions are in inches)

6x6B (3.0% Enrichment [†] , Boral Fixed neutron absorber ¹⁰ B minimum loading of 0.0067 g/cm ²) 35 or 36 fuel rods ^{††} (up to 9 MOX rods), 1 or 0 water rods ^{††} , pitch=0.694 to 0.710 ^{††} , Zr clad													
Fuel Assembly Designation	maximum k_{eff}	calculated k_{eff}	standard deviation	EALF	pitch	fuel rods	cladding OD	cladding ID	cladding thickness	pellet OD	fuel length	water rod thickness	channel thickness
6x6B01	0.7604	0.7563	0.0007	0.2461	0.694	36	0.5645	0.4945	0.0350	0.4820	110	n/a	0.060
6x6B02	0.7618	0.7577	0.0007	0.2450	0.694	36	0.5625	0.4925	0.0350	0.4820	110	n/a	0.060
6x6B03	0.7619	0.7578	0.0007	0.2439	0.696	36	0.5625	0.4925	0.0350	0.4820	110	n/a	0.060
6x6B04	0.7686	0.7644	0.0008	0.2286	0.696	35	0.5625	0.4925	0.0350	0.4820	110	0.0	0.060
6x6B05	0.7824	0.7785	0.0006	0.2184	0.710	35	0.5625	0.4925	0.0350	0.4820	110	0.0	0.060
Dimensions Listed for Authorized Contents					0.710 (max.)	35 or 36	0.5625 (min.)	0.4945 (max.)		0.4820 (max.)	120 (max.)	0.0	0.060 (max.)
bounding dimensions (B6x6B01)	0.7822 ^{†††}	0.7783	0.0007	0.2190	0.710	35	0.5625	0.4945	0.0340	0.4820	120	0.0	0.060

Note:

1. These assemblies contain up to 9 MOX pins. The composition of the MOX fuel pins is given in Table 6.3.4.

[†] The ²³⁵U enrichment of the MOX and UO₂ pins is assumed to be 0.711% and 3.0%, respectively.

^{††} This assembly class was analyzed and qualified for a small variation in the pitch and a variation in the number of fuel and water rods.

^{†††} The k_{eff} value listed for the 6x6B05 case is slightly higher than that for the case with the bounding dimensions. However, the difference (0.0002) is well within the statistical uncertainties, and thus, the two values are statistically equivalent (within 1 σ). Therefore, the 0.7824 value is listed in Tables 6.1.2 and 6.1.3 as the maximum.

Table 6.2.39
 MAXIMUM K_{EFF} VALUES FOR THE 6X6C ASSEMBLY CLASS IN THE MPC-68F
 (all dimensions are in inches)

6x6C (3.0% Enrichment [†] , Boral Fixed neutron absorber ¹⁰ B minimum loading of 0.0067 g/cm ²)											
36 fuel rods, 0 water rods, pitch=0.740, Zr clad											
Fuel Assembly Designation	maximum k_{eff}	calculated k_{eff}	standard deviation	EALF	cladding OD	cladding ID	cladding thickness	pellet OD	fuel length	water rod thickness	channel thickness
6x6C01	0.8021	0.7980	0.0007	0.2139	0.5630	0.4990	0.0320	0.4880	77.5	n/a	0.060
Dimensions Listed for Authorized Contents					0.5630 (min.)	0.4990 (max.)		0.4880 (max.)	77.5 (max.)	n/a	0.060 (max.)

[†] Although the calculations were performed for 3.0%, the enrichment is limited in the specification for authorized contents to 2.7%.

Table 6.2.40
 MAXIMUM K_{EFF} VALUES FOR THE 7X7A ASSEMBLY CLASS IN THE MPC-68F
 (all dimensions are in inches)

7x7A (3.0% Enrichment [†] , Boral Fixed neutron absorber ¹⁰ B minimum loading of 0.0067 g/cm ²)											
49 fuel rods, 0 water rods, pitch=0.631, Zr clad											
Fuel Assembly Designation	maximum k_{eff}	calculated k_{eff}	standard deviation	EALF	cladding OD	cladding ID	cladding thickness	pellet OD	fuel length	water rod thickness	channel thickness
7x7A01	0.7974	0.7932	0.0008	0.2015	0.4860	0.4204	0.0328	0.4110	80	n/a	0.060
Dimensions Listed for Authorized Contents					0.4860 (min.)	0.4204 (max.)		0.4110 (max.)	80 (max.)	n/a	0.060 (max.)

[†] Although the calculations were performed for 3.0%, the enrichment is limited in the specification for authorized contents to 2.7%.

Table 6.2.41
MAXIMUM K_{EFF} VALUES FOR THE 8X8A ASSEMBLY CLASS IN THE MPC-68F
 (all dimensions are in inches)

8x8A (3.0% Enrichment [†] , Boral Fixed neutron absorber ¹⁰ B minimum loading of 0.0067 g/cm ²)												
63 or 64 fuel rods ^{††} , 0 water rods, pitch=0.523, Zr clad												
Fuel Assembly Designation	maximum k_{eff}	calculated k_{eff}	standard deviation	EALF	fuel rods	cladding OD	cladding ID	cladding thickness	pellet OD	fuel length	water rod thickness	channel thickness
8x8A01	0.7685	0.7644	0.0007	0.2227	64	0.4120	0.3620	0.0250	0.3580	110	n/a	0.100
8x8A02	0.7697	0.7656	0.0007	0.2158	63	0.4120	0.3620	0.0250	0.3580	120	n/a	0.100
Dimensions Listed for Authorized Contents					63	0.4120 (min.)	0.3620 (max.)		0.3580 (max.)	110 (max.)	n/a	0.100 (max.)
bounding dimensions (8x8A02)	0.7697	0.7656	0.0007	0.2158	63	0.4120	0.3620	0.0250	0.3580	120	n/a	0.100

[†] Although the calculations were performed for 3.0%, the enrichment is limited in the specification for authorized contents to 2.7%.

^{††} This assembly class was analyzed and qualified for a variation in the number of fuel rods.

Table 6.2.42

SPECIFICATION OF THE THORIA ROD CANISTER AND THE THORIA RODS

Canister ID	4.81"
Canister Wall Thickness	0.11"
Separator Assembly Plates Thickness	0.11"
Cladding OD	0.412"
Cladding ID	0.362"
Pellet OD	0.358"
Active Length	110.5"
Fuel Composition	1.8% UO ₂ and 98.2% ThO ₂
Initial Enrichment	93.5 wt% ²³⁵ U for 1.8% of the fuel
Maximum k_{eff}	0.1813
Calculated k_{eff}	0.1779
Standard Deviation	0.0004

Table 6.2.43
 MAXIMUM K_{EFF} VALUES FOR THE 14X14E ASSEMBLY CLASS IN THE MPC-24
 (all dimensions are in inches)

14x14E (5.0% Enrichment, Borated Fixed neutron absorber ^{10}B minimum loading of 0.02 g/cm ³)										
173 fuel rods, 0 guide tubes, pitch=0.453 and 0.441, SS clad [†]										
Fuel Assembly Designation	maximum k_{eff}	calculated k_{eff}	standard deviation	EALF	cladding OD	cladding ID	cladding thickness	pellet OD	fuel length ^{††}	guide tube thickness
14x14E01	0.7598	0.7555	0.0008	0.3890	0.3415	0.3175 0.2845 0.3015	0.0120 0.0285 0.0200	0.3130 0.2800 0.2970	102	0.0000
14x14E02	0.7627	0.7586	0.0007	0.3607	0.3415	0.3175	0.0120	0.3130	102	0.0000
14x14E03	0.6952	0.6909	0.0008	0.2905	0.3415	0.2845	0.0285	0.2800	102	0.0000
Dimensions Listed for Authorized Contents					0.3415 (min.)	0.3175 (max.)		0.3130 (max.)	102 (max.)	0.0000 (min.)
Bounding dimensions (14x14E02)	0.7627	0.7586	0.0007	0.3607	0.3415	0.3175	0.0120	0.3130	102	0.0000

[†] This is the IP-1 fuel assembly at Indian Point. This assembly is a 14x14 assembly with 23 fuel rods omitted to allow passage of control rods between assemblies. Fuel rod dimensions are bounding for each of the three types of rods found in the IP-1 fuel assembly.

^{††} Calculations were conservatively performed for a fuel length of 150 inches.

Table 6.2.44
 MAXIMUM K_{EFF} VALUES FOR THE 9X9G ASSEMBLY CLASS IN THE MPC-68 and MPC-68FF
 (all dimensions are in inches)

9x9G (4.2% Enrichment, Boral Fixed neutron absorber ^{10}B minimum loading of 0.0279 g/cm ²)											
72 fuel rods, 1 water rod (square, replacing 9 fuel rods), pitch=0.572, Zr clad											
Fuel Assembly Designation	maximum k_{eff}	calculated k_{eff}	standard deviation	EALF	cladding OD	cladding ID	cladding thickness	pellet OD	fuel length	water rod thickness	channel thickness
9x9G01	0.9309	0.9265	0.0008	0.2191	0.4240	0.3640	0.0300	0.3565	150	0.0320	0.120
Dimensions Listed for Authorized Contents					0.4240 (min.)	0.3640 (max.)		0.3565 (max.)	150 (max.)	0.0320 (min.)	0.120 (max.)

6.3 MODEL SPECIFICATION

In compliance with the requirements of 10CFR71.31(a)(1), 10CFR71.33(a)(5), and 10CFR71.33(b), this section provides a description of the HI-STAR 100 System in sufficient detail to identify the package accurately and provide a sufficient basis for the evaluation of the package.

6.3.1 Description of Calculational Model

Figures 6.3.1 through 6.3.3 show representative horizontal cross sections of the four types of cells used in the calculations, and Figures 6.3.4 through 6.3.6 illustrate the basket configurations used. Four different MPC fuel basket designs were evaluated as follows:

- a 24 PWR assembly basket,
- an optimized 24 PWR assembly basket (MPC-24E/EF and Trojan MPC-24E/EF),
- a 32 PWR assembly basket, and
- a 68 BWR assembly basket.

For all basket designs, the same techniques and the same level of detail are used in the calculational models.

Full three-dimensional calculations were used, assuming the axial configuration shown in Figure 6.3.7, and conservatively neglecting the absorption in the overpack neutron shielding material (Holtite-A). Although the ~~Boral-fixed~~ neutron absorber panels are 156 inches in length, which is much longer than the active fuel length (maximum of 150 inches), they are assumed equal to the active fuel length in the calculations, except for the Trojan MPC-24E/EF. Due to the reduced height of the Trojan MPCs, there is the potential of a misalignment of about 1 inch between the active length and the ~~Boral-fixed neutron absorber~~ at the bottom of the active region. Conservatively, a misalignment of 3 inches is assumed in the calculational model for the Trojan MPCs. As shown on the drawings in Section 1.4, 16 of the 24 periphery ~~Boral-fixed neutron absorber~~ panels on the MPC-24 have reduced width (i.e., 6.25 inches wide as opposed to 7.5 inches). However, the calculational models for the MPC-24 conservatively assume all of the periphery ~~Boral-fixed neutron absorber~~ panels are 6.25 inches in width. ~~Note that Figures 6.3.1 through 6.3.3 show Boral as the fixed neutron absorber. The effect of using Metamic as fixed neutron absorber is discussed in Subsection 6.4.12.~~

The calculational model explicitly defines the fuel rods and cladding, the guide tubes (or water rods for BWR assemblies), the water-gaps and ~~Boral-fixed neutron absorber~~ panels on the

stainless steel walls of the basket cells. Under normal conditions of transport, when the MPC is dry, the resultant reactivity with the design basis fuel is very low ($k_{\text{eff}} < 0.5$). For the flooded condition (loading, unloading, and hypothetical accident condition), water was assumed to be present in the fuel rod pellet-to-clad gap regions (see Subsection 6.4.2.3 for justification). Appendix 6.D provides sample input files for the MPC-24 and MPC-68 basket designs in the HI-STAR 100 System.

The water thickness above and below the fuel is intentionally maintained less than or equal to the actual water thickness. This assures that any positive reactivity effect of the steel in the MPC is conservatively included.

As indicated in Figures 6.3.1 through 6.3.3 and in Tables 6.3.1 and 6.3.2, calculations were made with dimensions assumed to be at their most conservative value with respect to criticality. CASMO and MCNP4a were used to determine the direction of the manufacturing tolerances which produced the most adverse effect on criticality. After the directional effect (positive effect with an increase in reactivity; or negative effect with a decrease in reactivity) of the manufacturing tolerances was determined, the criticality analyses were performed using the worst case tolerances in the direction which would increase reactivity.

CASMO-3 and -4 were used for one of each of the two principal basket designs, i.e. for the fluxtrap design MPC-24 and for the non-fluxtrap design MPC-68. The effects are shown in Table 6.3.1 which also identifies the approximate magnitude of the tolerances on reactivity. The conclusions in Table 6.3.1 are directly applicable to the MPC-24E/EF and the MPC-32, due to the similarity in the basket designs.

Additionally, MCNP4a calculations are performed to evaluate the tolerances of the various basket dimensions of the MPC-68, MPC-24 and MPC-32 in further detail. The various basket dimensions are inter-dependent, and therefore cannot be individually varied (i.e., reduction in one parameter requires a corresponding reduction or increase in another parameter). Thus, it is not possible to determine the reactivity effect of each individual dimensional tolerance separately. However, it is possible to determine the reactivity effect of the dimensional tolerances by evaluating the various possible dimensional combinations. To this end, an evaluation of the various possible dimensional combinations was performed using MCNP4a, with fuel assemblies centered in the fuel storage locations. Calculated k_{eff} results (which do not include the bias, uncertainties, or calculational statistics), along with the actual dimensions, for a number of dimensional combinations are shown in Table 6.3.2 for the reference PWR and BWR fuel assemblies. Each of the basket dimensions are evaluated for their minimum, nominal and maximum values. Due to the close similarity between the MPC-24 and MPC-24E, the basket dimensions are only evaluated for the MPC-24, and the same dimensional assumptions are applied to both MPC designs.

Based on the MCNP4a and CASMO calculations, the conservative dimensional assumptions listed in Table 6.3.3 were determined for the MPC basket designs. Because the reactivity effect (positive or negative) of the manufacturing tolerances are not assembly dependent, these dimensional assumptions were employed for the criticality analyses.

The design parameters important to criticality safety are: fuel enrichment, the inherent geometry of the fuel basket structure, and the fixed neutron absorbing panels (~~Boral~~). None of these parameters are affected by the hypothetical accident conditions of transport.

During the hypothetical accident conditions of transport, the HI-STAR 100 System is assumed to be flooded to such an extent as to cause the maximum reactivity and to have full water reflection to such an extent as to cause the maximum reactivity. Further, arrays of packages under the hypothetical accident conditions must be evaluated to determine the maximum number of packages that may be transported in a single shipment. Thus, the only differences between the normal and hypothetical accident condition calculational models are the internal/external moderator densities and the boundary conditions (to simulate an infinite array of HI-STAR 100 Systems).

6.3.2 Cask Regional Densities

Composition of the various components of the principal designs of the HI-STAR 100 Systems are listed in Table 6.3.4. In this table, only the composition of fresh fuel is listed. For a discussion on the composition of spent fuel for burnup credit in the MPC-32 see Appendix 6.E.

The HI-STAR 100 System is designed such that the fixed neutron absorber (~~Boral~~) will remain effective for a period greater than 20 years, and there are no credible means to lose it. A detailed physical description, historical applications, unique characteristics, service experience, and manufacturing quality assurance of ~~Boral~~ *fixed neutron absorbers* are provided in Subsection 1.2.1.4.1.

The continued efficacy of the ~~Boral~~ *fixed neutron absorber* is assured by acceptance testing, documented in ~~Subsection 8.1.5.3~~ *Chapter 8*, to validate the ^{10}B (poison) concentration in the ~~Boral~~ *fixed neutron absorber*. To demonstrate that the neutron flux from the irradiated fuel results in a negligible depletion of the poison material, an MCNP4a calculation of the number of neutrons absorbed in the ^{10}B was performed. The calculation conservatively assumed a constant neutron source for 50 years equal to the initial source for the design basis fuel, as determined in Section 5.2, and shows that the fraction of ^{10}B atoms destroyed is only 2.6E-09 in 50 years. Thus, the reduction in ^{10}B concentration in the ~~Boral~~ *fixed neutron absorber* by neutron absorption is negligible. In addition, the structural analysis demonstrates that the sheathing, which affixes the ~~Boral~~ *fixed neutron absorber* panel, remains in place during all hypothetical accident conditions, and thus, the ~~Boral~~ *fixed neutron absorber* panel remains permanently fixed.

Therefore, there is no need to provide a surveillance or monitoring program to verify the continued efficacy of the neutron absorber.

6.3.3 Eccentric Positioning of Assemblies in Fuel Storage Cells

Up to and including Revision 9 of this SAR, all criticality calculations were performed with fuel assemblies centered in the fuel storage locations since the effect of credible eccentric fuel positioning was judged to be not significant. Starting in Revision 10 of this SAR, the potential reactivity effect of eccentric positioning of assemblies in the fuel storage locations is accounted for in a conservatively bounding fashion, as described further in this subsection, for all new or changed MPC designs or assembly classes. The calculations in this subsection serve to determine the highest maximum k_{eff} value for each of these assembly class and basket combinations, that is then reported in the summary tables in Section 6.1 and the results tables in Section 6.4. Further, the calculations in this subsection are used to determine the assembly class in each basket with the highest maximum k_{eff} that is then used to demonstrate compliance with the requirements of 10CFR71.55 and 10CFR71.59. All other calculations throughout this chapter, such as studies to determine bounding fuel dimension, bounding basket dimensions, or bounding moderation conditions, are performed with assemblies centered in the fuel storage locations.

To conservatively account for eccentric fuel positioning in the fuel storage cells, three different configurations are analyzed, and the results are compared to determine the bounding configuration:

- Cell Center Configuration: All assemblies centered in their fuel storage cell; same configuration that is used in Section 6.2 and Section 6.3.1;
- Basket Center Configuration: All assemblies in the basket are moved as closely to the center of the basket as permitted by the basket geometry; and
- Basket Periphery Configuration: All assemblies in the basket are moved furthest away from the basket center, and as closely to the periphery of the basket as possible.

It needs to be noted that the two eccentric configurations are hypothetical, since there is no known physical effect that could move all assemblies within a basket consistently to the center or periphery. Instead, the most likely configuration would be that all assemblies are moved in the same direction when the cask is in a horizontal position, and that assemblies are positioned randomly when the cask is in a vertical position. Further, it is not credible to assume that any such configuration could exist by chance. Even if the probability for a single assembly placed in the corner towards the basket center would be $1/5$ (i.e. assuming only the center and four corner positions in each cell, all with equal probability), then the probability that all assemblies would be located towards the center would be $(1/5)^{24}$ or approximately 10^{-17} for the MPC-24, $(1/5)^{32}$ or approximately 10^{-23} for the MPC-32, and $(1/5)^{68}$ or approximately 10^{-48} for the MPC-68. However, since the configurations listed above bound all credible configurations, they are

conservatively used in the analyses.

The results are presented in Table 6.3.5 for the MPC-24, Table 6.3.6 for the MPC-24E/EF, Table 6.3.7 for the Trojan MPC-24E/EF, and Table 6.3.8 for the MPC-68. For evaluations of eccentric fuel positions in the MPC-32 with burnup credit see Appendix 6.E. Each table shows the maximum k_{eff} value for centered and the two eccentric configurations for each of the assembly classes, and indicates the bounding configuration. The results are summarized as follows:

- In all cases, moving the assemblies to the periphery of the basket results in a reduction in reactivity, compared to the cell centered position.
- Most cases show the maximum reactivity for the basket center configuration, however, in some cases the reactivity is higher for the cell center configuration.

For each of the assembly class and basket combinations listed in Tables 6.3.5 through Table 6.3.8, the configuration showing the highest reactivity is used as the bounding configuration, and listed in the respective tables in Section 6.1. and 6.4. For evaluations of eccentric fuel positions in the MPC-32 with burnup credit see Appendix 6.E.

Table 6.3.1

CASMO-4 CALCULATIONS FOR EFFECT OF TOLERANCES AND TEMPERATURE

Change in Nominal Parameter [†]	Δk for Maximum Tolerance		Action/Modeling Assumption
	MPC-24	MPC-68 [‡]	
Reduce Boralfixed neutron absorber Width to Minimum	N/A ^{†††} min. = nom. = 7.5" and 6.25"	N/A ^{†††} min. = nom. = 4.75"	Assume minimum Boralfixed neutron absorber width
Increase UO ₂ Density to Maximum	+0.0017 max. = 10.522 g/cc nom. = 10.412 g/cc	+0.0014 max. = 10.522 g/cc nom. = 10.412 g/cc	Assume maximum UO ₂ density
Reduce Box Inside Dimension (I.D.) to Minimum	-0.0005 min. = 8.86" nom. = 8.92"	See Table 6.3.2	Assume maximum box I.D. for the MPC-24
Increase Box Inside Dimension (I.D.) to Maximum	+0.0007 max. = 8.98" nom. = 8.92"	-0.0030 max. = 6.113" nom. = 6.053"	Assume minimum box I.D. for the MPC-68
Decrease Water Gap to Minimum	+0.0069 min. = 1.09" nom. = 1.15"	N/A	Assume minimum water gap in the MPC-24

[†] Reduction (or increase) in a parameter indicates that the parameter is changed to its minimum (or maximum) value.

[‡] Calculations for the MPC-68 were performed with CASMO-3 [6.3.1 – 6.3.4].

^{†††} The ~~Boralfixed~~ neutron absorber width for the MPC-68 is 4.75" +0.125", -0", the ~~Boralfixed~~ neutron absorber widths for the MPC-24 are 7.5" +0.125", -0" and 6.25" +0.125" -0" (i.e., the nominal and minimum values are the same).

Table 6.3.1 (continued)

CASMO-4 CALCULATIONS FOR EFFECT OF TOLERANCES AND TEMPERATURE

Change in Nominal Parameter	Δk Maximum Tolerance		Action/Modeling Assumption
	MPC-24	MPC-68 [‡]	
Increase in Temperature			Assume 20°C
20°C	Ref.	Ref.	
40°C	-0.0030	-0.0039	
70°C	-0.0089	-0.0136	
100°C	-0.0162	-0.0193	
10% Void in Moderator			Assume no void
20°C with no void	Ref.	Ref.	
20°C	-0.0251	-0.0241	
100°C	-0.0412	-0.0432	
Removal of Flow Channel (BWR)	N/A	-0.0073	Assume flow channel present for MPC-68

[‡] Calculations for the MPC-68 were performed with CASMO-3 [6.3.1 – 6.3.4].

Table 6.3.2

MCNP4a EVALUATION OF BASKET MANUFACTURING TOLERANCES[†]

Pitch		Box I.D.		Box Wall Thickness		MCNP4a Calculated k_{eff}
MPC-24 ^{††} (17x17A01 @ 4.0% Enrichment)						
nominal	(10.906")	maximum	(8.98")	nominal	(5/16")	0.9325±0.0008 ^{†††}
minimum	(10.846")	nominal	(8.92")	nominal	(5/16")	0.9300±0.0008
nominal	(10.906")	nom. -0.04"	(8.88")	nom. + 0.05"	(0.3625")	0.9305±0.0007
MPC-68 (8x8C04 @ 4.2% Enrichment)						
minimum	(6.43")	minimum	(5.993")	nominal	(1/4")	0.9307±0.0007
nominal	(6.49")	nominal	(6.053")	nominal	(1/4")	0.9274±0.0007
maximum	(6.55")	maximum	(6.113")	nominal	(1/4")	0.9272±0.0008
nom. + 0.05"	(6.54")	nominal	(6.053")	nom. + 0.05"	(0.30")	0.9267±0.0007

Note: Values in parentheses are the actual value used.

[†] Tolerance for pitch and box I.D. are $\pm 0.06"$.
Tolerance for box wall thickness is $+0.05"$, $-0.00"$.

^{††} All calculations for the MPC-24 assume minimum water gap thickness (1.09").

^{†††} Numbers are 1σ statistical uncertainties.

Table 6.3.2 (cont.)

MCNP4a EVALUATION OF BASKET MANUFACTURING TOLERANCES[†]

Pitch		Box I.D.		Box Wall Thickness		MCNP4a Calculated k_{eff}
MPC-32 (17x17A @ 4.0% Enrichment)						
minimum	(9.158")	minimum	(8.73")	nominal	(9/32")	later
nominal	(9.218")	nominal	(8.79")	nominal	(9/32")	later
maximum	(9.278")	maximum	(8.85")	nominal	(9/32")	later
nominal+0.05"	(9.268")	nominal	(8.79")	nominal+0.05"	(0.331")	later
minimum+0.05"	(9.208")	minimum	(8.73")	nominal+0.05"	(0.331")	later
maximum	(9.278")	Maximum-0.05"	(8.80")	nominal+0.05"	(0.331")	later

Notes:

1. Values in parentheses are the actual value used.

[†] Tolerance for pitch and box I.D. are $\pm 0.06"$.
Tolerance for box wall thickness is $+0.05"$, $-0.00"$.

Table 6.3.3

BASKET DIMENSIONAL ASSUMPTIONS

Basket Type	Pitch	Box I.D.	Box Wall Thickness	Water-Gap Flux Trap
MPC-24	nominal (10.906")	maximum (8.98")	nominal (5/16")	minimum (1.09")
MPC-24E	nominal (10.847")	maximum (8.81", 9.11" for DFC Positions, 9.36" for DFC Positions in Trojan MPC)	nominal (5/16")	minimum (1.076", 0.776" for DFC Positions, 0.526" for DFC Positions in Trojan MPC)
MPC-32	minimum (9.158")	minimum (8.73")	nominal (9/32")	N/A
MPC-68	minimum (6.43")	minimum (5.993")	nominal (1/4")	N/A

Table 6.3.4

COMPOSITION OF THE MAJOR COMPONENTS OF THE HI-STAR 100 SYSTEM

MPC-24		
UO₂ 4.0% ENRICHMENT, DENSITY (g/cc) = 10.522		
Nuclide	Atom-Density	Wgt. Fraction
8016	4.693E-02	1.185E-01
92235	9.505E-04	3.526E-02
92238	2.252E-02	8.462E-01
BORAL (0.02 g ¹⁰B/cm sq), DENSITY (g/cc) = 2.660		
Nuclide	Atom-Density	Wgt. Fraction
5010	8.707E-03	5.443E-02
5011	3.512E-02	2.414E-01
6012	1.095E-02	8.210E-02
13027	3.694E-02	6.222E-01
MPC-32		
BORAL (0.0279 g ¹⁰B/cm sq), DENSITY (g/cc) = 2.660		
Nuclide	Atom-Density	Wgt. Fraction
5010	8.071E-03	5.089E-02
5011	3.255E-02	2.257E-01
6012	1.015E-02	7.675E-02
13027	3.805E-02	6.467E-01

Table 6.3.4 (continued)

COMPOSITION OF THE MAJOR COMPONENTS OF THE HI-STAR 100 SYSTEM

MPC-68		
UO₂ 4.2% ENRICHMENT, DENSITY (g/cc) = 10.522		
Nuclide	Atom-Density	Wgt. Fraction
8016	4.697E-02	1.185E-01
92235	9.983E-04	3.702E-02
92238	2.248E-02	8.445E-01
UO₂ 3.0% ENRICHMENT, DENSITY (g/cc) = 10.522		
Nuclide	Atom-Density	Wgt. Fraction
8016	4.695E-02	1.185E-01
92235	7.127E-04	2.644E-02
92238	2.276E-02	8.550E-01
MOX FUEL[†], DENSITY (g/cc) = 10.522		
Nuclide	Atom-Density	Wgt. Fraction
8016	4.714E-02	1.190E-01
92235	1.719E-04	6.380E-03
92238	2.285E-02	8.584E-01
94239	3.876E-04	1.461E-02
94240	9.177E-06	3.400E-04
94241	3.247E-05	1.240E-03
94242	2.118E-06	7.000E-05

[†] The Pu-238, which is an absorber, was conservatively neglected in the MOX description for analysis purposes.

Table 6.3.4 (continued)

COMPOSITION OF THE MAJOR COMPONENTS OF THE HI-STAR 100 SYSTEM

BORAL (0.0279 g ¹⁰B/cm sq), DENSITY (g/cc) = 2.660		
Nuclide	Atom-Density	Wgt. Fraction
5010	8.071E-03	5.089E-02
5011	3.255E-02	2.257E-01
6012	1.015E-02	7.675E-02
13027	3.805E-02	6.467E-01
FUEL IN THORIA RODS, DENSITY (g/cc) = 10.522		
Nuclide	Atom-Density	Wgt. Fraction
8016	4.798E-02	1.212E-01
92235	4.001E-04	1.484E-02
92238	2.742E-05	1.030E-03
90232	2.357E-02	8.630E-01

Table 6.3.4 (continued)

COMPOSITION OF THE MAJOR COMPONENTS OF THE HI-STAR 100 SYSTEM

COMMON MATERIALS		
ZR CLAD, DENSITY (g/cc) = 6.550		
Nuclide	Atom-Density	Wgt. Fraction
40000	4.323E-02	1.000E+00
MODERATOR (H₂O), DENSITY (g/cc) = 1.000		
Nuclide	Atom-Density	Wgt. Fraction
1001	6.688E-02	1.119E-01
8016	3.344E-02	8.881E-01
STAINLESS STEEL, DENSITY (g/cc) = 7.840		
Nuclide	Atom-Density	Wgt. Fraction
24000	1.761E-02	1.894E-01
25055	1.761E-03	2.001E-02
26000	5.977E-02	6.905E-01
28000	8.239E-03	1.000E-01
ALUMINUM, DENSITY (g/cc) = 2.700		
Nuclide	Atom-Density	Wgt. Fraction
13027	6.026E-02	1.000E+00

Table 6.3.5

EFFECT OF ECCENTRIC FUEL POSITIONING IN THE MPC-24

Fuel Assembly Class	Maximum k_{eff}			Bounding Configuration	Bounding Maximum k_{eff}
	Cell Center Configuration	Basket Center Configuration	Basket Periphery Configuration		
14x14A	0.9296	0.9271	0.8951	Cell Center	0.9296
14x14B	0.9228	0.9207	0.8904	Cell Center	0.9228
14x14C	0.9287	0.9307	0.9068	Basket Center	0.9307
14x14D	0.8507	0.8498	0.8225	Cell Center	0.8507
14x14E	0.7627	0.7608	0.7003	Cell Center	0.7627
15x15A	0.9204	0.9227	0.9037	Basket Center	0.9227
15x15B	0.9388	0.9388	0.9240	Basket Center	0.9388
15x15C	0.9361	0.9351	0.9218	Cell Center	0.9361
15x15D	0.9367	0.9364	0.9248	Cell Center	0.9367
15x15E	0.9368	0.9392	0.9264	Basket Center	0.9392
15x15F	0.9395	0.9410	0.9271	Basket Center	0.9410
15x15G	0.8876	0.8907	0.8761	Basket Center	0.8907
15x15H	0.9337	0.9335	0.9214	Cell Center	0.9337
16x16A	0.9287	0.9284	0.9051	Cell Center	0.9287
17x17A	0.9368	0.9362	0.9221	Cell Center	0.9368
17x17B	0.9324	0.9355	0.9204	Basket Center	0.9355
17x17C	0.9336	0.9349	0.9225	Basket Center	0.9349

Table 6.3.6

EFFECT OF ECCENTRIC FUEL POSITIONING IN THE MPC-24E/EF

Fuel Assembly Class	Maximum k_{eff}			Bounding Configuration	Bounding Maximum k_{eff}
	Cell Center Configuration	Basket Center Configuration	Basket Periphery Configuration		
14x14A	0.9380	0.9327	0.9080	Cell Center	0.9380
14x14B	0.9312	0.9288	0.9029	Cell Center	0.9312
14x14C	0.9356	0.9365	0.9189	Basket Center	0.9365
14x14D	0.8875	0.8857	0.8621	Cell Center	0.8875
14x14E	0.7651	0.7536	0.7001	Cell Center	0.7651
15x15A	0.9336	0.9304	0.9188	Cell Center	0.9336
15x15B	0.9465	0.9487	0.9367	Basket Center	0.9487
15x15C	0.9462	0.9452	0.9348	Cell Center	0.9462
15x15D	0.9440	0.9445	0.9343	Basket Center	0.9445
15x15E	0.9455	0.9471	0.9372	Basket Center	0.9471
15x15F	0.9468	0.9495	0.9406	Basket Center	0.9495
15x15G	0.9054	0.9062	0.8970	Basket Center	0.9062
15x15H	0.9423	0.9455	0.9365	Basket Center	0.9455
16x16A	0.9341	0.9358	0.9183	Basket Center	0.9358
17x17A	0.9447	0.9443	0.9355	Cell Center	0.9447
17x17B	0.9421	0.9438	0.9303	Basket Center	0.9438
17x17C	0.9433	0.9431	0.9347	Cell Center	0.9433

Table 6.3.7

EFFECT OF ECCENTRIC FUEL POSITIONING IN THE TROJAN MPC-24E/EF

Fuel Assembly Class	Maximum k_{eff}			Bounding Configuration	Bounding Maximum k_{eff}
	Cell Center Configuration	Basket Center Configuration	Basket Periphery Configuration		
17x17B (Intact Fuel)	0.9161	0.9187	0.9059	Basket Center	0.9187
17x17B (Intact Fuel and Damaged Fuel/Fuel Debris)	0.9377	0.9353	0.9338	Cell Center	0.9377

Table 6.3.8

EFFECT OF ECCENTRIC FUEL POSITIONING IN THE MPC-68

Fuel Assembly Class	Maximum k_{eff}			Bounding Configuration	Bounding Maximum k_{eff}
	Cell Center Configuration	Basket Center Configuration	Basket Periphery Configuration		
8x8F	0.9411	0.9459	0.9193	Basket Center	0.9459
9x9E/F	0.9401	0.9486	0.9166	Basket Center	0.9486
9x9G	0.9309	0.9383	0.9124	Basket Center	0.9383

6.4 CRITICALITY CALCULATIONS

6.4.1 Calculational or Experimental Method

The principal method for the criticality analysis is the general three-dimensional continuous energy Monte Carlo N-Particle code MCNP4a [6.1.4] developed at the Los Alamos National Laboratory. MCNP4a was selected because it has been extensively used and verified and has all of the necessary features for this analysis. MCNP4a calculations used continuous energy cross-section data based on ENDF/B-V[†], as distributed with the code [6.1.4]. Independent verification calculations were performed with NITAWL-KENO5a [6.1.5], which is a three-dimensional multigroup Monte Carlo code developed at the Oak Ridge National Laboratory. The KENO5a calculations used the 238-group cross-section library, which is based on ENDF/B-V data and is distributed as part of the SCALE-4.3 package [6.4.1], in association with the NITAWL-II program [6.1.6], which adjusts the uranium-238 cross sections to compensate for resonance self-shielding effects. The Dancoff factors required by NITAWL-II were calculated with the CELLDAN code [6.1.13], which includes the SUPERDAN code [6.1.7] as a subroutine.

The convergence of a Monte Carlo criticality problem is sensitive to the following parameters: (1) number of histories per cycle, (2) the number of cycles skipped before averaging, (3) the total number of cycles and (4) the initial source distribution. The MCNP4a criticality output contains a great deal of useful information that may be used to determine the acceptability of the problem convergence. This information was used in parametric studies to develop appropriate values for the aforementioned criticality parameters to be used in the criticality calculations for this submittal. Based on these studies, calculations assuming fresh fuel used a minimum of 5,000 simulated histories per cycle, a minimum of 20 cycles were skipped before averaging, a minimum of 100 cycles were accumulated, and the initial source was specified as uniform over the fueled regions (assemblies). For parameters used in the burnup credit calculations see Appendix 6.E. Further, the output was examined to ensure that each calculation achieved acceptable convergence. These parameters represent an acceptable compromise between calculational precision and computational time. Appendix 6.D provides sample input files for the MPC-24 and MPC-68 basket in the HI-STAR 100 System.

CASMO-4 [6.1.10-6.1.12] was used for determining the small incremental reactivity effects of manufacturing tolerances. Although CASMO has been extensively benchmarked, these calculations are used only to establish direction of reactivity uncertainties due to manufacturing tolerances (and their magnitude). This allows the MCNP4a calculational model to use the worst combination of manufacturing tolerances. Table 6.3.1 shows results of the CASMO calculations. Additionally, CASMO-4 was used to determine the isotopic composition of spent fuel for burnup credit in the MPC-32 (see Appendix 6.E).

[†] For burnup credit calculations in the MPC-32, ENDF/B-VI cross sections are used for nuclides where ENDF/B-V cross sections are not available.

6.4.2 Fuel Loading or Other Contents Loading Optimization

The basket designs are intended to safely accommodate the candidate fuel assemblies with enrichments indicated in Tables 6.1.1 through 6.1.3 and 6.1.5 through 6.1.7. The calculations were based on the assumption that the HI-STAR 100 System was fully flooded with water. In all cases, the calculations include bias and calculational uncertainties, as well as the reactivity effects of manufacturing tolerances, determined by assuming the worst case geometry.

6.4.2.1 Internal and External Moderation

The regulations in 10CFR71.55 include the requirement that the system remains subcritical when assuming moderation to the most reactive credible extent. The regulations in 10CFR71.59 require subcriticality for package arrays under different moderation conditions. The calculations in this section demonstrate that the HI-STAR 100 System remains subcritical for all credible conditions of moderation, and that the system fulfills all requirements of 10CFR71.55 and 10CFR71.59. The following subsections 6.4.2.1.1 through 6.4.2.4 present various studies to confirm or identify the most reactive configuration or moderation condition. Specifically, the following conditions are analyzed:

- Reduced internal and external water density for single packages (6.4.2.1.1) and package arrays (6.4.2.1.2);
- Variation in package to package distance in package arrays (6.4.2.1.2);
- Partial internal flooding of package (6.4.2.2);
- Flooding of pellet to cladding gap of the fuel rods (6.4.2.3); and
- Preferential flooding, i.e. uneven flooding inside the package (6.4.2.4).

The calculations that specifically demonstrate compliance with the individual requirements of 10CFR71.55 and 10CFR71.59 are presented in Section 6.4.3. These calculations are performed for all MPCs.

The studies in subsections 6.4.2.1.1 through 6.4.2.4 have been performed for both principal basket designs (flux-trap and non-flux-trap) and for both fuel designs (BWR and PWR). Specifically, the studies are performed with the MPC-24 (flux-trap design / PWR fuel) and the MPC-68 (non-flux-trap design / BWR fuel). The results of the studies show a consistent behavior of the different basket designs and fuel types for different moderation conditions. Consequently, the conclusions drawn from these studies are directly applicable to the remaining baskets, namely the MPC-24E/EF (flux-trap design, PWR), MPC-32 (non-flux-trap design, PWR) and MPC-68F (non-flux-trap design, BWR), and no further studies are required for these baskets.

The studies in subsection 6.4.2.1.1 through 6.4.2.4 have been performed with the fuel assemblies centered in each storage location in the basket, which is not necessarily the most reactive position. However, this assumption is acceptable since the objective of these studies is to determine the most reactive moderation condition, not the highest reactivity. The calculations in Section 6.4.3 that demonstrate compliance with 10CFR71.55 and 19CFR71.59 are performed with the most reactive assembly position as discussed in Section 6.3.3.

Regarding the effect of low moderator density it is noted that with a neutron absorber present (i.e., the ~~Boral~~ *fixed neutron absorber* sheets on the steel walls of the storage compartments), the phenomenon of a peak in reactivity at a hypothetical low moderator density (sometimes called "optimum" moderation) does not occur to any significant extent. In a definitive study, Cano, et al. [6.4.2] has demonstrated that the phenomenon of a peak in reactivity at low moderator densities does not occur when strong neutron absorbing material is present or in the absence of large water spaces between fuel assemblies in storage. Nevertheless, calculations for a single reflected cask and for infinite arrays of casks were made to confirm that the phenomenon does not occur with low density water inside or outside the HI-STAR 100 Systems.

6.4.2.1.1 Single Package Evaluation

Calculations for a single package are performed for the MPC-24 and MPC-68. The Calculational model consists of the HI-STAR System surrounded by a rectangular box filled with water. The neutron absorber on the outside of the HI-STAR is neglected, since it might be damaged under accident conditions, and since it is conservative to replace the neutron absorber (Holtite-A) with a neutron reflector (water). The minimum water thickness on each side of the cask is 30 cm, which effectively represents full water reflection. The outer surfaces of the surrounding box are conservatively set to be fully reflective, which effectively models a three dimensional array of cask systems with a minimum surface to surface distance of 60 cm. The calculations with internal and external moderators of various densities are shown in Table 6.4.1. For comparison purposes, a calculation for a single unreflected cask (Case 1) is also included in Table 6.4.1. At 100% external moderator density, Case 2 corresponds to a single fully-flooded cask, fully reflected by water. Figure 6.4.9 plots calculated k_{eff} values ($\pm 2\sigma$) as a function of internal moderator density for both MPC designs with 100% external moderator density (i.e., full water reflection).

Results listed in Table 6.4.1 and plotted in Figure 6.4.9 support the following conclusions:

- The calculated k_{eff} for a fully-flooded cask is independent of the external moderator (the small variations in the listed values are due to statistical uncertainties which are inherent to the calculational method (Monte Carlo)), and

- Reducing the internal moderation results in a monotonic reduction in reactivity, with no evidence of any optimum moderation. Thus, the fully flooded condition corresponds to the highest reactivity, and the phenomenon of optimum low-density moderation does not occur and is not applicable to the HI-STAR 100 System.

6.4.2.1.2 Evaluation of Package Arrays

In terms of reactivity, the normal conditions of transport (i.e., no internal or external moderation) are bounded by the hypothetical accident conditions of transport. Therefore, the calculations in this section evaluate arrays of HI-STAR 100 Systems under hypothetical accident conditions (i.e., internal and external moderation by water to the most reactive credible extent and no neutron shield present).

In accordance with 10CFR71.59 requirements, calculations were performed to simulate an infinite three-dimensional square array of internally fully-flooded (highest reactivity) casks with varying cask spacing and external moderation density. The MPC-24 was used for this analysis. The maximum k_{eff} results of these calculations are listed in Table 6.4.2 and confirm that the individual casks in a square-pitched array are independent of external moderation and cask spacing. The maximum value listed in Table 6.4.2 is statistically equivalent (within three standard deviations) to the reference value (Case 1 shown in Table 6.4.1) for a single unreflected fully flooded cask.

To further investigate the reactivity effects of array configurations, calculations were also performed to simulate an infinite three-dimensional hexagonal (triangular-pitched) array of internally fully-flooded (highest reactivity) MPC-24 casks with varying cask spacing and external moderation density. The maximum k_{eff} results of these calculations are listed in Table 6.4.3 and confirm that the individual casks in a hexagonal (triangular pitched) array are effectively independent of external moderation and cask spacing. The maximum value listed in Table 6.4.3 is statistically equivalent (within two standard deviations) to the reference value (Case 1 shown in Table 6.4.1) for a single unreflected fully flooded cask.

To assure that internal moderation does not result in increased reactivity, hexagonal array calculations were also performed for 10% internal moderator with 10% and 100% external moderation for varying cask spacing. Maximum k_{eff} results are summarized in Table 6.4.4 and confirm the very low values of k_{eff} for low values of internal moderation.

The results presented thus far indicate that neutronic interaction between casks is not enhanced by the neighboring casks or the water between the neighboring casks, and thus, the most reactive arrangement of casks corresponds to a tightly packed array with the cask surfaces touching. Therefore, calculations were performed for an infinite hexagonal (triangular pitched) array of touching casks (neglecting the Holtite-A neutron shield). These calculations were performed for

the MPC-24 and the MPC-68 designs, in the internally flooded (highest reactivity) and internally dry conditions, with and without external flooding. The results of these calculations are listed in Table 6.4.5. For both the MPC-24 and MPC-68, the maximum k_{eff} values are shown to be statistically equivalent (within one standard deviation) to that of a single internally flooded unreflected cask and are below the regulatory limit of 0.95.

The calculations demonstrate that the thick steel wall of the overpack is more than sufficient to preclude neutron coupling between casks, consistent with the findings of Cano, et al. Neglecting the Holtite-A neutron shielding in the calculational model provides further assurance of conservatism in the calculations.

6.4.2.2 Partial Flooding

To demonstrate that the HI-STAR 100 System would remain subcritical if water were to leak into the containment system, as required by 10CFR71.55, calculations in this section address partial flooding in the HI-STAR 100 System and demonstrate that the fully flooded condition is the most reactive.

The reactivity changes during the flooding process were evaluated in both the vertical and horizontal positions for the MPC-24 and MPC-68 designs. For these calculations, the cask is partially filled (at various levels) with full density (1.0 g/cc) water and the remainder of the cask is filled with steam consisting of ordinary water at partial density (0.002 g/cc). Results of these calculations are shown in Table 6.4.6. In all cases, the reactivity increases monotonically as the water level rises, confirming that the most reactive condition is fully flooded. This conclusion is also true for the other baskets that were not analyzed under partial flooding conditions, since increasing the water level always improves the moderation condition of the fuel and therefore results in an increase in reactivity[†]. The fully flooded case therefore represents the bounding condition for all MPC basket types.

6.4.2.3 Clad Gap Flooding

The reactivity effect of flooding the fuel rod pellet-to-clad gap regions, in the fully flooded condition, has been investigated. Table 6.4.7 presents maximum k_{eff} values that demonstrate the positive reactivity effect associated with flooding the pellet-to-clad gap regions. These results confirm that it is conservative to assume that the pellet-to-clad gap regions are flooded. For all cases that involve flooding, the pellet-to-clad gap regions are assumed to be flooded.

6.4.2.4 Preferential Flooding

[†] The rate of increase in reactivity along the fuel length, though, could be different between different MPC designs. An example would be the MPC-32 with burnup credit where the reactivity is strongly affected by the lower burned ends of the fuel.

Two different potential conditions of preferential flooding are considered: preferential flooding of the MPC basket itself (i.e. different water levels in different basket cells), and preferential flooding involving Damaged Fuel Containers.

Preferential flooding of the MPC basket itself for any of the MPC fuel basket designs is not possible because flow holes are present on all four walls of each basket cell and on the two flux trap walls at both the top and bottom of the MPC basket. The flow holes are sized to ensure that they cannot be blocked by crud deposits. Because the fuel cladding temperatures remain below their design limits (as demonstrated in Chapter 3) and the inertial loading remains below 63g's (Section 2.9), the cladding remains intact. For damaged BWR fuel assemblies and BWR fuel debris, the assemblies or debris are pre-loaded into stainless steel Damaged Fuel Containers fitted with 250x250 fine mesh screens (20x20 for Trojan FFC) which prevent damaged fuel assemblies or fuel debris from blocking the basket flow holes. Therefore, the flow holes cannot be blocked and the MPC fuel baskets cannot be preferentially flooded.

However, when DFCs are present in the MPC, a condition could exist during the draining of the MPC, where the DFCs are still partly filled with water while the remainder of the MPC is dry. This condition would be the result of the water tension across the mesh screens. The maximum water level inside the DFCs for this condition is calculated from the dimensions of the mesh screen and the surface tension of water. The wetted perimeter of the screen openings is up to 50 ft per square inch of screen. With a surface tension of water of 0.005 lbf/ft, this results in a maximum pressure across the screen of 0.25 psi, corresponding to a maximum water height in the DFC of 7 inches. For added conservatism, a value of 12 inches is used. Assuming this condition, calculations are performed for the two possible DFC configurations:

- MPC-68 or MPC-68F with 68 DFCs (Assembly Classes 6x6A/B/C, 7x7A and 8x8A, see Subsection 6.4.4)
- MPC-24E or MPC-24EF with 4 DFCs and 20 intact assemblies (Bounding all PWR assembly classes, see Subsection 6.4.9)

For each configuration, the case resulting in the highest maximum k_{eff} for the fully flooded condition (see Subsections 6.4.4 and 6.4.9) is re-analyzed assuming the preferential flooding condition. For these analyses, the lower 12 inches of the active fuel in the DFCs and the water region below the active fuel (see Figure 6.3.7) are filled with full density water (1.0 g/cc). The remainder of the cask is filled with steam consisting of ordinary water at partial density (0.002 g/cc). All calculations are performed for a single unreflected cask. Table 6.4.10 lists the maximum k_{eff} for the configurations in comparison with the maximum k_{eff} for the fully flooded condition. For all configurations, the preferential flooding condition results in a lower maximum k_{eff} than the fully flooded condition. Thus, the preferential flooding condition is bounded by the fully flooded condition.

In summary, it is concluded that the MPC fuel baskets cannot be preferentially flooded, and that the potential preferential flooding conditions involving DFCs are bounded by the result for the fully flooded condition listed in Subsections 6.4.4 and 6.4.9.

6.4.2.5 Hypothetical Accidents Conditions of Transport

The analyses presented in Section 2.7 of Chapter 2 and Section 3.5 of Chapter 3 demonstrate that the damage resulting from the hypothetical accident conditions of transport are limited to a loss of the neutron shield material as a result of the hypothetical fire accident. Because the criticality analyses do not take credit for the neutron shield material (Holtite-A), this condition has no effect on the criticality analyses.

As reported in Table 2.7.1, the minimum factor of safety for all MPCs as a result of the hypothetical accident conditions of transport is larger than 1.0 against the Level D allowables for Subsection NG, Section III of the ASME Code. Therefore, because the maximum box wall stresses are well within the ASME Level D allowables, the flux-trap gap change in the MPC-24 and MPC-24E/EF will be insignificant compared to the characteristic dimension of the flux trap.

Regarding the fuel assembly integrity, SAR Section 2.9 contains an evaluation of the fuel under accident conditions that concludes that the fuel rod cladding remains intact under the design basis deceleration levels set for the HI-STAR 100.

In summary, the hypothetical transport accidents have no adverse effect on the geometric form of the package contents important to criticality safety, and thus, are limited to the effects on internal and external moderation evaluated in Subsection 6.4.2.1.

6.4.3 Criticality Results

In calculating the maximum reactivity, the analysis used the following equation:

$$k_{eff}^{max} = k_c + K_c \sigma_c + Bias + \sigma_B$$

where:

- ⇒ k_c is the calculated k_{eff} under the worst combination of tolerances;
- ⇒ K_c is the K multiplier for a one-sided statistical tolerance limit with 95% probability at the 95% confidence level [6.1.8]. Each final k_{eff} value calculated by MCNP4a (or KENO5a) is the result of averaging 100 (or more) cycle k_{eff} values, and thus, is based on a sample size of 100. The K multiplier corresponding to a sample size of 100 is 1.93.

However, for this analysis a value of 2.00 was assumed for the K multiplier, which is larger (more conservative) than the value corresponding to a sample size of 100;

- ⇒ σ_c is the standard deviation of the calculated k_{eff} , as determined by the computer code (MCNP4a or KENO5a);
- ⇒ **Bias** is the systematic error in the calculations (code dependent) determined by comparison with critical experiments in Appendix 6.A; and
- ⇒ σ_B is the standard error of the bias (which includes the K multiplier for 95% probability at the 95% confidence level; see Appendix 6.A).

Appendix 6.A presents the critical experiment benchmarking and the derivation of the bias and standard error of the bias (95% probability at the 95% confidence level).

The studies in sections 6.4.2.1 through 6.4.2.4 demonstrate that the moderation by water to the most reactive credible extent corresponds to the internally fully flooded condition of the MPC, with the pellet-to-clad gap in the fuel rods also flooded with water. The external moderation and/or the presence of other surrounding packages, however, has a statistically negligible effect. To demonstrate compliance with 10CFR71.55 and 10CFR71.59, the following set of four calculations is performed for each of the MPC designs:

- Single containment with full internal and external water moderation. The full external water moderation is modeled through an infinite array of containments with a 60cm surface to surface distance. The containment system corresponds to the 2.5 inch inner shell of the overpack. This case addresses the requirement of 10CFR71.55 (b).
- Single cask with full internal and external water moderation. As for the single containment, the full external water moderation is modeled through an infinite array. The external neutron moderator is conservatively neglected in the model. This case also addresses the requirement of 10CFR71.55 (b).
- Hexagonal array of touching casks with full internal and external water reflection. This addresses the requirement of 10CFR71.59 (a)(2) and the determination of the transport index based on criticality control according to 10CFR71.59 (b).
- Hexagonal array of touching casks, internally and externally dry. This addresses the requirement of 10CFR71.59 (a) (1) and the determination of the transport index based on criticality control according to 10CFR71.59 (b). This also addresses the requirement of 10CFR71.55 (d)(1).

To satisfy the requirements of 10CFR71.55 (b)(1), the calculations are performed

- with the assembly type that results in the highest reactivity in the MPC. This is the assembly class 15x15F for the MPC-24, MPC-24E/EF and MPC-32, the assembly class 17x17B with intact and damaged assemblies in the Trojan MPC-24E/EF, the assembly class 9x9E/F in the MPC-68, and the assembly class 6x6C for the MPC-68F; and

- with the bounding basket dimensions as determined in Section 6.3.1 for each basket; and
- with eccentric fuel positioning as necessary, as discussed in Section 6.3.3.

The maximum k_{eff} values for all these cases, calculated with 95% probability at the 95% confidence level, are listed in Table 6.4.12. Results of the criticality safety calculations for other assembly classes under the condition of full internal flooding with water are summarized in Section 6.1. Corresponding detailed results including the maximum k_{eff} , standard deviation and energy of the average lethargy causing fission (EALF) are listed for all MPCs except the MPC-32 in Tables 6.4.13 through 6.4.17. Results for the MPC-32 are presented in Appendix 6.E. Overall, these results confirm that for each of the candidate fuel assemblies and basket configurations the effective multiplication factor (k_{eff}), including all biases and uncertainties at a 95-percent confidence level, do not exceed 0.95 under all credible normal and hypothetical accident conditions of transport. Therefore, compliance with 10CFR71.55 for single packages and 10CFR71.59 for package arrays in both normal and hypothetical accident conditions of transport is demonstrated for all of the fuel assembly classes and basket configurations listed in Tables 6.1.1 through 6.1.3 and 6.1.5 through 6.1.7. It further demonstrates that the transportation index for criticality control is zero because an infinite number of HI-STAR 100 casks will remain subcritical ($k_{\text{eff}} < 0.95$) under both normal and hypothetical accident conditions of transport.

Additional calculations (CASMO-4) at elevated temperatures confirm that the temperature coefficients of reactivity are negative as shown in Table 6.3.1. This confirms that the calculations for the storage baskets are conservative.

Tables listing the maximum k_{eff} , calculated k_{eff} , standard deviation, and energy of the average lethargy causing fission (EALF) for each of the candidate fuel assemblies in each assembly class for the MPC-24, MPC-68 and MPC-68F basket configurations, and with assemblies centered in the fuel storage locations, are provided in Section 6.2.

6.4.4 Damaged Fuel Container for BWR Fuel

Both damaged BWR fuel assemblies and BWR fuel debris are required to be loaded into Damaged Fuel Containers (DFCs). Two different DFC types with slightly different cross sections are analyzed. DFCs containing fuel debris ~~must be stored~~ *are only analyzed* in the MPC-68F. DFCs containing damaged fuel assemblies may be stored in either the MPC-68 or MPC-68F. Evaluation of the capability of storing damaged fuel and fuel debris (loaded in DFCs) is limited to very low reactivity fuel in the MPC-68F. Because the MPC-68 has a higher specified ^{10}B loading, the evaluation of the MPC-68F conservatively bounds the storage of damaged BWR fuel assemblies in a standard MPC-68. Although the maximum planar-average enrichment of the damaged fuel is limited to 2.7% ^{235}U as specified in Chapter 1, analyses have been made for

three possible scenarios, conservatively assuming fuel^{††} of 3.0% enrichment. The scenarios considered included the following:

1. Lost or missing fuel rods, calculated for various numbers of missing rods in order to determine the maximum reactivity. The configurations assumed for analysis are illustrated in Figures 6.4.1 through 6.4.7.
2. Broken fuel assembly with the upper segments falling into the lower segment creating a close-packed array (described as a 8x8 array). For conservatism, the array analytically retained the same length as the original fuel assemblies in this analysis. This configuration is illustrated in Figure 6.4.8.
3. Fuel pellets lost from the assembly and forming powdered fuel dispersed through a volume equivalent to the height of the original fuel. (Flow channel and clad material assumed to disappear).

Results of the analyses, shown in Table 6.4.8, confirm that, in all cases, the maximum reactivity is well below the regulatory limit. There is no significant difference in reactivity between the two DFC types. Collapsed fuel reactivity (simulating fuel debris) is low because of the reduced moderation. Dispersed powdered fuel results in low reactivity because of the increase in ²³⁸U neutron capture (higher effective resonance integral for ²³⁸U absorption).

The loss of fuel rods results in a small increase in reactivity (i.e., rods assumed to collapse, leaving a smaller number of rods still intact). The peak reactivity occurs for 8 missing rods, and a smaller (or larger) number of intact rods will have a lower reactivity, as indicated in Table 6.4.8.

The analyses performed and summarized in Table 6.4.8 provides the relative magnitude of the effects on the reactivity. This information in combination with the maximum k_{eff} values listed in Table 6.1.3 and the conservatism in the analyses, demonstrate that the maximum k_{eff} of the damaged fuel in the most adverse post-accident condition will remain well below the regulatory requirement of $k_{\text{eff}} < 0.95$.

Appendix 6.D provides sample input files for the damaged fuel analysis.

6.4.5 Fuel Assemblies with Missing Rods

For fuel assemblies that are qualified for damaged fuel storage, missing and/or damaged fuel rods are acceptable. However, for fuel assemblies to meet the limitations of intact fuel assembly storage, missing fuel rods must be replaced with dummy rods that displace a volume of water that is equal to, or larger than, that displaced by the original rods.

^{††} 6x6A01 and 7x7A01 fuel assemblies were used as representative assemblies.

6.4.6 Thoria Rod Canister

The Thoria Rod Canister is similar to a DFC with an internal separator assembly containing 18 intact fuel rods. The configuration is illustrated in Figure 6.4.10. The k_{eff} value for an MPC-68F filled with Thoria Rod Canisters is calculated to be 0.1813. This low reactivity is attributed to the relatively low content in ^{235}U (equivalent to UO_2 fuel with an enrichment of approximately 1.7 wt% ^{235}U), the large spacing between the rods (the pitch is approximately 1", the cladding OD is 0.412") and the absorption in the separator assembly. Together with the maximum k_{eff} values listed in Tables 6.1.2 and 6.1.3 this result demonstrates, that the k_{eff} for a Thoria Rod Canister loaded into the MPC68 or the MPC68F together with other approved fuel assemblies or DFCs will remain well below the regulatory requirement of $k_{\text{eff}} < 0.95$.

6.4.7 Sealed Rods Replacing BWR Water Rods

Some BWR fuel assemblies contain sealed rods filled with a non-fissile instead of water rods. Compared to the configuration with water rods, the configuration with sealed rods has a reduced amount of moderator, while the amount of fissile material is maintained. Thus, the reactivity of the configuration with sealed rods will be lower compared to the configuration with water rods. Any configuration containing sealed rods instead of water rods is therefore bounded by the analysis for the configuration with water rods and no further analysis is required to demonstrate the acceptability. Therefore, for all BWR fuel assemblies analyzed, it is permissible that water rods are replaced by sealed rods filled with a non-fissile material.

6.4.8 Neutron Sources in Fuel Assemblies

Fuel assemblies containing start-up neutron sources are permitted for storage in the HI-STAR 100 System. The reactivity of a fuel assembly is not affected by the presence of a neutron source (other than by the presence of the material of the source, which is discussed later). This is true because in a system with a k_{eff} less than 1.0, any given neutron population at any time, regardless of its origin or size, will decrease over time. Therefore, a neutron source of any strength will not increase reactivity, but only the neutron flux in a system, and no additional criticality analyses are required. Sources are inserted as rods into fuel assemblies, i.e. they replace either a fuel rod or water rod (moderator). Therefore, the insertion of the material of the source into a fuel assembly will not lead to an increase of reactivity either.

6.4.9 PWR Damaged Fuel and Fuel Debris

The MPC-24E, MPC-24EF, and Trojan MPC-24E and MPC-24EF are designed to contain damaged fuel and fuel debris, loaded into Damaged Fuel Containers (DFCs) or Failed Fuel Cans (FFCs). There is one generic DFC for the MPC-24E/EF, and two containers, a Holtec DFC and a

Trojan FFC for the Trojan MPC-24E/EF. In this section, the term "DFC" is used to specify either of these components. In any case, the number of DFCs is limited to 4, and the permissible locations of the DFCs are shown in Figure 6.4.11.

Only the Trojan MPC-24E/EF is certified for damaged fuel and fuel debris. However, the generic MPC-24E/EF is also designed to accommodate damaged *fuel and* fuel debris, and the majority of criticality evaluations for damaged fuel and fuel debris are performed for the generic MPC-24E/EF, with only a smaller number of calculations performed for the Trojan MPCs. Therefore, criticality evaluations for both the generic MPC-24E/EF and the Trojan MPC-24E/EF are presented in this subsection, even though the Trojan MPC-24E/EF are the only MPCs authorized to transport damaged fuel and fuel debris.

Damaged fuel assemblies are assemblies with known or suspected cladding defects greater than pinholes or hairlines, or with missing rods, but excluding fuel assemblies with gross defects (for a full definition see Chapter 1). Therefore, apart from possible missing fuel rods, damaged fuel assemblies have the same geometric configuration as intact fuel assemblies and consequently the same reactivity. Missing fuel rods can result in a slight increase of reactivity. After a drop accident, however, it can not be assumed that the initial geometric integrity is still maintained. For a drop on either the top or bottom of the cask, the damaged fuel assemblies could collapse. This would result in a configuration with a reduced length, but increased amount of fuel per unit length. For a side drop, fuel rods could be compacted to one side of the DFC. In either case, a significant relocation of fuel within the DFC is possible, which creates a greater amount of fuel in some areas of the DFC, whereas the amount of fuel in other areas is reduced. Fuel debris can include a large variety of configurations ranging from whole fuel assemblies with severe damage down to individual fuel pellets.

In the cases of fuel debris or relocated damaged fuel, there is the potential that fuel could be present in axial sections of the DFCs that are outside the basket height covered with ~~Boral~~ *fixed neutron absorber*. However, in these sections, the DFCs are not surrounded by any intact fuel, only by basket cell walls, non-fuel hardware and water. Studies have shown that this condition does not result in any significant effect on reactivity, compared to a condition where the damaged fuel and fuel debris is restricted to the axial section of the basket covered by ~~Boral~~ *fixed neutron absorber*. All calculations for damaged fuel and fuel debris are therefore performed assuming that fuel is present only in the axial sections covered by ~~Boral~~ *the fixed neutron absorber*, and the results are directly applicable to any situation where damaged fuel and fuel debris is located outside these sections in the DFCs.

To address all the situations listed above and identify the configuration or configurations leading to the highest reactivity, it is impractical to analyze a large number of different geometrical configurations for each of the fuel classes. Instead, a bounding approach is taken which is based

on the analysis of regular arrays of bare fuel rods without cladding. Details and results of the analyses are discussed in the following sections.

All calculations for generic damaged fuel and fuel debris are performed using a full cask model with the maximum permissible number of Damaged Fuel Containers. For the MPC-24E and MPC-24EF, the model consists of 20 intact assemblies, and 4 DFCs in the locations shown in Figure 6.4.11. The bounding assumptions regarding the intact assemblies and the modeling of the damaged fuel and fuel debris in the DFCs are discussed in the following sections.

6.4.9.1 Bounding Intact Assemblies

Intact PWR assemblies stored together with DFCs in the MPC-24E/EF are limited to a maximum enrichment of 4.0 wt% ^{235}U , regardless of the fuel class. Results presented in Table 6.1.5 for the MPC-24E/EF loaded with intact assemblies only are for different enrichments for each class, ranging between 4.2 and 5.0 wt% ^{235}U , making it difficult to directly identify the bounding assembly. However, the assembly class 15x15H is among the classes with the highest reactivity, but has the lowest initial enrichment. Therefore, the 15x15H assembly is used as the intact PWR assembly for all calculations with DFCs.

The Trojan MPC-24E/EF is only certified for the assembly class 17x17B, which bounds the fuel types used at the Trojan plant. Consequently, the assembly class 17x17B is used as the intact assembly in all calculations for the Trojan MPC-24E/EF.

6.4.9.2 Bare Fuel Rod Arrays

A conservative approach is used to model both damaged fuel and fuel debris in the DFCs, using arrays of bare fuel rods:

- Fuel in the DFCs is arranged in regular, rectangular arrays of bare fuel rods, i.e. all cladding and other structural material in the DFC is replaced by water.
- The active length of these rods is chosen to be the maximum active fuel length of all fuel assemblies listed in Section 6.2, which is 150 inch for PWR fuel.
- To ensure the configuration with optimum moderation and highest reactivity is analyzed, the amount of fuel per unit length of the DFC is varied over a large range. This is achieved by changing the number of rods in the array and the rod pitch. The number of rods are varied between 64 (8x8) and 729 (27x27) for PWR fuel.
- Analyses are performed for the minimum, maximum and typical pellet diameter of the fuel.

This is a very conservative approach to model damaged fuel, and to model fuel debris configurations such as severely damaged assemblies and bundles of individual fuel rods, as the absorption in the cladding and structural material is neglected.

This is also a conservative approach to model fuel debris configurations such as bare fuel pellets due to the assumption of an active length of 150 inch. For some of the analyzed cases, this assumption results in more uranium mass being modeled in the DFCs than is permitted by the uranium mass loading restrictions listed in Chapter 1.

To demonstrate the level of conservatism, additional analyses are performed with the DFC containing various realistic assembly configurations such as intact assemblies, assemblies with missing fuel rods and collapsed assemblies, i.e. assemblies with increased number of rods and decreased rod pitch.

As discussed in Subsection 6.4.9, all calculations are performed for full cask models, containing the maximum permissible number of DFCs together with intact assemblies.

Graphical presentations of the calculated maximum k_{eff} for each case as a function of the fuel mass per unit length of the DFC are shown in Figure 6.4.12. The results for the bare fuel rods show a distinct peak in the maximum k_{eff} at about 3.5 kgUO₂/inch.

The realistic assembly configurations are typically about 0.01 (delta-k) or more below the peak results for the bare fuel rods, demonstrating the conservatism of this approach to model damaged fuel and fuel debris configurations such as severely damaged assemblies and bundles of fuel rods.

For fuel debris configurations consisting of bare fuel pellets only, the fuel mass per unit length would be beyond the value corresponding to the peak reactivity. For example, for DFCs filled with a mixture of 60 vol% fuel and 40 vol% water the fuel mass per unit length is 7.92 kgUO₂/inch for the PWR DFC. The corresponding reactivities are significantly below the peak reactivities. The difference is about 0.01 (delta-k) or more for PWR fuel. Furthermore, the filling height of the DFC would be less than 70 inches in these examples due to the limitation of the fuel mass per basket position, whereas the calculation is conservatively performed for a height of 150 inch. These results demonstrate that even for the fuel debris configuration of bare fuel pellets, the model using bare fuel rods is a conservative approach.

To demonstrate that the bare fuel rod approach also bounds the potential presence of fuel fragments in the DFCs, additional calculations were performed with fuel fragments in the DFCs instead of bare fuel rods. The fuel fragments are modeled as regular 3-dimensional arrays of fuel cubes positioned inside water cubes. Both the dimension of the fuel cubes and the fuel-to-water-

volume ratio are varied over a wide range. Calculations are performed for the MPC-24E/EF Trojan, and the results are presented in Table 6.4.18. The highest maximum k_{eff} is 0.9320 for a fragment outer dimension of 0.2 inches and a fuel to water volume ratio of 0.4. This maximum k_{eff} value is lower than the corresponding value for the bare fuel rod model, which is 0.9377 as shown in Table 6.4.17. The damaged fuel and fuel debris model based on bare fuel rods therefore bounds any condition involving fuel fragments in the DFCs.

6.4.9.3 Results for MPC-24E and MPC-24EF

The MPC-24E/EF is designed for the storage of up to four DFCs with damaged fuel *or fuel debris* in the four outer fuel baskets cells shaded in Figure 6.4.11. ~~The MPC-24EF allows storage of up to four DFCs with damaged fuel or fuel debris in these locations.~~ These locations are designed with a larger box ID to accommodate the DFCs. For an enrichment of 4.0 wt% ^{235}U for the intact fuel, damaged fuel and fuel debris, the results for the various configurations outlined in Subsection 6.4.9.2 are summarized in Figure 6.4.12 and in Table 6.4.11. Figure 6.4.12 shows the maximum k_{eff} , including bias and calculational uncertainties, for various actual and hypothetical damaged fuel and fuel debris configurations as a function of the fuel mass per unit length of the DFC. For the intact assemblies, the 15x15H assembly class was chosen (see Subsection 6.4.9.1). Table 6.4.11 lists the highest maximum k_{eff} for the various configurations. All maximum k_{eff} values are below the 0.95 regulatory limit.

6.4.9.4 Results for Trojan MPC-24E and MPC-24EF

For the Trojan MPC-24E/EF, bare fuel rod arrays with arrays sizes between 11x11 and 23x23 were analyzed as damaged fuel/fuel debris, with a pellet diameter corresponding to the 17x17B assembly class. The highest maximum k_{eff} value is shown in Table 6.1.6, and is below the 0.95 regulatory limit. The realistic damaged fuel assembly configurations in the DFC, such as assemblies with missing rods, were not analyzed in the Trojan MPC-24E/EF since the evaluations for the generic MPC-24E/EF demonstrate that these conditions are bounded by the fuel debris model using bare fuel pellets.

6.4.10 Non-fuel Hardware in PWR Fuel Assemblies

Non-fuel hardware such as Thimble Plugs (TPs), Burnable Poison Rod Assemblies (BPRAs), Rod Cluster Control Assemblies (RCCAs) and similar devices are permitted for storage with the PWR fuel assemblies in the Trojan MC-24E/EF. Non-fuel hardware is inserted in the guide tubes of the assemblies. For pure water, the reactivity of any PWR assembly with inserts is bounded by (i.e. lower than) the reactivity of the same assembly without the insert. This is due to the fact that the insert reduces the amount of moderator in the assembly, while the amount of fissile material remains unchanged.

Therefore, from a criticality safety perspective, non-fuel hardware inserted into PWR assemblies are acceptable for all allowable PWR types, and, depending on the assembly class, can increase the safety margin.

6.4.11 Reactivity Effect of Potential Boral Fixed Neutron Absorber Damage

During the manufacturing process of the fuel baskets, it is possible that minor damage to Boral fixed neutron absorber panels occurs during welding operations. Criticality calculations have been performed for all basket types to determine whether this condition could have an effect on the reactivity of the system. Since the potential Boral fixed neutron absorber damage is typically the result of welding operations, the damage would occur in a narrow area along the edge of the panel, and would only be present in a few panels within each basket. However, in order to maximize the potential reactivity effect of the damage in the calculations, it is assumed that the damage occurs in an area with a diameter of 1 inch at the center of the Boral fixed neutron absorber panel, and that this condition exists in every panel in the basket. It is further assumed that the Boral fixed neutron absorber in this area is completely replaced by water, while in reality only a relocation of the Boral fixed neutron absorber would occur, since the Boral fixed neutron absorber is completely covered by the sheathing. Calculations performed under these assumption demonstrate that the conservatively modeled Boral fixed neutron absorber damage has a negligible effect on the reactivity, i.e. the difference to the condition without the damage is less than 2 standard deviations. For example, for the MPC-24 and MPC-24E, the change in reactivity is +0.0006 and -0.0004, respectively, for a standard deviation between 0.0004 and 0.0005. In the MPC-24E for Trojan, a specific potential damage was identified that is not bounded by the generic approach described above. To demonstrate that this condition is acceptable, a specific calculation was performed assuming a damage of 5 square-inches in a specific location in up to 8 Boral fixed neutron absorber panels in the basket, and was found to have again a negligible effect on reactivity. In summary, these calculations demonstrate that Boral fixed neutron absorber damage bounded by the configurations assumed in the analyses is acceptable and does not affect the reactivity of the HI-STAR System.

6.4.12 Fixed Neutron Absorber Material

The MPCs in the HI-STAR 100 System can be manufactured with one of two possible neutron absorber materials: Boral or Metamic. Both materials are made of aluminum and B₄C powder. Boral has an inner core consisting of B₄C and aluminum between two outer layers consisting of aluminum only. This configuration is explicitly modeled in the criticality evaluation and shown in Figures 6.3.1 through 6.3.3 for each basket. Metamic is a single layer material with the same overall thickness and the same credited ¹⁰B loading (in g/cm²) for each basket. The majority of the criticality evaluations documented in this chapter are performed using Boral as the fixed neutron absorber. For a selected number of bounding cases, analyses are also performed using Metamic instead of Boral. The results for these cases are listed in Table 6.4.19, together with the

~~corresponding result using Boral and the difference between the two materials for each case. Individual cases show small differences for the two materials. However, the differences are mostly below two times the standard deviation (the standard deviation is about 0.0008 for all cases in Table 6.4.19), indicating that the results are statistically equivalent. Furthermore, the average difference is well below two standard deviations, and all cases are below the regulatory limit of 0.95. The calculations therefore demonstrate that the two fixed neutron absorber materials are identical from a criticality perspective. All results obtained for Boral are therefore directly applicable to Metamic and no further evaluations using Metamic are required.~~

6.4.13 Reactivity Effect of Manufacturing Variations

~~For additional flexibility in manufacturing neutron absorber panels, two options or conditions for the poison panel are evaluated to demonstrate that these options or conditions are acceptable and do not lead to an increase in reactivity. The conditions are:~~

~~Neutron absorber panels are manufactured in two pieces. A maximum gap of 1/4 inch is permitted between the panels. To conservatively model this condition, the maximum gap of 1/4 inch is assumed to exist in all panels in a basket, located at the axial center of the active length of the fuel.~~

~~A poison panel might show a reduced width in a small section along the length, while the average width is equal to or larger than the required minimum. To conservatively model this condition, it is assumed that all panels have a width reduction below the minimum by 1/32 inch over a length of 12 inches at the axial center of the active length. The width of the remainder of the panel is increased slightly to maintain the minimum width on average for a panel length of 156 inches.~~

~~For simplification, both conditions are considered in the same analytical model, and are analyzed for a selected number of bounding cases. The conditions are conservatively assumed to be present at the axial center of all panels in the basket. The results for these cases are listed in Table 6.4.20, together with the corresponding results for the design basis, i.e. with a single panel and minimum panels width, and the reactivity difference for each case is shown. The differences are either below two times the standard deviation (the standard deviation is between 0.0004 and 0.0008 for all cases in Table 6.4.20), or the conditions result in a reduction in reactivity. Furthermore, the average difference is well below two standard deviations, and all cases are below the regulatory limit of 0.95. The calculations therefore demonstrate that the conditions stated above have a negligible effect on reactivity and are therefore acceptable.~~

6.4.14 Reactivity Effect of Inhomogeneties in Neutron Poison Plates

~~The reactivity of the fuel basket is more a global value, depending on the number and~~

~~*B₄C loading of the poison panels than on local inhomogeneities in the B₄C distribution. To demonstrate this, calculations were performed with conservatively modeled inhomogeneities in the panels. The modeling consisted of dividing all panels in the basket into axial sections, and assigning different B₄C levels to the sections in an alternating fashion. The B₄C levels chosen were 80% and 120% of the level in the reference calculation. This way, the total amount of B₄C in the basket of the reference case is maintained. This is a very conservative modeling approach, since it models a condition that would actually be rejected in the acceptance test, since areas of the panel are below the acceptable B₄C content limit. The parameter that is varied in these calculations is the axial length of the sections with the reduced and increased B₄C content. This length is varied between 1 cm and almost 100 cm. In the latter case, each panel would consist of only four axial sections, two of which are at 80% of the B₄C loading, with the two other at 120%. The calculations were performed for the MPC 68 and the MPC 24 with design basis fuel. For the MPC 68, the results show that up to a section length of 8 cm, there is no significant effect on reactivity, and even at a section length close to 100cm, the reactivity effect is small, around 0.0025 delta k. For the MPC 24, there is no statistically significant effect on reactivity even at section length close to 100 cm. This confirms that the reactivity of the basket is a more global value, and local differences in the B₄C amount are inconsequential as long as the total B₄C amount is maintained. Consequently, the acceptance tests for the poison plates do not require sampling of small sections (below 8 cm) of the panels to confirm acceptability.*~~

Table 6.4.1

MAXIMUM REACTIVITIES WITH REDUCED WATER DENSITIES FOR CASK ARRAYS[†]
WITH MPC-24 AND MPC-68

Case Number	Water Density		MCNP4a Results					
	Internal	External	MPC-24 (17x17A01 @ 4.0%)			MPC-68 (8x8C04 @ 4.2%)		
			Max. $k_{eff}^{\dagger\dagger}$	1 σ	EALF (eV)	Max. k_{eff}	1 σ	EALF (eV)
1	100%	single cask	0.9368	0.0008	0.2131	0.9348	0.0007	0.2915
2	100%	100%	0.9354	0.0009	0.2136	0.9339	0.0005	0.2922
3	100%	70%	0.9362	0.0008	0.2139	0.9339	0.0006	0.2921
4	100%	50%	0.9352	0.0008	0.2144	0.9347	0.0004	0.2924
5	100%	20%	0.9372	0.0008	0.2138	0.9338	0.0005	0.2921
6	100%	10%	0.9380	0.0009	0.2140	0.9336	0.0005	0.2920
7	100%	5%	0.9351	0.0008	0.2142	0.9333	0.0006	0.2936
8	100%	0%	0.9342	0.0008	0.2136	0.9338	0.0005	0.2922
9	70%	0%	0.8337	0.0007	0.4115	0.8488	0.0004	0.6064
10	50%	0%	0.7426	0.0008	0.8958	0.7631	0.0004	1.4515
11	20%	0%	0.5606	0.0007	15.444	0.5797	0.0006	26.5
12	10%	0%	0.4834	0.0005	160.28	0.5139	0.0003	241
13	5%	0%	0.4432	0.0004	1133.9	0.4763	0.0003	1770
14	10%	100%	0.4793	0.0005	171.79	0.4946	0.0003	342

[†] For an infinite square array of casks with 60 cm spacing between cask surfaces.

^{††} Maximum k_{eff} includes the bias, uncertainties, and calculational statistics, evaluated for the worst case combination of manufacturing tolerances.

Table 6.4.2

REACTIVITY EFFECTS OF SPACING AND WATER MODERATOR DENSITY FOR
 SQUARE ARRAYS OF MPC-24 CASKS
 (17x17A01 @ 4.0% E)

Cask-to-Cask External Spacing (cm)					
External Moderator Density (%)	2	10	20	40	60
5	0.9352	0.9389	0.9356	0.9345	0.9351
10	0.9366	0.9353	0.9338	0.9357	0.9380
20	0.9368	0.9371	0.9359	0.9366	0.9372
50	0.9363	0.9363	0.9371	0.9352	0.9352
100	0.9355	0.9369	0.9354	0.9354	0.9354

Note:

1. All values are maximum k_{eff} which include the bias, uncertainties, and calculational statistics, evaluated for the worst case combination of manufacturing tolerances.
2. The standard deviation (σ) of the calculations ranges between 0.0007 and 0.0010.

Table 6.4.3

REACTIVITY EFFECTS OF SPACING AND WATER MODERATOR DENSITY FOR
 HEXAGONAL (TRIANGULAR-PITCHED) ARRAYS OF MPC-24 CASKS
 (17x17A01 @ 4.0% E)

Cask-to-Cask External Spacing (cm)					
External Moderator Density (%)	2	10	20	40	60
5	0.9358	0.9365	0.9369	0.9354	0.9354
10	0.9363	0.9372	0.9351	0.9368	0.9372
20	0.9354	0.9357	0.9345	0.9358	0.9381
50	0.9347	0.9361	0.9371	0.9365	0.9370
100	0.9373	0.9381	0.9354	0.9354	0.9354

Note:

1. All values are maximum k_{eff} which include the bias, uncertainties, and calculational statistics, evaluated for the worst case combination of manufacturing tolerances.
2. The standard deviation (σ) of the calculations ranges between 0.0007 and 0.0009.

Table 6.4.4

REACTIVITY EFFECTS OF SPACING AND EXTERNAL MODERATOR DENSITY FOR
 HEXAGONAL (TRIANGULAR-PITCHED) ARRAYS OF MPC-24 CASKS (17x17A01 @
 4.0% E) INTERNALLY FLOODED WITH WATER OF 10% FULL DENSITY

Cask-to-Cask External Spacing (cm)					
External Moderator Density (%)	2	10	20	40	60
10	0.4818	0.4808	0.4798	0.4795	0.4789
100	0.4798	0.4788	0.4781	0.4793	0.4793

Note:

1. All values are maximum k_{eff} which include the bias, uncertainties, and calculational statistics, evaluated for the worst case combination of manufacturing tolerances.
2. The standard deviation (σ) of the calculations ranges between 0.0004 and 0.0005.

Table 6.4.5

CALCULATIONS FOR HEXAGONAL (TRIANGULAR-PITCHED) ARRAYS OF
TOUCHING CASKS WITH MPC-24 AND MPC-68

MPC-24 (17x17A01 @ 4.0% ENRICHMENT)		
Internal Moderation (%)	External Moderation (%)	Maximum k_{eff}
0	0	0.3910
0	100	0.3767
100	0	0.9366
100	100	0.9341
MPC-68 (8x8C04 @ 4.2% ENRICHMENT)		
Internal Moderation (%)	External Moderation (%)	Maximum k_{eff}
0	0	0.4036
0	100	0.3716
100	0	0.9351
100	100	0.9340

Note:

1. All values are maximum k_{eff} which include bias, uncertainties, and calculational statistics, evaluated for the worst case combination of manufacturing tolerances.
2. The standard deviation (σ) of the calculations ranges between 0.0007 and 0.0008 for 100% internal moderation, and between 0.0002 and 0.0003 for 0% internal moderation.

Table 6.4.6

REACTIVITY EFFECTS OF PARTIAL CASK FLOODING FOR MPC-24 AND MPC-68

MPC-24 (17x17A01 @ 4.0% ENRICHMENT)			
Flooded Condition (% Full)	Vertical Orientation	Flooded Condition (% Full)	Horizontal Orientation
25	0.9157	25	0.8766
50	0.9305	50	0.9240
75	0.9330	75	0.9329
100	0.9368	100	0.9368
MPC-68 (8x8C04 @ 4.2% ENRICHMENT)			
Flooded Condition (% Full)	Vertical Orientation	Flooded Condition (% Full)	Horizontal Orientation
25	0.9132	23.5	0.8586
50	0.9307	50	0.9088
75	0.9312	76.5	0.9275
100	0.9348	100	0.9348

Notes:

1. All values are maximum k_{eff} which include bias, uncertainties, and calculational statistics, evaluated for the worst case combination of manufacturing tolerances.
2. The standard deviation (σ) of the calculations ranges between 0.0007 and 0.0010.

Table 6.4.7

REACTIVITY EFFECT OF FLOODING THE PELLET-TO-CLAD GAP FOR MPC-24 AND MPC-68

Pellet-to-Clad Condition	MPC-24 17x17A01 4.0% Enrichment	MPC-68 8x8C04 4.2% Enrichment
dry	0.9295	0.9279
flooded	0.9368	0.9348

Notes:

1. All values are maximum k_{eff} which includes bias, uncertainties, and calculational statistics, evaluated for the worst case combination of manufacturing tolerances.
2. The standard deviation (σ) of the calculations ranges between 0.0007 and 0.0010.

Table 6.4.8

MAXIMUM k_{eff} VALUES[†] IN THE DAMAGED FUEL CONTAINER

Condition	MCNP4a Results					
	DFC Dimensions: ID 4.93" THK. 0.12"			DFC Dimensions: ID 4.81" THK. 0.11"		
	Max. ^{††} k_{eff}	1 σ	EALF (eV)	Max. ^{††} k_{eff}	1 σ	EALF (eV)
<u>6x6 Fuel Assembly</u>						
6x6 Intact Fuel	0.7086	0.0007	0.3474	0.7016	0.0006	0.3521
w/32 Rods Standing	0.7183	0.0008	0.2570	0.7117	0.0007	0.2593
w/28 Rods Standing	0.7315	0.0007	0.1887	0.7241	0.0006	0.1909
w/24 Rods Standing	0.7086	0.0007	0.1568	0.7010	0.0008	0.1601
w/18 Rods Standing	0.6524	0.0006	0.1277	0.6453	0.0007	0.1288
Collapsed to 8x8 array	0.7845	0.0007	1.1550	0.7857	0.0007	1.1162
Dispersed Powder	0.7628	0.0007	0.0926	0.7440	0.0007	0.0902
<u>7x7 Fuel Assembly</u>						
7x7 Intact Fuel	0.7463	0.0007	0.2492	0.7393	0.0006	0.2504
w/41 Rods Standing	0.7529	0.0007	0.1733	0.7481	0.0007	0.1735
w/36 Rods Standing	0.7487	0.0007	0.1389	0.7444	0.0006	0.1406
w/25 Rods Standing	0.6718	0.0007	0.1070	0.6644	0.0007	0.1082

[†] These calculations were performed with a planar-average enrichment of 3.0% and a ¹⁰B loading of 0.0067 g/cm², which is 75% of a minimum ¹⁰B loading of 0.0089 g/cm². The minimum ¹⁰B loading in the MPC-68F is 0.010 g/cm². Therefore, the listed maximum k_{eff} values are conservative.

^{††} Maximum k_{eff} includes bias, uncertainties, and calculational statistics, evaluated for the worst case combination of manufacturing tolerances.

Table 6.4.9

DELETED

Table 6.4.10

REACTIVITY EFFECT OF PREFERENTIAL FLOODING OF THE DFCs

DFC Configuration	Preferential Flooding	Fully Flooded
MPC-68 or MPC-68F with 68 DFCs (Assembly Classes 6x6A/B/C, 7x7A and 8x8A)	0.6560	0.7857
MPC-24E or MPC-24EF with 4 DFCs (Bounding All PWR Assembly Classes)	0.7895	0.9480

Notes:

1. All values are maximum k_{eff} which includes bias, uncertainties, and calculational statistics, evaluated for the worst case combination of manufacturing tolerances.

Table 6.4.11

MAXIMUM k_{eff} VALUES IN THE GENERIC PWR DAMAGED FUEL CONTAINER FOR A
 MAXIMUM INITIAL ENRICHMENT OF 4.0 wt% ^{235}U .

Model Configuration inside the DFC	Maximum k_{eff}
Intact Assemblies (2 assemblies analyzed)	0.9340
Assemblies with missing rods (4 configurations analyzed)	0.9350
Collapsed Assemblies (6 configurations analyzed)	0.9360
Regular Arrays of Bare Fuel Rods (36 configurations analyzed)	0.9480

Notes:

1. All values are maximum k_{eff} which includes bias, uncertainties, and calculational statistics, evaluated for the worst case combination of manufacturing tolerances.
2. The standard deviation (σ) of the calculations ranges between 0.0007 and 0.0010.

Table 6.4.12
SUMMARY OF THE CRITICALITY RESULTS FOR THE MOST REACTIVE ASSEMBLY FROM
THE MOST REACTIVE ASSEMBLY CLASS IN EACH MPC-24
TO DEMONSTRATE COMPLIANCE WITH 10CFR71.55 AND 10CFR71.59

MPC-24, Assembly Class 15x15F, 4.1 wt% ²³⁵U					
Configuration	% Internal Moderation	% External Moderation	Max. [‡] k _{eff}	1 σ	EALF (eV)
Single Package, unreflected	100%	0%	0.9410	0.0007	0.2998
Single Package, fully reflected	100%	100%	0.9397	0.0008	0.3016
Containment, fully reflected	100%	100%	0.9397	0.0008	0.3006
Infinite Array of Damaged Packages	100%	100%	0.9436	0.0009	0.2998
Infinite Array of Undamaged Packages	0%	0%	0.3950	0.0004	82612.0
MPC-68, Assembly Class 9x9E/F, 4.0 wt% ²³⁵U					
Configuration	% Internal Moderation	% External Moderation	Max. k _{eff}	1 σ	EALF (eV)
Single Package, unreflected	100%	0%	0.9486	0.0008	0.2095
Single Package, fully reflected	100%	100%	0.9470	0.0008	0.2079
Containment, fully reflected	100%	100%	0.9461	0.0007	0.2092
Infinite Array of Damaged Packages	100%	100%	0.9468	0.0008	0.2106
Infinite Array of Undamaged Packages	0%	0%	0.3808	0.0003	85218.0
MPC-68F, Assembly Class 6x6C, 2.7 wt% ²³⁵U					
Configuration	% Internal Moderation	% External Moderation	Max. k _{eff}	1 σ	EALF (eV)
Single Package, unreflected	100%	0%	0.8021	0.0007	0.2139
Single Package, fully reflected	100%	100%	0.8033	0.0008	0.2142
Containment, fully reflected	100%	100%	0.8033	0.0008	0.2138
Infinite Array of Damaged Packages	100%	100%	0.8026	0.0008	0.2142
Infinite Array of Undamaged Packages	0%	0%	0.3034	0.0002	99463.0

[‡] The maximum k_{eff} is equal to the sum of the calculated k_{eff}, two standard deviations, the code bias, and the uncertainty in the code bias.

Table 6.4.12 (continued)
SUMMARY OF THE CRITICALITY RESULTS FOR THE MOST REACTIVE ASSEMBLY FROM
THE MOST REACTIVE ASSEMBLY CLASS IN EACH MPC-24
TO DEMONSTRATE COMPLIANCE WITH 10CFR71.55 AND 10CFR71.59

MPC-24E/EF, Assembly Class 15x15F, 4.5 wt% ²³⁵U					
Configuration	% Internal Moderation	% External Moderation	Max. ‡ k _{eff}	1 σ	EALF (eV)
Single Package, unreflected	100%	0%	0.9495	0.0008	0.3351
Single Package, fully reflected	100%	100%	0.9485	0.0008	0.3313
Containment, fully reflected	100%	100%	0.9486	0.0008	0.3362
Infinite Array of Damaged Packages	100%	100%	0.9495	0.0008	0.3335
Infinite Array of Undamaged Packages	0%	0%	0.4026	0.0004	87546.0
MPC-24E/EF TROJAN, Trojan Intact and Damaged Fuel, 3.7 wt% ²³⁵U					
Configuration	% Internal Moderation	% External Moderation	Max. k _{eff}	1 σ	EALF (eV)
Single Package, unreflected	100%	0%	0.9377	0.0008	n/c†
Single Package, fully reflected	100%	100%	0.9366	0.0008	n/c
Containment, fully reflected	100%	100%	0.9377	0.0008	n/c
Infinite Array of Damaged Packages	100%	100%	0.9383	0.0007	n/c
Infinite Array of Undamaged Packages	0%	0%	0.3518	0.0003	n/c
MPC-32, Assembly Class 15x15F, 4.0 wt% ²³⁵U					
Configuration	% Internal Moderation	% External Moderation	Max. k _{eff}	1 σ	EALF (eV)
Single Package, unreflected	100%	0%	later	later	later
Single Package, fully reflected	100%	100%	later	later	later
Containment, fully reflected	100%	100%	later	later	later
Infinite Array of Damaged Packages	100%	100%	later	later	later
Infinite Array of Undamaged Packages	0%	0%	later	later	later

‡ The maximum k_{eff} is equal to the sum of the calculated k_{eff}, two standard deviations, the code bias, and the uncertainty in the code bias.

† n/c = not calculated

Table 6.4.13

RESULTS FOR EACH ASSEMBLY CLASS IN THE MPC-24

Fuel Assembly Class	Maximum Allowable Enrichment (wt% ²³⁵ U)	Max. [†] k _{eff}	1 σ	EALF (eV)
14x14A	4.6	0.9296	0.0008	0.2093
14x14B	4.6	0.9228	0.0008	0.2675
14x14C	4.6	0.9307	0.0008	0.3001
14x14D	4.0	0.8507	0.0008	0.3308
14x14E	5.0	0.7627	0.0007	0.3607
15x15A	4.1	0.9227	0.0007	0.2708
15x15B	4.1	0.9388	0.0009	0.2626
15x15C	4.1	0.9361	0.0009	0.2385
15x15D	4.1	0.9367	0.0008	0.2802
15x15E	4.1	0.9392	0.0008	0.2908
15x15F	4.1	0.9410	0.0007	0.2998
15x15G	4.0	0.8907	0.0008	0.3456
15x15H	3.8	0.9337	0.0009	0.2349
16x16A	4.6	0.9287	0.0008	0.2704
17x17A	4.0	0.9368	0.0008	0.2131
17x17B	4.0	0.9355	0.0008	0.2659
17x17C	4.0	0.9349	0.0009	0.2677

[†] The term "maximum k_{eff}" as used here, and elsewhere in this document, means the highest possible k-effective, including bias, uncertainties, and calculational statistics, evaluated for the worst case combination of manufacturing tolerances.

Table 6.4.14

RESULTS FOR EACH ASSEMBLY CLASS IN THE MPC-68

Fuel Assembly Class	Maximum Allowable Enrichment (wt% ²³⁵ U)	Max. [†] k _{eff}	1 σ	EALF (eV)
7x7B	4.2	0.9386	0.0007	0.3983
8x8B	4.2	0.9416	0.0007	0.3293
8x8C	4.2	0.9425	0.0007	0.3081
8x8D	4.2	0.9403	0.0006	0.2778
8x8E	4.2	0.9312	0.0008	0.2831
8x8F	4.0	0.9459	0.0007	0.2361
9x9A	4.2	0.9417	0.0008	0.2236
9x9B	4.2	0.9436	0.0008	0.2506
9x9C	4.2	0.9395	0.0008	0.2698
9x9D	4.2	0.9394	0.0009	0.2625
9x9E	4.0	0.9486	0.0008	0.2095
9x9F	4.0	0.9486	0.0008	0.2095
9x9G	4.2	0.9383	0.0008	0.2292
10x10A	4.2	0.9457	0.0008	0.2212
10x10B	4.2	0.9436	0.0007	0.2366
10x10C	4.2	0.9433	0.0007	0.2416
10x10D	4.0	0.9376	0.0008	0.3355
10x10E	4.0	0.9185	0.0007	0.2936

[†] The term "maximum k_{eff}" as used here, and elsewhere in this document, means the highest possible k-effective, including bias, uncertainties, and calculational statistics, evaluated for the worst case combination of manufacturing tolerances.

Table 6.4.15

RESULTS FOR EACH ASSEMBLY CLASS IN THE MPC-68F

Fuel Assembly Class	Maximum Allowable Enrichment (wt% ²³⁵ U)	Max. [†] k _{eff}	1 σ	EALF (eV)
6x6A	2.7 ^{††}	0.7888	0.0007	0.2310
6x6B ^{†††}	2.7	0.7824	0.0006	0.2184
6x6C	2.7	0.8021	0.0007	0.2139
7x7A	2.7	0.7974	0.0008	0.2015
8x8A	2.7	0.7697	0.0007	0.2158

[†] The term "maximum k_{eff}" as used here, and elsewhere in this document, means the highest possible k-effective, including bias, uncertainties, and calculational statistics, evaluated for the worst case combination of manufacturing tolerances.

^{††} These calculations were performed for 3.0% planar-average enrichment; however, the authorized contents are limited to a maximum planar-average enrichment of 2.7%. Therefore, the listed maximum k_{eff} values are conservative.

^{†††} Assemblies in this class contain both MOX and UO₂ pins. The composition of the MOX fuel pins is given in Table 6.3.4. The maximum allowable planar-average enrichment for the MOX pins is given in the specification of authorized contents, Chapter 1.

Table 6.4.16

RESULTS FOR EACH ASSEMBLY CLASS IN THE MPC-24E/EF

Fuel Assembly Class	Maximum Allowable Enrichment (wt% ²³⁵ U)	Max. [†] k _{eff}	1 σ	EALF (eV)
14x14A	5.0	0.9380	0.0008	0.2277
14x14B	5.0	0.9312	0.0008	0.2927
14x14C	5.0	0.9365	0.0008	0.3318
14x14D	5.0	0.8875	0.0009	0.4026
14x14E	5.0	0.7651	0.0007	0.3644
15x15A	4.5	0.9336	0.0008	0.2879
15x15B	4.5	0.9487	0.0009	0.3002
15x15C	4.5	0.9462	0.0008	0.2631
15x15D	4.5	0.9445	0.0008	0.3375
15x15E	4.5	0.9471	0.0008	0.3242
15x15F	4.5	0.9495	0.0008	0.3351
15x15G	4.5	0.9062	0.0008	0.3883
15x15H	4.2	0.9455	0.0009	0.2663
16x16A	5.0	0.9358	0.0008	0.3150
17x17A	4.4	0.9447	0.0007	0.2374
17x17B	4.4	0.9438	0.0008	0.2951
17x17C	4.4	0.9433	0.0008	0.2932

[†] The term "maximum k_{eff}" as used here, and elsewhere in this document, means the highest possible k-effective, including bias, uncertainties, and calculational statistics, evaluated for the worst case combination of manufacturing tolerances.

Table 6.4.17

RESULTS FOR THE MPC-24E/EF TROJAN

Fuel Assembly Class	Maximum Allowable Enrichment (wt% ²³⁵U)	Content	Max.[†] k_{eff}	1 σ	EALF (eV)
17x17B	3.7	Intact Fuel	0.9187	0.0009	not calculated
17x17B	3.7	Intact Fuel, Damaged Fuel and Fuel Debris	0.9377	0.0008	not calculated

[†] The term "maximum k_{eff}" as used here, and elsewhere in this document, means the highest possible k-effective, including bias, uncertainties, and calculational statistics, evaluated for the worst case combination of manufacturing tolerances.

Table 6.4.18

RESULTS FOR THE MPC-24E/EF TROJAN USING A FUEL FRAGMENT MODEL FOR DAMAGED FUEL AND FUEL DEBRIS

Fuel Cube OD (Inches)	Maximum k_{eff}			
	Fuel Volume / Water Volume			
	0.2	0.4	0.6	0.8
1	0.9098	0.9223	0.9260	0.9204
0.5	0.9156	0.9310	0.9273	0.9168
0.2	0.9254	0.9320	0.9216	0.9137
0.1	0.9253	0.9274	0.9183	0.9135
0.05	0.9224	0.9228	0.9168	0.9126
0.02	0.9183	0.9213	0.9140	0.9122

Table 6.4.19

COMPARISON OF MAXIMUM k_{eff} VALUES FOR DIFFERENT FIXED NEUTRON ABSORBER MATERIALS

<i>CASE</i>	<i>Maximum k_{eff}</i>		<i>Reactivity Difference</i>
	<i>BORAL</i>	<i>METAMIC</i>	
<i>MPC 68</i>	<i>0.9486</i>	<i>0.9470</i>	<i>-0.0016</i>
<i>MPC 68F with 68 DFCs</i>	<i>0.8021</i>	<i>0.8019</i>	<i>-0.0002</i>
<i>MPC 24</i>	<i>0.9410</i>	<i>0.9425</i>	<i>+0.0015</i>
<i>MPC 24E, Intact Assemblies</i>	<i>0.9495</i>	<i>0.9494</i>	<i>-0.0001</i>
<i>MPC 24E, with 4 DFCs</i>	<i>0.9480</i>	<i>0.9471</i>	<i>-0.0009</i>
<i>Average Difference</i>			<i>-0.0003</i>

Table 6.4.20

COMPARISON OF MAXIMUM k_{eff} VALUES FOR DIFFERENT FIXED NEUTRON ABSORBER CONDITIONS

CASE	Maximum k_{eff}		Reactivity Difference
	DESIGN BASIS (SINGLE PART PANEL AND MINIMUM WIDTH)	TWO PART PANELS AND WIDTH REDUCTION	
<i>MPC 68</i>	0.9486	0.9464	-0.0022
<i>MPC 68F with 68 DFCs</i>	0.8021	0.8023	+0.0002
<i>MPC 24</i>	0.9410	0.9411	+0.0001
<i>MPC 24E, Intact Assemblies</i>	0.9495	0.9494	-0.0001
<i>MPC 24E, with 4 DFCs</i>	0.9480	0.9470	-0.0010
Average Difference			-0.0006

SUPPLEMENT 6.I

CRITICALITY EVALUATION OF HUMBOLDT BAY FUEL IN THE MPC-HB

6.I.0 INTRODUCTION

This supplement is focused on providing criticality evaluations for fuel from the Humboldt Bay Power Plant (HBPP) in the HI-STAR HB. The evaluation presented herein supplements those evaluations contained in the main body of Chapter 6 of this SAR, and information in the main body of Chapter 6 is not repeated in this supplement. To aid the reader, the sections in this supplement are numbered in the same fashion as the corresponding sections in the main body of this chapter, i.e., Sections 6.I.1 through 6.I.6 correspond to Sections 6.1 through 6.6. Tables and figures in this supplement are labeled sequentially. The results of the evaluations in this supplement demonstrate that, for the designated fuel assembly classes and basket configurations, an infinite number of HI-STAR 100 Systems remain subcritical with a margin of subcriticality greater than $0.05\Delta k$. This corresponds to a Criticality Safety Index (CSI) of zero (0) and demonstrates compliance with 10CFR71 criticality requirements for normal and hypothetical accident conditions of transport.

6.I.1 DISCUSSION AND RESULTS

Fuel from the HBPP is qualified in the main body of Chapter 6 of this SAR for transport in the HI-STAR 100 using the MPC-68 and MPC-68F. The assembly classes corresponding to this fuel are 6x6C and 7x7A. However, subsequent to these analyses, an additional basket design was developed for the HBPP fuel. Taking advantage of the smaller physical size of these assemblies, the capacity of the basket was increased to 80 assemblies while maintaining the same outer MPC diameter. The designated name of this MPC version is MPC-HB. Section 6.I.3 of this supplement provides the relevant details for this design. The MPC-HB is placed into the HI-STAR HB overpack, which is a shorter version of the HI-STAR 100 overpack. Also, revised assembly classes, designated 6x6D and 7x7C, are used in this supplement for the calculations with the MPC-HB. Finally, the number of cell locations for damaged fuel is increased to up to 40 per basket for the MPC-HB, compared to only 16 in the MPC-68. This is necessary since it is possible that a larger number of HBPP assemblies need to be loaded as damaged fuel.

The principal calculational results from this supplement, which address the following conditions:

- A single package, under the conditions of 10 CFR 71.55(b), (d), and (e);*
- An array of undamaged packages, under the conditions of 10 CFR 71.59(a)(1); and*
- An array of damaged packages, under the conditions of 10 CFR 71.59(a)(2)*

are summarized in Table 6.1.1 for all MPCs-HB and for the most reactive configuration and fuel condition in each MPC. Results are shown for both intact or undamaged assemblies only, and the bounding condition for intact or undamaged and damaged fuel (see Section 6.1.4.1 for a discussion on undamaged assemblies). The results demonstrate that the HI-STAR 100 System is in full compliance with 10CFR71 (71.55(b), (d), and (e) and 71.59(a)(1) and (a)(2)). The calculations for package arrays are performed for infinite arrays of HI-STAR 100 Systems under flooded conditions. Therefore, the CSI is zero (0). In addition, the table shows the result for an unreflected, internally flooded cask for each MPC. This configuration is used in many calculations and studies throughout this chapter, and is shown to yield results that are statistically equivalent to the results for the corresponding reflected package.

6.1.2 SPENT FUEL LOADING

The evaluations in Section 6.2 of the main body of Chapter 6 demonstrate that the bounding fuel dimensions consist of maximum active fuel length, maximum fuel pellet diameter, minimum cladding outside diameter (OD), maximum cladding inside diameter (ID), minimum guide tube/water rod thickness, and maximum channel thickness. A detailed review of the HBPP fuel information indicated that not all assemblies were bounded by the specification of the assembly classes 6x6C and 7x7A defined in Section 6.2. Therefore, expanded assembly classes, designated 6x6D and 7x7C, are used in this supplement for the calculations with the MPC-HB. The characteristics of these assembly classes are provided in Table 6.1.2.

6.1.3 MODEL SPECIFICATION

6.1.3.1 Calculational model

Figure 6.1.1 shows a representative horizontal cross section of the MPC-HB cells used in the calculations, and Figure 6.1.2 illustrates the basket configuration used. Based on the evaluations performed for the MPC-68 described in Section 6.3 of the main body of Chapter 6, the calculations use the minimum cell pitch and cell ID, and nominal cell wall thickness. The same techniques and the same level of detail are used in the calculational models as described in the main body of this chapter. Although the neutron absorber panels are 88 inches in length, which is much longer than the active fuel length (maximum of 80 inches), they are assumed equal to the active fuel length in the calculations.

6.1.3.2 Regional Densities

The densities and material compositions unique to the calculations in the MPC-HB are for the fuel and for the neutron absorber. These are listed in Table 6.1.3. All other compositions are the same as listed in Section 6.3 of the main body of this chapter. Note that the calculations conservatively take credit for only 75% of the minimum B-10 areal density of the neutron

absorber, which is less than the maximum value of 90% supported by the tests and qualifications prescribed in Chapter 8.

6.1.4 CRITICALITY CALCULATIONS

6.1.4.1 Intact and Undamaged Assemblies

Intact Assemblies

Results for calculation with intact assemblies of assembly class 6x6D and 7x7C are summarized in Table 6.1.4. The following conditions are evaluated:

- *Standard: Corresponds to assemblies located in the center of each cell, without DFCs*
- *Assemblies in DFCs: It might be beneficial to place not only damaged, but also intact assemblies into DFCs.*
- *Potential Poison Plate Damage: This condition is consistent with the condition evaluated in Section 6.4.11 of the main body of this chapter, assuming a 1 inch diameter at the center of each poison plate is replaced by water.*
- *Eccentric positioning: All assemblies are placed closest to the basket center*

The results demonstrate that the assembly class 6x6D, with eccentric positioning and assumed poison plate damage is the bounding condition for intact assemblies.

Undamaged Assemblies

Fuel inspection for HB fuel is limited to visual inspection, focusing predominantly on the rods on the periphery of the fuel assemblies. Assemblies with defects are considered damaged, and need to be placed into DFCs. The modeling of those assemblies is discussed in detail in the following subsection. However, even if no defects are detected in the inspection, some defects could exist in the inner rods of the assemblies that are not easily visible in the inspection. This means that even if no defects are detected, the assemblies may not be intact. This condition could later result in rod-breakage, which could potentially result in local relocation of fuel, creating areas with larger or smaller fuel amounts in the assembly. Note that any lateral relocation would be limited by the outer row of intact rods, and axial relocation would be limited by the grid spacers. To ensure such assemblies are qualified for loading without DFCs, additional calculations were performed where potential defects in those assemblies are modeled. The assemblies qualified this way are considered undamaged in respect to the criticality function of the cask, but not intact. In these models, the fuel rods on the periphery of the assembly remain in its original location, whereas inside the assembly various arrays of fuel rods are assumed. The array size is varied between a 3x3 array and a 7x7 array, which conservatively represents various rod damages, including axial relocation of fuel within the assembly. For each array size, two different rod pitch values are analyzed, one which spaces the rods evenly within the bounds of

the peripheral rods, and one with an enlarged pitch where the outer rods of the array are closer to the peripheral rods of the assembly. The higher of the two results is then used, which is typically that for the enlarged pitch. This variation in pitch is the reason that the undamaged 6x6 assembly with a 4x4 array of rods inside the peripheral rods has a higher k_{eff} than the corresponding intact assembly, despite the fact that the number of fuel rods is the same. To maximize any reactivity effect of these conditions, they are simultaneously assumed to be present in all assemblies in the basket, and along the entire active length. In the model for damaged fuel (see Section 6.1.4.2 below) it is conservatively assumed that all cladding has disappeared. This is not a credible condition for the defects in the interior rods of the assemblies, since there is no path for the cladding to get out of the interior of the assemblies. The various arrays used to represent the result of defects in the interior of the assembly are therefore modeled as cladded rods. Results of the analyses are shown in Table 6.1.4, and indicate a slight increase in reactivity for both assembly types compared to the intact condition. The maximum k_{eff} is determined for a 4x4 and 5x5 array within the fuel assembly for the 6x6 and 7x7 assemblies, respectively, ~~which is the condition with the highest k_{eff} value.~~ As for intact fuel, the 6x6 assembly presents the higher k_{eff} value.

The condition with assembly class 6x6D, undamaged fuel, eccentric positioning, and assumed poison plate damage is therefore used for ~~This condition is then used to perform~~ the calculations demonstrating compliance with the regulatory requirements shown in Table 6.1.1 for intact and undamaged fuel, except for the condition of the single unreflected package, which was analyzed without the assumed poison damage.

6.1.4.2 Damaged Assemblies

To conservatively model conditions of damaged fuel and fuel debris, the same approach is used as in Section 6.4.9 of the main body of this chapter, i.e., the fuel is represented by arrays of bare fuel rods in the DFC. Both the fuel rod diameter of the 6x6D fuel and 7x7C fuel is analyzed. A total of 6 different array sizes are analyzed for each condition. Additionally, two different DFC patterns are evaluated. The first pattern allows damaged fuel/fuel debris in DFCs in the 28 peripheral cells of the basket only. This first configuration is shown in Figure 6.1.3. For the second configuration, a checkerboard array of cells with intact and damaged fuel is analyzed, resulting in a total of 40 cells qualified for damaged fuel and fuel debris. This second configuration is shown in Figure 6.1.4. The calculations are performed in several steps, where in each step some of the principal parameters are varied such that the k_{eff} value is maximized. In all cases, the intact or undamaged assemblies are assumed to be assembly class 6x6D, which is bounding as shown in the previous subsection. For the damaged fuel and fuel debris in the DFCs, it is assumed that the fuel is present along the entire length of the DFC, including the areas that are not covered by the poison in the basket. Results for the two patterns, two pellet diameters, and various array sizes are listed in Table 6.1.5 for damaged and intact fuel. The results show that the bounding condition exists for the checkerboard array with the larger pellet ID, and a 7x7 array of bare rods. For this condition, further calculations were performed with assumed poison plate damage and eccentric positioning, as for intact fuel in the previous subsection. These results are listed in Table 6.1.6. As for the intact assemblies, the eccentric

~~damaged~~ for a single fully reflected package. The intact assembly in all cases is from array class 6x6D. The results are presented in Table 6.1.87, and show that reducing the water density results in a monotonic reduction of the reactivity. Optimum moderation at lower water densities does therefore not exist, and the fully flooded condition is bounding.

6.1.5 CRITICALITY BENCHMARKS

Fuel design, fuel conditions, basket design and moderation conditions are bounded by the corresponding conditions in the main body of Chapter 6. The benchmark calculations in the main body are therefore directly applicable to the calculations performed in this supplement.

6.1.6 REGULATORY COMPLIANCE

In summary, the evaluation presented in this supplement demonstrates that the HI-STAR HB System with fuel of the assembly classes 6x6D and 7x7C in the MPC-HB is in full compliance with the criticality requirements of 10CFR71.

Table 6.1.1

SUMMARY OF THE CRITICALITY RESULTS FOR THE MOST REACTIVE ASSEMBLY FROM THE ASSEMBLY CLASSES 6x6D AND 7x7C IN THE MPC-HB TO DEMONSTRATE COMPLIANCE WITH 10CFR71.55 AND 10CFR71.59

MPC-HB, Assembly Class 6x6D, 2.6 wt% ²³⁵U, all Intact or Undamaged Assemblies				
<i>Configuration</i>	<i>% Internal Moderation</i>	<i>% External Moderation</i>	<i>Applicable Requirement</i>	<i>Maximum k_{eff}</i>
<i>Single Package, unreflected</i>	100%	0%	n/a	0.84010.8464
<i>Single Package, fully reflected</i>	100%	100%	10CFR71.55 (b), (d), and (e)	0.84100.8480
<i>Containment, fully reflected</i>	100%	100%		0.83940.8472
<i>Infinite Array of Damaged Packages</i>	100%	100%	10CFR71.59 (a)(2)	0.84000.8477
<i>Infinite Array of Undamaged Packages</i>	0%	0%	10CFR71.59 (a)(1)	0.38040.3790
MPC-HB, Assembly Class 7x7C, 2.6 wt% ²³⁵U, Intact or Undamaged and Damaged Assemblies				
<i>Configuration</i>	<i>% Internal Moderation</i>	<i>% External Moderation</i>	<i>Applicable Requirement</i>	<i>Maximum k_{eff}</i>
<i>Single Package, unreflected</i>	100%	0%	n/a	0.89810.9018
<i>Single Package, fully reflected</i>	100%	100%	10CFR71.55 (b), (d), and (e)	0.89900.9017
<i>Containment, fully reflected</i>	100%	100%		0.89860.9026
<i>Infinite Array of Damaged Packages</i>	100%	100%	10CFR71.59 (a)(2)	0.90030.9022
<i>Infinite Array of Undamaged Packages</i>	0%	0%	10CFR71.59 (a)(1)	0.38570.3858

Table 6.1.2
BWR FUEL CHARACTERISTICS AND ASSEMBLY CLASS DEFINITIONS FOR HBPP FUEL
(all dimensions are in inches)

<i>Fuel Assembly Designation</i>	<i>Clad Material</i>	<i>Pitch</i>	<i>Number of Fuel Rods</i>	<i>Cladding OD</i>	<i>Cladding Thickness</i>	<i>Pellet Diameter</i>	<i>Active Fuel Length</i>	<i>Number of Water Rods</i>	<i>Water Rod OD</i>	<i>Water Rod ID</i>	<i>Channel Thickness</i>	<i>Channel ID</i>
<i>6x6D Assembly Class</i>												
<i>6x6D01</i>	<i>Zr</i>	<i>0.740</i>	<i>36</i>	<i>0.5585</i>	<i>0.02675</i>	<i>0.4880</i>	<i>80</i>	<i>0</i>	<i>n/a</i>	<i>n/a</i>	<i>0.060</i>	<i>4.542</i>
<i>7x7C Assembly Class</i>												
<i>7x7C01</i>	<i>Zr</i>	<i>0.631</i>	<i>49</i>	<i>0.4860</i>	<i>0.0300</i>	<i>0.4110</i>	<i>80</i>	<i>0</i>	<i>n/a</i>	<i>n/a</i>	<i>0.060</i>	<i>4.542</i>

Table 6.1.3

COMPOSITION OF THE MAJOR COMPONENTS OF THE HI-STAR HB SYSTEM

METAMIC (0.0075 g ¹⁰B/cm²), DENSITY = 2.667 g/cm³	
Nuclide	Atom Density (atoms/(barn*cm))
¹⁰ B	3.5529E-03
¹¹ B	1.4721E-02
C	4.5656E-03
Al	5.0402E-02
UO₂, 2.6 wt% INITIAL ENRICHMENT, DENSITY = 10.522 g/cm³	
Nuclide	Wgt. Fraction
²³⁵ U	0.02292
²³⁸ U	0.85858
O	0.11850

Table 6.1.4

MAXIMUM k_{eff} VALUES FOR ASSEMBLY CLASSES 6x6D AND 7x7C IN THE MPC-HB FOR INTACT AND UNDAMAGED FUEL WITH AN AVERAGE ENRICHMENT OF 2.6 wt% ^{235}U .

<i>Assembly Class</i>	<i>Configuration</i>	<i>Maximum k_{eff}</i>
6x6D	<i>Intact, Standard</i>	0.8318
7x7C	<i>Intact, Standard</i>	0.8237
6x6D	<i>Intact Assemblies in DFCs</i>	0.8069
6x6D	<i>Intact, Potential Poison Plate Damage</i>	0.8335
6x6D	<i>Intact, Eccentric Fuel Positioning</i>	0.8401
6x6D	<i>Undamaged, Eccentric Fuel Positioning</i>	0.8464
7x7C	<i>Undamaged</i>	0.8333
7x7C	<i>Undamaged, Eccentric Fuel Positioning</i>	0.8400

Table 6.1.5

MAXIMUM k_{eff} VALUES FOR THE MPC-HB WITH INTACT FUEL AND DAMAGED FUEL/FUEL DEBRIS WITH AN AVERAGE ENRICHMENT OF 2.6 wt% ^{235}U

DFC Pattern	Maximum k_{eff}			
	Basket Periphery (28 DFCs)		Checkerboard (40 DFCs)	
Pellet Diameter	0.411"	0.488"	0.411"	0.488"
DFC Rod Array				
5x5	n/c [†]	0.8307	n/c	0.8092
6x6	0.8324	0.8389	0.8234	0.8682
7x7	0.8383	0.8444	0.8684	0.8906
8x8	0.8433	0.8422	0.8875	0.8846
9x9	0.8449	0.8372	0.8875	0.8602
10x10	0.8400	0.8331	0.8742	0.8343
11x11	0.8352	n/c	0.8512	n/c

[†] n/c = not calculated

Table 6.1.6

MAXIMUM k_{eff} VALUES FOR THE MPC-HB WITH INTACT FUEL AND DAMAGED FUEL/FUEL DEBRIS WITH AN AVERAGE ENRICHMENT OF 2.6 wt% ^{235}U

<i>Configuration</i>	<i>Maximum k_{eff}</i>
<i>Standard</i>	<i>0.8906</i>
<i>Potential Poison Plate Damage</i>	<i>0.8896</i>
<i>Eccentric Fuel Positioning</i>	<i>0.8981</i>

Table 6.1.7

MAXIMUM k_{eff} VALUES FOR THE MPC-HB WITH UNDAMAGED FUEL AND DAMAGED FUEL/FUEL DEBRIS WITH AN AVERAGE ENRICHMENT OF 2.6 wt% ^{235}U

Rod Array inside undamaged assemblies	Maximum k_{eff}	
	Fuel and DFCs Centered in Basket Cells	Eccentric positioning of Fuel and DFCs
3x3	0.8784	0.8849
4x4	0.8938	0.9018
5x5	0.8786	0.8874
6x6	0.8601	0.8671

Table 6.I.78

MAXIMUM k_{eff} VALUES FOR ASSEMBLY CLASSES 6x6D AND 7x7C
WITH REDUCED WATER DENSITY IN THE MPC.

Water Density (% of Full Density)	Maximum k_{eff} for Assembly Class 6x6D, all intact assemblies	Maximum k_{eff} for Assembly Class 7x7C, intact and damaged assemblies
100 (Reference)	0.8410	0.9003
98	0.8385	0.8997
95	0.8380	0.8951
90	0.8304	0.8857
80	0.8127	0.8717
70	0.7963	0.8513
50	0.7444	0.8113
30	0.6549	0.7870
10	0.5045	0.5832
5	0.4470	0.4782

Figure Withheld Under 10 CFR 2.390

FIGURE 6.1.1; TYPICAL CELL IN THE CALCULATION MODEL (PLANAR CROSS-SECTION)
WITH REPRESENTATIVE FUEL IN THE MPC-HB BASKET
(SEE CHAPTER 1 FOR TRUE BASKET DIMENSIONS)

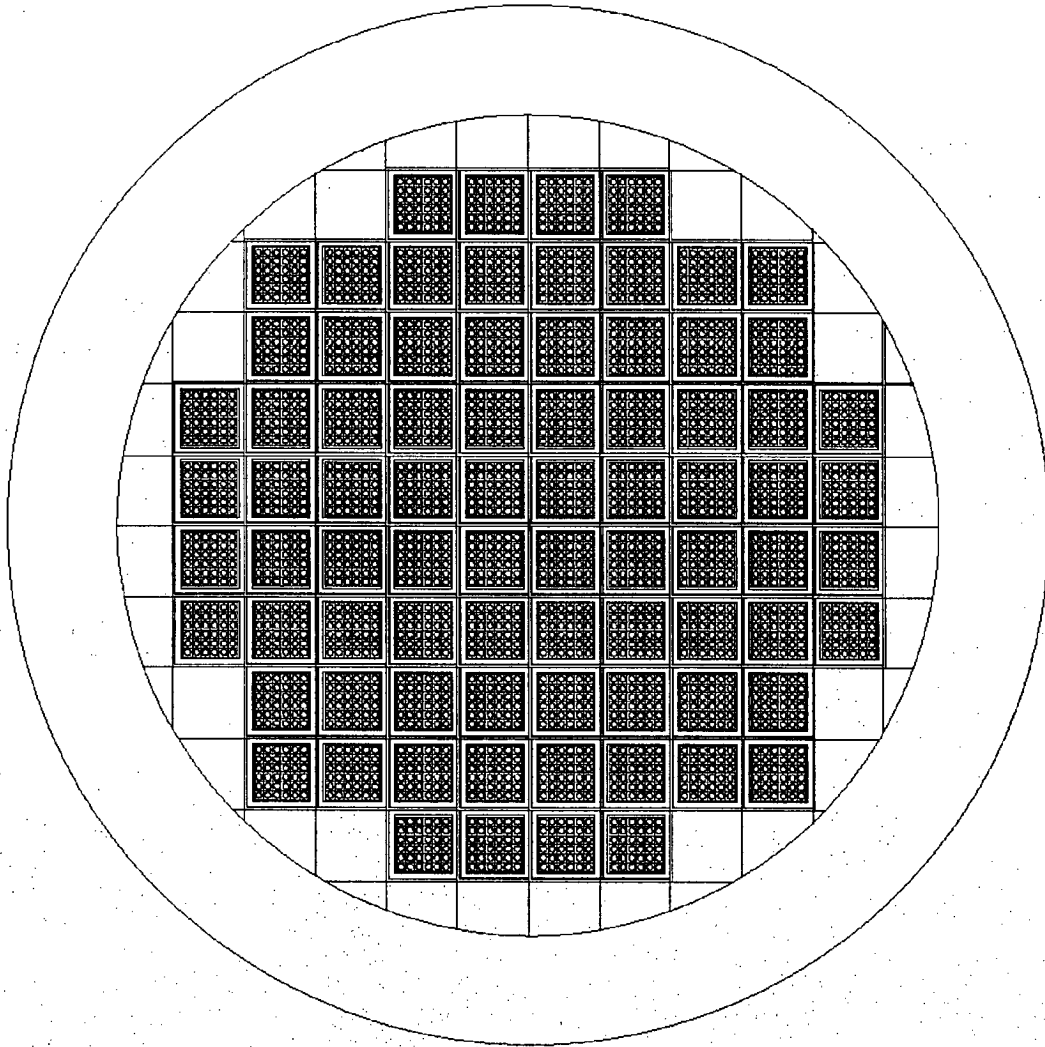
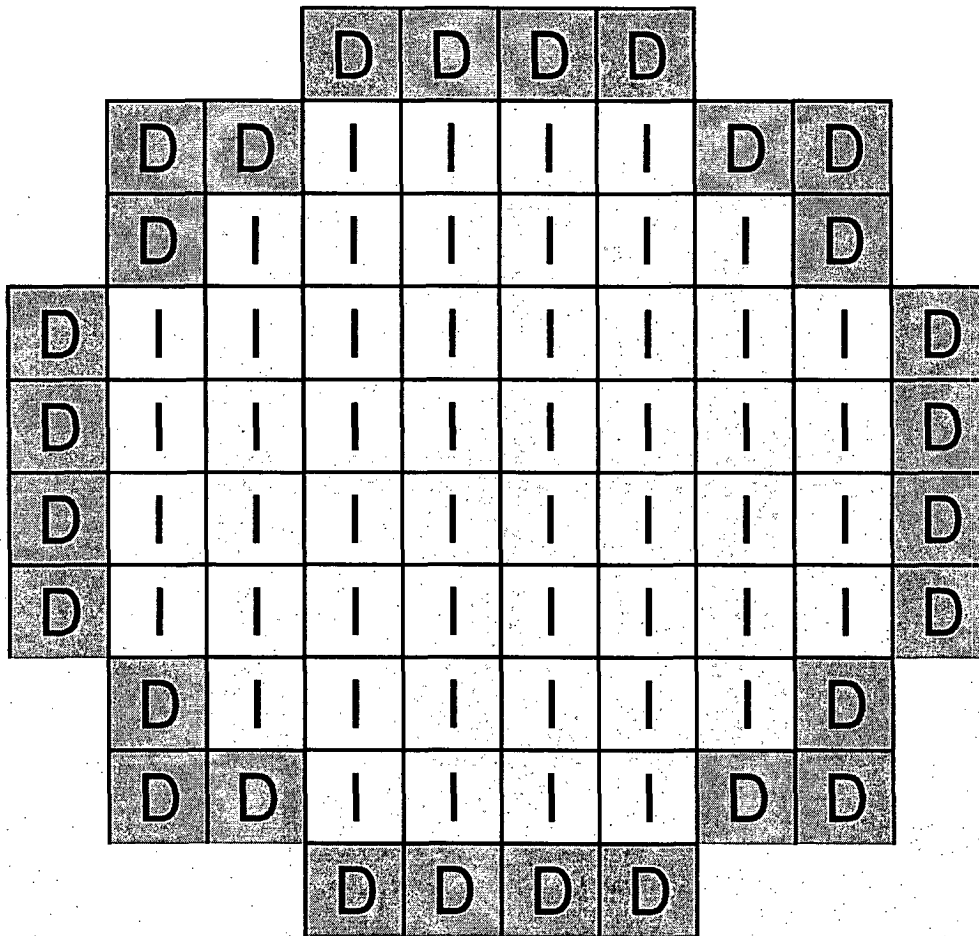
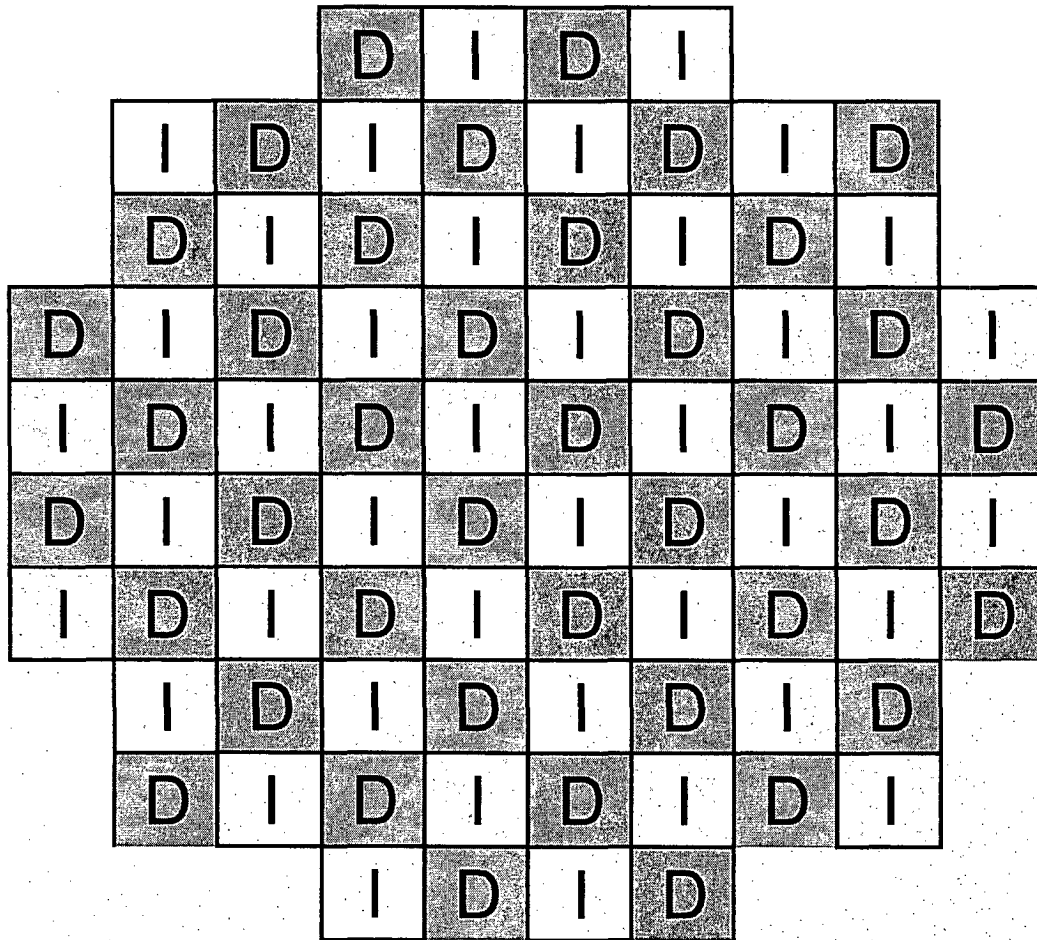


Figure 6.I.2 Radial Cross Section of Criticality Model (Intact Assemblies) generated by MCNP



I	Intact Assembly (with or w/o DFC)
D	Damaged Fuel/Fuel Debris in DFC

Figure 6.I.3: Damaged Fuel/Fuel Debris in Peripheral Cells of Basket only. Note that undamaged assemblies are permitted in all locations for intact assemblies.



I	Intact Assembly (with or w/o DFC)
D	Damaged Fuel/Fuel Debris in DFC

Figure 6.I.4: Checkerboard of Damaged Fuel/Fuel Debris and Intact Fuel. Note that undamaged assemblies are permitted in all locations for intact assemblies.

CHAPTER 7: OPERATING PROCEDURES

7.0 INTRODUCTION

This chapter provides the high level description of the essential elements necessary to prepare the system for shipment and to ensure that its performance under normal and accident conditions will be as described in the system evaluation. The information described in the chapter contains the minimum requirements that will ensure that the HI-STAR 100 System is operated in a safe and reliable manner consistent with the evaluation in the SAR. Holtec will use the information presented in this chapter along with their knowledge of the technical basis of the system design described in chapters 2 through 6 to develop more detailed generic procedures for the HI-STAR 100 System. Equipment specific operating details such as valve manipulation and onsite transporter operation will be provided to users based on the specific equipment selected and the configuration of the site. Licensees will utilize the information provided in this chapter, (understanding that it provides the essential operation elements that must be included in the detailed operating procedures), the conditions of the Certificate of Compliance (CoC), equipment-specific operating instructions, and plant working procedures and apply them to develop the site-specific written loading, unloading, and handling procedures to ensure that the system is operated in accordance with the system CoC and all applicable government regulatory requirements. Users may add, modify the sequence of, perform in parallel, or delete steps as necessary, provided that the intent of this chapter and the requirements of the CoC are met.

The operations described in this chapter assume that the fuel will be loaded into, or unloaded from, an MPC while in the HI-STAR overpack submerged in a spent fuel pool. With some modifications, the information presented herein can be used to develop site-specific procedures for loading or unloading fuel into the system within a hot cell or other remote handling facility. Because the HI-STAR is a dual-use cask certified for use as a dry storage cask under 10 CFR 72, the descriptions below include the steps required to transport the cask after a period of storage. The chapter also provides a description of the essential elements necessary to transfer a Holtec MPC from a dry storage system into the HI-STAR system for transportation.

It is the cask user's responsibility to develop the site-specific operating procedures in accordance with the system CoC, the information presented in this chapter, and applicable regulatory requirements. Users will be required to develop or modify existing programs and procedures to account for the transport operation of the HI-STAR 100 System. Written procedures are required and will be developed or modified to account for such things as nondestructive examination (NDE) of the MPC welds, handling and storage of items and components identified as important to safety, heavy load handling, specialized instrument calibration, special nuclear material accountability, fuel handling procedures, training, equipment and process qualifications. Users shall implement controls to ensure that the lifted weights do not exceed the HI-STAR 100 lifting trunnion design limit. Users shall implement controls to monitor the time limit from the removal of the HI-STAR 100 from the spent fuel pool to the commencement of MPC draining to prevent boiling. Users shall also implement controls to ensure that the HI-STAR 100 overpack cannot be subjected to a fire in excess of design limits during loading operations.

Control of system operation shall be performed in accordance with the licensee's Quality Assurance (QA) program to ensure critical steps are not overlooked and that the MPC and overpack, as applicable, have been confirmed to meet all requirements of the Part 71 CoC before being released for shipment.

Table 7.1.1 provides the HI-STAR 100 System bolt torque and sequencing requirements. Fuel assembly selection and verification shall be performed by the licensee in accordance with written, approved procedures that ensure that only SNF assemblies authorized in the CoC are loaded into the HI-STAR 100 System. Fuel handling, including the handling of fuel assemblies in the Damaged Fuel Container (DFC) shall be performed in accordance with written site-specific procedures. Damaged fuel and fuel debris, as defined in the CoC, shall be loaded in DFCs.

ALARA notes and warnings are included to alert users to radiological issues. Actions identified with these notes and warnings are not mandatory and shall be implemented based on a determination by radiation protection.

Supplementary guidance for each of the sections in Chapter 7 that are specific to HI-STAR HB operations are found in Supplement 7.I.

7.1 PROCEDURE FOR LOADING AND PREPARATION FOR TRANSPORT OF THE HI-STAR 100 SYSTEM

7.1.1 Overview of HI-STAR Loading Operations

The MPC loading operations described herein are for HI-STAR 100 systems prepared for "load-and-go" directly into transportation under 10CFR71. HI-STAR 100 systems that are loaded and stored on an ISFSI site must be prepared in accordance with the applicable Part 72 HI-STAR FSAR or HI-STORM FSAR license and respective Certificate of Compliance (CoC). Any HI-STAR overpack and/or MPC deployed at an ISFSI must be confirmed to meet all conditions of the 10CFR71 CoC prior to shipment. The dryness criteria under the Part 72 CoC shall be considered acceptable for use in transport under Part 71 [7.1.2], [7.1.6].

The HI-STAR 100 System (HI-STAR) is used to load and transport spent nuclear fuel (SNF). The essential elements required to prepare the HI-STAR for fuel loading, to load the fuel, to ready the system for transport, and to ship the HI-STAR are described below.

7.1.2 Preparation of HI-STAR for Loading

- 1. If the HI-STAR overpack has previously been used to transport SNF, the HI-STAR overpack is received and the personnel barrier, if attached, is removed. The security seals, if used, are inspected to verify there was no tampering and that they match the corresponding shipping documents.*
- 2. The HI-STAR is visually receipt inspected to verify that there are no outward visual indications of impaired physical condition except for superficial marks and dents. Any road dirt is washed off and any foreign material is removed.*
- 3. Radiological surveys are performed in accordance with 49CFR173.443 [7.1.3] and 10CFR20.1906 [7.1.4]. Any issues are identified to site management and the overpack is decontaminated as directed by site radiation protection and make appropriate notifications as detailed in the surveillance requirements.*
- 4. The impact limiters, if attached, are removed and a second visual inspection to verify that there are no outward visual indications of impaired physical condition is performed.*
- 5. The HI-STAR overpack is upended and the neutron shield relief devices are inspected to confirm that they are installed, intact, and not covered by tape or any other covering.*

7.1.3 Loading of Contents into HI-STAR

7.1.3.1 Loading of SNF into HI-STAR from a Spent Fuel Pool

- 1. The HI-STAR is positioned in the MPC loading area.*
- 2. An empty MPC is upended and prepared for loading. The MPC is subjected to receipt*

inspection (inspected for cleanliness and outward visual indications of impaired physical condition except for superficial marks and dents). Road dirt/debris and any foreign material are removed from the MPC prior to placement in the spent fuel pool. Verification is made to ensure that the appropriate fuel spacers, as necessary, are used to position the active fuel zone within the neutron absorber plates of the MPC, and limit axial movement of the fuel assemblies in the MPC cavity. The empty MPC is raised and inserted into the HI-STAR overpack while being careful not to damage the HI-STAR sealing surface. The MPC is inspected to ensure that the neutron absorber panel sheathing is present and there are no signs of potential damage to the neutron absorber.

- 3. The annulus is filled with clean (uncontaminated) water and the annulus seal is installed in the annulus between the MPC and the HI-STAR overpack.*

ALARA Note:

A bottom protective cover may be attached to the cask bottom or placed in the designated preparation area or spent fuel pool. This will help prevent embedding contaminated particles in the cask bottom surface and ease the decontamination effort. Waterproof tape placed over empty bolt holes, and bolt plugs may also reduce the time required for decontamination. Wetting the components that enter the spent fuel pool may reduce the amount of decontamination work to be performed later.

- 4. The MPC is filled with either spent fuel pool water or clean water and the HI-STAR is raised and lowered into the spent fuel pool for fuel loading.*
- 5. Prior to loading the fuel into the MPC, the user identifies the fuel to be loaded. A pre-loading verification is made to assure that damaged fuel and fuel debris will be placed in damaged fuel containers and that the DFCs will occupy authorized locations in the MPC. The fuel is independently verified to see that it meets the conditions of the CoC. The pre-selected assemblies are loaded into the MPC using DFCs as required, and a visual verification of the assembly identification is performed.*
- 6. While still underwater, a thickly shielded lid (the MPC lid) is positioned over the pool surface and the drain line is installed. The MPC lid drain line is guided into its receiver and the MPC lid is installed. The upper surface of the MPC lid will seat approximately flush with the top edge of the MPC shell when properly installed. The lid may be removed and the drain line replaced should it be damaged during installation of the MPC lid. The user performs a site-specific Time-to-Boil analysis. This determines a time limit that ensures water in the MPC will not boil prior to the start of the draining operations. If it appears that the Time-to-Boil limit will be exceeded prior to draining the MPC, the user shall take appropriate action to prevent water from boiling.*

ALARA Note:

Activated debris may have settled on flat surfaces of the cask during fuel loading. Cask surfaces suspected of carrying activated debris should be kept under water until a preliminary dose rate scan clears the cask for removal.

7. *The lift attachment engages the HI-STAR overpack lifting trunnions to lift the HI-STAR overpack and loaded MPC close to the spent fuel pool surface.*

ALARA Note:

Radiation and contamination surveys are performed on the overpack and MPC lid as the overpack is removed from the spent fuel pool. To reduce decontamination time, the surfaces of the cask and lift yoke should be kept wet until decontamination begins. Decontamination of the cask bottom should be performed using pole-mounted cleaning devices.

8. *The HI-STAR is removed from the spent fuel pool. If a lid retention system is being used, it is installed to secure the MPC lid for the transfer to the cask preparation area. The lift attachment and HI-STAR overpack are sprayed with clean water to help remove contamination as they are removed from the spent fuel pool.*
9. *The HI-STAR overpack is placed in the designated preparation area and the lift attachment and lid retention system, as applicable, are removed.*
10. *The top surfaces of the MPC lid, upper accessible regions of the MPC external shell and the upper flange of the HI-STAR overpack are decontaminated.*

ALARA Note:

The water in the HI-STAR 100 overpack-to-MPC annulus provides personnel shielding. The level should be checked periodically and refilled accordingly. Pocket trunnions, if present and not used are plugged to reduce radiation levels around the lower region of the overpack.

11. *The temporary shield ring, if used, is installed. The annulus seal is removed, and an annulus shield is installed. The temporary shield ring provides additional personnel shielding around the top of the HI-STAR overpack during MPC closure operations. The annulus shield also provides additional personnel shielding at the top of the annulus and prevents small items from being dropped into the annulus.*
12. *Dose rates are measured at the MPC lid and around the HI-STAR overpack to establish appropriate radiological control.*

ALARA Warning:

Personnel should remain clear of the drain lines any time water is being pumped or purged from the cask. Assembly crud, suspended in the water, may create a radiation hazard to workers. Dose rates will rise as water is drained from the cask. Continuous dose rate monitoring is recommended.

ALARA Warning:

The use of manual welding should be minimized and only used when deemed advantageous from an ALARA perspective. If manual welding is elected, it should only be performed under conditions consistent with ALARA principals (e.g., utilizing temporary shielding).

13. *The MPC water level and water level in the annulus are lowered slightly; the MPC is vented or purged and checked for combustible gas concentrations. The MPC lid is seal welded using an automated welding system, by manual welding, or a combination of both.*
14. *Visual examinations are performed on the tack welds. Liquid penetrant (PT) examinations are performed on the root and final passes. A volumetric examination is performed on the MPC welds using the ultrasonic method to ensure that the completed weld is satisfactory. As an alternative to volumetric examination of the MPC lid-to-shell weld, a multi-layer PT may be performed including intermediate examinations after approximately every three-eighth inch of weld depth. Any unsatisfactory indications are repaired in accordance with the code requirements [7.1.1].*
15. *At the appropriate time in the sequence of activities, based on the type of test performed (hydrostatic or pneumatic), an ASME pressure test of the MPC enclosure vessel is performed in accordance with the requirements of Section III, Subsection NB, Article NB-6000 and applicable subarticles [7.1.1]. Any non-satisfactory conditions require the user to determine the cause of the leak and make repairs as necessary to achieve a successful result.*

ALARA Note:

Dose rates will rise as water is drained from the MPC. Continuous dose rate monitoring is recommended.

16. *The MPC water is displaced from the MPC and the water is drained from the annulus area.*
17. *The Forced Helium Dehydration (FHD) is connected to the MPC and is used to remove moisture from the MPC. To ensure that the MPC cavity is suitably dry either the temperature or the dew point of the helium exiting the FHD demoisturizer shall be less*

than or equal to 22.9 °F for no less than 30 minutes.

18. *The MPC helium backfill is adjusted to the pressure equivalent of greater than 0 psig and less than 44.8 psig at a reference temperature of 70 degrees Fahrenheit.*
19. *Cover plates are installed and seal welded over the MPC vent and drain ports and PT examinations are performed on the root (for multi-pass welds) and final passes. Any unsatisfactory indications are repaired in accordance with the code requirements.*
20. *The MPC closure ring is placed on the MPC.*
21. *The closure ring is aligned, tacked in place, and seal welded. Tack welds are visually examined and PT examinations are performed on the root (for multi-pass welds) and final welds.*
22. *The annulus shield and the temporary shield ring (if used) are removed.*

7.1.3.2 Not Used

7.1.3.3 Loading a Loaded and Sealed MPC into HI-STAR Overpack

1. *After the HI-STAR overpack has been prepared in accordance with Section 7.1.2 above, it is placed in the MPC transfer location and is fitted with a mating device to interface with the transfer cask.*
2. *The transfer cask with loaded MPC is brought to the MPC transfer location and placed atop the HI-STAR overpack and mating device.*
3. *The mating device is used to open the bottom of the transfer cask and the MPC is lowered into the HI-STAR overpack.*
4. *The transfer cask and mating device are removed from the HI-STAR.*

7.1.4 Closure of HI-STAR

1. *The MPC lid and accessible areas at the top of the MPC shell are smeared for removable contamination. Decontamination of the MPC lid and accessible areas at the top of the MPC may be performed at any time prior to closure of the HI-STAR overpack.*
2. *The sealing surfaces for the HI-STAR overpack are inspected for signs of damage. Any damage that would prevent a seal is remedied, any old seals are discarded, new seals are inserted for the closure plate, and the closure plate is installed with the bolts torqued in accordance with requirements in Table 7.1.1 and the order prescribed in Figure 7.1.1.*
3. *The HI-STAR overpack annulus is dried by evacuating to a pressure of less than or equal to 3 torr. The overpack annulus shall be considered dry when it can hold a stable pressure of less than or equal to 3 torr for at least 30 minutes.*

4. *The HI-STAR overpack is then backfilled with helium gas to a pressure of greater than or equal to 10 psig and less than or equal to 14 psig.*
5. *Any old seals are removed from the HI-STAR overpack vent and drain plugs and the plugs are installed with new seals and torqued in accordance with Table 7.1.1.*
6. *All HI-STAR overpack containment boundary seals, e.g. closure plate, vent and drain ports, are leak tested to assure they will provide long-term retention of the annulus helium. All HI-STAR overpack containment boundary seals shall be leak tested in accordance with ANSI N14.5 [7.1.5] and shall demonstrate compliance with the leakage rate acceptance criterion in SAR Section 4.1. Unacceptable leakage rates will require repair and re-testing of the seals. The leak test shall be performed within the 12-month period prior to each shipment and after de-tensioning one or more overpack lid bolts, drain port, or the vent port plug;*
7. *The HI-STAR 100 overpack vent and drain port cover plates are installed.*
8. *The HI-STAR 100 overpack is surveyed for removable contamination per 49CFR173.443 [7.1.3]. If necessary, the overpack is further decontaminated to meet the surveillance requirements.*

7.1.5 Preparation of HI-STAR for Transport

1. *Verify the HI-STAR has been leak tested within the past 12 months and no overpack lid bolts and vent and drain port plugs have been de-tensioned. If not, the HI-STAR is leak tested in accordance with Step 6 of Section 7.1.4 above.*
2. *The relief devices on the neutron shield vessel are verified that they have been replaced within the past 5 years. If not, the relief devices are replaced.*

ALARA Warning:

Dose rates around the unshielded bottom end of the cask may be higher than other locations around the cask. After the cask is downended on the transport frame, the bottom impact limiter should be installed promptly. Personnel should remain clear and exercise other appropriate ALARA controls when working around the bottom end of the cask.

3. *Buttress plate is installed and the HI-STAR overpack is moved to the transport location. The HI-STAR is down-ended and placed on the transport vehicle. Pocket trunnions are plugged if present and not in use on the transport vehicle.*
4. *HI-STAR is visually inspected for signs of impaired condition.*
5. *Contamination surveys are performed on the HI-STAR per 49CFR173.443 [7.1.3]. If necessary, the overpack is further decontaminated to meet the surveillance requirements.*

6. *The impact limiters are installed on the HI-STAR and the bolts are torqued in accordance with Table 7.1.1.*
7. *The tie-down system is installed and a security seal, one per impact limiter is installed and the seal numbers are recorded in the shipping documents.*
8. *Final radiation surveys of the package surfaces per 10CFR71.47 [7.1.4] and 49CFR173.443 [7.1.3] are performed and recorded in the shipping documents.*
9. *The personnel barrier is installed.*
10. *The assembled package is given a final inspection to verify that all conditions for transport have been met (inspection steps may be performed in any order):*
 - a. *Verify that required radiation survey results are properly documented on the shipping documentation.*
 - b. *Perform a HI-STAR overpack surface temperature check. The accessible surfaces of the HI-STAR Package (impact limiters and personnel barrier) shall not exceed the Exclusive Use temperature limits of 49CFR173.442 [7.1.3].*
 - c. *Verify that all required leakage testing has been performed, the acceptance criteria have been met, and the results have been documented on the shipping documentation.*
 - d. *Verify that the receiver has been notified of the impending shipment and that the receiver has the appropriate procedures and equipment available to safely receive and handle the HI-STAR (10CFR20.1906(e)) [7.1.4].*
 - e. *Verify that the carrier has the written instructions and a list of appropriate contacts for notification of accidents or delays.*
 - f. *Verify that the carrier has written instructions that the shipment is to be Exclusive Use in accordance with 49CFR173.441 [7.1.3].*
 - g. *Verify that route approvals and notification to appropriate agencies have been completed.*
 - h. *Verify that the appropriate labels have been applied in accordance with 49CFR172.403 [7.1.3].*
 - i. *Verify that the appropriate placards have been applied in accordance with 49CFR172.500 [7.1.3].*
 - j. *Verify that all required information is recorded on the shipping documentation.*
11. *Following the above checks, the HI-STAR 100 System is released for transport.*

Table 7.1.1
HI-STAR 100 SYSTEM TORQUE REQUIREMENTS

Fastener	Torque (ft-lbs)	Pattern
<i>Overpack Closure Plate Bolts^{†, ††}</i>	<i>First Pass – Hand Tight Second Pass – Wrench Tight Third Pass – 860 +25/-25 Fourth Pass – 1725 +50/-50 Final Pass - 2000 +250/-0</i>	<i>See Figure 7.1.1</i>
<i>Overpack Vent and Drain Port Plugs</i>	<i>45+5/-2</i>	<i>None</i>
<i>Closure Plate Test Port Plug</i>	<i>45+5/-2</i>	<i>None</i>
<i>Top Impact Limiter Attachment Bolt</i>	<i>256+10/-0</i>	<i>None</i>
<i>Bottom Impact Limiter Attachment Bolt</i>	<i>1500+45/-0</i>	<i>None</i>

† *Detorquing shall be performed by turning the bolts counter-clockwise in 1/3 turn +/- 30 degrees increments per pass according to Figure 7.1.1 for three passes. The bolts may then be removed.*

†† *Bolts shall be cleaned and inspected for damage or excessive wear (replaced if necessary) and coated with a light layer of Fel-Pro Chemical Products, N-5000, Nuclear Grade Lubricant (or equivalent).*

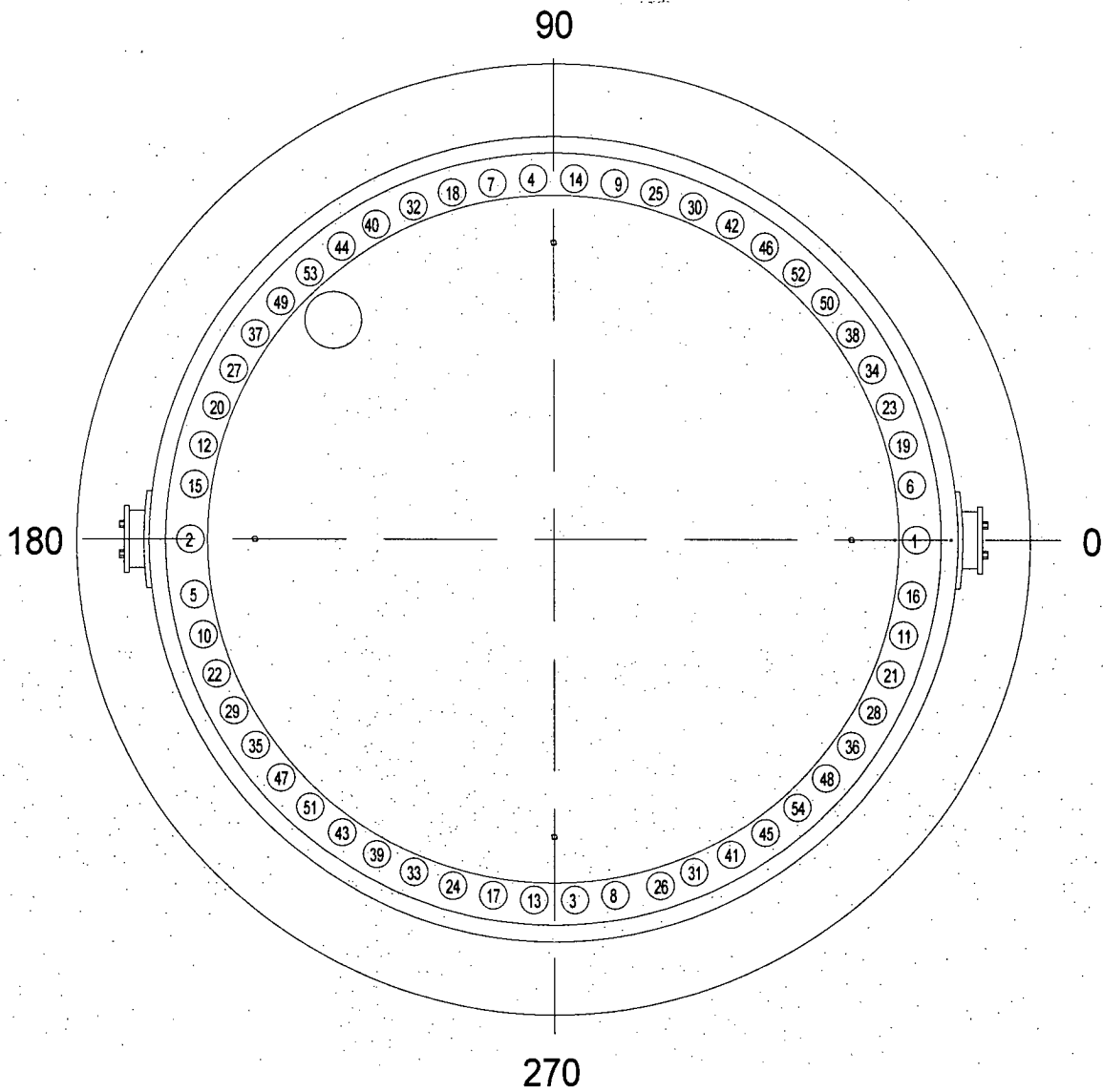


Figure 7.1.1; HI-STAR Closure Plate Bolt Torquing Pattern

7.2 PROCEDURE FOR UNLOADING THE HI-STAR 100 SYSTEM

The essential elements required to prepare the system for fuel unloading, to cool the stored fuel assemblies in the MPC, to flood the MPC cavity, to remove the lid welds, to unload the spent fuel assemblies, and to recover the HI-STAR 100 overpack and empty MPC are described below.

7.2.1 Receipt of Package from Carrier

1. *The HI-STAR 100 overpack is received from the carrier and inspected to verify that there are no outward visual indications of impaired physical conditions except for superficial marks and dents. Any road dirt is washed off and any foreign material is removed.*
2. *The personnel barrier is removed and the security seals are inspected to verify there was no evidence of tampering and that they match the corresponding shipping documents. Any discrepancies are identified to the site management and appropriate authorities.*

ALARA Warning:

Dose rates around the unshielded bottom end of the HI-STAR 100 cask may be higher than other locations around the cask. After the impact limiter is removed, the cask should be upended promptly. Personnel should remain clear of the bottom of the unshielded cask and exercise other appropriate ALARA controls.

3. *The impact limiters are removed.*
4. *The HI-STAR is visually inspected to verify there are no outward visual indications of impaired physical conditions except for superficial marks and dents, the neutron shield relief devices are inspected to confirm that they are installed, intact, and not covered, and radiation survey and removable contamination survey are performed per 49CFR173.443 [7.1.3]. Any issues are identified to site management and the overpack is decontaminated as directed by site radiation protection. Note that portions of the inspections, surveys, and decontamination activities described here-in may be performed prior to removal of the impact limiters.*
5. *The HI-STAR 100 overpack is upended and returned to the fuel building or other unloading area.*
6. *The buttress plate is removed and the HI-STAR 100 overpack is placed in the designated preparation area. Removal of the buttress plate may be performed prior to placing the HI-STAR in the designated preparation area.*

7.2.2 Removal of Contents

1. *The HI-STAR 100 overpack vent port cover plate is removed and a gas sample is drawn from the HI-STAR 100 overpack annulus to determine the condition of the MPC confinement boundary.*
2. *The annulus is depressurized in accordance with Radiation Protection directions and the HI-STAR 100 overpack closure plate is removed.*
3. *The annulus is filled with clean water and an annulus shield is installed to protect the annulus from debris produced from the lid removal process.*
4. *The MPC closure ring above the vent and drain ports and the vent and drain port cover plates are core-drilled and removed to access the vent and drain ports.*

ALARA Warning:

Gas sampling is performed to assess the condition of the fuel cladding. If a leak is discovered in the fuel cladding, the user's Radiation Control organization may require special actions to vent the cask cavity.

5. *A temporary attachment is connected to the vent port to open the vent port and collect a gas sample from inside the MPC. A gas sample analysis is performed to assess the condition of the fuel assembly cladding.*
6. *If the MPC is to be unloaded under water, the MPC is cooled as necessary to reduce the MPC internal temperature. This allows water flooding without thermally shocking the fuel assemblies or over-pressurizing the MPC from the formation of steam. The MPC is then filled with water.*
7. *The MPC lid to MPC shell weld is removed using an automated weld removal system or other suitable equipment. The weld removal equipment is removed with the MPC lid left in place.*
8. *The top surfaces of the HI-STAR 100 overpack and MPC are cleared of metal shavings.*
9. *The annulus shield is removed and if necessary, the annulus is re-filled with clean water and an annulus seal is installed.*
10. *The MPC lid is rigged to the lift equipment and the lift attachment is engaged to the HI-STAR 100 overpack lifting trunnions.*

ALARA Note:

Wetting the components that enter the spent fuel pool may reduce the amount of decontamination work to be performed later.

11. *The HI-STAR 100 overpack is placed in the spent fuel pool or other appropriate unloading area and the MPC lid is removed.*
12. *All fuel assemblies are returned to the spent fuel storage racks and the MPC fuel cells are vacuumed to remove any assembly debris and crud.*
13. *The fuel cells are inspected for any remaining items and these are removed as appropriate.*

ALARA Warning:

Activated debris may have settled on flat surfaces of the cask during fuel unloading. Surfaces suspected of carrying activated debris should be kept under water until a preliminary dose rate scan clears the cask for removal. To reduce contamination of the cask, the surfaces of the cask and lift yoke should be kept wet until decontamination can begin.

14. *The HI-STAR 100 overpack and MPC are returned to the designated preparation area where any water in the MPC is pumped back into the spent fuel pool, liquid radwaste system or other approved location as necessary.*
15. *The annulus water is drained and the MPC and overpack are decontaminated.*

The essential elements for preparing an empty package (previously used) for transport are similar to those required for transporting the loaded package with several exceptions. A survey for removable contamination is performed to verify that the removable contamination on the internal and external surfaces of the HI-STAR 100 overpack are ALARA and that the limits of 49CFR173.428 [7.1.3] and 10CFR71.87(i) [7.1.4] are met. At the user's discretion, impact limiters are installed and the personnel barrier is installed and locked. The installation of the impact limiters and personnel barrier are described in this Section. These steps may be omitted.

1. The Seal Surface Protector is removed from the HI-STAR 100 overpack if necessary.
2. HI-STAR 100 Overpack is surveyed for contamination and verified to be empty and contain less than 15 gm U-235 in accordance with 49CFR173.421(a)(5) [7.1.3].
3. The closure plate is installed on the HI-STAR 100 overpack and the bolts are torqued in accordance with requirements in Table 7.1.1 and the order prescribed in Figure 7.1.1.
4. The vent and drain port cover plates are installed if necessary.
5. The HI-STAR 100 overpack is downended and positioned on the transport equipment.
6. A final inspection of the HI-STAR 100 overpack is performed and includes the following:
 - A final survey for removable contamination on the accessible external surfaces of the HI-STAR 100 overpack in accordance with 49CFR173.443(a) [7.1.3]. If necessary, the overpack is further decontaminated to meet the surveillance requirements.
 - A radiation survey of the HI-STAR 100 overpack to confirm that the radiation levels on any external surface of the overpack do not exceed the levels required by 49CFR173.421(a)(2) [7.1.3]. Any issues are identified to site management and the overpack is decontaminated as directed by site radiation protection.
 - A visual inspection of the HI-STAR 100 overpack to verify that there are no outward visual indications of impaired physical condition except for superficial marks and dents and that the package is securely closed in accordance with 49CFR173.428(b) [7.1.3].
 - Verification is made that the HI-STAR 100 overpack neutron shield relief devices are installed, intact, and are not covered by tape or other covering.
7. If desired, the impact limiters are installed and the impact limiter bolts are torqued in accordance with requirements in Table 7.1.1.
8. A security seal is installed either on the closure plate or on both impact limiters, if installed. The security seal number(s) is(are) recorded on the shipping documentation.

9. *Final radiation surveys of the package surfaces are performed per 10CFR71.47 [7.1.4], and 49CFR173.428(a) [7.1.3].*
10. *If desired, the personnel barrier and personnel barrier locks are installed and the personnel barrier keys are transferred to the carrier.*
11. *A final check to ensure that the package is ready for release is performed and includes the following checks:*
 - *Verification that the receiver has been notified of the impending shipment.*
 - *Verification that any labels previously applied in conformance with Subpart E of 49CFR172 [7.1.3] have been removed, obliterated, or covered and the "Empty" label prescribed in 49CFR172.450 [7.1.3] is affixed to the packaging in accordance with 49CFR173.428(d) [7.1.3].*
 - *Verification that the package for shipment is prepared in accordance with 49CFR173.422 [7.1.3].*
 - *Verification that all required information is recorded on the shipping documentation.*
12. *The HI-STAR 100 System is then released for transport.*

7.4

*PROCEDURE FOR PREPARING THE HI-STAR 100 OVERPACK FOR
TRANSPORT FOLLOWING A PERIOD OF STORAGE*

The operations for preparing the loaded HI-STAR 100 Overpack for transport following a period of storage (in excess of one year from the date of completion of HI-STAR 100 overpack mechanical seal leakage testing) are identical to the cask loading and preparation for transport described in Section 7.1.5.

7.5

REFERENCE

- [7.1.1] *American Society of Mechanical Engineers "Boiler and Pressure Vessel Code". 1995 Edition with 1996 and 1997 Addenda.*
- [7.1.2] *Holtec International Report HI-2012610, HI-STAR 100 System Final Safety Analysis Report.*
- [7.1.3] *U.S. Code of Federal Regulations, "Shippers – General Requirements for Shipments and Packages," Part 49, "Transportation."*
- [7.1.4] *U.S. Code of Federal Regulations, "Standards for Protection Against Radiation", Part 10, "Energy."*
- [7.1.5] *American National Standards Institute, Institute for Nuclear Materials Management, "American National Standard for Radioactive Materials – Leakage Tests on Packages for Shipment," ANSI N14.5-19897, January 1987.*
- [7.1.6] *Holtec International Report HI-2002444, Final Safety Analysis Report for the HI-STORM 100 Cask System.*

SUPPLEMENT 7.I

OPERATING PROCEDURES OF THE HI-STAR HB SYSTEM

7.I.0 INTRODUCTION

This chapter outlines the procedures for loading, preparation for shipment, unloading, and preparation for empty cask shipment of the HI-STAR HB System where it differs from the HI-STAR 100 System in accordance with 10CFR71 [7.0.1].

7.I.1 PROCEDURE FOR LOADING AND PREPARATION FOR TRANSPORT OF THE HI-STAR HB SYSTEM

7.I.1.1 Loading of Contents into HI-STAR HB

7.I.1.1.1 Loading of SNF into HI-STAR HB from a Spent Fuel Pool

Steps 1 through 17 as well as 19 through 22 are equivalent to HI-STAR 100 in Section 7.1.3.1. The following is an exception for HI-STAR HB:

- 18. The helium backfill is adjusted to the pressure equivalent of ≥ 0 psig and ≤ 48.8 psig at a reference temperature of 70 degrees Fahrenheit.*

CHAPTER 8: ACCEPTANCE TESTS AND MAINTENANCE PROGRAM

8.0 INTRODUCTION

This chapter identifies the acceptance tests and maintenance program to be conducted on the HI-STAR 100 Package to verify that the structures, systems, and components (SSCs) classified as important to safety have been fabricated, assembled, inspected, tested, accepted, and maintained in accordance with the requirements set forth in this Safety Analysis Report (SAR), the applicable regulatory requirements, and the Certificate of Compliance (CoC). The acceptance criteria and maintenance program described in this chapter fully comply with the requirements of 10CFR Part 71 [8.0.1].

8.1 ACCEPTANCE TESTS

This section provides the workmanship inspections and acceptance tests to be performed on the HI-STAR 100 Package prior to or during use. These inspections and tests provide assurance that the HI-STAR 100 Package has been fabricated, assembled, inspected, tested, and accepted for use and loading under the conditions specified in this SAR and the CoC issued by the NRC in accordance with the requirements of 10CFR Part 71.

8.1.1 Visual Inspections and Measurements

The following visual inspections and measurements shall be performed on the HI-STAR 100 Package, including the MPCs, in order to assure compliance with this SAR and the Certificate of Compliance. Inspections and measurements shall be performed in accordance with written and approved procedures and results shall be documented and become part of the quality documentation package. Any area found to be under the specified minimum thickness shall be repaired in accordance with the applicable ASME code requirements.

- 1. Visual inspections and measurements shall be made and controls shall be exercised to ensure that the packaging conforms to the dimensions and tolerances specified on the applicable drawings referenced in the CoC, specifically the following:
 - a. The radial neutron shield minimum thickness*
 - b. The impact limiter neutron shield minimum thickness.*
 - c. The minimum flux trap sizes, if applicable.*
 - d. The minimum fuel cell pitch, if applicable.*
 - e. Correct thickness of top flange, closure plate, and bottom plate for gamma shielding.*
 - f. Correct total measured thickness of inner shell plus intermediate shells over the total surface area.**
- 2. The packaging shall be inspected for cleanliness and proper preparation for shipping in accordance with written and approved procedures.*
- 3. The sealing surfaces (including the lid and all penetrations) shall be inspected to ensure that there are no gouges, cracks, or scratches that could result in unacceptable leakage.*

4. *The locations, types, and sizes of welds shall be confirmed by measurement to be as specified on the drawings.*
5. *The packaging will be visually inspected to ensure it is conspicuously and durably marked with the proper markings/labels in accordance with 10CFR71.85(c) and if applicable also in accordance with 10CFR 72.236(k).*
6. *Visual inspections shall be made to verify that neutron absorber panels are present on the basket cell walls as required by the basket design.*

8.1.2 Weld Examinations

All weld examinations shall be performed in accordance with the applicable ASME Code sections as specified on the drawings [8.1.1]. Examination of MPC components shall be performed per ASME Code Section III, Subsections NB, NF, and NG, per NB-5300, NF-5300, and NG-5300 and the code alternatives listed in Table 1.3.2, as applicable. Examination of the overpack shall be performed per ASME Code, Subsection NB, NB-5300 for containment boundary components, and Subsection NF, NF-5300 and the code alternatives listed in Table 1.3.2 for non-containment boundary components.

The MPC lid-to-shell weld shall be verified by either volumetric examination using ultrasonic methods or by surface examination using multi-layer liquid penetrant methods. Regardless of which method is used, the root and final layers shall be examined by liquid penetrant. If liquid penetrant alone is used, additional intermediate examinations shall be conducted after each approximately 3/8 inch of the weld is completed.

All weld examinations shall be performed in accordance with written and approved procedures, by qualified personnel, in accordance with SNT-TC-1A [8.1.2]. All results, including relevant indications, shall be made a permanent part of the quality records by video, photographic, or other means providing an equivalent retrievable record of weld integrity.

8.1.3 Structural and Pressure Tests

The HI-STAR 100 system containment boundary shall be examined and tested using pressure testing, ultrasonic testing, MT and/or PT, as applicable, to verify that it is free of cracks, pinholes, uncontrolled voids or other defects that could significantly reduce the effectiveness of the packaging.

8.1.3.1 Lifting Trunnions

Two trunnions (located near the top of the HI-STAR overpack) are provided for vertical lifting and handling of the HI-STAR 100 Package without the impact limiters installed. The trunnions are designed and shall be inspected and tested in accordance with ANSI N14.6 [8.1.3] as detailed in this Subsection. The trunnions are fabricated using a high-strength and high-ductility material (see overpack drawing in Section 1.4). The trunnions contain no welded components.

In order to ensure that the lifting trunnions do not have any hidden material flaws, the

trunnions shall be tested at 300% of the maximum design (service) lifting load. The load shall be applied for a minimum of 10 minutes to the pair of lifting trunnions. The accessible parts of the trunnions (areas outside the HI-STAR overpack), and the local HI-STAR 100 cask areas shall then be visually examined to verify no deformation, distortion, or cracking has occurred. Any evidence of deformation, distortion or cracking of the trunnion or adjacent HI-STAR 100 cask areas shall require replacement of the trunnion and/or repair of the HI-STAR 100 cask. Following any replacements and/or repair, the load testing shall be re-performed and the components re-examined in accordance with the original procedure and acceptance criteria. Testing shall be performed in accordance with written and approved procedures. Certified material test reports verifying trunnion material mechanical properties meet ASME Code Section II requirements provide further verification of the trunnion load capabilities. Test results shall be documented and shall become part of the final quality documentation package.

8.1.3.2 Pressure Testing

8.1.3.2.1 HI-STAR 100 Containment Boundary

The containment boundary of the HI-STAR Package shall be hydrostatically or pneumatically pressure tested to 150 psig +10/-0 psig, in accordance with the requirements of the ASME Code Section III, Subsection NB, Article NB-6000 and the code alternatives listed in Table 1.3.2. The test pressure of 150 psig is 150% of the Maximum Normal Operating Pressure (MNOP).

The overpack pressure test may be performed at any time during fabrication after the containment boundary is complete. The HI-STAR overpack shall be assembled for this test with the closure plate mechanical seal (only one required) or temporary test seal installed.

The test pressure shall be maintained for ten minutes. During this time period, the pressure gauge reading shall not fall below 150 psig. At the end of ten minutes, and while the pressure is being maintained at a minimum of 150 psig, the overpack shall be observed for leakage. In particular, the closure plate-to-top forging joint (the only credible leakage point) shall be examined. If a leak is discovered, the overpack shall be emptied and an evaluation shall be performed to determine the cause of the leakage. Repairs and retest shall be performed until the pressure test acceptance criterion is met.

After completion of the pressure testing, the overpack closure plate shall be removed and the internal surfaces shall be visually examined for cracking or deformation. Any evidence of cracking or deformation shall be cause for rejection or repair and retest, as applicable. The overpack shall be required to be pressure tested until the examinations are found to be acceptable.

Test results shall be documented and shall become part of the final quality documentation package.

8.1.3.2.2 MPC Pressure Boundary

Pressure testing (hydrostatic or pneumatic) of the MPC pressure boundary shall be performed in accordance with the requirements of the ASME Code Section III, Subsection NB, Article NB-6000, applicable sub-articles, and the code alternatives listed in Table 1.3.2 when field welding of the MPC lid-to-shell weld is completed. If hydrostatic testing is used, the MPC shall be pressure tested to 125% of design pressure. The minimum hydrostatic test pressure shall be 125 psig. If pneumatic testing is used, the MPC shall be pressure tested to 120% of the design pressure. The minimum pneumatic test pressure shall be 120 psig. Following completion of the required hold period at the test pressure, and after determining the leakage acceptance criterion is met, the surface of the MPC lid-to-shell weld shall be re-examined by liquid penetrant examination performed in accordance with ASME Code Section V, Article 6, with acceptance criteria per ASME Code Section III, Subsection NB, Article NB-5350.

Test results shall be documented and shall become part of the final quality documentation record package.

8.1.3.3 Pneumatic Testing of the Neutron Shield Enclosure Vessel

A pneumatic pressure test of the neutron shield enclosure vessel shall be performed following final closure welding of the enclosure shell returns and enclosure panels. The pneumatic test pressure shall be 37.5 +2.5, -0 psig, which is 125 percent of the relief device set pressure. The test shall be performed in accordance with approved written procedures.

During the test, the relief devices on the neutron shield enclosure vessel shall be removed. One of the relief device threaded connections is used for connection of the air pressure line and the other connection will be used for connection of the pressure gauge.

Following the introduction of pressurized gas into the neutron shield enclosure vessel, a 15-minute pressure hold time is required. If the neutron shield enclosure vessel fails to hold pressure, an approved soap bubble solution shall be applied to determine the location of the leak. The leak shall be repaired using weld repair procedures prepared in accordance with the ASME Code Section III, Subsection NF, Article NF-4450. The pneumatic pressure test shall be re-performed until no pressure loss is observed.

Test results shall be documented and shall become part of the final quality documentation package.

8.1.4 Leakage Tests

Leakage testing shall be performed in accordance with the requirements of ANSI N14.5-1997 [8.1.4]. Testing shall be performed in accordance with written and approved procedures. A leakage test of the HI-STAR overpack shall be performed at any time after the containment boundary fabrication is complete. The leakage test instrumentation shall have a minimum test sensitivity of 2.15×10^{-6} atm cm^3/s (helium). Containment boundary welds shall have indicated leakage rates not exceeding 4.3×10^{-6} atm cm^3/s (helium).

8.1.5 Component and Material Tests

The majority of materials used in the HI-STAR overpack are ferritic steels. ASME Code Section III and Regulatory Guides 7.11 [8.1.5] and 7.12 [8.1.6] require that certain materials be tested in order to assure that these materials are not subject to brittle fracture failures.

Each plate or forging for the HI-STAR 100 Package containment boundary (overpack inner shell, bottom plate, top flange, and closure plate) shall be required to be drop weight tested in accordance with the requirements of Regulatory Guides 7.11 and 7.12, as applicable. Additionally, per the ASME Code Section III, Subsection NB, Article NB-2300, Charpy V-notch testing shall be performed on these materials. Weld material used in welding the containment boundary shall be Charpy V-notch tested in accordance with ASME Section III, Subsection NB, Articles NB-2300 and NB-2430.

Non-containment portions of the overpack, as required, shall be Charpy V-notch tested in accordance with ASME Section III, Subsection NF, Articles NF-2300, and NF-2430. The non-containment materials to be tested include the intermediate shells, overpack port cover plates, and applicable weld materials.

Tables 2.1.22 and 2.1.23 provide the test temperatures or T_{NDT} , and test requirements to be used when performing the testing specified above.

8.1.5.1 Valves, Relief Devices, and Fluid Transport Devices

There are no fluid transport devices associated with the HI-STAR 100 Package. The only valve-like components in the HI-STAR 100 Package are the specially designed caps installed in the MPC lid for the drain and vent ports. These caps are recessed inside the MPC lid and covered by the fully welded vent and drain port cover plates. No credit is taken for the caps' ability to confine helium or radioactivity. After completion of drying and backfill operations, the drain and vent port cover plates are welded in place on the MPC lid and are leak tested to verify the MPC pressure boundary.

There are two relief devices (rupture discs) installed in the upper ledge surface of the neutron shield enclosure vessel of the HI-STAR overpack. These relief devices are provided for venting purposes under hypothetical fire accident conditions in which vapor formation from neutron shielding material degradation may occur. The relief devices are designed to relieve at 30 psig (± 5 psig).

8.1.5.2 Seals and Gaskets

Two concentric mechanical seals are provided on the HI-STAR overpack closure plate to provide containment boundary sealing. Mechanical seals are also used on the overpack vent and drain port plugs of the HI-STAR overpack containment boundary. Each primary seal is individually leak tested, in accordance with Subsection 8.1.4, prior to the HI-STAR 100 Package's first use and during each loading operation. An independent and redundant seal is

provided for each penetration (e.g., closure plate, port cover plates, and closure plate test plug). No containment credit is taken for these redundant seals and they are not leakage tested. Details on these seals are provided in Chapter 4.

8.1.5.3 Transport Impact Limiter

The removable HI-STAR transport impact limiters consist of aluminum honeycomb crush material arranged around a carbon steel structure and enclosed by a stainless steel shell. The drawings in Chapter 1 specify the crush strength of the aluminum honeycomb materials (nominal +/- 7%) for each zone of the impact limiter. For manufacturing purposes, verification of the impact limiter material is accomplished by performance of a crush test of sample blocks of aluminum honeycomb material for each large block manufactured. The verification tests are performed in accordance with approved procedures. The certified test results shall be submitted to Holtec International with each shipment of material.

All welds on the HI-STAR impact limiter shall be visually examined in accordance with the ASME Code, Section V, Article 9, with acceptance criteria per ASME Section III, Subsection NF, Article NF-5360.

8.1.5.4 Neutron Shielding Material

Neutron shield properties of Holtite-A are provided in Chapter 1. Each manufactured lot of neutron shield material shall be tested to verify that the material composition (aluminum and hydrogen), boron concentration, and neutron shield density (or specific gravity) meet the requirements specified in Chapter 1. A manufactured lot is defined as the total amount of material used to make any number of mixed batches comprised of constituent ingredients from the same lot/batch identification numbers supplied by the constituent manufacturer. Testing shall be performed in accordance with written and approved procedures and/or standards. Material composition, boron concentration, and density (or specific gravity) data for each manufactured lot of neutron shield material shall become part of the quality record documentation package.

The installation of the neutron shielding material shall be performed in accordance with written, approved, and qualified procedures. The procedures shall ensure that mix ratios and mixing methods are controlled in order to achieve proper material composition, boron concentration and distribution, and that pours are controlled in order to prevent gaps or voids from occurring in the material. Holtec International shall maintain samples of each manufactured lot of neutron shield material.

Users shall implement procedures which verify the integrity of the Holtite-A neutron shield once for each overpack. Neutron shield integrity shall be verified via measurements either at first use or with a check source using, at a maximum, a 6x6 inch test grid over the entire surface of the neutron shield, including the impact limiters.

Following the first fuel loading of each HI-STAR 100 Package, a shielding effectiveness test shall be performed to verify the effectiveness of the neutron shield using written and approved

procedures. Calibrated radiation detection equipment shall be used to take measurements at the surface of the HI-STAR overpack. Measurements shall be taken at three cross sectional planes through the radial shield and at four points along each plane's circumference. The average measurement results from each sectional plane shall be compared to calculated values to assess the continued effectiveness of the neutron shield. The calculated values shall be representative of the loaded contents (i.e., fuel type, enrichment, burnup, cooling time, etc...) or the particular check source used for the measurements. Measurements shall be documented and become part of the quality documentation package.

8.1.5.5 Neutron Absorber Material

Each plate of neutron absorber shall be visually inspected for damage such as scratches, cracks, burrs, peeled cladding, foreign material embedded in the surfaces, voids, delamination, and surface finish.

8.1.5.5.1 Boral

After manufacturing, a statistical sample of each lot of neutron absorber shall be tested using wet chemistry and/or neutron attenuation testing to verify minimum ^{10}B content (areal density) in samples taken from the ends of the panel. The minimum ^{10}B loading of the neutron absorber panels for each MPC model must comply with the limits specified on the drawings. Any panel in which ^{10}B loading is less than the minimum allowed shall be rejected. Testing shall be performed using written and approved procedures. Results shall be documented and become part of the cask quality records documentation package.

8.1.5.5.2 METAMIC[®]

NUREG/CR-5661 identifies the main reason for a penalty in the neutron absorber B-10 density as the potential of neutron streaming due to non-uniformities in the neutron absorber, and recommends comprehensive acceptance tests to verify the presence and uniformity of the neutron absorber for credits more than 75%. Since a 90% credit is taken for METAMIC[®], the following criteria must be satisfied:

- The boron carbide powder used in the manufacturing of METAMIC[®] must have small particle sizes to preclude neutron streaming.
- The ^{10}B areal density must comply with the limits specified on the drawings.
- The B_4C powder must be uniformly dispersed locally i.e. must not show any particle agglomeration. This precludes neutron streaming.
- The B_4C powder must be uniformly dispersed macroscopically i.e. must have a consistent concentration throughout the entire neutron absorber panel.
- The maximum B_4C content in METAMIC[®] shall be less than or equal to 33.0 weight percent.

To ensure that the above requirements are met the following tests shall be performed:

- All lots of boron carbide powder are analyzed to meet particle size distribution requirements.
- The following qualification testing shall be performed on the first production run of METAMIC[®] panels for the MPCs in order to validate the acceptability and consistency of the manufacturing process and verify the acceptability of the METAMIC[®] panels for neutron absorbing capabilities:
 - 1) The boron carbide powder weight percent shall be verified by testing a sample from forty different mixed batches. (A mixed batch is defined as a single mixture of aluminum powder and boron carbide powder used to make one or more billets. Each billet will produce several panels.) The samples shall be drawn from the mixing containers after mixing operations have been completed. Testing shall be performed using the wet chemistry method.
 - 2) The ¹⁰B areal density shall be verified by testing a sample from one panel from each of forty different mixed batches. The samples shall be drawn from areas contiguous to the manufactured panels of METAMIC[®] and shall be tested using the wet chemistry method. Alternatively, or in addition to the wet chemistry tests, neutron attenuation tests on the samples may be performed to quantify the actual ¹⁰B areal density.
 - 3) To verify the local uniformity of the boron particle dispersal, neutron attenuation measurements of random test coupons shall be performed. These test coupons may come from the production run or from pre-production trial runs.
 - 4) To verify the macroscopic uniformity of the boron particle distribution, test samples shall be taken from the sides of one panel from five different mixed batches before the panels are cut to their final sizes. The sample locations shall be chosen to be representative of the final product. Wet chemistry or neutron attenuation shall be performed on each of the samples.
- During production runs, testing of mixed batches shall be performed on a statistical basis to verify the correct boron carbide weight percent is being mixed.
- During production runs, samples from random METAMIC[®] panels taken from areas contiguous to the manufactured panels shall be tested via wet chemistry and/or neutron attenuation testing to verify the ¹⁰B areal density. This test shall be performed to verify the continued acceptability of the manufacturing process.

The measurements of B₄C particle size, ¹⁰B isotopic assay, uniformity of B₄C distribution and ¹⁰B areal density shall be made using written and approved procedures. Results shall be documented and become part of the cask quality records documentation package.

8.1.5.6 Gamma Shielding

The gamma shielding (steel) in the construction of the HI-STAR 100 package is dimensionally inspected to assure compliance with the applicable drawings referenced in the CoC and as required in Subsection 8.1.1.

8.1.6 Thermal Tests

The first fabricated HI-STAR 100 overpack was tested to confirm its heat transfer capability. The test was performed and documented in Holtec Document DOC-5014-01 [8.1.7]. The tests have shown that the HI-STAR 100 system is within acceptable limits and future thermal testing is no longer required.

8.2 MAINTENANCE PROGRAM

An ongoing maintenance program is defined and incorporated in the HI-STAR 100 System Operations Manual that will be prepared and issued to each user prior to delivery and first use of the HI-STAR 100 Package. This document shall delineate the detailed inspections, testing, and parts replacement necessary to ensure continued radiological safety, proper handling, and containment performance of the HI-STAR 100 Package in accordance with 10CFR71 regulations, conditions in the Certificate of Compliance (CoC), and the design requirements and criteria contained in this Safety Analysis Report (SAR).

The HI-STAR 100 Package is totally passive by design. There are no active components or systems required to assure the continued performance of its safety functions. As a result, only minimal maintenance will be required over its lifetime, and this maintenance would primarily result from weathering effects, and pre- and post-usage requirements for transportation. Typical of such maintenance would be the reapplication of corrosion inhibiting materials on accessible external surfaces, and seal replacement and leak testing following replacement. Such maintenance requires methods and procedures are no more demanding than those currently in use at power plants.

The maintenance program schedule for the HI-STAR 100 Package is provided in Table 8.2.1.

8.2.1 Structural and Pressure Tests

Prior to each fuel loading, a visual examination in accordance with a written and approved procedure shall be required of the following HI-STAR 100 Package components: lifting trunnions (area outside of the overpack); overpack internals and externals; and impact limiters. The examination shall inspect for indications of overstress such as cracking, deformation or wear marks, gross damage to components, or areas of chipped or missing surface coatings. Repairs or replacement in accordance with written and approved procedures shall be required if unacceptable conditions are identified.

No periodic structural or pressure tests on the overpack or MPCs following the initial acceptance tests are required to verify continuing performance.

8.2.2 Leakage Tests

Mechanical seals are used on the HI-STAR 100 overpack containment boundary to ensure the retention of the radioactive material contents in the HI-STAR 100 Package. These seals are not temperature sensitive within the design temperature range, are resistant to corrosion and radiation environments, and are helium leak tested after fuel loading. The containment system has been designed to withstand normal and accident conditions of transport without loss of containment integrity. The overpack containment penetration seals shall be leakage tested in accordance with Chapter 7 and the acceptance criteria of Subsection 8.1.4.

The mechanical seals on the overpack containment boundary shall be replaced as defined in Table 8.2.1. After each replacement, the helium leak test of the overpack containment seals

described in Chapter 7 shall be performed. Prior to replacement of each seal, the mating surfaces shall be cleaned and visually inspected for scratches, pitting or roughness, and affected surface areas shall be polished smooth or repaired as necessary in accordance with written and approved procedures. The bolting for the closure plate and the vent and drain port cover plates, and port plugs shall also be inspected for indications of wear, galling, or indentations on the threaded surfaces prior to reinstallation and closure torquing. Any bolt or port plug showing any of these indications shall be replaced.

8.2.3 Component and Material Tests

The relief devices on the overpack neutron shield enclosure shell shall be visually inspected prior to each use of the HI-STAR 100 Package for damage or indications of excessive corrosion. If the inspection determines an unacceptable condition, the relief devices shall be replaced. The relief devices shall be replaced with approved spares every five years while the cask is in transport service.

8.2.4 Shielding

Periodic verification of the neutron shield integrity shall be performed within 5 years prior to each shipment. The periodic verification shall be performed by radiation measurements with either loaded contents or a check source. Measurements shall be taken at three cross sectional planes through the radial shield and at four points along each plane's circumference. The average measurement results from each sectional plane shall be compared to calculated values to assess the continued effectiveness of the neutron shield. The calculated values shall be representative of the loaded contents (i.e., fuel type, enrichment, burnup, cooling time, etc...) or the particular check source used for the measurements.

8.2.5 Thermal Tests

For each package, a periodic thermal performance test shall be performed within 5 years prior to each shipment, to demonstrate that the thermal capabilities of the cask remain within its design basis.

8.2.6 Miscellaneous Tests

The impact limiters shall be visually inspected in accordance with a written procedure prior to each use to inspect for surface denting, surface penetrations, and weld cracking. Any areas found to not meet the defined acceptance criteria shall be repaired and/or replaced in accordance with written and approved procedures.

Table 8.2.1

MAINTENANCE AND INSPECTION PROGRAM SCHEDULE

Task	Frequency
<i>Overpack cavity and external surface (accessible) visual inspection</i>	<i>Prior to each fuel loading</i>
<i>Overpack bolting and port plug visual inspection</i>	<i>Prior to installation and prior to each transport</i>
<i>Lifting trunnion and pocket trunnion recess visual inspection</i>	<i>Prior to each fuel loading and prior to each transport</i>
<i>Containment System Periodic Leakage Test of closure plate, and vent and drain port plugs</i>	<i>Following each fuel loading, and prior to off-site transport if period from last test exceeds 1 year</i>
<i>Containment System Fabrication Verification Leakage Test of containment boundary closures</i>	<i>After third use</i>
<i>Transport impact limiter visual inspection</i>	<i>Prior to each transport</i>
<i>Closure plate mechanical seal replacement</i>	<i>Following removal of closure plate bolting</i>
<i>Closure plate bolt replacement</i>	<i>Every 240 bolting cycles (assumes 20 years at 12 cycles per year)</i>
<i>Port plug seal replacement</i>	<i>Following removal of applicable port plug</i>
<i>Port cover plate seal replacement</i>	<i>Following removal of applicable cover plate</i>
<i>Relief Device visual inspection</i>	<i>Prior to each transport</i>
<i>Relief Device replacement</i>	<i>Every five years</i>
<i>Thermal Test</i>	<i>Within 5 years prior to each shipment</i>
<i>Shielding Test</i>	<i>Within 5 years prior to each shipment</i>

8.3 REFERENCES

- [8.0.1] U.S. Code of Federal Regulations, Title 10, "Energy", Part 71, "Packaging and Transportation of Radioactive Materials."
- [8.1.1] American Society of Mechanical Engineers, "Boiler and Pressure Vessel Code," Sections II, III, V, IX, and XI, 1995 Edition with 1996 and 1997 Addenda.
- [8.1.2] American Society for Nondestructive Testing, "Personnel Qualification and Certification in Nondestructive Testing," Recommended Practice No. SNT-TC-1A, December 1992.
- [8.1.3] American National Standards Institute, Institute for Nuclear Materials Management, "American National Standard for Radioactive Materials - Special Lifting Devices for Shipping Containers Weighing 10,000 Pounds (4500 kilograms) or More", ANSI N14.6, September 1993.
- [8.1.4] American National Standards Institute, Institute for Nuclear Materials Management, "American National Standard for Radioactive Materials Leakage Tests on Packages for Shipment", ANSI N14.5, 1997.
- [8.1.5] U.S. Nuclear Regulatory Commission, "Fracture Toughness Criteria of Base Material for Ferritic Steel Shipping Cask Containment Vessels with a Maximum Wall Thickness of 4 Inches (0.1m)," Regulatory Guide 7.11, June 1991.
- [8.1.6] U.S. Nuclear Regulatory Commission, "Fracture Toughness Criteria of Base Material for Ferritic Steel Shipping Cask Containment Vessels with a Wall Thickness Greater than 4 Inches (0.1m) But Not Exceeding 12 Inches (0.3m)," Regulatory Guide 7.12, June 1991.
- [8.1.7] Holtec International Document DOC-5014-03, "Acceptance Testing of First HI-STAR Overpack (Thermal and He Leak Tests)", September 2006.

SUPPLEMENT 8.I

ACCEPTANCE TEST & MAINTENANCE PROGRAM

The main body of this chapter remains fully applicable for the HI-STAR HB configuration of the HI-STAR 100 System.